University of East Anglia

Atmospheric Halocarbon Measurements with a focus on East and South-East Asia

By

Lauren Jane Gooch

July 2016

A thesis submitted to the School of Environmental Sciences of the Univeristy of East Anglia, in partial fulfilment of the requirements for the degree of Doctor of Philosophy

For Dad

Abstract

A large variety of halocarbon species are present in the atmosphere and can significantly impact stratospheric ozone depletion and/or global warming. Compound use has been phased out, reduced and replaced for some species under global control measures such as the Montreal and Kyoto Protocols. However, relatively long atmospheric lifetimes, imperfect substitutes and incomplete reductions in usage mean that global abundances of halocarbon species still require regular monitoring. This is especially true for the rapidly developing East and South-East Asian regions where widespread emissions have been repeatedly reported in recent years.

To detect a variety of halocarbon mixing ratios, air samples are cryotrapped and analysed via gas chromatography couple with mass spectrometry (GC-MS). Highly sensitive and precise instrumentation widens this range further and the automation of the analysis system would improve and extend sample throughput. A semi-automated inlet system for a GC-MS set-up was constructed and cryotrapping with liquid nitrogen was tested successfully.

In the atmosphere, anthropogenic emissions are the main source of many halocarbons, however methyl halides also have large natural sources including from cultivated crops like rice. Using genetically mapped and altered *Arabidopsis thaliana* and *Physcomitrella patens*, methyl halide emission rates were calculated. Differences found when compared to wild type plants indicated the potential for developing 'ozone-safe' crops through manipulation of the HOL-gene, which may particularly benefit Asian emissions.

Three short-term sampling campaigns based in Taiwan assessed abundances of mainly anthropogenically-sourced halocarbons in East Asia. Backwards trajectory modelling was used to estimate potential source regions and both enhanced and close to background mixing ratios were observed for a range of species. Pollution events and interspecies correlations were found for many halocarbons with poorly understood sources such as CFC-113a and HCFC-133a.

A further short-term campaign based in Bachok, Malaysia assessed long-range transport of ozone-depleting species to South-East Asia during the cold surge phenomenon of the winter monsoon, when rapid vertical transport may occur. Short-lived species were observed at significantly high abundances suggesting their potential impact on stratospheric ozone may have been previously underestimated.

Acknowledgements

I have to start by thanking my supervisor Johannes Laube for all his support and patience throughout the long process that has been this thesis. Thanks must also go to Bill Sturges and David Oram, for their considerable help and direction as co-supervisors, as well as the many tangent-filled meetings.

This work would have been impossible without the generosity and support of so many other people, particularly the teams in both Taiwan and Bachok, for collecting samples and sharing their data, and Matt Ashfold for all of the modelling.

In the lab, thanks to Graham Mills for the many technical (and some not so technical) solutions, Stephen Humphrey for all the Entech samples and Adam Wisher for the support during the inlet system construction. I am also extremely grateful to Sam Allin for teaching me the ways of the AutoSpec and all the administrative help. Finally, the electronics and mechanics workshops at UEA deserve a huge thank you for putting up with my destructive tendencies; Nick and Gareth - you guys saved me more times than I can count!

On a more personal note, I would like to thank Anna for all the company in the lab, the unintentional 3-hour coffee breaks and all of the pep talks – I'm not sure I would have got this far without you! To my Glen Lodge family, especially Emma, thanks for the much needed distraction and friendship throughout my research. Whilst I don't recommend going straight from a 12-hour lab day to a 7-hour bar shift, there's no one else I'd rather do it with.

Bryony – thank you for keeping me sane, listening to my rants and ensuring I left the house from time to time when I was writing. As best friends go, there's no doubt in my mind that you are the very best. And Lee – you were only subjected to last parts of this process but I think that meant you saw some of the worst moments. Thank you for your patience during my frustration, procrastination and general stressing. You're still here so it can't have been all bad. Here's to the future.

Finally, Dad. You and Jill have been there for me throughout the whole of my university career and I can't thank you both enough. Your unending faith that one day I would complete this thesis and that I would eventually stop being a student has kept pushing me up to the end (and of course, because it's us, it has to be right up to the deadline). You proofread a large amount of this monstrosity and I don't think I can every repay you except to say that this work is entirely dedicated to you. After all, it is your fault that it ended up so long; I was following your advice:

"Why use 3 words when 27 will do."

Table of Contents

Chapter 1: General Introduction

Chapter 2: Experimental Theory and Methods

Chapter 3: Analysis of Methyl Halide Emissions from Plants

Chapter 4: Halocarbon Observations in Taiwan

Chapter 5: Long-range transport of Ozone Depleting Substances to Bachok, Malaysia

Chapter 6: Conclusions and Outlook

Appendices

Chapter 1: General Introduction

Atmospheric environmental concerns have, in the past few decades, come to the forefront of scientific and public interest. Air pollution, anthropogenic climate change and the ozone hole are just some of the issues that, given their negative effect on the environment and human health, have led to the implementation of both local and global control measures. Legislation of this type aims to minimise further man-made impact by reducing emissions of the chemical compounds and trace gases responsible, whilst encouraging industry to develop and implement less damaging alternatives. Regardless, policy-makers and the scientific community alike are required to continually monitor atmospheric composition to ensure current measures are being followed and to identify new or recurring potential threats.

This thesis will focus on the halocarbon family of atmospheric trace gases, carbon-based species that also contain fluorine, chlorine, bromine and/or iodine atoms, which contribute to stratospheric ozone depletion and global warming. This chapter will cover the basic concepts of atmospheric structure and the related chemistry as well as introducing the subgroups of halocarbon species and the global legislation that affects their production and use.

1.1 The Atmosphere

Although mainly composed of nitrogen (78% by volume) and oxygen (21%), the Earth's atmosphere contains a wide variety of what are known as 'trace' gases due to their relatively low atmospheric abundances. Whilst carbon dioxide (CO_2) and methane (CH_4) can be measured in parts-per-million (ppm) and parts-per-billion (ppb) respectively, only in recent years have reliable measurements been capable for species in the parts-per-trillion (ppt) range. The origin of these species may be natural, anthropogenic or a combination of the two.

There are generally four major regions of the atmosphere, known as the troposphere, stratosphere, mesosphere and thermosphere (see Figure 1). Closest to the surface is the troposphere and this extends to a height of approximately 8 to 18km depending on global location and the season. Most known weather effects occur in this region due to the dynamic surface-heat-driven mixing and water vapour availability. Above this is the stratosphere, which encompasses the region from the top of the troposphere to around 45-55km altitude, and the transition between these regions is known as the tropopause. The stratosphere sees much slower vertical mixing (approximately 1 year in the lower stratosphere) than is found in the troposphere (around 3-4 weeks) (Warneck, 1999) and is where the formation of ozone, the species that absorbs most of the ultraviolet radiation from the sun, dominates. This work investigates species with chemistry only relevant to these two regions.

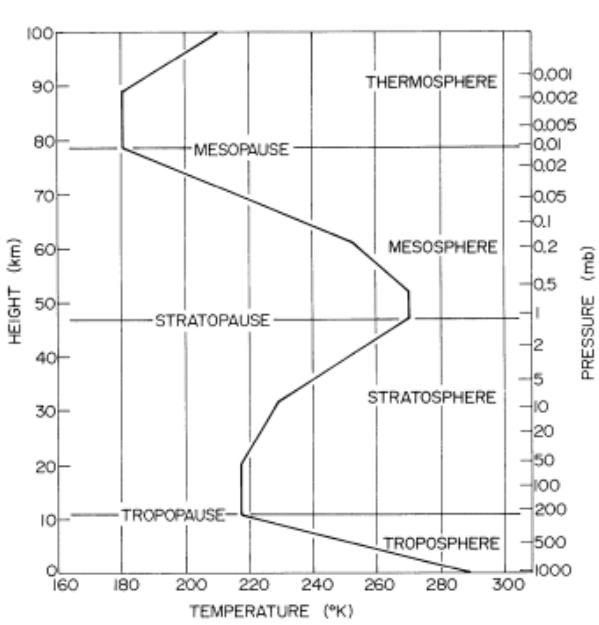

Figure 1.1: The layers of the atmosphere and the typical vertical temperature profiles a for midlatitude U.S. Standard Atmosphere (Wallace and Hobbs, 1977)

1.2 Transport

In the troposphere, temperature decreases with height at a rate of ~6.5Kkm^{-1} since the main heat source is emitted radiation from the Earth's surface. This results in convective vertical transport where hot, moist air rises and is then dried through condensation with increasing altitude, creating instability and causing further uplift. When the tropopause is reached, the presence of ozone in the stratosphere causes a temperature inversion, which inhibits further convective transport. However, air may be driven through the tropopause if it has enough latent heat energy and, when this is encountered, often the air masses were originally those of warm, water-saturated air from the tropics.

The temperature difference between the warmer tropical regions and the cold polar-regions is the driving force behind atmospheric circulation in the troposphere. It is attempted equilibration between these areas that results in the transport from the equator to the tropics. The Intertropical Convergence Zone (ITCZ) is a region close to the equator where air masses are transported across the subtropic surface and then undergo strong vertical transport at the tropics. This is the main region considered in this work as the deep convection may result in trace gases being transported from the marine boundary layer (MBL) to the tropical tropopause layer (TTL) and so to the stratosphere much quicker than through general transport (Hossaini *et al*. 2012a, Krysztofiak *et al.* 2012, Takahashi and Luo, 2014), potentially in a matter of hours.

The TTL is a layer found below the cold point tropopause (~17km) and above the maximum convective outflow level (~12km) that acts a source region for the lowermost stratosphere.

Uplift from this region results in transport to the stratosphere in the Brewer-Dobson circulation where slow, pole-ward transport takes place. At the mid-latitudes, air descends meaning mixing and transport with the tropopause occurs again.

As such, some substances that entered in the tropics may be recycled back into the troposphere and those that enter at the mid-latitudes are unlikely to be transported to the upper stratosphere. The majority of halocarbon species considered in this study are substantially broken down before an altitude of 30km, with the breakdown of most short-lived species occurring below 19km (Laube et al. 2008).

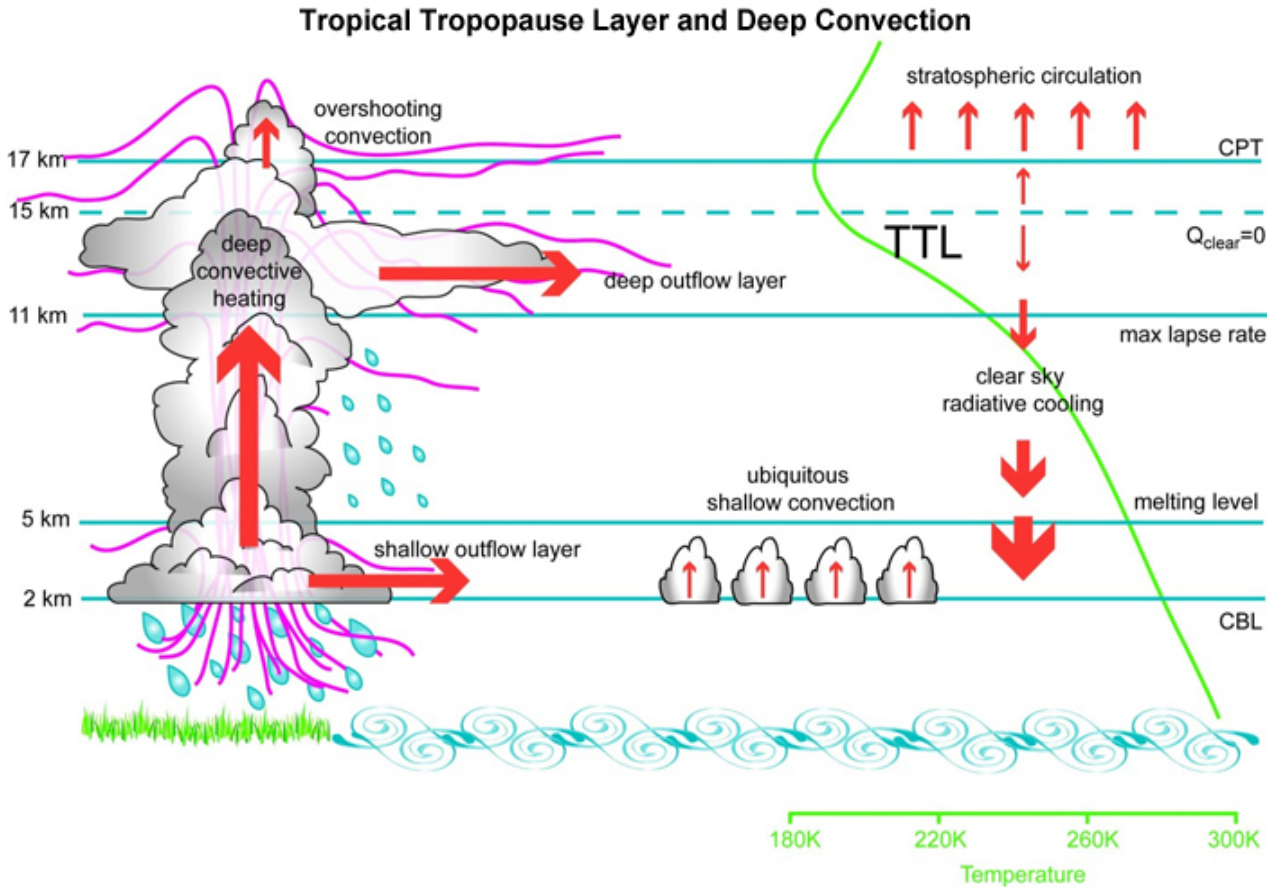

Figure 1.2: Schematic of tropical deep convection and interaction with the Tropical Tropopause Layer (TTL). (Carpenter and Reimann, 2014)

1.3 Ozone

Although mostly located in the stratosphere, naturally occurring ozone (O_3) is also present nearer the Earth's surfaces in the tropospheric atmosphere. At low altitudes O_3 can be damaging to both public health and plant life due to its highly reactive nature. However, in the stratosphere where it forms the 'ozone layer', O_3 absorbs UVB (280-315nm) and UVC (10-280nm) radiation from the sun, preventing most of this potentially harmful radiation from reaching the surface. As such, comprehension of the formation and destruction of O_3 that controls its atmospheric abundance is particularly important in order to maintain stratospheric O_3 whilst minimising near-surface O_3.

Global distribution of ozone varies significantly as a number of factors impact the mechanisms for production and loss, including latitude and season (see Figure 1.3), as well as atmospheric circulation.

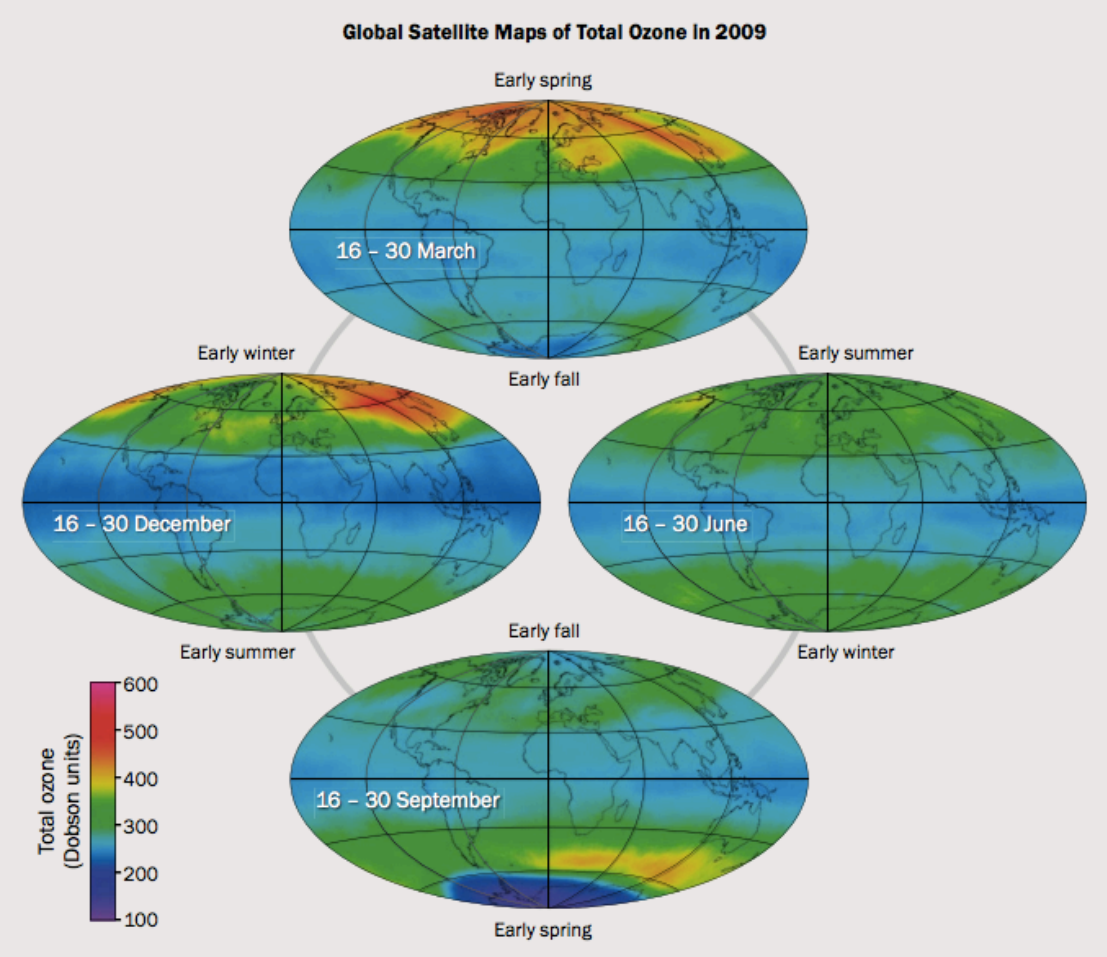

Figure 1.3: Typical seasonal and latitudinal variations in Total Ozone abundance, measured in Dobson units, from global satellite maps in 2009. The lowest values of ozone can be found over Antarctica during late winter and early spring, when the ozone hole forms each year. (Hegglin *et al.* 2015)

The discovery of the 'ozone hole' over the Antarctic (Farman et al. 1985) was the first step in increasing both public and scientific awareness of the damage being done in the stratosphere by ozone-depleting gases. This occurs during the late winter and early spring when ozone destruction by chlorine- and bromine-containing gases is increased due to the meteorological and chemical conditions of the region.

Firstly, stratospheric transport results in these gases be transported pole-wards via Brewer Dobson circulation. During the winter, a polar vortex is formed around the poles, preventing significant transport or mixing of air in or out of the polar stratospheres. As the temperature decreases, the circulation of the vortex strengthens and, as winter temperatures are lower in the Antarctic, the southern polar vortex is more effective of the two. Once the polar temperatures drop low enough, this causes the formation of liquid and solid polar stratospheric clouds (PSCs) over the Antarctic. These increase the relative abundance of reactive chlorine gases, through reactions on their surfaces, that convert reservoir species to the more reactive chlorine monoxide (ClO) (see Section 1.4 for more details). This heightened abundance of ClO results in the catalytic cycles that destroy ozone becoming active as soon as sunlight is available, causing severe depletion. The geographical region known as the 'ozone hole' is the usually defined as the area where ozone concentration falls below 220-Dobson units, averaged between 21-30th September each year.

The discovery of this phenomenon and the work of Molina and Rowland (1974) on the role of chlorofluorocarbons in ozone depletion led to the creation and primary implementation of global legislation, namely the Montreal Protocol, to reduce and ultimately counteract this phenomenon. For these control measures to be most effective, atmospheric O_3 chemistry needs to be understood.

1.3.1 Production

Tropospheric O_3 may be transported from the stratosphere, through the tropopause, or be produced by near-surface chemical reactions. Whilst these reactions may involve natural or anthropogenic gases, the production of pollutant gases like mono-nitrogen oxides (NO_x), through the combustion of fossil fuels, is a main source of low altitude O_3 production. Equation 1.1 shows how the breakdown of NO_2 by photolysis can result in oxygen atom formation. This atom is highly reactive and may combine with O_2 to form O_3 (see Equation 1.2, Liu and Ridley, 1999). *M* is representative of a third body, often N_2 or O_2 although particles or trace gases may also serve, which absorb the excess energy from the reaction as heat (Coffey and Brasseur, 1999).

$$NO_2 + h\nu \longrightarrow O + NO \quad (\lambda < 400\text{nm}) \qquad \text{Equation 1.1}$$

$$O + O_2 + M \longrightarrow O_3 + M \qquad \text{Equation 1.2}$$

In the stratosphere, photolysis by ultraviolet radiation splits molecules of O_2 into O atoms as shown in Equation 1.3. Again, as in Equation 1.2, these atoms may react with further O_2 and produce O_3. For every three O_2 split, the overall reaction produces two O_3 molecules.

$$O_2 + h\nu \longrightarrow O + O \quad (\lambda < 242\text{nm}) \qquad \text{Equation 1.3}$$

1.3.2 Loss

In the troposphere, the main loss process is where O_3 is photolysed in the presence of water vapour (see Equation 1.4) to an excited state oxygen atom, $O(^1D)$, and O_2. This $O(^1D)$ may then go on to combine with water vapour to produce 2 hydroxyl radicals (Equation 1.5). O_3 may also be lost by surface deposition.

$$O_3 + h\nu \longrightarrow O(^1D) + O_2 \qquad \text{Equation 1.4}$$
$$O(^1D) + H_2O \longrightarrow 2OH \qquad \text{Equation 1.5}$$

Stratospheric O_3 may be converted back to O_2 and atomic O by solar radiation (see Equation 1.6, Coffey and Brasseur, 1999) and these processes are part of a reaction series put forward by Chapman (1930) to describe the production and destruction of the ozone layer. The net reaction of this cycle can be seen in Equation 1.7, however abundance of O_3 is overestimated by this oxygen-only mechanism, indicating that further loss reactions must be taking place.

$$O_3 + h\nu + M \longrightarrow O_2 + O + M \qquad \text{Equation 1.6}$$
$$2O_3 \longrightarrow 3O_2 \text{ (net)} \qquad \text{Equation 1.7}$$

These additional loss mechanisms are from a number of catalytic cycles that result in ozone destruction. The basic processes can be seen in Equations 1.8 and 1.9 and the net reaction is shown in Equation 1.10. Here, *X* can represent a variety of catalytic species present in the natural atmosphere, including H, OH and NO, as well as the halogens Cl, Br and to a lesser extent I. Whilst HO_x species (H, OH and HO_2) are mostly produced in the stratosphere from the reaction of energetically excited oxygen, $O(^1D)$, with CH_4 and H_2O, NO_x species (NO and NO_2) are produced through the breakdown of nitrous oxide (N_2O). The breakdown of both natural and anthropogenic halocarbon trace gases is responsible for the presence of stratospheric Cl and Br. However, the vertical gradient of I in the troposphere is uncertain and variable and, likely due to its shorter photochemical lifetime and the lower abundance of source gases, very little I reaches the stratosphere.

$$X + O_3 \longrightarrow XO + O_2 \qquad \text{Equation 1.8}$$
$$XO + O \longrightarrow X + O_2 \qquad \text{Equation 1.9}$$
$$O + O_3 \longrightarrow 2O_2 \text{ (net)} \qquad \text{Equation 1.10}$$

This work is focussed on chlorine and bromine based halocarbon species that deplete ozone and so only the chlorine and bromine ozone chemistry will be discussed further.

1.4 Chlorine and Ozone

The increased application of halogenated species in industry led to Stolarski and Cicerone proposing the chlorine-catalysed destruction of stratospheric ozone in 1974. These species breakdown through photolysis in the upper stratosphere and release chlorine atoms, an example of which is shown in Equation 1.11 using the compound CFC-12 (CCl_2F_2).

$$CCl_2F_2 + h\nu \longrightarrow CClF_2 + Cl \qquad \text{Equation 1.11}$$

Chlorine atoms participate in the chlorine catalytical cycle which is shown in Equation 1.12 and 1.13, and may be natural or anthropogenic in origin. Since there is increased solar radiation at tropical and mid-latitudes in the stratosphere, the O_3 destruction cycle is also increased resulting in the formation of more atomic oxygen. This can then be used by the process in Equation 1.13 to recycle the Cl atom, which in turn can go on to potentially destroy 100,000 ozone molecules (Chiras, 2001). As such, each Cl atom in the stratosphere has a very high potential for O_3 destruction.

$$Cl + O_3 \longrightarrow ClO + O_2 \qquad \text{Equation 1.12}$$
$$ClO + O \longrightarrow Cl + O_2 \qquad \text{Equation 1.13}$$

This catalytic cycle may be terminated via reactions with a number of species that result in the formation of 'reservoir' compounds. These are compounds that retain ozone-destroying species in an inactive form. Chlorine nitrate ($ClONO_2$) is produced by reactions with NO_x (Equation 1.14) to form a temporary reservoir for ClO and reactions with HO_x do the same with the formation of hypochlorous acid (HOCl, Equation 1.15). These can lead to non-linear response of ozone to chlorine transport (Holloway and Wayne, 2010) and so, when assessing the potential impact of ozone destroying chemical, the reservoir load must be included in the quantification. If the reservoirs are removed from the stratosphere, these mechanisms may act as sinks for ClO_x, where ClO_x refers to the involved chlorinated species (with x = 0, 1 or 2).

$$ClO + NO_2 + M \longrightarrow ClONO_2 + M \qquad \text{Equation 1.14}$$
$$ClO + HO_2 \longrightarrow HOCl + O_2 \qquad \text{Equation 1.15}$$

However, the main reservoir for ClO_x is through the formation of hydrochloric acid (HCl), which acts as a sink by removal from the stratosphere via slow transport into the troposphere. At this point it is dissolved by water and released in rainfall. HCl is thought to account for around 70% of stratospheric chlorine (Holloway and Wayne, 2010) and the production and regeneration reactions are shown in Equations 1.15 and 1.16.

$$Cl + CH_4 \longrightarrow CH_3 + HCl \qquad \text{Equation 1.16}$$
$$OH + HCl \longrightarrow Cl + H_2O \qquad \text{Equation 1.17}$$

1.5 Bromine and Ozone

On a per-atom basis, compared to chlorine, bromine is around 60 times more efficient at ozone destruction (Daniel and Velders, 2007) and there are three associated factors that contribute to this:

1. Longer wavelengths photolyse bromine compounds resulting in a higher percentage of free bromine atoms than chlorine.
2. Inefficient formation of bromine reservoir species and these are readily photolysed.
3. Free chlorine and bromine are produced through coupling between chlorine- and bromine-catalysed reactions.

There are also three branches of these coupling cycles of ClO and BrO processes and Equations 1.18 and 1.19 indicate the two that produce Cl and Br atoms directly. BrCl is formed by the third branch of the cycle (Equation 1.20) and this can be further broken down by photolysis to atomic Br and Cl. Equations 1.20 and 1.21 show the mechanism by which these atoms from the ClO-BrO cycle may go on to react with O_3.

$$ClO + BrO \longrightarrow Cl + Br + O_2 \qquad \text{Equation 1.18}$$
$$ClO + BrO \longrightarrow OClO + Br \qquad \text{Equation 1.19}$$
$$ClO + BrO \longrightarrow BrCl + O_2 \qquad \text{Equation 1.20}$$

$$Cl + O_3 \longrightarrow ClO + O_2 \qquad \text{Equation 1.21}$$
$$Br + O_3 \longrightarrow BrO + O_2 \qquad \text{Equation 1.22}$$

1.6 Heterogeneous Chemistry

Gas phase reactions, such as those described in the previous sections (1.3, 1.4 and 1.5), are not the only ones that occur in the stratosphere. Stratospheric particles including ice, sulphuric acid and nitric acid hydrate, all play a role in stratospheric chemistry, particularly in the re-partitioning of reservoir species. $ClONO_2$, as formed in Equation 1.13, may react with HCl to form Cl_2 (Equation 1.23) that can then be photolysed (Equation 1.24) or it can also be hydrolysed on stratospheric particles (Equation 1.25). A variety of other reactions involving reservoir species and stratospheric particles also occur but will not be expanded on here.

$$ClONO_2 + HCl \xrightarrow{on\ ice} Cl_2 + HNO_3 \qquad \text{Equation 1.23}$$
$$Cl_2 + h\nu \longrightarrow 2Cl \qquad \text{Equation 1.24}$$

$$ClONO_2 + H_2O_{(s)} \longrightarrow HOCl + HNO_3 \qquad \text{Equation 1.25}$$

1.7 The Importance of Halogenated Trace Gases

The relative abundance of chlorine and bromine in the stratosphere is dependent upon the surface emissions of halogenated trace gases such as chlorofluorocarbons (CFCs) and halons, along with considerations as to their reactivity and that of other related species. Halocarbon compounds such as these are known to contribute to ozone depletion. Knowledge of their concentrations can be key to identifying past and future changes to the ozone layer, although other factors such as carbon dioxide trends must also be considered to give a complete picture. Many halocarbons are greenhouse gases as well so predictions as to changes in global warming, be they past or future, can be made given abundancy data for known contributing species. In short, measurements of halogenated trace gases provide the foundation for understanding and anticipating pivotal changes to the atmospheric environment and as such regular global monitoring is required.

1.8 Atmospheric Lifetimes

The total atmospheric lifetime of a species is calculated as a ratio of its global atmospheric burden (C_{Global}) to the global loss rate (L_{Total}) which encompasses all the processes that remove a gas from the atmosphere (see Equations 1.26 and 1.27 below). These can include photodissociation, reaction with OH and heterogeneous removal along with oceanic and land uptake that leads to permanent removal (Carpenter and Reimann, 2014).

$$\tau_{\text{Total}} = {}^{C_{\text{Global}}}/_{L_{\text{Total}}} \qquad \text{Equation 1.26}$$

$$\text{Where } L_{\text{Total}} = L_{\text{Atm}} + L_{\text{Soil}} + L_{\text{Ocean}} \dots L_x \qquad \text{Equation 1.27}$$

Lifetimes are regularly used in the computation of other atmospherically relevant values such as ozone depleting potentials and global warming potentials. The upcoming tables 1.1 – 1.10 include the total atmospheric lifetimes for the species measured in this study, most of which are measured in years aside from the very short-lived species which range from days to months. Atmospheric lifetimes are regularly re-evaluated and updated to reflect increased knowledge in chemistry and removal processes.

1.9 Ozone Depleting Potentials (ODPs)

In order for the relative impacts of ozone depletion to be compared for halogenated gases, a standardised method was developed. The calculated ozone depletion potential (ODP) for a species is used to quantify the potential to destroy stratospheric ozone when said species is released at the Earth's surface. All compounds are assessed relative to a similar mass of CFC-11 (CCl_3F), which is given an ODP of 1.0. A high ODP indicates a more effective ozone depleting substance per mass emitted.

The equation for calculating ODP can be seen below:

$$\mathrm{ODP} = \Phi \cdot \alpha \cdot \frac{\tau_x}{\tau_{\mathrm{CFC-11}}} \frac{M_{\mathrm{CFC-11}}}{M_x} \frac{n_x}{3} \qquad \text{Equation 1.28}$$

Where **Φ** is the fractional release factor (representing the factor of inorganic halogen release into the stratosphere relative to CFC-11), and **α** indicates the relative effectiveness for ozone destruction of any halogen compared with chlorine (e.g. 60 would be used here for bromine (Daniel and Velders, 2006)). $\boldsymbol{\tau_x}$ represents the global lifetime of the halogen gas, $\boldsymbol{M_x}$ is the molecular weight and $\boldsymbol{n_x}$ indicates the number of halogen atoms (Montzka and Fraser, 2003). Uncertainties in atmospheric lifetimes and understanding of stratospheric chemistry and dynamics can lead to the adjustment of ODPs for affected species.

Of the halocarbon species discussed in this work chlorofluorocarbons (CFCs) and halons have high ODPs whereas their replacements, hydrochlorofluorocarbons (HCFCs) and hydrofluorocarbons (HFCs) have much lower or near-zero ODPs thus their use reduces the negative impact to stratospheric ozone abundance.

1.10 Radiative Forcing

This concept is used to compare natural and anthropogenic conditions that can influence climate change, as a simple method that enables their quantification. It can be defined as 'the change in net (down minus up) irradiance (solar plus longwave; in W m^{-2}) due to an imposed change. More simply, it is the difference in the irradiation absorbed by the Earth and the energy the radiated back into space, measured as power (watts) per square meter of Earth surface. A positive radiative forcing indicates a warming effect on the Earth's climate whereas a negative forcing indicates a cooling effect. Whilst it does not represent overall climate response, it is more easily calculable than response to other external forcings and so it is useful in providing estimates of climate impact (Myhre *et al*. 2013).

The amount of radiation retained in the Earth's atmosphere can be altered through the greenhouse effect. This is where some of the infrared radiation travelling back into space from the Earth's surface is absorbed by gases in the atmosphere, which produces a warming effect.

The natural greenhouse effect is very important as the Earth's average temperature without it would be -18°C. However, the addition of further greenhouse gases (GHGs) to the atmosphere will, over time, shift the balance of energy entering and leaving the Earth's system further and increase the warming effect.

Whilst trace gases like CO_2, CH_4 and water vapour, along with all of the halocarbon species considered in this work, are significantly less abundant than N_2 and O_2, they make large contributions in terms of radiative forcing. This is because these species, known as GHGs, have strong absorption bands in the infrared spectrum. Whilst these absorption bands differ between species, halocarbons cover the areas where CO_2 absorbs weakly, effectively closing the atmospheric 'windows' where radiation may escape into space. As such all GHGs have a direct positive radiative forcing value. However, indirect effects such as their contribution to ozone depletion resulting in cooling effects may compensate for this and, in the case of some species like the halons, lead to negative radiative forcing values. Figure 1.4 shows the evolution of radiative forcing for a range of GHGs, including many of the halocarbons featured in this work, between 1850 and 2011. Control measures have slowed and in some cases begun to reverse the additional forcing of some species, however the long atmospheric lifetimes associated with many halocarbons mean impacts are still likely to be seen for many decades to come.

Radiative forcing values alone are not enough to assess the climate response to a specific species; the temporal and spatial evolution of emissions need to be considered, along with atmospheric lifetimes (Forster *et al*. 2007). As such, global warming potentials (GWPs) are frequently utilised to evaluate the impact to climate from a particular substance.

1.11 Global Warming Potentials (GWPs)

Similar to that of ODP, a standardised method was developed in order to compare the radiative forcing of a GHG emission to a reference gas, on a per kilogram basis, so relative impact could be assessed between species. This global warming potential (GWP) takes into account both the atmospheric lifetime and radiative forcing effect of a specific gas (see equation 1.29) and compares it to a reference gas. As such, GWP is dependent on the time-horizon over which it is calculated (e.g. 20, 100 or 500 years). Compounds with atmospheric short atmospheric lifetimes (e.g. less than 1 year) but with high radiative forcing may have a considerable impact over a 20-year period but this reduces to a negligible impact over a 100-year period. Carbon dioxide is used as the reference gas and so has a GWP of 1.0 and 100 years is the most commonly utilised time-horizon.

$$GWP(x) = \frac{\int_0^{TH} a_x \bullet [x(t)]\, dt}{\int_0^{TH} a_r \bullet [r(t)]\, dt} \qquad \text{Equation 1.29}$$

Where *TH* is the time-horizon, a_x represents the radiative forcing due to a unit increase in atmospheric abundance of the species and $[x(t)]$ is the loss rate (atmospheric lifetime) of said species. The corresponding quantities for the reference gas, CO_2, are inserted into the denominator (Boucher *et al*. 2001).

The GWPs for the range of halocarbon species discussed in this work can be found in the upcoming Tables 1.1 – 1.10. Again, like ODPs, uncertainties in chemistry, dynamics and atmospheric lifetimes can alter the GWPs of specific compounds.

GWP and ODP do not strongly correlate for halocarbon species as they values depend on different properties, chemical and physical, within a compound. As such, whilst hydrofluorocarbon (HFC) species have near zero ODPs due to their lack of chlorine and bromine atoms, their GWPs range between 2 and 13,000 times more effective at climate forcing than the same mass of CO_2 (Hegglin *et al*. 2015). The implementation of global control measures resulted in a slowing of radiative forcing (see Figure 1.4) due to the decline in emissions of CFCs. However, emissions of HFCs, perfluorocarbons (PFCs) and SF_6 continue to increase, all of which are strong GHGs. Figure 1.5 shows emissions of ODS and ODS replacement, weighted by 100-yr GWPs into equivalent CO_2 emissions between 1980 and 2012. This indicates that CO_2 equivalent emissions of HCFCs and HFCs are near equal to those of CFCs and are still increasing. As such, climate forcing from halocarbons will begin to increase again until these species are similarly controlled (Carpenter and Reimann, 2014). However, even though its GWP is lower than many halocarbon species, CO_2 itself is the most abundant greenhouse gas and so the most important in the control of climate forcing (Hegglin *et al*. 2015).

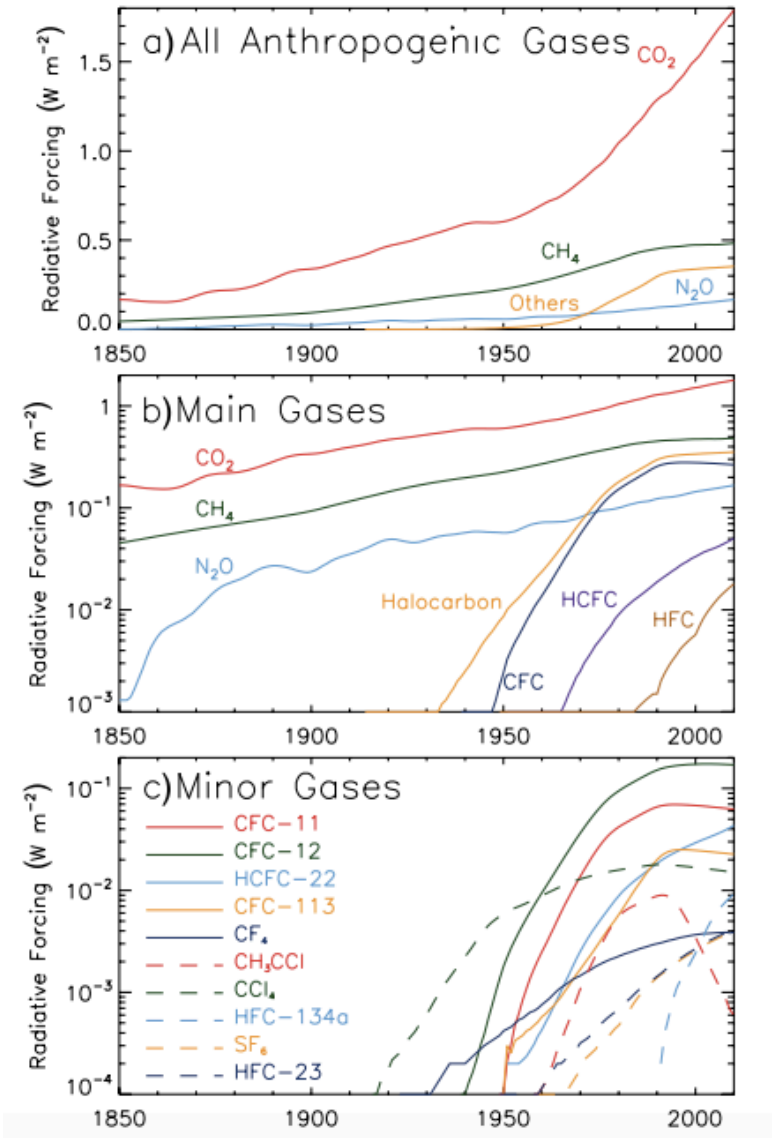

Figure 2.4: A comparison of the radiative forcing of a number of well mixed greenhouse gases between 1850 and 2011. A) Summary of the change in radiative forcing of all contributing anthropogenic gases. B) Utilises a logarithmic scale to further display the same information as A and displays the contributing of several halocarbon groups. C) Displays the change in radiative forcings of a number of specific halocarbon species, utilising a logarithmic scale (Myhre et al. 2013).

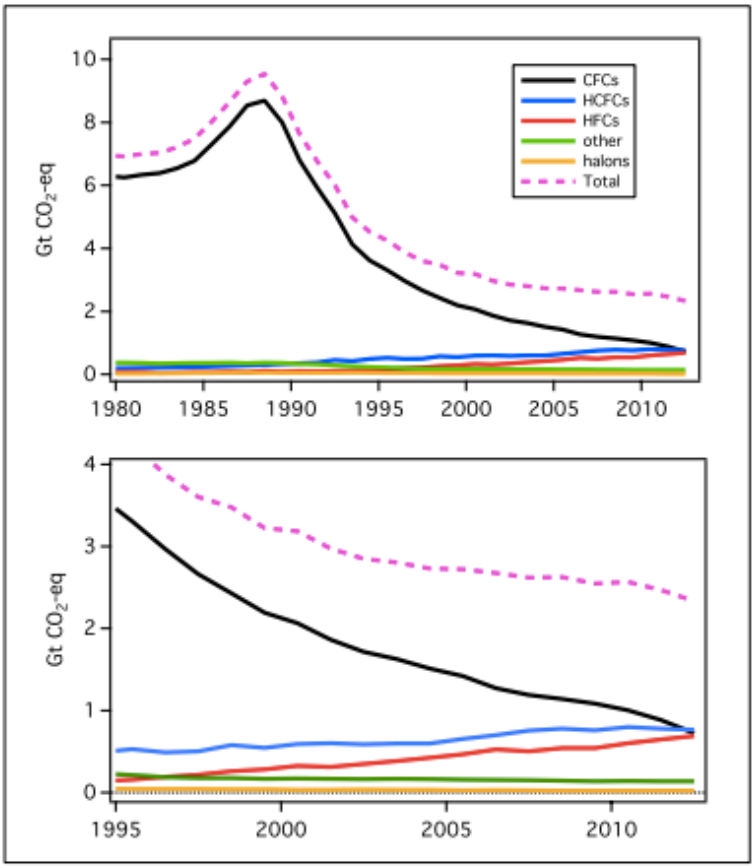

Figure 1.5: The change in emissions of ozone depleting substances and their replacements, weighted by 100-yr global warming potential (GWP) to equivalent emissions of carbon dioxide between 1980 and 2012. The lower panel is an expansion of the 1995-2012 period from the upper panel, showing the increasing emissions of HCFCs and HFCs near equally the decreasing emissions of CFCs, the group of compounds they were developed to replace (Carpenter and Reimann, 2014).

1.12 Equivalent Effective Stratospheric Chlorine (EESC) and Equivalent Chlorine (ECl)

EESC is an estimate of the total stratospheric amount of effective chlorine and bromine and ECl is an estimate of total tropospheric chlorine and bromine. They are both calculated using the sum of chlorine and bromine from tropospheric abundances (Montzka and Reimann, 2011). These are weighted to reflect the expected impact on stratospheric ozone; for EESC using each compounds ODP and for ECl (as utilised in section 6.6.5) by multiplying any bromine atoms included in the calculation by 60 (as they are on average 60 times more effective than chlorine atoms at depleting stratospheric ozone (Daniel and Velders, 2007)). Bromine gases are also scaled accordingly and included in EESC. Time of year and latitude can impact both EESC and ECl values. For EESC, assumptions on transport times into the upper atmosphere are used and so this value will vary between the different regions of the stratosphere (Carpenter and Reimann, 2014). For ECl, atmospheric lifetimes, particularly for the short-lived species, will result in variations in abundance between different regions of the troposphere.

EESC has been regularly used to assess changes in anthropogenic ODS emissions and predict the impact of control measures on stratospheric chlorine and bromine, providing insight into potential future ozone recovery. This is shown in Figure 1.6, which includes a graph indicating the relative amounts of EESC contributed by different halocarbon groups or species up to 2012 and predicts the likely change up to 2100, following compliance with global control measures. 1980 levels are marked on the graphand EESC is not predicted to return to this point until 2050 in the midlatitudes.

Figure 1.7 gives an overview of only the total stratospheric bromine abundances between 1977 and 2009, showing the increase during the uncontrolled use of halons and other bromine-based ODS and then reversal after control measures came into effect. The increased impact of stratospheric bromine is weighted and factored in to the equivalent effective stratospheric chlorine levels shown in Figure 1.6. Figure 1.8 highlights the relationship between EESC and ozone abundance, indicating that as EESC has been decreasing in recent years, polar ozone has begun to increase again.

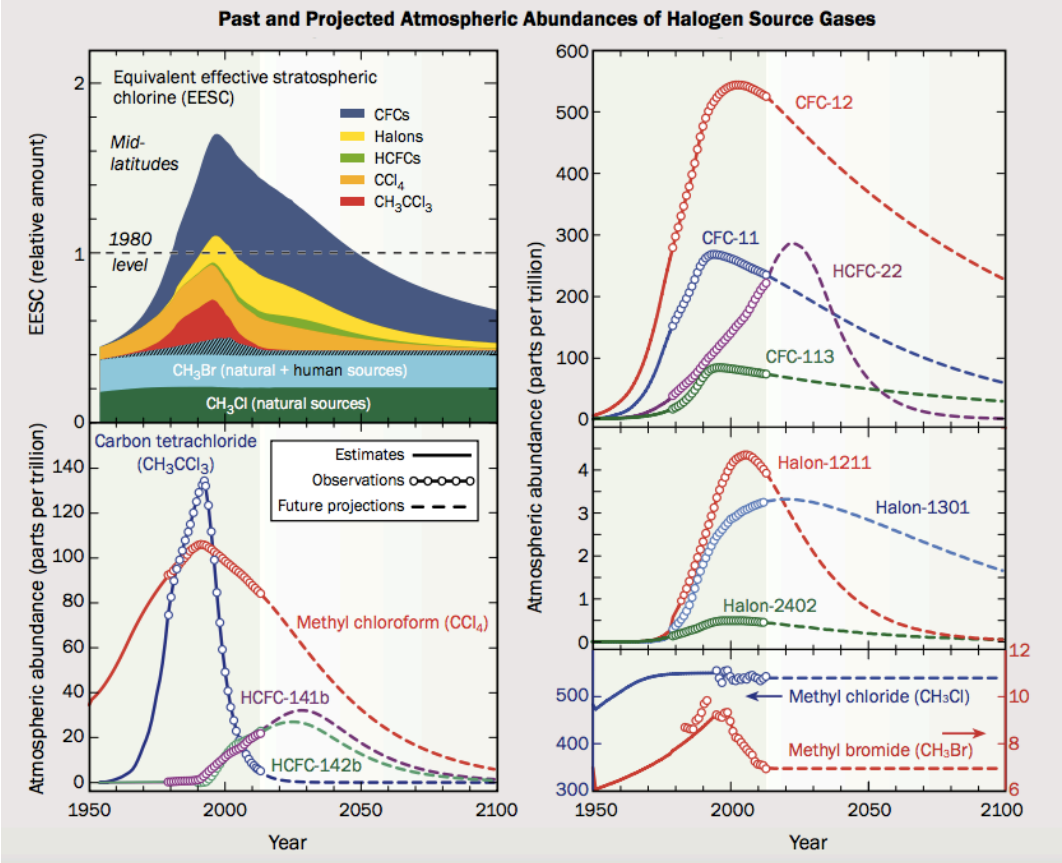

Figure 3.6: The top left panel summarises change in equivalent effective stratospheric chlorine (EESC) between 1950 and 2100. From 1950 to 2012, historical abundance and atmospheric measurements were used to calculate the EESC value and the coloured shading reflects the contribution of different groups of halogenated species. The period saw a distinct rise in EESC before slowing and reversing in the last 20 years. EESC values after 2012 are predicted assuming continued compliance with the Montreal Protocol restrictions on ozone depleting substances (ODS) and thus further decreasing EESC levels.
The other three panels of the figure display observations and estimates of key ODS abundances, measured in parts per trillion, up to 2012. Many of these species saw significant rises in abundance in the late 20th century, followed by a reversal after control measures took effect. Again, after this point predictions are utilised following Montreal protocol compliance. Species such as the hydrochloroflurocarbons (HCFCs) begin their reversal later due to the differences in phase-out schedules compared to chlorofluorocarbons (CFCs) and halons (Hegglin et al. 2015).

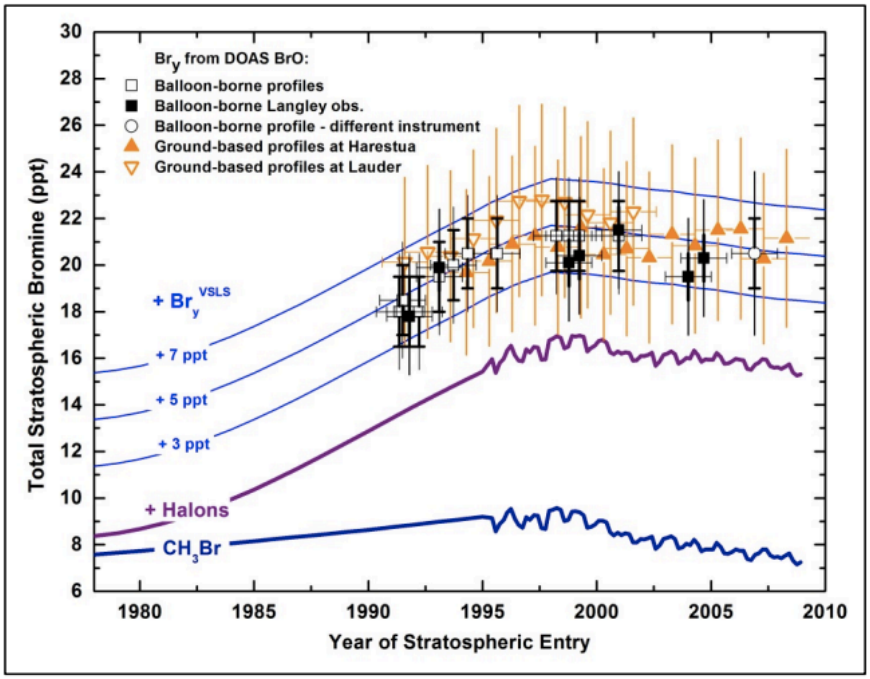

Figure 1.7: Comparison of time of stratospheric entry with total stratospheric bromine abundances, reflecting the contributions of methyl bromide (CH_3Br), halons and a range of potential impacts from very short lived bromine-containing species. Firn measurements were utilised prior to 1995, after which ambient air measurements were used. The pronounced increase attributed to halon after 1980 is unsurprising due to their widespread industrial applications during this period. Methyl bromide has many natural sources and so an industrial related increase is less pronounced however there is a clear decrease after phase-outs in the Montreal Protocol took affect indicating a reduction in sources. The contribution of halons also decreases after the mid to late 1990's, although at a slower rate due to the long-lived nature of halon species. Observation of stratospheric bromine from balloons and ground based measurements suggest that between 3 to 7 ppt of stratospheric bromine may be due to the use of very short lived species (Carpenter and Reimann, 2014).

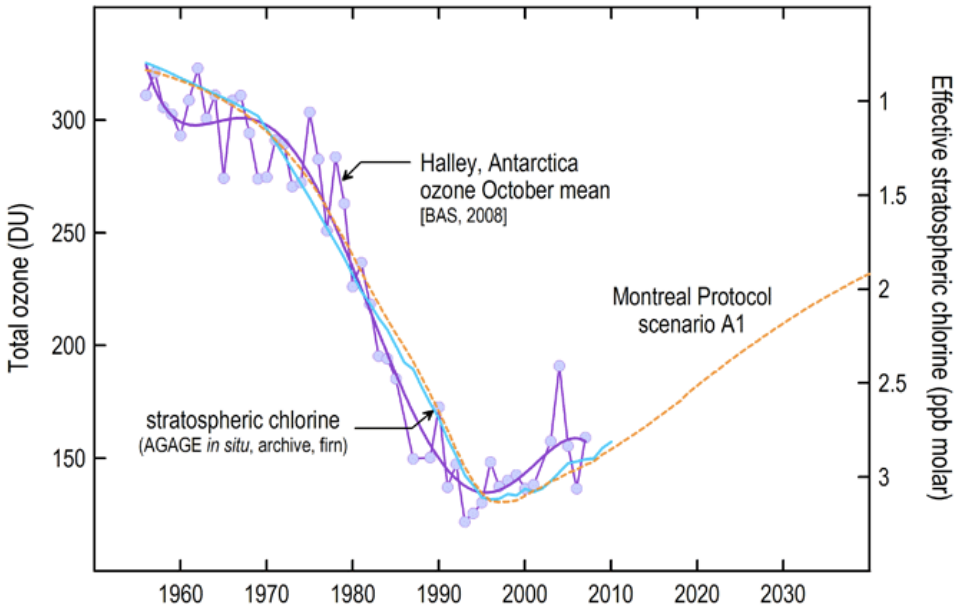

Figure 1.8: A graph comparing observed and predicted effective stratospheric chlorine abundances to those of observed Antarctic ozone. The purple circles represent October mean Antarctic ozone abundances, the blue line represents observed effective stratospheric chlorine concentrations and the dotted orange line represents the predicted effective stratospheric chlorine abundance given Montreal Protocol compliance.

Observed effective stratospheric chlorine can be seen to increase significantly up to the mid to late 1990's with total ozone having decreased over the same time frame. A reversal, due to the influence of the Montreal Protocol control measures, occurred after this point for both effective stratospheric chlorine and total ozone. The observed effective stratospheric chlorine follows closely with the predicted compliance scenario suggesting as stratospheric chlorine decreases, ozone concentrations should continue to increase (CSIRO, 2012)

1.13 Global Legislation

After the identification of the ozone hole, development of global control measures began to reduce and ultimately replace the anthropogenic use of ozone depleting substances (ODS) in industry. This was in the form of the Montreal Protocol, which was first signed by 20 participating nations in 1987. It came into effect on 1st January 1989 and set phase-out schedules for the use of specific groups of ODS for both developed and developing nations (Hegglin *et al*. 2014). Since then, 8 amendments to the Protocol have been made, mainly to increase the range of compounds covered, and it has now been ratified by all 197 parties, making it one of the first universally ratified treaties in UN history. Specific uses of a number of compounds are excluded from being phased out at this time and these, along with the schedules for halocarbon groups, will be discussed further in section 1.14.1 (UNEP, 2017a). The successful reduction of ODS from this legislation has resulted in the ozone hole no longer increasing in size during recent years and ozone mixing ratios are estimated to return to those of 1980 during the 21st century (UNEP, 2014). Figure 1.9 shows the impact on EESC the Montreal Protocol and its amendments made between 1980 and 2012.

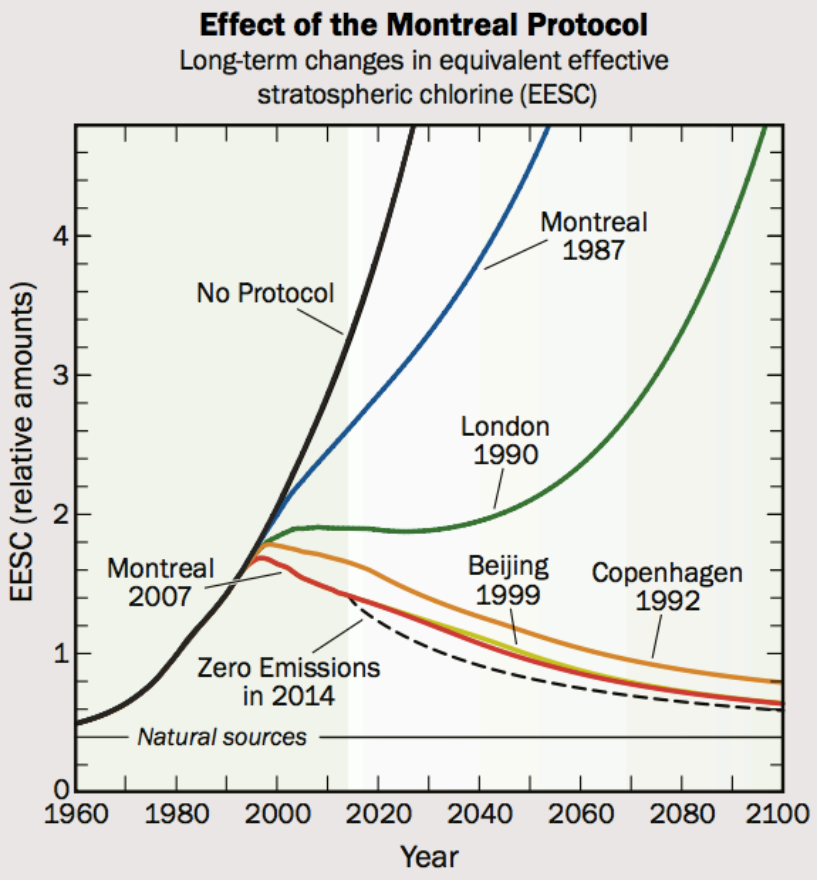

Figure 1.9: The impact of the Montreal Protocol and its amendments on equivalent effective stratospheric chlorine (EESC). This combines and weights the chlorine and bromine content of the ozone depleting substances controlled by the Protocol. EESC values include past observations and projections of a number of scenarios including no provisions, the original 1987 Montreal Protocol provisions and its more recent amendments. The city names and years indicate when and where agreements were reached as to adjusting the 1987 provisions (Hegglins et al. 2015).

There are a number of halocarbon species that do not deplete ozone but they are still GHGs. The Kyoto Protocol was an international treaty, developed in 1997 and entered into force in 2005, in which ratifying nations agreed to reduce GHG emissions. It extended the commitment of the 1992 United Nations Framework Convention on Climate Change (UNFCCC) and set out country-specific targets over a commitment period, the first of which was between 2008 and 2012. These targets covered emissions of CO_2, CH_4 and N_2O (which also depletes ozone) as well as the halocarbon compound groups of hydrofluorocarbons (HFCs), perfluorocarbons (PFCs) and SF_6, which will be expanded on in section 1.12.2. Notable nations that did not ratify the Kyoto Protocol included the United States of America and Canada, the latter of which withdrew in December 2012. The second commitment period was agreed upon in 2012, in the Doha Amendment (UNFCCC, 2012), however not enough states have accepted this amendment for it to have entered into force.

In December 2015, within the framework of the UNFCCC, the Paris Agreement was adopted by consensus and will enter into force in 2017, as long as 55 countries that produce 55% of global greenhouse gas emissions have ratified or accepted the agreement. The aim of this legislation is to keep increases in global temperature "well below 2°C" comparative to pre-industrial levels. National determined contributions (NDCs) will be agreed upon for individual countries and will be reported to and recorded by the UNFCCC Secretariat every 5 years. Whilst this is widely considered a good step towards reducing global warming, there is currently no binding enforcement for the targets set out (UNFCCC, 2015).

In October 2016, the Kigali Amendment was added to the Montreal Protocol, adding HFCs to the list of controlled substances, scheduled to be phased-out. Whilst not generally considered ODS due to their near-zero ODPs, HFCs were utilised in the replacement of CFCs, halons and HCFCs and their increasing use poses a distinct risk to the environment as they have high GWPs. The Kigali Amendment enters into force on the 1st January 2019 and intends to reduce HFC use by 80-85% by the late 2040s. As previously utilised, developed and developing countries have different phase-out schedules in order to allow time and funding to make necessary adjustments to industry and technology. This phase-out process is expected to avoid up to 0.5°C global temperature increase by 2100 (UNEP, 2017b). The universal ratification of the Montreal Protocol and its previous success is hoped to continue with the addition of this landmark amendment.

1.14 Halocarbons

Halocarbon is the general term that represents a large family of fluorine, chlorine, bromine and iodine-containing carbon-based species that can be separated into a number of subgroups. Whilst the majority of halocarbon compounds are greenhouse gases that contribute to global warming, only some groups contain species that deplete stratospheric ozone. The following sections will summarise the various halocarbon subgroups and their properties along with anthropogenic sources, atmospheric sinks and global contributions.

1.14.1 Ozone Depleting Substances

1.14.1.1 Chlorofluorcarbons (CFCs)

The combination compounds of halogens and volatile methane and ethane derivatives, known as chlorofluorocarbons (CFCs), were first developed in the early 1930s for diverse applications both domestically and industrially (Kim *et al*. 2011). Due to their volatility and stability, low toxicity (McCulloch, 1999) and low corrosiveness, as well as zero flammability and reasonable cost, they were used mainly as refrigerants, aerosol propellants, solvents and foam blowing agents (Kim *et al*. 2011).

CFC-12 (CCl_2F_2) and CFC-11 (CCl_3F) were first produced commercially in 1931 and 1932 respectively (Calm, 2008) along with CFC-13 ($CClF_3$), a side product of their manufacture (Montzka and Fraser, 2003). Later followed the development and use of CFC-113 (CCl_2FCClF_2). As the most abundant CFC species in the atmosphere, CFC-12 (524.4 ppt, 2012), CFC-11 (236.3ppt, 2012) and CFC-113 (73.8 ppt, 2012) are known as the major CFCs ([NOAA] Carpenter and Reimann, 2014). CFC-13, which had an abundance of 4 ppt in 1998 (Ehhalt et al. 2001), is considered one of the minor CFC species along with CFC-114 (CF_2ClCF_2Cl) and CFC-115 (CF_3CClF_2) (McCulloch, 1999) as well as the isomers CFC-113a (CCl_3CF_3) and CFC-114a (CF_3CCl_2F). CFC-113a was first detected in atmospheric samples in recent years, owing to its low abundance, along with CFC-112 ($CFCl_2CFCl_2$) and CFC-112a (CF_2ClCCl_3) (Laube et al 2014). The longer-chain, propane-derived CFCs, -216ba ($CF_3CClFCClF_2$) and -216ca ($CClF_2CF_2CClF_2$) were also first observed in 2014 (Kloss et al. 2014). Table 1.1 summarises the uses, atmospheric lifetimes and GWPs of these compounds.

Due to their chemical stability and a minimum of decades long atmospheric lifetimes, CFCs are transported into the stratosphere from the troposphere where they undergo photolysis. There the chlorine atoms are released into the catalytic cycles that destroy ozone. Hydrogen chloride (see equation 1.16) is also a major reservoir for these chlorine atoms. As well as this, all CFCs are good absorbers of infrared radiation, particularly at 1000 to 1400 cm^{-1} (McCulloch, 2003), making them strong GHGs.

Gradual phase out schedules for CFCs under the Montreal Protocol were implemented through the use of alternative compounds such as hydrochlorofluorocarbons (HCFCs – section 1.14.1.3) and hydrofluorocarbons (HFCs – section 1.14.2.1) (McCulloch, 1999), as well as through technological advancement (IPCC/TEAP, 2005). For developed countries, the phase out was mandated for 1st January 1996 whereas developing countries could continue to purchase and produce CFCs until 2010.

Table 1.1: Anthropogenic Uses and Sources, Atmospheric Lifetimes and Global Warming Potentials of Chlorofluorocarbons

Name[a]	Formula[a]	Uses/Sources	Total Lifetime (years)[a]	GWPs relative to CO_2 at 100 years[b]
CFC-11	CCl_3F	Aerosol Propellant, Refrigerant[e]	52	4660
CFC-12	CCl_2F_2	Refrigerant, Aerosol Propellant[e]	102	10200
CFC-113	CCl_2FCClF_2	Aerosols, Cleaning, Drying, Dry-clearing, Blowing agent, Phenolic foams, Heat transfer fluid[f], Solvents[e]	93	5820
CFC-13	$CClF_3$	Side product[g]	640	13900
CFC-114	$CClF_2CClF_2$	Blowing agent, Polyolefin foams[f], Propellants[e]	189	8590
CFC-114a	CCl_2FCF_3	Chemical Processes[f]	~100	6510[d]
CFC-115	$CClF_2CF_3$	Refrigerant, Dieclectric fluid[e]	540	7670
CFC-113a	CCl_3CF_3	Chemical Intermediate[g]	59	3650[d]
CFC-112	$CFCl_2CFCl_2$	Chemical Feedstock, Solvents[g]	59	4260[d]
CFC-112a	CF_2ClCCl_3	Chemical Feedstock, Solvents[g]	51	3330[d]
CFC-216ba	$CF_3CClFCClF_2$	Chemical Processes, Refrigerant[c]	135[c]	-
CFC-216ca	$CF_2ClCF_2CF_2Cl$	Chemical Processes, Refrigerant[c]	135[c]	-

a – Carpenter and Reimann, 2014 b – Hodnebrog et al. 2013 c – Kloss et al. 2014
d – Davis et al. 2016 e – Kim et al. 2011 f – EIA, 2009
g – Montzka and Fraser, 2003

Although global production of CFCs has decreased substantially since the Montreal Protocol was introduced (Kim *et al*. 2011), large volumes remain unreleased in banks such as closed-cell foam products (CFC-11) and non-hermetically sealed refrigeration (CFC-12) (Qin, 2007). Tropospheric chlorine levels have, in recent years, begun to decrease with 2.02 ppb (61%) in 2012 being accounted for from CFCs, a 1% reduction globally from levels in 2008. Hydrogen chloride levels in the stratosphere have also shown, on average, a decline of 0.6% yr^{-1} between 1997 and 2012, reflecting the effect of controls on chlorinated gases (Mahieu *et al*. 2013).

1.14.1.2 Halons

First introduced in the 1960's, bromine containing halogenated hydrocarbons, known as halons, were utilised for fire-fighting and explosion protection (HTOC, 2007) applications. Due to their volatility and electrical non-conductivity along with a lack of damaging residue or toxicity and inexpensive production costs, their use grew worldwide (IPCC/TEAP, 2005).

The major halons (see Table 1.2) developed were halon 1211 (CF_2ClBr) and halon 1301 ($CBrF_3$), with their global production peaking in 1988 at 43,000 and 13,000 tonnes respectively (HTOC, 1991). Their abundances in 2015 were 3.8 ppt and 3.4 ppt respectively (Vollmer et al. 2016). The production of halon 1211 also may have led to the non-deliberate production of the halon 1202 (CBr_2F_2) as a side product, potentially due to over-bromination (Reeves *et al.* 2005). At mixing ratios of 0.019 ppt in 2012 ([UEA Cape Grim] Carpenter and Reimann, 2014), this is considered to be a minor halon species along with halon 2402 ($C_2Br_2F_4$), which was utilised mainly in the former Soviet Republic (IPCC/TEAP, 2005) and had an abundance of 0.42 ppt in 2015 (Vollmer et al. 2016).

Table 1.2: Anthropogenic Uses and Sources, Atmospheric Lifetimes and Global Warming Potentials of Halons

Name[a]	Formula[a]	Uses/Sources[c]	Total Lifetime (years)[a]	GWPs relative to CO_2 at 100 years[b]
Halon-1211	$CBrClF_2$	Fire extinguisher	16	1750
Halon-1301	$CBrF_3$	Fire extinguisher, Feedstock	72	6290
Halon-2402	$CBrF_2CBrF_2$	Fire extinguisher, Chemical Processes	28	1470
Halon-1202	CBr_2F_2	By-product of Halon 1211 production[d]	2.5	231

a – Carpenter and Reimann, 2014 b – Hodnebrog et al. 2013 c – TEAP, 2009
d – Reeves et al. 2005

Like CFCs, halon use results in the destruction of stratospheric ozone through photolysis in the upper stratosphere and the release of Br atoms into catalytic cycles. However, as previously mentioned, bromine is around 60 times more effective than chlorine at destroying ozone (Daniel and Velders, 2007). Also, only relatively small amounts of bromine are held in acid (HBr) and nitrate ($BrONO_2$) non-ozone-destroying reservoirs (Solomon, 1999). Again, halons are good absorbers of infrared radiation, making them strong GHGs although they have relatively low abundance.

Halons were part of the original Montreal Protocol in 1987 and this required that developed countries cease production and consumption by 1996 (UNEP, 1987).

Developing countries were given until 2010 to phase out production and consumption although halon 1301 is still produced in China and France as a feedstock for pesticide manufacture (HTOC, 2011). As such halon 1301 mole fractions are still growing in the atmosphere, with only small emissions required to maintain this growth, given its long lifetime of 72 years (Vollmer et al 2016). Other relatively recent studies have suggested there may be currently unknown sources or banks that are continuing to emit halon 1202 (Newland *et al*. 2013) and this will be discussed further in section 5.11.1. After their addition to the Montreal Protocol, halon replacements were developed including HFCs, HCFC blends and inert gases such as nitrogen and argon, as well as non-gaseous agents such as dry powder aerosols, water mist and foam systems (HTOC, 2011).

Again, similar to CFCs, global production of halons has decreased substantially since the introduction of the Montreal Protocol but large volumes remain unreleased in fire protection application banks. In 2010 these banks were estimated to be 65 Gg for halon 1211 and 43 Gg for halon 1301. However uncertainties in atmospheric lifetimes, particularly for halon 1211, means there may be relative discrepancies. As such, these banks may not be depleted for decades and the effect of the 2010 phase out may not be observable atmospherically for some time (Carpenter and Reimann, 2014).

1.14.1.3 Hydrochlorofluorocarbons (HCFCs)

Developed in the 1980s as substitutes for long-lived ozone-depleting substances, hydrochlorofluorocarbons (HCFCs) are similarly structured to CFCs but contain at least one hydrogen atom. This means that, while they share many of the physiochemical properties of CFCs such as low toxicity, low flammability and reasonable cost (Kim *et al.* 2011), their impact on chlorine levels in the stratosphere is relatively low (Tsai, 2002).

HCFCs are mainly used as CFC replacements and so have applications in the same commercial industries, employing a number of different species (see Table 1.3). Of the more commonly used, major HCFC species, HCFC-22 ($CHClF_2$), HCFC-123 ($CHCl_2CF_3$) and HCFC-124 ($CHClFCF_3$) are all used as refrigerants (McCulloch, 1999). HCFC-141b (CH_3CCl_2F) has applications as a cleaning solvent (Tsai, 2002) as well as a foam-blowing agent along with HCFC-142b (CH_3CClF_2) (McCulloch, 1999).

For the more minor species, HCFC-225ca ($CF_3CF_2CHCl_2$) is utilised as a cleaning agent as well as in adhesives and coatings (Kloss et al. 2014) and HCFC-21 ($CHCl_2F$) is produced by the anaerobic degradation of CFC-11 that may occur in landfills (Kjeldsen *et al*. 2003, Scheutz *et al*. 2010). Knowledge surrounding the applications of the newly observed species HCFC-133a (CF_3CH_2Cl) and HCFC-31 (CH_2ClF) (Laube et al., 2014, Schoenenberger et al., 2015) is limited. However, both are known intermediates in the production of more widely used species, HFCs -125 and -134a for HCFC-133a and HFC-32 for HCFC-31 (Vollmer et al. 2015, Schoenenberger et al., 2015). Two refrigerant blends (R-505 and -506) have also utilised HCFC-31 (Agarwal et al. 2002) but production was not extensive (Schoenenberger et al., 2015).

Due to the carbon-hydrogen bonds present in HCFCs, they are readily susceptible to attack by hydroxyl radicals (OH) in the troposphere. This breakdown means they have considerably shorter atmospheric lifetimes than CFCs and halons (Tsai, 2002) with a maximum lifetime of 18 years, compared to a maximum of 640 years for CFCs and 72 years for halons (Carpenter and Reimann, 2014). Once oxidized, the chlorine subsequently released combines with other tropospheric chemicals and forms soluble compounds that are removed from the atmosphere by precipitation. However, a portion of HCFC molecules will reach the stratosphere and are destroyed in the same way as CFCs, by photolysis. This means they also release chlorine that can participate in the ClO_x catalytic cycle and deplete ozone. As well as this, HCFCs partially contribute to global warming as they too are strong absorbers of infrared radiation. Again, due to tropospheric destruction, the GWPs of HCFCs are still lower than those of CFCs (listed in Table 1.3 and Table 1.1 respectively).

Since HCFCs still contribute some way to stratospheric chlorine levels and global warming, they are only considered to be interim replacements for CFCs and are to be phased out under the Montreal Protocol (Tsai, 2002). HCFCs were originally added to the Protocol under the Copenhagen Amendment in 1992 (UNEP, 1992) and the current schedule for developed countries is that the phase out should be completed by 2020. Developing countries have until 2030 to reach a 97.5% reduction (100% by 2040) whilst consumption and production was to be 'frozen' by 2013 (UNEP, 2007). Replacements for HCFCs vary by application but include CO_2, isobutane, ammonia and HFCs, all of which have disadvantages such as toxicity and high GWP (UNIDO, 2009).

As the phase out of HCFCs is only in the beginning stages, there have been increased emissions over recent years due to their continued use in developing nations. However the growth rates of global mixing ratios for two of the most abundant HCFCs, HCFC-22 and -142b, were found to have declined between 2008 and 2012, by ~30% and ~60% respectively; this is indicative of reduced emissions. The resulting mole fractions were 218 ppt for HCFC-22 and 21.3 ppt for HCFC-142b in 2012 ([NOAA flasks] Carpenter and Reimann, 2014). HCFC-141b growth rates, on the other hand, had increased by ~70% over this period, in line with reported production and consumption by developing countries. As such, global mole fractions reached 22.3 ppt ([NOAA flasks] Carpenter and Reimann, 2014).

Global and regional studies have also suggested that HCFC emissions have shifted to the lower latitudes, where most developing countries are located, reflecting the earlier phase out schedule of developed nations. As well as this, abundances of the minor HCFC-133a were also observed to be increasing between 2008 (0.275 ppt) and 2012 (0.365 ppt), however analysis of more recent air samples by Vollmer et al. (2015) indicates this may now be decreasing (see section 5.10.1 for more information). Finally, contributions from HCFCs to total tropospheric chlorine have increased from 212 ppt (6.3%) in 2004 to 286 ppt (8.7%) in 2012 (Carpenter and Reimann, 2014).

Table 1.3: Anthropogenic Uses and Sources, Atmospheric Lifetimes and Global Warming Potentials of Hydrochlorofluorocarbons

Name[a]	**Formula**[a]	**Uses/Sources**	**Total Lifetime (years)**[a]	**GWPs relative to CO_2 at 100 years**[b]
HCFC-22	$CHClF_2$	Refrigerant[c], foam applications, feedstock[d]	11.9	1760
HCFC-123	$CHCl_2CF_3$	Refrigerant[c], cleaning solvent, fire extinguisher, feedstock[d]	1.3	79
HCFC-124	$CHClFCF_3$	Refrigerant[c], sterilant, fire extinguisher[d]	5.9	527
HCFC-141b	CH_3CCl_2F	Foam blowing agent[c], cleaning solvent[d]	9.4	782
HCFC-142b	CH_3CClF_2	Foam blowing agent[c], refrigerant, feedstock[d]	18	1980
HCFC-225ca	$CHCl_2CF_2CF_3$	Cleaning agent[d], solvent, adhesives/coatings[i]	1.9	127
HCFC-21	$CHCl_2F$	By-product[e], Anaerobic degradation of CFC-11[f]	1.7	148
HCFC-133a	CH_2ClCF_3	Chemical Processes[g]	4	340
HCFC-31	CH_2ClF	Refrigerant[h]	1.2	-

a – Carpenter and Reimann, 2014 b – Hodnebrog et al. 2013 c – McCulloch, A. 1999
d – Tsai, W.T. 2002 e – Noakes, T. 2002 f – Scheutz et al. 2010
g – Vollmer et al. 2015 h – Schoenenberger et al. 2015 i – Kloss et al. 2014

1.14.1.4 Chlorocarbons

These chlorinated compounds have atmospheric lifetimes longer than 6 months (see Table 1.4) and a variety of applications. Their contribution to stratospheric ozone depletion has led to their inclusion under the Montreal Protocol and so atmospheric abundances are decreasing.

Table 1.4: Anthropogenic Uses and Sources, Atmospheric Lifetimes and Global Warming Potentials of Chlorocarbons

Name[a]	Formula[a]	Uses/Sources	Total Lifetime (years)[a]	GWPs relative to CO_2 at 100 years[b]
Methyl Chloroform	CH_3CCl_3	Cleaning solvent, Feedstock[a]	5	160[ε]
Carbon Tetrachloride	CCl_4	Cleaning solvent, Feedstock[d], Fumigant, Fire extinguisher[e]	26	1730[ε]
Halothane	$CHBrClCF_3$	Anaesthetic[c]	1[c]	50[c]

a – Carpenter and Reimann, 2014 b – Hodnebrog et al. 2013 c – Vollmer et al. 2015b
d – Sturrock et al. 2002 e – Kim et al. 2011

1.14.1.4.1 Carbon Tetrachloride

From as early as 1912, carbon tetrachloride (CCl_4) was used as a cleaning solvent before being used as a feedstock in CFC-11 and CFC-12 manufacture from 1931 (Sturrock *et al.* 2002). It also has had applications as a fumigant and fire extinguisher (Kim et al. 2011). Whilst it is no longer used for these purposes, carbon tetrachloride is still a feedstock and process agent for a number of minor but essential chemical reactions. Efforts have been made to minimise fugitive emissions from these processes and alternatives have been sought and implemented where possible (TEAP, 2013). Firn samples have suggested that there may be small natural sources of carbon tetrachloride (Butler *et al*. 1999) but anthropogenic sources dominate emissions.

Stratospheric photolysis is the major destruction pathway of carbon tetrachloride, causing chlorine atom release and resulting in ozone depletion. As such, carbon tetrachloride was added to the Montreal Protocol as part of the London Amendment in 1990 (Kim *et al.* 2011). Degradation in oceans and soils are also potential sinks for this compound (Carpenter and Reimann, 2014). Carbon tetrachloride is also a greenhouse gas (see Table 1.4).

Atmospheric abundances have declined slowly since control measures began and the mole fraction has continued to decrease at a rate 1.6% (NOAA) from 2011 to 2012. In 2004, carbon tetrachloride contributed 11.1% to the total tropospheric chlorine levels and this had reduced to 10.3%, equivalent to 339 ppt, in 2012.

There are discrepancies between emissions suggested by 'bottom up' approaches (production records minus feedstock use and destruction) and the emissions calculated from observed atmospheric levels or 'top down' methodologies. Top down results have been larger indicating potentially unknown emission sources. Hemispheric gradients have been found and may be evidence of continued emissions in the northern hemisphere, however the larger oceanic area in the southern hemisphere that can act as a sink may impact this gradient.

Potential sources of the emissions could be from abandoned industrial sites as well as contaminated soils (Carpenter and Reimann, 2014) and uncapped landfills (Hu et al. 2016). Feedstock usage may also contribute but, given the magnitude of the discrepancy (30-70 Gg yr^{-1}), full responsibility from fugitive emissions would seem unlikely (Montzka and Reimann, 2011). A recent study in the United States suggested that emissions there were more consistent with industrial sources, likely associated with chlorine production and processing (Hu et al. 2016). There is also potential for higher emissions from these sources in developing countries, especially during methane chlorination, where higher rates of CCl_4 coproduction have been reported (UNEP, 2009).

However, the recent SPARC report (2016) has reduced the discrepancy from 54 Gg yr^{-1} (Carpenter and Reimann, 2014) to 15 Gg yr^{-1} which does reconcile the difference within uncertainties for the 'top down' and 'bottom up' estimates (SPARC, 2016).

1.14.1.4.2 Methyl Chloroform

Although firn samples indicate the presence of small natural sources of methyl chloroform (Butler *et al*. 1999, Sturrock *et al*. 2002), the majority of emissions are from industrial production. The first deliberate production occurred in the 1950's (Sturrock *et al*. 2002) and it's used as a solvent for metal and electronic part cleaning and as a feedstock for HCFC-141b and HCFC-142b production.

Due to the carbon-hydrogen bonds, methyl chloroform is susceptible to hydroxyl radical attack and so is mostly destroyed in the troposphere. Some does reach the stratosphere and is photolysed so, in this respect, methyl chloroform was added to the Montreal Protocol as part of the London Amendment in 1990 (Kim *et al.* 2011). Methyl chloroform is also a greenhouse gas (see Table 1.4).

The global abundance of methyl chloroform reached a peak in the early 1990s but has been decreasing steadily and substantially ever since. By 2012 it had declined to 4% of the maximum value, at ~5.4 ppt, and global emissions had decreased to ~2 Gg. The tropospheric chlorine contribution from methyl chloroform in 2012 was only 16 ppt, just 0.5% of the total chlorine level, down from 1.9% in 2004. Limited small banks and feedstock use, however, could result in some continued emissions and so the slowing down of this decline in forthcoming years (Carpenter and Reimann, 2014).

1.14.1.4.3 Halothane

With use as an inhalation anaesthetic, halothane ($CHBrClCF_3$) was first clinically introduced in 1956. Although it was used extensively through the 1960s and 1970s, it has been replaced in developed countries by other flurane compounds such as isoflurane, desflurane and sevoflurane (Vollmer et al. 2015), because of its liver damaging potential (Halpern, D.F., 1993).

Halothane is susceptible to hydroxyl radical attack in the troposphere, resulting in its relatively short atmospheric lifetime of 1 year (see Table 1.4). However, photolytic breakdown of the portion that does reach the stratosphere releases both chlorine and bromine atoms and so halothane has an ODP of 1.56. The bromine content of this species more than compensates for its short lifetime and so this means the ODP is comparable to that of CFC-12 (1.55, Langbein, 1999) although its abundance is significantly lower. As such, halothane is controlled under the Montreal Protocol.

A recent study by Vollmer et al. (2015) detected declining abundances of halothane in the parts-per-quadrillion (ppq) range, resulting in a global average of 9.2 ppq or 0.0092 ppt for 2014. Continued emissions were suggested by the observation of a hemispheric gradient. However, the lack of pollution events detected at European stations indicates these emissions are more likely from developing nations that still utilise halothane medically (Vollmer et al. 2015).

1.14.1.5 Very Short-Lived Substances (VSLS)

These halogenated species are those with atmospheric lifetimes under 6 months and, as such, are not controlled under global legislation and are not greenhouse gases. Although short-lived, studies have found that these species can be transported to the stratosphere (Hossaini *et al*. 2015, Ashfold *et al*. 2015) where they are able to contribute to ozone depletion. This transport mostly occurs through convection in tropical regions but there is significant seasonal and inter-annual variation. Chapter 6 expands further on convective transport and VSLS in the tropics. This section focuses on the chlorinated and brominated VSLS rather than the iodine-based compounds as these are considered more important for stratospheric ozone and so measured in this work.

1.14.1.5.1 Chlorinated VSLS

Whilst natural sources of short-lived chlorinated VSLS include biomass burning (Simpson et al. 2011), phytoplankton production (Ooki and Yokouchi, 2011) and peat land (Worton et al. 2006, Khan et al. 2012), there are a wide range of industrial applications for these species (see Table 1.5). Dichloromethane (CH_2Cl_2) is utilised as a solvent and foam-blowing agent whereas chloroform ($CHCl_3$) is used in the production of HCFC-22 and is released as a by-product of the paper industry (Montzka and Reimann, 2011).

Around 50% of chloroform emissions can be accounted for by anthropogenic sources (Trudinger et al. 2004, Worton et al. 2006). Tetrachloroethene (perchloroethylene, PCE, C_2Cl_4) has applications as a dry-cleaning solvent and is used in metal degreasing, along with trichloroethene (trichloroethylene, TCE, C_2HCl_3). Polymer and rubber production utilises 1,2-dichloroethane (CH_2ClCH_2Cl) whilst chloroethane (C_2H_5Cl) is used as part of the manufacturing procedure for ethyl cellulose and some pharmaceuticals (Montzka and Reimann, 2011).

Table 1.5: Anthropogenic Uses and Sources, Atmospheric Lifetimes and Global Warming Potentials of Chlorinated Very Short-lived Substances

Name[a]	**Formula**[a]	**Uses/Sources**[c]	**Total Lifetime (days)**[a]	**GWPs relative to CO_2 at 100 years**[b]
Dichloromethane	CH_2Cl_2	Paint Remover, Foam Blowing Agent	144	9
Chloroform	$CHCl_3$	Chemical Processes, By-product	149	16
PCE	C_2Cl_4	Solvent, Chemical Processes	90	-
TCE	C_2HCl_3	Chemical Processes	4.9	-
1,2-DCE	CH_2ClCH_2Cl	Chemical Processes	65	1
Chloroethane	C_2H_5Cl	Chemical Processes	39	-

a – Carpenter and Reimann, 2014 b – Hodnebrog et al. 2013 c – Montzka and Reimann, 2011

In the troposphere, chlorinated VSLS loss is dominated by hydroxyl radical oxidation. Other minor tropospheric sinks include slow tropospheric photolysis (mainly in tropical regions) and potential oxidation by chlorine atoms. Once in the stratosphere, photolysis becomes the major sink for chlorinated VSLS.

Large hemispheric and regional variability is found in observed levels of VSLS species but of the most abundant chlorinated VSLS species, dichloromethane mole fractions have increased by 67%, to 30.7 ppt, from 2001 to 2012 ([NOAA] Carpenter and Reimann, 2014). Conversely, PCE has been found to have decreased in the atmosphere, with an abundance of 1.18 ppt in 2012, 63% lower than when observations began in 1994 ([NOAA] Carpenter and Reimann, 2014). Chloroform observations also began in this year, however no significant trend has been seen in this time and an average annual mole fraction for 2012 was found to be 7.53 ppt ([AGAGE] Carpenter and Reimann, 2014). Overall, chlorinated VSLS contributed around 91 ppt to the total tropospheric chlorine levels in 2012 (Carpenter and Reimann, 2014).

1.14.1.5.2 Brominated VSLS

These compounds are primarily natural in origin although small emissions of bromoform ($CHBr_3$) occur from water chlorination (Worton et al. 2006). Trends of dibromomethane (CH_2Br_2) analysed from firn suggested this species was of entirely natural origin. 1-bromopropane (C_3H_7Br) and 1,2-dibromoethane (CH_2BrCH_2Br) both have minor anthropogenic sources (see Table 1.6, Montzka and Reimann, 2011) but were not measured in this work. $CHBrCl_2$ and $CHBr_2Cl$ were measured but are not currently known to have anthropogenic emissions. Natural sources of brominated VSLS include marine phytoplankton, seaweed and terrestrial vegetation (Law and Sturges, 2007).

Table 1.6: Anthropogenic Uses and Sources, Atmospheric Lifetimes and Global Warming Potentials of Brominated Very Short-lived Substances

Name[a]	Formula[a]	Uses/Sources[a]	Total Lifetime (days)[d]	GWPs relative to CO_2 at 100 years[b]
Bromoform	$CHBr_3$	Water Treatment	24	-
1-bromopropane	C_3H_7Br	Metal/Electronic Cleaning	12.8	-
1,2-dibromoethane	CH_2BrCH_2Br	Fumigant, Chemical Processes	70	-
Dibromomethane	CH_2Br_2	Natural	123	1
Bromochloromethane	CH_2BrCl	Natural	137[d]	-
Bromodichloromethane	$CHBrCl_2$	Natural	67[c]	-
Dibromochloromethane	$CHBr_2Cl$	Natural	50[c]	-

a – Montzka and Reimann, 2011 b – Hodnebrog et al. 2013 c – Orkin et al. 2013
d – Carpenter and Reimann, 2014

Like the chlorinated VSLS, tropospheric loss is dominated by hydroxyl radical oxidation, however photolysis is more important for multi-brominated species like bromoform. Studies have indicated that photolysis accounts for 50-70% of bromoform removal in the tropical troposphere (Papanastasiou et al. 2014). Stratospheric photolysis dominates brominated VSLS sinks once compounds are transported out of the troposphere.

Although there have been a wide range of studies, sources of brominated VSLS vary seasonally and temporally presenting difficulties in consistently quantifying global emissions (Leedham *et al*. 2013, Ziska *et a.l* 2013, Ashfold *et al*. 2014). As such estimates for brominated VSLS are still not satisfactory to constrain budgets and more global-scale observational data is required.

1.14.1.6 Methyl Halides

There are three methyl halide species – methyl chloride (CH_3Cl), methyl bromide (CH_3Br) and methyl iodide (CH_3I), all of which have relatively short atmospheric lifetimes (see Table 1.7). They all can deplete ozone and are greenhouse gases although since methyl iodide is particularly short-lived (~7 days), its impact on stratospheric chemistry is small and so discussion of this compound will be limited.

Table 1.7: Anthropogenic Uses and Sources, Atmospheric Lifetimes and Global Warming Potentials of Methyl Halides

Name[a]	Formula[a]	Anthropogenic Uses/Sources[a]	Total Lifetime (years)[a]	GWPs relative to CO_2 at 100 years[b]
Methyl Chloride	CH_3Cl	Coal Combustion, Chemical Processes[c]	0.9	12
Methyl Bromide	CH_3Br	Coal Combustion, Fumigant, Chemical Feedstock	0.8	2
Methyl Iodide	CH_3I	Pesticide	7 days	-

a – Carpenter and Reimann, 2014 b – Hodnebrog et al. 2013 c – ATSDR, 1998

1.14.1.6.1 Methyl Chloride

This compound is of primarily natural origin with sources including the ocean, fungi, marshes and wetlands as well as tropical forests, mangroves and rice paddies. Biomass burning is also a source however this may originate either naturally or anthropogenically. Coal combustion is another major anthropogenic source (Carpenter and Reimann, 2014) and methyl chloride has been used in chemical processes including the production of silicones (ATSDR, 1998). Given the large proportion of natural sources (~3028 Gg yr^{-1} out of 3658 Gg yr^{-1} estimated emissions sources, Carpenter and Reimann, 2014), methyl chloride production and consumption is not controlled by global legislation.

The major sink for this species is oxidation by hydroxyl radicals in the troposphere however there is also loss by soil uptake, oceanic degradation and reaction with chlorine radicals. Methyl chloride reaching the stratosphere will be broken down by photolysis. These sinks, however, outweigh the estimates of known sources of methyl chloride meaning the atmospheric budget for this compound is currently unbalanced.

Atmospheric mole fractions have been slowly declining with a 4.4 ppt decrease from 2008 to an abundance of 542.2 ppt in 2012 ([NOAA] Carpenter and Reimann, 2014). This is equivalent to 16.4% of the total tropospheric chlorine level for the same year (Carpenter and Reimann, 2014).

1.14.1.6.2 Methyl Bromide

This species has a very similar range of natural sources as methyl chloride, however the anthropogenic sources of methyl bromide are more extensive and, as such, are controlled as part of the Montreal Protocol after being added in the Copenhagen Amendment of 1992. Its main use was as an agricultural fumigant and this was subject to a phase out schedule to be completed by 2005 and 2015 for developed and developing nations respectively. Some critical agricultural uses are exempt from this restriction as well as quarantine and pre-shipping fumigant applications. However, emissions from this have been relatively stable for the past two decades. Other more minor uses include biofuel production and as a chemical feedstock.

Sinks for methyl bromide include tropospheric hydroxyl radical breakdown, degradation by oceans and soil microbial uptake as well as photolysis in the stratosphere. Again, like methyl chloride, sinks outweigh the estimated known sources of methyl bromide (Carpenter and Reimann, 2014).

Since 2008, methyl bromide mole fractions have declined to 6.95 ppt ([NOAA flasks] Carpenter and Reimann, 2014), a decrease of 0.38 ppt. However, this value is still 27% higher than the estimated natural background (Carpenter and Reimann, 2014).

1.14.1.6.3 Methyl Iodide

Oceanic sources make up 80% of methyl iodide emissions however it is a registered pesticide and may have very minor anthropogenic sources. The short lifetime (~7 days) of methyl iodide is due to photolysis in the troposphere.

There are some disagreements between regional top down and bottom up estimates for this compound suggesting potential source and/or sink uncertainty. However, quantifying emissions is challenging due to abundances widely varying with spatial and temporal differences and its very short lifetime. As such, impact on stratospheric ozone and global warming are thought to be small (Carpenter and Reimann, 2014).

1.14.2 Greenhouse Gases

1.14.2.1 Hydrofluorocarbons (HFCs)

These species were the second-generation replacements for CFCs and other ozone depleting compounds. As such, hydrofluorocarbons (HFCs) have similar structures to the compounds they replace but contain only hydrogen, fluorine and carbon atoms (Laube *et al.* 2010). They share many chemical and physical properties to CFCs and HCFCs including low toxicity, high volatility and, in most cases, non-flammability so they are utilised in the same variety of applications(Lindley and McCulloch, 2005).

The most widely used compound in this group is HFC-134a, which is utilised globally for mobile air conditioning in vehicles. HFC-23 (CHF_3) is mainly emitted during HCFC-22 production but it does have some minor uses, along with HFC-125 (CHF_2CF_3) and HFC-227ea (CF_3CHFCF_3), as a fire extinguisher. HFC-23 and HFC-125 also have applications as dry etching agents, like HFC-32 (CH_2F_2). This compound is also employed as a refrigerant, along with HFC-152a (CH_3CHF_2) and HFC-143a (CH_3CF_3). Other uses for HFCs include blowing agents, solvents and aerosol inhaler propellants (see Table 1.8) and other minor HFCs include HFC-245fa ($CF_3CH_2CHF_2$), HFC-365mfc ($CF_3CH_2CF_2CH_3$) and HFC-43-10mee ($CF_3CHFCHFCF_2CF_3$).

Like HCFCs, the carbon-hydrogen bonds in HFCs allow for tropospheric attack by hydroxyl radicals and thus they have shorter atmospheric lifetimes than CFCs and halons. However, unlike HCFCs, they do not contain chlorine and so have near-zero ozone depleting potential. This causes them to not be covered under the Montreal Protocol (Tsai, W.T., 2005). HFCs can break down to trifluoroacetic acid (TFA), due to the CF_3 groups present, by photolytic degradation. This can accumulate and damage eco-systems, particularly aquatic ones (Montzka and Reimann, 2011). Stratospheric reservoir species for these compounds include hydrogen fluoride (HF) and carbonyl fluoride (COF_2). HFCs are also GHGs as, like the other fluorocarbons discussed before, they are good absorbers of infrared radiation and so contribute to global warming (McCulloch, 2003). In this respect, they are controlled by the Kyoto Protocol and the new Paris Agreement (see section 1.11).

Globally, emissions of HFCs have continued to increase in recent years. In 2012, HFC-134a emissions were ~176 Gg, a 4% yr^{-1} increase on those found in 2008, and the average global mole fraction reached 67.8 ppt ([AGAGE] Carpenter and Reimann, 2014), HFC-23 emissions decreased between 2006 and 2009 to 8.6 Gg however, by 2012, this increased again to 12.8 Gg, resulting in a global mole fraction of 25 ppt ([AGAGE] Carpenter and Reimann, 2014). Near-doubling emissions between 2009 and 2012 were seen for HFC-32 (to 19 Gg yr-1) and HFC-125 (to 40 Gg yr-1) along with ~50% increases in HFC-143a emissions (24 Gg yr-1) as well. HFC-152a emissions, on the other hand, have stabilised at ~50 Gg yr^{-1} since 2010 and increases in abundance have slowed to a rate of 0.28 ppt yr^{-1} resulting in a mole fraction of 6.8 ppt for 2012.

Table 1.8: Anthropogenic Uses and Sources, Atmospheric Lifetimes and Global Warming Potential of Hydrofluorocarbons

Name[a]	Formula[a]	Anthropogenic Uses/Sources[c]	Total Lifetime (years)[a]	GWPs relative to CO_2 at 100 years[b]
HFC-134a	CH_2FCF_3	Refrigerant, Blowing agent, Aerosol inhaler, Dry-etching agent	14	1300
HFC-125	CHF_2CF_3	Fire extinguisher, Dry-etching agent, Refrigerant Blend[d]	31	3170
HFC-227ea	CF_3CHFCF_3	Aerosol propellant, Fire fighting, Plasma-etching[e]	36	3350
HFC-23	CHF_3	Fire extinguisher, Dry-etching agent, By-product[f]	228	12400
HFC-32	CH_2F_2	Refrigerant, Dry-etching agent	5.4	677
HFC-143a	CH_3CHF_2	Refrigerant	51	4800
HFC-152a	CH_3CHF_2	Refrigerant, Blowing agent, Aerosol propellant[g]	1.6	138
HFC-245fa	$CHF_2CH_2CF_3$	Foams[h], Blowing agent, Refrigerant	7.9	858
HFC-365mfc	$CH_3CF_2CH_2CF_3$	Foams[h], Blowing agent	8.7	804
HFC-43-10mee	$CF_3CHFCHFCF_2CF_3$	Solvent, Electronics Industry[i]	16.1	1650

a – Carpenter and Reimann, 2014 b – Hodnebrog et al. 2013 c – Tsai, W.T. 2005
d – O'Doherty et al. 2013 e – Bernstien et al. 2007 f – EIA, 2009
g – Montzka and Fraser, 2003 h – Montzka and Reimann, 2011 i – Arnold et al. 2014

Mixing ratios of the very minor HFCs, -245fa, -227ea and -365mfc all increased between 2008 and 2012, reaching 1.44 ppt. 0.74 ppt and 0.65 ppt respectively. Emissions of HFC-245fa and -365mfc had levelled off in 2006 but have increased again since 2012 to 8.2 Gg yr^{-1} for HFC-245fa and 3.1 Gg yr^{-1} for HFC-365mfc. Estimated emissions of HFC-227ea appear to have been increasing since the 1990s and in 2012 were 3.3 Gg yr^{-1}.

In order to decrease these emissions, a variety of methods are required (Montzka and Reimann, 2011). In some circumstances they can be replaced with compounds that have similar properties such as hydrocarbons, ammonia and carbon dioxide, but these all have disadvantages including high flammability and toxicity (Lindley and McCulloch, 2005). Hydrofluoroethers (HFEs) and hydrofluoropolyethers (HFPEs) can be used as replacements as well but these have similar atmospheric lifetimes and GWPs to some HFCs (Tsai, 2005b). Measures to improve containment and reduce leakages by improved engineer training and increased equipment checks have also been introduced (EIA, 2009).

1.14.2.2 Perfluorocarbons (PFCs)

Fully-fluorinated hydrocarbons are known as perfluorocarbons (PFCs) (Laube *et al.* 2012) and they possess several properties, such as being non-flammable, non-toxic and inert, that have led to their use in a wide range of applications (see Table 1.9). PFC-14 (CF_4) and PFC-116 (C_2F_6) were mainly used for dry-etching and cleaning prior to the mid-1990's before being substituted by PFC-218 (C_3F_8) and PFC-C318 (C_4F_8) (Tsai *et al.* 2002). PFC-218 also has some emissions from the aluminium industry, where it can be produced as a by-product of the smelting process (Carpenter and Reimann, 2014). Of the larger compounds, PFC-31-10 (C_4F_{10}) and PFC-41-12 (C_5F_{12}) have reported usage in semiconductor manufacturing, fire suppressions and refrigeration where as PFC-51-14 (C_6F_{14}) and PFC-61-16 (C_7F_{16}) have uses as heat transfer fluids and solvents (Laube *et al*. 2012, Ivy et al. 2012). Perfluorodecalin ($C_{10}F_{18}$) has several medicinal and industrial applications (Tsai, 2011).

Similar to CFCs, PFCs are strong absorbers of infrared radiation. Their atmospheric lifetimes are very long as well (in the range of thousands of years) which means the global warming effect they contribute is large relative to their emissions. The global warming potentials (GWPs) of PFCs are calculated to be several orders of magnitude higher than CO_2 (Ivy *et al*. 2012) and by the end of 2009 their emissions had added the equivalent of 325 million tonnes of CO_2 to global warming (Laube *et al.* 2012).

Due to the stability of the hydrogen fluoride formed when PFC decomposes in the atmosphere, it acts as a permanent sink and does not deplete ozone (McCulloch, 1999). This means that PFCs are not covered under the Montreal Protocol however they are regulated by the Kyoto Protocol and the Paris Agreement.

Of the short chain PFCs, CF_4 is the most abundant and in 2012 had an average annual mole fraction of 79.7 ppt. C_2F_6 is the second most abundant PFC but has a significantly lower mole fraction, only 4.2 ppt, for the same year. The only other PFC observed at over 1 ppt was cyclic-C_4F_8 (1.24 ppt, [UEA Cape Grim] Carpenter and Reimann, 2014). Emissions of this compound were estimated to be 1.1 Gg yr^{-1} in 2007 (Oram et al. 2012) and, for the long chain PFCs, emissions of recent years appear stable at less than 0.5 Gg yr^{-1} (Carpenter and Reimann, 2014).

Table 1.9: Anthropogenic Uses and Sources, Atmospheric Lifetimes and Global Warming Potentials of Perfluorocarbons

Name[a]	Formula[a]	Anthropogenic Uses/Sources	Total Lifetime (years)[a]	GWPs relative to CO_2 at 100 years[b]
PFC-14	CF_4	Dry etching, CVD chamber cleaning[c], aluminium production[d]	>50,000	6630
PFC-116	C_2F_6	Dry etching, CVD chamber cleaning[c], aluminium production[d]	>10,000	11100
PFC-218	C_3F_8	Refrigerants, Fire Suppressant, Semiconductor manufacturing[e], aluminium production[d]	~7000	8900
PFC-c318	c-C_4F_8	Refrigerant[e], Semiconductor manufacturing[d]	3200	9540
PFC-31-10	C_4F_{10}	Refrigerants, Fire Suppressant, Semiconductor manufacturing[f]	2600	9200
PFC-41-12	C_5F_{12}	Refrigerants, Fire Suppressant, Semiconductor manufacturing[f]	4100	8550
PFC-51-14	C_6F_{14}	Solvents, Heat transfer fluids[f]	3100	7910
PFC-61-16	C_7F_{16}	Solvents, Heat transfer fluids[f]	~3000	7820
PFC-71-18[ε]	C_8F_{18}	Heat transfer fluids, Semiconductor manufactuting[g]	~3000	7620
Perfluorodecalin[h]	$C_{10}F_{18}$[h]	Medicinal uses[h]	~2000	7190

a – Carpenter and Reimann, 2014 b – Hodnebrog et al. 2013 c – Tsai, W.T., 2002
d – O'Doherty et al. 2013 e – Montzka and Fraser, 2003 f – Laube et al. 2012
g – Ivy et al. 2012b h – Tsai, W.T. 2011

Replacements for PFCs, such as nitrogen trifluoride (NF_3), carbonyl fluoride (COF_2) and iodofluorocarbons (IFCs), have all been developed for the dry etching and cleaning applications. However, these alternatives have the disadvantages of being potentially highly toxic, reactive and more expensive than those they would be replacing. More immediately, effective techniques for reducing PFC emissions include recovery and recycling, process optimization and conversion of PFCs to non-PFCs (destruction) (Tsai *et al.* 2002). The combination of these techniques has led to a decrease in the emissions of several PFC species in recent years (Laube *et al*. 2012).

1.14.2.3 Other

The compounds in this section are those that are not technically halocarbons but may be utilised in similar industries or act as replacements for previously used halocarbon species. Table 1.10 summarises their uses, lifetimes and global warming potentials.

1.14.2.3.1 Sulphur Hexafluoride (SF_6)

First emitted in 1953 (Ko *et al*. 1993), and almost exclusively of anthropogenic origin, sulphur hexafluoride has several industrial emission sources (Levin *et al*. 2010). Its major uses are as a dielectric gas for high voltage smelting, as an electrical insulating fluid, and as a deliberately released tracer to study oceanic and atmospheric transport processes (Bernstein et al. 2007). Emissions of SF_6 originally grew at a similar rate relative to SF_5CF_3 (Sturges *et al*. 2012) but have continued to rise after the late 1990s, most likely due to increased emissions from developing countries (Levin *et al*. 2010). In 2012, SF_6 had a global mixing ratio of 7.6ppt (Carpenter and Reimann, 2014).

With a contribution to radiative forcing of 4.3 mWm^{-2} in 2012 and, due to its similar structure and so atmospheric loss process as the PFCs, very long atmospheric lifetime, SF_6 is another gas controlled by the Kyoto Protocol and Paris Agreement. Several methods have been implemented in an attempt to reduce emissions including changes to equipment and servicing procedures, which have reduced leakage to less than 0.5% per annum (Lindley and McCulloch, 2005). Other recycling measures include membrane separation, cryogenic concentration distillation and pressure swing adsorption (Tsai, 2002). Mixing ratios, however, have continued increasing at a rate of ~0.28 ppt yr^{-1} since 2007 (Carpenter and Reimann, 2014).

Table 1.10: Anthropogenic Uses and Sources, Atmospheric Lifetimes and Global Warming Potentials of Other Species similar to Halocarbons

Name[a]	Formula[a]	Anthropogenic Uses/Sources	Total Lifetime (years)[a]	GWPs relative to CO_2 at 100 years[b]
Sulphur Hexafluoride	SF_6	High voltage dielectric[e], Tracer[g]	3200	23500
Trifluoromethyl-sulphurpentafluoride	SF_5CF_3	Side product[e]	650-950	17400
Carbonyl Sulphide	COS	Oxidation of carbon disulphide, Domestic stoves, heating systems[f]	35[c]	27[c]
Sulphuryl Fluoride	SO_2F_2	Fumigant[d]	36	4090
Nitrogen Trifluoride	NF_3	Etching[h], Semiconductor manufactuiring[d]	569	16100

a – Carpenter and Reimann, 2014 b – Hodnebrog et al. 2013 c – Bruhl et al. 2012
d – Montzka and Reimann, 2011 e – Sturges et al. 2012 f – Mu et al. 2002
g – Bernstien et al. 2007 h – Tsai, W.T. 2002

1.14.2.3.2 Trifluoromethyl sulphur pentafluoride (SF_5CF_3)

With emissions first thought to have begun in the 1950s, trifluoromethyl sulphur pentafluoride is a compound of anthropogenic origin that grew in the atmosphere up to the late 1990s. Since 1999, however, emissions decreased to be indistinguishable from zero after 2003. Its major source was as a by-product of electrochemical fluorination during the production of fluorosurfactants used in foam and stain-resist coating manufacture, a process that was discontinued in 2000 (Sturges *et* al. 2012).

When first detected (Sturges *et al*. 2000), SF_5CF_3 was found to have the highest radiative forcing efficiency (0.57 Wm^{-2} ppb^{-1}) of any gas measured in the atmosphere. However its contribution to global warming is currently only small due to a maximum atmospheric abundance of 0.15ppt globally (Sturges *et al*. 2012). The long lifetime of the molecule means these concentrations are unlikely to decline considerably in the foreseeable future (Montzka and Reimann, 2011).

1.14.2.3.3 Carbonyl Sulphide (COS)

Carbonyl sulphide is the most abundant sulphur containing trace-gas in the troposphere and contributes to stratospheric ozone destruction through being a precursor for stratospheric sulphate aerosols that catalyse this depletion (Andreae and Crutzen, 1997). It has a GWP 27 times higher than CO_2 (100 year time horizon) however sulphate aerosols reflect solar radiation away from the surface and thus cool the planet.

These converse effects were calculated to approximately cancel one another out, in a study by Bruhl et al (2012), and so COS is not considered a net contributor to global warming though it is technically a GHG.

Sources include the oxidation of carbon disulphide (CS_2), which is emitted naturally and in the production of artificial fibres and dimethyl sulphide (DMS), which is emitted from marine phytoplankton. Domestic stoves and heating systems have been suggested as direct sources of COS (Mu et al. 2002) and natural sources include biomass burning, volcanoes and wetlands (Aydin et al. 2008). Sinks for COS include uptake by vegetation, soils and oceans as well as reaction with hydroxyl radicals and stratospheric photolysis.

Tropospheric mole fractions of COS in 2012 were ~490 ppt and are significantly higher than pre-industrial values (300-400 ppt, Montzka et al. 2004). Comparison of observations from the NOAA network suggests changes in COS since 2000 have been less that 3% and an increase of only 0.4% was calculated between 2011 and 2012 (Carpenter and Reimann, 2014).

The following species were not measured as part of the analysis in this work as they are not easily measured without compromising additional compounds. These are also regularly monitored by global networks so other species were prioritised.

1.14.2.3.4 Sulphuryl Fluoride (SO_2F_2)

Although commercially available since the 1960s, sulphuryl fluoride emissions have increased since its use as a replacement fumigant, for the Montreal Protocol regulated methyl bromide, began after 1986 (Papadimitiriou *et al*. 2008). Though volcanoes and fluorite minerals may be possible natural sources, their emissions are thought to be extremely small. Emissions calculated from atmospheric observations are around a third lower than those reported from global production, which suggests that, like CH_3Br, some SO_2F_2 is destroyed during application or through additional loss pathways.

SO_2F_2 has a global warming potential similar to that of CFC-11 and, although its atmospheric lifetime is slightly lower, it can still contribute to global warming and is currently not controlled under any legislation. With a global mole fraction of 1.8ppt in 2012, the contribution to radiative forcing is currently small, however emissions were 3.1 Gg in 2012, around double what they were in 2008 (Carpenter and Reimann, 2014).

1.14.2.3.5 Nitrogen Trifluoride (NF_3)

Originally seen as a niche product used for rocket fuel and lasers (Prather, 2008), nitrogen trifluoride found uses in plasma etching and semi-conductor manufacture (Montzka and Reimann, 2011) as replacement for CF_4 and C_2F_6, PFCs controlled by the Kyoto Protocol (Muhle *et al.* 2010), as well as in photovoltaic manufacture (Fthenakis *et al*. 2010). The use and emissions of NF_3 are not currently controlled by any legislation.

Though a portion of the NF_3 used in manufacturing applications is destroyed during the process, some will escape into the atmosphere (Prather and Hsu, 2008). Increased production, and uses coupled with both a high global warming potential and a long atmospheric lifetime, means that the radiative forcing caused by NF_3 will also increase. In 2008, NF_3 was first measured in the atmosphere (Weiss *et al.* 2008) and a global mean mixing ratio of 0.45ppt was established with a growth rate of +0.05ppt/yr (Montzka and Reimann, 2011). Molecular fluorine (F_2) has been suggested as a replacement for NF_3 in some applications as it has lower bond energy and zero global warming potential, however there are other issues with high toxicity and reactivity (Oh *et al*. 2012).

1.15 Key Themes

Throughout this study, the individual chapters are linked by their relevance and relation to the East and South East regions of Asia, and their production of halocarbon species.

Comparative to Europe and the United States, the industrial revolution that took place in East and South East Asia was markedly more recent. This 'late' industrialisation resulted in a more rapid development due to the ability to borrow, learn and adapt already commercialised technology from other countries rather than only developing propriety ideas. Government intervention, in the form of subsidies, market distortion and the control of imports and exports also played a key part in the region's growth (Amsden, 1995).

The shift away from largely agriculturally based industry has resulted in the increased use and production of a large number of anthropogenic compounds, particularly halocarbons, that have environmental impacts. As the halocarbon family contains both ozone depleting species and greenhouse gases, this swift expansion has attracted international interest as well as concern as to the control and monitoring of these substances.

Nevertheless, there is still agricultural industry in East and South East Asia and this remains widespread to address the ever-increasing population. This area encompasses some the highest rice production globally (see Figure 1.10), both for consumption and exportation (see Figure 1.11). Whilst this industry may not utilise large amounts of anthropogenic halocarbons, rice production can also contribute to potential environmental damage due to the release of naturally produced halocarbon species, notably the methyl halides. As such the control of cultivated sources needs to be considered and monitored along with industrial sources to fully assess global impact.

However, it is not only the increasing size and quantity of halocarbon sources that is of importance to the scientific community for this region but the atmospheric transport within the area after they are released. Weather patterns, known as cold surges, which occur during the winter monsoon season have been found to rapidly transport air masses from East Asia towards the tropics and South East Asia. Convection is also increased during cold surges which may result in the rapid vertical transport to the upper tropical troposphere, the entry region for the stratosphere. With increased halocarbon sources in East Asia, this transport mechanism could result in even short-lived species being conveyed and potentially depleting stratospheric ozone.

Chapter 3 discusses a preliminary study into the genetic modification of plants to minimise their methyl halide production and the potential impact to global halocarbon emissions this could have if it were implemented across the East Asian rice crop. Chapters 4 and 5 examine the results of a number of campaigns monitoring the abundance of halocarbon species through air sampling. Chapter 4 explores campaigns based in two sites in Taiwan (see Figure 1.12) and considers potential source locations of halocarbons in East Asia. Chapter 5 analyses the

results of a sampling campaign based in Bachok, Malaysia (see Figure 1.12) that measured the abundance of ozone depleting species during and after a cold surge. Measurements are then used to suggest the increase in equivalent chlorine transported to the upper troposphere during these conditions of increased convection.

Overall, this study seeks to further highlight this region as playing a key role in the global production and transport of atmospheric halocarbons and their potential to damage the environment, through both depletion of ozone and the increase of greenhouse gases. From this work it is hoped that key compounds and prospective patterns may be identified that could lead, through further monitoring and investigation, to effective control measures and, ultimately, replacement chemical species utilised in industry.

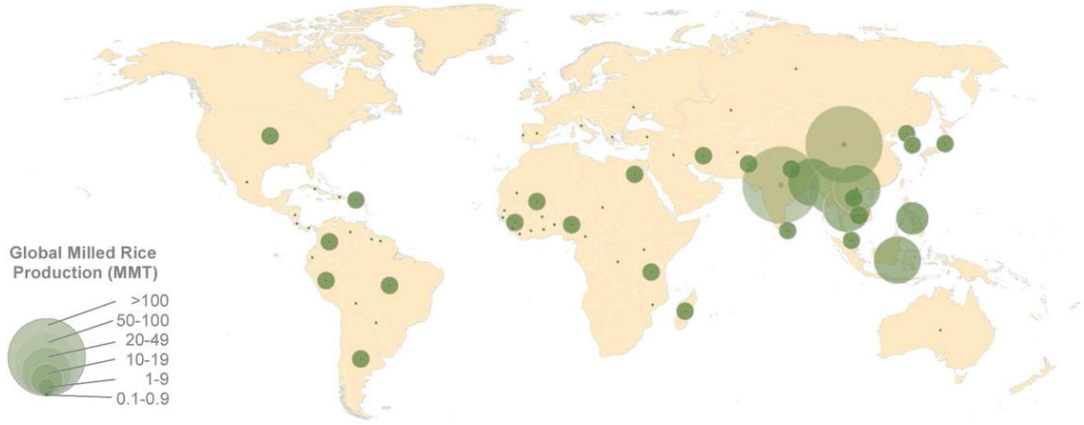

Figure 1.10: Global map of rice production for 2011. (Muthayya *et al*. 2014)

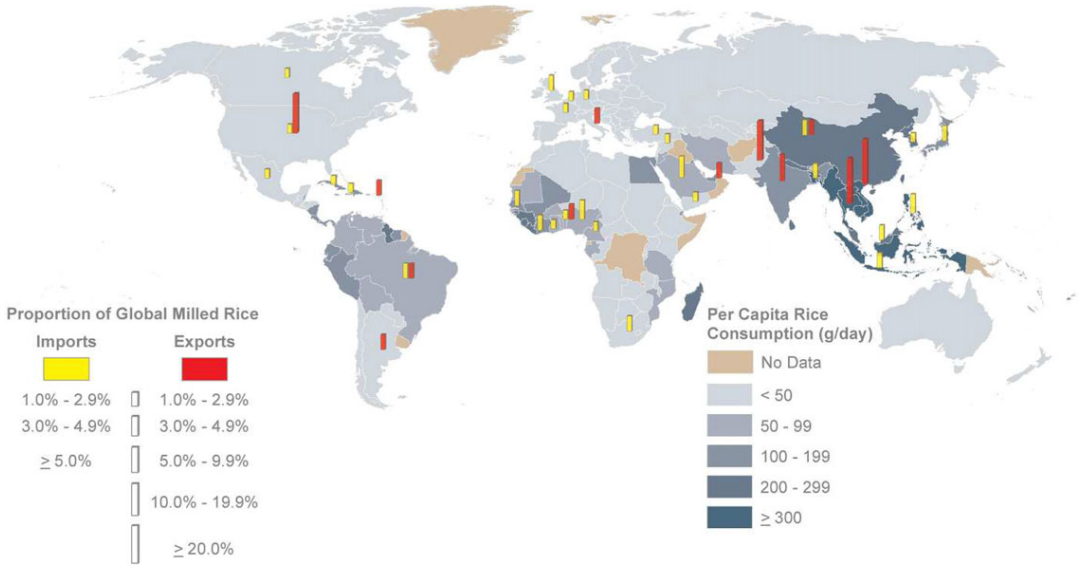

Figure 1.11: Global map of consumption, import and export of rice for 2009-2010. (Muthayya *et al.* 2014)

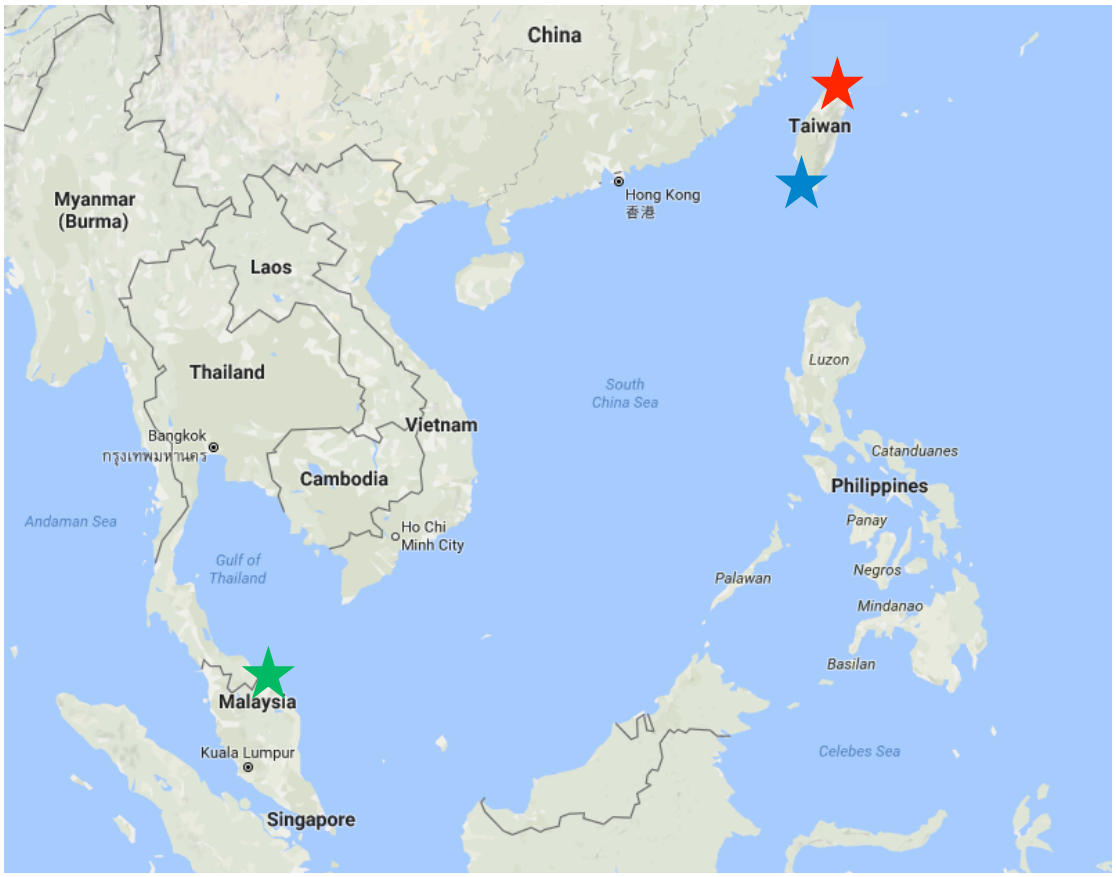

Figure 1.12: Map of parts of East and South East Asia showing the approximate locations of the three sampling sites utilised in this study. The blue star indicates the location of the 2013 and 2015 campaigns in southern Taiwan whereas the red star indicates the location of the 2014 northern campaign (Chapter 4). The green star indicates the location of the 2014 Bachok sampling campaign in Malaysia (Chapter 5). Information on more specific locations can be found in the respective chapters.

1.16 Aims and Objectives

This section outlines the aims and objectives of this study and summarises the overall structure of this thesis. Each chapter includes a description of the methodology specifically utilised as there were variations, however a general overview of the overriding techniques can be found in Chapter 2.

Chapter 3: Analysis of methyl halide emissions from plants

The general aim of this chapter was to assess the emissions of methyl halides from a range of genetically modified plant species as part of a wider project in conjunction with the John Innes Centre.

The main objectives were:

- Compare emissions of methyl halide species from wild type *Arabidopsis thaliana* with genetically modified *hol*-mutants.
- Compare emissions of methyl halide species of transgenic *A. thaliana* lines produced using genetic code from rice, moss and diatoms.
- Compare emissions of methyl bromide from wild type *Physcomitrella patens* with genetically modified Pphol knockout lines.
- Assess the effect of varying growth temperatures on wild type *A. thaliana* and *hol*-mutants.
- Assess the effect of varying growth temperatures on wild type *P. patens* and Pphol knockout lines.
- Identify any relationships requiring further investigation.

Chapter 4: Halocarbon observations in Taiwan

The overall aim of this chapter was to improve our knowledge as to the abundances of a wide range of halocarbon species in the East Asian region over a three-year period.

The main objectives were:

- Identify and quantify a variety of halocarbon species, including newly detected and minor compounds, in air samples collected during three ground-based sampling campaigns in Taiwan.
- Assess trends in mixing ratios over the three years sampled and compare this with reported global trends.
- Compare mixing ratios with reported background abundances and quantify any enhancement observed.
- Use modelled back-trajectories to assess potential source locations for species-specific pollution events.
- Calculate interspecies correlations to assess potential co-location of sources or co-emission.
- Identify specific species with relationships of interest and interpret these further in separate case studies.

- Identify species and relationships in need of further monitoring due to lack of comparable data sets or potential contributions towards global legislation.

Chapter 5: Long-range transport of Ozone depleting substances to Bachok, Malaysia

The general aim of this chapter was to compare the mixing ratios of ozone depleting substances transported to Bachok, Malaysia during weather systems known as cold surges with those abundances after these systems have passed.

The main objectives were:

- Identify and quantify a wide range of ozone-depleting substances in air samples collected during and after a cold surge period at Bachok.
- Compare mixing ratios of these species during and after the cold surge.
- Compare abundances with reported backgrounds and quantify any enhancement.
- Use modelled back-trajectories to assess potential source locations for distinct pollution events.
- Calculate interspecies correlations to assess potential co-location of species.
- Calculate equivalent chlorine levels using the Bachok data and compare this with estimates from recent reports.
- Estimate emissions of species found to have good correlation with carbon monoxide identified as originating from latitudes above 20°N.
- Identify species and relationships in need of further investigation due to lack of comparable data sets or potential contributions towards global legislation.

Chapter 2: Experimental Theory and Methods

In recent years, the use and sensitivity of coupled gas chromatography-mass spectrometry (GC-MS) systems has increased making them invaluable in the detection of trace gases, including those at parts per trillion (ppt) and parts per quadrillion (ppq) concentrations, in atmospheric samples. This chapter will give a general overview of the theory behind this technique (summarised from Skoog et al. (2004), Williams (2006) and Hubschmann (2009) where more detailed descriptions can be found) and describe the methods used for analysis in Chapters 3, 4 and 5.

2.1 Gas Chromatography (GC)

First introduced by James and Martin (1952), the basic principle of gas chromatography as an analytical technique involves the separation of volatilised compounds by injection on to a prepared column. This column may contain a porous layer or packing known as the stationary phase and analytes are moved through this system by a carrier gas mobile phase such as helium or hydrogen. The chemical or physical interaction of compounds with the stationary phase is what causes the separation; those with weak interactions will pass through the column more quickly than those that strongly interact. The column itself is contained within an oven and regulation of column temperature is important in ensuring predictable compound elution. Once they have passed through the column, a connected detector is used to record eluting species.

2.1.1 GC Columns

Of the two main types of GC columns, packed columns and capillary columns, the analysis of atmospheric trace gases predominantly uses those of the capillary variety as they have greater efficiency due to their lack of eddy diffusion. This is where, in packed columns, there is variation in path lengths between molecules as they pass through the liquid stationary phase which coats an inert support material within the column, thus causing the solute band to broaden. As capillary columns consist of a long narrow tube, usually made of fused silica with an internal coating instead of packing, eddy diffusion is not a factor. Other advantages over packed columns include higher resolution with shorter run times, however injected sample volume is limited due to distortion through overloading caused by the narrower internal diameters (ID) of capillary columns.

Capillary columns are usually between 20 and 100m long and internal diameters range from 100-560µm. These columns may be wall coated open tubular (WCOT), where the internal coating is a liquid film, or porous layer open tubular (PLOT) where there is a solid (e.g. alumina) or molecular sieve layer on the inner walls.

For the trace gas analysis carried out for this research, two types of PLOT column were utilised. The Agilent GS-GasPro (length 30-50m, ID 0.32mm, Agilent Technology, 2016) is the standard column installed due to its wide working-temperature range (-80 to 260/300°C, Agilent Technology, 2016b) and extensive halocarbon separation (see Figure 2.1). The Agilent CP-Al2O3/KCl column (length 50m, ID 0.32mm) was also used for a period and this has aluminium oxide (Al_2O_3) deactivated by potassium chloride as a stationary phase. Its installation enabled isomeric separation of a number of halocarbon species that is not possible with the GasPro column as it utilises their polarities rather than boiling points.

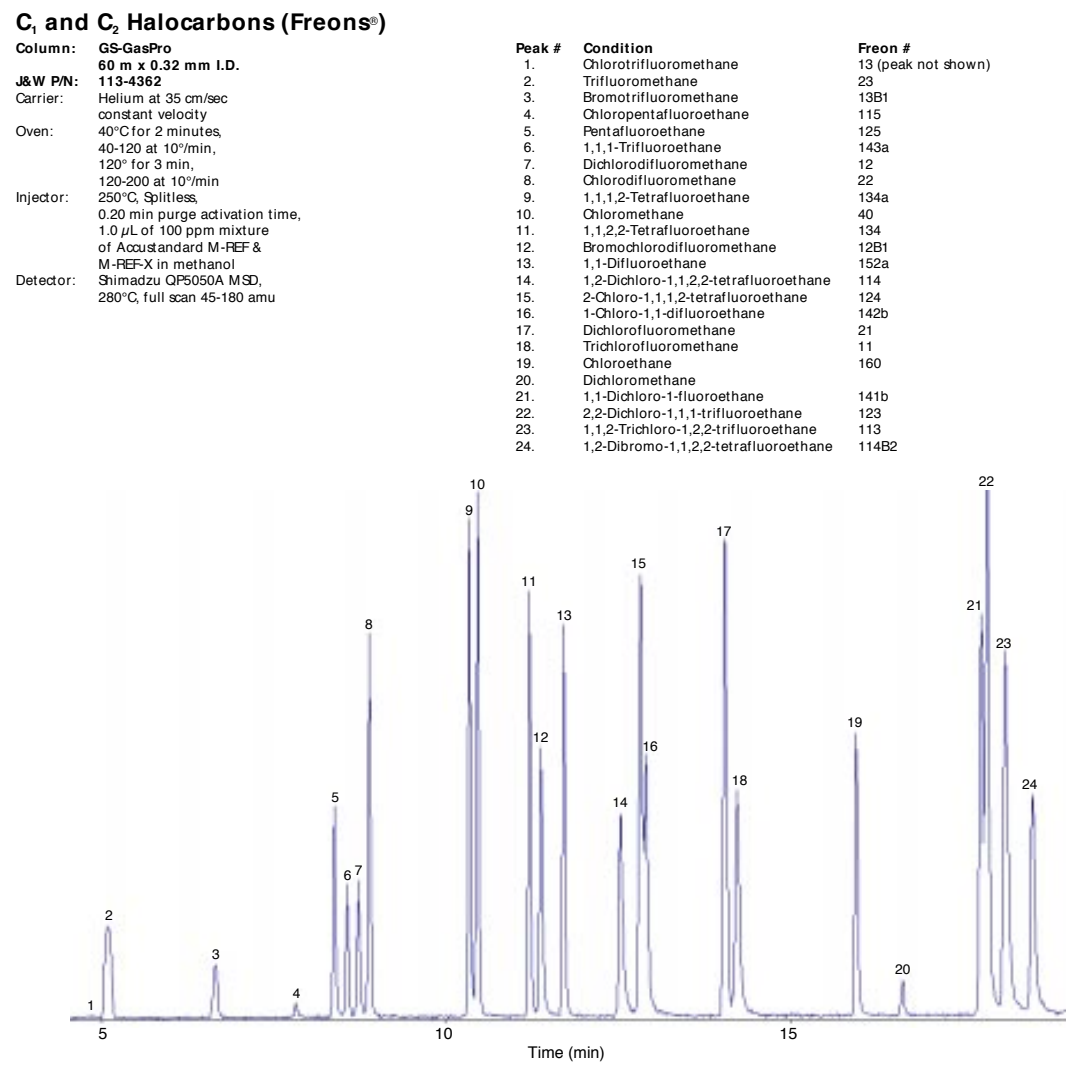

Figure 1.1: Test mixture of C1-C2 Halocarbons run on a GS-GasPro column (instrument specifications found at the top left of the figure). Published by Agilent, available from: http://www.chem.agilent.com/cag/cabu/pdf/c664.pdf

However, retention times of compounds analysed with the CP-Al2O3/KCl were regularly found to shift, most likely due to adsorbing CO_2, which alumina columns are known to accumulate (Armstrong *et al.* 1996, Agilent Technology, 2016b). Also, HCFC species detection was limited so this remains a secondary column to the GasPro for atmospheric trace gas analysis.

The columns for this work were all housed in Agilent GC ovens with specific temperature programs (see sections 2.2.5 and 2.2.6.1 for details) that enabled further control of individual compound elution.

2.1.2 Carrier Gases

Helium is the most common mobile phase for most GC-MS analysis of atmospheric trace gases and was utilised in this research. Hydrogen is less commonly used due to the risks associated with its flammability. For optimal analysis, the flow rate of the carrier gas has to balance speed and separation efficiency. For helium, this flow rate is ~25cms^{-1} however a velocity of 30cms^{-1} is utilised in practice in order to compensate for low starting temperatures in the GC oven program.

2.1.3 Detectors

A range of detectors can be combined with gas chromatography including electron capture detectors (ECDs), flame ionisation detectors (FIDs) and flame photometric detectors (FPDs). Whilst these are utilised, particularly for specific compound groups such a hydrocarbons (FID) and sulphur-species (FPD), they rely on retention time as the main method of compound identification. This limits their ability, particularly with polluted atmospheric samples, as both known and unknown species may cause interference. The thousands of trace gases present in these samples along further adds to these limitations.

Gas chromatography in combination with mass spectrometric detection on the other hand, enables identification of chemical species in conjunction with separation. This means interferences occur less frequently and are more easily identified, hence why this technique is widely utilised for atmospheric trace gas detection.

2.2 Mass Spectrometry

A. J. Dempster and F. W. Aston first developed modern mass spectrometry techniques in 1918 and 1919 respectively. The basic principles involve the ionisation of samples that may cause the formation of charged fragments. These ions are then accelerated and subjected to an electric or magnetic field in order to separate them by deflection according to their mass-to-charge (*m/z*) ratios. These ions are then recorded using the current induced when the ions strike the detector surface and spectra showing relative abundance against *m/*z ratio are produced.

The mass spectrometry carried out for this work utilised electron ionisation to charge species eluting from the gas chromatography column and then mass selection occurred via either a quadrupole or tri-sector mass analyser, the details of which are explained in the upcoming sections.

2.2.1 Electron Ionisation

After travelling through the GC capillary column, compounds are transported to the ionisation source of the mass spectrometer. Here, a heated metal filament (usually tungsten) thermoelectrically emits a beam of high-energy electrons that are accelerated by a potential difference, generally of 70 electron volts (eV). These electrons then enter the source through a slit and then bombard molecules of the sample gas. Collisions between accelerated electrons and neutral molecules (M) may result in an electron being ejected from the molecule causing the formation of a positively charged radical ion (see Equation 2.1). This $M^{+\cdot}$ ion is commonly referred to as the molecular ion and ~10eV is required to remove one electron from most organic molecules.

$$M + e^- \longrightarrow M^{+\cdot} + 2e^- \qquad \text{Equation 2.1}$$

Impacting ions with larger energies may result in enough excess energy for the molecular ion to fragment into a lower mass ion. Equations 2.2-2.4 show examples of the potential fragmentations from the molecular ion of methyl chloride, CH_3Cl. The energy of the impacting electron directly affects the number of ions produced and the fragmentation pattern so, providing this energy is known, similar compound fragmentation should be found between instruments utilising electron ionisation.

$$CH_3Cl + e^- \longrightarrow CH_3Cl^{+\cdot} + 2e^- \qquad \text{Equation 2.2}$$
$$CH_3Cl^{+\cdot} \longrightarrow CH_3^+ + Cl^{\cdot} \qquad \text{Equation 2.3}$$
$$CH_3Cl^{+\cdot} \longrightarrow CH_3^{\cdot} + Cl^+ \qquad \text{Equation 2.4}$$

Whilst electron ionisation is the most common method used, the fragmentation process can result in reduced information about the molecular ion. Chemical ionisation (CI) is an alternative technique that utilises an ion transfer process or dissociative electron capture to ionise sample molecules to molecular ions. However, since no fragment ions are produced by this method, there is a loss of structural information obtained and this is essential in the identification of isomeric compounds.

2.2.2 Quadrupole Mass Filter

With their low cost, durability, simple operation and maintenance, quadrupole mass filters (QMFs) have found widespread use in GC application since commercial development began in the 1960s. Consisting of four, ideally hyperbolic, parallel rods (see Figure 2.2), QMF analysers induce a fluctuating field in the central space using oscillating direct current (DC) and radio frequency (RF) electrical potentials. Ions from the ion source are accelerated into this central space and the electrical field magnitude and frequency can be varied.

This variation allows only the passage of specific *m/z* values to reach the detector at the other end of the space whilst any other ions collide with the quadrupole surface.

In the mass selective detector, the ions of interest impact with the detector surface resulting in the emission of electrons. This causes the induction of a current, which due to its small size particularly when dealing with trace gases, is amplified using an electron multiplier. This is where repeated collisions with a curved dynode surface causes the production of secondary electrons, which collide and cause a cascade effect. This amplifies the signal, typically in the order of one million to one, and the induced current is then recorded and converted to spectra for interpretation (Larsson and Odham, 1984).

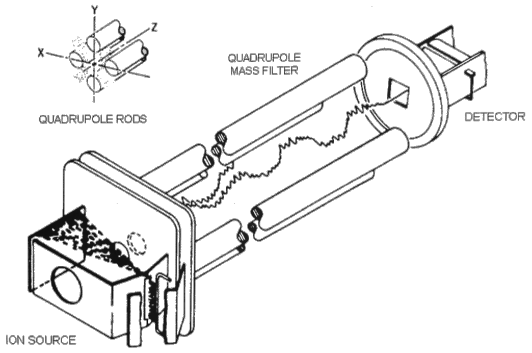

Figure 2.2: Quadrupole Mass Filter schematic. The trajectories of ions of only one *m/z* are stable enough to reach the detector. From Watson and Sparkman (2007).

There are two modes that QMFs allow for analysis in: scan mode or single ion monitoring (SIM) mode. For preliminary identification of compounds, scan mode is most commonly used and this is where a range of *m/z* values are scanned for in each time window. Sensitivity is reduced in this mode since a large number of ions need to be measured and so the time spent acquiring them is limited. In SIM mode, a small number of ions can be selected and filtered in each window of time. Generally, <10 ions may be measured in each window in order to maintain a useful number of spectra collected per second. As such, this means sensitivity is much higher than that of scan mode, theoretically by a factor of 100 but practically closer to a factor of 30-50 (Hubschmann, H.J., 2009). However, creating a SIM method requires more preparation prior to analysis in identifying compounds of interest and ensuring reliable detection by selecting appropriate ions and time windows.

The Entech system described in section 2.2.5 and utilised for analysis in chapters 5 and 6 contains a QMF, as does the GC-MS system used for the preliminary assessment of the inlet system described in chapter 3.

2.2.3 Tri-sector Mass Spectrometry

The AutoSpec instrument (description in section 2.2.6), used for the majority of the halocarbon trace gas analysis detailed in chapters 4, 5 and 6, utilises a tri-sector mass spectrometer as opposed to a quadrupole-based system.

In this set up, ions pass from the source through two electric sectors that are either side of a magnetic sector (EBE). These electric sectors reduce background noise and improve sensitivity by the respective removal of metastable ions and the de-magnification of optics. The magnetic sector deflects analyte ions towards the detector and the degree of deflection corresponds with the *m/z* ratio of each ion. Air molecules are prevented from interacting with or deflecting sample ions through the vacuum created and maintained by scroll and diffusion pumps.

Ions are recorded by the AutoSpec system using an off-axis ion detector that prevent neutral ions from striking it, thus further reducing background noise level. When sample ions strike the surface, electrons are released by a dual conversion dynode configuration and, unlike with the quadrupole system, these then impact a phosphor screen resulting in the emission of photons. A photomultiplier tube then converts these to a signal able to be detected electronically via the photoelectric effect and the secondary emission of electrons. This is where electrons are released through the impact of photons on a surface and the release of several electrons through an electron striking an electrode surface. The signals produced are then converted to spectra for interpretation.

Like the quadrupole system, the tri-sector analyser can be run in both scan and SIM mode and the pros and cons of both modes are consistent between instruments. The major difference between the two analysers is the higher resolution and sensitivity achievable when using the tri-sector system. The AutoSpec instrument used for this work is capable of high precision measurements of pmol mol^{-1} trace gases from low volume air samples. The Entech quadrupole system requires larger sample volumes (~500mL) and higher trace gas concentrations (limits of detection are generally in ppt rather than in ppq) to achieve similar precision data.

2.2.4 Calibration

In order to assign mixing ratios for individual species in the samples analysed in this work, compound specific response factors were determined by comparison with working standards of known concentrations. These standards vary between instruments but are all supplied by the Global Monitoring Division of National Oceanic and Atmospheric Administration Earth System Research Laboratory (NOAA ESRL). These come in 34L electro-polished stainless steel or Aculite-treated aluminium canisters (Essex Cryogenics, St. Louis, MO, US). A range of compounds from these standards have mixing ratios determined by comparison to primary standards, prepared using dilutions of pure compound vapour or liquid, at the Central Comparison Laboratory of the Global Monitoring Division of NOAA ESRL.

NOAA does not calibrate for a number of trace and recently detected atmospheric species and so a similar process utilising pure vapour or liquid standards is followed by the University of East Anglia (UEA, see Laube et al. 2012 for details). Accuracies with these calibrations are better than 7% (Laube et al. 2012).

Some compounds are not stable when stored for prolonged periods in these canisters and regular inter-comparisons between all the in-use and a number of previously working standards are carried out. This allows for any drift in concentration to be quantified and so the mixing ratios of affected species can be time-corrected.

2.2.5 Entech System

Several of the more abundant halocarbon species were detected using the Entech system for the samples analysed in chapters 5 and 6.

This consists of a gas chromatography-electron ionisation mass spectrometer (GC-EI-MS, GC model Agilent 5973 and MS model Agilent 6890) attached to an Entech™ 7100A Pre-concentrator inlet system. Accurately measured samples (~500ml, flow rate ~100 ml/min) were passed through a magnesium perchlorate ($Mg(ClO_4)_2$) drier prior to pre-concentration. Separation was carried out using an Agilent GS-GasPro™ capillary column (length 30m, ID 0.32mm) utilising research grade helium (>99.9995% purity) as the carrier gas. Following injection, the column was held at -10°C for two minutes and then ramped at 10°C per minute to 145°C followed by a further ramp of 20°C per minute to a final temperature 200°C, which was held for a further two minutes. This was coupled to a quadrupole mass selective detector, using electron ionisation and operating with a SIM mode method designed to detect a wide range of halocarbon trace gas species.

Mixing ratios were determined by comparison with the 34L, electro-polished stainless steel canister, SX-706070 working standard. Analytical uncertainties are 1σ standard deviation of duplicate samples analysed the same day and were calculated on a per-run basis.

All samples analysed on this system were run, interpreted and the resulting data provided by Stephen Humphreys, Adam Wisher and David Oram for further analysis and comparison in this work.

2.2.6 AutoSpec

The majority of halocarbon species measured in this work and described in chapters 3, 4 and 5 were analysed using the high performance AutoSpec GC-MS suite. The full measurement procedure is described in the following sections.

2.2.6.1 Instrument Setup

The software package 'MassLynx', provided by Waters®, is the interface between the user and the instrument that controls all aspects of the pre-analysis instrument setup.

The MS was operated in EI and SIM modes with a mass resolution of 1000 at 5% peak height determined using the internal reference compound. Ion *m/z* corresponding to known source ionisation products of compounds of interest were selected and added to defined time windows, or functions of the SIM method, that cover the period that species will elute from the GC column. These were previously determined using static dilutions of pure compounds and/or comparison with the NIST spectral library (NIST/EPA/NIH, 2005).

In order to be selected, these *m/z* must produce peaks large enough to be detected but not so large as to overload the detector. Each function must also not contain too wide a *m/z* range or sensitivity may decrease. As such the largest *m/z* should not be more than 1.5 times the smallest *m/z* in that particular function. Multiple fragments of the same species may be measured during a single acquisition meaning isotopologues, molecules that only differ by their isotope composition, or fragments that corroborate the identification of a particular compound can be detected. Thorough testing of each SIM method was carried out before sample analysis occurred using known standards to ensure the response of key compounds was optimised. Adjustments were made and tested as necessary to reflect changes in instrumentation, procedure or methodology.

During every analysis, pure hexadecane was injected continuously into the source to act as a reference gas for the calculation of *m/z* as it produces a wide range of fragment ions (*m/z* 29 to 226). As such, each function includes a hexadecane lock-mass, chosen to have a *m/z* close to those of the ions of interest. The most abundant hexadecane mass (57) is used to tune the instrument at the beginning of each analysis day to confirm optimal settings are in place to achieve the desired mass resolution and sensitivity. This, and the other hexadecane masses, are also used for the daily mass calibration of the SIM method.

Table 2.1 gives an overview of a halocarbon trace gas SIM method developed for the AutoSpec, showing the variety of *m/z* measured over a range of different functions and their corresponding compounds.

2.2.6.2 Sample Preparation

Figure 2.3 gives an overview of the inlet system, all of which is evacuated and under vacuum, specially designed for the cryotrapping and injection of atmospheric samples into the GC-MS system. A glass tube containing hygroscopic $Mg(ClO_4)_2$ was used in this system to remove any water from samples before they undergo the cryotrapping pre-concentration procedure. To cryotrap the samples, a stainless steel sample loop (external diameter $1/16^{th}$ inch) filled with a Hayesep D (80/100 mesh) adsorbent was immersed in a dry ice/ethanol mixture and cooled to -78°C. Between 200ml and 300ml of dried air was then passed through the loop, trapping trace gases but not oxygen, nitrogen or the more volatile noble gases. As such, a 6L reference volume and Baratron pressure sensor were used to accurately measure the specific volume trapped.

The sample loop would then be opened to the helium (research grade) carrier gas, the dry ice/ethanol mixture removed and replaced immediately with hot water (~95°C). This releases the trapped gases into the constant 2 mL/min helium flow and transports them into the GC oven. The Agilent 6890 GC instrument connected to the inlet system contained either an Agilent GS-GasPro column (length 30-50m, ID 0.32mm) or Agilent CP-Al2O3/KCl column (length 50m, ID 0.32mm) as described previously. The column temperature was held at -10°C for two minutes and then ramped from -10°C to 200°C at 10°C per minute. This temperature programme was used to produce a reproducible set of retention times for the pre-concentrated species.

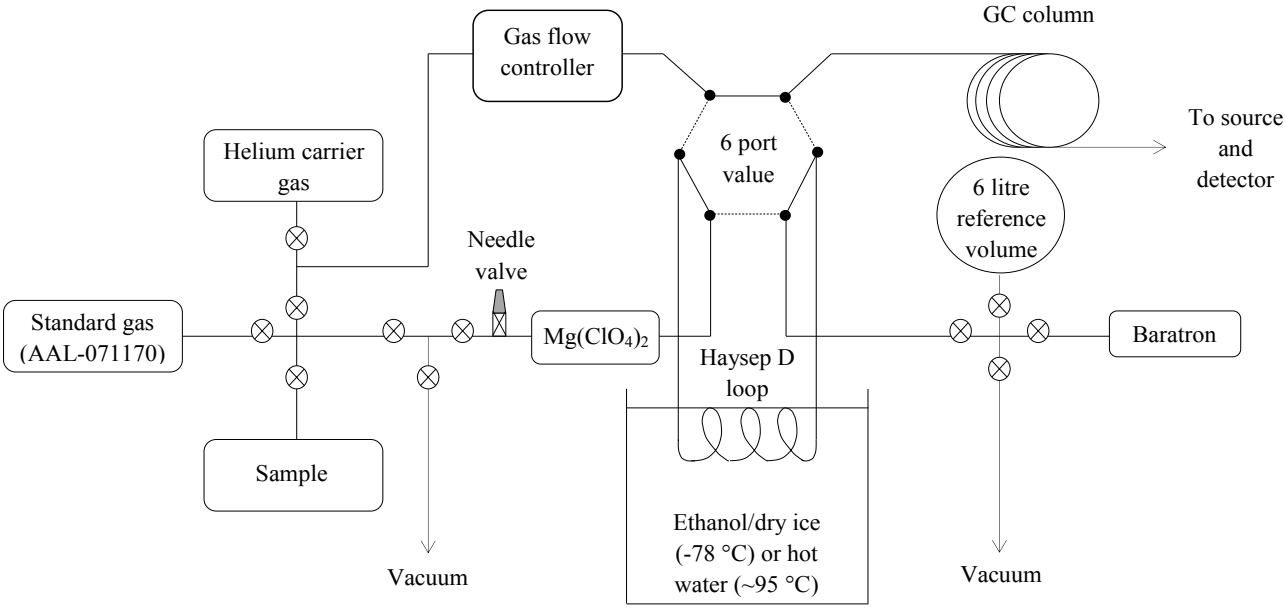

Figure 2.3: A schematic diagram of the AutoSpec manual inlet system. Valves are indicated by a cross within a circle. Courtesy of (Allin, 2015.)

Table 2.1: Overview of a halocarbon trace gas selective ion monitoring (SIM) method developed for the AutoSpec mass spectrometry suite

Function	Time (mins)	Compound	Ion Mass 1	2	3
1	4.7-5.8	CFC-13	86.9627		
		C_2F_6	118.9920		
		SF_6	126.9641		
2	5.8-8.5	HFC-23	51.0046		
		HFC-32	51.0046	52.0125	
		COS	61.9623		
3	8.5-9.45	C_3F_8	168.9888		
4	9.45-11.8	CFC-115	86.9627		
		SF_5CF_3	88.9673		
		C_2F_3Cl	115.9641		
5	11.8-12.5	CH_3Cl	49.9923	50.9957	51.9894
6	12.5-12.95	C_2H_3Cl	61.9923	63.9894	
7	12.95-13.8	Halon 1211	128.9151	130.9131	
8	13.8-14.35	CH_3Br	93.9418	95.9398	
9	14.35-14.6	CH_2CCl_2	95.9534	97.9504	
10	14.6-15.18	*n*-C_5F_{12}	168.9888		
11	15.18-15.9	Halon 1202	128.9131	130.9131	
12	15.9-16.4	C_2H_5Cl	64.0080	66.0050	102.9332
13	16.4-17.05	CH_2Cl_2	82.9455		
		t-CHClCHCl	95.9534	97.9504	
14	17.05-17.42	*n*-C_6F_{14}	168.9888	218.9856	
15	17.42-18.4	C_2H_5Br	107.9575	109.9554	
		CFC-113	116.9066		
		CFC-113a	116.9066		
16	18.4-18.95	C_3H_7Cl	78.0236	80.0207	
17	18.95-19.62	*n*-C_7F_{16}	168.9888	218.9856	
		Halothane	195.8902		
18	19.62-20.3	Isoflurane	114.9762	149.0026	
		HCFC-225cb	166.9687		
19	20.3-20.8	C_3H_7Br	121.9731	123.9711	
20	20.8-22.2	DCE	61.9923	63.9894	

2.2.6.3 Sample Analysis

As well as to determine sample mixing ratios, the working standard is used to track any drift in detector response that would result in a bias when comparing samples and standards run at very different times of the same day (see section 2.2.6.4). For the AutoSpec, this standard is AAL-071170, a 34L Aculife-treated aluminium canister, containing air collected at Niwot Ridge, Colorado in 2006 by NOAA. On each day of analysis, this standard is run twice to allow the instrument to settle and, once stable peaks are achieved, samples may be run. A maximum of three samples are run consecutively with standards bracketing either side. One sample per day is also repeated three times to assess the standard deviation of sample response that is then used in the calculation of analytical uncertainty for the data (see section 2.2.6.4).

A 'blank' run is also carried out at the beginning of a measurement day on the instrument. This is where 200-300 mL of helium carrier gas is passed through the inlet system, cryotrapped, injected into the GC-MS and analysed. Any peaks detected from this run are subtracted from subsequent standard and sample runs as these represent contaminations or emissions from within the system that are not representative of standard or sample data. Table 2.2 summarises the average mixing ratios of a range of routinely measured species detected in the helium blanks analysed during the three Taiwan campaigns on the GS-GasPro column. These compounds are those that consistently had responses in the blank sample and none of these made up more than 1.5% of the average sample response. Unexpected larger peaks in the helium blank may be an indication of a leak in the system.

Table 2.2: Average Mixing Ratios detected in the Helium Blank samples for a range of halocarbon species from the analysis of the Taiwan campaigns of 2013, 2014 and 2015 along with their percentage relative to the AAL-071170 standard and standard deviations.

Compound	Average Blank Response								
	2013			2014			2015		
	(ppt)	(%)	SD	(ppt)	(%)	SD	(ppt)	(%)	SD
CH_3Cl	1.49	0.26	0.10				3.67	0.62	1.18
CH_3Br	0.01	0.13	0.00	0.22	2.71	0.37	0.02	0.24	0.01
DCM	0.32	1.02	0.30	0.11	0.33	0.04	0.55	1.70	0.33
DCE	0.08	1.48	0.01	0.04	0.68	0.02	0.20	3.44	0.17
C_2H_5Cl	0.41	5.15	0.01	0.20	2.56	0.09	0.49	6.18	0.46
HFC-23	0.06	0.05	0.04	0.08	0.07	0.01	0.44	0.38	0.43
C_3F_8	0.01	2.20	0.01	0.02	3.70	0.02	0.01	1.59	0.01
COS	0.64	0.10	0.13	0.40	0.06	0.21	1.93	0.29	1.88

2.2.6.4 Data Processing

The program TargetLynx is a part of the Mass Lynx software used to control the instrument and this was used to integrate and export the raw peak data from the AutoSpec analysis. Methods were set up to automatically integrate the peak areas for compounds of interest for each analysis. However, these were all manually checked and adjusted for accuracy and consistency before the data was exported from the programme for further analysis and interpretation.

Once exported, for each compound, these peak areas were normalised according to the exact sample volume injected and then compared to the equivalent peak from the working standard (AAL-071170). To factor in any instrumental drift during the measurement day (see Figure 2.4), each sample was compared to a combination of the surrounding standard responses, each of which was weighted by proximity to the sample. This weighting is used to produce a combined standard value, which is compared to the normalised sample peak areas, and sample to standard ratio is calculated. This ratio is then multiplied by the known mole fraction of the compound in the standard to establish the sample mole fraction.

A 1σ total precision for these mole fractions is also calculated, using the standard deviation (SD) of the sample and the SD of the standard (see Equation 2.5). If repeat analysis of a sample was unsuccessful or not carried out for a particular day, the standard SD for that day was used instead for both terms in the equation to produce an estimate of total precision.

$$\text{Total uncertainty} = \sqrt{(\text{SD}_{sample}{}^2 + \text{SD}_{standard}{}^2)} \qquad \text{Equation 2.5}$$

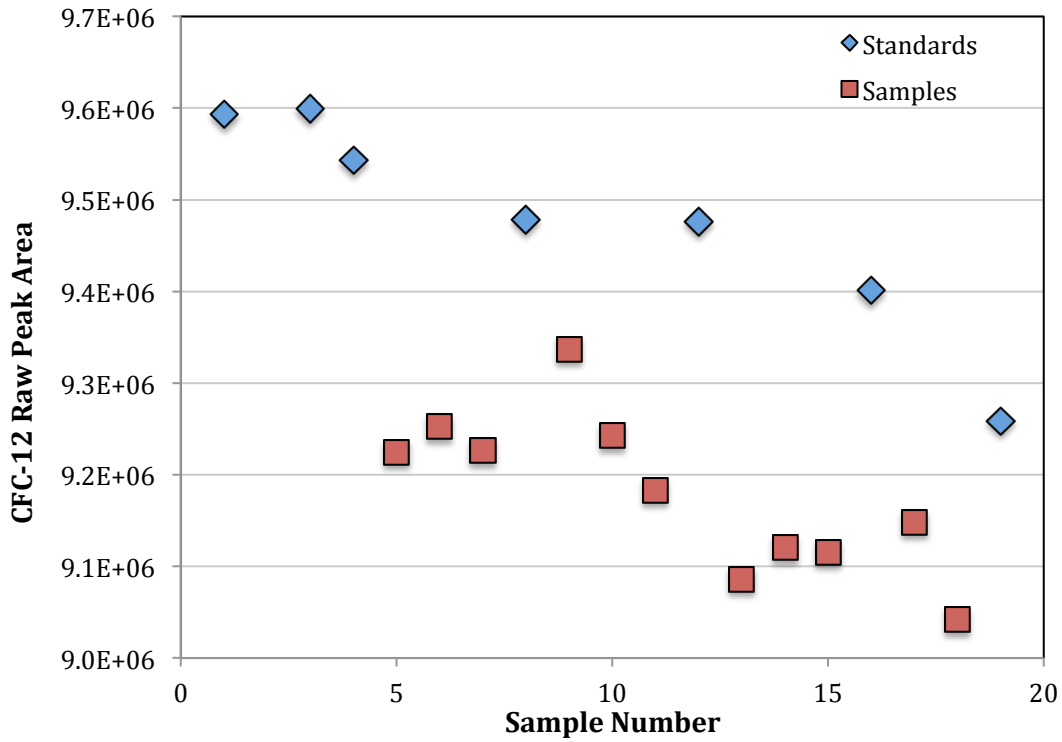

Figure 2.4: A graph showing the variation in the detected raw peak area of CFC-12 during sampling on the 23rd September 2014 for both standards and samples. The decrease in peak area seen, particularly for the standard, as the day goes on is due to instrumental drift. This is normalised during data processing.

2.3 Air Mass Backwards Trajectory Modelling

In chapters 4 and 5, computer modelling is used to estimate the backward trajectories of the air masses that were sampled. This was carried out using the UK Meteorological Office Numerical Atmospheric Modelling Environment (NAME v4) and Matt Ashfold, University of Nottingham, performed the model runs. NAME is a Lagrangian dispersion model that utilises three-dimensional wind fields and can track ensembles of particles forwards or backwards in time.

NAME was developed by 1988 and was intended as an emergency response model to predict the transport and deposition of radioactive materials released during a nuclear accident. Subsequent updates and expansion of the model, including the introduction of chemistry schemes, increased its capabilities and enabled its use for a wider range of applications (Jones *et al.* 2007). Forwards trajectory prediction modelling has been used to asses potential impact from volcanic ash clouds (Devenish *et al*. 2012) and forest fires (ref) as well as the viral transmission of foot and mouth disease (Gloster *et al*. 2003). Backwards dispersion modelling has been utilised to identify sources responsible for specific pollution events or emission patterns based on observed data (Manning *et al*. 2003).

NAME can be utilised to understand the origin of sampled air masses and has previously been used extensively for the estimation of emissions of long-lived trace gases on a national scale (such as Manning et al. 2011). In Ashfold *et al.* (2015), 12-day backwards trajectories were calculated for perchloroethene (C_2Cl_4), starting from two measurement sites in Borneo. Here they compare the back-trajectory routes visible on the particle density maps produced by the model with the observed mixing ratios, thus indicating potential source regions. A similar qualitative approach is taken in chapters 4 and 5 of this study.

NAME can be used quantitatively for inversion modelling, in a 'top down' approach, using observational data to estimate emissions of a specific species which in turn can be compared to inventory estimates as a method of independent assessment. However, the location and quality of measurement sites and the dynamics of the modelled dilution process can all introduce uncertainties that are difficult to quantify. As such, only large differences in trend or magnitude are indications that inventory assessment need re-examining (Manning *et al.* 2011). Sulphur dioxide (SO_2) mass concentrations in European and North Atlantic airspace from Icelandic volcanic eruptions have also be modelled by NAME. Whilst the likely presence or absence of SO_2 in a specific region is readily available, the uncertainties with more quantitative measurements are again quite large, mainly due to the accuracy and high resolution needed to fully constrain the source terms of the model (Schmidt *et al.* 2014). The complexity and magnitude of information needed to minimise the uncertainties produced in a more quantitative analysis utilising the NAME model was not readily available for this study and as such a qualitative outlook was taken in this work.

Since NAME is a Lagrangian model is takes the perspective of an 'air parcel' and calculates the its position and properties over time utilising mean wind field data. Eulerian models, such as MEDIA (Sandu *et al.* 2003) and CANERM (D'Amours, 1998) which have also been used for forecasting volcanic ash (Witham *et al*., 2007), monitor specific reference points for atmospheric properties. Simple Lagrangian models such as FRAME (Singles *et al*. 1998) and HARM (Metcalfe *et al*. 2001) have advantages over NAME in that their run times are much faster and so allow for the calculation of multiple simulations. However, the more complex NAME model is better representative of the chemistry and concentrations of the particles in question, as well as being able to simultaneously portray other pollutants that may interact (Dore *et al*. 2015). HYPLIT, a hybrid puff-particle/trajectory model (Stein *et al*. 2015), and FLEXPART, a regional to global scale dispersion model (Stohl *et al*. 2005), have both been used for many similar applications to NAME but both are more open source than NAME which is only available for external research use under licence. NAME also utilises the Unified Model for meteorological data (Jones *et al*. 2007) whereas FLEXPART uses the European Centre for Medium-range Weather Forecasts (Stohl *et al*. 2005) and HYSPLIT utilises the U.S. National Weather Service (Stein *et al*. 2015).

NAME does encounter some limitations in terms of resolution of the atmospheric boundary layer (ABL). This is the region of the atmosphere directly in proximity to the Earth's surface (Bonner *et al*. 2010) and so is subject to rapid changes in height, composition and turbulence depending on any number of factors including season, temperature and weather (Hennemuth and Lammert, 2006). The ABL plays an important role in particle and pollutant dispersion however its complexity means that assumptions and averages have to be used to constrain the model algorithms (Lateb et al. 2016). Whilst the resolution of the ABL has improved through the different iterations of the NAME model (Jones et al., 2007), there is still progress to be made. Local ground level wind data was collected during the campaigns discussed in Chapters 4 and 5 in order to compare with suggested NAME trajectories and identify potential influences from ABL variation. Similarly, a further limitation may be in the difficulties of global models in reproducing the complex meteorological conditions of mountainous regions (Travnikov *et al.* 2016), specifically the Central Mountain Range in Taiwan which influenced the campaigns of Chapter 4. Again, local wind data was utilised to indicate differences in sampled air masses potentially impacted by mountainous meteorological conditions.

In this work, for each air sample, batches of 60,000 inert particles were released and trajectories were calculated by NAME backwards from the measurement site within an altitude of 0-100m. These were started throughout a 3-hour period encompassing the sampling time and the mid-point of this is recorded on trajectory plots. These trajectories ran backwards in time for 12 days and are associated with an arbitrary mass. The location of all the trajectories within the lowest 100m of the modelled atmosphere was recorded every 15 minutes on a grid with a resolution of 0.5625° longitude and 0.375° latitude.

The trajectories are calculated using three-dimensional meteorological fields produced by the UK Met Office's Numerical Weather Prediction tool, the Unified Model (UM). Each field has a horizontal grid resolution of 0.35° longitude by 0.23° latitude (improved to 0.23° longitude by 0.16° latitude for the 2015 Taiwan campaign) as well as 59 vertical levels below ~30km. These are available in 3 hour intervals. Vertical velocities are obtained from the UM while NAME parameterises the sub-grid-scale process of turbulence.

From this information, a map of time-integrated particle density (in g s m^{-3}) can be created and these are the plots utilised in chapters 5 and 6. Essentially, these are a measurement of the amount of trajectory mass (g) and the length of time (s) all the trajectories spend near the surface (below 100m) of each grid cell (m^3). It is also possible to calculate modelled emissions for species using this particle density and this will be discussed in more detail in section 6.6.4.

Chapter 3: Analysis of Methyl Halide Emissions from Plants

3.1 Natural Sources of Methyl Halides

The methyl halides – methyl chloride (CH_3Cl), methyl bromide (CH_3Br) and methyl iodide (CH_3I) (see Figure 3.1), are volatile organic species that, unlike most other halocarbon compounds, have large natural sources and few anthropogenic ones. Although atmospheric lifetimes for these species are relatively short in comparison to compounds such as CFCs and halons, both methyl chloride and methyl bromide can still reach the stratosphere and so do contribute to ozone depletion (Santee *et al*. 2013, Hossaini *et al*. 2012b). For methyl iodide this contribution is thought to be near zero due to its very short lifetime. Methyl chloride accounted for 540±5 ppt (~16%) of the total tropospheric chlorine in 2012 (Carpenter and Reimann, 2014). Whilst this value has remained essentially constant since 2008, due to the predominantly natural sources, tropospheric mole fractions of methyl bromide decreased from 7.33 ppt in 2008 to 6.95 ppt in 2012 (equivalent to ~400 ppt of chlorine), reflecting the continued reduction in production, consumption and emissions from industrial sources in line with global control measures (Carpenter and Reimann, 2014). Section 1.14.1.6 discusses these anthropogenic applications as well as those for the other methyl halides in more detail.

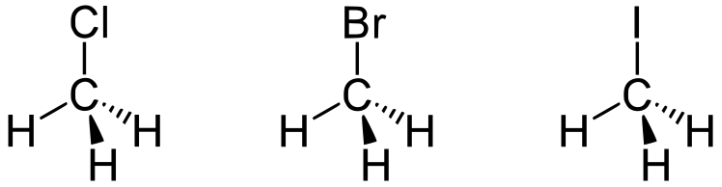

Methyl chloride **Methyl bromide** **Methyl iodide**

Figure 3.1: Chemical structures of the three methyl halides: methyl chloride, methyl bromide and methyl iodide. Courtesy of Koerner, 2012.

In terms of natural emissions, the ocean is the main source of methyl iodide, contributing to over 80% of total global emissions (including anthropogenic sources), as well as methyl bromide, which corresponds to total global emissions of ~38% from oceanic sources (Carpenter and Reimann, 2014). For methyl chloride, oceanic sources (19% [~700 Gg yr^{-1}], Hu et al. 2013) are secondary only to those from tropical and subtropical forests (56% [~2040 Gg yr^{-1}], Carpenter and Reimann, 2014). Figure 3.2 and Table 3.1 summarise the natural and anthropogenic sources that make up the total global emissions of the methyl halides.

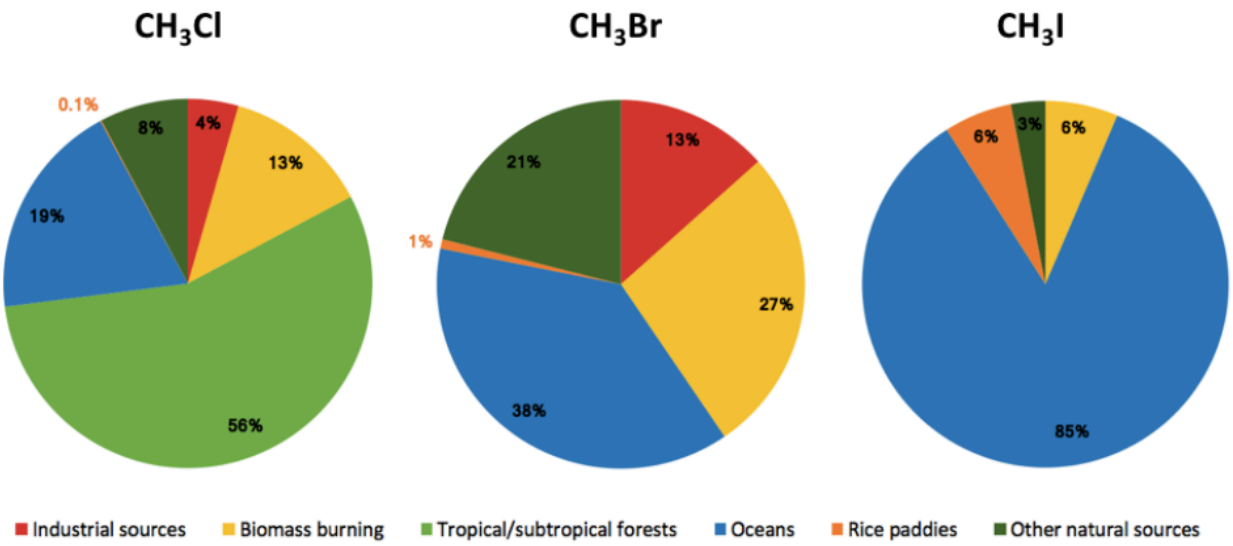

Figure 3.2: Contribution of natural and anthropogenic sources to the total global emissions of methyl halides in the atmosphere for 2012. Sources of CH_3Cl and CH_3Br are based on Carpenter and Reimann (2014), sources of CH_3I are based on Youn *et al.* (2010).

All three compounds have emission sources of plant-based origin, however the contributions from agriculturally grown crops are of particular interest when considering potential impact to the ozone layer. In 2012, global emissions from rice paddies were estimated at 3.7 Gg yr^{-1} (0.1%) for methyl chloride and 0.7 Gg yr^{-1} (1%) for methyl bromide. Lee-Taylor and Redeker (2005) also suggested emissions of 22.5 Gg yr^{-1} (6% of the total global emissions) for methyl iodide from rice cultivation however, due to the very short atmospheric lifetime of this compound (7 days, Carpenter and Reimann, 2014) there is likely no impact to ozone depletion. Rapeseed crops contribute to methyl bromide sources as well, with global emissions of 5.1 Gg yr^{-1} (6%) being estimated for 2012 (Carpenter and Reimann, 2014).

Table 3.1: Emissions contributions in Gg yr^{-1} of methyl halides from natural and anthropogenic sources.

Source	Emissions (Gg yr^{-1})		
	Methyl Chloride[a]	**Methyl Bromide[a]**	**Methyl Iodide[b]**
Industrial	162	11.4	n.q
Biomass Burning	468	23	0.017
Oceans	700	32	0.224
Tropical/subtropical forests	2040	n.q.	n.q
Rice Paddies	3.7	0.7	0.016
Other natural sources	284	17.9	0.008
Total	3658	85	0.265

a – Carpenter and Reimann, 2014 b – Youn *et al.* 2010

Although these agricultural sources may seem negligible (0.1-1% of total global emissions), particularly in comparison to other biogenic emissions, given that the global human population is steadily increasing, demand for cultivated crops will also rise. Since 1961, rice production has increased from 215 million tonnes to 746 million tonnes in 2013 (see Figure 3.3a) as it still remains a staple food source, particularly in Asia. Rapeseed production has similarly increased, from 3.6 million tonnes in 1961 to 72.5 million tonnes in 2013 (see Figure 3.3b, FAOSTAT, 2014). Between 2012 and 2013 there was a notable increase of around 8 million tonnes, which may reflect expanded production due to the use of rapeseed in biofuels and, as such, further annual increases are likely.

Methyl halide production from cultivated crops could also be influenced by climate change itself, as well as contributing to it. Redeker and Cicerone (2004) found emissions from rice to be influenced by temperature, with a later study estimating that an increase of 1°C could see emissions of methyl bromide and methyl iodide rise by 10% (Lee-Taylor and Redeker, 2005).

The development of salt tolerant crops (Flowers, 2004, Rozema and Flowers, 2008) to expand agricultural land, and help meet increased crop demands, also poses potential risks in terms of methyl halide emissions. Previous studies have found positive correlation between the production of methyl halides and the concentration of halide ions in the growth medium for both rice and rapeseed (Gan *et al*. 1998, Rhew *et al*. 2003). Redeker and Cicerone (2004) estimated in rice an increase of 0.21 mg yr-1 methyl chloride for every part-per-million (ppm) increase in soil chloride, as well as an increase of 0.3 mg yr^{-1} methyl bromide and 160 mg yr^{-1} methyl iodide for every ppm increase in soil bromide and soil iodide respectively. This implies that emissions would further increase with salt tolerant crop use, potentially causing additional damage to the ozone layer.

A possible method for reducing this impact is the development of 'ozone-safe' varieties of crop species. The identification of the genes that control and regulate methyl halide production was the first step in the process. Understanding the function and links between these genes, as well as the results of manipulations to them, may then enable the growth of species producing zero or low methyl halide emissions, without constraining desirable properties such as crop yield or disease resistance.

Crops of this type would be particularly beneficial in Asia where the majority of global rice production occurs (Muthayya *et al*. 2014). As discussed in chapters 1 and 5, the region experiences rapid vertical transport, from the boundary layer to the stratosphere, in a matter of days (Ashfold et al. 2015). This means that methyl halides produced by rice paddies in this area are more likely to reach the stratosphere and so contribute to ozone depletion, despite short atmospheric lifetimes.

The increasing global population is intensifying pressure on the Asian region to produce higher yielding crops rather than clear more land for farming. However, if recent trends continue, demand is unlikely to be met.

Ray et al. (2013) predicted an increase in global production of 42% by 2050 due to increased crop yields but the projected shortfall is still 394 million tonnes. As such a combination of increasing crop yields and increasing plant numbers may have to be utilised to ensure needs are met. With more rice paddies in Asia, the ozone depleting impact of this region is likely to increase and more rapidly than that of other areas due to the local atmospheric transport conditions. It is therefore important for methods that may counteract this impact, such as 'ozone-safe' rice crops, to be developed and tested in the near future so they may be successfully implemented before further damage to the ozone layer occurs.

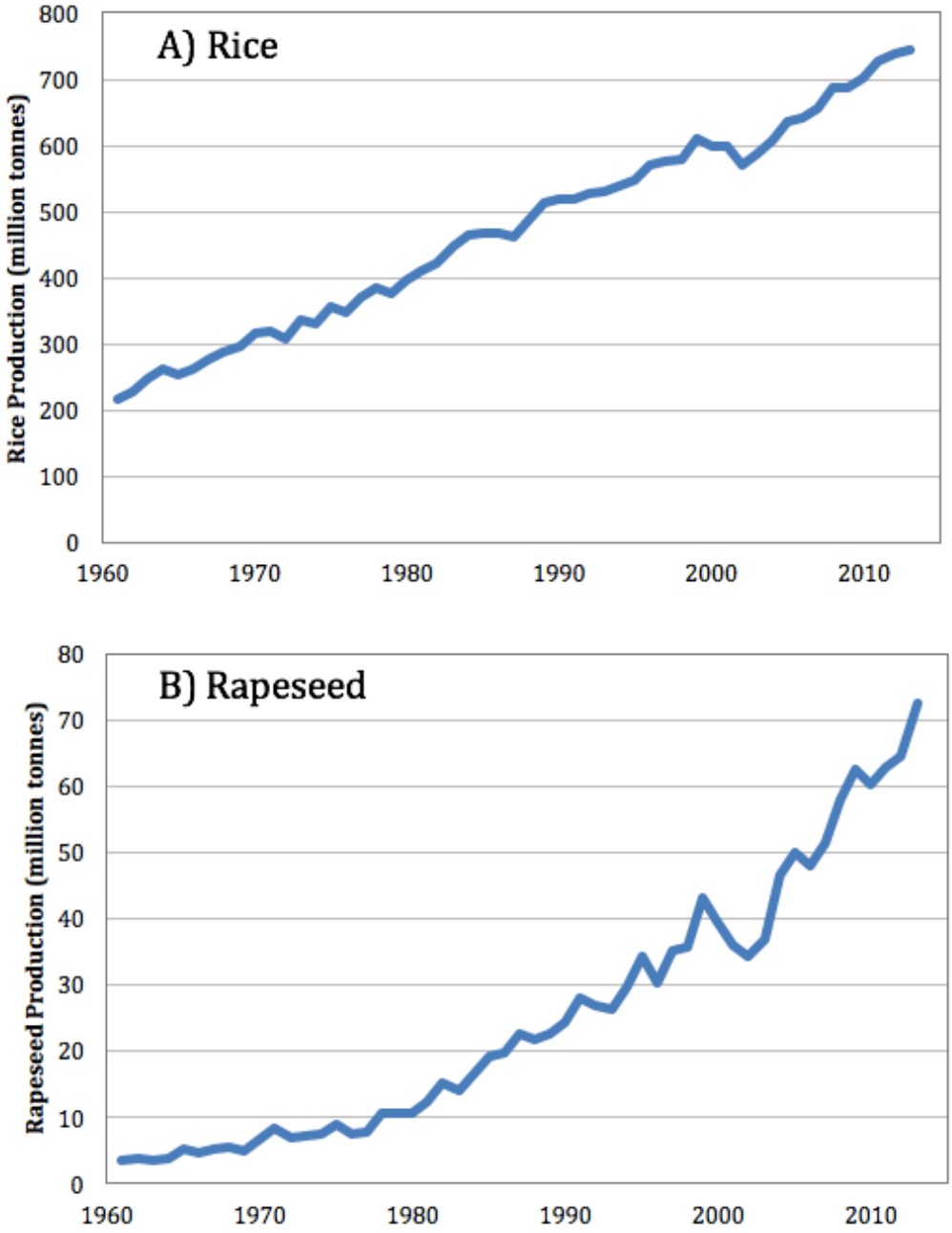

Figure 3.3: Global production between 1961 and 2013 of A) Rice and B) Rapeseed. Data available from http://faostat.fao.org

3.2 Methyl Halide Production in Plants

For a long time, the specific mechanism for methyl halide production by living organisms was relatively unknown. Wuosmaa and Hager (1990) discovered that S-Adenosyl-L-methionine (SAM)-dependent methyl transferases (MTs) catalysed the transfer of a methyl group from SAM to halide ions (Figure 3.4a) in examples of fungi (*Phellinus pomaceus*), marine algae (*Endocladia muricata*) and plants (*Mesembryanthemum crystallium*). Various other species and bacteria were subsequently found to exhibit methyl transferase activity with halide ions (Amachi et al. 2001) and the same enzymes were determined to be able to catalyse the methylation of sulphur-containing ions, including bisulphide (HS^-) and thiocyanate (SCN^-) (Attieh et al. 1995, Attieh et al. 2000) (Figure 3.4b). A study into the rate of this enzymatic reaction indicated a high Michaelis-Menten (K_m) value suggesting a low affinity of halides to methyl transferases (Manley, 2002). This may imply that halides are not the target substrate and the methylation of thiols is actually the primary function.

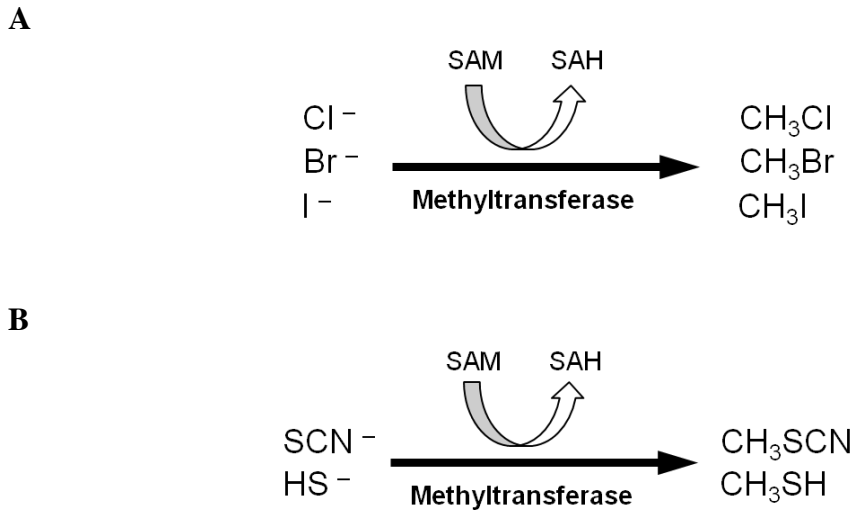

Figure 3.4: Methyl halide (A) and volatile sulphur species (B) production through S-Adenosyl-L-methionine (SAM)-dependent methyltansferases (MTs). Courtesy of Koerner, 2012.

The gene encoding for a methyl chloride transferase was first cloned from *Batis maritime* (Ni and Hager et al. 1998) and other halide/thiol MTs (HTMTs) have since been cloned in *Brassica oleracea* (Attieh et al. 2002), *Arabidopsis thaliana* (Rhew et al. 2003, Nagatoshi and Nakamura, 2009), rice (*Oryza sativa*) (Takekawa and Nakamura, 2012) and the diatom *Phaeodactylum tricornutum* (Toda and Itoh, 2011). Rhew et al. (2003) displayed *in vivo* that HTMTs catalyse methyl halide formation. The identified gene encoding for an HTMT from *A. thaliana* was named *HARMLESS TO OZONE LAYER (HOL)* after the expected effect of loss of function once the gene is deactivated. The *HOL* control over methyl halide production was confirmed as mutant plants (termed as *hol)* had detected emissions less than 1% of wild type (WT) levels in adult plants (Figure 3.5).

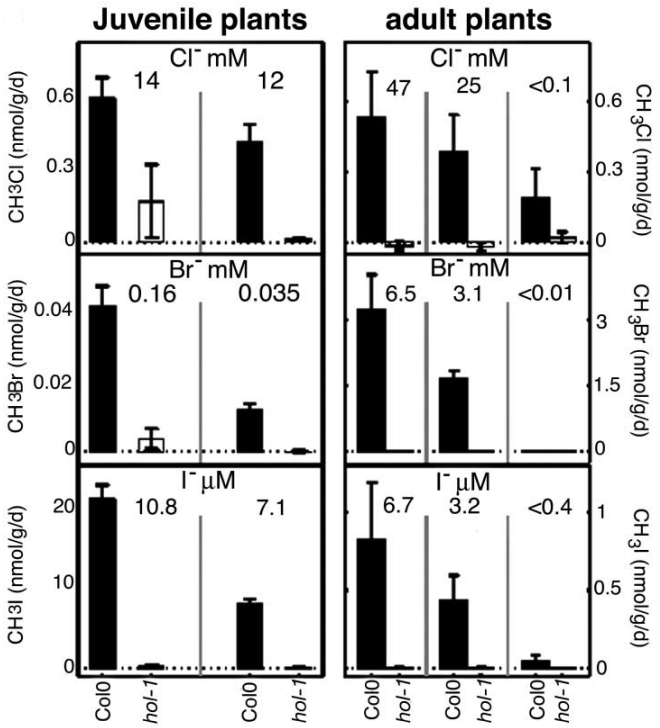

Figure 3.5: Control of methyl halide production in *A. thaliana* by the *HOL* gene is shown by the differences in observed emissions between wild type (*Col0*) and mutant species (*hol*). The numbers above each graph indicate the average halide ion concentration in the growth medium. Image from Rhew et al. 2003.

However, the function of methyl halide production in plants is still unknown. No major role in plant development was obvious in *A. thaliana* as *hol* mutants exhibited no noticeable growth defects (Rhew *et al*. 2003). Hypotheses and supporting evidence as to the potential purpose of methyl halide production include:

- **Resistance to biotic stress including plant pathogens, insects and nematodes** (Taylor, R.W.D., 1994, Ohr et al. 1996, Ristaino and Thomas, 1997). Methyl bromide and methyl iodide have been utilised in industry as pesticides and post-harvest treatment of perishable items, and so naturally they may potentially act as a defence mechanism. One study showed *hol* mutant seedlings had lower survival rates when exposed to a bacterial pathogen (Nagatoshi and Nakamura, 2009), however this experiment has been criticised for its bacterial growth monitoring procedure (Koerner, 2012).

- **Disposal of excessive halide ions to maintain homeostasis for plants growing in high salinity** (Ni and Hager, 1998, Ni and Hager, 1999). Several studies have shown positive correlation between halide ion concentrations in soils with methyl halide emissions in a variety of plants (Redeker and Cicerone, 2004, Rhew et al. 2003, Gan et al. 1998, Armeanu-D'Souza, 2009). Environments such as salt marshes and mangrove forests, where there is high soil salinity, have been reported as being significant methyl halide emitters (Rhew et al. 2000, Yokouchi et al. 2000, Manley et al. 2006, Manley et al. 2007).

- **Detoxification of glucosinolate (GL) hydrolysis products**. SCN^- and HS^- occur naturally after wounding through GL hydrolysis in *Brassicaceae* (Attieh et al. 2000). The HOL gene was confirmed as catalysing the conversion of SCN^- to CH_3SCN in *A. thaliana* as *hol* mutants did not produce CH_3SCN upon wounding and plant development was hindered comparative to wild type plants when grown in a SCN^- rich medium (Nagatoshi and Nakamura, 2009).

- **'Accidents of metabolism'** attributed to non-specific methylation of halide ions (Manley, S.L. 2002).

- **Attraction of bacteria to act as biocontrol by impairing pathogen growth** (Lindlow and Brandl, 2003, Bais et al. 2006, Raaijakers et al. 2009). Methyl halide utilising bacteria have been found in both soils (Schafer et al. 2007) and on *A. thaliana* leaves (Nadalig et al. 2011). These could act as competition for resources such as nutrients with pathogens (Lindlow and Brandi, 2003, Bais et al. 2006, Raaijakers et al. 2009).

No clear consensus has been reached and so investigations continue into the purpose of methyl halide production. The work in this study collaborates with the John Innes Centre (JIC) and focuses on the effect of *HOL* gene manipulation on methyl halide emissions using *A. thaliana*. Whilst this work aims to identify and quantify the results of successful mutations and thus contribute to the development of 'ozone-safe' species, the JIC hope that continued experimentation may also shed some light onto the overall purpose of methyl halide emissions from plants.

3.3 *Arabidopsis thaliana* and the *HOL* gene

The *Arabidopsis* genome has been entirely sequenced and near-saturation mutant collections are available making it very useful in the investigation of genetic-based regulation. After the *HOL* gene was identified, a mutant (*hol)* was found in the SALK T-DNA collection, a compilation of stable loss-of-function mutations developed for nearly all the genes of *A. thaliana*. T-DNA (transfer DNA) is a section of DNA code which can be inserted into the DNA strands of a host plant using a bacterial plasmid. The insertion utilised in this case consisted of 160 nucleotides (DNA bases) in the intron 2 section, which is found before the

coding of the gene itself. This change renders the resulting HTMT inactive and so dramatically reduces methyl halide production (Rhew et al. 2003).
As deactivation of the *HOL* gene results in decreased methyl halide emissions, overexpression of the gene was expected to cause increased emissions. In order to test this hypothesis the cauliflower mosaic virus (CaMV) 35S promoter was utilised to cause *HOL* gene overexpression. This increased transcription (enzyme production) by 60-fold and 140-fold in two independently created lines (196-9 and 196-11 respectively). As anticipated, emissions of methyl chloride and methyl bromide in the two lines increased, by 20-fold and 50-fold respectively, when compared to wild type (WT) levels. Methyl iodide also increased 3-fold in comparison to WT. This confirmed there is a positive correlation between the expression of the *HOL* gene and the production levels of methyl halides in *A. thaliana*.

Characterisation of *HOL* reporter lines indicated strong expression in the roots of *A. thaliana* suggesting this is where the majority of methyl halide production occurs. This, in turn, appeared to support the hypotheses that HOL function was either related to salt tolerance (disposal of excess halide ions) or plant-insect/plant-microbe interactions. Testing resulted in no supporting evidence for either hypothesis, as *hol* mutants were no more sensitive to salinity than WT plants. No significant differences in the herbivore performance or microbial community between *hol* mutant, WT and overexpressed *35S::HOL* plants were detected. Thus further investigation into the purpose of methyl halide production is still necessary.

Multiple *A. thaliana HOL*-homologous genes, those with the same structure, position and organisation, were identified in both *Brassica rapa* and *Oryza sativa*. These were tested to determine those with the most similarities to *A. thaliana HOL* in terms of methyl halide regulation. One *A. thaliana HOL*-homologous gene was identified in the moss *Physcomitrella patens,* referred to as *PpHOL* hereafter. These homologous genes can help the understanding of the phylogeny and the evolutionary process behind methyl halide production. Multiple copies can be indicative of specific events after divergence from a common ancestor, and the presence of a homologous gene in a moss suggests that methyl halide production is an ancient mechanism in land plants.

From these homologous genes, transgenic *A. thaliana* lines were able to be produced. Plasmids containing the gene coding sequence of interest were inserted into the *Agrobacterium* strain AGLI. A modified floral dip method (Clough and Bent, 1998) was used to transform *Arabidopsis* and full details of this process can be found in Koerner, (2012). Successful transformation was verified via polymerase chain reaction (PCR) and homozygous third generation plants (T3) were used for experimentation (Koerner, 2012). The lines were created to see if overexpressed un-mutated *HOL* genes from other species would mediate methyl halide production the same way in *A. thaliana*. As such, mutant *A. thaliana* was used for the transformation to minimise background emissions. The results of some of these tests will be discussed in section 3.4.2.

To investigate the regulation of methyl halide in *P. patens* further, *PpHOL* knockout lines were generated. These are where protoplasts from WT *P. patens* are transformed along with a gene targeting construct that uses homologous recombination to replace the endogenous *HOL* gene with an antibiotic resistance cassette (Koerner, 2012). Transformed mosses should no longer produce methyl halides via the *HOL* controlled mechanism and the gained antibiotic resistance properties may aid the identification of moss samples that have undergone successful transformation. As with the transgenic lines, homozygous third generation mosses were used for experimentation. Results of tests on WT and *PpHOL* knockout line samples will be discussed in section 3.4.3.

Using genetic manipulation and transgenic lines to investigate the purpose of HTMTs and methyl halide regulation, furthers both understanding and the potential development of 'ozone-safe' crop species. Around 90% of methyl halide emissions from rice paddies originate in South-central and Southeast Asia as well as mainland China (Lee-Taylor and Redeker, 2005). Given some of these areas have proximity to the tropics, where vertical transport of emissions to the upper troposphere and stratosphere occurs more rapidly, these regions in particular could greatly benefit from methods to reduce the global impact from their rice cultivation, especially with the growing demand of an increasing global population.

This chapter will summarise a range of *A. thaliana* and moss (*Physcomitrella patens*) based experiments, carried out in collaboration with the John Innes Centre and University of East Anglia, that monitored the production of methyl halides between WT and *hol* mutant plants as well as with rice, diatom and moss transgenic lines. High sensitivity GC-MS was used to quantify and compare emissions from these samples and potential relationships were identified.

3.4 Sample Preparation

Samples were prepared by Nicola Stacey at the John Innes Centre under the same method used in Koerner, (2012).

3.4.1 *Arabidopsis thaliana*

Seeds were surface-sterilised for 2 minutes in 70% ethanol, then in a bleach solution (15% bleach, 0.01% Tween 20) for 10 minutes before being washed 5 times with sterile water. The seeds were then sown on MS media (4.4 g/L Murashige and Skoog basal salt mixture (Murashige and Skoog, 1962) [Duchefa] (see Appendix 3.1a for composition), 10 g/L sucrose, 0.5 g/L LMES (2-(N-morpholino)ethanesulfonic acid), 8 g/L agar, pH 5.7) and the plates were stratified for 3 days at 4°C. They were then transferred to growth chambers at 22°C with a 16hr/8hr day/night cycle (Koerner, 2012). For the experiments assessing temperature effect, some samples were grown at 27°C with the same day/night cycle.

3.4.2 *Physcomitrella patens*

One mL spore solution (~20 spores) of the Gransden wild-type strain of *Physcomitrella patens* (Hedw.) Bruch and Schimp was plated on PPNO3 media (see Appendix 3.1b for composition). Cultures were placed in a 22°C growth chamber and grown with a 16hr/8hr day/night cycle (Koerner, 2012). For the experiments assessing temperature effect, some samples were grown at 27°C with the same day/night cycle.

3.4.3 Experiment Design

As the results discussed in this study are also part of a wider project, in collaboration with the John Innes Centre (JIC), the initial experiments were designed through discussion between Prof. Bill Sturges and Dr. Lars Østergaard, heads of the project from UEA and JIC respectively. As the results featured below were achieved, I also participated in these meetings to better understand the project itself and to suggest areas that may benefit from further experimentation given my previous analysis. Whilst this allowed for some control over the range of samples that would be analysed, ultimately the time, availability and success of the genetic manipulation necessary for the growth of these plants was the key factor in controlling and limiting the experimentation process.

3.5 Sample Collection

Air samples were collected by fully enclosing the plants in Teflon bags for several hours (see Appendix 3.2 for specific timings), which were sealed to the beakers or plates using electrical tape (see Figure 3.6). Petri dishes containing growth medium but no plants were also bagged and left under the same conditions to act as controls and provide background methyl halide concentrations for the air. Samples were extracted via a Teflon valve on the bags and were transferred to 1L SilcoCans via Teflon tubing. These cans were first evacuated, and so under negative pressure, causing when opened the air from the Teflon bags to travel along the tubing and into the canister. A battery-operated pump was also used to facilitate this air extraction and pressurise the canisters; between 1 and 2 litres of air was collected per sample.

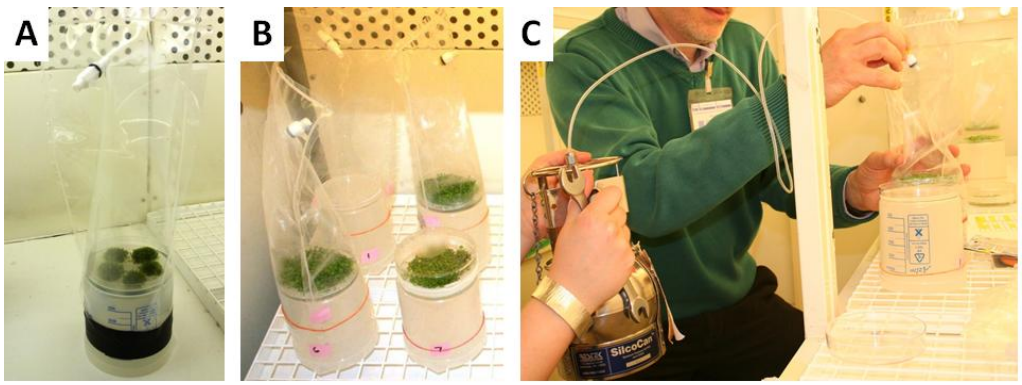

Figure 3.6: *Arabidopsis* (A) and moss (B) were grown on petri dishes with agar growth medium and enclosed in Teflon bags for several hours. Teflon tubing (C), attached to the valve on the bags, was used to collect samples in evacuated SilcoCans.

3.6 Sample Analysis

The air samples were analysed using the high-sensitivity Waters AutoSpec GC-MS suite, as described in section 2.2.6, however only ~8mL of air was trapped per run. A specific selective ion method was set up for the analysis of these samples and the compounds included, masses measured and the associated time windows can be found in Table 3.2.

Table 3.2: Selective ion method developed for the AutoSpec analysis of the plants samples to establish methyl halide emissions.

Function	Time (mins)	Compound	Ion Mass 1	2	3
1	5.5-7.4	SF_6	126.9641		
		C_2F_4	99.9936		
2	7.4-9.9	COS	59.9670	60.9664	61.9623
		HFC-32	51.0046		
3	9.9-11.3	SO_2F_2	82.9603		
		CFC-115	84.9657	86.9627	
4	11.3-12.4	CFC-12	100.9361	101.9395	102.9332
5	12.4-13.4	CH_3Cl	49.9923	50.9957	51.9894
6	13.4-14.6	CS_2	75.9441	77.9399	
7	14.6-15.5	CH_3Br	93.9418	94.9452	95.9398
8	15.5-16.4	CFC-11	100.9361	101.9395	102.9332
9	16.4-17.7	CH_3I	126.9045		
10	17.7-19.1	CFC-113	100.9361	101.9395	102.9332
11	19.1-20.1	$CHCl_3$	82.9455	84.9426	
		CCl_4	116.9066	118.9036	

3.7 Data Interpretation

The peak areas of mass ions corresponding to compounds of interest were extracted from the chromatograms produced by the analysis of each sample. Similar to the method of data processing described in section 2.2.6.4, the raw areas were first corrected to reflect the volume of air trapped per sample. Multiple standards were run on each day of analysis, two at the beginning of each session, one after every two samples and one for the final run. Each day, the areas of these standards were averaged for each compound and any areas not within two standard deviations were removed from the average calculation as outliers. The sample areas were then normalised by dividing them by this average standard value.

The normalised areas were converted to mixing ratios (ppt) through multiplication by the individual compound mixing ratios found in the standard. At this point, the mixing ratios of the control samples collected during each experiment were averaged and these values were subtracted from the sample mixing ratios. Again, values not within two standard deviations were removed from the average as outliers but only for experiments where four control samples were measured. Those with only three controls were all included.

Although mixing ratios give a good representation of the differences between the sets of samples measured, further processing is required to calculate emission rates. The mixing ratios were converted, via the ideal gas law, into the number of moles of each compound for every sample measured. Boyle's Law was used to calculate the extracted air volume for this calculation, and where canister pressures were not recorded, a value of 2 bar was used as this represents the maximum pressure the pump can deliver.

The corresponding value was then converted to nanomoles and the time the plants were covered by the Teflon bags was utilised to produce a value in nmol $hour^{-1}$. The emissions were then normalised to each plant samples' fresh weights to produce a rate in nmol $hour^{-1}$ $kgFW^{-1}$.

3.8 Results

In this section, five experimental sampling sets are described and a summary of the methyl halide emissions rates can be found in Table 3.3. Due to the nature of producing genetically modified plants, each sampling set contains a maximum of 4 plants per genetic alteration, all of which exhibit natural biological variation. As such, statistically significant conclusions are very limited from the current data when errors and standard deviations are considered. However, it should also be noted that these experiments are part of a wider, long-running project in collaboration with the John Innes Centre. This project will continue after the analysis in this work and so testing to further confirm or refute the results and relationships proposed will take place after the completion of this thesis.

Table 3.3: Methyl halide emissions summary from the 5 sets of experiments discussed in this chapter. Sample groups marked with an asterisk were analysed at a different time to the rest of that experiment. Emissions rates recorded in red had samples removed from the average calculation due to outlying results which will be discussed further in section 3.8.3.

Experiment	Sample Group	Average Emission Rate (nmol hour^{-1} kgFW^{-1})		
		CH_3Cl	CH_3Br	CH_3I
A. thaliana Wild Type and *hol*-mutant lines	COL	16.521	0.338	12.597
	hol-1	0.874	0.009	0.421
	hol-1*	1.424	0.004	1.075
A. thaliana based Transgenic Lines	OsHOL*	0.824	0.005	0.381
	PpHOL	2.533	0.015	1.394
	PtHOL	1.901	0.007	2.130
P. patens Wild Type and PpHOL Knockout Lines	WT	0.273	0.025	0.008
	PpHOL4	0.496	0.009	0.007
	PpHOL9	0.096	0.010	0.001
Effect of Temperature: *P. patens* Wild Type and PpHOL	WT 22°C	0.076	0.033	0.006
	WT 27°C	0.203	0.053	0.015
	PpHOL4 22°C	0.044	0.002	0.001
	PpHOL4 27°C	0.231	0.008	0.005
Effect of Temperature: *A. thaliana* Wild Type and *hol*-mutant	WT 22°C	16.244	0.484	47.291
	WT 27°C	20.076	0.552	54.401
	hol 22°C	1.822	0.017	1.012
	hol 27°C	0.625	0.015	0.877

3.8.1 *Arabidopsis thaliana* Wild Type and *hol*-mutants

For this experiment, both wild type (COL) *A. thaliana* and *hol*-mutant (*hol*-1 and *hol*-1*) lines were grown and their methyl halide emissions monitored. The *hol*-1* plants were grown from the same line and conditions as the *hol*-1 plants, however these were grown and analysed a month later so some variation was expected. Table 3.3 indicates the average emission rate detected for each set of samples and each methyl halide.

What is clear, when the emission rates are plotted for all three of the methyl halides (see Figures 3.7a, 3.7b and 3.7c), is that the wild type *A. thaliana* has significantly higher emissions than the *hol*-mutants and Table 3.4 summarises the percentage reduction in emission rates. For both methyl chloride and methyl iodide, the *hol*-1 mutant rate of emission was, on average, 94.7% and 96.7% lower respectively than the wild type. The *hol*-1* mutant rate was detected at a rate ~91% lower than the wild type for both methyl chloride and methyl iodide. This is less of a reduction than was seen with the previous samples however, for methyl bromide, the *hol*-1 mutant exhibited an average 97.2% reduction whereas the *hol*-1* reduction was found to be slightly larger at 98.7%.

Table 3.4: Reduction in emission rates found with *hol*-mutants when compared to wild type *A. thaliana*.

	Average Percentage Reduction in Emission Rate when compared with Wild Type *A.thaliana* (%)		
	CH_3Cl	**CH_3Br**	**CH_3I**
hol-1	94.7	97.2	96.7
hol-1*	91.4	98.7	91.5

Whilst conditions for both experiments were kept as similar as possible, slight differences during plant growth as well as storage of the mutant line between experiments may have been a factor. More likely, however, particularly since emissions rates are not consistently higher for all the methyl halide in the *hol*-1* mutant, is either biological or instrument variation. Biological variation is seen between individual plants in all experiments and is why average emission rates are considered, in an attempt to minimise the impact of plants that may be predisposed to under- or overexpress particular features or characteristics (see COL-03 in Figure 3.7C as an example).

However, none of the *hol*-1* plants were calculated to have significantly higher or lower emission rates than the others measured at the same time, so the average value has not been particularly skewed. This means all four plants would have had to be predisposed to under-express methyl chloride and methyl iodide and over-express methyl bromide, comparative to the previously analysed *hol*-1 plants which, whilst possible, seems less likely than instrument variation. Sensitivity on the AutoSpec varies daily and the instrument is re-tuned and calibrated before each analysis session begins to minimise any impact from this.

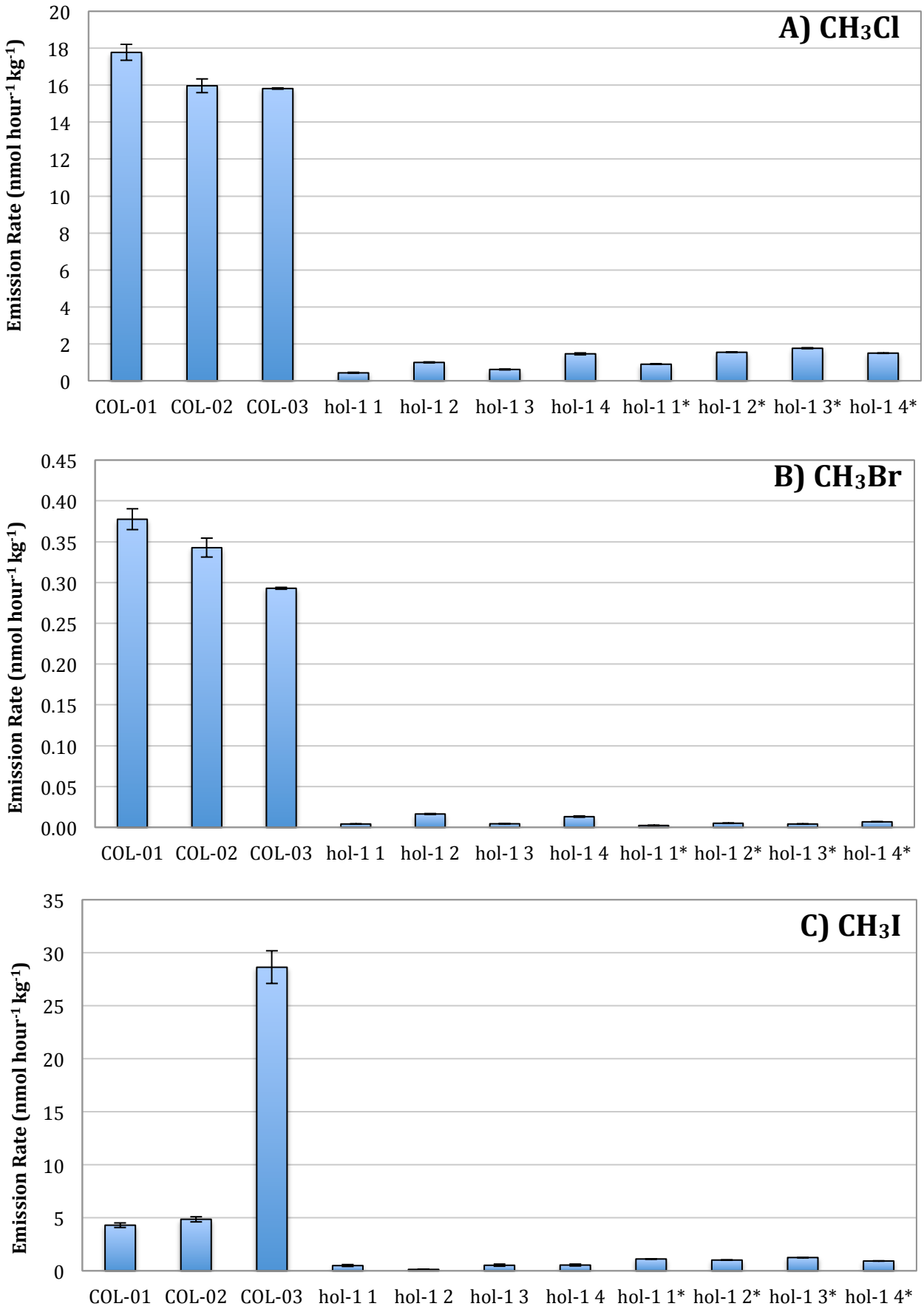

Figure 3.7: Comparison of emission rates of A) methyl chloride, B) methyl bromide and C) methyl iodide from wild type *A. thaliana* and *hol*-mutants.

As no other lines were repeated in both analyses, there is no way to confirm whether there was a difference with the instrument or analysis that caused this effect. However, there are still significant differences between the wild type emissions and those of both mutant lines indicating that the loss-of-function of the *HOL*-gene was achieved, regardless of these variations.

3.8.2 Transgenic Lines – Rice, Moss and Diatom

This experiment was carried out to assess whether *HOL* genes from other species would mediate methyl halide production when inserted into *A. thaliana*. Similar to the previous section, the rice transgenic line (OsHOL*) was analysed a month earlier than the moss (PpHOL) and diatom (PtHOL) lines and some differences in emissions, due to biological variation, may be expected. Table 3.5 shows the difference between the average emission rates for these transgenic lines for each methyl halide and those averaged from both *hol*-mutant lines previously discussed.

Table 3.5: Overview of the difference in emission rates between the transgenic lines from rice, moss and diatoms, and the *hol*-mutants.

	Difference between emission rates from Transgenic lines and average *A. thaliana hol*-mutants					
	CH_3Cl ((nmol hour^{-1} kgFW^{-1})	**%**	**CH_3Br (nmol hour^{-1} kgFW^{-1})**	**%**	**CH_3I (nmol hour^{-1} kgFW^{-1})**	**%**
OsHOL*	-0.32	-28	0.00	+24	-0.37	-49
PpHOL	1.39	+120	0.01	+110	0.65	+86
PtHOL	0.75	+65	0.00	+7	1.38	+180

For the rice, OsHOL, low emission rates for all three methyl halides are seen (Figures 3.8a, 3.8b and 3.8c) indicating that this gene, whilst over 50% identical to that found in *A. thaliana*, does not function the same way and so is unable to produce methyl halides in this plant. The negative rates seen for methyl chloride and iodide may suggest that the insertion of this gene actually disrupted the methyl halide production process, although further investigation would be needed to confirm this.

For the moss, PpHOL, emission rates for all three methyl halides are, on average, higher than both the *hol*-mutant lines analysed previously (by 120% for methyl chloride, 110% for methyl bromide and 86%for methyl iodide). This suggests that the 47% identical gene is able to mediate some methyl halide production in *A. thaliana,* however it is still significantly less efficient than the wild type gene.

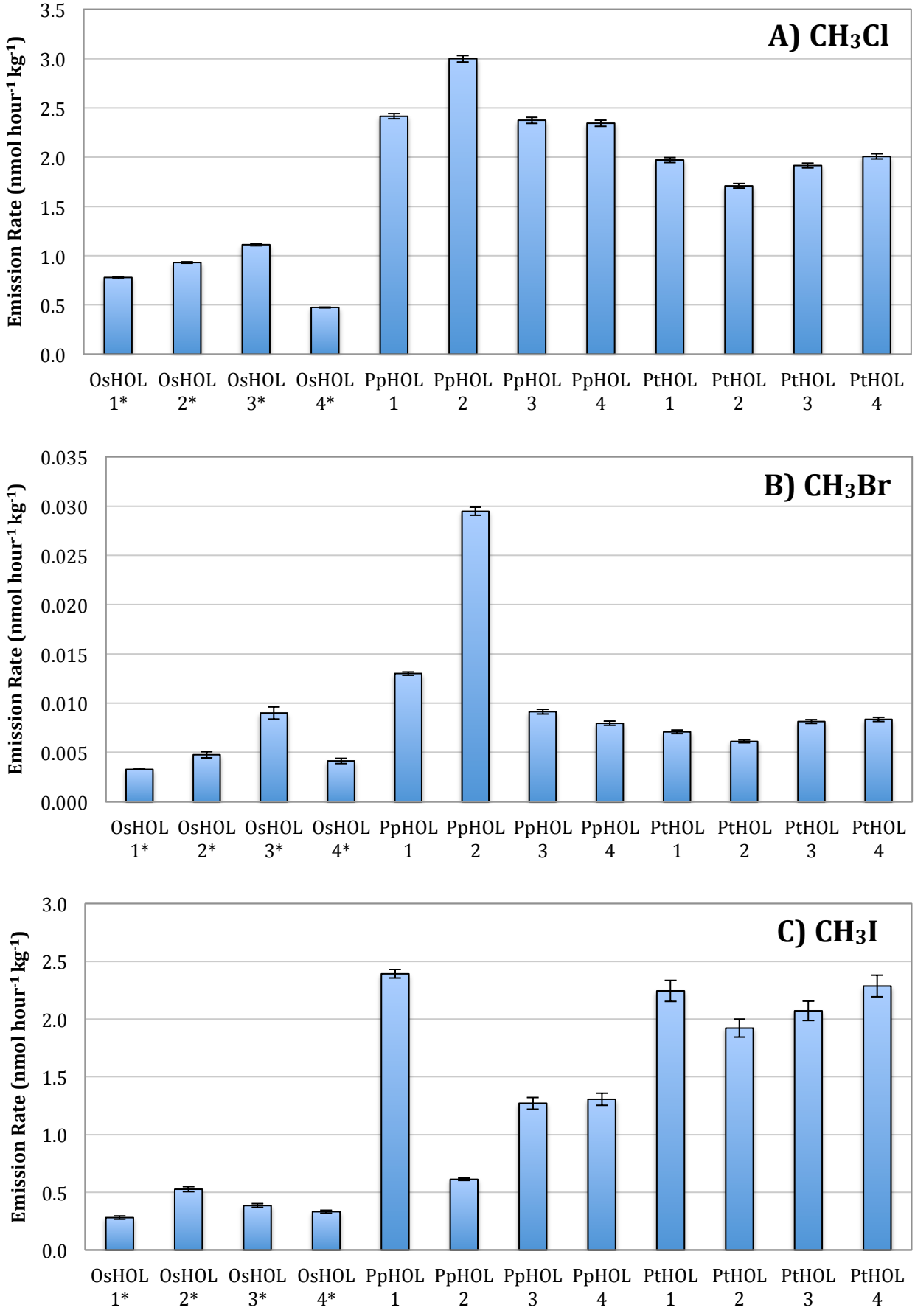

Figure 3.8: Comparison of emission rates of A) methyl chloride, B) methyl bromide and C) methyl iodide from *A. thaliana* based rice (OsHOL), moss (PpHOL) and diatom (PtHOL) transgenic lines.

In the case of the diatom gene, (PtHOL), emission rates for methyl bromide were, on average, no different than from the previously detected *hol*-mutants, however methyl chloride and methyl iodide saw increases (65% and 180% respectively). This suggests that, similar to moss, this gene in *A. thaliana* can produce some methyl halides. However emissions are still notably lower than the wild type.

Overall, this suggests that whilst the *HOL* gene from rice does not mediate methyl halide production in *A. thaliana*, the moss and diatom *HOL* genes do so for some methyl halides – most notably methyl chloride for the moss gene and methyl iodide for the diatom gene.

This indicates that the sections of coding for this gene, that are homologous between these species, and *A. thaliana* are different and so further comparison of similarities between the coding may help identify key sections related to function.

3.8.3 *Physcomitrella patens* Wild Type and Pp-HOL Knockout Lines

In previous experiments with moss, it was found that the wild type emits very low mixing ratios of all three methyl halides that were similar to background abundances assessed by control plates. This was attributed to the lack of halide ions in the moss due its growth on a minimal medium and so a 5mM KBr solution was added and found to successfully boost methyl bromide production (Koerner, 2012). As such, although both methyl chloride and methyl iodide were measured for this assessment of moss wild type and knockout line emissions (see Appendix 3.3), only methyl bromide emissions will be discussed.

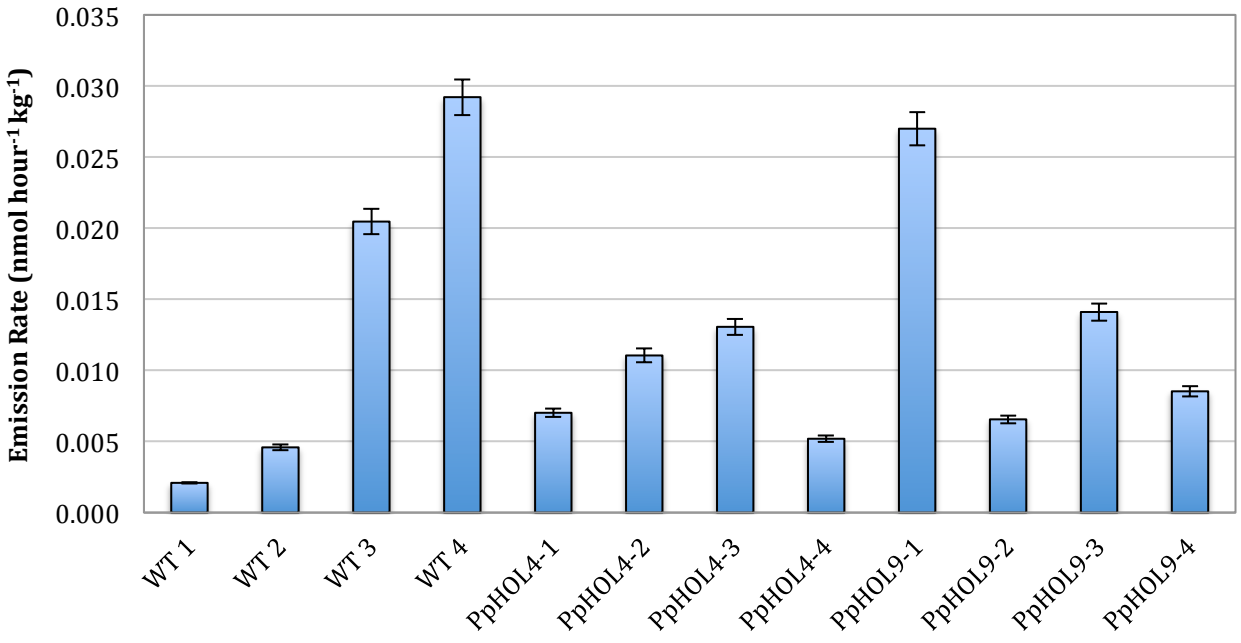

Figure 3.9: Comparison of Methyl Bromide emissions from moss *Physcomitrella patens* wild type (WT) and two independent Pp-HOL knockout lines (Pp-HOL4 and Pp-HOL9).

Figure 3.9 shows a comparison of the plotted emission rates for the wild type moss and the two independently generated PpHOL knockout lines for methyl bromide. From this graph, it can be seen that two of the wild type rates were significantly lower than the others and also disagree with the previous experiments.

As such, WT1 and WT2 were removed from the data set (after personal communication with Dr. Lars Østergaard, head of the project at JIC) due to them outlying anticipated biological variation. This cause of this was not clear but could suggest issues during spore germination or early growth, resulting in reduced development. As such, these results not included in the average rate found in Table 3.3. Also, sample PpHOL-1 was calculated to have a similar rate to that of these two wild type mosses, unlike the other knockout line samples and so this too was removed from the average calculations for Table 3.3.

What is apparent from this experiment is that both PpHOL knockout lines produce emissions ~2.5 times lower than those seen with the unmodified genome. This indicates that the PpHOL gene is partially responsible for methyl halide production in mosses, which in turn demonstrates that the emission of methyl halides from plants is an ancient mechanism. Figure 3.10 shows that this must have evolved over 350 million years ago, before the divergence of species that resulted in the evolution of *A. thaliana*.

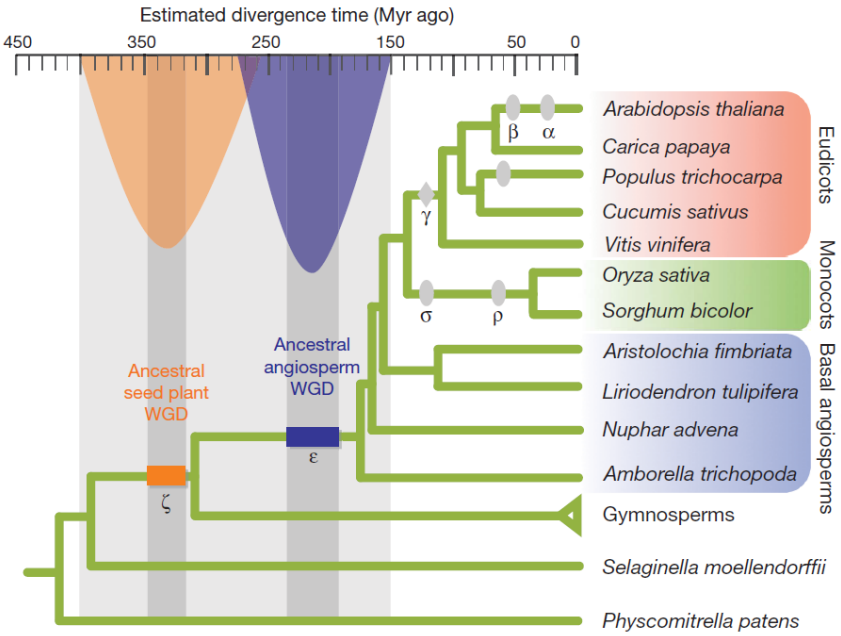

Figure 3.10: Divergence of flowering and seed plants showing whole gene duplication (WGD) events, including ancestral WGDs (orange and blue boxes) and other duplication (oval) and triplication (diamond) events in flowering plants. Image from Jiao et al. 2010.

3.8.4 Effect of Temperature - *Physcomitrella patens* and *Arabidopsis thaliana*

With the previous experiment indicating methyl halide production to be an ancient process, the effect of temperature was considered to see if an increased global temperature, as expected during the period when mosses first developed, would impact on emissions. As such, samples of the *P. patens* wild type and PpHOL4 knockout line were grown at 22°C and 27°C and compared. The experiment was then repeated with the *A. thaliana* wild type and *hol*-mutant to see if any impact was apparent in more modern species.

Figures 3.11a, 3.11b and 3.11c show the results of the *P. patens* experiment for the three methyl halides, with the rates from the 22°C growth being in blue and the 27°C growth being in red.

Although the emissions from methyl bromide are the only ones boosted to show a clear distinction between the wild type and knockout line, it is still apparent that for all three methyl halides there is an increase in emission rates at 27°C (see Table 3.6).

Table 3.6: Difference between emission rates from *P. patens* grown at 27°C and 22°C

	Difference between emission rates (nmol hour^{-1} kgFW^{-1})		
	CH_3Cl	CH_3Br	CH_3I
WT	0.127	0.020	0.009
PpHOL4	0.187	0.006	0.004

One explanation for this may be that 27°C is a more optimal temperature for the HTMT enzymes and so slight differences in folding and bonding mean the active sites work more efficiently. Since mosses evolved during a period when the global temperature was higher than today, this would suggest that the enzymes would have developed to be more effective when warmer.

However, when comparing the two lines using methyl bromide, the wild type *P. patens* sees an increase in average emissions over 3 times higher than that found for the PpHOL4 knockout line (0.020 nmol hour^{-1} kgFW^{-1} and 0.006 nmol hour^{-1} kgFW^{-1} respectively). Whilst there is clear biological variation between samples, this is similar to the average relative-fold difference detected in the previous experiment. This may be an indication that, in moss, the process that causes increases in methyl halide production due to increased temperature is separate from the *HOL*-gene. As such, this suggests an explanation for the increase in emissions at 27°C is unlikely to be related to the HTMT enzyme coded for by the *HOL*-gene.

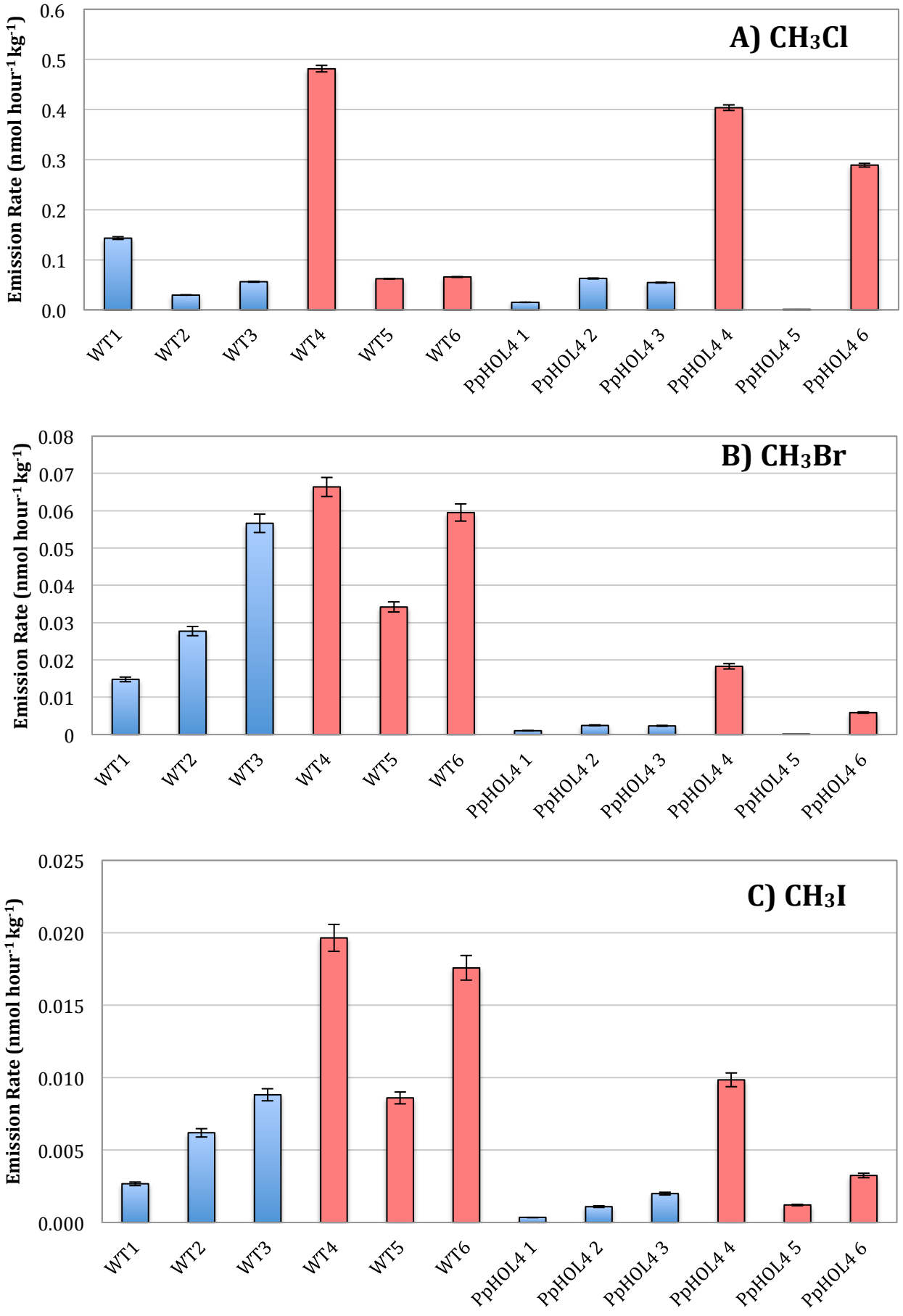

Figure 3.11: Comparison of A) methyl chloride, B) methyl bromide and C) methyl iodide emissions from moss *Physcomitrella patens* wild type (WT) and Pp-HOL knockout line (Pp-HOL4) grown at 22°C (blue bars) and 27°C (red bars).

To assess if the same effect was seen in modern plants, the experiment was repeated using wild type and *hol*-mutant *A. thaliana*. Figure 3.12a, 3.12b and 3.12c show the results, again with the rates from the 22°C growth being in blue and the 27°C growth being in red. Whilst the response from the wild type *A. thaliana* does show an increase in emissions at 27°C for all three methyl halides (although only marginally for methyl bromide - see Table 3.7), the *hol*-mutant was found to have decreasing emissions at 27°C for all three species. However, neither of these changes were found to be statistically significant (over two sigma) which may, in part be contributed to by the small sample size. Had there been even a somewhat significant (between 1 and 2 sigma) relationship this could suggest, unlike moss, that any temperature dependent aspect to the production of methyl halides is linked to the *HOL*-gene in modern plants and so may be connected to the HTMT enzyme. As such, repetition of this experiment with a larger sample size is necessary to clarify any potential relationships and further highlight differences between modern and ancient plant mechanisms.

Finally, both the *A. thaliana* and the *P. patens* wild type species do show an increase in emissions rates of over 10% at the higher temperature, which is larger than that suggested by Lee Taylor and Redeker's (2005) study of rice plants. As such, the effect of increased temperatures due to global warming may result in enhanced emissions of methyl halides from plant species and so further study into this is necessary.

Table 3.7: Difference between emission rates from *A. thaliana* samples grown at 22°C and 27°C

	Difference between emission rates (nmol hour^{-1} kgFW^{-1})		
	CH_3Cl	**CH_3Br**	**CH_3I**
WT	3.832	0.068	7.110
hol	-1.197	-0.002	-0.135

In summary, these two experiments found that increasing temperatures does positively impact emissions in both *P. patens* and *A. thaliana*, however the exact cause of this appears to have changed between ancient and modern plants and so further investigation is required.

Overall, the results from the experiments described previously have increased the understanding of the effects of the *HOL*-gene and development of methyl halide production in plants. Although additional research is required before conclusions drawn can be confirmed, it is possible to make some estimations as to the impact of utilising this gene to reduce emissions from crop species.

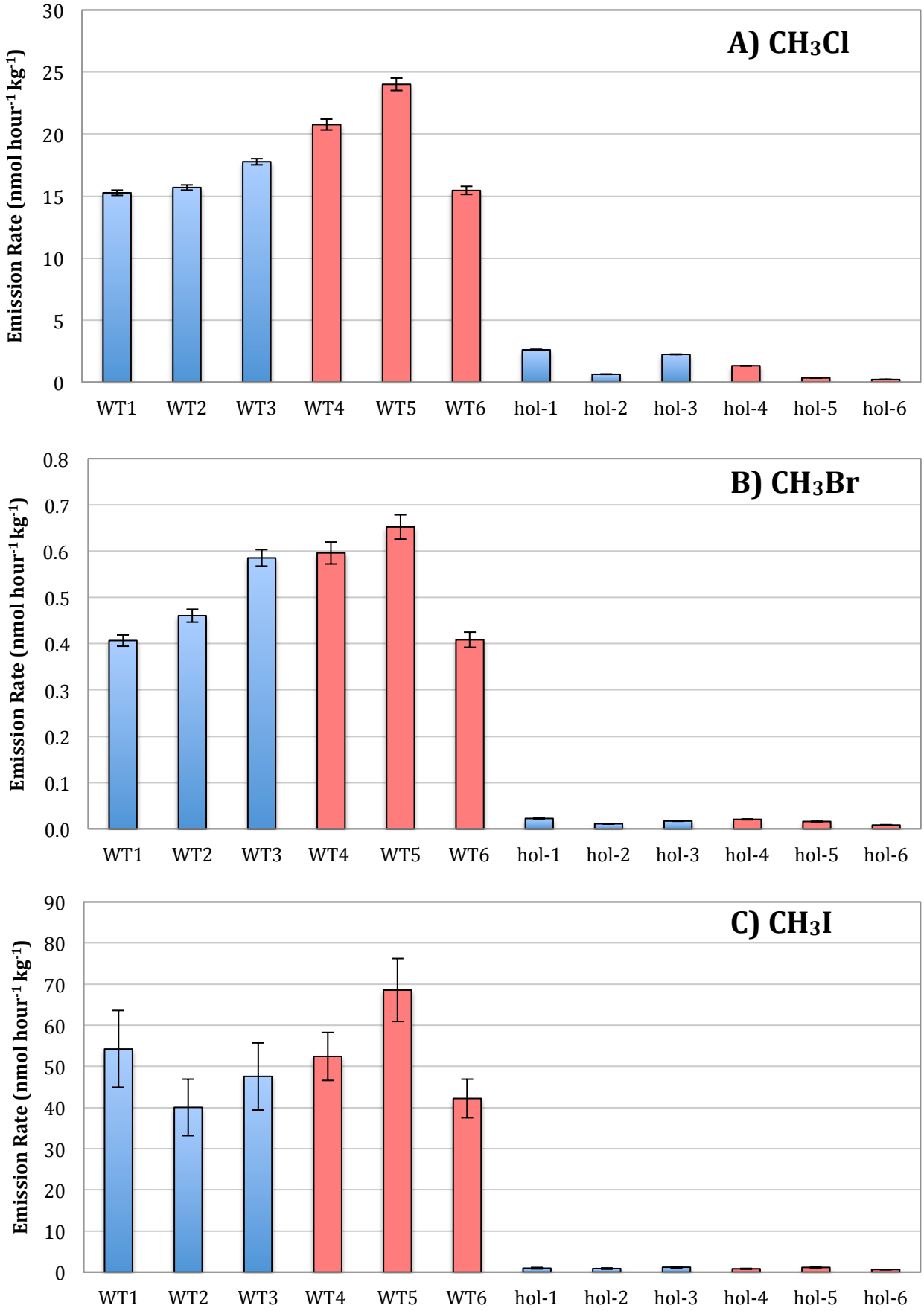

Figure 3.12: Comparison of A) methyl chloride, B) methyl bromide and C) methyl iodide emissions from *Arabidopsis thaliana* wild type (WT) and HOL-mutant line (HOL) grown at 22°C (blue bars) and 27°C (red bars).

3.9 Potential Impact of 'Ozone Safe' Species

As a staple food source, along with the expanding global population that will only increase its contribution as a source of methyl halide emission, rice is a strong candidate to undergo modification to produce an ozone-safe variety. Though the estimated emissions of methyl iodide from rice paddies are more substantial, the longer-lived nature of methyl chloride and methyl bromide, and so their impact on ozone depletion, make these species of more current concern. This section will focus on estimating how utilising a modified rice crop may reduce the levels of emissions from these two species.

Though two *HOL*-homologous genes in *Oryza sativa* have been identified, previous attempts to produce loss-of-function mutants *in vivo* were unsuccessful (Koerner, 2012). Results from the experiments on transgenic lines using the OsHOL gene to mediate methyl halide production in *A. thaliana* also proved ineffective (see section 3.4.2). Thus the potential for 'ozone-safe' (OZS) rice is still in the very early stages of development and there is little data to work from. However, estimations can be made if assumed that the relationship between the *A. thaliana* wild type and the *hol*-mutant would be proportional between that of wild type *O. sativa* and an OZS-mutant.

As such, average emission rates of wild type *A. thaliana* and *hol*-mutant (grown during the same sampling period) were calculated for methyl chloride and methyl bromide from the experiment in section 3.8.1. These values were then converted from nmol hour^{-1} g^{-1} to mol yr^{-1} tonne^{-1} (see Table 3.8) and a ~20 fold and ~35 fold reduction in emissions from wild type to mutant was calculated for methyl chloride and methyl bromide respectively.

Table 3.8: Average emission rates of *A. thaliana* wild type and *hol*-mutants for methyl chloride and methyl bromide.

	Average emission rates of *A. thaliana*			
	CH_3Cl		CH_3Br	
	nmol hour^{-1} kgFW^{-1}	mol yr^{-1} tonne^{-1}	nmol hour^{-1} kgFW^{-1}	mol yr^{-1} tonne^{-1}
WT	16.521	144.722	0.338	2.958
hol-1	0.874	7.652	0.009	0.083
Reduction	94.70%		97.20%	

The reported emissions of these species in Capenter and Reimann (2014) from rice paddies for 2012 was then used and converted from Gg yr^{-1} to mol yr^{-1} tonne^{-1} using the molecular weights and rice production number for 2012 (Table 3.9, FAOSTAT, 2014). These values were then divided by the reduction relationship previously calculated to give estimate emissions of methyl chloride and methyl bromide for 2012, if the global rice crop had been an OZS-variety.

In Table 3.10, these values were converted back to Gg yr^{-1} to aid comparison with the published numbers from Carpenter and Reimann (2014), with methyl chloride emission reduced to 0.2 Gg yr^{-1} from 3.7 Gg yr^{-1} and methyl bromide reduced to 0.02 Gg yr^{-1} from 0.7 Gg yr^{-1}. In terms of the total global emissions, this would reduce rice paddy emissions from 0.1% to 0.005% for methyl chloride and 0.5% to 0.016% for methyl bromide. These changes would not only decrease ozone depletion but also enable expansion of cultivation to meet growing demand with only negligible risk to atmospheric concentrations.

Table 3.9: Calculated emissions rates from rice of methyl chloride and methyl bromide for 2012

	Average emission rates from Rice			
	CH_3Cl		**CH_3Br**	
	Gg yr^{-1}	**mol yr^{-1} $tonne^{-1}$**	**Gg yr^{-1}**	**mol yr^{-1} $tonne^{-1}$**
Rice	3.70	0.099	0.70	0.010

Table 3.10: Estimated emissions rates from 'Ozone-safe' rice of methyl chloride and methyl bromide for 2012.

	Estimated emission rates from 'Ozone-safe' Rice			
	CH_3Cl		**CH_3Br**	
	Gg yr^{-1}	**mol yr^{-1} $tonne^{-1}$**	**Gg yr^{-1}**	**mol yr^{-1} $tonne^{-1}$**
OZS Rice	0.20	0.0053	0.02	0.0003

This would be of particular importance for areas in Asia, namely South-central Asia, Southeast Asia and Mainland China, as Lee-Taylor and Redeker (2005) modelled these areas as being the origins of the majority of global methyl halide emission from rice paddies. In fact, combined modelled contributions from these areas made up 88% and 90% of the respective methyl chloride and methyl bromide global rice paddy emissions for 2002. Using these percentages, if the whole rice crop in 2012 was replaced by OZS rice instead, emissions of methyl chloride would reduce from 3.26 Gg yr^{-1} to 0.17 Gg yr^{-1} and methyl bromide would reduce from 0.63 Gg yr^{-1} to 0.017 Gg yr^{-1} (see Table 3.11).

Table 3.11: Estimated emissions of methyl chloride and methyl bromide from rice paddies (using data from Carpenter and Reimann, 2014) and 'ozone-safe' rice in Asia for 2012.

	Estimated Rice Emissions from Asia		
	Global Contribution (%)	**2012 (Gg yr^{-1})**	**OZS (Gg yr^{-1})**
CH_3Cl	88	3.26	0.17
CH_3Br	90	0.63	0.02

As such, these preliminary estimates indicate that further investigation into the *HOL*-gene in agricultural crop species, and from that development and implementation of 'ozone-safe' varieties, may be a significant method for reducing methyl halide emissions whilst still meeting ever-expanding cultivation demands.

3.10 Summary and Further Investigations

Analysis of the *HOL*-gene in *Arabidopsis thaliana* using wild type and *hol*-mutant lines found that methyl halide emissions were significantly reduced in the halide/thiol methyl transferase-inactive mutant, as expected.

Transgenic lines using *HOL*-genes from rice, moss and diatoms inserted into *A. thaliana* were also analysed. The results from these tests suggested that the *HOL* gene from rice does not mediate methyl halide production in *A. thaliana*. However, the moss and diatom *HOL* genes do appear to for some but not all methyl halides.
This indicates that the sections of coding for this gene that are homologous between these species and *A. thaliana* are different. Comparisons of the coding may help identify key sections related to function that may be useful for future developments.

Wild type moss, *Physcomitrella patens*, and lines with the PpHOL gene knocked out were also assessed, but only for methyl bromide emissions. Both knockout lines were found to have emission rates ~2.5 times lower than those seen in the wild type, indicating that the PpHOL gene is partially responsible for methyl halide production in mosses. This suggests that the emission of methyl halides from plants is an ancient mechanism.

A final experiment found that increasing temperatures does have a positive effect on the emission rates of methyl halides in *P. patens* and somewhat in *A. thaliana,* but the exact cause of this appears to have changed between ancient and modern plants.

As well as this, preliminary estimates as to the impact of *HOL*-gene manipulated crops indicates that reductions in emissions would be significant and so further research towards this goal is essential. Before this can be achieved, however, knowledge about the *HOL* gene still needs increasing and as such more testing is required.

In order to confirm the relationship, the temperature experiments with both moss and *A. thaliana* should be repeated, with larger sample sizes to better constrain statistically significant relationships from biologically variation . To test this theory further, as well as establish more information about the evolution of methyl halide production in plants, tests with a more ancient species such as Liverwort should be considered.

Further study into glucosinolate pathway in plants may also help explain why plants produce methyl halides and measurement of other related species, such as acetonitrile, potentially in real time, could aid this.

Previous attempts at overexpressing the *HOL* gene in rice and moss were unsuccessful unlike in *A. thaliana*. Repeating this process may again increase understanding of function and enable further testing to be carried out that could aid 'ozone-safe' crop development.

Chapter 4: Halocarbon Observations in Taiwan

Methyl halides are not the only important halocarbons with anthropogenically-influenced emissions in East Asia. The region has widespread agricultural industry but also contains manufacturing and production hubs for a large range of marketable commodities. These industries utilise many of the halocarbon species previously described and so may be large-scale emission sources for these compounds. Previous studies and continuous measurements of halocarbons in East Asia has been limited. Species with high global warming potentials (GWPs), such as the PFCs, or high ozone depleting potentials (ODP), such as the minor CFCs, may still have a large atmospheric impact despite relatively low mole fractions. This study aims to provide new data for the East Asian region and extend current knowledge as to the recent mixing ratios and trends of a wide range of species, particularly newly detected compounds and those with low atmospheric abundances. The data set produced can also contribute towards the global assessment of emerging greenhouse gases (GHGs) and ozone depleting substances (ODS) and ultimately, may influence global control measures.

4.1 Introduction

As a sub-region of the Asian continent, East Asia geographically covers a number of countries including China, Hong Kong and Japan, as well as both North and South Korea and Taiwan. With a total population of over 1.6 billion (CIA, 2016) and some of the world's most densely populated areas (Figure 4.1, Zifan, 2015), this is a region where anthropogenic emissions can impact the atmospheric environment at a global level. In recent decades, rapid industrialisation has taken place across this area (Kim et al. 2010), generating further international interest into the widespread use of halocarbons in East Asian industry.

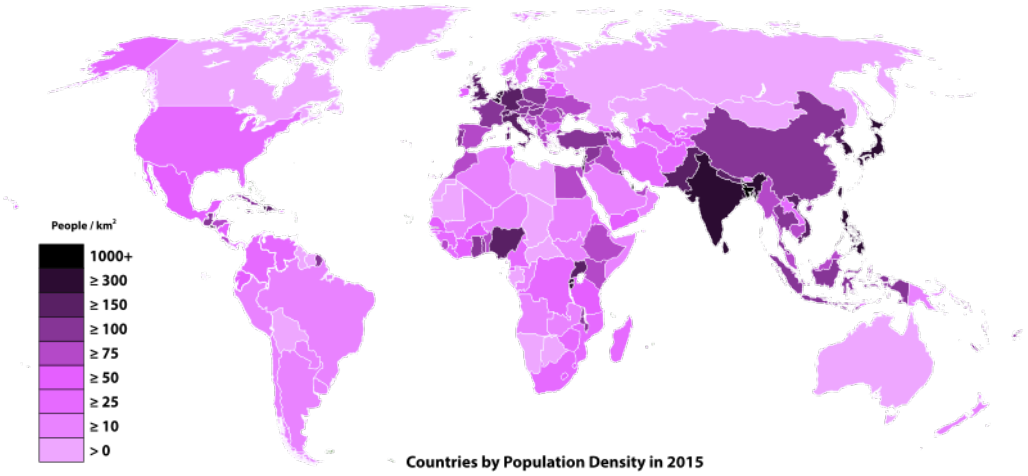

Figure 4.1: Global map of population density by country in 2015 (Zifan, 2015).

With the introduction of global control measures on halocarbon production and emissions, namely the Montreal Protocol and to some extent the Kyoto Protocol, many countries in the region have ratified these agreements and followed the appropriate schedules (UNEP, 2013). Whilst the Montreal Protocol is concerned with the cessation of production and use of ozone depleting substances (ODS), the Kyoto Protocol is related to reducing emissions of greenhouse gases (GHGs) only. More detailed descriptions of both of these control measures can be found in section 1.13.

Under the Montreal Protocol, Japan is considered a developed country, unlike China and both North and South Korea, which are given developing status (Article 5, UNEP, 2015). This allows these countries to have longer timescales to use and replace controlled compounds. For example, developed nations completed their phase-out of CFC and Halon species in 1996 whereas developing nations had until 2010 to undertake and fulfil the conditions (UNEP, 2016). Other projects like the Clean Development Mechanism (CDM), one of the flexible mechanisms defined by the Kyoto Protocol, have also been utilised by developing countries like China to incentivise emissions reductions (UNFCCC, 2014).

Taiwan, officially the Republic of China, is considered to be included under the ratification of the People's Republic of China (Mainland China), as a province (UNEP, 2013), due to the ambiguous political situation between the two states. Taiwan is not individually recognised by the UN, though steps by the current government towards autonomy from Mainland China are carefully being taken (EPA R.O.C, 2015b). As such, the Taiwanese position is that, since they have not individually ratified the Montreal Protocol, they are not technically part of it, but they have instead voluntarily reduced and controlled emissions of ODS in-line with the schedule for developed nations (EPA R.O.C, 2015a). A similar position towards GHGs and the Kyoto protocol has also been taken (EPA R.O.C., 2015b).

Within East Asia, these differing phase-out agendas, along with the use of a wide variety of replacement species, has resulted in enhanced halocarbon abundances across the region and in continental outflows (Kim et al. 2010). However, accurate evaluations regarding the extent of this halocarbon use are difficult due to the limited knowledge of emissions and a lack of official usage reports to regulating bodies. As such, the monitoring of a large range of these compounds in this region is particularly important to help identify and quantify East Asian contributions to ODS and GHGs concentrations. This, in turn, may help assess the impact of this region on a global scale and highlight specific compounds or areas requiring further regulation.

In this work, a comprehensive assortment of halocarbon species, including both long and short-lived ODS and GHG species, were measured in East Asia during three short-term campaigns. The potential implications of the detected concentrations are discussed, and possible sources and source locations are considered.

4.2 Previous Studies in East Asia

In the past decade, a number of field campaigns have been carried out in the region to help assess halocarbon emissions and their implications for the atmosphere. Continuous measurements of a number of halocarbon species are collected by the AGAGE network that has sites in Shangdianzi (China), Gosan (Korea) and Hateruma (Japan) and results from some of these are included in the studies discussed below. However, this network does not measure all of compounds of interest and is limited by location as to local influences and wider impacts and sources for the region. As such, these field campaigns help provide further information as to the extent of potential sources and emissions of halocarbon across the whole of East Asia. A summary of the results achieved, organised by halocarbon group, can be found as follows:

- Table 4.1a CFCs
- Table 4.1b Halons
- Table 4.1c HCFCs
- Table 4.1d Chlorocarbon
- Table 4.1e Very Short Lived Substances (VSLS)
- Table 4.1f Methyl Halides
- Table 4.1g HFCs
- Table 4.1h PFCs and SF_6

Some of these studies focused purely on Chinese emissions that, due to its size and extensive industrial areas, can dominate the region. Shao *et al.* (2011) and Guo *et al.* (2009) focused their campaigns on the Pearl River Delta, a rapidly industrialising area of South China, whilst Fang et al (2012a and 2012b) and Wang et al (2014) both sampled a range of over 40 cities across China. Aircraft measurements were also collected for the Wang (2014) study but this was still more focused on Chinese emissions than the aircraft campaigns of Palmer et al (2003) and Barletta et al (2009). These both used aircraft measurement data as part of the TRACE-P and INTEX-B campaigns respectively. Whereas Palmer *et al.* (2003) operated out of Hong Kong and sampled fresh outflow from the region near to the emission source, Barletta *et al.* (2009) was carried out across the Pacific Ocean along the North American coast and so reflects more long-range transport. This results in a dilution that can be seen by the lower mixing ratios detected but enhancements from background levels are still identifiable.

Other campaigns calculated regional emissions for China and other countries in East Asia as well. The main methods used for this were the comparison of back trajectories using particle dispersion models (Barletta et al. 2009, Guo et al. 2009, Stohl et al. 2010, Yao et al, 2012) and the use of specific compounds as tracers for different regions (Li et al. 2011, Kim et al. 2012).

FLEXPART and HYSPLIT are both Lagrangian transport models that use meteorological data to simulate both forwards and backwards atmospheric trajectories for air parcels.

In the studies considered here, FLEXPART was more commonly applied for regional and source location analysis (Barletta et al. 2009, Saito et al. 2010, Stohl et al. 2010, Yao et al. 2012, An et al. 2012, Fang et al. 2014) with only Guo et al (2009) (a more localised China-based study) utilising HYSPLIT. Whilst there are many similarities between the two models, FLEXPART has been suggested to perform better overall (Pagano, 2010). As for tracer compounds, some studies used HCFC-22 as a tracer of air masses from China, Korea and Taiwan, whereas HFC-134a was utilised as a tracer of air from Japan (Li et al. 2011, Kim et al. 2012). CO was also used as an indication of Chinese air since its emissions have been extensively studied. However, CO is both produced and destroyed in the atmosphere resulting in a transport time of weeks (as opposed to months/years for many halocarbons); this could be a minor source of error (Yao et al. 2012).

Another variation between studies was the method used to estimate emissions. Several utilised the correlation of different halocarbon species with CO (Palmer et al. 2003, Yokouchi et al. 2006, Guo et al. 2009, Shao et al. 2011, Yao et al. 2012) since, as mentioned before, its emissions are well known. However, one of the most common sources of CO is biomass burning, unlike most other halocarbon compounds, and whilst sources of CO may be co-located with those of halocarbon species, it is not emitted from the same processes. This means that emissions may be less well related (Yao et al. 2012, Fang et al. 2012b) than when using an interspecies correlation method with tracer compounds such as HCFC-22 (Kim et al. 2010, Li et al. 2011, Fang et al. 2012b, Kim et al. 2012, Wang et al. 2014). However, given the variety of measurable species and potential sources, there is no ideal tracer compound for all halocarbons and selection of an appropriate tracer for specific compounds of interest is required.

Tracer methods may result in overestimations due to poorer regional representation of less industrialised and populated areas (Saito et al. 2010). As well as this, and since there is a lack of 'top down' emissions estimates for the majority of the East Asian region, some campaigns applied analytical inverse algorithms instead (specific details of these can be found in the studies subsequently cited). These work in conjunction with atmospheric modelling (such as FLEXPART as well as MOZART (Saikawa et al. 2012), LMDz-SACS (Fortems-Cheiney et al. 2013) and NIES_TM (Fang et al. 2012b) and meteorological station data (Vollmer et al. 2009, Saito et al. 2014, Stohl et al. 2010, Saikawa et al. 2012, An et al. 2012, Fortems-Cheiney et al. 2013, Fang et al. 2014).

These inversion methods can include *a priori* (theoretical deduction) emissions, source-receptor relationships and observed mixing ratios to give *a posteriori* (observational induction) emissions estimates. They can also be designed to regulate and consider population density (Vollmer et al. 2009) in an effort to minimise one of the previously mentioned disadvantages to utilising a tracer methodology. The resulting differences between these two methods can be seen visually in Figure 4.2, which shows a comparison of regional emissions for the major HCFCs and HFCs from the overlapping campaigns of Stohl *et al*. (2010), who used an inversion algorithm method, and Li *et al*. (2011) that utilised the tracer method.

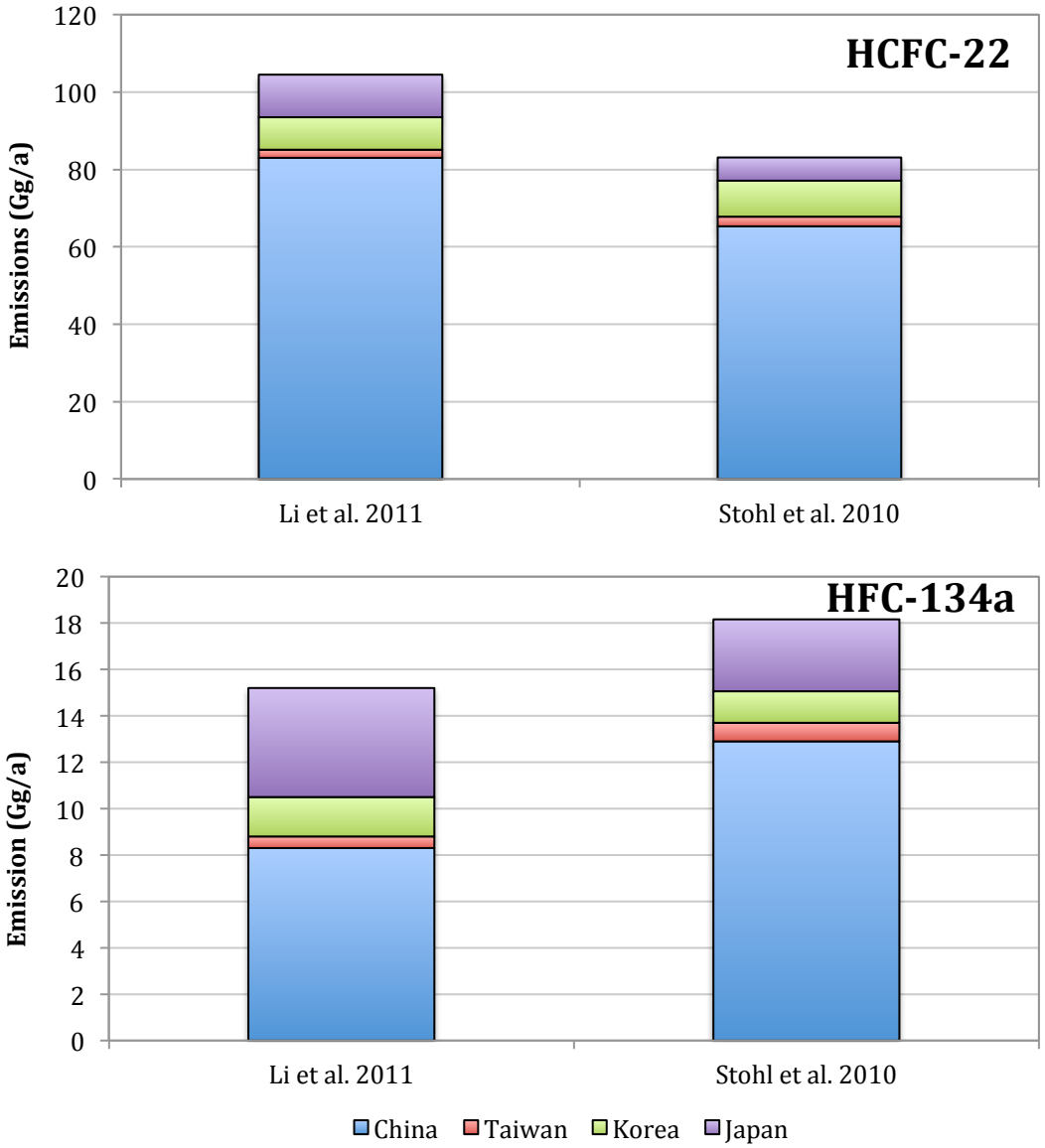

Figure 4.2: Comparison of regional emissions of HCFC-22 and HFC-134a as estimated from two overlapping studies, Li et al. 2011 and Stohl et al. 2010. These studies utilise different methods of estimation; a tracer method in Li *et al.* (2011) and an inversion algorithm in Stohl *et al.* (2010), and as such noticeable difference in the results are seen.

Below is a further comparison and overview of some of the results produced by the studies previously cited, organised by country. A number of species briefly discussed in this summary were not measured during the campaigns that make up this chapter, however several other species not present in the studies discussed below were measured for this work instead.

4.2.1 China

As the largest industrialised country in East Asia, China has a substantial influence on the overall halocarbon emissions in the area and the majority of studies focus on this region.

In 2008, 80% of the total halocarbons emissions estimated in East Asia were regionally identified as originating from China (Li *et al.* 2011).

4.2.1.1 **Chlorofluorocarbons** (see Table 4.1a)

With their wide range of applications, including as refrigerants and foam blowing agents, CFC species were used extensively across China but their production and consumption was completely phased out by 2010 under the Montreal Protocol.

Aircraft data from 2001, found CFC-11 and CFC-12 to have estimated emissions of 22.3 Gg a^{-1} and 28.3 Gg a^{-1} respectively. Whilst manufacturing records agreed with the CFC-12 estimate, records for CFC-11 accounted for less than half of the emissions detected (Palmer *et a*l. 2003) suggesting the possibility of unrecorded sources. By 2008, Li *et al.* (2011) found that Chinese emissions of CFC-11 and CFC-12 had decreased since 2001, by 50% and 80% respectively (see Figure 4.3). This decrease agreed with bottom up estimates (those calculated from production and usage data) and reflected the expected phase out of CFCs. However, although they agreed that CFC-12 emissions had declined, Vollmer *et al.* (2009), whose campaign finished in early 2008, reported that CFC-11 emissions had actually increased by 40% since 2001 suggesting that it may still be in use. Further data from 2008 by Kim *et al.* (2010) and later campaigns in 2010 (Fang et al 2012b, Wang et al 2014) also found emission decreases for CFC-11 suggesting that there may have been an overestimation in Vollmer *et al*. (2009). This could potentially be due to local bias given the proximity of the campaign to Beijing as well as a lack of data from South China.

Fang et al (2012a) measured mixing ratios of the major CFCs (those most widely used and so with the highest atmospheric concentrations e.g. CFC-11, -12 and -113) in urban and industrialised areas in 2010. When compared to the mixing ratios recorded by Guo et al (2009) in 2001 (see Figure 4.4), small decreases can be seen. Whilst, at first glance, these differences do not appear to reflect the magnitude of emissions decreases inferred over this time period by other campaigns, the decades-long atmospheric lifetimes, and so stability of these compounds, must be factored in (Guo et al, 2009). As such, it will take considerable time for mixing ratios for these compounds to decrease substantially and so the small differences seen are representative of substantial decreases in Chinese emissions under the Montreal Protocol.

CFC-114 mixing ratios were also measured by Barletta et al. (2009), Fang et al. 2012a and Wang et al. 2014. The increase seen in these results between 2006 and 2010 likely reflects the difference in campaign location so potential dilution and mixing of emissions rather than a global trend. Abundances observed during the later studies are comparable within uncertainties.

Table 4.1a: Overview of the reported mixing ratios and emissions estimates of chlorofluorocarbons from previous studies in the East Asian region.

Compound	Year	Region	Mixing Ratio (ppt)	Emissions estimate (Gg yr^{-1})	Study
CFC-11	2001	East Asia		30.1	Palmer *et al*. 2003
		China		22.3	
		Japan		2.3	
		Korea		2.9	
	2001-2002	Hong Kong	294 ± 7	0.03 ± 0.005	Guo *et al*. 2009
		S. China	298 ± 11	0.031 ± 0.010	
	2004	S. China	300	0.4 ± 0.2	Shao *et a*l. 2011
	2006	China	248 ± 4		Barletta *et al*. 2009
		Asia	250 ± 3		
	2006-2008	China		33	Vollmer *et al* 2009
	2007-2008	China		12 (9.4-17)	Kim *et al*. 2010
	2007-2008	China		11 (9-15)	Li *et al*. 2011
		Taiwan		0.3 (0.2-0.4)	
		Korea		0.9 (0.8-1.1)	
		Japan		1.1 (0.7-1.4)	
	2009	China		15.8 ± 7.2	Xingqin et al. 2012
	2009-2010	China		10 (8.4-11.7)	Fang et al. 2012b
	2010	China	268 ± 41		Fang *et al*. 2012a
	2010-2011	China	257 ± 27	7.1 ± 5	Wang et al. 2014
CFC-12	2001	East Asia		39.4	Palmer *et al*. 2003
		China		28.3	
		Japan		3.4	
		Korea		3.6	
	2001-2002	Hong Kong	615 ± 17	0.05 ± 0.02	Guo *et al*. 2009
		S. China	616 ± 17	1.5 ± 0.4	
	2004	S. China	700	1.6 ± 1.0	Shao *et al*. 2011
	2006	China	529 ± 5		Barletta *et al*. 2009
		Asia	529 ± 6		
	2006-2008	China		14 (9-19)	Vollmer *et al*. 2009
	2007-2008	China		6.3 (4.7-8.5)	Kim *et al*. 2010
	2007-2008	China		6.1 (4.4-8.5)	Li *et al*. 2011
		Taiwan		0.2 (0.1-0.3)	
		Korea		0.8 (0.7-0.9)	
		Japan		0.9 (0.7-1.1)	
	2009-2010	China		7.2 (6-8.4)	Fang et al. 2012b
	2010	China	558 ± 37		Fang *et al*. 2012a
	2010-2011	China	540 ± 49	13.1 ± 10.3	Wang et al. 2014

Table 4.1a continued: Overview of the reported mixing ratios and emissions estimates of chlorofluorocarbons from previous studies in the East Asian region.

Compound	Year	Region	Mixing Ratio (ppt)	Emissions estimate (Gg yr^{-1})	Study
CFC-113	2001-2002	Hong Kong S. China	96 ± 6 98 ± 7	0.03 ± 0.007 0.9 ± 0.3	Guo *et al.* 2009
	2004	S. China	97		Shao *et al.* 2011
	2006	China Asia	77.4 ± 0.9 77.1 ± 1.3		Barletta *et al.* 2009
	2006-2008	China		0.8 (0.4-1.7)	Vollmer *et al.* 2009
	2007-2008	China		3.2 (2.5-3.8)	Li *et al.* 2011
	2009-2010	China		0.2 (-0.3-0.6)	Fang et al. 2012b
	2010	China	78 ± 6		Fang et al. 2012a
	2010-2011	China	82 ± 5		Wang et al. 2014
CFC-114	2004	S. China	18		Shao *et al.* 2011
	2006	China Asia	14.8 ± 0.2 14.8 ± 0.2		Barletta *et al.* 2009
	2007-2008	China		1.3 (0.9-1.8)	Kim *et al.* 2010
	2007-2008	China		1.3 (0.9-1.8)	Li *et al.* 2011
	2009-2010	China		0.0 (-0.1-0.1)	Fang et al. 2012b
	2010	China	17 ± 2		Fang et al. 2012a
	2010-2011	China	16 ± 1		Wang et al. 2014

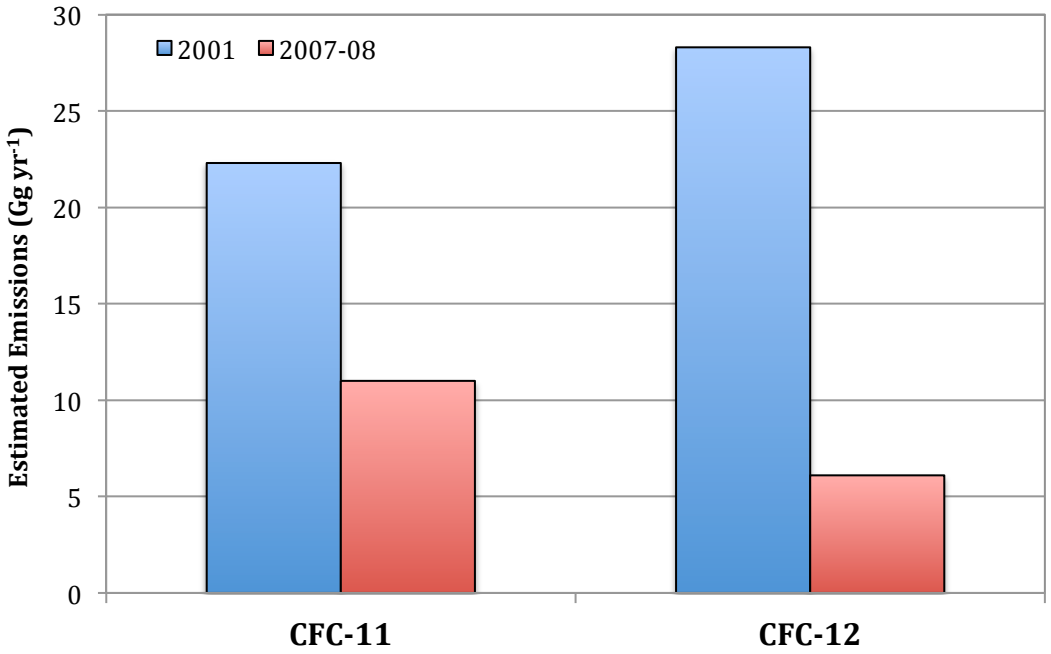

Figure 4.3: Emissions estimates for CFC-11 and CFC-12 for 2001 (blue bars) and 2007-2008 (red bars), showing the decline reflective of the Montreal Protocol's impact.

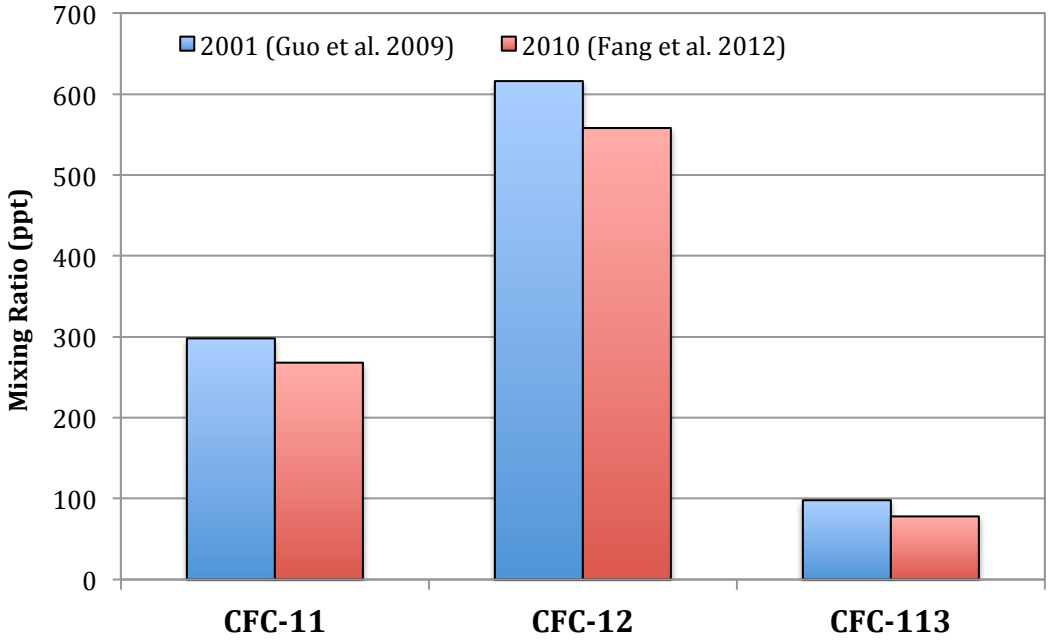

Figure 4.4: Observed mixing ratios of CFC-11, CFC-12 and CFC-113 for 2001 (Guo et al. 2009, blue bars) and 2010 (Fang et al. 2012a, red bars). Again, the decline indicates the impact of the Montreal Protocol phase out of these species.

4.2.1.2 **Halons** (see Table 4.1b)

The bromine-based halon species have been less widely measured in East Asia than their chlorine based counterparts, the CFCs, though their use in fire extinguishers and explosion protection was extensive. As such, data for the three main compounds (halon-1211, -1301 and -2402) is mainly only available for China.

For halon-1211, Barletta *et al*. (2009) detected mixing ratios of 4.49ppt in Chinese pollution plumes during 2006, whilst the more general Asian plumes were detected at 4.38 ppt. This suggests China was most likely the significant source of this compound in the region which is consistent with known emissions sources. This was also seen for halons -1301 and -2402 where the mixing ratios detected (3.06 ppt and 0.48 ppt respectively) were the same as the as those seen in the Asian plumes.

Emissions of -1211 for 2007-2008 were estimated at ~1.5 Gg a^{-1} (Kim *et al*. 2010, Li *et al.* 2011), slightly lower than those calculated by Vollmer *et al*. (2009) over a similar period (2.1 Gg a^{-1}). Halon-1301 was also estimated at 0.09 Gg a^{-1} by this study however there are no estimates for halon-2402, likely due to its less extensive sources.

Table 4.1b: Overview of the reported mixing ratios and emissions estimates of halons from previous studies in the East Asian region.

Compound	Year	Region	Mixing Ratio (ppt)	Emissions estimate (Gg/a)	Study
H1211	2006	China	4.49 ± 0.31		Barletta *et al*. 2009
		Asia	4.38 ± 0.10		
	2006-2008	China		2.1 (1.7-2.5)	Vollmer *et al*. 2009
	2007-2008	China		1.4 (1.0-1.9)	Kim *et al*. 2010
	2007-2008	China		1.5 (1.0-2.0)	Li *et al*. 2011
		Korea		0.1 (0.09-0.12)	
H1301	2006	China	3.06 ± 0.07		Barletta *et al*. 2009
		Asia	3.06 ± 0.06		
	2006-2008	China		0.09 (0.07-0.11)	Vollmer *et al*. 2009
H2402	2006	China	0.48 ± 0.01		Barletta *et al*. 2009
		Asia	0.48 ± 0.2		

4.2.1.3 Hydrochlorofluorocarbons (see Table 4.1c)

The phase out of CFCs and halons in favour of HCFC utilisation was noticeable by 2008 as these were dominant species detected from China (Li *et al.* 2011). Vollmer *et al*, (2009) estimated emissions at 165 Gg a^{-1} for HCFC-22 (substantially higher than previous studies), which does reflect this increase in consumption. Whilst Stohl *et al.* (2010) also found emissions to be higher than in previous years, the estimated 65 Gg a^{-1} is notably different from that found by Vollmer *et al*. (2009). This difference could be due to the use of data from only a single station, which may introduce bias, but Kim *et al.* (2010) also detected lower levels of 83.4 Gg a^{-1} over the same time period which again, similar to CFC-11, suggests that the Vollmer *et al.* (2009) result might have been overestimated. This is further confirmed by later campaigns from 2009 and 2010, when further increases would have been expected, but only detected emissions of 87.9 Gg a^{-1} and 103.4 Gg a^{-1} respectively (Fang et al, 2012b, Wang et al, 2014).

Similarly to the CFCs, comparison of detected mixing ratios between Guo et al (2009) and Fang et al. (2012a) reflects the changes in emissions of HCFCs seen in this period (Figure 4.5). The differences in detected mixing ratios, however, are generally more pronounced due to the shorter lifetimes of these compounds. As such, mixing ratios of all three major HCFCs (HCFC-22, -141b and 142b) have increased between 2001 and 2010.

Table 4.1c: Overview of the reported mixing ratios and emissions estimates of hydrochlorofluorocarbons from previous studies in the East Asian region.

Compound	Year	Region	Mixing Ratio (ppt)	Emissions estimate (Gg yr^{-1})	Study
HCFC-22	2001-2002	Hong Kong	322 ± 41	0.06 ± 0.03	Guo *et al*. 2009
		S. China	304 ± 59	2.2 ± 1.2	
	2004	S. China	464	3.5 ± 2.2	Shao *et al*. 2011
	2004-2005	China		52 ± 34	Yokouchi *et al*. 2006
	2006	China	181 ± 11		Barletta *et al*. 2009
		Asia	180 ± 4		
	2006-2008	China		165	Vollmer *et al*. 2009
	2007-2008	China		83 (64-109)	Kim et al. 2010
	2007-2008	China		83 (64-109)	Li *et al*. 2011
		Taiwan		2.1 (1.6-2.7)	
		Korea		8.4 (8-8.8)	
		Japan		11 (10-13)	
	2008	China		65.3	Stohl *et al*. 2010
		Taiwan		2.5	
		S. Korea		2.1	
		N. Korea		7.2	
		Japan		6	
	1997	East Asia		46 ± 4	Fortems-Cheiney et al. 2013
	2002			84 ± 6	
	2007			176 ± 5	
	2009	China		98.3 ± 47.4	Xingqin et al. 2012
	2009-2010	China		87.6 (77.2-98)	Fang et al. 2012b
	2010	China	508 ± 208		Fang et al. 2012a
	2010-2011	China	743 ± 603	103.4 ± 64	Wang et al. 2014
HCFC-141b	2001-2002	Hong Kong	56 ± 13	0.05 ± 0.008	Guo *et al*. 2009
		S. China	43 ± 13	0.9 ± 0.3	
	2006	China	19.9 ± 2.3		Barletta *et al*. 2009
		Asia	19.9 ± 0.7		
	2007-2008	China		15 (12-21)	Kim *et al*. 2010
	2007-2008	China		15 (11-21)	Li *et a*l. 2011
		Taiwan		0.5 (0.2-0.8)	
		Korea		2.2 (2.0-2.3)	
		Japan		1.6 (1.2-2.0)	
	2008	China		12.1	Stohl *et al*. 2010
		Taiwan		0.5	
		S. Korea		0.6	
		N. Korea		1.8	
		Japan		1.1	
	2009-2010	China		8.6 (7-10.2)	Fang et al. 2012b
	2010	China	57 ± 65		Fang et al. 2012a

Table 4.1c continued: Overview of the reported mixing ratios and emissions estimates of hydrochlorofluorocarbons from previous studies in the East Asian region.

Compound	Year	Region	Mixing Ratio (ppt)	Emissions estimate (Gg yr^{-1})	Study
HCFC-142b	2001-2002	Hong Kong S. China	32 ± 16 18 ± 2		Guo *et al*. 2009
	2006	China Asia	17.0 ± 1.3 16.4 ± 0.6		Barletta *et al*. 2009
	2006-2008	China		12 (10-18)	Vollmer *et al*. 2009
	2007-2008	China		10 (7.6-13)	Kim *et al*. 2010
	2007-2008	China Taiwan Korea Japan		9 (6.9-13) 0.12 (0.07-0.18) 0.8 (0.7-0.9) 0.9 (0.7-1.1)	Li *et al*. 2011
	2008	China Taiwan S. Korea N. Korea Japan		7.3 0.08 0.2 0.8 0.6	Stohl *et al*. 2010
	2009-2010	China		10.3 (8.6-12)	Fang et al. 2012b
	2010	China	65 ± 60		Fang et al. 2012a

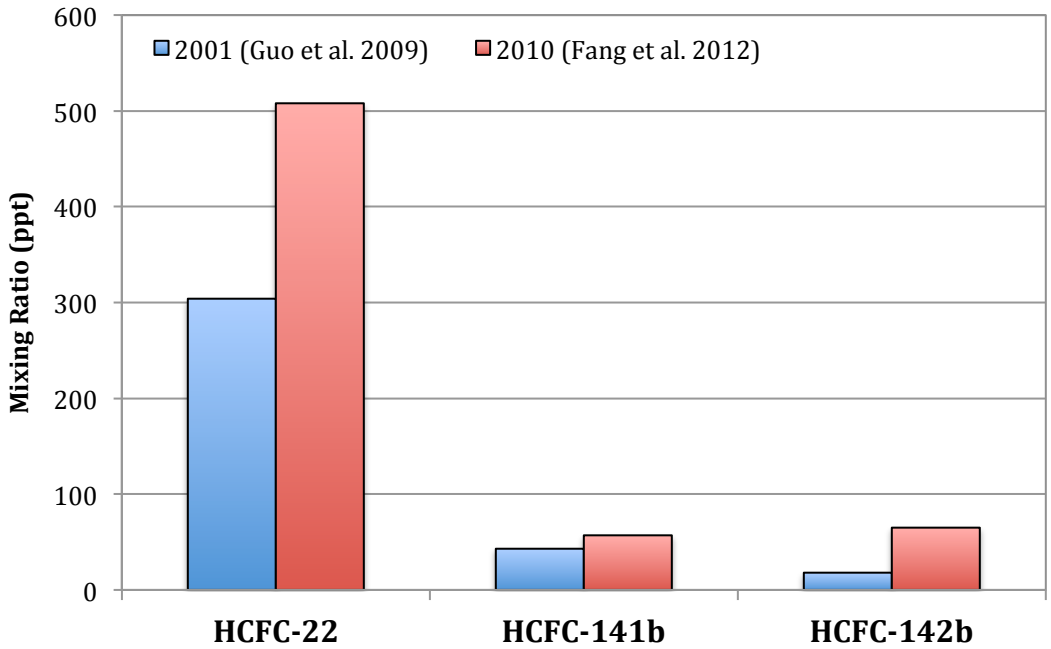

Figure 4.5: Observed mixing ratios of HCFC-22, HCFC-141b and HCFC-142b for 2001 (Guo et al. 2009, blue bars) and 2010 (Fang et al. 2012a, red bars). The increase in abundance indicates the expansion of their use due to the phase out of CFCs and halons under the Montreal Protocol.

4.2.1.4 **Chlorocarbons** (see Table 4.1d)

Carbon tetrachloride (CCl_4) mainly has uses as a cleaning solvent and as a feedstock for a number of minor chemical processes, although there are known discrepancies between bottom up and top down estimates that suggest there are other currently unknown sources (Carpenter, L.J. and Reimann, S., 2014). Palmer *et al*. (2003) estimated emissions of CCl_4 to be 17.6 Gg a-1 in 2001, which is considerably different from the 0.1Gg a^{-1} suggested by UNEP in 2002, but this disparity can most likely be attributed to a lack of source knowledge, as previously mentioned. In 2004, the Shao *et al.* (2011) study of the Pearl River delta detected elevated mixing ratios suggesting there was substantial regional use. However, by 2008, total Chinese emissions were reported to have fallen to 15 Gg a^{-1} (Vollmer et al. 2009). Mixing ratios (seen in Figure 4.6) from 2010 also show a slight drop in atmospheric concentrations since 2001, along with a number of short-lived chlorinated species (see section 4.2.1.5) used in similar applications. Whilst emissions may have decreased, these mixing ratios suggest there is still considerable consumption of these compounds in China.

Methyl chloroform was used as a solvent, as well as electronics cleaning and since its addition to the Montreal Protocol in 1990, steady and substantial decreases in emissions have been inferred across the globe, and China is no exception. In 2001, Palmer *et al*. (2003) estimated Chinese emissions to be 10.4 Gg a^{-1} and for 2006-2008 emissions had decreased to 3.3 Gg a^{-1} (Vollmer *et al*. 2009). By 2010-2011 these were calculated to be 2.8 Gg a^{-1} and mixing ratios were detected at 9 ppt (Wang *et al*. 2014) compared to 62 ppt in 2004 (Shao *et al*. 2011).

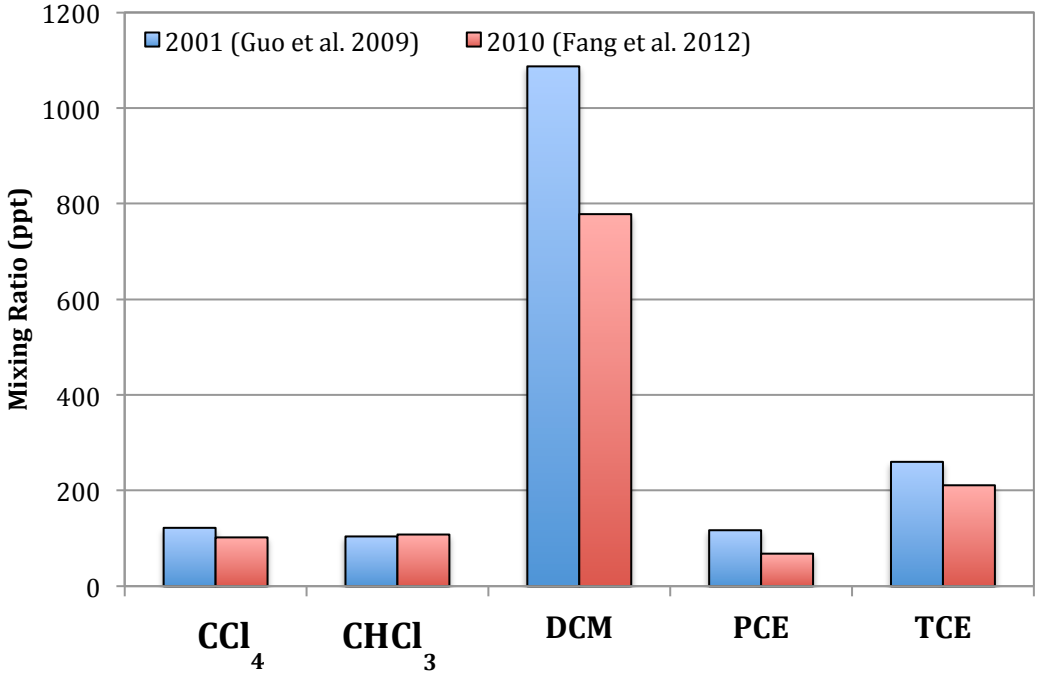

Figure 4.6: Observed mixing ratios of carbon tetrachloride, chloroform, dichloromethane, PCE and TCE for 2001 (Guo et al. 2009, blue bars) and 2010 (Fang et al. 2012a, red bars). All but chloroform show decreases in abundance although this may be due to the differences in the location of the studies. Continued considerable consumption of the VSLS species in China is apparent however.

Table 4.1d: Overview of the reported mixing ratios and emissions estimates of chlorocarbons from previous studies in the East Asian region

Compound	Year	Region	Mixing Ratio (ppt)	Emissions estimate (Gg yr^{-1})	Study
CCl_4	2001	East Asia		21.5	Palmer *et al.* 2003
		China		17.6	
		Japan		1.3	
		Korea		2.3	
	2001-2002	Hong Kong	121 ± 4	0.02 ± 0.004	Guo *et al*. 2009
		S. China	122 ± 7	0.7 ± 0.2	
	2004	S. China	194	1.1 ± 0.7	Shao *et a*l. 2011
	2006	China	95 ± 2		Barletta *et al*. 2009
		Asia	94 ± 2		
	2006-2008	China		15 (10-22)	Vollmer *et a*l. 2009
	2010-2011	China	102 ± 22	4.4 ± 3.4	Wang et al. 2014
$CHCl_2CHCl_2$	2004	S. China	34	0.6 ± 0.4	Shao *et al*. 2011
CH_3CCl_3	2001	China		10.4	Palmer *et al*. 2003
		Japan		1	
		Korea		1.8	
	2004	S. China	62	0.4 ± 0.2	Shao *et al*. 2011
	2006-2008	China		3.3 (3.1-4)	Vollmer *et al*. 2009
	2007-2008	China		1.7 (1.3-2.4)	Li *et al*. 2011
		Taiwan		0.13 (0.08-0.18)	
		Korea		1.5 (1.3-1.7)	
		Japan		0.6 (0.5-0.7)	
	2010-2011	China	9 ± 1	2.8 ± 2	Wang et al. 2014
$CH_3CHClCH_2Cl$	2004	S. China	53	0.4 ± 0.3	Shao *et al*. 2011
	2010-2011	China	181 ± 225	92.0 ± 69.9	Wang et al. 2014

4.2.1.5 Very Short-Lived Substances (see Table 4.1e)

Though it has some natural sources, chloroform is utilised in HCFC-22 production and is released by the paper industry. In China, emissions have been found to be increasing, from 2.4 Gg a^{-1} in 2001-2002 (Guo *et al*. 2009) to 57.1 Gg a^{-1} in 2010-2011 (Wang *et al*. 2014). Vollmer *et al*. (2009) estimated emissions of 86 Gg a^{-1} in 2006-2008 however, as mentioned previously, there may have been local bias in the campaign. Estimates from both Kim *et al*. (2010) and Li *et al*. (2011) for 2007-2008 appear to confirm this, as they are in line with the Wang *et al.* (2014) estimate.

Table 4.1e: Overview of the reported mixing ratios and emissions estimates of very short-lived substances from previous studies in the East Asian region.

Compound	Year	Region	Mixing Ratio (ppt)	Emissions estimate (Gg yr^{-1})	Study
$CHCl_3$	2001-2002	Hong Kong S. China	43 ± 7 104 ± 62	0.03 ± 0.004 2.4 ± 1.8	Guo *et al*. 2009
	2004	S. China	96	0.8 Gg ± 0.6	Shao *et al*. 2011
	2006	China Asia	14.9 ± 6.0 12.4 ± 1.5		Barletta *et al*. 2009
	2006-2008	China		86 (51-140)	Vollmer *et al*. 2009
	2007-2008	China		49 (38-66)	Kim *et al*. 2010
	2007-2008	China Korea Japan		44 (33-60) 2.1 (1.7-2.5) 3.4 (2.8-4.2)	Li *et al*. 2011
	2010-2011	China	108 ± 99	57.1 ± 42.7	Wang et al. 2014
CH_2Cl_2	2001-2002	Hong Kong S. China	948 ± 306 1087 ± 558	42.8 ± 7.2	Guo *et al*. 2009
	2004	S. China	1028	7.0 ± 4.6	Shao *et al*. 2011
	2006	China Asia	54.2 ± 24.4 48.8 ± 7.4		Barletta *et al*. 2009
	2007-2008	China		176 (133-234)	Kim *et al*. 2010
	2007-2008	China Korea Japan		169(126-230) 18 (16-20) 17 (14-20)	Li *et al*. 2011
	2010-2011	China	778 ± 731	235.4 ± 169.2	Wang et al. 2014
CHClCHCl	2006	China Asia	39.7 ± 34.7 18.4 ± 5.4		Barletta *et al*. 2009
PCE	2001-2002	Hong Kong S. China	167 ± 47 117 ± 53	0.26 ± 0.084 7.3 ± 1.5	Guo *et al*. 2009
	2004	S. China	170	2.3 ± 1.5	Shao *et al*. 2011
	2006	China Asia	5.9 ± 4.8 5.7 ± 1.9		Barletta *et al*. 2009
	2010-2011	China	68 ± 68	44.9 ± 32.4	Wang et al. 2014

With a variety of applications including paint removal and foam blowing (Carpenter and Reimann, 2014), substantial increases in emissions of dichloromethane were found from 2001-2002, where 42.8 Gg a^{-1} was estimated (Guo *et al*. 2009), to ~170 Gg a^{-1} in 2007-2008 (Kim *et al*. 2010, Li *et al*. 2011). However, the Guo *et al*. (2009) campaign was based in industrial South China near potential dichloromethane sources and, given the short-lived nature of this species, may not be reflective of the whole country. Still, emissions do appear to be increasing as Wang *et al*. (2014) calculated 235.4 Gg a^{-1} for 2010-2011 Chinese dichloromethane emissions.

Tetrachloroethene (PCE) and trichloroethene (TCE) are utilised as solvents, mainly in dry cleaning (Carpenter and Reimann, 2014), and have also been found to have increasing emissions in China. For PCE, these were estimated at 7.3 Gg a^{-1} in 2001-2002 (Guo *et al*. 2009) to 44.9 Gg a^{-1} in 2010-2011 (Wang *et al*. 2014) and, for TCE, from 12.8 Gg a^{-1} in 2001-2002 (Guo *et al*. 2009) to 121.1 Gg a^{-1} in 2010-2011 (Wang *et al*. 2014).

4.2.1.6 **Methyl Halides** (see Table 4.1f)

Methyl chloride and methyl bromide have primarily natural sources and are both produced in biomass burning, however methyl chloride is used in a number of chemical processes, including silicone production, and methyl bromide has applications as a fumigant and chemical feedstock. Shao et al. (2011) estimated emissions of 0.6 Gg a^{-1} and 0.1 Gg a^{-1} for methyl chloride and methyl bromide respectively in South China in 2004. These are considerably lower than later studies and most likely suggest a lack of sources in that region. Wang *et al*. (2014) calculated 41.8 Gg a^{-1} and 2.4 Gg a^{-1} respectively for Chinese emissions in 2010-2011, however Kim *et al*. (2010) and Li *et al*. (2011) inferred emissions of ~250 Gg a^{-1} for methyl chloride and ~5.6 Gg a^{-1} for methyl bromide during 2007-2008. Whilst these are notably higher than those estimated 3 years later, the variation and lack of control of natural sources is more likely to have impacted this difference than a significant change in anthropogenic emissions, particularly since methyl chloride is not controlled under the Montreal Protocol and the methyl bromide phase out was not completed until 2015 in China.

Table 4.1f: Overview of the reported mixing ratios and emissions estimates of the methyl halides from previous studies in the East Asian region.

Compound	Year	Region	Mixing Ratio (ppt)	Emissions estimate (Gg yr^{-1})	Study
CH_3Cl	2001-2002	Hong Kong S. China	940 ± 89 899 ± 64	0.68 ± 0126 2.8 ± 0.5	Guo *et al*. 2009
	2004	S. China	1165	0.6 ± 0.4	Shao *et al.* 2011
	2006	China Asia	604 ± 57 584 ± 21		Barletta *et al*. 2009
	2007-2008	China		265 (200-354)	Kim *et al*. 2010
	2007-2008	China Korea		239 (176-327) 5.7 (4.6-6.9)	Li *et al*. 2011
	2010-2011	China	941 ± 304	41.8 ± 30.1	Wang et al. 2014
CH_3Br	2001-2002	Hong Kong S. China	19 ± 4 18 ± 2		Guo *et al*. 2009
	2004	S. China	47	0.1 ± 0.1	Shao *et al*. 2011
	2006	China Asia	8.9 ± 1.1 8.8 ± 0.5		Barletta *et al*. 2009
	2007-2008	China		5.8 (4.3-7.9)	Kim *et al*. 2010
	2007-2008	China Korea		5.4 (3.9-7.5) 1.1 (0.9-1.4)	Li *et al*. 2011
	2010-2011	China	17 ± 10	2.4 ± 1.9	Wang et al. 2014
CH_3I	2006	China Asia	0.12 ± 0.1 0.19 ± 0.17		Barletta *et al.* 2009

4.2.1.7 **Hydrofluorocarbons** (see Table 4.1g)

As a by-product of HCFC-22 manufacture, HFC-23 is one of the major HFCs with around 98% of the emissions in the East Asian region originating from China (Li *et al.* 2011). Nevertheless, emissions were reduced significantly due to the introduction of the CDM Project (Stohl *et al.* 2010), which funded the destruction capabilities needed in HCFC-22 production for developing countries. Yao *et al.* (2012) estimated emissions to be 3.6 Gg a^{-1} for 2010-2011, which is considerably smaller than the 10 Gg a^{-1} estimated by Yokouchi *et al.* (2006) for 2004-2005. However this does still indicate the presence of significant sources (Kim *et al.* 2010).

Both Kim *et al.* (2010) and Li *et al.* (2011) report HFC-134a levels in emissions from China have increased sharply since 2005, and these are expected to continue to increase as the Chinese automotive industry expands due to its use in mobile air conditioning. Yao *et al.* (2012) reported HFC-134a as having the highest growth rate of all compounds studied, however the correlation between this compound and CO was found to be insignificant.

Table 4.1g: Overview of the reported mixing ratios and emissions estimates of hydrofluorocarbons from previous studies in the East Asian region.

Compound	Year	Region	Mixing Ratio (ppt)	Emissions estimate (Gg yr^{-1})	Study
HFC-23	2004-2005	China		10 ± 4.6	Yokouchi *et al*. 2006
	2007-2008	China		12 (8.6-15)	Kim *et al*. 2010
	2007-2008	China		10 (7.2-13)	Li *et al*. 2011
		Taiwan		0.07 (0.04-0.10)	
		Korea		0.11 (0.08-0.13)	
		Japan		0.3 (0.2-0.3)	
	2008	China		6.2	Stohl *et al*. 2010
		Taiwan		0.03	
		S. Korea		0.04	
		N. Korea		0.19	
		Japan		0.21	
	2010-2011	China		3.6 ± 3.2	Yao *et al*. 2012
HFC-32	2007-2008	China		4.3 (3.2-5.9)	Kim *et al*. 2010
	2007-2008	China		4.0 (2.9-5.6)	Li *et al*. 2011
		Taiwan		0.05 (0.03-0.07)	
		Korea		0.21 (0.18-0.23)	
		Japan		0.4 (0.3-0.5)	
	2010-2011	China		4.3 ± 3.6	Yao *et al*. 2012
HFC-125	2007-2008	China		3.2 (2.4-4.4)	Kim *et al*. 2010
	2007-2008	China		3.1 (2.3-4.3)	Li *et al*. 2011
		Taiwan		0.07 (0.04-0.1)	
		Korea		0.27 (0.24-0.31)	
		Japan		0.7 (0.7-0.9)	
	2010-2011	China		2.7 ± 2.3	Yao *et al*. 2012
HFC-143a	2007-2008	China		0.59 (0.44-0.8)	Kim *et al*. 2010
	2007-2008	China		0.6 (0.4-0.8)	Li *et al*. 2011
		Taiwan		0.04 (0.02-0.06)	
		Korea		0.08 (0.07-0.09)	
		Japan		0.4 (0.3-0.4)	

Table 4.1g continued: Overview of the reported mixing ratios and emissions estimates of hydrofluorocarbons from previous studies in the East Asian region.

Compound	Year	Region	Mixing Ratio (ppt)	Emissions estimate (Gg yr^{-1})	Study
HFC-134a	2004-2005	China		3.9 ± 2.4	Yokouchi *et al*. 2006
	2006	China Asia	36.1 ± 4.0 36.7 ± 1.9		Barletta *et al*. 2009
	2007-2008	China		8.7 (6.5-12)	Kim *et al*. 2010
	2007-2008	China Taiwan Korea Japan		8.3 (6.2-11) 0.5 (0.3-0.8) 1.7 (1.5-1.8) 4.7 (4.5-5	Li *et al*. 2011
	2008	China Taiwan S. Korea N. Korea Japan		12.9 0.8 0.46 1.9 3.1	Stohl *et al*. 2010
	2010-2011	N. China China		3.2 ± 2.9 6.0 ± 5.6	Yao *et al*. 2012
	2005 2010	China		5.0 (3.1-7.0) 16.7 (10.5-22.7)	Su et al. 2015
	2009-2010	China		5.7 (4.7-6.7)	Fang et al. 2012b
	2010	China	87 ± 57		Fang et al. 2012a
HFC-152a	2004-2005	China		4.3 ± 2.3	Yokouchi *et al*. 2006
	2007-2008	China		5.7 (4.3-7.6)	Kim *et al*. 2010
	2007-2008	China Taiwan Korea Japan		5.4 (4.0-7.4) 0.08 (0.04-0.13) 0.11 (0.08-0.13) 1.2 (1.0-1.4)	Li *et al*. 2011
	2008	China Taiwan S. Korea N. Korea Japan		3.4 0.02 0.15 0.19 0.9	Stohl *et al*. 2010
	2010-2011	N. China China		1.0 ± 0.9 2.0 ± 1.8	Yao *et al*. 2012
	2010	China	17 ± 7		Fang et al. 2012a
HFC-365mfc	2007-2008	Taiwan Japan		0.01 (0.007-0.017) 0.2 (0.2-0.3)	Li *et al*. 2011

As such, the emissions calculated could be considered questionable and are lower than would be expected (at only 6 Gg a^{-1} for 2010-11). Su et al. (2015) used bottom up manufacturing data, as well as leaks rates, to estimate emissions of 5 Gg a^{-1} in 2005, further increasing to 16.7 Gg a^{-1} in 2010.

Of the other more minor HFC species measured (HFC-125, -152a, -32 and -143a), emissions are summarised in Table 4.1g but generally appear consistent between studies.

4.2.1.8 Perfluorocarbons and SF_6 (see Table 4.1h)

The PFCs mainly have uses in aluminium and semiconductor manufacture (see section 1.14.2.2), and CF_4 and C_2F_6 had estimated emissions in 2007-2008 that were found to be in-line with previously extrapolated rates, however C_3F_8 had increased (Kim *et al.* 2010). In 2010-2011, estimates only had small differences to earlier studies for CF_4 and C_3F_8 but emissions for C_2F_6 were almost half of those reported by Kim *et al.* (2010) (Yao *et al.* 2012). Since PFC emissions are comparatively small (less than 0.5 Gg a^{-1} for C_2F_6 and C_3F_8), these disparities may be due to the use of differing estimation methods. A more recent study by Kim *et al.* (2014) inferred that differences between emissions, calculated using inventories and those using atmospheric observations, may have been due to previous underestimation of the Chinese aluminium and semiconductor industries. Saito et al. (2010) still found China to have the largest emissions of PFCs in the East Asian region.

SF_6 is mainly used in high-voltage switchgears in electrical equipment and was also found to be in agreement with other investigations (Vollmer *et al*. 2009, EC-JRC/PBL, 2009), which confirms that substantial emissions are still being produced (Kim *et al*. 2010). Fang et al. (2014) found emissions had doubled between 2006 and 2012 from 1.43 Gg a^{-1} to 2.87 Gg a^{-1}.

Although the emissions of the PFCs and SF_6 are relatively small compared to many of the other halocarbon species, their atmospheric lifetimes of several thousand years and global warming potentials several orders of magnitude higher than that of CO_2 mean that their combined emissions are equivalent to millions of tonnes of CO_2 permanently added to the atmosphere.

Finally, Figure 4.7 gives an overview of the percentage of Chinese emissions estimated for a number of halocarbon compound groups from the Li et al. (2011) 2007-2008 campaign. This study was chosen as it covered the largest range of compound groups measured over several regions. Since this campaign took place during the phase-out of CFCs and Halons, HCFCs have larger emissions than the groups they are used to replace. Anthropogenic VSLS, not controlled under the Montreal Protocol, are also found to make up a large portion of Chinese emissions, as do the methyl halides although some emissions of these may be natural in origin. HFC emissions would be expected to increase in upcoming years as to counteract the upcoming phase out of HCFCs by 2030.

Table 4.1h: Overview of emissions estimates of perfluorocarbons and sulphur hexafluoride from previous studies in the East Asian region.

Compound	Year	Region	Emissions estimate (Gg yr^{-1})	Study
CF_4	2007-2008	China	2.3 (1.7-3.1)	Kim *et al*. 2010
	2007-2008	China	2.1(1.4-2.9)	Li *et al*. 2011
		Korea	0.22 (0.19-0.26)	
		Japan	0.3 (0.2-0.3)	
	2010-2011	China	2.4 ± 2.1	Yao *et al*. 2012
C_2F_6	2007-2008	China	0.49 (0.37-0.66)	Kim *et al*. 2010
	2007-2008	China	0.5 (0.4-0.7)	Li *et al*. 2011
		Korea	0.10 (0.09-0.12)	
		Japan	0.2 (0.1-0.2)	
	2009	China	0.499 ± 0.038	Saito et al. 2010
		Taiwan	0.059 ± 0.004	
		N. Korea	0.013 ± 0.002	
		S. Korea	0.092 ± 0.006	
		Japan	0.196 ± 0.018	
	2010-2011	China	0.27 ± 0.026	Yao *et al*. 2012
C_3F_8	2007-2008	China	0.09 (0.07-0.12)	Kim *et al*. 2010
	2007-2008	China	0.09 (0.06-0.13)	Li *et al*. 2011
		Korea	0.04 (0.03-0.04)	
	2009	China	0.157 ± 0.030	Saito et al. 2010
		Taiwan	0.024 ± 0.012	
		N. Korea	0.07 ± 0.002	
		S. Korea	0.031 ± 0.008	
		Japan	0.091 ± 0.019	
	2010-2011	China	0.061 ± 0.095	Yao *et al*. 2012
c-C_4F_8	2009	China	0.422 ± 0.045	Saito et al. 2010
		Taiwan	0.009 ± 0.001	
		N. Korea	0.010 ± 0.001	
		S. Korea	0.032 ± 0.002	
		Japan	0.089 ± 0.006	

Table 4.h continued: Overview of emissions estimates of perfluorocarbons and sulphur hexafluoride from previous studies in the East Asian region

Compound	Year	Region	Emissions estimate (Gg yr^{-1})	Study
SF_6	2006-2008	China	0.8 (0.53-1.10)	Vollmer *et al.* 2009
	2007-2008	China	1.3 (0.93-1.7)	Kim *et al.* 2010
	2007-2008	China	1.2 (0.9-1.7)	Li *et al.* 2011
		Korea	0.38 (0.33-0.44)	
		Japan	0.4 (0.3-0.5)	
	2006	China	1.434 ± 0.247	Fang et al. 2014
		Taiwan	0.123 ± 0.06	
		N. Korea	0.057 ± 0.06	
		S. Korea	0.395 ±0.104	
		Japan	0.387 ± 68	
		East Asia	2.404 ± 325	
	2009	China	2.741 ± 0.472	
		Taiwan	0.184 ± 0.09	
		N. Korea	0.065 ± 0.069	
		S. Korea	0.546 ± 0.143	
		Japan	0.215 ± 0.038	
		East Asia	3.787 ± 0.512	
	2012	China	2.868 ± 0.494	
		Taiwan	0.301 ± 0.148	
		N. Korea	0.038 ± 0.04	
		S. Korea	0.657 ± 0.172	
		Japan	0.185 ± 0.032	
		East Asia	4.063 ± 0.549	

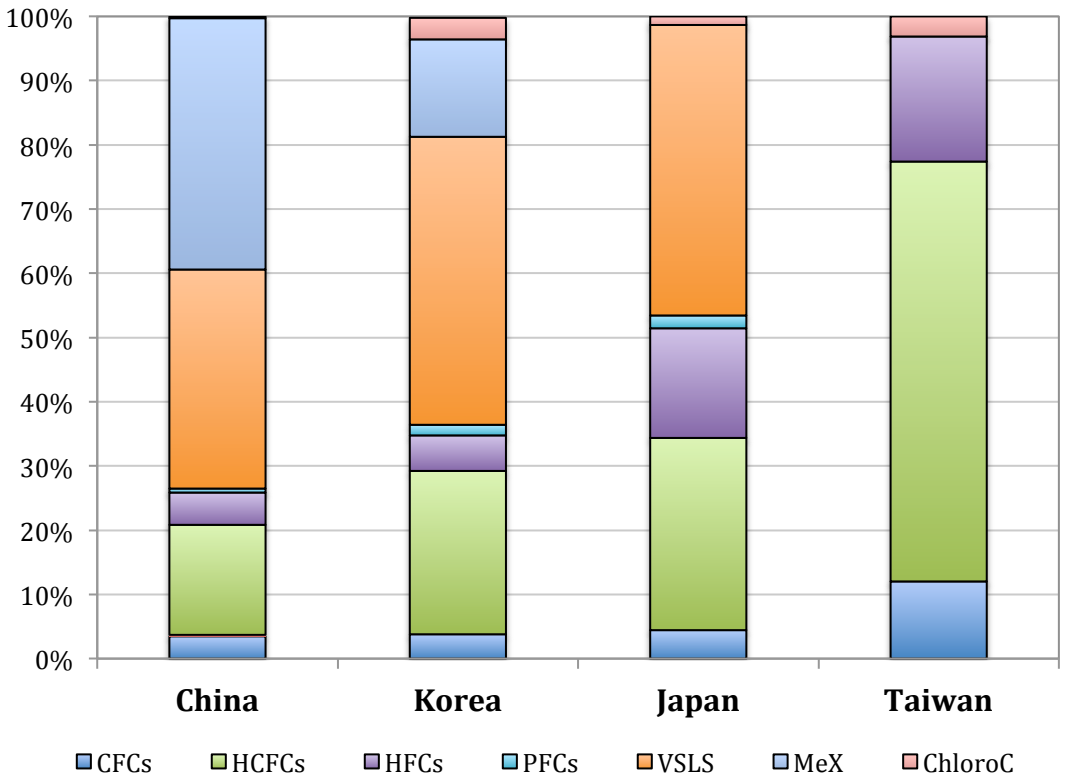

Figure 4.7: Overview of emissions from the main regions of East Asia, separated by compound group, for 2007-2008 (Li et al. 2011). Data was not available for all groups for all countries. Species not controlled by legislation (i.e. VSLS and methyl halides) make up large proportions of emissions. Larger emissions of HCFC than those of CFCs reflect the impact of the Montreal Protocol regulations.

4.2.2 Japan

Unlike China, Japan is not an 'Article 5' party under the Montreal Protocol and so is further into the ODS phase-out schedule, namely the reduction of HCFC use. This is apparent from the emissions estimated, in 2008 when CFC and HCFC emissions were both found to have decreased (by 70% and 30% respectively) since 2002 (Li *et al.* 2011) (see Figure 4.2 as well as Table 4.1a and 4.1c). No studies including Japanese halon emissions were available for comparison.

Stohl *et al.* (2010) detected decreases in HCFC emissions compared to previous studies (Table 4.1c), including a rapid decrease in HCFC-141b, which suggests that their phase-out is well underway. However interspecies correlations, particularly with HFC species found by Li *et al.* (2011), suggest that consumption of HCFC-142b has still continued.

Limited data is available on Japanese emissions of carbon tetrachloride (see Table 4.1d), however methyl chloroform emissions have decreased from 1 Gg a^{-1} in 2001 (Palmer *et al*. 2003) to 0.6 Gg a^{-1} by 2007-2008 (Li *et al*. 2011) in agreement with global trends. There is also a lack of studies including emissions of VSLS and the methyl halides from Japan.

Whilst emissions of HFC-23 and -152a were comparable between the two studies, HFC-134a emissions were estimated at 3.1 Gg a^{-1} by Stohl *et al*. (2010) for 2008 and 4.7 Gg a^{-1} by Li *et al.* (2011) for 2007-2008. Differences in methodology may be part of the reason for this discrepancy, although given the agreement of other species this would likely be minimal. However, the estimate from Stohl *et al*. (2010) is in line with bottom up calculations, suggesting the emissions from Li *et al*. may be overestimated. The very minor HFC-365mfc (not measured for China) was also found and its emissions estimated at 0.2 Gg a^{-1}, although the use of this compound in Japan had not been reported to the UNFCCC at the time (Li *et al.* 2011).

Saito et al. (2010) found Japan to be the second biggest emitter of PFCs in the East Asian region, but the estimates were lower than expected given the size of its semiconductor industry. This is most likely caused by successful adherence to a voluntary PFC reduction plan set in place by Japanese members of the World Semiconductor Council. However, emissions calculated for C_2F_6 and C_3F_8 were consistent with those from a 2003 study (Yokouchi et al. 2005) at 0.19 Gg a^{-1} and 0.06 Gg a^{-1} respectively. Fang et al. (2014) found Japanese SF_6 emissions to contribute between 5-16% of East Asian emissions between 2006 and 2012, though overall emissions from Japan in this period have been decreasing, from 0.387 Gg a^{-1} to 0.185 Gg a^{-1}, unlike China, Taiwan and South Korea.

Figure 4.7 again shows an overview of the halocarbon make-up of Japanese emissions during 2007-2008 (Li et al. 2011). While there was no available data on the Halons or Methyl Halides for this campaign, Japan's status as a developed country under the Montreal Protocol and its position further along the phase-out timeline is reflected. The integration of HCFCs into industry is clear from the high proportion of emissions detected, as is the further shift to HFCs. Similarly to China, the uncontrolled VSLS make up the largest portion of emissions estimated by this campaign.

The limited data available for several halocarbon groups further emphasises why the East Asian region requires increased monitoring of wide range of species if trends and impacts of emissions are to be assessed on both a regional and global scale.

4.2.3 Korea

Like China, both North and South Korea are considered "Article 5" countries under the Montreal Protocol and have had to phase out the use of certain halocarbon groups accordingly. Separate emissions from each country however are not easily determined and do spill over (Stohl *et al.* 2010), so the results discussed below refer to both North and South Korea together unless otherwise stated.

In 2008, Li *et al.* (2011) detected a 70% decrease in the emissions of CFCs since 2001 (see Figure 4.2 and Table 4.1a), however CFC-11 and CFC-12 still correlate with a number of halocarbon species potentially indicating their release from banks as HCFC compounds dominate the emissions. Stohl *et al.* (2010) found overall decreases in the emission of HCFC-22, HCFC-141b and HCFC-142b (see Table 4.1c), but noted that the emissions for HCFC-22 were lower than the reported consumption suggesting the build-up of banks (unreleased volumes of gas, e.g. in fire extinguishers or foams).

As with Japan, there is limited data for comparison regarding Korean emissions for halons, chlorocarbons, VSLS and methyl halides (see Tables 4.1b, 4.1d, 4.1e and 5.1f). However, methyl chloroform emissions estimates were found to agree with global trends and decreased from 1.8 Gg a^{-1} in 2001 (Palmer *et al.* 2003) to 1.5 Gg a^{-1} in 2007-2008 (Li *et al*. 2011).

Comparisons of HFC emissions estimates between the studies of Stohl *et al*. (2010) and Li *et al*. (2011), where possible (see Table 4.1g), generally found that the emissions calculated were higher from the Stohl *et al*. (2010) campaign. As they both covered a very similar time period, this difference may partially be due to the appropriation of emissions to both North and South Korea in Stohl *et al*. (2010).

Li et al (2011) found the semiconductor and electronics industries of Korea were reflected by the correlation between PFC emissions of C_2F_6 and C_3F_8, however larger emissions of SF_6 indicate that other sources of this compound exist elsewhere, such as high voltage switchgear as well as the magnesium industry. Fang et al (2014) noted South Korea was the second largest contributor to SF_6 emissions in the region, with 8-16% between 2006 and 2012, whereas North Korea only contributed less than 3%. North Korea was also found to have the lowest PFC emissions, which is consistent with the minimal semiconductor industry there, however this may still be an overestimation due to limited model resolution resulting in South Korean emissions spill over (Saito et al. 2010).

Though total halocarbon emissions from Korea are not as high as China, per capita the emissions are the highest in the region. Figure 4.7 shows the proportions of these emissions attributable to each of the halocarbon groups though, again, no data for the Halons was available in this study. The emissions detected were very similar to China in that there are large proportions of HCFC and HFCs found compared to CFCs, consistent with Montreal Protocol impact. However, contributions from the methyl halides appear less than those found in Chinese emissions, VSLS, namely dichloromethane and chloroform, make up the bulk of emissions, likely due to widespread solvent use (Li et al, 2011).

4.2.4 Taiwan

Taiwan's 'voluntary' phase-out of CFCs is apparent from the low emissions (0.3Gg a^{-1}, Table 4.1a) and the lack of correlation between the CFCs and other halocarbon species seen by Li *et al.* (2011), which suggests they were mostly phased out by 2008. HCFC-22, -141b and -142b emissions all show good agreement between the Stohl *et al.* (2010) and the Li *et al.* (2011) campaigns although, like Japan and Korea, there is no data from a different time period to compare with to assess any regional emission trends.

As has been seen for other countries, limited data on Taiwanese emissions of chlorocarbons is available and can be found in Table 4.1d. No studies have included regional emissions estimates for halons, VSLS or the methyl halides for Taiwan.

HFC-134a *a posteriori* emissions in 2008 (Stohl *et al.* 2010) were found to be lower than previous extrapolated estimates (Tsai, 2006). This was suggested as potentially being due to decreased imports of HFC-134a since 2004 and thus not reflecting the previous estimate. Decreased emissions of HFC-152a suggest there are no substantial regional sources and this agrees with the low consumption levels reported (Stohl *et al*. 2010). Similarly, low usage of HFC-365mfc has been documented and this too is reflected by the emissions calculated. Table 4.1g indicates the emissions of the other HFCs (-23, -32, -125 and 143a) also estimated during this campaign (Li *et al.* 2011).

Similarly to Japan, Taiwan was found to have notable PFC emissions, but these were less than originally expected given its extensive semiconductor and electronics manufacturing industries (Saito et al, 2010). Fang et al. (2014) found Taiwanese SF_6 emissions to only contribute between 4-7% of those from the East Asian Region though, per capita, this is still more than 5 times the global per capita average.

Again, Figure 4.7 shows the make-up of halocarbon emissions detected by Li et al. (2011), however data for Taiwan was only available for a much smaller range of compounds. It still can be seen that the proportion of emissions from HCFCs and HFCs outweighs those of CFCs, reflecting the voluntary phase-out undertaken.

4.3 The Research Gap

Whilst many of these campaigns and studies focus on particular groups or a selection of halocarbon compounds, none cover the full range of detected species. This is especially true for some of the more minor and/or novel compounds such as Halon 1202, CFC-113a or HCFC-133a, which have little known about their production and uses that analysis and monitoring would only aid. VSLS species also would benefit from increased monitoring, as their high emissions in the East Asian region and lack of global control measures mean their impact on the atmosphere may be significant, but assessment is currently limited through lack of observational data.

Further to this, comparisons between levels of compounds detected each year are hindered by the lack of multi-year campaigns. Whilst halocarbons have been measured in the region for over a decade by different campaigns, differing analysis and interpretation techniques make the identification of regional emissions trends more complex to assess. By factoring in the diversity of methods utilised, multiple uncertainties have to be considered making statistically significant relationships that could reflect the impact of global control measures or their shortcomings less clear.

4.4 This Study

This study aims to use a short-term, ground-based, air sampling campaign carried out over 3 years to analyse the widest range of halocarbon species in the region. By collaborating with campaigns organised and carried out by the National Central University (NCU) of Taiwan, access to meteorological data as well as mixing ratios of non-halocarbon species, such as ozone and CO was also available for comparison. The results from these campaigns will be able to contribute to assessments of halocarbon levels in the East Asian region as well as potentially highlighting groups or specific compounds in need of further monitoring or, ultimately, further regulation.

4.5 Location

In order to assess halocarbon concentrations in East Asia, Taiwan was chosen as a suitable base for air sample collection.

Taiwan is situated around 180km off the south-eastern coast of mainland China and is one of the most densely populated countries in the world (Zinfan, 2015). It is a largely industrialised area and is involved in the production of electronics and semiconductors as well as chemicals, textiles and consumer products. As a manufacturing hub, the Taiwanese economy relies on global exportation of its products (CIA, 2016).

During the springtime, Taiwan experiences winter monsoon wind patterns that are typically predominant over East Asia. These coincide with strong continental outflows of pollution, particularly from Mainland China, Korea and Japan (Ou-Yang et al. 2012). This means that air masses, which pass over sampling collection sites in Taiwan, are likely to contain halocarbon species from long-range transport as well as possible examples of more local pollution. Analysis of samples collected during the spring, and comparison with air mass back trajectories, should enable the identification of compounds emitted from across the East Asian region as well as establishing potential source areas.

4.6 Sample Collection

Sampling sites were selected by NCU for their campaigns and, following input and instructions from UEA, their staff collected the samples recording the times and approximate pressures each canister was filled to.

During 2013 and 2015, samples were collected at a coastal site in the Hengchun province of southern Taiwan, 22.0547N, 120.6995E (see Figures 4.8 and 4.9), at an inlet height of 7m above sea level. In 2013, samples were collected once per day on 19 days between the 7th March and 5th April, at approximately 11:00am local time. In 2015, 23 samples were collected between 12th March and 25th April. Throughout the period of the 12th March to 31st March, 16 samples were collected, once per day at approximately 10:30am local time. Due to staffing constraints, the further 7 samples were collected between 22nd April and 25th April, twice per day (except on the 22nd April), once in the morning and once in the evening.

Figure 4.8: Location of the 2013 and 2015 sampling site in Southern Taiwan. The satellite image shows that there are some residential areas near to the site. Taken from Google Maps.

Figure 4.9: Photograph taken at the Southern Taiwanese sampling site during the 2015 campaign showing some of the instrumentation of the NCU campaign taking place simultaneously.

In 2014, samples were collected at a coastal site on the Fue-Gue cape in Northern Taiwan, 25.297N, 121.538E (see Figures 4.10 and 4.11), at an inlet height of 52m above sea level. Collection of one sample per day took place on 24 days between the 11th March and 4th April at approximately 2:15pm local time.

Though both sites are coastal, there are some notable differences between the North and South of the island. Whilst the South is a lot less industrialised and more rural, this site is on the west coast and is quite close to a number of residential buildings. During the winter monsoon, the area experiences wind conditions known as katabatic, strong winds that travel from the east, down from the peaks of the Central Mountain Range and across the more populated areas towards the coast. Whilst Taiwan also experiences Foehn winds during the year, the strong downslope winds associated with the winter monsoon do not exhibit the adibatical warming that would identify them as Foehn winds (Kusky, T., 2005). The cold, dry, katabatic winds can reach up to 20 m/s and may pick up local pollution before reaching the sampling site.

Figure 4.10: Location of the 2014 sampling site in Northern Taiwan. The satellite image shows that this site is more remote and there is very limited construction nearby. Taken from Google Maps.

Figure 4.11: Photograph taken at the Northern Taiwanese sampling site in March 2015.

As for the Northern site, though very local sources are limited, it is closer to some of the major industrial parks in Taiwan, which are situated at the northern part of the island and along the west coast. There is no land between the sampling site and China, Korea and Japan so, if the air masses travel down from north of Taiwan, then these samples should give a good representation of outflow from these areas. However, if winds are from the south or south-west of the site, there could be considerable local influence from industry. As such, local wind direction and speeds were measured at the sites during sampling so any impact from potential local pollution could be assessed. The timing in which samples were collected was limited and so it was not possible to wait for changes to wind direction in order to collect a sample that may better reflect continental outflow as opposed to local emissions.

Throughout all 3 campaigns, samples were collected directly into 3L Silcosteel-treated stainless steel canisters (Restek Corp) at a pressure of approximately 2.5 bar using a diaphragm pump. A number of studies into long term trends and reconstructing atmospheric histories of a range of halocarbons using similar methods, (Fraser et al, 1999, Muhle et al. 2010 and Oram et al. 2012, Sturges *et al*. 2012, Laube et al. 2012, Newland et al. 2013 and Laube et al. 2014), have found that long-lived halocarbons are able to be stored this way for extended periods without significant changes in their concentrations. Potential contamination from within the canisters was also assessed by filling several with nitrogen as blanks and analysing samples of these using the same GC-MS method. For the majority of halocarbon species, the results of this were indistinguishable from the instrument background however, where relevant, further detail will be given.

A full list of the dates and times that samples were collected at can be found in Table 4.2a-c. The sample denoted with an asterisk in the 2013 campaign was one for which the collection time was not recorded and so an approximate time was used, in line with other samples from the same campaign.

Table 4.2a: 2013 Campaign data on sample collection, local winds and NAME source analysis.

Collection:			Local Winds			NAME Source Location	
Date	Time (Local)	Time (UTC)	Degrees	Direction	Speed (m/s)	Major	Minor
07/03/13	11:20	04:20	313.83	WNW	4.18	China	Taiwan
08/03/13	11:00*	04:00*	3.20	NNE	5.16	China	Japan Taiwan
11/03/13	11:33	04:33	212.94	SSW	4.96	China/Korea	Taiwan Pacific
12/03/13	10:56	03:56	76.92	ENE	6.92	Korea	China Taiwan Pacific
13/03/13	10:40	03:40	315.67	NNW	3.53	Pacific Ocean	Japan
14/03/13	11:00	04:00	69.77	ENE	15.21	China	Taiwan
15/03/13	09:50	02:50	110.31	ESE	7.64	Korea	China Taiwan
18/03/13	09:55	02:55	281.88	WNW	11.85	Pacific Ocean	Japan Philippines Korea
19/03/13	10:30	03:30	164.02	SSE	3.08	Taiwan	Korea Japan Pacific
20/03/13	09:30	02:30	303.38	WNW	7.30	South China Sea Philippines	Korea Japan Pacific
21/03/13	09:20	02:20	63.06	ENE	15.62	China/Korea	South China Sea
22/03/13	10:45	03:45	278.61	WNW	3.77	Pacific Korea	China
25/03/13	09:50	02:50	68.45	ENE	13.95	China	Korea
27/03/13	11:20	04:20	305.41	WNW	2.69	Pacific Korea	China Taiwan
28/03/13	10:40	03:40	273.88	WSW	3.87	China/Korea	Taiwan
01/04/13	10:40	03:40	324.40	NNW	3.88	Japan	Korea China
03/04/13	10:27	03:27	65.09	ENE	15.88	China	Korea
04/04/13	10:15	03:15	74.11	ENE	7.23	China Pacific	Korea
05/04/13	11:02	04:02	275.06	WNW	6.70	South China Sea Philippines	Pacific

Table 4.2b: 2014 Campaign data on sample collection, local winds and NAME source analysis.

Collection:			Local Winds			NAME Source Location	
Date	Time (Local)	Time (UTC)	Degrees	Direction	Speed (m/s)	Major	Minor
11/03/14	10:22	03:22	N/A	N/A	N/A	China	
12/03/14	14:20	07:20	264.12	WSW	2.01	Taiwan China	Korea
13/03/14	15:50	08:50	49.71	ENE	3.11	China	
14/03/14	14:15	07:15	97.37	ESE	7.30	China	
15/03/14	14:30	07:30	204.45	SSW	0.43	China	
16/03/14	14:22	07:22	123.04	ESE	1.71	China Taiwan	
17/03/14	14:23	07:23	262.33	WSW	3.04	China Taiwan	
18/03/14	14:27	07:27	118.54	ESE	1.82	China Taiwan	
19/03/14	14:40	07:40	238.25	WSW	1.55	China Taiwan	Pacific
21/03/14	14:21	07:21	85.51	ENE	8.69	China	
22/03/14	14:20	07:20	94.31	ESE	8.30	China/Korea	
23/03/14	14:30	07:30	94.58	ESE	8.18	Korea	
24/03/14	14:15	07:15	113.43	ESE	1.89	Korea	Japan
25/03/14	14:15	07:15	223.62	SSW	2.04	Taiwan	Japan Korea China
26/03/14	14:25	07:25	236.44	WSW	7.23	Taiwan Pacific	Japan Korea China
27/03/14	14:20	07:20	151.40	SSE	4.38	China Pacific	Taiwan Japan
28/03/14	14:15	07:15	131.52	ESE	1.48	Taiwan Pacific	China Japan
29/03/14	14:05	07:05	131.53	ESE	0.91	Taiwan Pacific Philippines	Japan
30/03/14	15:20	08:20	96.59	ESE	7.70	China	Korea
31/03/14	14:20	07:20	290.93	WNW	2.14	China	Korea
01/04/14	14:25	07:25	36.44	NNE	1.96	China/Korea	Japan
02/04/14	14:10	07:10	94.54	ESE	4.08	China Korea Japan	
03/04/14	14:25	07:25	71.63	ENE	3.77	China Korea Japan	
04/04/14	14:15	07:15	103.53	ESE	5.39	China/Korea	

Table 4.2c: 2015 Campaign data on sample collection, local winds and NAME source analysis.

Collection:			Local Winds			NAME Source Location	
Date	Time (Local)	Time (UTC)	Degrees	Direction	Speed (m/s)	Major	Minor
12/03/15	17:35	10:35	72.00	ENE	6.18	China Taiwan	
17/03/15	11:26	04:26	137.20	SSE	4.56	Pacific	Japan
18/03/15	10:40	03:40	114.00	ESE	4.17	Pacific	Japan
19/03/15	10:40	03:40	277.33	WNW	3.53	Taiwan Pacific Philippines	Japan
20/03/15	10:42	03:42	295.40	WNW	3.50	Pacific Philippines	Taiwan
21/03/15	08:45	01:45	77.75	ENE	7.00	Taiwan Pacific	
22/03/15	10:20	03:20	48.00	ENE	8.93	China/Korea	Japan
23/03/15	10:11	03:11	71.92	ENE	14.18	China	Korea
24/03/15	13:03	06:03	129.05	ESE	15.95	Korea	Japan
25/03/15	10:20	03:20	237.67	WSW	10.60	Korea	China
26/03/15	10:10	03:10	79.50	ENE	4.12	Korea	
27/03/15	09:45	02:45	330.75	NNE	0.65	Korea Japan Pacific	Taiwan
28/03/15	13:07	06:07	62.12	ENE	4.35	China Japan	Korea Taiwan
29/03/15	08:50	01:50	75.17	ENE	2.95	China Taiwan Japan	Korea
30/03/15	09:38	02:38	86.67	ENE	3.16	China Taiwan Japan	Korea
31/03/15	10:12	03:12	143.80	SSE	3.62	Japan Pacific	
22/04/15	19:45	12:45	69.75	ENE	11.75	Korea/Japan	China Taiwan
23/04/15	10:04	03:04	60.33	ENE	8.96	Korea Taiwan	China Japan
23/04/15	17:50	10:50	77.50	ENE	4.54	Korea	China Japan
24/04/15	10:40	03:40	288.00	WNW	4.00	Korea Taiwan	China Japan
24/04/15	17:40	10:40	157.00	SSE	2.23	Korea Taiwan	China Japan
25/04/15	10:40	03:40	187.00	SSW	3.53	Korea/Japan	
25/04/15	17:20	10:20	63.67	ENE	7.83	Japan	Korea

4.7 Sample Analysis

All samples were analysed on two different systems, both utilising gas chromatography separation and mass spectrometry detection (GC-MS).

In all 3 campaigns many of the major halocarbons species, i.e. CFCs, halons, HCFCs and HFCs, were analysed using a gas chromatography-electron ionisation mass spectrometer (GC-EI-MS), referred to as the Entech system (see section 2.2.5 for full description).

To identify the more 'exotic' and so less abundant species, such as the PFCs and minor CFCs, a higher sensitivity mass spectrometry suite, with a proven detection limit of <1 attomole, was used. This is referred to as the AutoSpec and a full description of the set up can be found in section 2.2.6. As part of the analysis of the 2015 campaign, samples were evaluated using two different GC columns to extend the range of detectable species and aid separation of several isomers, such as CFC-114 and -114a. An example of the MS method used on the AutoSpec can be found in section 2.2.6.3.

A number of species were analysed on both GC-MS systems and on both GC columns during the 2015 campaign to assess comparability of the resulting data sets. When available, AutoSpec data was prioritised over Entech system data due to its lower detection limits, higher mass resolution and better precision.

A full list of halocarbon compounds analysed during the Taiwan campaigns can be found in Tables 4.3a-e along with which campaigns, instruments and columns were used and the corresponding average precisions. The majority of major halocarbons were calibrated on a NOAA scale (see section 2.2.6.4) but several of the more minor compounds used in-house UEA calibrations instead. For some compounds, the calibrations are still considered estimates and others are awaiting full calibration and, as such are only relative to the standard at present (this information can also be found in Tables 4.3a-e). In the results section of this chapter, those halocarbons without confirmed calibrations are calculated relative to the standard and so will not be intensely interpreted. However, it should be noted that the data for these compounds will be made available for future investigations should the relevant calibration scales be developed.

4.8 NAME Analysis

Backward trajectories of the air masses sampled were estimated using the UK Met. Office Numerical Atmospheric Modelling Environment (NAME v4). This is a Lagrangian dispersion model and for each sample batches of 60,000 inert particles were released from the corresponding measurement site. The model then calculated the trajectories backwards from the site, recording those particles within an altitude of 0-100m every 15 minutes. Each trajectory was started throughout a 3-hour period that encompassed the actual sampling time and continued for 12 days. A full description of the NAME model and its set up for this analysis can be found in section 2.3.

Table 4.3a: Overview of the CFCs and halons measured during the 2013, 2014 and 2015 campaigns including the average precisions and ions used in analysis.

Compound		Calibration Scale	Taiwan Campaign										Ions Measured		
			2013			2014			2015						
			Entech	AutoSpec	Average	Entech	AutoSpec	Average	Entech	AutoSpec		Average			
Group	Name		✓	✓	Precision (%)	✓	✓	Precision (%)	✓	GasPro	AlPlot	Precision (%)	1	2	3
CFCs	11	NOAA	✓		1.66	✓		1.6	✓	✓	✓	1.84	101	103	
	12	NOAA	✓		1.66	✓		0.63	✓		✓	1.24	101	103	
	13	UEA		✓	1.87			-			✓	1.11	85	87	
	112	NOAA			-	✓		-	✓			-	101	103	
	113	NOAA	✓	✓	0.83	✓	✓	2.25	✓	✓	✓	-	101	103	117
	113a	UEA		✓	1.91	✓	✓	4.63			✓	6.15	103	117	
	114	UEA			-			-			✓	1.48	85	87	135
	114a	UEA			-			-			✓	1.8	85	87	135
	115	UEA	✓	✓	1.82	✓	✓	0.98	✓	✓	✓	2.36	85	87	
Halons	1211	NOAA	✓	✓	1.09	✓		1.5	✓		✓	1.47	85	129	131
	1202	UEA		✓	4.16		✓	3.49			✓	2.24	129	131	
	1301	NOAA	✓		1.44	✓		1.23	✓		✓	2.71	69	129	131
	2402	UEA	✓		3.08	✓	✓	3.11	✓		✓	10.5	129	179	181

Table 4.3b: Overview of the HCFCs and chlorocarbons measured during the 2013, 2014 and 2015 campaigns including the average precisions and ions used in analysis.

Compound		Calibration Scale	Taiwan Campaign									Ions Measured		
			2013			2014			2015					
			Entech	AutoSpec	Average Precision (%)	Entech	AutoSpec	Average Precision (%)	Entech	AutoSpec		Average Precision (%)			
Group	Name		✓	✓		✓	✓		✓	GasPro	AlPlot		1	2	3
HCFCs	21	No Scale	✓		-	✓		-	✓			-	67	102	
	22	NOAA	✓		3.1	✓	✓	1.44	✓	✓		0.75	67		
	31	No Scale			-		✓	-		✓		-	68	70	
	123	Estimate			-		✓	-		✓		-	133		
	124	No Scale			-	✓	✓	-	✓	✓		-	67		
	133a	UEA	✓		11.7	✓	✓	1.34	✓	✓		2.48	118	120	
	141b	NOAA	✓		2.83	✓		3.85	✓	✓		3.46	81	101	103
	142b	NOAA	✓		2.99	✓		1.07	✓	✓		1.38	65		
	225cb	No Scale		✓	-		✓	-				-	167		
Chloro-carbons	CCl_4	NOAA	✓		1.83	✓		2.05	✓		✓	1.82	117	119	
	CH_3CCl_3	NOAA	✓		0.72	✓		0.82	✓			4.14	97	117	
	Halothane	UEA			-		✓	0.86		✓		1.79	196	198	
	Isoflurane	No Scale		✓	-		✓	-		✓		-	115	149	
	C_3H_7Cl	No Scale		✓	-		✓	-		✓		-	78	80	
	C_2H_3Cl	No Scale		✓	-		✓	-		✓		-	62	64	
	C_2F_3Cl	No Scale		✓	-	✓	✓	-				-	116	118	

Table 4.3c: Overview of the chlorinated and brominated VSLSs and methyl halides measured during the 2013, 2014 and 2015 campaigns including the average precisions and ions used in analysis.

Compound		Calibration Scale	Taiwan Campaign									Ions Measured		
			2013			2014			2015					
			Entech	AutoSpec	Average Precision (%)	Entech	AutoSpec	Average Precision (%)	Entech	AutoSpec		Average Precision (%)			
Group	Name		✓	✓		✓	✓		✓	GasPro	AlPlot		1	2	3
VSLS-Cl	PCE	NOAA	✓		2.21	✓		2.83	✓			7.36	129	166	
	DCE	UEA		✓	2.77	✓	✓	3.13	✓	✓		1.67	62	64	
	CH_2Cl_2	NOAA	✓	✓	2.04	✓	✓	2.41	✓	✓		1.17	83	84	
	Chloroform	No Scale	✓		6.06	✓		9.84	✓	✓		2.73	83	117	119
	C_2H_5Cl	UEA	✓	✓		✓	✓		✓	✓			64	66	
	CHClCHCl	No Scale		✓	-		✓	-		✓		-	96	98	
	CH_2CCl_2	No Scale		✓	-		✓	-		✓		-	96	98	
VSLS-Br	CH_2Br_2	NOAA	✓		-	✓		-	✓			-	174		
	Bromoform	NOAA	✓		16.19	✓		13.4	✓			9.58	173		
	$CHClBr_2$	NOAA			-	✓		-				-	127	129	
	C_2H_5Br	UEA		✓	-		✓	-		✓		-	108	110	
	CH_2ClBr	NOAA			-		✓	-				-	128	130	
Methyl Halides	CH_3Cl	NOAA	✓	✓	0.87	✓		1.31	✓	✓		4.66	49	50	51
	CH_3Br	NOAA	✓	✓	2.20	✓	✓	2.69	✓	✓		4.36	94	96	
	CH_3I	NOAA	✓		1.81	✓		35.73	✓			4.34	142		

Table 4.3d: Overview of the HFCs measured during the 2013, 2014 and 2015 campaigns including the average precisions and ions used in analysis.

Compound		Calibration Scale	Taiwan Campaign										Ions Measured		
			2013			2014			2015						
			Entech	AutoSpec	Average Precision (%)	Entech	AutoSpec	Average Precision (%)	Entech	AutoSpec		Average Precision (%)			
Group	Name		✓	✓		✓	✓		✓	GasPro	AlPlot		1	2	3
HFCs	23	UEA	✓	✓	7.28	✓	✓	5.12		✓		2.71	51	69	
	32	No Scale	✓	✓	-	✓	✓	-	✓	✓		-	51		
	125	Estimate	✓		3.07	✓		3.12	✓	✓		2.11	101		
	134a	NOAA	✓		2.11	✓	✓	1.98	✓		✓	1.91	83	102	
	143a	Estimate	✓		1.85	✓		2.58	✓	✓		3.81	65	69	
	152a	NOAA	✓		0.73	✓		3.66	✓			1.97	65		
	227ea	UEA	✓		3.6	✓		3.5	✓	✓		1.19	69	101	151
	245fa	Estimate	✓		3.11	✓		2.84	✓			3.23	115		
	365mfc	Estimate	✓		2.73	✓		16.6	✓	✓		8.10	133		

Table 4.3e: Overview of the PFCs and other species measured during the 2013, 2014 and 2015 campaigns including the average precisions and ions used in analysis

Compound		Calibration Scale	Taiwan Campaign									Ions Measured		
			2013			2014			2015					
			Entech	AutoSpec	Average Precision (%)	Entech	AutoSpec	Average Precision (%)	Entech	AutoSpec		Average Precision (%)			
Group	Name		✓	✓		✓	✓		✓	GasPro	AlPlot		1	2	3
PFCs	C_2F_4	NOAA	✓		-	✓		-				-	81	100	
	C_2F_6	UEA		✓	1.77		✓	2.15		✓	✓	0.76	119		
	C_3F_8	UEA		✓	3.11		✓	1.71	✓	✓	✓	1.91	169		
	C_4F_{10}	UEA			-		✓	3.04	✓		✓	1.69	119		
	c-C_4F_8	UEA	✓		2.61	✓	✓	0.93	✓		✓	1.7	100	131	
	C_5F_{12}	UEA		✓	6.06		✓	3.82	✓		✓	3.25	169		
	c-C_5F_{10}	No Scale			-			-			✓	3.22	131		
	C_6F_{14}	UEA		✓	4.12			-	✓		✓	5.31	169	219	
	iso-C_6F_{14}	No Scale			-			-			✓	3.67	169	219	
	C_7F_{16}	UEA		✓	4.38		✓	4.75	✓		✓	3.78	169	219	
	SF_6	No Scale		✓	0.7		✓	0.49		✓	✓	1.91	89	127	
Other	COS	NOAA	✓	✓	1.29	✓	✓	1.24	✓	✓		1.75	60	62	
	SF_5CF_3	UEA		✓	1.85		✓	2.84		✓	✓	3.94	89		
	C_3H_7Br	No Scale		✓	-		✓	-				-	122	124	
	Benzene	Estimate	✓		-	✓		-	✓			-	78		

4.9 Results

4.9.1 NAME Analysis

Matt Ashfold (University of Nottingham) ran the NAME model for the full sampling periods of each of the three Taiwanese campaigns. Back trajectories were calculated starting over a three-hour period around the sampling time and continuing for 12 days. The following analysis utilises these trajectories and copies can be found in Appendix 4.1-4.3. The date of each trajectory is noted at the top of each plot along with the mid-point time (in UTC) of the trajectory start window.

Each trajectory was assessed to consider which countries were passed over, or were closest, and so could have contributed emissions that were then transported to the sampling site. Figure 4.12 indicates the approximate areas on each trajectory associated with different potential source regions used for this assessment. Table 4.2 includes the possible major and minor source locations for the air masses sampled during each campaign, assessed from analysis of the NAME trajectories as follows:

Major being where the **particle density** in the model **is high (>10^{-7} g s m^{-3})** and over the **majority (>70%)** of a previously defined **country-associated area,**

Minor being where a **significant proportion (50-70%) of a country-associated area** is covered by a **relatively high density of particles (10^{-7} – 10^{-6} g s m^{-3}).**

Emissions from major potential source locations would be expected to dominate the air masses sampled and spikes in mixing ratios for specific compounds to reflect this would be anticipated. Identification of possible minor source locations were intended to aid in the explanation of enhanced mixing ratios that are not clearly associated with emissions from the major source location (given comparison with previous studies and literature).

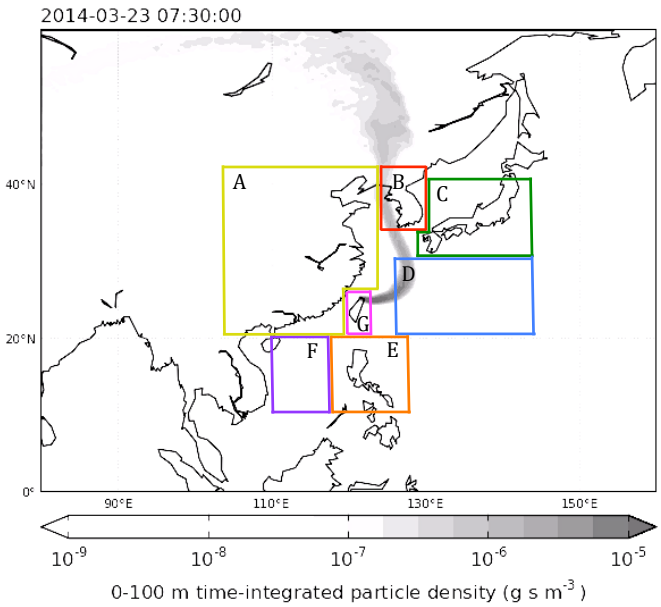

Figure 4.12: Potential source regions established from NAME trajectories. Air masses were determined as possibly originating from A) China, B) Korea, C) Japan, D) Pacific Ocean, E) Philippines, F) South China Sea or G) Taiwan.

For some trajectories, one country was clearly the major influence (see Figure 4.13a) whereas for others there were several potential major and minor sources (see Figure 4.13b). Potential major sources were selected for all samples, however not all saw minor influences as well. A maximum of three joint-major or three joint-minor countries were chosen. If more than three met the criteria set out above, those with the highest particle densities were selected as this would suggest their contribution to the modelled air mass would be proportionally larger.

Overviews and examples for each campaign can be found below, however further comparisons with detected mixing ratios will be considered later in the Results section.

4.9.1.1 2013

In the 2013 campaign, the largest range of potential sources was seen (see Appendix 4.1) with 7 distinct areas contributing to the air masses sampled. Figure 4.14a shows the percentage frequency each area was found to possibly be a major influence to the sampled air mass. Figure 4.14b indicates the percentage frequency of potential minor influences.

In terms of major source locations, emissions from China and Korea appear, from this modelling, to be the most heavily sampled (Figures 4.15 and 4.16) as they made up 37% and 24% of the trajectories respectively. With both being developing countries that only completed the CFC and Halon phase out three years previously, samples collected on these days would be expected to be predominantly HCFC based. Japan and Taiwan (Figures 4.17 and 4.18), on the other hand, both only contribute 5% of the potential major source locations for this campaign, but these would be expected to contain a larger proportion of HFCs as they are further into their HCFC phase-out schedules. 19% of sample days showed major oceanic influences (Figure 4.19) from the Pacific and, as such, closer to background levels from similar latitudes (e.g. Mauna Loa, Hawaii [NOAA] and Ragged Point, Barbados [AGAGE]) would be anticipated for most anthropogenic compounds in these cases.

The assessment of minor source locations for the 2013 campaign indicated that emissions from Taiwan and Korea (28% and 24% respectively) were likely to be sampled alongside those from major sources most frequently. This suggests that regional Taiwanese sources may impact mixing ratios more often than originally anticipated and so comparisons with local wind data were required to ensure this was attributed where appropriate. China, Japan and the Pacific Ocean also see similar percentage frequencies (15%, 13% and 13% respectively) as minor potential influences but, as previously mentioned, there are differences between their expected emissions and so impact on observed mixing ratios.

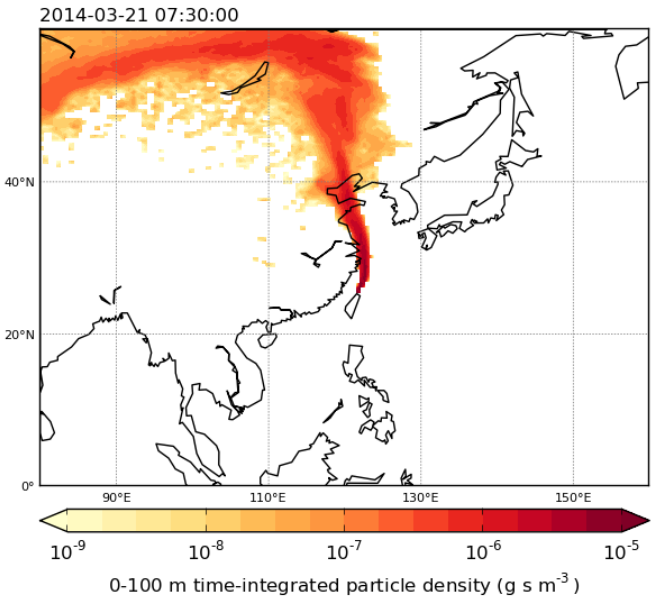

Figure 4.13a: NAME trajectory from the 21st March 2013 suggesting China as a potential major emission source.

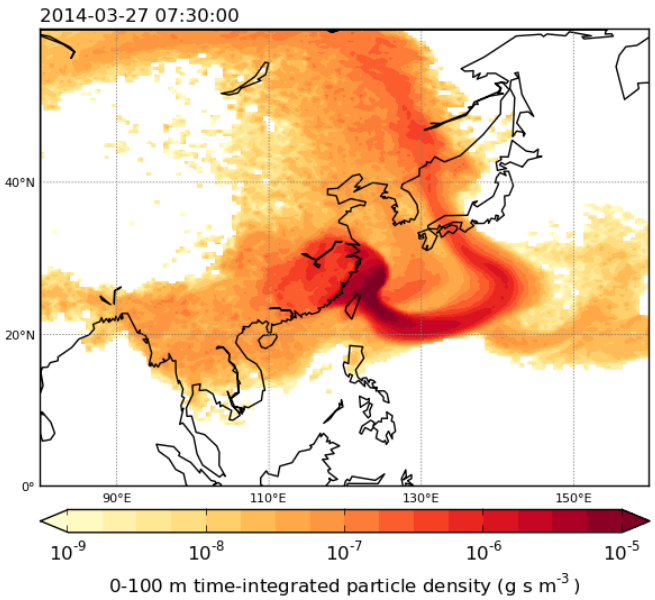

Figure 4.13b: NAME trajectory from the 27th March 2014 suggesting China, Taiwan, Japan and the Pacific Ocean as potential emission sources.

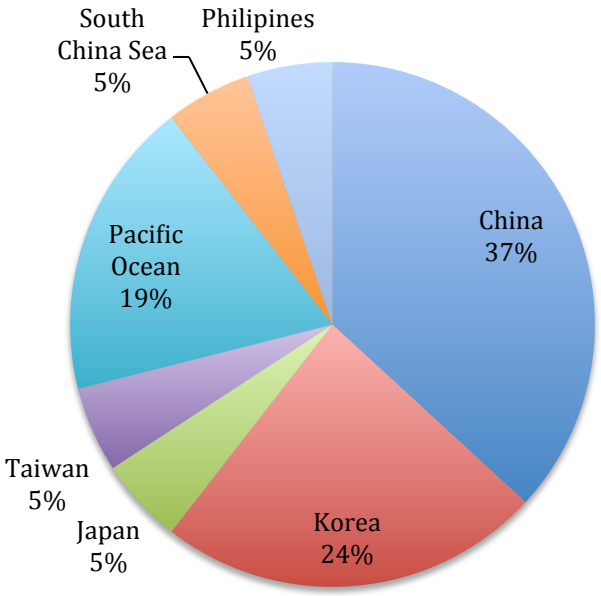

Figure 4.14a: Frequency of potential major emissions contributions from different regions using NAME backwards trajectories for the 2013 Taiwan Campaign.

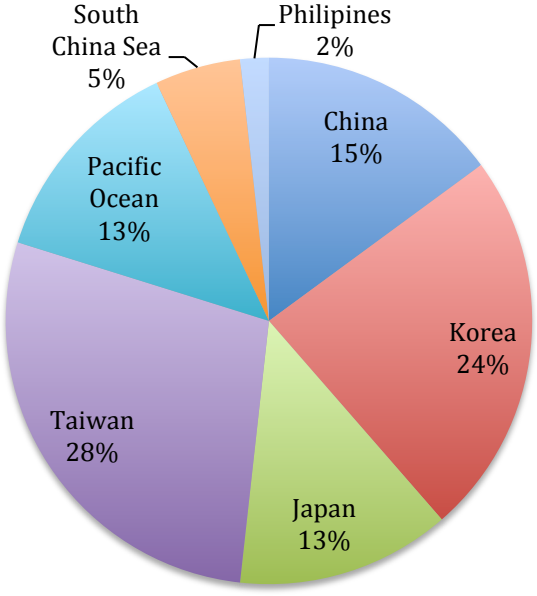

Figure 4.14b: Frequency of potential minor emissions contributions from different regions using NAME backwards trajectories for the 2013 Taiwan Campaign.

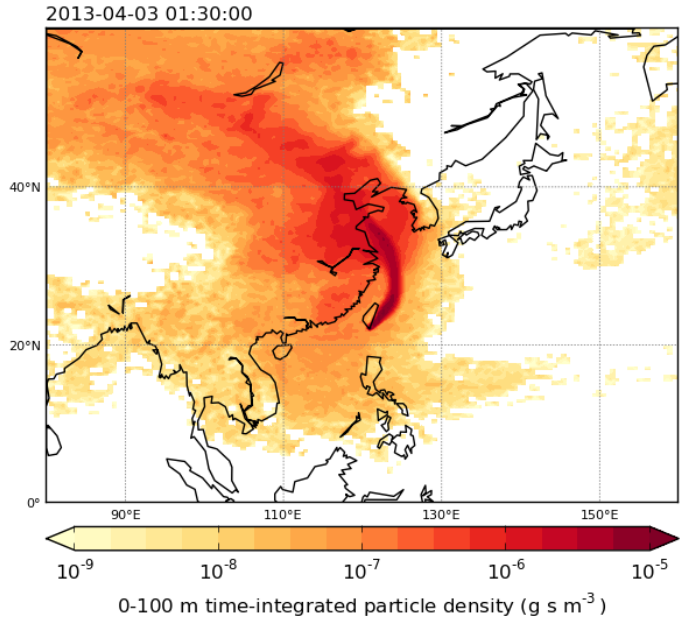

Figure 4.15: NAME back trajectory from the 2013 Taiwan campaign indicating potential emissions from China.

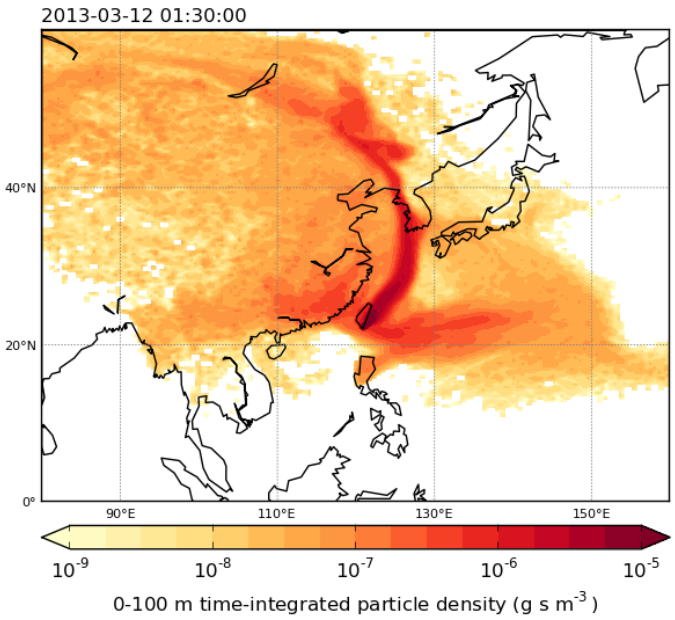

Figure 4.16: NAME back trajectory from the 2013 Taiwan campaign indicating potential emissions from Korea.

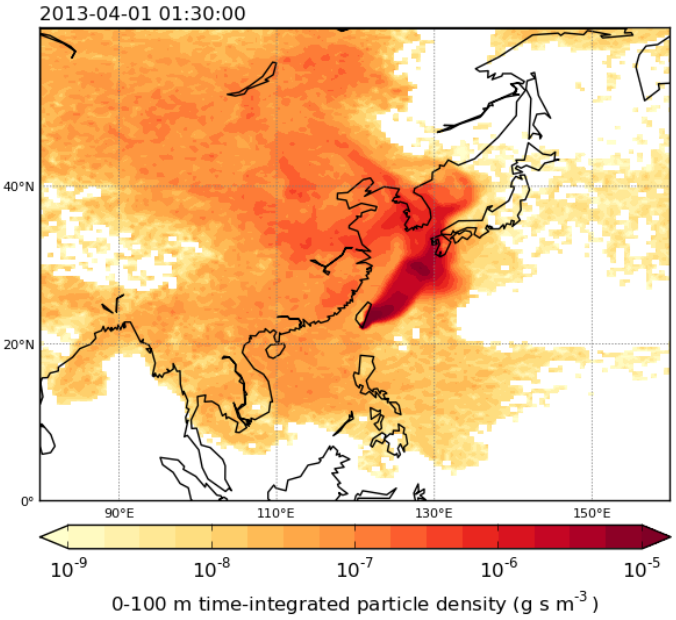

Figure 4.17: NAME back trajectory from the 2013 Taiwan campaign indicating potential emissions from Japan.

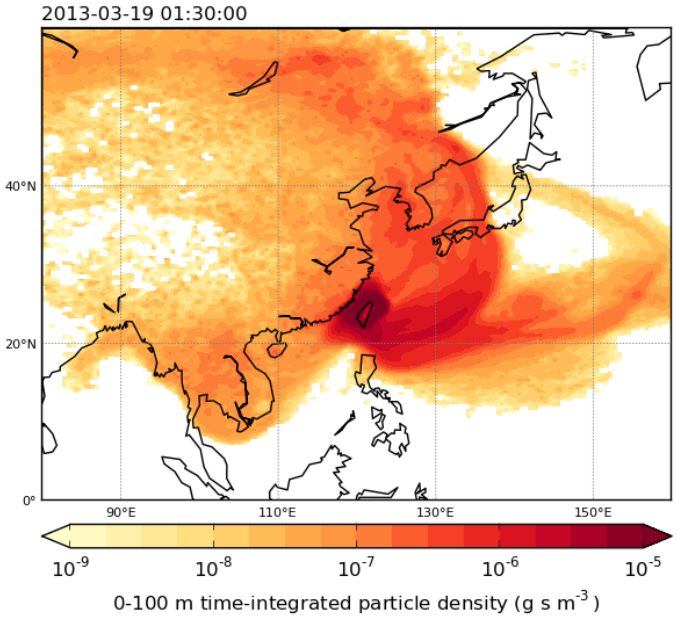

Figure 4.18: NAME back trajectory from the 2013 Taiwan campaign indicating potential emissions from Taiwan.

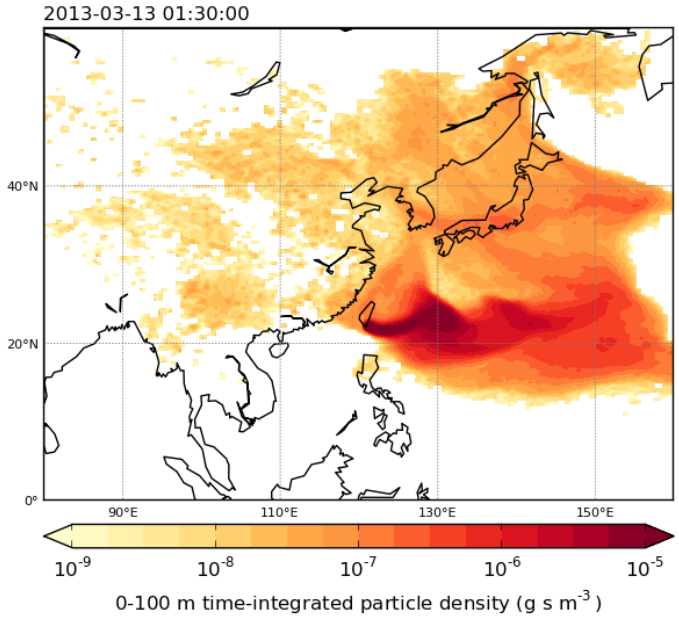

Figure 4.19: NAME back trajectory from the 2013 Taiwan campaign indicating potential emissions from the Pacific Ocean.

4.9.1.2 2014

In 2014 (see Appendix 4.2), only 6 distinct areas were found for both major or minor possible source locations, with no trajectories indicating emissions from the South China Sea during this campaign. The percentage frequency these areas were potentially sampled can be seen in Figures 4.20a (major) and 4.20b (minor). Chinese emissions (see Figure 4.12) contributed to just over half of the days analysed, whereas Korea and Taiwan were all considerably less (17% and 20% respectively). This means, similar to 2013, higher HCFC emissions would be expected in the majority of samples. However, the potential contribution of Taiwanese emissions (Figure 4.21) is comparatively higher in this campaign, most likely due to the difference in the sampling site and associated wind patterns (i.e. no katabatic winds). This could result in particularly high levels of some halocarbons used in Taiwanese industry over a number of days as they would not have undergone dilution during transport unlike emissions from areas further away. Days with oceanic influence were seen again (8%) so background levels were also expected.

Whilst Japan contributed as a major potential source for only 3% of the 2014 campaign, it dominates the minor locations with a frequency of 42%. This suggests that mixing ratios, particularly those of the HFCs, may see enhancement due to Japanese emissions. Korea also makes up a significant proportion (33%) of the minor possible source locations and China contributes another 11%. This indicates, along with frequencies from the major possible sources, that most of days sampled would mainly be influenced by air masses travelling from China and Korea.

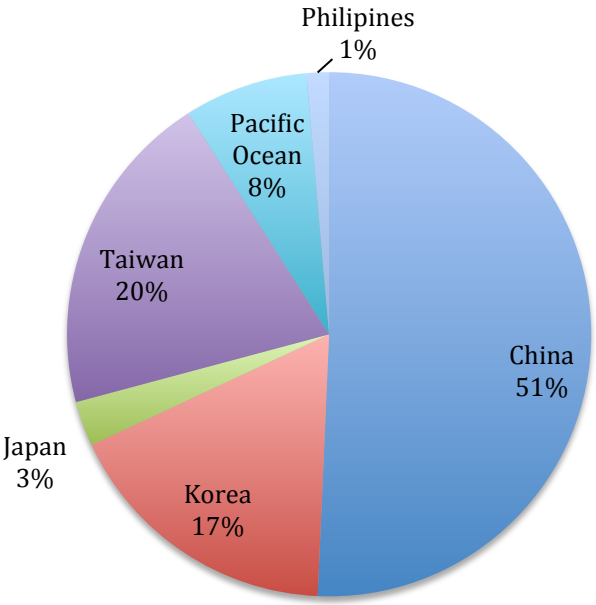

Figure 4.20a: Frequency of potential major emissions contributions from different regions using NAME backwards trajectories for the 2014 Taiwan Campaign.

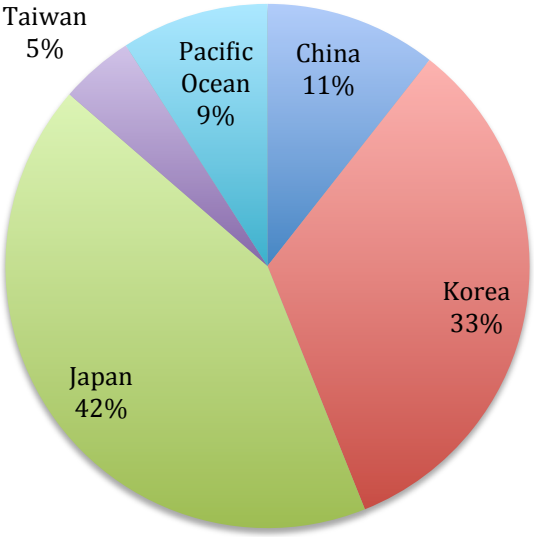

Figure 4.20b: Frequency of potential minor emissions contributions from different regions using NAME backwards trajectories for the 2014 Taiwan Campaign.

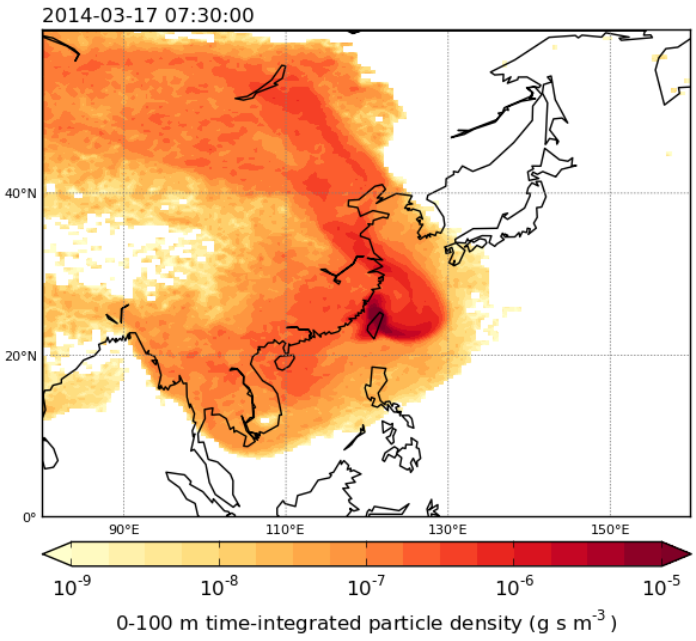

Figure 4.21: NAME back trajectory from the 2014 Taiwan campaign indicating potential emissions from Taiwan.

4.9.1.3 2015

Finally, in 2015 (see Appendix 4.3), the same 6 distinct areas were seen as in 2014 and Figures 4.22a and 4.22b show the percentage frequency breakdown for major and minor potential source locations respectively. Korea (see Figure 4.23) appears to have been a major contributor of emissions in 32% of the days whereas China, Taiwan, Japan and the Pacific Ocean all were assessed at similar frequencies (between 14-18%) for this campaign. These back trajectories suggest enhanced levels of HCFCs and HFCs are to be anticipated, as are background levels, given a number of oceanic-influenced days (18%). Regional major contributions from Taiwan (15%) are lower than in 2014 so impact is less likely but still needs to be assessed in comparison with local wind data.

Minor potential source locations were again mainly Japanese (39%) and Korean (25%), indicating overall that emissions from these areas may be more apparent from observed mixing ratios than those of China or Taiwan.

Whilst NAME analysis is very useful in estimating emission sources of long-range halocarbon transport, the resolution is not sufficient for very local air movement and, as previously mentioned, local influences still need to be considered.

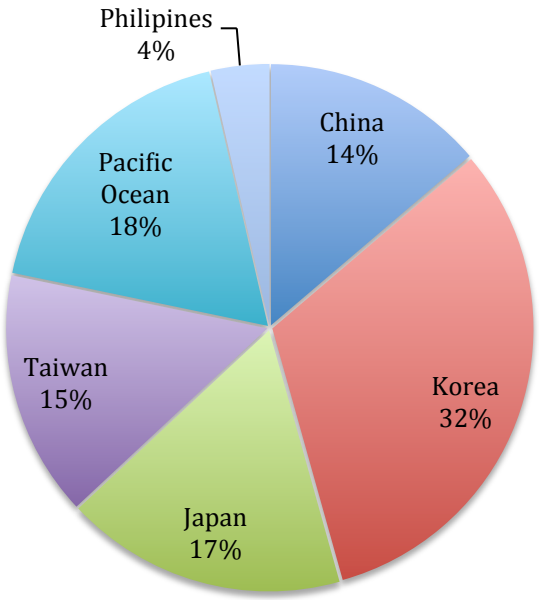

Figure 4.22a: Frequency of potential major emissions contributions from different regions using NAME backwards trajectories for the 2015 Taiwan Campaign.

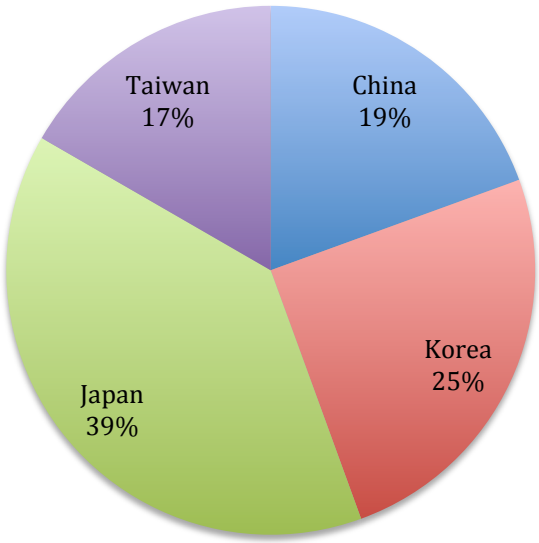

Figure 4.22b: Frequency of potential minor emissions contributions from different regions using NAME backwards trajectories for the 2015 Taiwan Campaign.

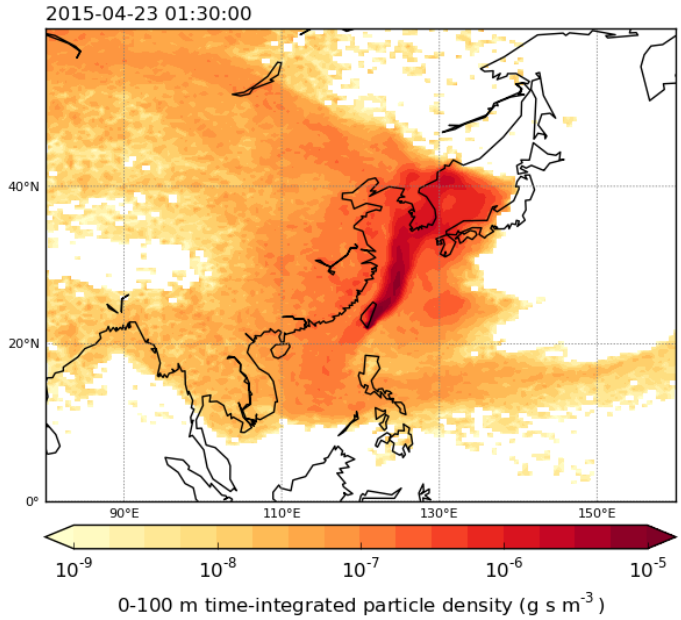

Figure 4.23: NAME back trajectory from the 2015 Taiwan campaign indicating potential emissions from Korea.

4.9.2 Local Wind Data Analysis

For each campaign, local meteorological data was collected throughout the sampling period, including wind speed and wind direction, and an overview can be found in Table 4.2. The meteorological data was collected hourly and the results in the table have been time-averaged in an effort to more accurately reflect conditions at the time of sampling. Similar to the NAME analysis, a brief summary for each campaign can be found below and more specific comparisons to detected levels will be considered later.

This data was important in assessing influence of potential local emissions and possible impact of atmospheric boundary layer dynamics that would not be resolved through the NAME modelling. Whilst the results of NAME suggest the air mass likely to have been sampled, fluctuations and turbulence associated with the instability of the boundary during the daytime may have resulted in other air masses being sampled. As such, wind direction and speed, particularly in association with influence of katabatic winds from the Central Mountain range, was considered as well as NAME modelling. Temperature profiles, which could have been used to assess boundary layer height and better constrain potential impact were unfortunately not available during the three campaign.

In 2013, local winds were mainly detected from the NNW or the ENE. Due to the coastal sampling site, those days with winds coming from a westerly direction are not likely to have picked up local emissions. This means the influences suggested by the NAME trajectories on these should be the main sources of the halocarbon levels detected.

Those days with winds coming from an easterly direction would have travelled over populated areas and so could have contributions from local emissions. However, since this site is at the southern tip of the island and away from the major industrial sites, these emissions are most likely more residential in origin making them minimal in both quantity and variety. Also, as previously mentioned, this area does experience katabatic winds that bring air from the eastern side of the island down across the mountains to the west coast. Many of the NAME trajectories show the air masses travelling from the eastern side (see Figure 4.24) and so this implies they undergo this transport across the mountains. In turn, this again means that the long-range emissions sources suggested by the trajectories are still likely to be the major influences in the abundances detected on these days. Wind speeds were consistently detected above 2m/s which also suggests influence from very local sources should be minimal. The strongest winds were found to be from the ENE, consistent with the katabatic winds, reaching over 15m/s on two occasions.

For the 2014 campaign, the majority of local winds were detected from the ESE. With the sampling site at the tip of the northern coastline, this is not unexpected and will still be largely due to more northerly winds swinging around as they meet the land. Although the northern site is much closer to some of the major Taiwanese industrial parks, the sample collection point was still relatively remote; the nearest populated areas were further away than at the southern site so influence from local emissions most days should have been minimal. As such the NAME trajectories for these days should indicate the major emissions sources. However, 4 days have local winds detected as from the WSW and Taiwanese industry is mainly situated to the west and south of the sampling site. For samples collected on these days, there may be notable enhancements in halocarbons commonly used in Taiwan, such as the PFCs and HFCs. The levels detected are also likely to be larger than those seen from other areas, due to the lack of dilution during transport, since they are of local origin. Wind speeds during this campaign are lower than in 2013, with only 14 days being detected at over 2m/s and only three days reaching over 8m/s. This could result in local emissions having more of impact on calculated halocarbon mixing ratios for some days.

Due to taking place in the same location, it is unsurprising that the 2015 campaign saw very similar conditions meteorologically to the 2013 campaign. The majority of local winds were detected from the ENE interspersed with a few days of more westerly winds. Again, these winds from the west are not likely to be influenced by local emissions since they are coming from over the ocean. The easterly winds can also be put down to the katabatic wind conditions, bringing air down from over the mountains along with the NAME trajectories showing air mass movement down the east coast (Figure 4.25). This again suggests the long-range emissions sources from the modelling are likely to be the major contributors to the abundances seen on these days. As for the wind speed detected, all but one day saw speeds over 2m/s with two days seeing speeds over 14m/s, in-line with the katabatic winds.

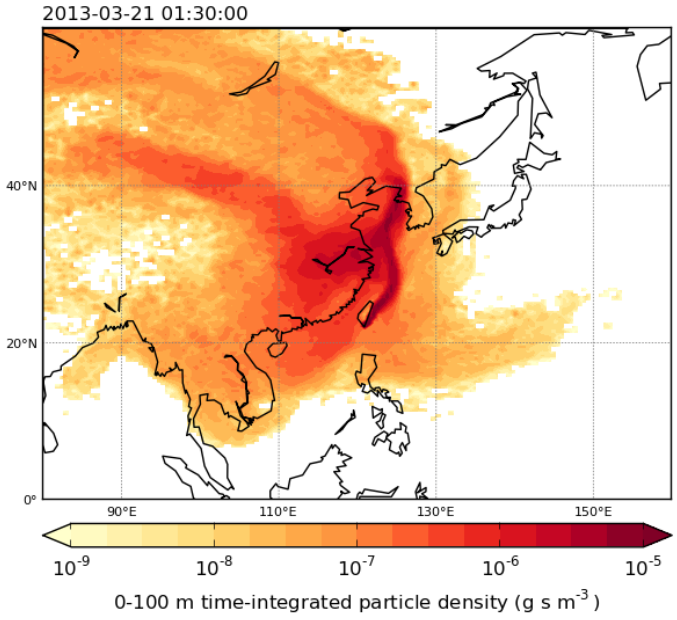

Figure 4.24: NAME back trajectory from the 2013 Taiwan campaign showing air mass movement along the east coast of the island.

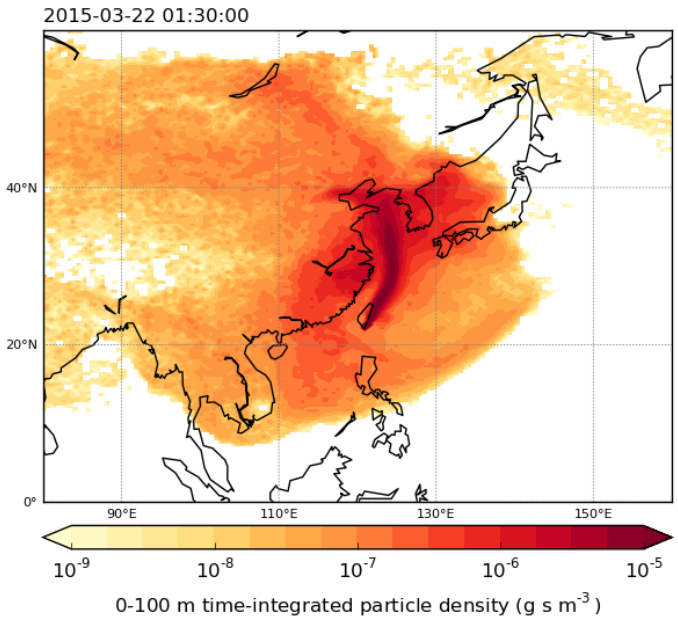

Figure 4.25: NAME back trajectory from the 2015 Taiwan campaign showing air mass movement along the east coast of the island

In conclusion, for the campaigns at the southern site in 2013 and 2015, the impact of local emissions is expected to be minimal and the areas indicated by the NAME back trajectories are likely to be the major sources of halocarbons detected. For the 2014 campaign at the northern site, the NAME back trajectories are expected to denote the potential origins of identified halocarbon mixing ratios. However, several days see marked enhancements in a number of compounds due to local emissions.

4.9.3 Overview of Halocarbon Mixing Ratios

This section will give an overview for all of the major and a number of more minor halocarbons, organised by compound group, for all three campaigns. Several compounds will be covered in more detail in further case studies.

In total, 69 halocarbon compounds were measured over the three Taiwan campaigns; 56 in 2013, 62 in both 2014 and 2015. Appendix 4.4a-e gives a summary of these compounds for each campaign, and shows the median and range of mixing ratios in parts per trillion (ppt) detected for each. The median was calculated for each species, instead of the mean, in an attempt to minimise bias by significant spikes in mixing ratios likely caused by transported emissions. Compounds highlighted in yellow are those currently without calibration scales and, although the relative abundances of these species will not change so inter-species comparisons can be carried out, a full assessment is not possible at this time. Appendix 4.5a-c utilises the mixing ratio data to give a percentage value of enhancement above background mixing ratios as this allows for the direct comparison of different species.

Since not all of the compounds analysed have background data available presently, these tables are reduced to 41 calibrated species and again shows the median and range for each campaign. The background mixing ratios are coloured coded by origin and the uncertainties for these can be found in Appendix 4.6.

Backgrounds are primarily taken from the NOAA Mauna Loa Observatory in Hawaii (19.536°N, 155.576°W), during March of each campaign year, due to its similar latitude to Taiwan. This is a remote station and so sees very minimal influences from anthropogenic emissions unlike Taiwan, which is located in a major source region. As such, these mixing ratios can act as baseline values and observed data from Taiwan would not generally be expected to be detected beneath them. However, given the proximity to the southern hemisphere and the large hemispheric gradients for many halocarbon species, where changes in average mixing ratios observed in the northern hemisphere are only detected in the southern hemisphere a year later, lower than background air masses may reach the Taiwanese sampling sites.

Similarly, AGAGE backgrounds are taken from Ragged Point, Barbados (13.165°N, 59.432°W), another remote station closest in latitude, again for March of the campaign year. AGAGE background mixing ratios are used when NOAA data is not available for a specific species. NOAA backgrounds are prioritised as UEA utilises a NOAA calibration. Further compounds use values extrapolated from literature or the Air Archive from Cape Grim, Tasmania (40.683°S, 144.690°E) and are referenced accordingly. The calculations for the extrapolations assume that previously detected growth rates stayed the same, which may not be the case for all species. Those backgrounds extrapolated from Cape Grim are likely to be lower than observed mixing ratios due to the southern hemispheric location of this station.

Whilst the sources of this background data are robust, one of the limitations faced by this study was the unavailability of robust background mixing ratios for the East Asian region. For the long-lived species, this is less problematic however short-lived species do exhibit latitudinal variation and as such regional backgrounds can vary. Data was requested from the AGAGE stations located in Gosan, Korea and Hateruma Island, Japan in an attempt to constrain a more regionally accurate background however, no response was forthcoming from this request. Interpolating or extrapolating backgrounds for the area was also hindered by both the lack of regionally station data and the lack of species data for a number of compounds of interest. As such, the decision was made to utilise background data from the sources described above which generally reflect remote northern hemispheric (aside from Cape Grim) mixing ratios in the lower latitudes, closest to Taiwan.

Correlations between species are also considered, and will be discussed where relevant, as high levels of correlation indicate combined emissions or source locations and so are useful in assessing interspecies relationships. Pearson correlation coefficients were calculated utilising the equation 4.1.

$$r = \frac{\sum (x - \bar{x})(y - \bar{y})}{\sqrt{\sum (x - \bar{x})^2 \sum (y - \bar{y})^2}}$$ Equation 4.1

Where ***r*** is the Pearson correlation coefficient, ***x*** is the mixing ratio of one halocarbon species and ***y*** is the mixing ratio of a second halocarbon species. The coefficient quantifies the linear correlation between the two variables and is a built-in function of Excel which aided data processing. For this study species were separated as having some, good or excellent correlation using the following criteria:

Some correlation = Pearson coefficient **between 0.5 and 0.75**

Good correlation = Pearson coefficient **between 0.75 and 0.95**

Excellent correlation = Pearson coefficient **above 0.95**

For each year, Table 4.4a-c lists those species determined to have good correlation and Table 4.5 lists those with excellent correlation. Good correlation suggests the potential of co-location of species sources, whereas excellent correlation can be indicative of co-emission from the same source.

Table 4.4a: Halocarbon compounds with good interspecies correlation during the 2013 Taiwan campaign, as assessed by Pearson correlation coefficients.

Species found to have good (0.75-0.95) Pearson correlation coefficients during 2013						
CFC-113	CFC-113a	Halon 1202	HCFC-133a	HCFC-142b	HFC-227ea	
	HFC-23	DCM	PCE			
CFC-113a	CFC-113	Halon 1202	HCFC-133a	HCFC-141b	HCFC-142b	
	HFC-227ea	DCM	PCE	CH_3Cl	COS	
Halon 1211	HCFC-225cb	HFC-134a	HFC-143a	HFC-125	C_2F_6	
	C_3F_8	c-C_4F_8	SF_6	Bromoform		
Halon 1202	CFC-113	CFC-113a	HCFC-133a	HCFC-141b	HCFC-142b	
	HFC-227ea	HFC-23	DCM	PCE		
HCFC-133a	CFC-113	CFC-113a	Halon 1202	HCFC-142b	HFC-227ea	
	HFC-23	HFC-365mfc	DCM	PCE		
HCFC-141b	CFC-113a	Halon 1202	HFC-125	DCM	PCE	CH_3Cl
HCFC-142b	CFC-113	CFC-113a	Halon 1202	HCFC-133a	HFC-227ea	
	DCM	PCE	COS			
HFC-134a	Halon 1211	HCFC-225cb	C_2F_6	C_3F_8	c-C_4F_8	
	SF_6	CH_3I				
HFC-143a	Halon 1211	HFC-125	DCE			
HFC-227ea	CFC-113	CFC-113a	Halon 1202	HCFC-133a	HCFC-142b	
	DCM	CH_3Cl				
HFC-23	CFC-113	Halon 1202	HCFC-133a	HFC-227ea	HFC-365mfc	
	DCM	CH_3Cl	COS			
HFC-125	Halon 1211	HCFC-141b	HFC-143a	HFC-32	cC4F8	
	DCM	CH_3I	CO			
HFC-365mfc	HCFC-133a	HFC-23	PCE			
C_2F_6	Halon 1211	HFC-134a	c-C_4F_8	SF_6	CH_3I	
C_3F_8	Halon 1211	HFC-134a				
c-C_4F_8	Halon 1211	HFC-134a	HFC-125	C_2F_6	SF_6	CH_3I
SF_6	Halon 1211	HCFC-225cb	HFC-134a	C_2F_6	c-C_4F_8	
	Bromoform	CH_3I				
DCM	CFC-113	CFC-113a	Halon 1202	HCFC-133a	HCFC-141b	
	HCFC-142b	HFC-227ea	HFC-23	HFC-125	PCE	
PCE	CFC-113	CFC-113a	Halon 1202	HCFC-133a	HCFC-141b	
	HCFC-142b	HCFC-21	DCM	CH_3Cl	COS	
DCE	HFC-143a	C_2H_5Cl				
C_2H_5Cl	DCE					
Bromoform	Halon 1211	SF_6				
CH_3Cl	CFC-113a	HCFC-141b	HFC-227ea	HFC-23	PCE	COS
CH_3I	HFC-134a	C_2F_6	c-C_4F_8	SF_6		
COS	CFC-113a	HCFC-142b	HCFC-21	HFC-23	PCE	CH_3Cl
CO	HFC-125					

Table 4.4b: Halocarbon compounds with good interspecies correlation during the 2014 Taiwan campaign, as assessed by Pearson correlation coefficients.

Species found to have good (0.75-0.95) Pearson correlation coefficients during 2014						
CFC-11	Chloroform	C_2H_5Cl	CCl_4	CH_3Cl	COS	
CFC-113	HCFC-133a	HCFC-142b	HFC-23	C_7F_{16}	PCE	Chloroform
	CH_3Cl	COS				
CFC-113a	HCFC-142b	HFC-227ea	HFC-23	C_7F_{16}	PCE	Chloroform
	C_2H_5Cl	CCl_4	CH_3Cl	COS		
Halon 1211	HCFC-22	HFC-134a	HFC-143a			
Halon 1202	HCFC-22	HFC-143a	HFC-125	HFC-152a	C_4F_{10}	C_7F_{16}
	PCE	CCl_4	CH_3Cl	COS		
Halon 1301	HCFC-142b					
HCFC-22	Halon 1211	Halon 1202	HCFC-141b	HFC-134a	HFC-143a	HFC-23
	HFC-125	HFC-152a	C_4F_{10}	C_7F_{16}	DCE	PCE
	Chloroform	CH_3Cl	CH_3Br	COS		
HCFC-133a	CFC-113	HCFC-142b	HFC-227ea	HFC-23	HFC-365mfc	C_7F_{16}
	PCE	Chloroform	CH_3Cl	COS		
HCFC-141b	HCFC-22	HFC-143a	HFC-125	HFC-152a	HFC-245fa	C_2F_6
	C_3F_8	c-C_4F_8				
HCFC-142b	CFC-113	CFC-113a	Halon 1301	HCFC-133a	HFC-23	PCE
	Chloroform	CH_3Cl	COS			
HFC-134a	H1211	HCFC-22	HFC-143a	HFC-125	C_2F_6	c-C_4F_8
	SF_6					
HFC-143a	Halon 1211	Halon 1202	HCFC-22	HCFC-141b	HFC-134a	HFC-125
	C_2F_6	c-C_4F_8	SF_6			
HFC-227ea	CFC-113a	HFC-365mfc	CH_3Cl			
HFC-23	CFC-113	CFC-113a	HCFC-22	HCFC-133a	HCFC-142b	HFC-152a
	C_7F_{16}	PCE	Chloroform	CCl_4	CH_3Cl	COS
HFC-125	Halon 1202	HCFC-22	HCFC-141b	HFC-134a	HFC-143a	HFC-152a
	HFC-245fa	C_2F_6	C_3F_8	c-C_4F_8	C_4F_{10}	C_7F_{16}
	DCM	DCE	CH_3Cl	CH_3Br		
HFC-152a	HCFC-22	HCFC-141b	HFC-125	HFC-23	DCM	DCE
	PCE	CH_3Cl	COS			
HFC-245fa	HCFC-141b	HFC-125	C_2F_6	c-C_4F_8	DCM	DCE

Table 4.4b continued: Halocarbon compounds with good interspecies correlation during the 2014 Taiwan campaign, as assessed by Pearson correlation coefficients.

Species found to have good (0.75-0.95) Pearson correlation coefficients during 2014						
C_2F_6	HCFC-141b DCM	HFC-134a DCE	HFC-143a	HFC-125	HFC-245fa	SF_6
C_3F_8	HCFC-141b	HFC-125	SF_6	DCM	DCE	
c-C_4F_8	HFC-134a	HFC-143a	HFC-125	HFC-245fa		
C_4F_{10}	Halon 1202	HCFC-22	HFC-125	C_7F_{16}	PCE	
C_7F_{16}	CFC-113 C_4F_{10}	CFC-113a	Halon 1202	HCFC-22	HCFC-133a	HFC-125
SF_6	HFC-134a	HFC-143a	C_2F_6	C_3F_8	c-C_4F_8	
DCM	HFC-125	HFC-152a	HFC-245fa	C_2F_6	C_3F_8	c-C_4F_8
DCE	HCFC-22 c-C_4F_8	HFC-125	HFC-152a	HFC-245fa	C_2F_6	C_3F_8
PCE	CFC-113 HFC-23 CCl_4	CFC-113a HFC-152a CH_3Cl	Halon 1202 C_4F_{10} COS	HCFC-22 C_7F_{16}	HCFC-133a Chloroform	HCFC-142b C_2H_5Cl
Chloroform	CFC-11 HFC-23 COS	CFC-113 C_7F_{16}	CFC-113a PCE	HCFC-22 C_2H_5Cl	HCFC-133a CCl_4	HCFC-142b CH_3Cl
C_2H_5Cl	CFC-11 Chloroform	CFC-113a CCl_4	HCFC-133a CH_3Cl	HFC-23 COS	C_7F_{16}	PCE
CCl_4	CFC-11 C2H5Cl	CFC-113a CH_3Cl	Halon 1202 COS	HFC-23	PCE	Chloroform
CH_3Cl	CFC-11 HCFC-142b PCE	CFC-113 HFC-227ea Chloroform	CFC-113a HFC-23 C_2H_5Cl	Halon 1202 HFC-125 CCl_4	HCFC-22 HFC-152a COS	HCFC-133a C_7F_{16}
CH_3Br	HCFC-22	HFC-125				
COS	CFC-11 HCFC-142b C_2H_5Cl	CFC-113 HFC-23 CCl_4	CFC-113a HFC-152a CH_3Cl	Halon 1202 C_7F_{16}	HCFC-22 PCE	HCFC-133a Chloroform

Table 4.4c: Halocarbon compounds with good interspecies correlation during the 2015 Taiwan campaign, as assessed by Pearson correlation coefficients.

Species found to have good (0.75-0.95) Pearson correlation coefficients during 2015						
CFC-113a	CFC-114a PCE	Halon 1202	HCFC-133a	HCFC-142b	HFC-227ea	DCM
CFC-114a	CFC-113a	HCFC-133a	HCFC-142b	PCE		
Halon 1211	HCFC-141b	HFC-134a	HFC-143a	SF_6		
Halon 1202	CFC-113a	HFC-227ea	DCM			
Halon 1301	Chloroform					
HCFC-22	DCE	C2H5Cl				
HCFC-133a	CFC-113a PCE	CFC-114a	HCFC-142b	HCFC-124	HFC-227ea	DCM
HCFC-141b	Halon 1211 Bromoform	HFC-134a	HFC-143a	SF_6	DCE	Chloroform
HCFC-142b	CFC-113a COS	CFC-114a	HCFC-133a	HCFC-124	DCM	PCE
HFC-134a	Halon 1211	HCFC-141b	HFC-143a	SF_6	DCE	
HFC-143a	Halon 1211	HCFC-141b	HFC-134a	SF_6	DCE	
HFC-227ea	CFC-113a	Halon 1202	HCFC-133a	DCM		
HFC-23	CFC-113a	CFC-114a	HCFC-142b	PCE	COS	
C_2F_6	C_3F_8	c-C_4F_8	SF_6			
C_3F_8	C_2F_6	c-C_4F_8	SF_6			
c-C_4F_8	C_2F_6	C_3F_8				
C_6F_{14}	iso-C_6F_{14}					
iso-C_6F_{14}	C_6F_{14}					
C_7F_{16}	DCM	DCE	Chloroform			
SF_6	Halon 1211	HCFC-141b	HFC-134a	HFC-143a	C_2F_6	C_3F_8
DCM	CFC-113a PCE	Halon 1202	HCFC-133a	HCFC-142b	HCFC-227ea	C_7F_{16}
PCE	CFC-113a	CFC-114a	HCFC-133a	HCFC-142b	HFC-23	DCM
DCE	HCFC-22	HCFC-141b	HFC-143a	C_7F_{16}	Chloroform	CH_3Cl
Chloroform	Halon 1301	HCFC-141b	C_7F_{16}	DCE	CCl_4	CH_3Cl
CCl_4	Chloroform	CH_3Cl				
CH_3Cl	DCE	Chloroform	CCl_4			
COS	HCFC-142b					
Bromoform	HCFC-141b					
C_2H_5Cl	HCFC-22					

Table 4.5: Halocarbon compounds with excellent interspecies correlation during the Taiwan campaigns, as assessed by Pearson correlation coefficients.

Species found to have Excellent (0.95+) Pearson Correlation Coefficients					
2013		**2014**		**2015**	
HCFC-142b	HFC-23	**CFC-113**	CFC-113a	**Halon 2402**	HFC-125
HFC-23	HCFC-142b PCE	**CFC-113a**	CFC-113 HCFC-133a	**HFC-125**	Halon 2402 HFC-152a HFC-245fa
C_3F_8	SF_6	**HCFC-141b**	DCM DCE		
C_5F_{12}	C_6F_{14}			**HFC-152a**	HFC-125 HFC-245fa
C_6F_{14}	C_5F_{12} C_7F_{16}	**HCFC-133a**	CFC-113a		
C_7F_{16}	C_6F_{14}	**C_2F_6**	C_3F_8 c-C_4F_8	**HFC-245fa**	HFC-125 HFC-245fa
SF_6	C_3F_8	**C_3F_8**	C_2F_6 c-C_4F_8		
PCE	HFC-23				
Chloroform	CCl_4	**c-C_4F_8**	C_2F_6 C_3F_8		
CCl_4	Chloroform				
		DCM	HCFC-141b DCE		
		DCE	HCFC-141b DCM		

In general, across all three campaigns, over 30 species were measured at both enhanced and near background abundances. This suggests that both clean and polluted air masses were sampled and distinct spikes in the concentration of a species are likely due to pollution transported to the site in these air masses. Local emissions may influence these spikes, however the likelihood of this was assessed by considering the local wind speed (over 2 ms^{-1} in order to minimise local impact) and local wind direction (whether industrial or residential areas were travelled over). When local emissions are considered minimal, it is these spikes that are mainly considered in estimating potential source locations using the NAME back trajectories. Significant mixing ratios (over 2 sigma) above background abundances, both spikes and extended periods, for individual species will be expanded on within the compound assessments ahead.

A high number of species also were found to have a larger proportion of good to excellent interspecies correlation during the 2014 campaign. This was the year with the highest frequency of Chinese originating trajectories, as well as the site closest to the Chinese mainland. As such, emissions from China during this year may have had a larger impact and undergone less dilution in transport thus this correlation was more evident. This site was also closer to areas of Taiwanese industry, which too may have contributed to the abundances and interspecies relationships detected. Specific correlations between compounds will be discussed in the upcoming sections.

Finally, inter-annual variation across the three years of campaigns was established by looking at the median mixing ratios for each compound (found in Appendix 4.4a-e) and comparing these with the published global trends. Whilst any similarities with global trends of species and variation between campaigns is discussed, it should be noted that this is likely influence by atmospheric variability and so is not indicative of any long-term trends. Any assessment of species trends is not possible due to the short-term nature of these campaigns as well as the variation of measurement site. Continuous measurement at one site over a period of at least 5- would be necessary in order to accurately represent potential atmospheric trends. For any species that was found to have potential contamination throughout a campaign, the corresponding years median would not be considered during this assessment, although correlation and back trajectory assessments would not be affected as long as distinct pollution events were visible. Site differences and the frequency of trajectory origins are also considered for their potential impact. Where available, comparisons to mixing ratios from previous campaigns in the East Asian region are made as well.

The next sections summarise the data collected and conclusions drawn for the 41 halocarbon species previously mentioned plus a number of other species of interest, organised by compound group. Included in these sections are a number of recently detected species, some of which are only currently measured at UEA, including CFC-113a, CFC-114a, HCFC-133a, c-C_5F_{10} and iso-C_6F_{14}.

4.9.3.1 Ozone Depleting Substances

The species discussed in the following sections contain chlorine and bromine and so can participate in the stratospheric destruction of ozone molecules. As such, the production and consumption of many of these compounds is controlled under the Montreal Protocol (see section 1.11 for further information).

4.9.3.1.1 Chlorofluorocarbons

Given their global phase-out under the Montreal Protocol, concentrations for the CFCs were expected to be detected at close to background mixing ratios. A slight declining shift in medians was anticipated over the three campaigns due to only minimal regional emissions from refrigerant and foam banks as well as long atmospheric lifetimes.

In general, all of the CFCs measured were detected at mostly enhanced above background abundances. Comparison with NAME back trajectories indicates mainly Chinese and Korean emissions influencing the sampled air masses when distinct spikes in concentration were found. Since these are countries that only finished their phase-out of CFCs in 2010, they are likely to have larger banks remaining than, for example, Japan. Here the phase out was completed by 1997 and, as such, banks of CFCs should have decreased in size and had time to stabilise. Correlations and overall variabilities between the campaigns appear to vary with species and so, along with specific events or features found during analysis, will be discussed individually below.

CFC-11 – Figure 4.26a

This major CFC was utilised mainly in refrigeration and foam-blowing before its production and consumption was successfully phased out under the Montreal Protocol, resulting in a decreasing trend in global abundance. In order to compare the overall inter-annual variability seen across the campaigns, the median mixing ratios were compared with those in literature from 2001 and 2010 (for China as no East Asia data is available) and this can be seen in Figure 4.27. An overall decrease from 2001 can be seen, which agrees with the global trend. The median mixing ratios for 2014 and 2015 are very similar (237 ppt and 238 ppt respectively) and an increase of 1 ppt is seen between campaigns, although this is within the margin of error. This lack of discernable difference could, however, indicate a slow down or plateau in the regional variability. The difference in sampling location may have had some impact, however the 2013 median mixing ratio (256 ppt) was nearly 20 ppt higher than 2014, suggesting a larger difference would be expected regardless of location. As such, overall CFC-11 appears to have followed the global trend between 2001 and 2015.

In 2013, mixing ratios were consistently over 5% above background (236 ppt) throughout the campaign, although distinct spikes indicative of pollution events were seen. This on-going enhancement suggests the potential of contamination for this year, particularly as near background levels were measured in the latter campaigns. This enhancement could be caused by a steadily emitting source in close proximity to the site and thus relatively unaffected by changes in wind direction, however one was not identified. A direct contamination of the sampling equipment is also possible, although analysis of nitrogen blanks has ruled out canister contamination for CFC-11. Since pollution events are still identifiable, correlations and back trajectories for this campaign were still possible, however this data was not considered during the inter-annual variability assessment.

In 2015 there were 3 significant (over 2 sigma above the median) spikes in concentration on the 24th March and the 22nd and 23rd April. The biggest of these was over 200% higher than the background mixing ratio (757 ppt compared to a background of 234 ppt). Since this campaign took place at the southern site, local influences should be minimal, however 2013 also saw higher than expected abundances although this was generalised across the campaign. In 2015 distinct spikes in concentration were seen which suggests that these were caused by separate pollution events. The NAME back trajectories for all three days suggest emissions were mainly coming from Korea with some influence from Japan. Since Japan phased out CFCs by 1997 and Korea by 2010, the latter seems the more likely source region. However similar trajectories seen on days with comparative local winds are very close to background mixing ratios. The magnitude of these spikes may be indicative of more short-range transport, though local wind data is consistent with the katabatic winds seen for the majority the campaign, both in direction and speed. This means that similar winds travelled over the local populated area when close-to background abundances of CFC-11 were detected.

As such, the source of these high concentrations, if local, may have only been present for a short time and so caused by something like the destruction of foam on a particular day or it may have been due to boundary layer variation. The spikes on the 22nd and 23rd April were collected in the late afternoon/evening whereas a near background mixing ratio sample was collected during the morning between them. The boundary layer during the morning may have been more stable and less well mixed comparative to those in the afternoons. Whilst this does suggest that local human activity may have played a role in the causing these enhancements, these differences could suggest that the source was actually present for longer but was not consistently sampled due to boundary layer variation. Comparison with other species detected in this sample do not see spike of relative magnitude, only enhancement above magnitude. This further suggests that a specific local source of CFC-11 was sampled as opposed to a heavily polluted air mass.

Good interspecies correlation for CFC-11 was limited to 2014 and mainly to chlorocarbon species, however some correlation was observed for a wide range of halocarbons covering a range of different groups. Given that this correlation suggests some similarities in sources, this reflects the widespread use, and so locations of CFC banks. No compounds were found to have good or excellent correlation during the 2013 or 2015 campaigns and some correlation was only found with halon 2402 in 2013 and CFC-12 in 2015.

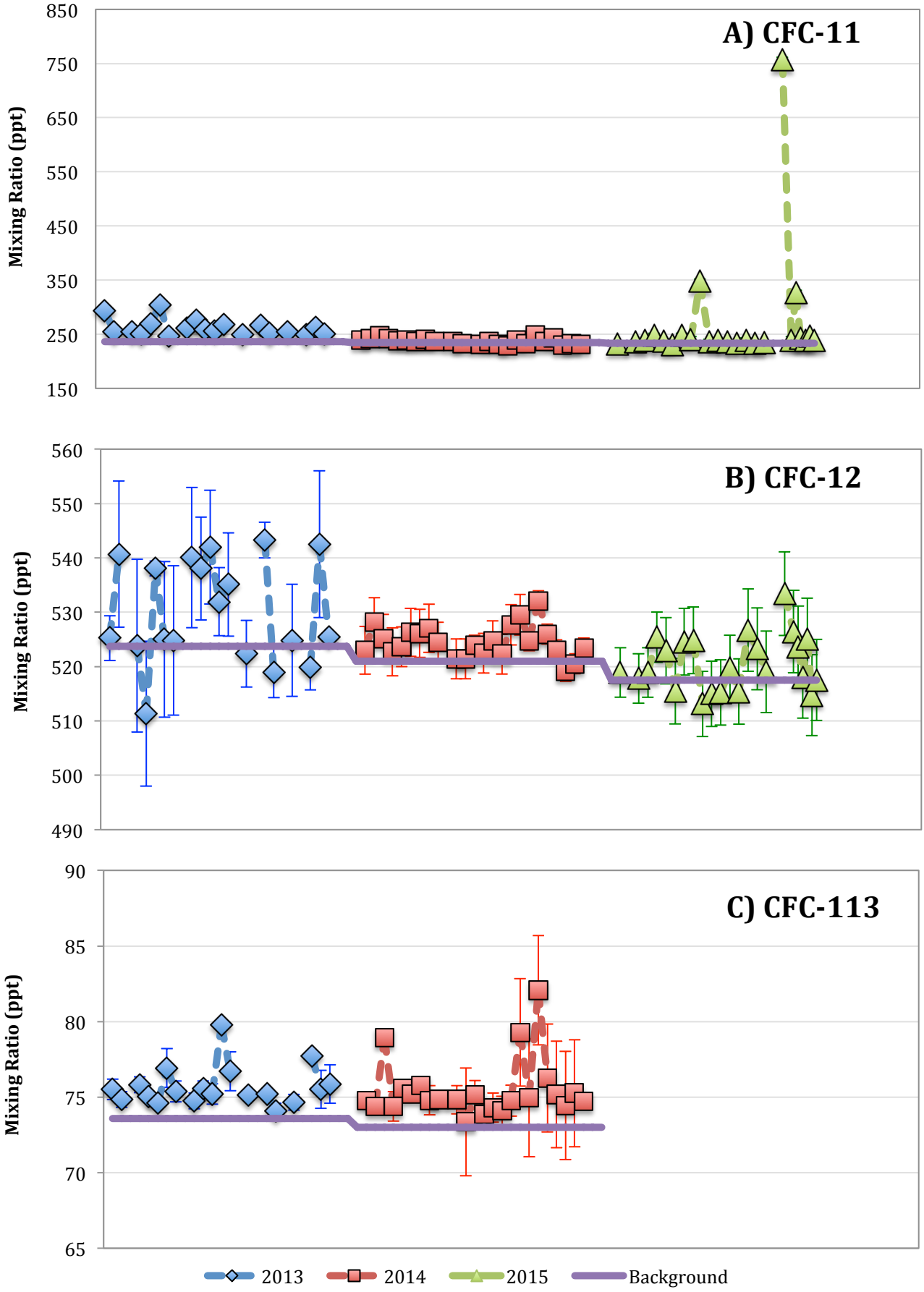

Figure 4.26: Time series spanning the three Taiwain campaigns for the major CFCs – A) CFC-11, B) CFC-12 and C) CFC-113. Data from 2013 is represtented in blue, 2014 in red and 2015 in green. Background abundances are shown in purple. Error bars indicate the total uncertainty calculated for the samples.

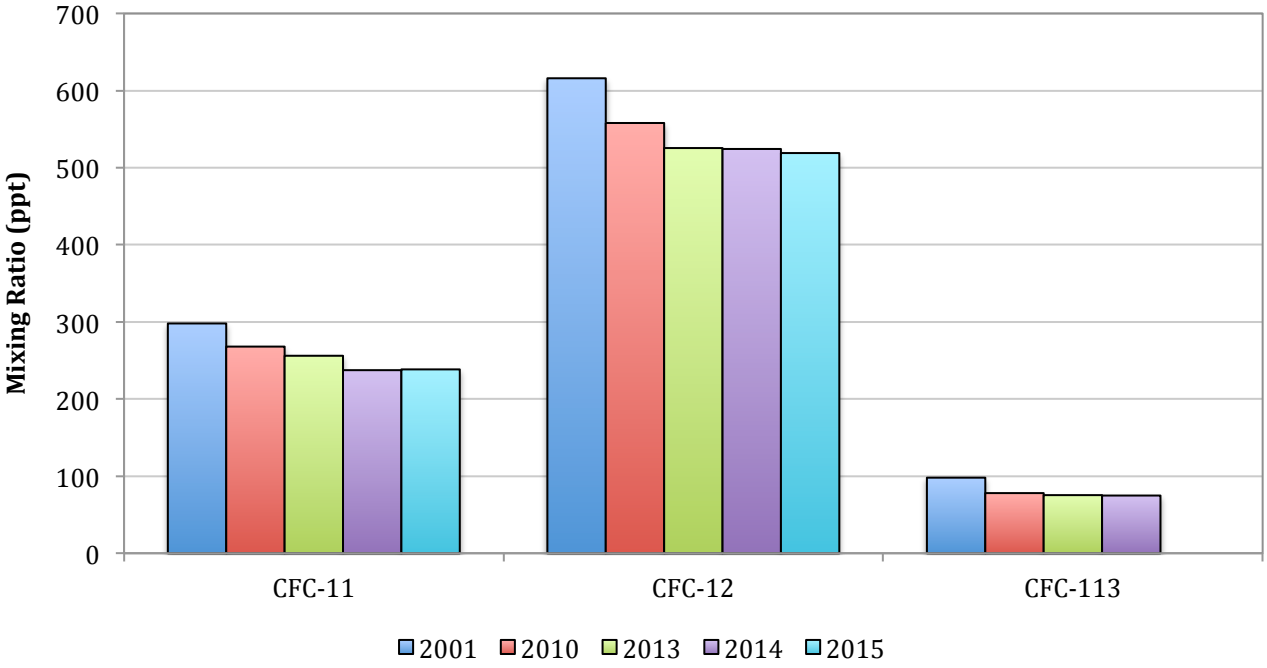

Figure 4.27: Comparison of mixing ratios of the major CFCs from literature (Guo et al. 2009 for 2001 and Fang et al. 2012a for 2010) and the Taiwan campaigns (2013, 2014 and 2015).

CFC-12 – Figure 4.26b

As the most abundant CFC, and with similar applications and control measures in place as CFC-11, CFC-12 also has a decreasing global trend in terms of atmospheric mixing ratios. When the median abundances for these campaigns and previous studies were compared (see Figure 4.27), CFC-12 followed this global trend between 2001 and 2015. Medians between the three campaigns were within 6 ppt of each other, and so within error margins, although a decrease each year was measured. As the decades-long atmospheric lifetimes of CFCs make them relatively stable in the atmosphere, the similarities between these mixing ratios reflect the minimal continued regional emissions of CFC-12.

Although the significant spike in abundance (533 ppt) detected during the 2015 campaign corresponds with the sample that had the highest CFC-11 enhancement, the other two samples that were observed do not. In fact, these CFCs only have a correlation coefficient of 0.50 during this campaign suggesting there is no co-emission or combined source of the two, despite emissions likely being released from similar refrigerant and foam banks. Another significant spike (532 ppt) was also detected in the 2014 campaign, on the 30th March, and this too corresponds with a significant spike in CFC-11, but again only some correlation between the species was observed (0.53). Comparison with NAME back trajectories suggests China as a major influence for this 2014 spike, however Korea and Japan are indicated to be the major emissions influences for the 2015 spike.

Given the extensive use of the major CFCs across the East Asian region, widespread banks are to be anticipated and this is likely being observed here. No clear source location for these notably larger abundances can be identified.

CFC-12 exhibited no good or excellent interspecies correlation during the 2013 or 2015 campaigns. Some correlation was observed in both these years, with halon 1301 in 2013 and with C_4F_{10}, COS and methyl chloroform in 2015. Again, like CFC-11, some correlation was found between a significant range of halocarbon species during the 2014 campaign, indicating the wide-ranging use and so banks of CFC-12 across the East Asian region.

CFC-113 – Figure 4.26c

Although this compound is also a major CFC, data is only available for 2013 and 2014 due to interference and inconsistencies with the 2015 analysis. Time constraints did not allow for re-analysis. For these two campaigns however, good correlation was seen with several species and this will be expanded on in Case Study 1 (section 4.10).

CFC-113 was also compared with previously detected mixing ratios from 2001 and 2010 (see Figure 4.27) and, like CFCs -11 and -12, the decreasing global trend was reflected by the 2013 and 2014 results. The median values for these two campaigns were similar (75.4 ppt and 74.8 ppt respectively), again reflecting the reduction of regional emissions since 2001 and the shift towards plateauing mixing ratios.

CFC-113a – Figure 4.28a

This species, a recently detected minor CFC and isomer of CFC-113, saw both good and excellent correlation each year with a number of other species and this will be discussed further in Case Study 1 (section 4.10).

Since CFC-113a is not yet regularly measured, background values were extrapolated from literature (Laube et al. 2014, 0.50 to 0.53 ppt from 2013 to 2015). Although median mixing ratios appear to increase between 2013 and 2014, by 0.42 ppt, this may be due to the increased Chinese influence at the 2014 site. Between 2013 and 2015 there is a decrease in the median value (1.2 ppt to 1.0 ppt) and this too will be further looked at in Case Study 1.

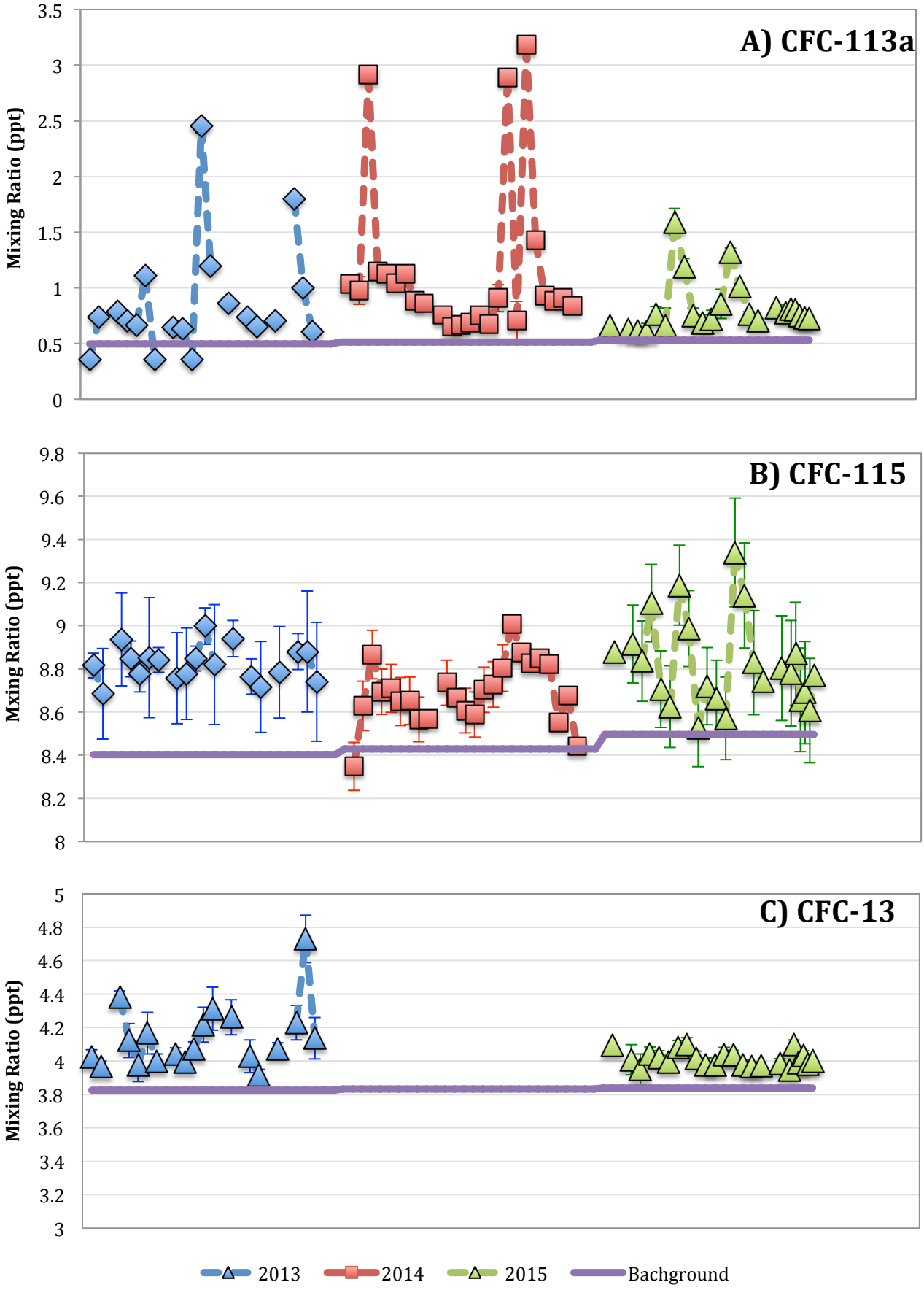

Figure 4.28: Time series spanning the three Taiwain campaigns for the minor CFCs – A) CFC-113a, B) CFC-115 and C) CFC-13. Data from 2013 is represtented in blue, 2014 in red and 2015 in green. Background abundances are shown in purple. Error bars indicate the total uncertainty calculated for the samples

CFC-114 – Figure 4.29a

The minor CFC with the highest global mixing ratio is CFC-114 and this too was utilised for foam blowing and refrigeration. This species was only measured during the 2015 campaign due to co-elution with its isomer, CFC-114a, when separated using the GasPro column. The AlPlot column enabled this separation and, as such, the only background available that reflects only CFC-114 and not a mixture of the isomers, is from the Cape Grim Air Archive (last available data – November 2014). Since this is representative of southern hemispheric air, some enhancement above the background (14.8 ppt) was expected and was seen for the majority of the campaign.

Significant spikes in mixing ratios were seen on the 26th March and 24th (pm) April and were over two sigma above the background, both at 15.3 ppt. Comparison with NAME back trajectories indicates that Korean emissions are potential major influences on both these days.

No good or excellent correlation with any other species was calculated for CFC-114.

CFC-114a – Figure 4.29b

Like its isomer, CFC-114a was only measured in 2015 and is compared to a Cape Grim November 2011-based background (1.02 ppt). More clearly than with CFC-114, this compound is consistently enhanced above the background throughout the campaign by at least 3%. This is likely, at least in part, due to hemispheric differences between the sampling and background sites. Significant spikes in mixing ratios (over 1.16 ppt) were measured on the 22nd and 23rd of March, with a further somewhat significant spike (between 1.12 ppt and 1.16 ppt) being observed on the 28th March.

What is noteworthy is that high mixing ratios are not found for CFC-114 in these samples and there is no correlation between the two species, which indicate separate sources. This can be seen visually in both Figure 4.30a, which compares the time series of these two species, and Figure 4.30b, which shows the trend line produced when the species are plotted against each other. Good correlations with CFC-114a were found with CFC-113a, HCFC-133a, HCFC-142b and PCE, implying some co-location of sources, and these compounds all show two main spikes in mixing ratios encompassed by 4 samples (22-23rd and 28-29th March). The correlation with CFC-113a and HCFC-133a is not unexpected as both of these can be produced as by-products, along with CFC-114a, in the production of HFC-125 (Kono et al. 2002) .

In the assessment of potential source regions for emissions that may have caused these spikes, local winds were found to be consistent with katabatic conditions. NAME back trajectories suggest Chinese emissions are dominant for the first spike and also present for the second. China also has a large HFC manufacturing industry and so is a likely source for CFC-114a.

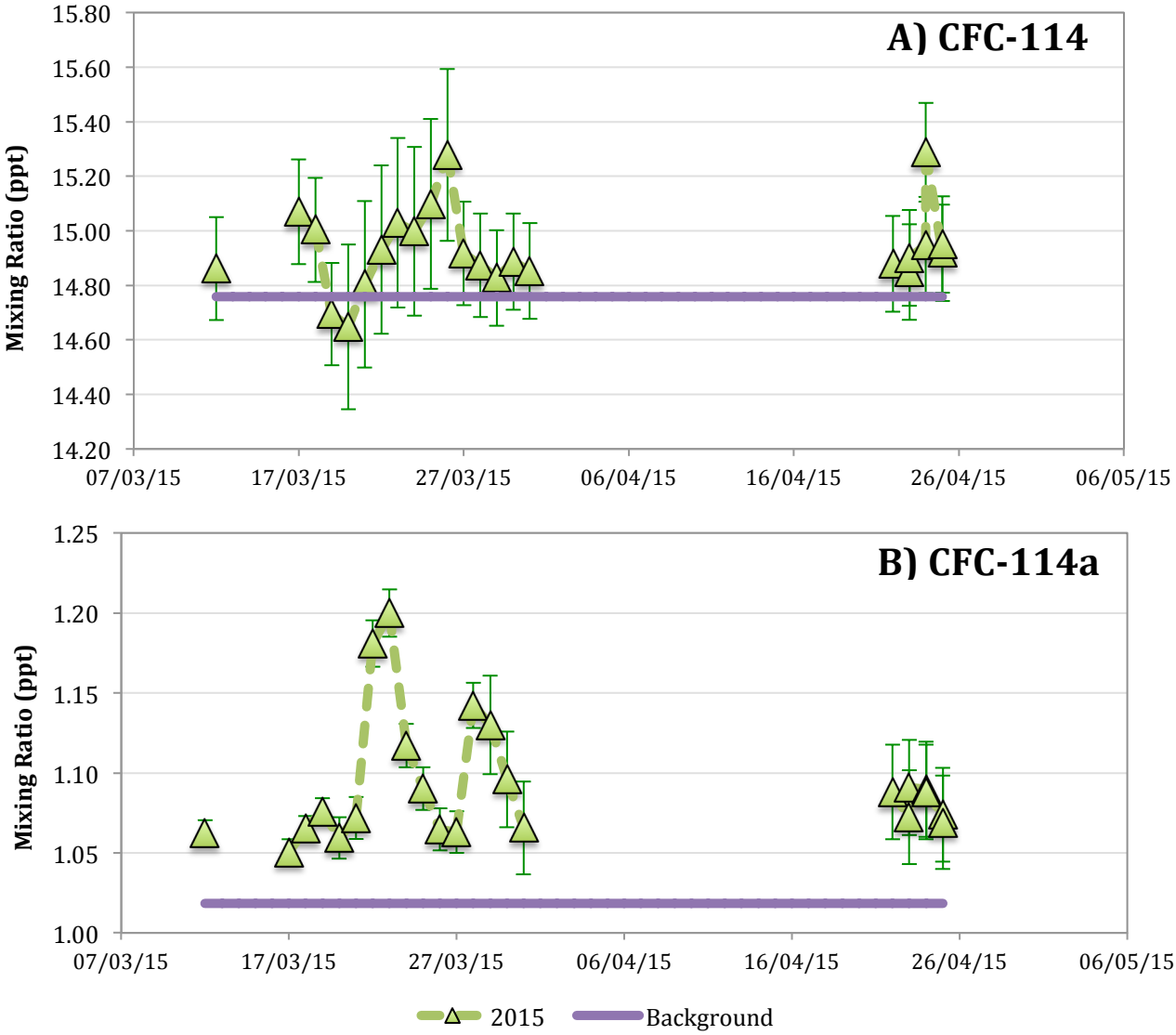

Figure 4.29: Time series for the 2015 Taiwain campaigns for A) CFC-114 and B) CFC-114a. Background abundances are shown in purple and error bars indicate the total uncertainty calculated for the samples

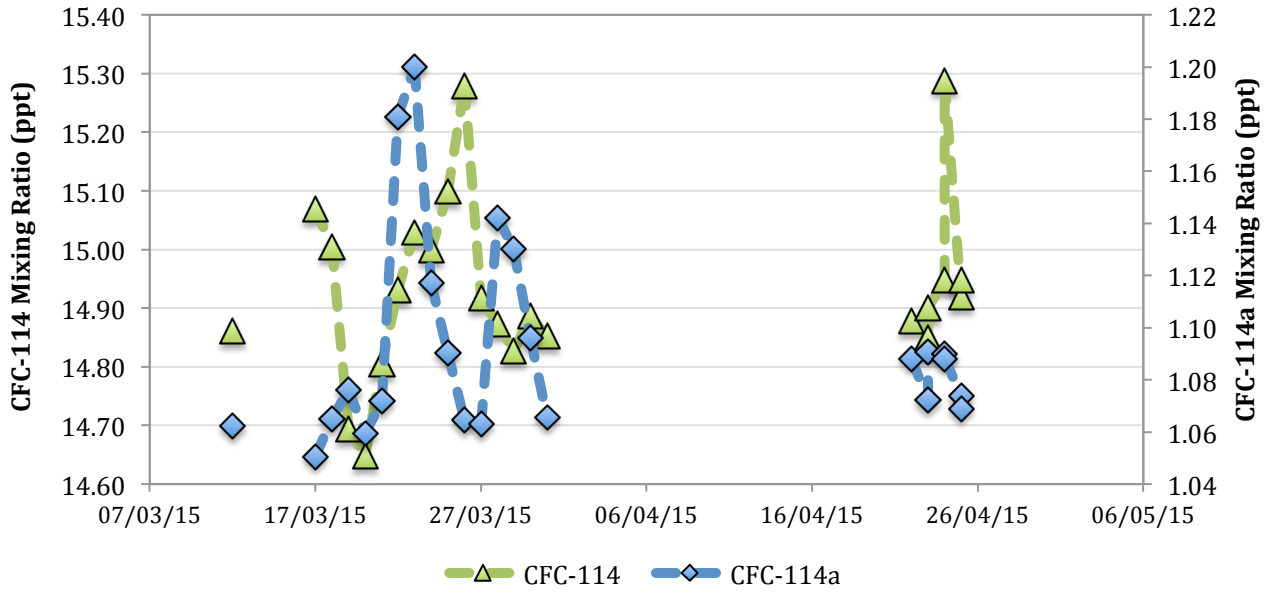

Figure 4.30a: Overlayed time series of the isomers CFC-114 (green) and CFC-114a (blue). The differences in the timing of spikes in mixing ratios suggest there are different sources for the two species.

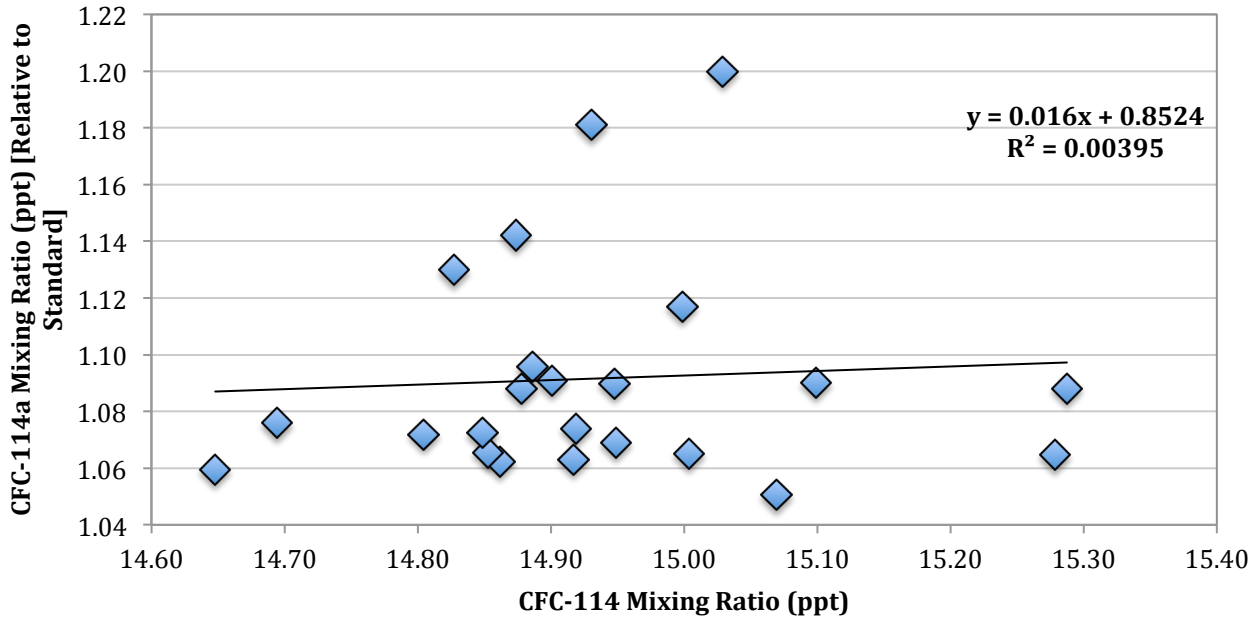

Figure 4.30b: Correlation between CFC-114 and CFC-114a during the 2015 Taiwan campaign. Addition of a linear trend line and the R^2 value indicate there is very minimal correlation between these species which, given their atmospheric lifetimes of over 100 years, likely suggests different sources.

CFC-115 – Figure 4.28b

CFC-115 is another of the minor CFCs and was measured during all three campaigns. Background mixing ratios for this species are taken from AGAGE's Ragged Point station in Barbados and, whilst in the same hemisphere as Taiwan, mixing ratios were predominantly observed above background for each year. This may in part be due to Taiwan's location in a less remote and source-rich region comparative to Barbados however, differences between calibration scales between AGAGE and UEA may be a factor in this difference as well.

Similar to CFC-12, median mixing ratios for CFC-115 decrease between 2013 and 2014 although this is against the apparent global trend and so likely due to atmospheric variability. This does increase again in 2015 however the difference between these concentrations is only 0.2 ppt and so within the margin of error for this species. This suggests that levels of CFC-115 were relatively stable over the three years measured and suggests minimal regional emissions. These are most likely from banks although, like CFC-113a and CFC-114a, production of CFC-115 as a by-product during HFC-125 manufacture is possible (Kono et al. 2002).

2015 saw the largest variation between detected mixing ratios (0.7 ppt, ~7% of background) and this may have been impacted by the use of the different column (AlPlot rather than GasPro) for this campaigns analysis. However, the other CFCs were measured using the same column and their results are comparable with previous years suggesting this would be the case for this species as well.

Only one of the spikes observed throughout the three campaigns is significant (over 2 sigma, 9.2 ppt) and this was from the 28th March. Comparisons with NAME back trajectories imply that the associated air mass may have been influenced by Chinese and/or Japanese emissions, both of which are likely to have banks of CFC-115.

Whilst CFC-115 was found to have some correlation with CFC-113a, CFC-114a and HCFC-133a across the three campaigns, this is only between 0.50-0.65 and so conclusions as to co-emission or co-location are less clear, though some relationship is not unexpected given the shared potential source.

CFC-13 – Figure 4.28c

As a known by-product of CFC-11 and -12 manufacture, CFC-13 is another minor CFC. It was only measured in 2013 and 2015 as its elution is very close to that of HFC-23 which, due to shifts in retention times, was prioritised in 2014. As these two campaigns were carried out at the same site, local influences should be similar and thus the results more directly comparable.

The background mixing ratios were taken from the Cape Grim Air Archive (March 2013, February 2014 and November 2014 samples) and were found to be increasing, from 3.8 ppt to 3.9ppt. Conversely, the data from the Taiwanese samples indicates a decreasing abundance, from median values of 6.6 ppt in 2013 to 4.1 ppt in 2015. Hemispheric gradients may account for some difference in the mixing ratios between the two sites. Whilst, the rate of increase in the Cape Grim samples appears relatively small, comparison with the rest of the data set does indicate mixing ratios have been increasing relatively steadily since the late 1990s and does not show signs of approaching a plateau or changing direction. This may instead indicate that whilst there are continued global sources of CFC-13, regional sources have reduced, a hypothesis supported further by the smaller range of mixing ratios detected in 2015, indicating less regionally affected variation.

A wider range of mixing ratios was detected in the 2013 campaign than in 2015, with a significant (over 2 sigma) spike detected on the 4th April. This day was assessed to have potential major influences from China as well as the Pacific Ocean, though significant mixing ratios of a minor CFC are more likely to have originated in a populated area. Korea was also a possible minor influence for this sample and meteorological data conformed with katabatic conditions, both in direction and speed, suggesting only minimal impact from the local area was likely. CFC-13 did have some uses as a refrigerant as well as potentially being emitted during some aluminium production (O'Doherty and Carpenter, 2007). China has a large aluminium industry and could have refrigerant banks of this species so is not an unreasonable suggestion for a potential source location.

4.9.3.1.2 Halons

Like the CFCs, the production and consumption of halons has been phased out globally and so a general stable or decreasing abundance was expected over the three campaigns along with relatively close to background levels. Though their mixing ratios are considerably lower than CFCs, their ODP is higher due to the bromine atoms which deplete ozone around 60 times more effectively than chlorine (Daniel and Velders, 2007) and as such, even small changes in concentration can be of significance.

Overall the Halons were mainly measured at enhanced above background levels aside from Halon 1301, which was observed at similar to background mixing ratios, within uncertainties. Comparisons with NAME back trajectories found no predominant source regions however influences from China were noted for all Halon species as well as some from Korea and Japan. Generally, global trends were followed and these as well as interspecies correlation will be discussed further below.

Halon 1211 – Figure 4.31a

As the major halon species, -1211 is the most abundant in the atmosphere of this group and had global applications in fire extinguishers and explosion protection. Since the Montreal Protocol phase out of production and consumption, emissions have reduced and the global trend for mixing ratios of -1211 is decreasing. Mixing ratios from the Taiwanese campaigns suggest this trend is being followed, with medians decreasing from 4.2 ppt in 2013 to 3.9 ppt in 2015. This is reflected in Figure 4.32 where the median abundances calculated for each campaign as compared with previous mixing ratio data from Barletta et al. (2009) in 2006. In this graph, the Taiwanese campaigns show an overall reduction of 0.5 ppt below the 2006 level (4.38 ppt) by 2015 suggesting the phase out has been successful.

Halon 1211 was found to be correlated with several species during each campaign and consistently with some of the most widely used HFCs, –134a and 143a. Given the previously extensive use of halon 1211 and so widespread banks, this correlation is more likely not related to a specific source or location but a combination of many similarly located emissions sites across East Asia. Further Halon 1211 correlations will be discussed in Case Study 2 (section 4.11).

Halon 1301 – Figure 4.31b

Conversely to the halon 1211, the other major halon species, -1301, has an increasing global trend despite the phase out of production and consumption. Its use as a feedstock however is exempt from the Montreal Protocol and both France and China are known to utilise this for the production of pesticides (HTOC, 2011). Other sources may include continued emissions from banks, namely those of fire prevention on aircraft and military aircraft, where suitable replacements have not been found (Montzka, 2011).

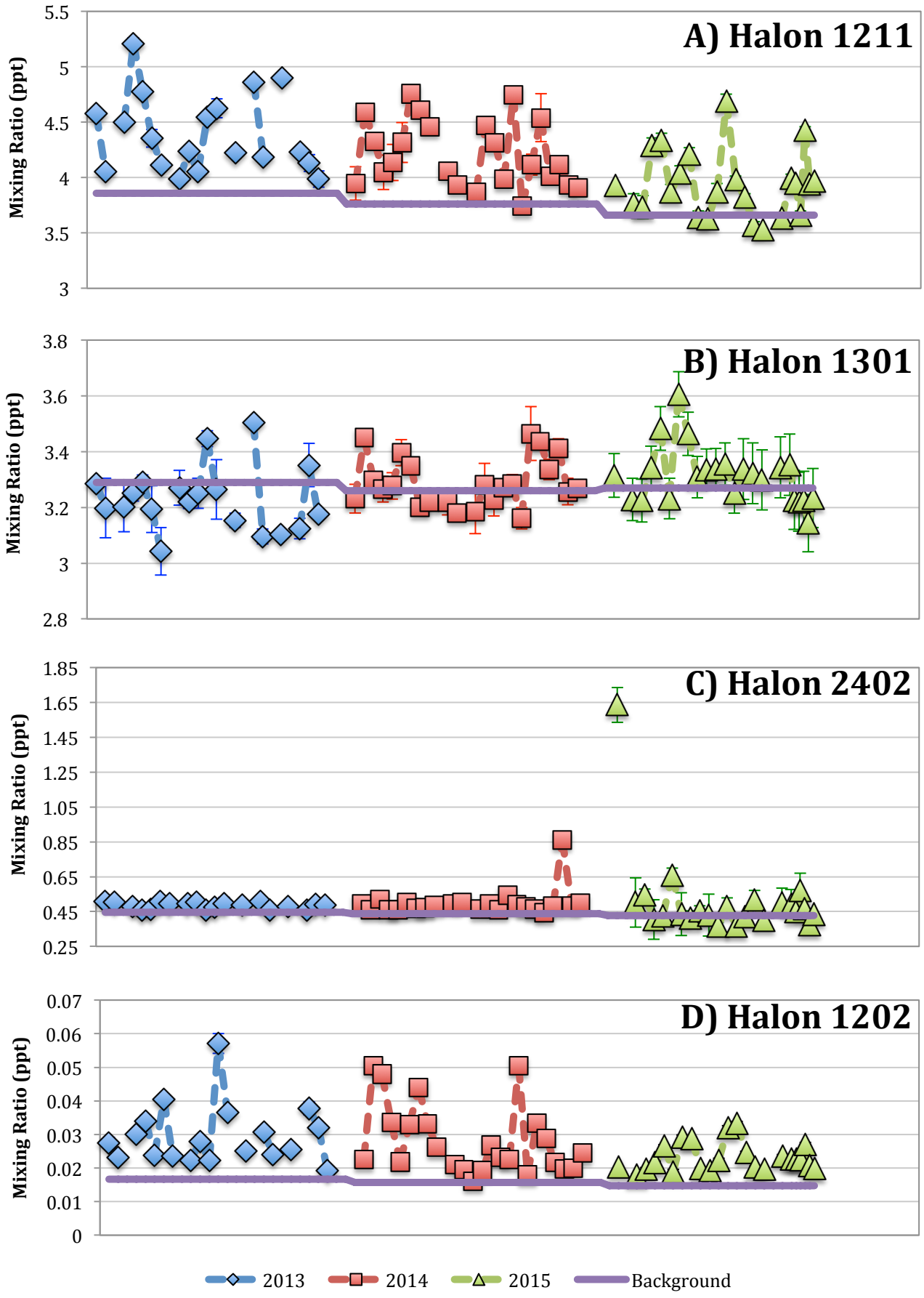

Figure 4.31: Time series spanning the three Taiwain campaigns for the halons – A) Halon 1211, B) Halon 1301, C) Halon 2402 and D) Halon 1202. Data from 2013 is represtented in blue, 2014 in red and 2015 in green. Background abundances are shown in purple. Error bars indicate the total uncertainty calculated for the samples

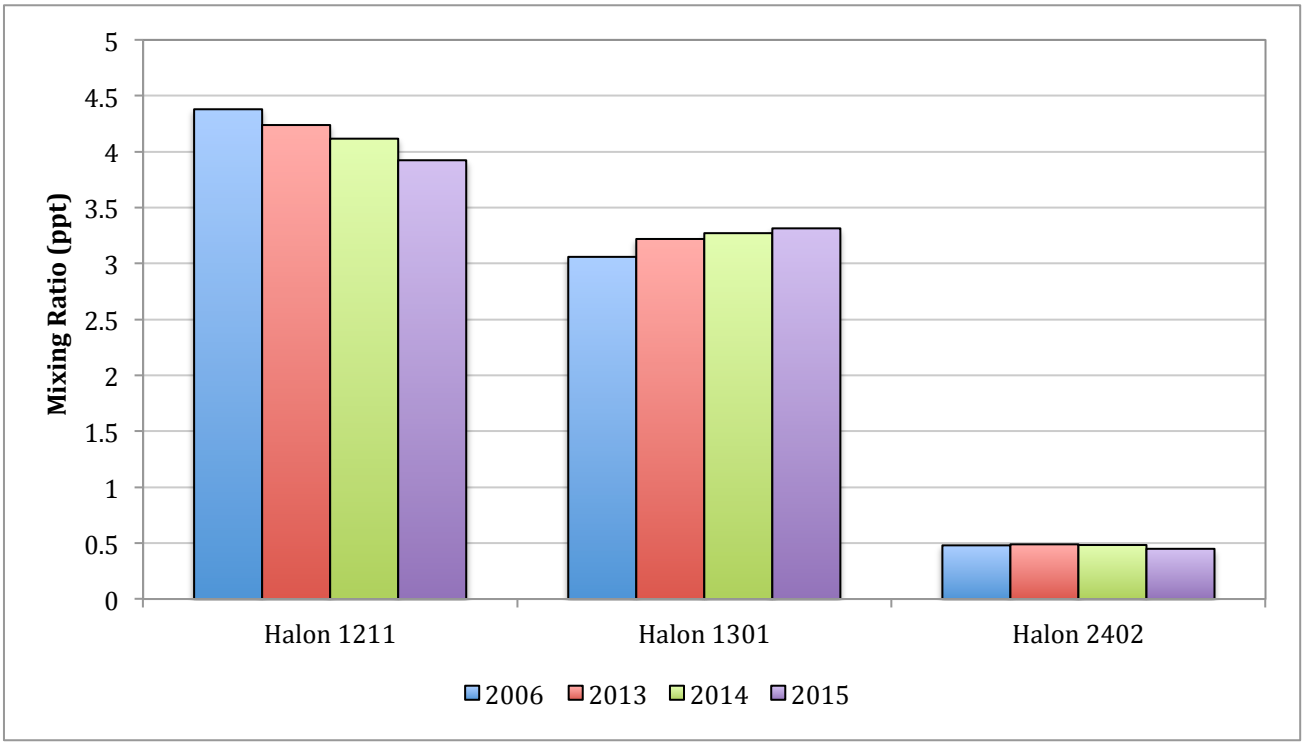

Figure 4.32: Comparison of mixing ratios of the halons from literature (Barletta et al. [2009] for 2006) and the Taiwan campaigns (2013, 2014 and 2015).

The median mixing ratios detected for each campaign do increase each year, following this global trend (see Figure 4.32).

Within calculated measurement uncertainties, Halon 1301 was detected at close to background abundances (~3.3 ppt in 2013, 2014 and 2015), with some spikes in mixing ratio indicative of pollution events. As most other species have seen more enhancements during these campaigns, the calibration was checked to ensure the significant portion of samples detected below background (before uncertainties were considered) to ensure this was an accurate reflection of the associated mixing ratios. Since the 2015 campaign was analysed using a different instrument and column but similarly spread data was observed, this suggests there is minimal impact from this and the calibrations are consistent.

One significant spike in abundance was measured for each campaign; 3.5 ppt on the 27th March 2013, 3.5 ppt on the 30th March 2014 and 3.6 ppt on the 22nd March 2015. Both 2013 and 2015 were assessed from NAME backwards trajectories as having potential major influences from Korea and minor influences from China whereas the 2014 trajectory indicated impact from Chinese emission as major and Korean as the minor. 2014 was the campaign with the largest influence from China and saw the lowest magnitude spike of the three, which together suggests that Korea may actually be the chief source.

In terms of interspecies correlation, good correlation is seen with HCFC-142b in 2014 and chloroform in 2015. Some correlation was seen each year with a number of HCFCs as well as several HFCs. Since these compound groups were implemented as replacements for halon species, these correlations likely suggest use in similar applications.

Some correlation was seen with other VSLS-Cl species as well however, given the different uses of these species, this may be coincidental.

Halon 2402 – Figure 4.31c

Halon 2402 is a minor halon species, mostly utilised for fire protection in the Soviet Republic, and has a decreasing global trend. The median results of the Taiwanese campaigns agree with this trend (see Figure 4.32) however comparison with literature suggests an increase in mixing ratio between 2006 (0.48 ppt) and 2013 (0.49 ppt). However, the Barletta et al. (2009) campaign sampled long range transport across the Pacific ocean and dilution would have occurred in this time, potentially causing the lower than 2013 level seen on the graph.

The 2015 campaign was observed to have the largest variation in mixing ratios including the biggest spike (1.6 ppt) and 4 samples below background even after uncertainties are included. The sampling of southern hemispheric air, given hemispheric gradients, could cause these below background samples, however comparison with back trajectories, particular for the lowest observed abundances (0.4 ppt) suggests air masses on these days travelled mostly from China, Korea and Japan. This corresponds with the findings of the Vollmer et al. (2016) study as this noted frequent pollution events for halon 2402 at Gosan, Korea suggesting the presence of sources in the East Asian region.

The 2015 campaign was analysed using the AlPlot column on the AutoSpec however it is Entech data represented in Figure 4.31c as mixing ratios observed from the AutoSpec were significantly lower than previous years. This could be due to column differences as the 2014 campaign was also analysed using the AutoSpec but with the GasPro column and these results appear comparable with the previous campaign, which was analysed on the Entech. As such, instrument or calibration bias was not anticipated to impact the 2015 Entech data and so these low mixing ratios may be accurate, although their cause is currently unknown.

No significant spikes in abundance were detected during 2013 however 0.9 ppt was observed on the 2nd April 2014 and, as previously mentioned, 1.6 ppt was measured on the 12th March 2015. Both these days have back trajectories that suggest impact from Chinese emissions. The 2015 trajectory also suggests potential regional influences from Taiwanese emissions, which may explain why this spike is almost double the 2014 as less dilution would occur during transport from Taiwanese sources as opposed to Chinese ones. Local wind direction and speed is consistent with katabatic winds and so indicates little impact from any local sources suggesting these Taiwanese emissions may be from a different area of the island.

Good correlation was only seen in 2015 and was with HFCs -152a (0.94) and -245fa (0.95) along with the short-lived dibromomethane (0.91). Excellent correlation during this campaign was seen with HFC-125 (0.96).

These correlations indicate co-located sources however the only interspecies correlation found during other campaigns was with CFC-11 in 2013 and that only had a coefficient of 0.52. This may indicate that this joint source of halon 2402 and the HFCs is relatively recent, as this relationship was not previously detected. Use of HFCs as replacement compounds due to the Montreal Protocol phase-outs has resulted in increasing emissions and more widespread sources across East Asia in recent years.

Halon 1202 – Figure 4.31d

As halon-1202 is a minor halon, with emissions potentially occurring from halon 1211 manufacture or release from US military based fire prevention, this species is not regularly measured. As such, this means the corresponding background mixing ratios are taken from the Cape Grim Air Archive and so the associated hemispheric gradient is at least partially responsible for the almost consistent enhancement seen over the three campaigns.

Since the a potential source of Halon 1202 is as a by-product of Halon 1211 production, there is some correlation with Halon 1211 seen each year. However, there are stronger correlations with a number of other compounds and these will be discussed in more detail in Case Study 2 (section 4.11).

As a by-product, levels were expected to decrease once Halon 1211 was phased-out and the results do follow this trend, with median mixing ratios decreasing from 0.03 ppt in 2013 to 0.02 ppt in 2015. Also, whilst spikes in abundance are seen for all three campaigns, the range of observed mixing ratios are around 10 ppt less in 2015, potentially indicating a reduction in regional sources.

4.9.3.1.3 Hydrochlorofluorocarbons

With HCFCs having replaced CFCs and Halons in many applications across the globe, emissions are expected to be more significantly HCFC based and so increasing abundances may be detected. However, though their use and production is still permitted in both developed and developing countries the phase-out has begun for these compounds and so emissions may have begun to decrease in some areas. Japan is further into the phase-out schedule and so sources are anticipated to be comparatively more minor in this area.

In general, all of the HCFCs measured were found at mainly enhanced levels and comparison with NAME back trajectories indicates emissions from China and Korea as having influenced the sampled air masses when higher concentrations were detected. As expected, correlations with other replacement compounds such as the HFCs were common as well as correlation with chlorinated VSLS. Variations in observed mixing ratios between the campaigns, however, appear to be decreasing suggesting the phase out of HCFCs is well underway and specifics for each species measured will be discussed further below.

HCFC-22 – Figure 4.33a

HCFC-22 is the most abundant HCFC species and is utilised as a CFC replacement compound, mainly as a refrigerant. Comparisons of the median mixing ratios for HCFC-22 with two previous campaigns from 2001 (Guo et al 2009) and 2010 (Fang et al 2012a) can be seen in Figure 4.34. Although the results from 2010 are significantly high in comparison, this is likely due to differences between the campaigns, particularly the proximity to sources and so lack of dilution during transport, a factor that impacts Guo et al (2009) as well. The relatively short lifetimes of HCFCs may also have an impact as, comparative to CFCs and halons, their lower atmospheric stability will reflect changes in emissions in the detected mixing ratios noticeably sooner. 2014 was found to have the highest median (266 ppt) of the three campaigns and this is most likely due to the larger proportion of trajectories from China, where HCFCs emissions are extensive. Comparisons between the 2013 and 2015 medians however are similar (261 ppt and 261 ppt respectively) potentially indicating that regional emission sources in East Asia may be decreasing causing atmospheric abundances in the area to begin to stabilise towards background mixing ratios.

2015 saw a significant spike, over 750% higher than the campaigns background abundance (237 ppt), of 2080 ppt on the 20th March. Comparison with the NAME trajectories does not indicate any obvious source, as the Philippines and Pacific Ocean were the main regions identified as potentially impacting this sample. The trajectories are also very similar to the surrounding days that were sampled and these were detected at levels consistent with the rest of the campaign. As for local influences on this day, winds were coming from the ocean to the west and so not over populated areas making local source unlikely.

However, the comparative magnitude of this spike is more indicative of a closer source, potentially only present on this day or for a short time due to boundary layer variation, similar to what was considered for the CFC-11 spikes previously mentioned. No other species detected in this sample were found to be have enhancements of a comparative magnitude and as such, this could potentially be a nearby leaking refrigeration unit but further campaigns would be required to fully explain this phenomenon.

Since HCFC-22 is often used as a tracer of Chinese and Korean emissions, good correlation with other compounds particularly associated with developing countries is not unexpected. For example, in 2014, HCFC-22 was found to have good correlation with 19 different species, more than during any other campaign. In 2015, only 5 species had good correlation with HCFC-22 and these were VSLS-Cl and chlorocarbon compounds and not the halons and HFCs as well, as was seen in 2014. This suggests that sources of HCFC-22 may be decreasing, in agreement with the global trend data.

HCFC-141b – Figure 4.33b

This species is mainly used as a replacement foam-blowing agent and, as such, has an increasing global trend. Figure 4.34 compares median mixing ratios of the three campaigns with previous studies and the apparent discrepancy in trend between literature and the Taiwanese data is likely due to the campaign differences previously mentioned as well as general atmospheric variation. As for HCFC-22, the 2014 had the highest observed median abundance (32 ppt) however the median for 2015 (29 ppt) is ~5% lower than that of 2013 (31 ppt). This again suggests Chinese emissions in particular impact HCFC-141b abundances, however Korean emissions are also influential, particularly in 2015 where less air masses from China were sampled (see Table 4.6) and also implies that regional sources may be decreasing and thus mixing ratios are shifting towards background in the area.

Table 4.6: Comparison of HCFC-141b mixing ratios with the percentage of samples with major emissions contributions from China and Korea for each campaign.

	2013	2014	2015
HCFC-141b mixing ratio (ppt)	31	32	29
Major Campaign Emissions contributions by China from NAME (%)	37	51	14
Major Campaign Emissions contributions by Korea from NAME (%)	24	17	32

All three campaigns saw spikes in abundance likely due to pollution however, the largest spike was seen during 2014 and was found to be enhanced over 280% above background (25 ppt) at ~95ppt. This was identified in a sample from the 12th March where local wind data does suggest potential influence from Taiwanese industry. The magnitude of this spike has not been replicated across the other campaigns unlike the smaller spikes, found at ~40ppt, suggesting a different source. Taiwan has phased out CFCs and halons in favour of HCFCs and HFCs and both Li et al. (2011) and Stohl et al. (2010) did identify Taiwanese emissions of HCFC-141b in 2008. However the other days in the 2014 campaign, where local wind data indicates potential local influence, do not see similar spikes though concentrations are ~10ppt above background. As such, there is likely a Taiwanese source of HCFC-141b that was measured during this campaign but only impacted significantly on the 12th March.

Along with several HFCs and some VSLS species, good correlation was found with the short chain PFCs, but only in 2014, and this gives credence to the reasoning that some of the HCFC-141b emissions detected were of local origin, as will be further explained in Case Study 3 (section 4.12).

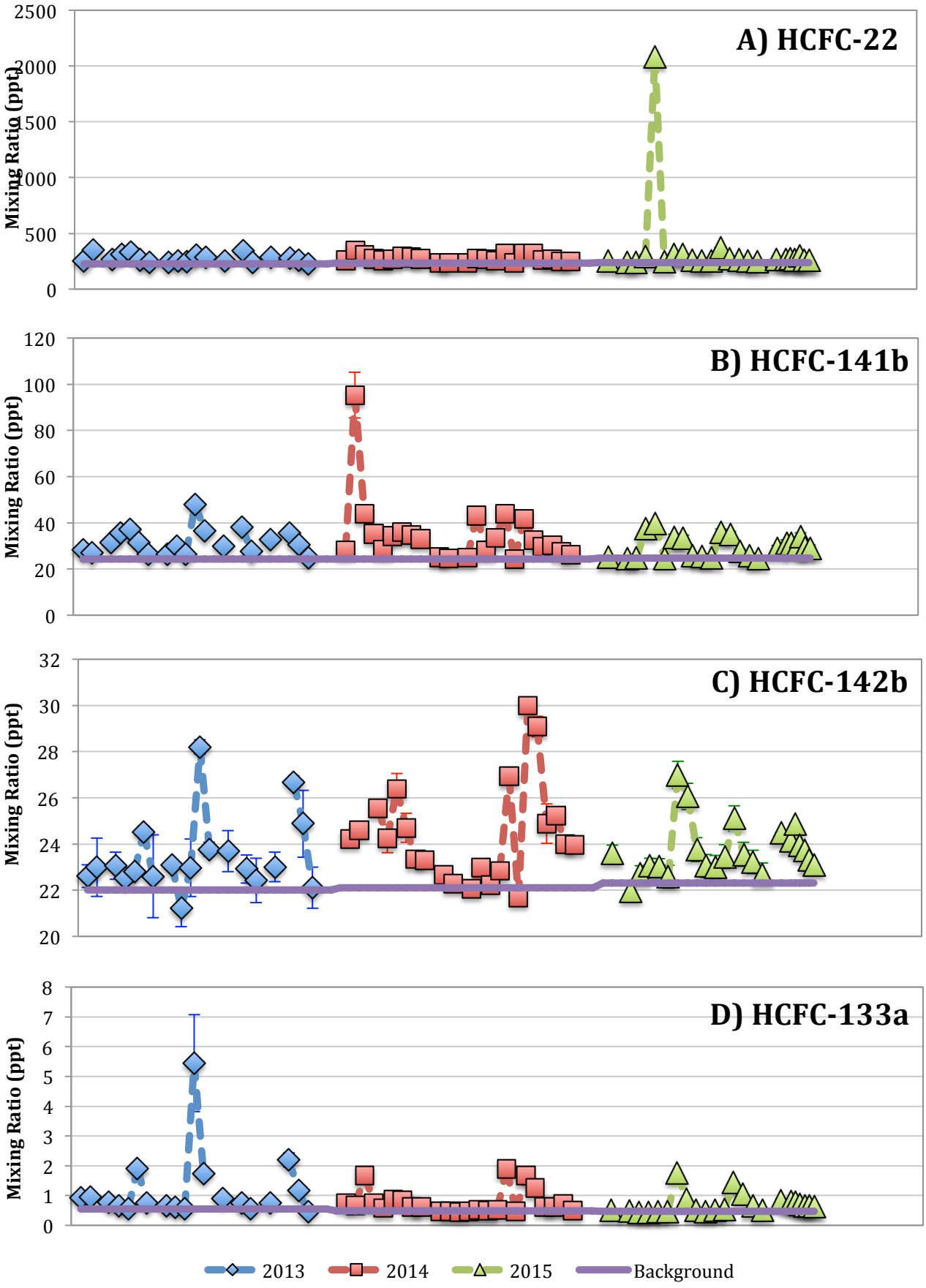

Figure 4.33: Time series spanning the three Taiwain campaigns for the HCFCs – A) HCFC-22, B) HCFC-141b, C) HCFC-142b and D) HCFC-133a. Data from 2013 is represtented in blue, 2014 in red and 2015 in green. Background abundances are shown in purple. Error bars indicate the total uncertainty calculated for the samples

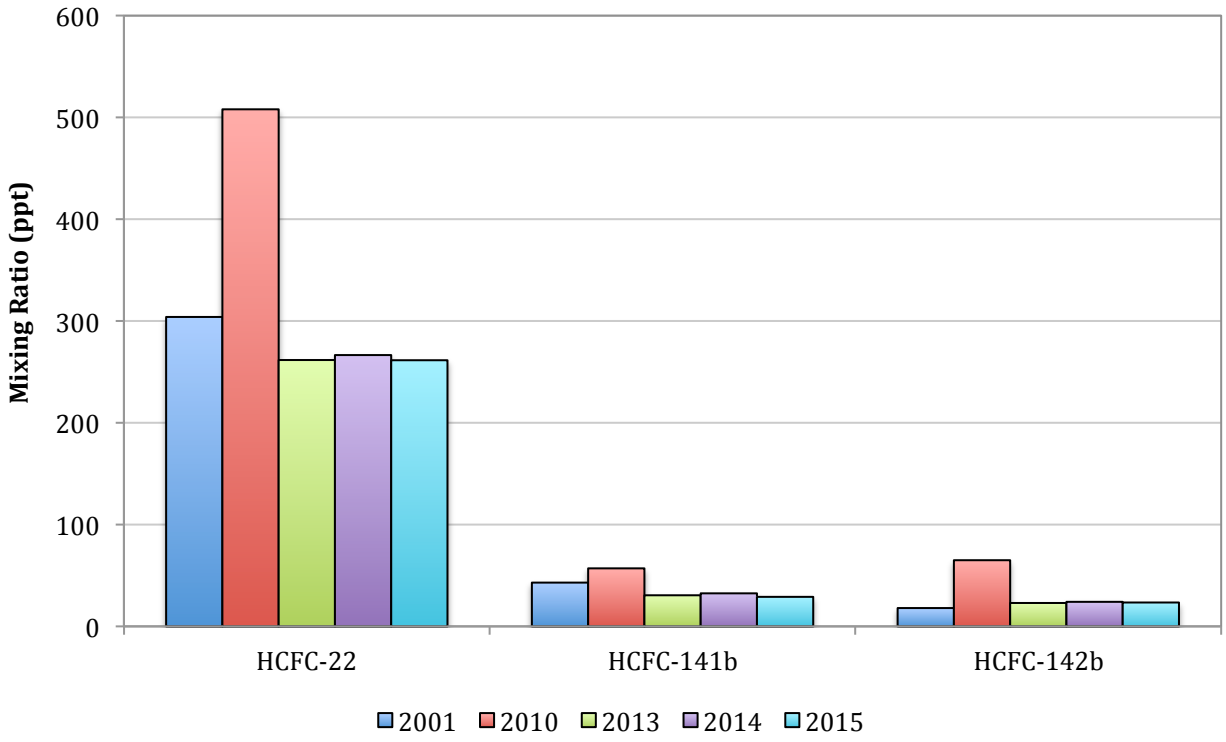

Figure 4.34: Comparison of mixing ratios of the halons from literature (Guo et al. 2009 for 2001 and Fang et al. 2012a for 2010) and the Taiwan campaigns (2013, 2014 and 2015).

HCFC-142b – Figure 4.33c

Another replacement foam-blowing agent, HCFC-142b also has an increasing growing trend and similar to the other major HCFCs, median mixing ratios were largest at 24.1 ppt in 2014 indicating particular impact from Chinese emissions. However, the 2015 median (23.5 ppt) is ~0.5 ppt higher than that measured in 2013. This would follow the global trend and would suggest that whilst regional emissions sources of the other HCFCs appear to declining, HCFC-142b emissions are continuing and so abundances are increasing accordingly.

Significant spikes were measured in all three campaigns: 28.2 ppt and 26.7 ppt on the 21st March and 3rd April 2013 respectively, 30 ppt and 29.1 ppt on the 30th and 31st March 2014 and 27 ppt and 26 ppt on the 20th and 21st March 2015. Comparison with NAME back trajectories for all these dates indicates consistent potential major influence from China.

Good correlation with HCFC-142b was found consistently with several HFCs and VSLS-Cl species but interestingly, good correlation was also identified each year with minor CFC-113a and, in 2015, CFC-114a. Emissions sources of these species are not well known however so the nature of this relationship is currently unclear.

HCFC-133a – Figure 4.33d

This is one of the recently detected compounds and a minor HCFC measured during the Taiwan campaigns. Uses of HCFC-133a includes in HFC-143a, agrochemical and pharmaceutical manufacture.

The background level for this HCFC-133a (0.54 ppt in 2013, 0.49 ppt in 2014 and 0.47 ppt in 2015) is taken from the recent Vollmer et al. (2015) paper but is reflective of northern hemispheric background mixing ratios at a considerably different latitude from Taiwan (47.5°N, Jungfraujoch, Switzerland as opposed to 22-25°N for Taiwan). The global trend of HCFC-133a had been increasing in recent years but this compound had periods of decrease before (see Figure 4.35). The Vollmer et al. (2015) paper, using a data set including these Taiwanese campaigns, has established the trend to be decreasing again and, even given the latitudinal difference, the three campaigns exhibit background mixing ratios in line with those from Jungfraujoch.

Significant spikes in abundance were seen across all three campaigns and will be discussed further in Case Study 1, along with the good and excellent correlation of HCFC-133a with CFC-113a. Good correlation is also seen with HCFC-142b, during each campaign, along with HFC-227ea and some VSLS-Cl species.

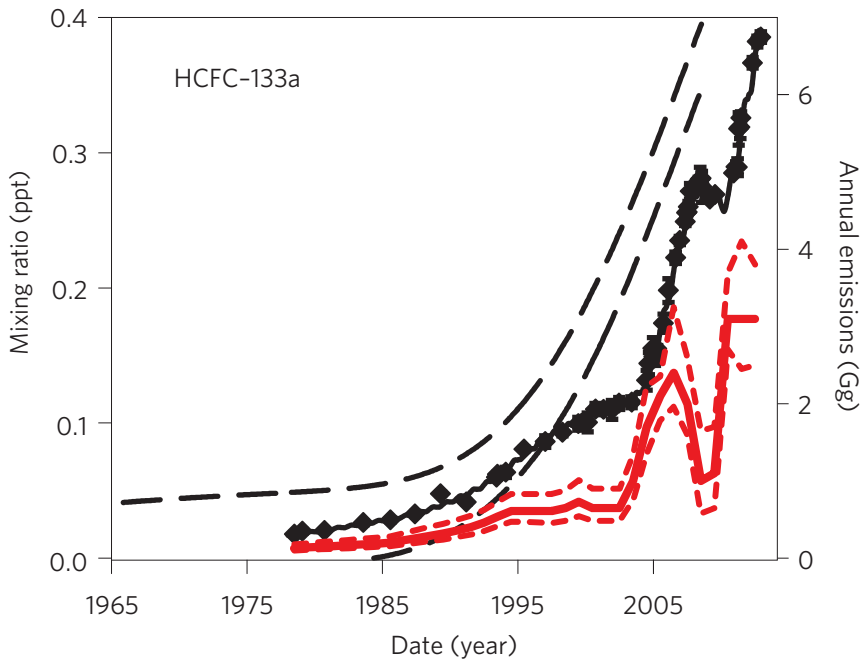

Figure 4.35: Atmospheric history and global trend of HCFC-133a. Black dashed lines reflect the range of northern hemispheric trend, reconstructed from firn samples. Black diamonds represent average individual samples collected at Cape Grim and the black solid line is the model fit through this data set that was used to estimate emissions (red line, right hand axis). Dashed red lines indicate 1σ uncertainties. From Laube et al. 2014

4.9.3.1.4 Chlorocarbons

These species are, as the name suggested, chlorinated compounds that do not contain fluorine and have lifetimes longer than 6 months. As such their production and use are controlled and so decreasing concentrations are expected across the three campaigns.

Overall, whilst carbon tetrachloride and methyl chloroform were detected at levels above background in 2013 and during the first half of the 2014 campaign, both were found at below background levels for the latter 2014 samples. Distinct spikes in concentration are still seen however and both compounds appear to be decreasing in-line with their global trends. Correlation and individual differences are discussed below along with a further chlorocarbon, halothane, for which background values are unknown.

Carbon Tetrachloride – Figure 4.36a

Whilst its uses as a feedstock for CFC-11 and CFC-12 production have been phased out due to the Montreal Protocol, carbon tetrachloride (CCl_4) does have applications in other chemical reactions however these do not fully explain the abundances being detected globally, even though the overall atmospheric trend is decreasing. Median mixing ratios for 2013 and 2014 reflect this trend (89.6 ppt to 85.5 ppt) however the 2015 median is very similar (85.7 ppt). However, a large portion of the 2014 campaign samples were detected at noticeably below background levels, which may have skewed the median. 2015 still saw several samples with near-background mixing ratios over the campaign suggesting that levels are decreasing as expected.

Significant spikes were seen during each campaign: 113 ppt and 134 ppt on the 20th March and 1st April 2013 respectively, 101 ppt on the 13th March 2014 and 94.4 ppt on the 22nd March 2015. Aside from the 1st April 2013, NAME backwards trajectories all suggest emission from China as the potential major influence on these days. For the 1st April, Japan is the suggested major influence although China was assessed as possibly having a minor impact as well. Given that this is the largest of all the spikes observed, this could suggest Japan as a significant source location however other days with similar trajectories see much closer to corresponding background abundances.

Carbon tetrachloride was found to have excellent correlation (0.95) with chloroform in 2013 indicating possible co-emission, however this reduces to only good correlation for 2014 (0.79) and 2015 (0.81). This may suggest that co-location is more likely for these species however chloroform does have some natural sources and as such, emissions of these may see more variance in magnitude and location than an anthropogenic source necessarily would.

Aside from chloroform, carbon tetrachloride does not exhibit good interspecies correlation consistently with any other compound except methyl chloride.

2014 saw the largest amount of correlation with other compounds and the majority of these are species found to have potential sources in China. However, whilst a number of minor species with potential Chinese sources such as CFC-113a, Halon 1202 and HFC-23 do correlate with carbon tetrachloride, related and significantly more major species have notably less correlation such as CFC-113, Halon 1211 and HCFC-22. This could be an indication that, while some of these compounds are by-products and so expected to have very similar sources to the major species, they could potentially have sources that are not co-located.

Methyl Chloroform – Figure 4.36b

Methyl Chloroform (CH_3CCl_3) was utilised as a feedstock for HCFC-141b and -142b production however, due to its inclusion in the Montreal Protocol, its production and consumption has been phased out and as such global abundances have been steadily declining since the mid-1990s. Figure 4.36b and the median mixing ratios for each campaign (5.0 ppt in 2013, 4.0 ppt in 2014 and 3.3 ppt in 2015) clearly indicate that the observed abundances are following the global trend.

Whilst 2013 mixing ratios were mostly enhanced above background (4.7 ppt) the later campaigns saw a number of samples detected in line with the corresponding background abundances (3.9 ppt in 2014 and 3.2 ppt in 2015). Only one significant spike was observed and that was on the 12th March 2014 at 4.4 ppt. NAME back trajectory assessment of this day indicated China and Taiwan as potential major influences and local wind data also suggest impact from nearby Taiwanese sources. Proximity of Taiwanese sources would account for the higher mixing ratio although other days with similar local wind conditions do not exhibit consistent enhancement.

No good or excellent interspecies correlations were seen with methyl chloroform however some correlation was seen in all three campaigns with a variety of species although the number this was with decreased from 14 in 2013, to 2 in 2015 with only halon 1301 showing some correlation in both (however not in 2014). This lack of consistent correlation is likely due to the fast rate at which methyl chloroform abundances are decreasing and its relatively short atmospheric lifetime (0.9 years, Carpenter and Reimann, 2014) compared to other halocarbon species.

Halothane – Figure 4.36c

The minor chlorocarbon species halothane, which was once utilised as an anaesthetic, was also measured in 2014 and 2015 however no background data was available so only limited assessment can be made. Median mixing ratios between the two campaigns are very similar (~0.01 ppt in both 2014 and 2015). Vollmer et al (2015b) observed similar abundances during 2014 however pollution events were not detected suggesting sources were outside of Europe but still northern hemispheric in origin.

Significant spikes in abundance from the Taiwan campaigns were observed on the 22nd and 23rd of April (AM and PM) 2015 and comparison with NAME backwards trajectories suggests Korea as the predominant major potential source for all three samples. Other days with similar trajectories however do not exhibit similar mixing ratios.

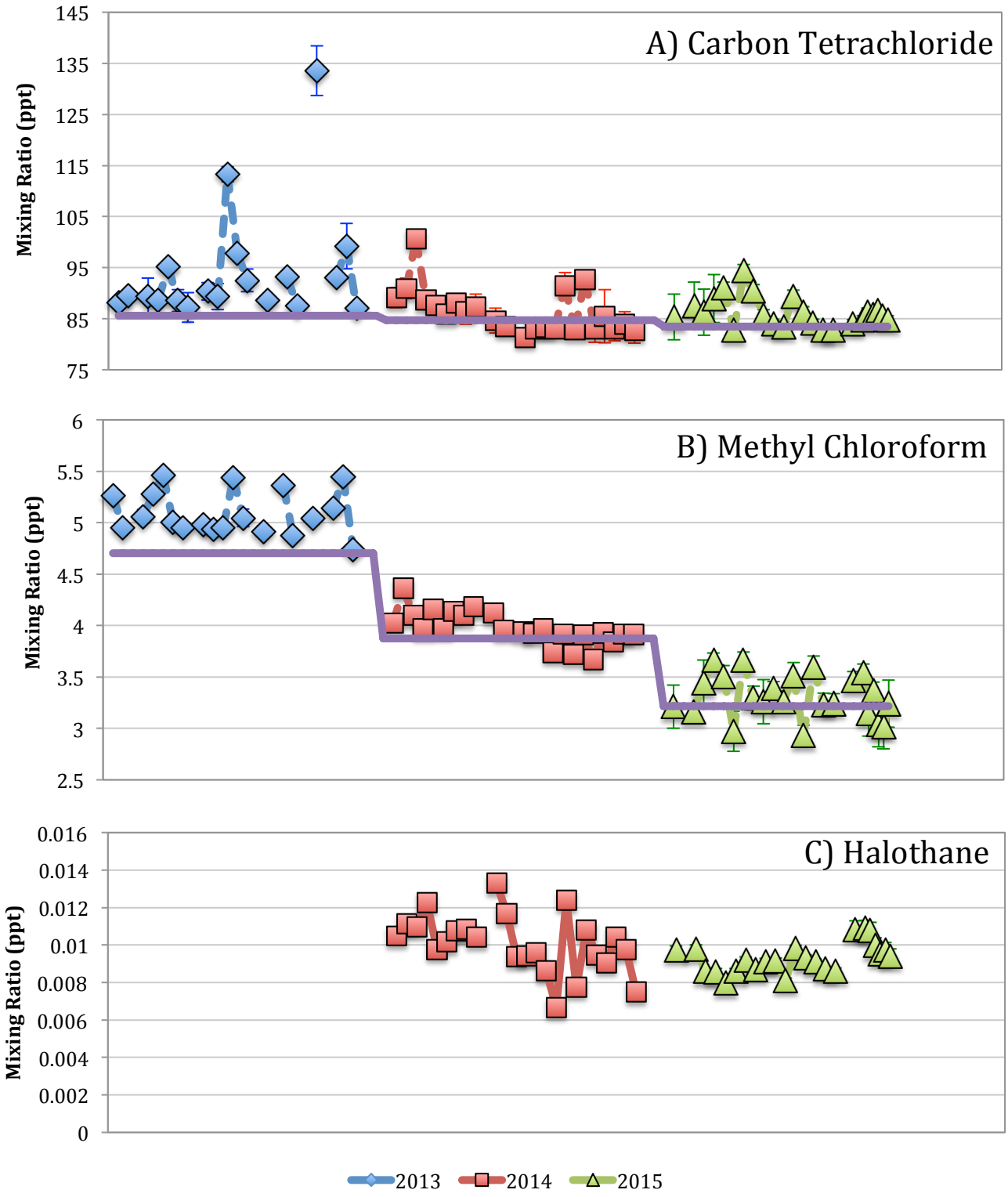

Figure 4.36: Time series spanning the three Taiwain campaigns for the chlorocarbons – A) carbon tetrachloride, B) methyl chloroform and C) halothane. Data from 2013 is represtented in blue, 2014 in red and 2015 in green. Background abundances are shown in purple. Error bars indicate the total uncertainty calculated for the samples

No good or excellent correlation was associated with halothane however some correlation was found with methyl chloroform (0.51) in 2014 and C_5F_{12} (0.54) in 2015. These are unlikely to indicate potential co-location of sources or related applications and so may be coincidental.

4.9.3.1.5 Very Short Lived Substances

The VSLS are a group of species not controlled under global legislation. Due to their short lifetimes of typically less than 6 months, high concentrations of these compounds are not expected to reach the stratosphere and impact ozone depletion as transport to this altitude take longer in most locations. However, as previously discussed, the East Asian region does experience deep convection which can transport compounds from ground level to the TTL in a matter of days (Ashfold *et al*. 2015) and as such the impact of these species may be larger than anticipated.

Chlorinated VSLS

The contribution to stratospheric chlorine from these species has previously been considered marginal but recent studies have found tropospheric levels of VSLS to be increasing (Leedham-Elvidge et al. 2014, Hossaini et al. 2015, Oram et al. in preparation, 2016) and that source location can significantly affect the impact of these species as ODS (Pisso et al. 2010, Brioude et al. 2010). Further information and explanation regarding these studies can be found in Chapter 6. These species are widely used in industry across the region and since their production is not controlled like other ODS, emissions are not expected to decrease.

For these compounds, concentrations are mainly enhanced across all three campaigns and NAME trajectories indicate China and Korea as the main sources of emissions however chloroform also shows some influence from Japan. Correlation and inter-annual variation suggest some differences between species and so are discussed individually below.

Dichloromethane (DCM) – Figure 4.37a

The most abundant VSLS-Cl species is dichloromethane, which has anthropogenic applications as a foam-blowing agent and paint remover. Globally, in recent years DCM mixing ratios have increased significantly (67% between 2001 and 2012, Carpenter and Reimann, 2014) although there is distinct seasonal variation in mixing ratios caused by hydroxyl radical concentration and photolysis frequency (see Figure 4.38). Medians for the three Taiwanese campaigns follow this trend between 2013 (239 ppt) to 2014 (265 ppt) but there is a significant decrease in 2015 (199ppt) potentially due to the shift in major emissions contributions from China to Korea or due to a reduction in regional sources enabling a shift towards stabilisation as DCM was detected at consistently enhanced abundances. Given the short-lived nature of this compound, the effect of changes in emissions on mixing ratio should be identifiable.

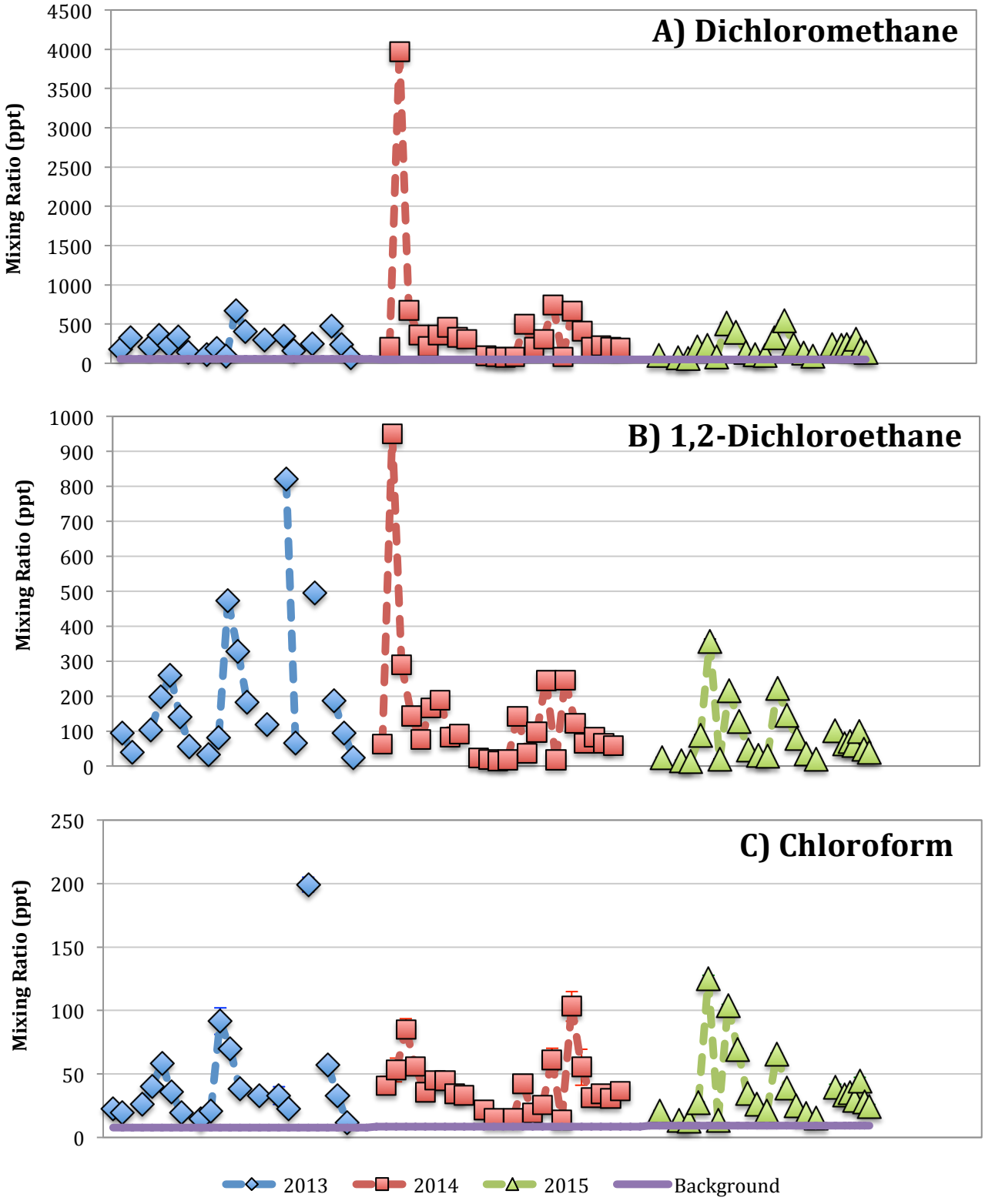

Figure 4.37: Time series spanning the three Taiwain campaigns for the major chlorinated VSLS – A) dichloromethane, B) 1,2-dichloroethane and C) chloroform. Data from 2013 is represtented in blue, 2014 in red and 2015 in green. Background abundances are shown in purple. Error bars indicate the total uncertainty calculated for the samples

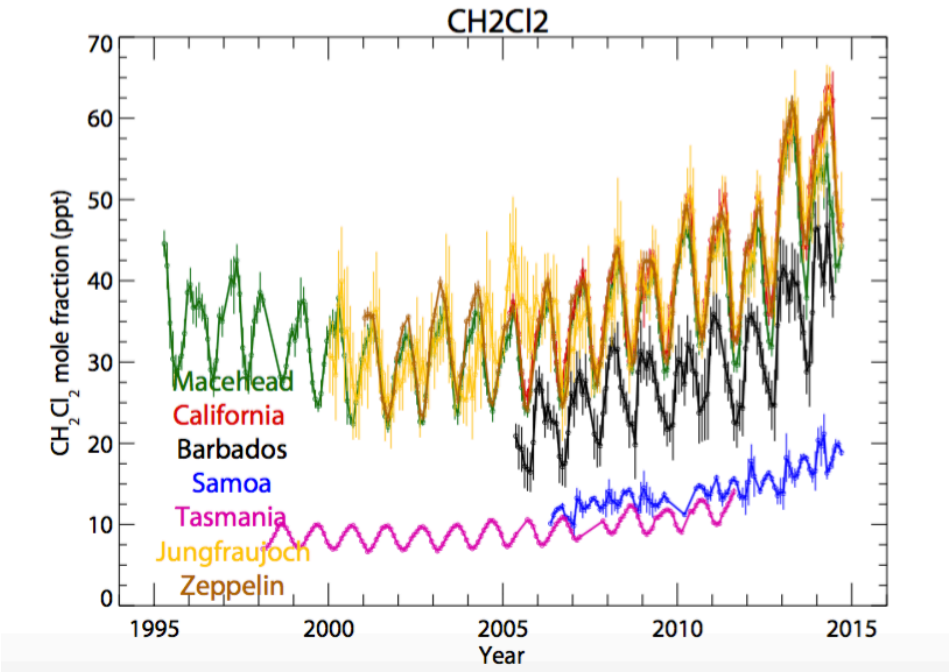

Figure 4.38: Seasonal variation of dichloromethane, up to September 2015, as measured by a range of sites in the AGAGE monitoring network.
Taken from: agage.mit.edu/data/agage-data

The most significant spike observed for DCM was the previously mentioned 12th March spike and was over 60 times the background mixing ratio (49.0 ppt). Several other compounds, including the short chain PFCs, were detected at particularly high levels on this day but none to this magnitude. Analysis of local winds for that day does imply that Taiwanese emissions may have been sampled however other days with significant spikes during this campaign (13th, 28th and 30th March with mixing ratios of 675 ppt, 741 ppt and 665 ppt respectively) do not correspond with days where meteorological data suggest impact from local sources (see Case Study 3, section 4.12 for further details). This implies that this huge peak, if caused by a local source, was likely due to one very near the sampling site and captured only on that day. Another possibility is that of multiple emissions sources being sampled and a potential combination of Taiwanese, Chinese and Korean emissions (as suggested by the NAME trajectory) causing this large spike however a very close local source seems more likely.

In terms of correlation, DCM showed good correlation with other compounds that were mainly found to be influenced by Chinese emissions including some HCFCs and CFC-113a, suggesting similarities in source location. In 2014 there was also found to be good correlation with the short-chain PFCs suggesting that some local sources of DCM were measured. Excellent correlation, implying potential coemission, was also seen during this campaign with HCFC-141b, another foam-blowing agent and 1,2-dichloroethene, another short lived species.

1,2-Dichloroethane (DCE) – Figure 4.37b

This short-lived species is utilised in polymer and rubber production but is not currently regularly measured in the atmosphere and so no background data is available to compare the results of the Taiwanese campaigns to. Median mixing ratios potentially suggest a decreasing atmospheric abundance since these reduced from 119 ppt in 2013, to 82.3 ppt in 2014 and 59.0 ppt in 2015. However a very wide range of mixing ratios were observed, particularly in the 2013 and 2014 campaigns, so general atmospheric and inter-annual variation is likely to have contributed as well.

All three campaigns each see a significant spike in mixing ratios but these are particularly dramatic in the first two campaigns. For 2013 this spike was measured on the 27th March and reached 820 ppt whilst in 2014 a mixing ratio of 950 ppt was reached on the 12th March. The significant spike during the 2015 campaign was observed on the 20th March at 356 ppt. Comparison with NAME backwards trajectories suggests that Chinese or Taiwanese emissions may have influenced the sampled air mass. Some likelihood of a local source of emissions is potentially indicated by local wind speeds, which were all comparatively low on these days (between 2 and 3.5 m s^{-1}) and, in the 2014 campaign, wind direction which suggested transport from industrialised areas of Taiwan. However, local wind directions for the 2013 and 2015 campaigns appeared oceanic in origin and with an atmospheric lifetime of 47 days (Carpenter and Reimann, 2014), a source in coastal China, where many chlorination-based industries are located, being transported across the ocean is plausible.

In terms of correlation, DCE was found to consistently have good correlation with HFC species across all three campaigns. In 2014, it also had good correlation with the short chain PFC species, which suggests potential local sources (see Case Study 3) and excellent correlation was found with HCFC-141b and DCM, both of which have major sources in China. 2015 saw good correlation with HCFC-141b as well as HCFC-22 and another short-lived species, chloroform.

Overall, the data from these campaigns indicates the presence of local emissions sources of DCE in both the North and South of Taiwan.

Chloroform – Figure 4.37c

Whilst chloroform has some natural sources, anthropogenic sources account for approximately 50% of its emissions. The global trend of chloroform is increasing, and the inter-annual variation for these campaigns showed the median detected mixing ratio was 33.0 ppt in 2013 and 35.7 ppt in 2014 but 28.0 ppt in 2015. Whilst the 2015 campaign was analysed using the AutoSpec instead of the Entech for this species, there is no clear evidence of significant instrument variation as the range of mixing ratios detected appears similar to that of the previous campaigns and no clear over- or underestimation is discernible between the data sets.

Given that this is a short-lived species, with a lifetime of 112 days in the boundary layer, variation in emissions may result in perceptible differences in mixing ratios much sooner than with other ODS which may have contributed to this lower median.

Significant spikes for chloroform were observed on the 1st April 2013 (199 ppt), the 13th and 30th March 2014 (85.1 ppt and 103 ppt respectively) and on the 20th and 22nd March 2015 (125 ppt and 104 ppt respectively). Background mixing ratios for chloroform are less than 10 ppt throughout the campaigns so these abundances are substantial in comparison. A potential source location of emissions given these spikes is not clear as the NAME back trajectories indicate Japan as a possible major source for the 2013 spike, China for 2014 and the Pacific Ocean as well as China for 2015. Including potential minor sources into the assessment adds Taiwan as an option however local winds speeds and directions do not suggest any consistent impact. Given there are natural sources of this species, emissions from these may have been influential as well and their locations may be more widespread.

In terms of good correlation, chloroform was found to be correlated with mainly other VSLS and chlorocarbons in all campaigns, particularly carbon tetrachloride which was found to have excellent correlation in 2013 (0.95). In 2014, good correlation was established with considerably more species and this may be due to the higher proportion of trajectories from China, where potential emission sources for these species have been suggested.

Tetrachloroethene (PCE) – Figure 4.39a

This minor short-lived chlorinated species, also known as perchloroethene (PCE), is utilised as a dry-cleaning solvent and in metal degreasing and has previously been observed to have a decreasing atmospheric abundance (Carpenter and Reimann, 2014). However, background abundances for Mauna Loa indicate that 2013 saw the lowest background at 2.20 ppt, which then increased to 2.65 ppt in 2014 and decreased again to 2.30 ppt in 2015. Median mixing ratios from the Taiwanese campaigns during 2013 and 2015 suggest a slight decrease from 4.38 ppt to 4.3 ppt however the 2014 median is substantially higher at 5.61 ppt. This increase is consistent with the change in background but is of a slightly larger magnitude. As has been seen for several previously mentioned species, medians are often higher during this campaign and this is likely due to the different sampling site, proximity to sources and the disparity in dilution that occurs given the variation in transport time between North and South Taiwan. This may be especially noticeable for short-lived species like PCE, which has a lifetime of 90 days in the boundary layer (Carpenter and Reimann, 2014), and so may have contributed to the higher abundance detected here.

Of the significant spikes observed, for all three campaigns these reached over 15 ppt and all occurred on days which, comparison with NAME back trajectories indicates, have potential major influences from Chinese emissions (21st March 2013, 12th, 13th and 30th March 2014 and 22nd March 2015).

Good correlation was consistently found with the HCFCs and CFC-113 and -113a, all of which have also been suggested to have emissions sources in China. Excellent correlation was seen with HFC-23 in 2013, indicating potential co-emission, however a combined source of these species is not currently known.

Chloroethane – Figure 4.39b

This species is not regularly measured and so no background or global trend data is available however it has uses in the production of ethyl cellulose and some pharmaceuticals. Median mixing ratios are notably higher in 2013 at 68.4 ppt compared to 20.6 ppt and 30.5 ppt in 2014 and 2015 respectively. Figure 4.39b indicates that there appears to be a consistent enhancement during this campaign, relative to the latter ones, and this could be indicative of contamination or, more likely, a local source. However, the 2014 and 2015 medians suggest that abundances of chloroethane may be increasing in the atmosphere.

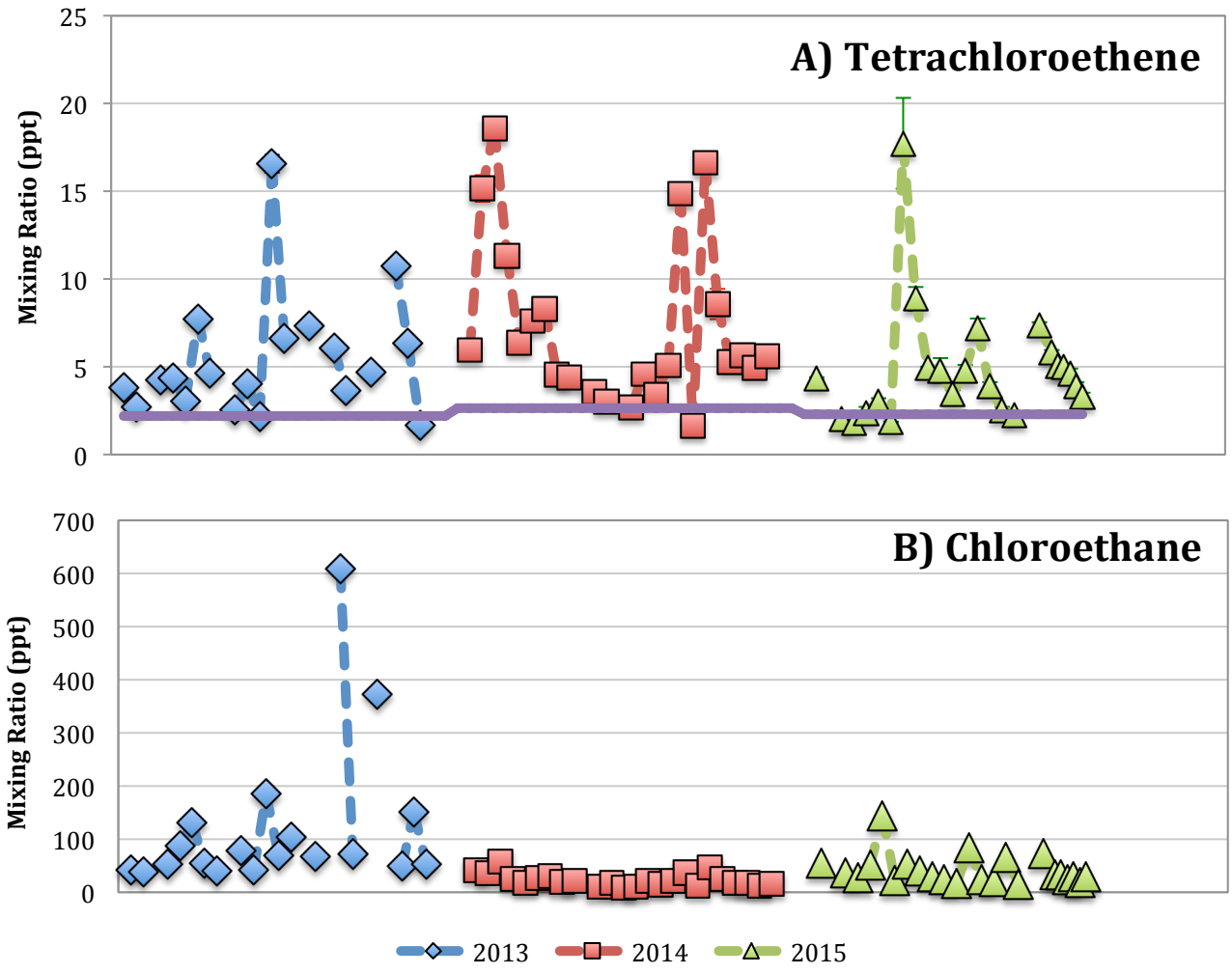

Figure 4.39: Time series spanning the three Taiwain campaigns for the other chlorinated VSLS – A) tetrachloroethen and B) chloroethane. Data from 2013 is represtented in blue, 2014 in red and 2015 in green. Background abundances are shown in purple. Error bars indicate the total uncertainty calculated for the samples

Significant spikes were detected on several days throughout the three campaigns, although those in 2014 are less clearly visible in Figure 4.39 than those in 2013 and 2015. These correspond with spikes in DCE abundance along with further spikes on the 1st April 2013 (372 ppt, although this includes the potential contamination suggested previously) and the 30th March 2014 (47 ppt). This similarity with DCE suggests the likelihood of a source in China, potentially coastal, for chloroethane and also indicates that these emissions are unlikely to be natural in origin. The other two spikes detected indicate a more long-range emissions source as well, potentially from China or Japan, when compared to the NAME back trajectories for the associated days.

No excellent correlation was seen with chloroethane throughout any of the campaigns however good correlation was found with DCE in 2013. This suggests that these emissions may be from chloroethane utilised in the Chinese industry, such as polymer and rubber production, as opposed to natural sources. Good correlations in 2014 were seen with a range of different compound groups, similar to many other ODS during this campaign, although several other short-lived species are included. Only HCFC-22 was shown to have good correlation in 2015.

Brominated VSLS

Similar to their chlorinated counterparts, VSLS-Br species have lifetimes under 6 months but are however, mostly natural in origin. Seasonal and temporal variations have resulted in difficulties in quantifying global emissions and as such little data is available. The only species discussed in this section will be bromoform, due to having some anthropogenic sources from water chlorination.

Bromoform – Figure 4.40

This species has an atmospheric lifetime of around 40 days in the boundary layer and around 46 days at 10km altitude. It primarily has oceanic natural sources however the anthropogenic process of water chlorination may result in bromoform emissions. Median mixing ratios fluctuate between the three campaigns from 2.4 ppt (2013) to 5.8 ppt (2014) and 2.0 ppt in 2015. As previously stated, there are difficulties associated with measuring VSLS-Br species consistently, and there is clear enhancement throughout the 2014 campaign which could be due to differences between the sampling sites or it may be indicative of a contamination issue. Chloroform saw a similar, at least partially, unexplained enhancement during this campaign and, given the related chemical structures, these instances may be related but further icampaigns would be required to confirm this.

Comparison with NAME back trajectories on days when significant spikes in mixing ratio were detected (12th March 2013, 25th and 27th March 2014 and 19th and 20th March 2015) all suggest Pacific Ocean influence which would correspond with a known natural source of bromoform.

Good correlation was found in 2013 with halon 1211 and SF_6 and in 2015 with HCFC-141b. Whilst these species are anthropogenic in origin, they do have widespread emissions sources across the East Asian region and so these relationships are more likely coincidental than associated with a specific anthropogenic source of bromoform.

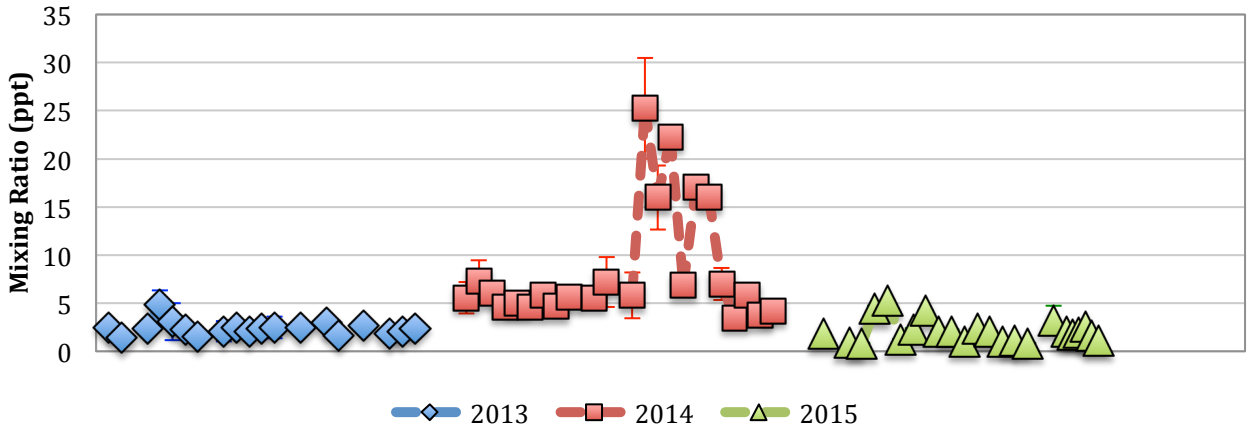

Figure 4.40: Time series spanning the three Taiwain campaigns for the brominated VSLS – Bromoform. Data from 2013 is represtented in blue, 2014 in red and 2015 in green.. Error bars indicate the total uncertainty calculated for the samples

4.9.3.1.6 Methyl Halides

Unlike many of the other species previously mentioned, the methyl halides have a number of natural sources and so are less indicative of anthropogenic emissions. However they do contribute to ozone depletion and so their levels should be monitored.

Methyl Chloride – Figure 4.41a

For methyl chloride, which has several anthropogenic sources, including coal combustion and silicone production, mixing ratios were found to be almost consistently above background across all three campaigns. The global trend suggests levels of methyl chloride are very slowly decreasing and the 2013 median abundance (924 ppt) is notably higher than the other two campaigns. However the later campaigns have median abundances much closer together (753 ppt in 2014 and 770 ppt in 2015) and the background did increase slightly between 2014 (546 ppt) and 2015 (554 ppt), which would have had some impact. However since there are natural sources of this species some fluctuations in levels are to be expected.

Significant spikes were seen on the 21st March 2013 (1240 ppt), 13th and 30th March 2014 (1090 ppt and 1050 ppt respectively) and 22nd March 2015 (1090 ppt). Comparison with NAME back trajectories suggests that emissions from China and Korea are the major influences on these days which could suggest anthropogenic sources however, given the wide range of natural sources including rice paddies and biomass burning, this is not clear.

Good correlation was seen with other species that have been suggested to have sources in China such as the VSLS and some HFCs. Correlation with methyl bromide (which could indicate biomass burning sources) was good in 2015 (0.86) but there was only some correlation between these species in 2013 (0.52) and 2014 (0.71). This suggests potential biomass burning sources in 2015 and these may have contributed to the higher median mixing ratio.

Methyl Bromide – Figure 4.41b

Methyl bromide shares many natural sources with methyl chloride however its anthropogenic use as a fumigant, now controlled under the Montreal Protocol, was extensive. In the Taiwanese campaigns, methyl bromide was consistently detected above background levels, notably more so in 2013 as seen with methyl chloride. This consistent enhancement, similar to that detected for the long chain PFCs during this campaign, could suggest either no background air masses were measured, which seems unlikely given the results of previously mentioned compounds, or potential contamination, either of the site or the sampling equipment. However, spikes in concentration on specific days were still clearly identifiable so while assessments of median mixing ratios and comparisons to long-term trends cannot be made with this campaigns data, potential source location and correlations can still be discussed.

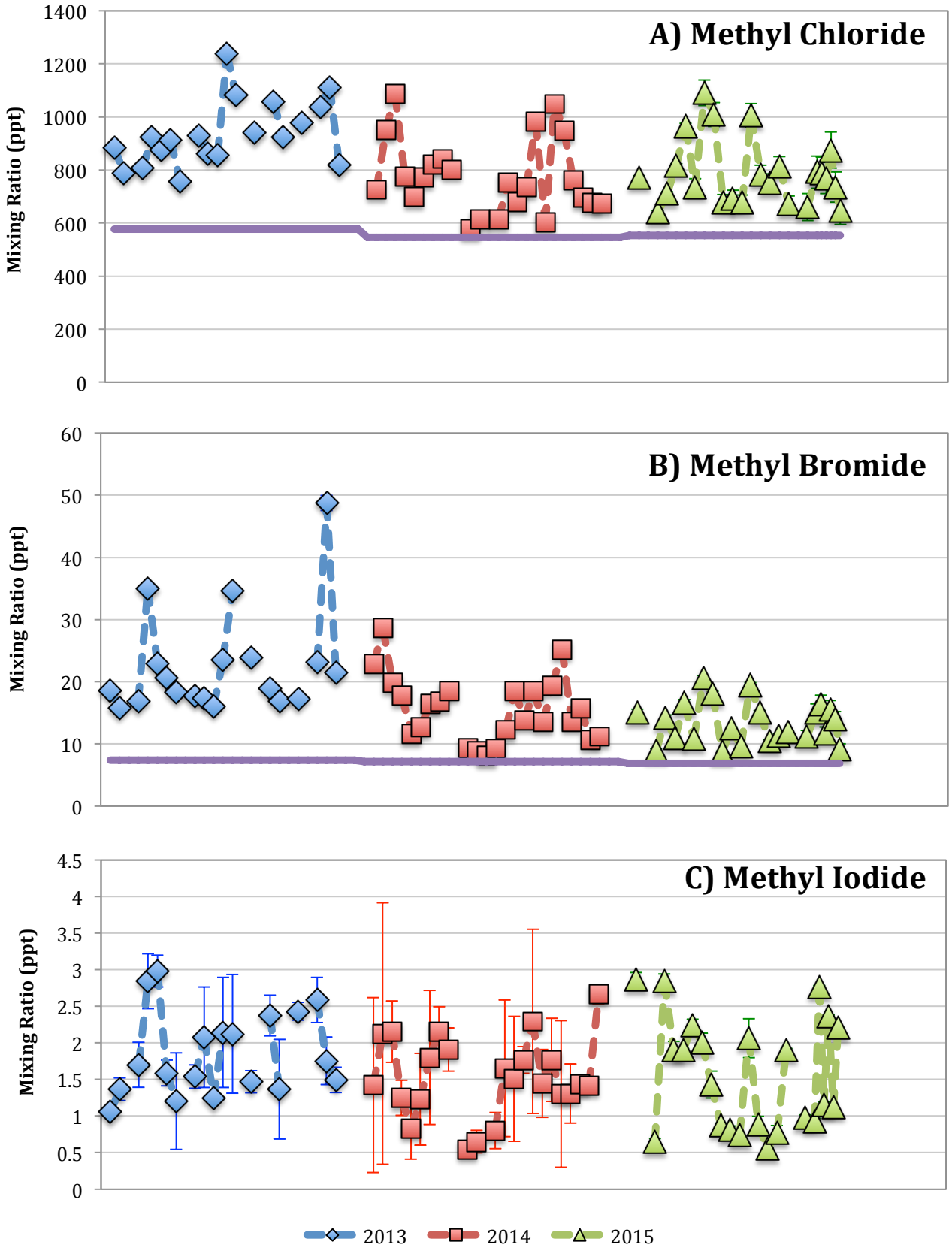

Figure 4.41: Time series spanning the three Taiwain campaigns for the methyl halides – A) methyl chloride, B) methyl bromide and C) methyl iodide. Data from 2013 is represtented in blue, 2014 in red and 2015 in green. Background abundances are shown in purple. Error bars indicate the total uncertainty calculated for the samples

The global trend for methyl bromide is decreasing and, whilst only considering the results of the 2014 and 2015 campaigns, median levels dropped from 14.8 ppt to 12.5 ppt, indicating the Taiwanese campaigns were consistent with the global trend.

Significant spikes in mixing ratios were observed on the 4th April 2013 (48.8 ppt), 12th March 2014 (28.6 ppt) and the 22nd and 27th March 2015 (20.6 ppt and 19.5 ppt respectively). Comparison with NAME back trajectories indicates a range of potential major sources including China, Korea, Taiwan and the Pacific Ocean. As such, little can be suggested as the main cause or location of the emissions leading to these measurable abundances.

With interspecies correlation, very few compounds had good correlation with methyl bromide except for HCFC-22 and HFC-125 in 2014. This lack of correlation is likely caused by the variation and widespread nature of the natural sources of methyl bromide.

Methyl Iodide – Figure 4.41c

Oceanic sources, particularly coastal sources, are responsible for the majority of methyl iodide emission and with its very short lifetime (~7 days), background data is not available for this compound. Median mixing ratios are similar for 2014 (1.5 ppt) and 2015 (1.4 ppt) although 2013 (1.7 ppt) is slightly higher but this was the case with the other methyl halides as well.

Significant mixing ratios were measured on the 13th March 2013 (3.0 ppt) and 4th April 2014 (2.7 ppt). The NAME back trajectory for the 13th March indicates the Pacific Ocean as a major source, which corresponds with known methyl iodide sources. The 4th April saw a Chinese and Korean influenced trajectory however a large proportion of that transport is over ocean and so emissions are likely to have been transported from there.

In 2015, methyl iodide does not see any interspecies correlation however in 2013 both some and good correlation are found with a wide range of species from different groups and with different applications, similarly for 2014 as well. This suggests, particularly due to the short atmospheric lifetime of this species, that these non-consistent correlations are probably coincidences from short-range transport of methyl iodide emissions from the ocean surrounding the island of Taiwan.

4.9.3.2 Greenhouse Gases

The species discussed in the following sections absorb infrared radiation and thus contribute to global warming making them greenhouse gases (GHGs). The previously discussed ODS species also absorb infrared but the following species do not contain chlorine or bromine and so do not deplete ozone. As such their production and consumption is not controlled under the Montreal Protocol however the Kyoto Protocol (see section 1.13) was set up as a control measure with an aim to reduce emissions of GHGs including those discussed below.

4.9.3.2.1 Hydrofluorocarbons

As the second generation of replacements for ODS, levels of HFCs in the East Asian region are expected to be increasing. Since their uses are widespread, emissions from China, Korea and Taiwan are anticipated as well as those from Japan where, due to their developed country status, HFCs are primarily used.

Overall, results for the HFCs were mostly found to be above background levels aside from HFC-245fa and -365mfc. NAME trajectories indicate Chinese and Korean emissions to be dominant for most of the spikes in concentrations detected for these compounds although some influence from Japan was noted for HFC-125, -227ea and -365mfc, as well as some Taiwanese impact for HFC-152a and -245fa. As expected due to its widespread emissions, HFC-134a saw no predominant trajectories and correlations were mainly with other extensively used species such as Halon 1211 and SF_6. Other HFCs were mainly found to have correlation with HCFCs and VSLS species. In terms of the variation established by these campaigns, the majority of HFCs were indicated to be increasing, reflecting their global levels except for HFC-23 and -152a. Discussed below are more species specifics found during the analysis.

HFC-134a – Figure 4.42a

With its main application in mobile air conditioning, an extensive and ever expanding industry, HFC-134a has an increasing global trend and the results of the Taiwanese campaigns reflect this. Median mixing ratios increased from 81.9 ppt in 2013 to 95.5 ppt in 2015. Figure 4.43 compares these medians with data from the 2010 Yao et al. (2012) campaign and this confirms mixing ratios in recent years have been continually increasing for this species.

Comparison with NAME back trajectories and those samples with significant spikes in abundance, suggests no consistent specific area as a potential source of emissions for HFC-134a. Since mobile air conditioning sources are widespread across the East Asian region, this is not unexpected. However, Taiwan is either a potential major or minor influence on most of the days with spikes in concentration possibly indicating that any proximity to sources in local area may have impacted mixing ratios. These spikes ranged from 104 ppt in 2013 to 132 ppt in 2015 when respective background mixing ratios were 72.8 ppt and 83.7 ppt.

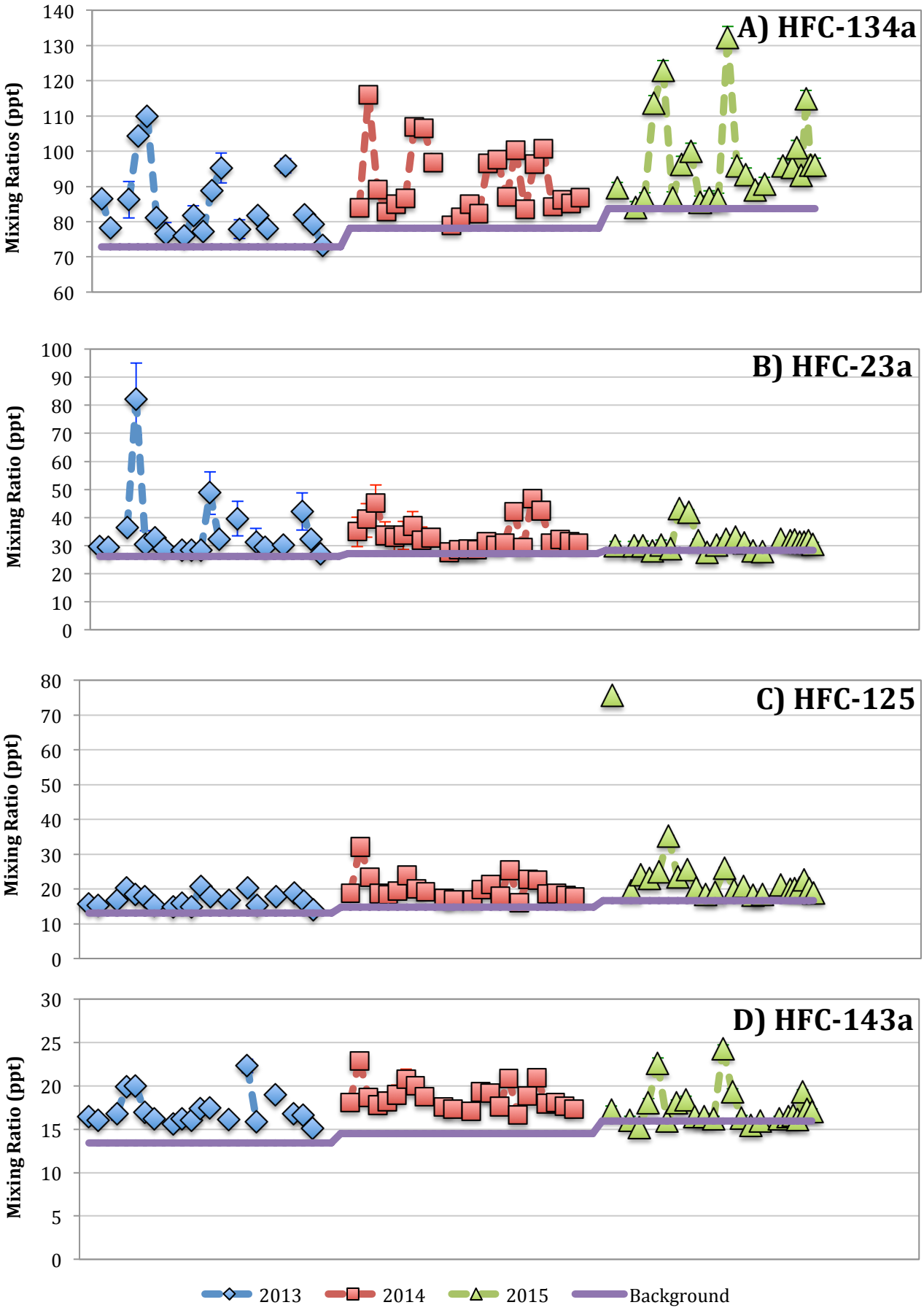

Figure 4.42: Time series spanning the three Taiwain campaigns for the major HFCS– A) HFC-134a, B) HFC-23, C) HFC-125 and D) HFC-143a. Data from 2013 is represtented in blue, 2014 in red and 2015 in green. Background abundances are shown in purple. Error bars indicate the total uncertainty calculated for the samples

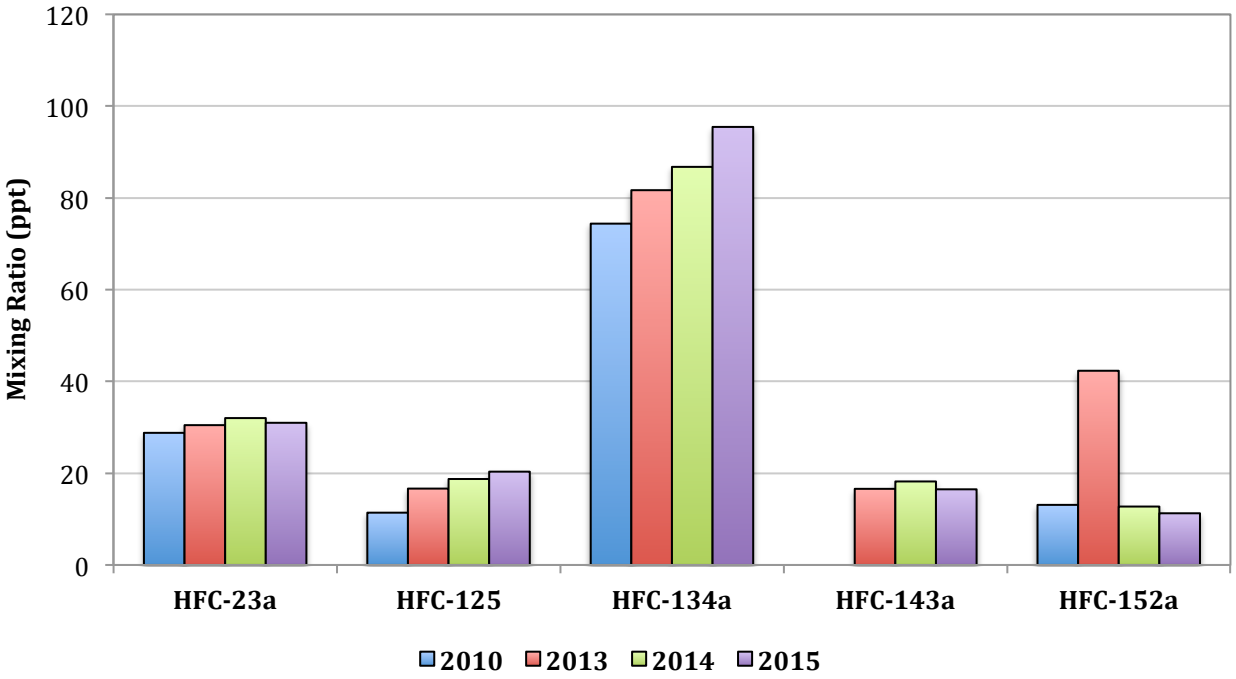

Figure 4.43: Comparison of mixing ratios of the major HFCs from literature (Fang et al. 2012a for 2010) and the Taiwan campaigns (2013, 2014 and 2015).

Interspecies correlation with HFC-134a varies between campaigns more than with the other HFC species and good correlation is only consistently seen with Halon 1211 and SF_6. This is most likely due to their widespread sources found across the region and similarities in source locations due to applications found in generally populated areas.

HFC-23a – Figure 4.42b

HFC-23a is mainly produced as a by-product of HCFC-22 manufacture however it does have some minor applications as a fire extinguisher and dry etching agent. Between 2013 and 2015 the background mixing ratio increased from 26 ppt to 28.3 ppt indicating the global trend is increasing. Median abundances from the Taiwan campaigns can be seen in Figure 4.43 and, whilst this trend is followed between 2013 and 2014 (and previously when compared with the 2010 data from literature), in 2015 the median was calculated to be 31 ppt, a 1 ppt decrease from 2014. More near-background (28.3 ppt) samples were observed in 2015 whilst 2014 saw more general enhancement, likely caused by the difference in sampling site and proximity to sources.

A number of significant spikes in abundance were measured during each campaign; 12th March 2013 (82 ppt), 13th and 30th March 2014 (45 ppt and 47 ppt respectively) and the 22nd and 23rd March 2015 (43.1 ppt and 41.9 ppt respectively). Back trajectories from the NAME model suggest, for all these spikes, that Chinese emissions potentially influenced the sampled air masses.

This is consistent with the general enhancement seen during the 2014 campaign, when the largest proportion of Chinese back trajectories were measured and so indicates this is a likely source of emissions. China is also known to manufacture HCFC-22, the main source of HFC-23.

Unsurprisingly, good correlation was found with other species that have suggested sources from Chinese emissions including HCFCs (-141b and -133a), and VSLS-Cl (DCM and PCE) however none of these are consistent throughout all three campaigns indicating potentially shifting source locations. Excellent correlation was only found in 2013 and this was with HCFC-142b and PCE, not HCFC-22 as would be expected from a by-product source. In fact, correlation with HCFC-22 was only found to be good in 2014 (0.88 [Pearson correlation coefficient]), which does indicate some co-location, likely from Chinese emissions sources. However, the other two campaigns also saw trajectories influenced by China but correlations with HCFC-22 were only 0.31 in 2013 and -0.02 [Pearson correlation coefficients] (see Figure 4.44 for graphical comparison), indicating no relationship between sources of these species. HCFC-22 data for 2013 and 2015 did suggest that regional sources may have been decreasing which may be related to the HCFC phase out beginning. This could result in other sources of HFC-23a starting to dominate observed mixing ratios, creating the lack of correlation found.

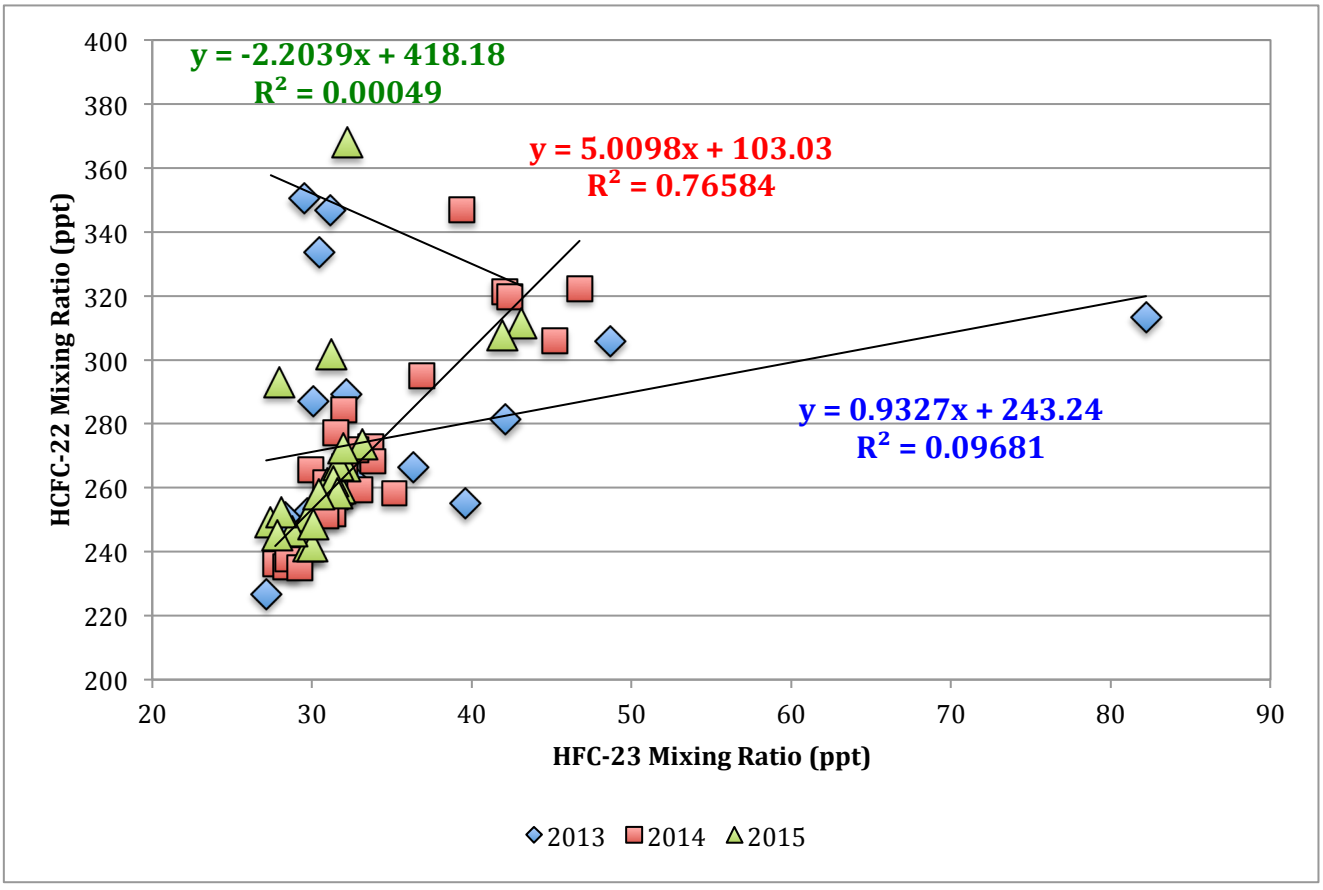

Figure 4.44: Correlation between HCFC-22 and HFC-23. Although HFC-23 is a known by-product of HCFC-22 production, good correlation (as shown by the R^2 values) is only seen during the 2014 campaign suggesting sources in the other years were not co-located and may vary given the widespread applications of these species.

However, as is noticeable on the graph, the R^2 values are likely to have been strongly influenced by one data point in 2013 (12th March) and potentially 3 data points in 2015 (19th and27th March, 24th April [PM)]. The removal of these data points sees the Pearson correlation coefficient for 2013 actually decrease to 0.22, however the coefficient for 2015 increases to 0.95. Whilst these data points and the 2013 campaign do suggest there may be sources of HFC-23a not co-located with HCFC-22, the 2014 and 2015 campaigns indicate there is still a clear relationship between the two species, even if regional sources may be decreasing.

HFC-125 – Figure 4.42c

Like HFC-23, applications of HFC-125 include as replacement species in fire extinguishers and dry etching agents, particularly in electronics manufacture. As such the global trend for this compound is increasing and this agrees with the median mixing ratios detected for the three Taiwanese campaigns. Figure 4.43 again compares these medians with a literature value from 2010 (11.4) and abundances have increased each year to 20.3 ppt in 2015. Background mixing ratios have increased from 13.1 ppt (2013) to 16.7 ppt (2015) and samples from the campaigns were mainly enhanced above this, likely due to the proximity of the sites to source regions, comparative to the remote location of the background site.

Significant spikes in mixing ratios were observed on the 21st March 2013 (20.7 ppt), 12th March 2014 (32.0 ppt) and 12th March 2015 (75.8 ppt) and all of these correspond to days where assessment of NAME trajectories suggest major influence from Chinese emissions. The notably larger abundance detected in 2015 also corresponds with similar relative spikes for many of the other HFCs and, whilst NAME also indicates Taiwan may be a major influence on this day as well, comparison with local winds is consistent with katabatic winds and so implies this may be regional Taiwanese emissions rather than local.

Good correlation was seen with HCFC-141b and other HFCs in 2013 and 2014 as well as DCM, all species assessed to have potential source locations in China. Only excellent correlation was seen in 2015 and this was with HFCs -152a (0.97) and 245fa (0.96), both utilised in foam blowing and may be combined in refrigerant blends. Halon 2402 (0.96) also saw excellent correlation with HFC-125 although a combined source of these species is unclear.

HFC-143a – Figure 4.42d

HFC-143a is mainly utilised as a replacement refrigerant and although background mixing ratios indicate an increasing global trend, the Taiwanese campaign medians indicate a slight decrease in abundance between 2013 and 2015 (16.6 ppt to 16.49 ppt, see Figure 4.43). In general however, the 2013 campaign was enhanced above background (13.4 ppt) by over 12% whereas 2015 saw mainly near background (16.0 ppt) samples. This may suggest East Asian sources are decreasing however further campaigns would be required to confirm this.

2014 also saw consistent enhancement of over 14% above background (14.5 ppt) however this is similar to many of the other HFCs and likely due to the higher proportion of Chinese influenced back trajectories combined with the different sampling site of this campaign.

Although the 2014 enhancement above background does suggest impact from China, assessment of the NAME back trajectories for samples observed to have significant spikes in abundance (27th March 2013, 12th March 2014, 20th and 27th March 2015) also indicates Taiwan is a major or minor possible source on these days as well. Local winds speeds on these days were 3.5 m s^{-1} or less, which could be indicative of impact from local sources. However local wind directions during those days in 2013 and 2015 is not consistent with populated areas and so impact from regional Taiwanese would seem more likely.

Good correlation was found consistently only with halon 1211 which may be coincidental to the widespread locations of banks since this species has been phased out. DCE also had good correlation with HFC-143a in 2013 and 2015 along with the short chain PFCs in 2014, which agrees with the assessment that some measured sources may be Taiwanese in origin.

HFC-152a – Figure 4.45a

This species is utilised as a refrigeration and foam blowing replacement. Observed backgrounds indicated mixing ratios decreased between 2013 (7.77 ppt) and 2014 (7.19 ppt) but increased again in 2015 (7.32 ppt). Comparison of the Taiwanese campaigns and 2010 mixing ratios from literature (Figure 4.43) indicates a general decreasing abundance although assessment ignores the 2013 campaign which was biased by several extremely large abundances, suggesting potential contamination, likely local given the magnitude, for at least the first half of the campaign. As such, only the 2014 and 2015 campaigns will be discussed further.

Significant spikes were detected on the 12th and 13th March 2014 (26.0 ppt and 22.0 ppt respectively) and the 12th March 2015 (38.1 ppt). NAME back trajectories imply that these days all were influenced by Chinese emissions and possibly Taiwanese sources. Given that both these regions utilise HFCs in industry this is unsurprising. Local meteorological data also only indicates potential impact from local sources on the 12th March 2014 and not the 13th.

Good correlation was detected during 2014 with several species assessed as having potential source locations in China including HCFC-22 and VSLS-Cl species. Correlation with HFC-125 was found to be good in 2014 but excellent in 2015, along with HFC-245fa. This may be due to the use of refrigerant blends containing these species in industry.

HFC-245fa – Figure 4.45b

For this minor HFC species, used as a blowing agent and refrigerant, results from the Taiwanese campaigns were consistently detected below background mixing ratios. This may be due to difference in calibration as the background is taken from the Ragged Point AGAGE station in Barbados whereas UEA calibrates using a NOAA scale and this is currently estimated for this species. Although exact abundances may not be comparable, the background does indicate an increasing trend across the three years and this is reflected by the calculated median mixing ratios, which increase from 1.3 ppt (2013) to 1.5 ppt (2014) and then to 1.6 ppt (2015).

Of the significant spike in abundances observed for this species, all three (21st March 2013, 12th March 2014 and 2015) were indicated to have major influences from Chinese emissions from comparisons with NAME back trajectories.
No good or excellent correlation was found in the 2013 campaign but several species including HCFC-141b, HFC-125 and DCM with potential source in China showed good correlation in 2014. Similarly, DCE and the short chain PFCs C_2F_6 and c-C_4F_8 had good correlation with HFC-245fa suggesting potential impact from local Taiwanese sources as well. In 2015 only excellent correlation was seen and this was with HFC-125 and -152a indicating possible use of refrigerant blends of these species.

HFC-227ea – Figure 4.45c

HFC-227ea is mainly utilised as an aerosol propellant or in fire fighting applications and background data indicates the abundance in the atmosphere is increasing, from 0.9 ppt in 2013 to 1.1 ppt in 2015. Comparison of the Taiwanese data for this compound suggests there are distinct differences in detected levels between the two sites. While the results from the campaigns at the southern site (2013 and 2015) saw below background levels and some pollution events, for the campaign at the northern site, all the days sampled were enhanced above the background (1.0 ppt). As such, median enhancement for the southern campaigns was under 10% but had increased to 24% during 2014.

This almost consistent increase in concentration could be indicative of a nearby local source however local wind direction and speed varies across the campaign making this unlikely. Also, comparison of NAME back trajectories during the 2013 and 2015 campaigns does not indicate particular influence from air travelling for the southern hemisphere which, due to the hemispheric gradient, may have resulted in lower than background value being observed. Potential contamination of the sampling equipment or canisters can most likely be ruled out due to the two near background samples and the lack of distinguishable from background mixing ratio in the analysed nitrogen blank. However, like many other species previously discussed, this site may see a bias due to its location and frequency of trajectory with major influences from Chinese sources.

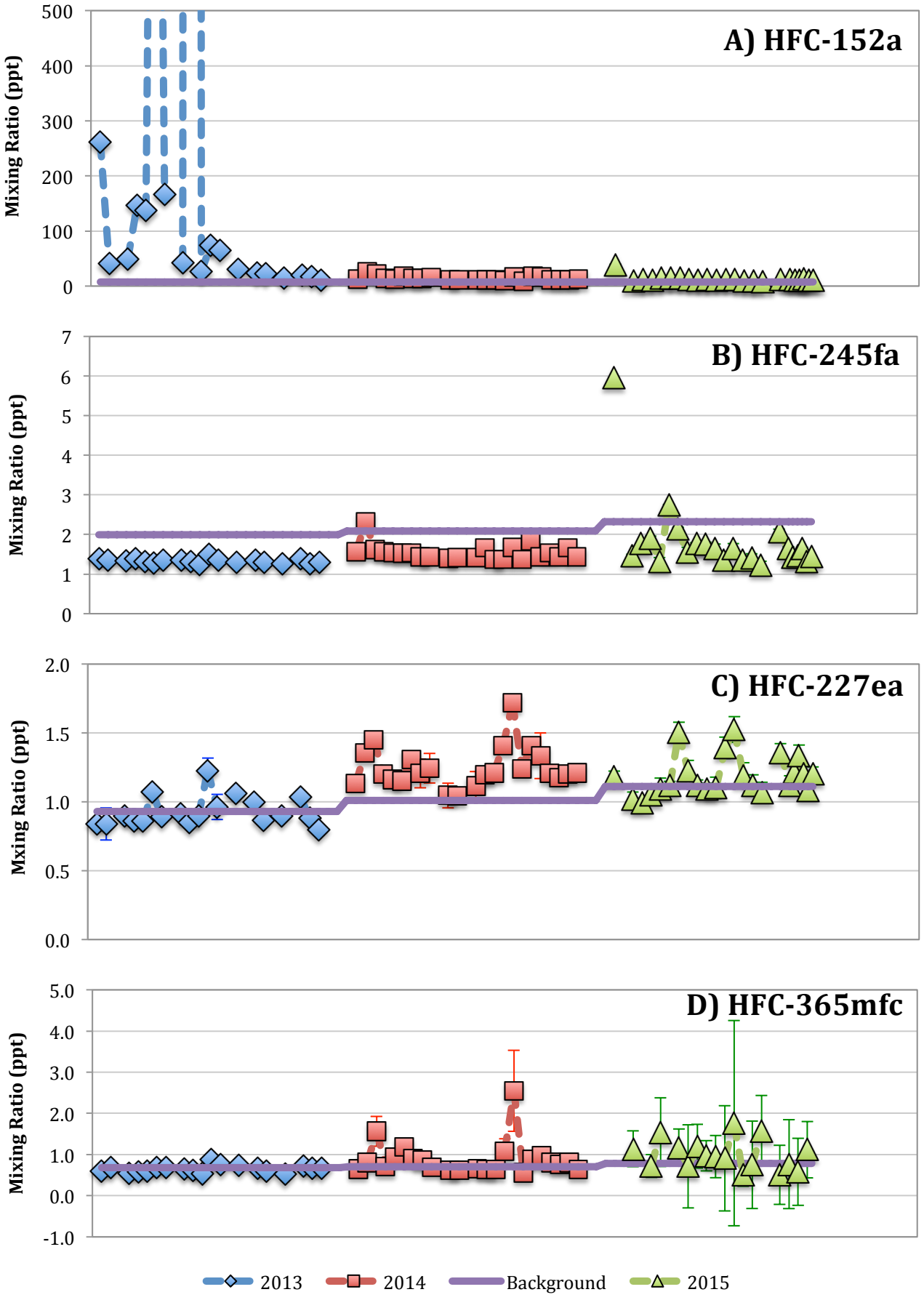

Figure 4.45: Time series spanning the three Taiwain campaigns for the minor HFCS– A) HFC-152a, B) HFC-245fa, C) HFC-227ea and D) HFC-365mfc. Data from 2013 is represtented in blue, 2014 in red and 2015 in green. Background abundances are shown in purple. Error bars indicate the total uncertainty calculated for the samples. Two samples from 2013 were found to contain mixing ratios much larger that those of the rest of the campaign for HFC-152a and so are not dispkayed on the graph.

As such, the 2014 median was not included in the inter-annual variation assessment for HFC-227ea. However, between 2013 and 2015, levels do appear to be increasing, as anticipated, along with the global trend.

Significant spikes in mixing ratios were measured on the 21st March 2013 (1.22 ppt), 28th March 2014 (1.72 ppt) and the 22nd and 28th March 2015 (1.50 ppt and 1.53 ppt respectively), all of which are impacted by back trajectories from China according to the NAME model.

Good correlation with CFC-113a was consistently seen across all three campaigns and for the 2013 and 2015 campaigns good correlation was also seen with halon 1202, HCFC-133a and DCM. These species have all been assessed as having potential source locations in China although specific applications vary between them. No excellent correlation for HFC-227ea was found.

HFC-365mfc – Figure 4.45d

Similar to HFC-245fa, most likely due to the estimated calibration scale, significant portions of all of campaigns are below background mixing ratios although distinct enhancements are identifiable. The global trend for HFC-365mfc appears to be increasing as background abundances have increased from 0.7 ppt in 2013 to 0.8 ppt in 2015. Although the exact mixing ratios for this species are not comparable with the background data, medians do suggest that this trend is being followed as they increase between each campaign from 0.7 ppt in 2013 to 0.8 ppt in 2014 and 1.0 ppt in 2015.

Spikes in abundance of significance were observed on 21st March 2013 and the 28th March 2014 and 2015. Comparison with NAME back trajectories suggest China and Taiwan as the major potential influences on these days and this agrees with previous studies (Li et al. 2011).

Good correlation with this compound was only seen in 2013 and this was with HCFC-133a, HFC-23 and PCE, all species that also have potential Chinese emissions sources.

4.9.3.2.2 Perfluorocarbons and SF_6

These are fully fluorinated compounds with applications in semiconductor and electronics manufacture, as heat transfer fluids and some species are produced during aluminium manufacturing. Most of the countries in the East Asian region have utilised these industries (Saito et al. 2010, Kim et al. 2014, Fang et al. 2014) and so relatively stable or increasing emissions are anticipated from a range of sources. For all the PFCs measured (except SF_6), the background concentrations are extrapolated from Cape Grim archive data or literature, assuming the most recent growth rates remain constant. Given the active effort by industry to reduce PFC emissions, this method may result in an overestimation of background abundances.

Short Chain PFCs and SF_6

For the short chain PFCs, mixing ratios were observed most frequently at above background levels aside from the 2013 results for cyclic-C_4F_8. This species is included with the short chain PFCs whilst C_4F_{10} is included under the long chain section due to similarities in applications and emissions with the other short chain compounds. Comparison with NAME back trajectories suggests the main source areas for the PFCs are China and Japan with some influence from Korea as well. Since they all have very similar uses, it is unsurprising that the short chain PFCs correlate with one another consistently throughout the three campaigns. This correlation is most pronounced in 2014 when local Taiwanese emissions also appear to have been detected and this is discussed further in Case Study 3 (section 4.12). Given the atmospheric lifetimes of PFCs are thousands of years, background abundances will only stabilise and not decrease and so variation in median mixing ratios reflects changes in the mixing of emissions and not a change in the long-term global emission trend of the species.

C_2F_6 – Figure 4.46a

This species is predominantly used in semiconductor manufacture and may be produced as a by-product of aluminium production. Growth rates from literature suggest the global trend is increasing and background mixing ratios were estimated at 3.70 ppt, 3.74 ppt and 3.78 ppt for 2013-2015 respectively. Figure 4.47 shows a comparison of the median mixing ratios of C_2F_6 detected in each campaign. Whilst median abundances decreased after 2013 from 4.16 ppt to 4.03 ppt, they increased again for 2015 to 4.05 ppt however, these values are quite similar and so within the margin of error. The decreasing abundances detected for these campaigns are reflections of less well-mixed emissions of PFCs.

Significant spikes were not observed in 2013 and those in 2015 (23rd and 27th March) correspond to NAME trajectories with major influences potentially from Korea and China respectively, both of which utilise the associated industries that could result in C_2F_6 emissions.

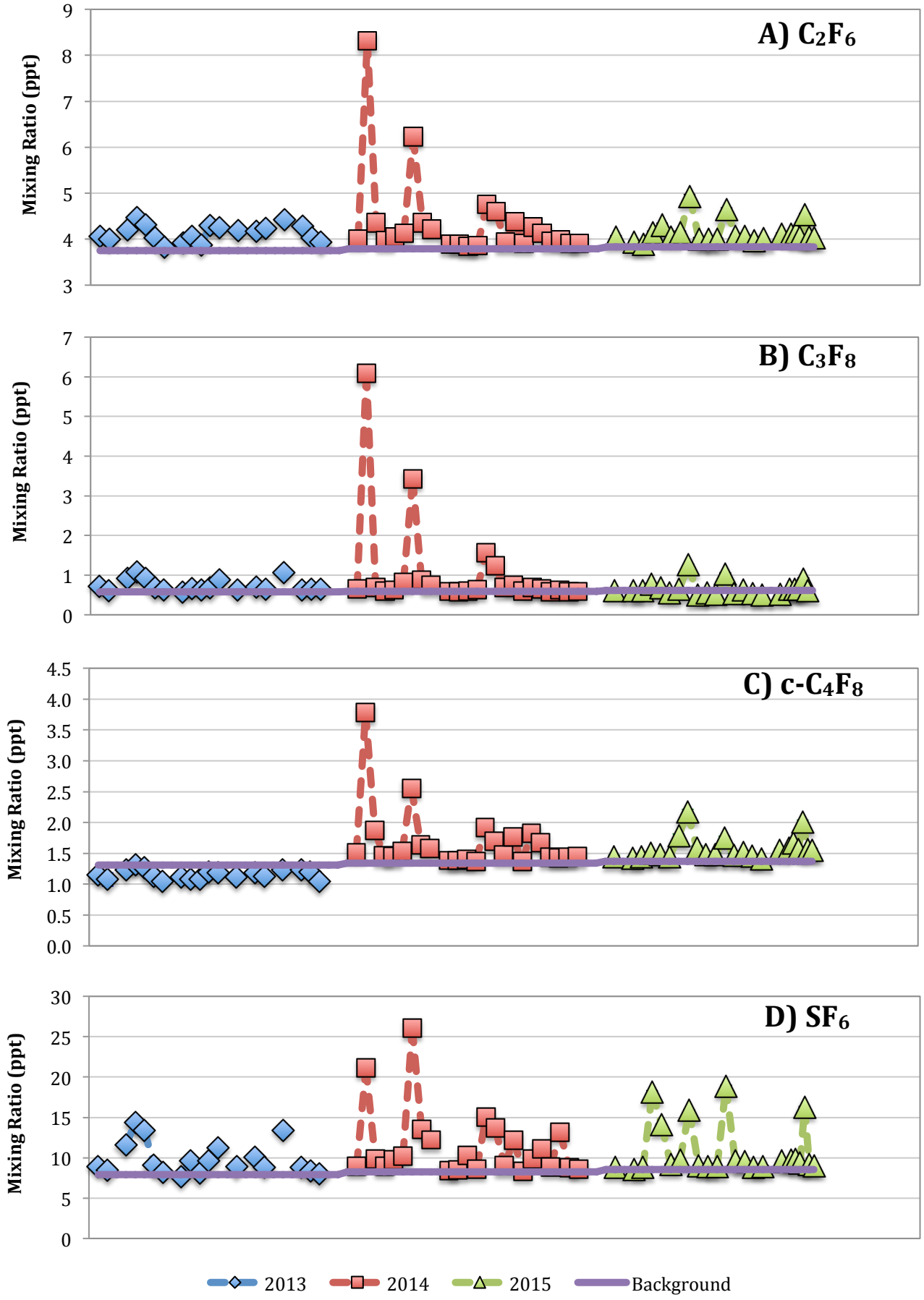

Figure 4.46: Time series spanning the three Taiwain campaigns for the short chain PFCS– A) C_2F_6, B) C_3F_8, C) c-C_4F_8 and D) SF_6. Data from 2013 is represtented in blue, 2014 in red and 2015 in green. Background abundances are shown in purple. Error bars indicate the total uncertainty calculated for the samples.

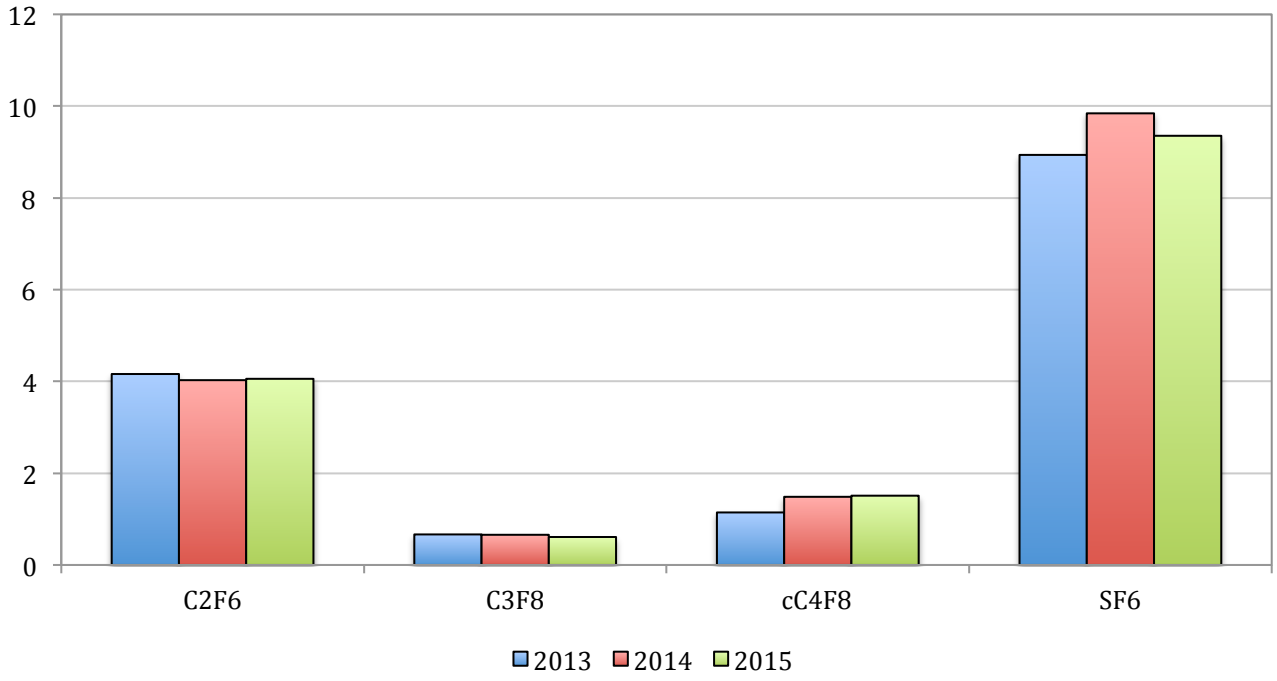

Figure 4.47: Comparison of mixing ratios of the short chain PFCs during the Taiwan campaigns (2013, 2014 and 2015).

Aside from correlation with the other short chain PFC species, good correlation was found with HFC-134a in 2013 and 2014, most likely due to its extensive sources across the region. 2014 also saw good correlation with several other HFCs, HCFC-141b, DCM and DCE, which suggests co-location with sources from China and local to Taiwan. No other good interspecies correlation was found for 2015.

C_3F_8 – Figure 4.46b

Like for C_2F_6, this species shares application in semiconductor manufacture and is a by-product of aluminium production and again, growth rates from literature suggest this global trend is increasing by ~0.02 ppt per year. Comparison of median mixing ratios for the three campaigns (Figure 4.47) show a slight decrease from 0.66 ppt (2013) to 0.61 ppt (2015). Again, this is likely caused by changes in the mixing of emissions and may suggest some reduction in regional emissions.

Conversely to C_2F_6, C_3F_8 was observed to have significant spikes in the 2013 campaign on the 12th March (1.1 ppt) and the 1st April (1.1 ppt). NAME back trajectories suggest major influences potentially from China and Japan respectively on these days. In the 2015 campaign significant spikes correspond with those of C_2F_6 and so indicate possible source from Korea as well as China.

Similar species to C_2F_6 were also found to have good correlation with C_3F_8 again suggesting the co-location of sources in both China and Taiwan for the 2013 and 2014 campaigns.

c-C_4F_8 – Figure 4.46c

Cyclic-C_4F_8 also has application in semiconductor manufacture and the growth rate suggested by literature (0.03 ppt yr^{-1}, Oram et al. 2012) resulted in extrapolated background mixing ratios of 1.3 ppt (2013) to 1.4 ppt (2015). Abundances of c-C_4F_8 were detected at mostly below background in 2013 but were consistently enhanced above background for 2014 and 2015. Although Figure 4.47 does indicate median mixing ratios have been increasing over the 3 years sampled, this species was analysed on the Entech during 2013 as opposed to the AutoSpec in the other years. Therefore, this variation is likely due to potential differences between instrument sensitivity and calibration scale offset for this compound rather than differences between the campaigns. The increase of ~0.02 ppt between the 2014 and 2015 campaigns is almost in line with the predicted growth rate.

Similar significant spikes to the other short chain PFCs were again observed although a further spike on the 24th April 2015 (PM, 2.0 ppt) was also detected. Assessment of the NAME back trajectory for this sample suggests potential major influences from China and/or Korea, which corresponds with the assessments of the other spikes.

Good correlation is seen in the 2013 and 2014 campaigns, predominantly with HFC species, further supporting potential source locations of c-C_4F_8 in China.

SF_6 – Figure 4.46d

Although not technically a PFC, SF_6 is another fully fluorinated compound that is used in semiconductor manufacture along with other PFC species since it shares properties such as being non-flammable and inert. It is also has applications as a dielectric gas in high-voltage switchgear. SF_6 mainly correlates with the short-chain species and this is particularly clear in the 2014 and 2015 samples. However, there are some slight differences in both these campaigns and the data from 2014 will be discussed further in Case Study 3. The global trend for SF_6, taken from NOAA background data, is increasing from 7.90 ppt in 2013 to 8.53 ppt in 2015. Figure 4.47 indicates that the median mixing ratios for the Taiwanese campaigns increases between 2013 and 2014 by ~1 ppt but then decreases by ~0.5 ppt between 2014 and 2015. This, as with the other short chain PFCs, likely reflects differences in atmospheric mixing for emissions and the proximity of the 2014 campaign to potential source locations may have impacted the abundances detected more than during other campaigns.

More significant spikes were measured for this species than for the other short chain PFCs however these all bar one correspond with spikes of these PFC species suggesting potential sources are also located in China, Korea and Japan. The other spike was detected on the 13th March 2013 (13.4 ppt) and NAME back trajectories suggest that emission from Japan may influence this sample. This difference in spikes is likely due to the variation in applications SF_6 has in comparison with the short chain PFCs.

Aside from the short chain PFCs, HFC-134a was the only species identified as having good correlation with SF_6 across all three campaigns and this may reflect the widespread applications across the region these species both have, particularly in populated areas.

4.9.3.2.3 Long Chain PFCs

For the long chain PFCs, mixing ratios were observed most frequently at above background levels particularly during 2013. The significant and consistent enhancement detected across all measured long chain PFCs in this campaign is indicative of contamination, either at the site or in the sampling equipment. As such, results from this campaign were not used when assessing the inter-annual variation for these species. However, though the exact cause of the contamination is unknown, it was not detected during the 2015 campaign carried out at the same site suggesting it was likely not due to local industry. Nitrogen blanks were also analysed and mixing ratios of the long chain PFCs were indistinguishable from background indicating the sampling equipment was not the source of the contamination for the 2013 campaign Finally, since the long chain PFCs have significantly lower emissions than their short chain counterparts, enhancements above background were considerably smaller and less distinct than those seen with the short chain PFCs.

Comparison with NAME back trajectories suggests the main source areas for these PFCs are China, Japan and Korea. Whilst they do have similar applications, there was distinctly less correlation between the long chain PFCs than was seen between the short chain, indicating their emissions are likely from different sources and so over a wider range of locations. Again atmospheric lifetimes of these PFCs species are thousands of years and so background abundances will not decrease but may stabilise. This means that any mixing ratio variation is only indicative of changes in the mixing of emissions of the species. Further individual species differences are also discussed below.

n-C_4F_{10} – Figure 4.48a

This long chain PFC it utilised in the manufacture of semiconductors and electronics and was not measured in 2013 due to method constraints on the AutoSpec system. Growth rates taken from literature (0.003 ppt yr^{-1}, Laube et al. 2012) resulted in background mixing ratios that increased from 0.178 ppt in 2013 to 0.181 ppt in 2015. Median mixing ratios between the two campaigns increase by 0.03 ppt, which, with uncertainties, is in line with the expected growth rate for C_4F_{10}.

The only significant spike in abundance detected for this species is on the 12th March 2014 (0.24 ppt) and this corresponds with a day where local wind data indicates influence from nearby Taiwanese sources and this was clearly seen with the short chain PFCs. Given that C_4F_{10} is also used in semiconductor manufacture, it is unsurprising that this spike corresponds to those the short chain PFCs used in the same industry with probable local sources.

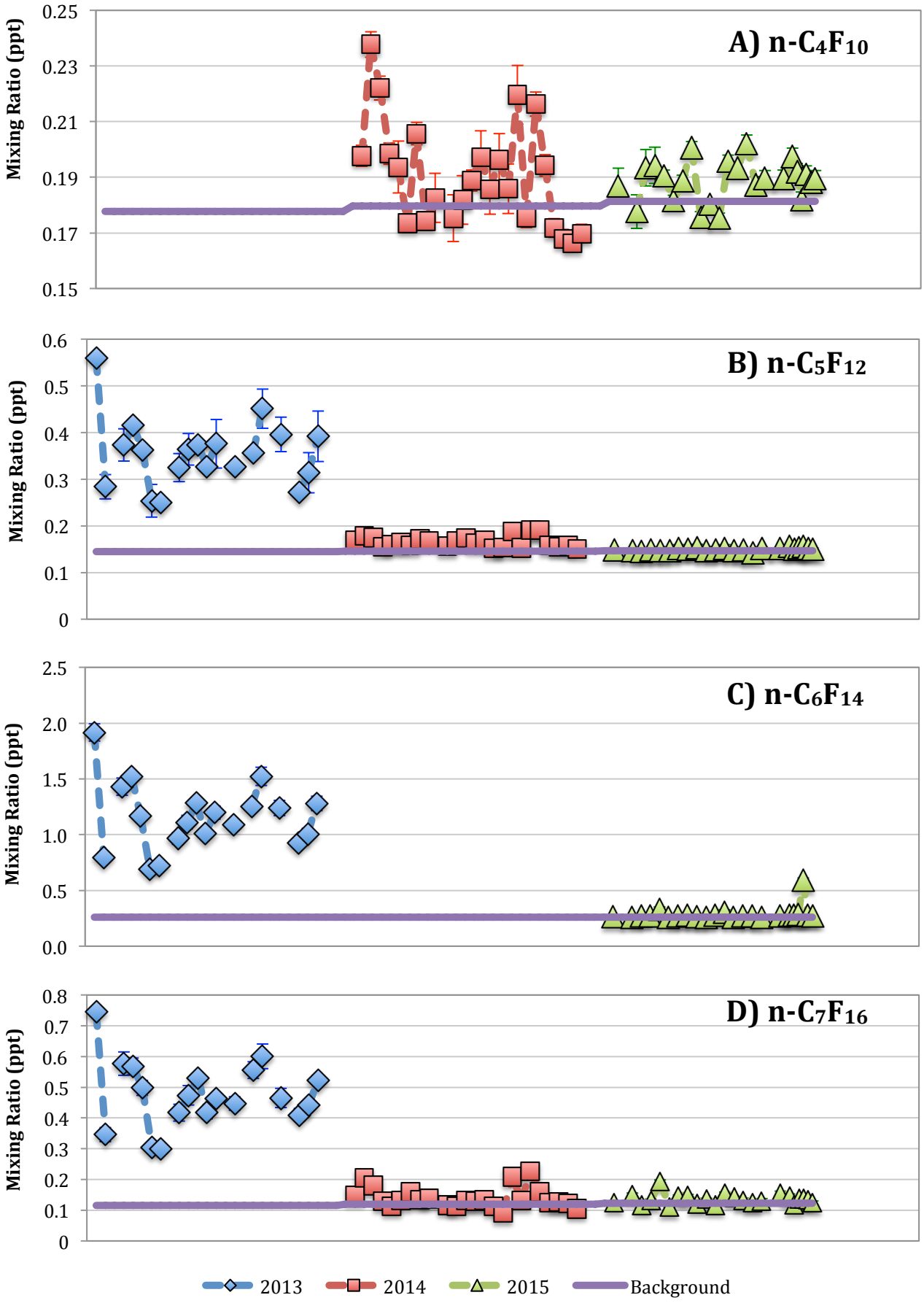

Figure 4.48: Time series spanning the three Taiwain campaigns for the long chain PFCS– A) C_4F_{10}, B) C_5F_{12}, C) C_6F_{14} and D) C_7F_{16}. Data from 2013 is represtented in blue, 2014 in red and 2015 in green. Background abundances are shown in purple. Error bars indicate the total uncertainty calculated for the samples.

However, other spikes that only suggest some significance (0.22 ppt on both the 27th and 29th March 2014) which are not seen for the short chain species indicate that there are unrelated sources in the region. Comparison with NAME back trajectories for these days suggests China and/or Japan as common potential source locations.

Good interspecies correlation was only found during the 2014 campaign and species include HCFC-22, HFC-125 and PCE, all of which have been previously assessed as having possible emissions sources in China.

n-C_5F_{12} – Figure 4.48b

The compound also has application in semiconductor manufacture and an extrapolated background of 0.146 ppt in 2014 and 0.147 ppt in 2015 was calculated using the growth rate from literature (0.0016 ppt yr^{-1}, Laube et al. 2012). Observed mixing ratios were consistently enhanced above this background by 3% in 2014 (median of 0.16 ppt) whilst 2015 saw mixing ratios more in line with the background abundance (median of 0.15 ppt). This is likely due to difference in sites and so closer proximity to potential sources in the 2014 campaign, as has been reflected for a variety of species.

Significant spikes in mixing ratios were only measured on the 30th and 31st March 2014 (0.19 ppt) and a slightly significant spike was detected on the 28th March 2014 (0.18 ppt). Even though C_5F_{12} is utilised in the same industry as C_4F_{10} and the short chain PFCs, the significant spikes do not correspond with these species suggesting that there are different sources although the slightly significant spike is shared with C_4F_{10}. Comparison with NAME back trajectories and local wind data implies emissions from China are potential major influences on this day.

However there is a lack of good correlation with C_5F_{12} and any other halocarbon species measured during both campaigns which indicates that any sources, if Chinese in origin as the back trajectories suggest, are located separately to other species like HCFCs, HFCs and VSLS-Cl.

n-C_6F_{14} – Figure 4.48c

n-C_6F_{14} is mainly utilised as a heat transfer fluid and was only measured in 2013 and 2015. However, as previously mentioned, significant enhancement above background during the 2013 campaign, potentially caused by contamination, was seen making these results unusable. This species was not measured in 2014 do to issues with co-elution during analysis, which was resolved by the introduction of a different GC column for the 2015 samples. Background mixing ratios were calculated using the growth rate of 0.004 ppt yr^{-1} to give a value of 0.26 ppt for 2015.

During this analysis, one significant spike in abundance was observed on the 24th April (PM) at 0.59 ppt. NAME back trajectories for this sample suggest Korea and/or Taiwan as possible major influences.

However, similar trajectories were modelled for the surrounding samples and these mixing ratios are much nearer to the median mixing ratio of 0.27 ppt for this campaign. This suggests that something affected only this sample and, as there is some variation in the local wind direction for the surrounding samples, emissions from a local source may have had a larger impact on this sample.

C_7F_{16} – Figure 4.48d

This species is also utilised predominantly as a heat transfer fluid and was measured successfully during the 2014 and 2015 campaigns. The background mixing ratio was extrapolated using a growth rate of 0.0035 ppt yr^{-1} from literature (Laube et al. 2012) and resulted in 0.119 ppt for 2014 and 0.123 ppt for 2015. Median mixing ratios increased by 0.004 ppt between the two campaigns and this is in line with the suggested growth rate. 5 samples during the 2014 campaign and 4 samples during the 2015 campaign were measured at below background abundances. This may suggest that growth rates may have slowed during the extrapolation period and so this background is an overestimate. Another explanation would be the sampling of southern hemispheric air due to the hemispheric gradient however back trajectories for these days do not suggest influence from this region.

Significant spikes in mixing ratios were observed on the 12th, 28th and 30th March in 2015 and the 20th March 2015. All but the 30th indicate potential major influences from Taiwanese sources when compared to NAME back trajectories. The 30th, as well as the 12th, suggests Chinese emissions are the major influence.

Interspecies correlation in 2014 was found to be good with several species assessed to have potential Chinese sources including CFC-113a, HCFC-22 and HFC-125. Good correlation was seen in 2015 with DCM, another species with emission likely from China, as well as DCE, which was found to have more local emissions. As such, these agree with the potential sources suggested by the NAME back trajectory assessment.

c-C_5F_{10} – Figure 4.49a

Cyclic-C_5F_{10} is a compound of anthropogenic production but with unknown uses or emissions, potentially as a by-product of another PFC reaction. It was only able to be measured in 2015 using the AlPlot column on the AutoSpec and is not calibrated so all mixing ratios are relative to the standard (AAL-071170). As all the relative abundances are over 1 this suggests that c-C_5F_{10} has been increasing in the atmosphere since 2006 when the standard was collected.

Spikes in relative abundance were detected for this species, one of which was significant, namely the 23rd March at ~1.5. Slightly significant mixing ratios were measured on the 22nd and 30th March (~1.5 and ~1.4 respectively) as well as on the 25th April (~1.5 in both the AM and PM samples). Comparison with NAME back trajectories for all of these samples suggests Korea or Japan as consistent influences on emissions for these days, although China was also a potential major influence but only for the 22nd and 23rd March.

However, the lack of spikes in abundance may suggest that East Asia is not a major source region of this species.

The only interspecies correlation found with c-C_5F_{10} was some correlation with CFC-113a (0.50), CFC-114a (0.62) and HFC-23 (0.51). These species all have been found to have potential emissions source in China but co-location is not clearly indicated from these correlations. The other cyclic PFC species, c-C_4F_8 only shows a correlation of 0.23 and Figure 4.50 shows a comparison of the time series of these species. Whilst both species do see higher abundances on the 22nd and 23rd March, other changes in mixing ratio are almost opposite one another for the majority of the campaign.

Iso-C_6F_{14} – Figure 4.49b

As an isomer of n-C_6F_{14}, similarities between the time-series observed for these two species was expected and can be found in Figure 4.51. Although iso-C_6F_{14} is not currently calibrated, it is assessed relative to the standard and the data can be compared to other species.

Unsurprisingly, the only significant spike is found on the 24th April, at 2.4 times the standard mixing ratio, which corresponds to that of n-C_6F_{14}. Correlation between these two species was found to be excellent (0.96), indicating likely co-emission of these species. Slight differences in the magnitude of changes in abundances indicate that the ratio these species are emitted at may favour iso-C_6F_{14}. The median ratio between these species suggests for every 1 ppt of n-C_6F_{14} (relative to standard), 1.1 ppt of iso-C_6F_{14} (relative to standard) is present. For the significant spike however, n-C_6F_{14} was detected more abundant than iso-C6F14 and this could indicate influence from another source that has a different isomeric ratio, favouring n-C_6F_{14}, potentially through separation and removal of the isomer before use in industry.

No other good or excellent interspecies correlation was found for this species.

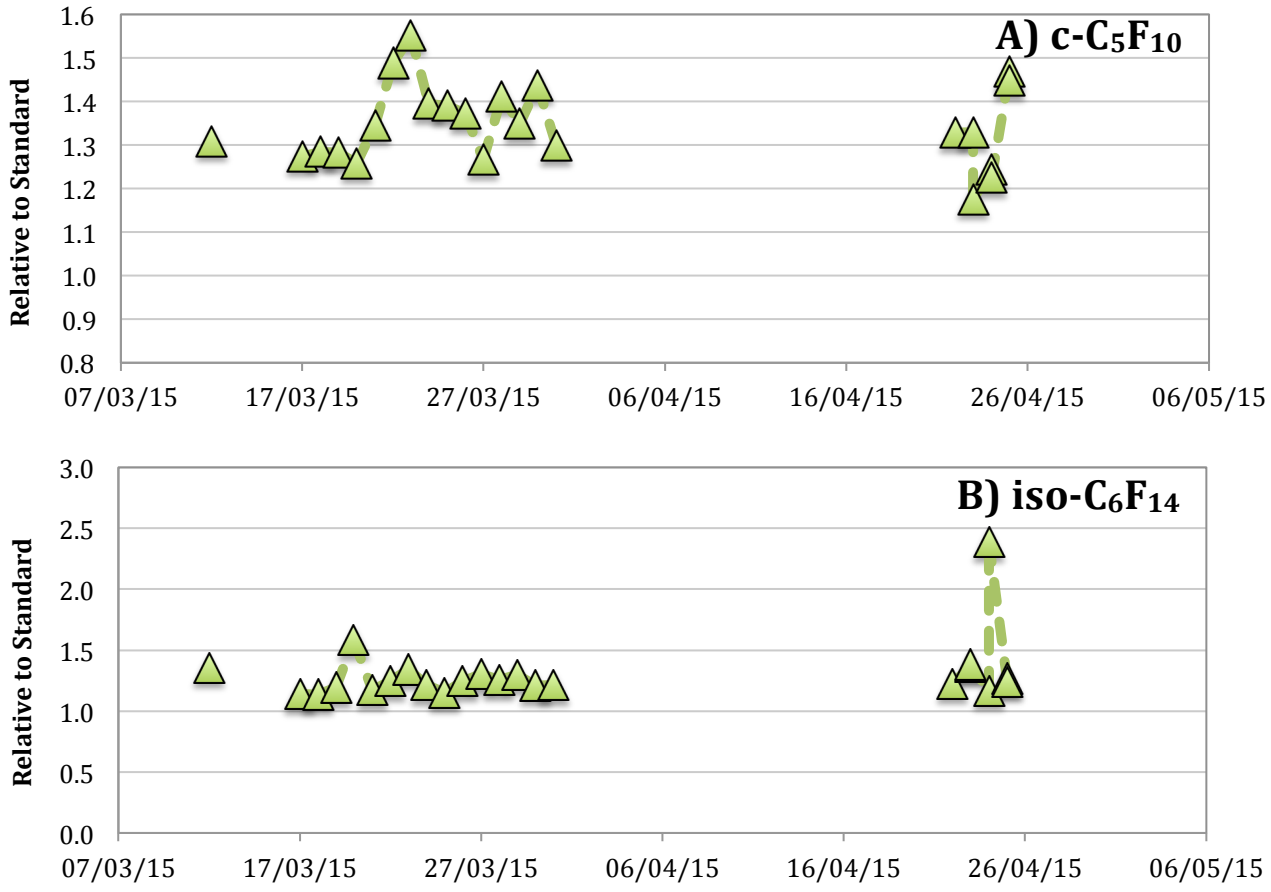

Figure 4.49: : Time series of the 2015 Taiwain campaign for the long chain PFCS– A) c-C_5F_{10} and B) iso-C_6F_{14}, C) C_6F_{14}.

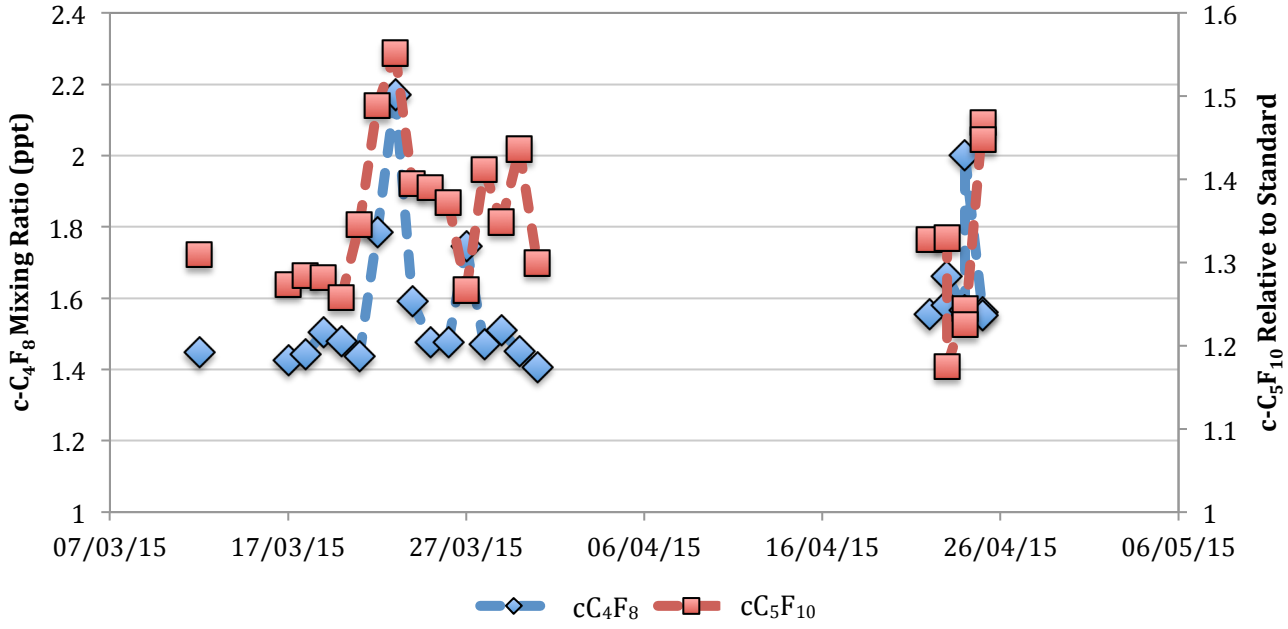

Figure 4.50: Comparison of the time series for the cyclic PFCs: c-C_4F_8 and c-C_5F_{10} during the 2015 Taiwan campaign. Whilst similar spikes in mixing ratios were observed on the 22nd and 23rd of March, little correlation is seen for the rest of the campaign.

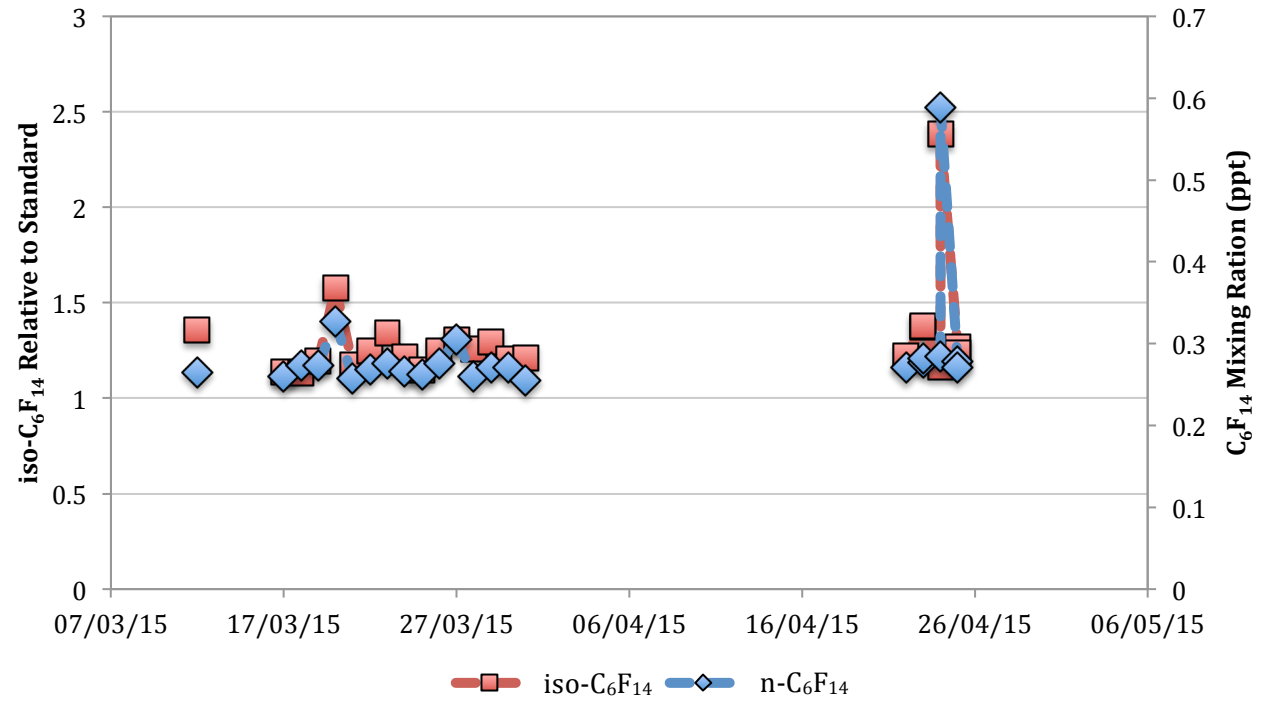

Figure 4.51: Comparison of the time series for the isomeric species: C_6F_{14} and iso-C_6F_{14} during the 2015 Taiwan campaign. Clear similarities in changes in abundance indicate likely co-emission of these species.

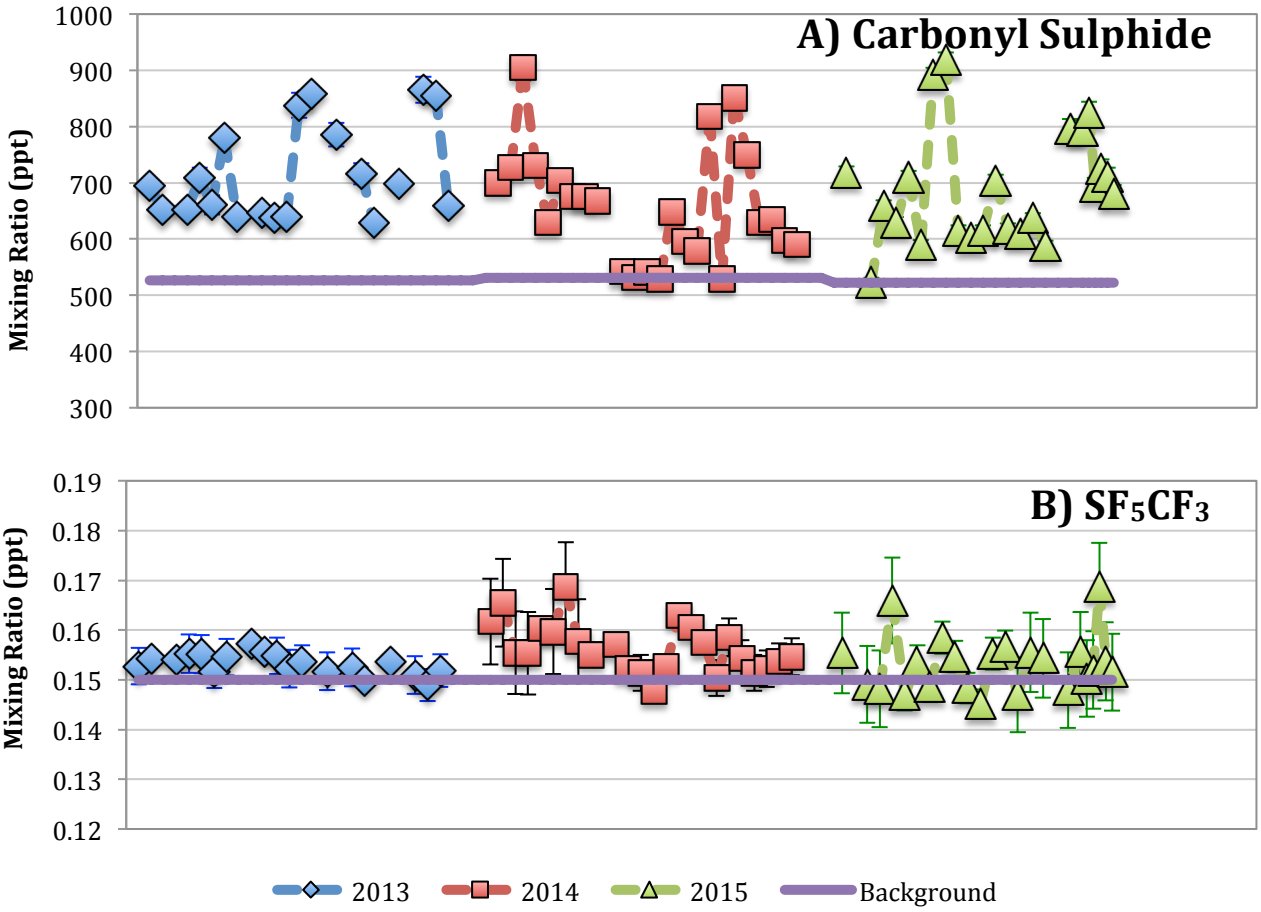

Figure 4.52: Time series spanning the three Taiwain campaigns for A) Carbonyl Sulphide and B) SF_5CF_3. Data from 2013 is represtented in blue, 2014 in red and 2015 in green. Background abundances are shown in purple. Error bars indicate the total uncertainty calculated for the samples.

4.9.3.2.4 Other Species

Like SF_6, some species that are not technically halocarbons but are still related to the group by potential applications or sources were also measured, namely COS and SF_5CF_3. A range of other compounds (CO, O_3, NO_x and PM_{10}), where high abundance is generally indicative of air pollution, were also measured by the Taiwanese research team who also collected the samples for halocarbon analysis. Ozone was measured using a UV photometer (EC9810, Ecotech, Australia), CO was measured using a nondispersive (NDIR) sensor (APMA-360, Horiba, Japan) and NO_x was measurements were taken using a chemiluminescent method (EC9841, Ecotech, Australia) (Ou-Yang *et al*. 2012). A Beta Attenuation Monitor (BAM-1020, MetOne Instruments Inc., USA) was utilised in the collection of PM_{10} data (Pantina *et al*. 2016). On-site data from these instruments was relayed as hourly averages, similarly to the local meteorological information, and so was selected to reflect sampling times accordingly.

Carbonyl Sulphide – Figure 4.52a

Carbonyl sulphide (COS) is the most abundant tropospheric sulphur-containing gas and, although it has natural sources such as volcanoes and biomass burning, anthropogenic sources include coal combustion and artificial fibre (e.g. rayon) production. COS was consistently detected above background levels, similar to the methyl halides. The majority of mixing ratios detected during all campaigns were notably higher than background. Near background abundances were only observed in 2014 (531 ppt background) for 5 samples and in 2015 (522 ppt background) for one sample. This suggests that background air masses were sampled during these campaigns but mostly air impacted by emission transport was collected. The 2013 campaign did not see any near-background (526 ppt) samples, which could be indicative of contamination, rather than only sampling polluted air masses. However, Nitrogen blanks indicate that canister contamination was not an issue for this compound as peaks detected were indistinguishable from the background signal.

Global atmospheric trends of COS have previously been found to be insignificant (Montzka et al. 2007), suggesting there was little change at the end of the twentieth century, indicating a balanced atmospheric budget for this species. However, more recent studies have indicated an increasing trend in the southern hemisphere (Kremser et al. 2015) and a global increase of 0.4% from 2011 to 2012 (Carpenter and Reimann, 2014). Median mixing ratios from the Taiwanese campaigns were similar for 2013 (695 ppt) and 2015 (680 ppt) however 2014 was lower (642 ppt). This is not entirely unexpected as near background levels were measured more frequently during this year.

Significant spikes in COS mixing ratios were only found in 2014 (851 ppt on the 30th March) and 2015 (891 ppt and 919 ppt on the 22nd and 23rd March respectively). Comparison with NAME back trajectories indicated China and Korea as major potential influence on these days and, given COS emissions from coal combustion, which is prevalent in China, this result was anticipated.

Whilst HCFC-142b was the only species found to have consistent good correlation with COS over the three campaigns, the number and range of correlating species increased in 2014 when the proportion of Chinese trajectories sampled also increased. These species, including CFC-113a, HCFC-22, HFC-152a and PCE all have been suggested to have potential sources in China which implies the same is true for COS.

Trifluromethyl sulphur pentafluoride (SF_5CF_3) – Figure 4.52b

Currently, the only known source of SF_5CF_3 is as a by-product of electrochemical fluorination during fluorosurfactant production, however this process was discontinued in 2000. Given the long atmospheric lifetime for this species and emissions indistinguishable from zero by 2003, the atmospheric background from 2011 of 0.15 ppt was utilised for all campaigns as no decline is expected (Sturges et al. 2012). Median mixing ratios from the campaigns reflect this as all are very similar (0.154 ppt for 2013 and 2015, 0.155 ppt for 2014) and median enhancements are ~3%, which is within uncertainty margins.

NAME back trajectories were assessed for samples where significant spikes in mixing ratios were detected and all three of these (17th March 2014, 19th March 2015 and 24th April (PM) 2015) suggested emissions from Taiwan were a major potential influence. Local winds were below 4 m s^{-1} on each of these days and direction during the 2014 spike only suggested local impact. Other samples with similar wind directions during this campaign saw somewhat significant abundances, possibly suggesting there could be an emissions source in Taiwan although further campaigns would be necessary to identify it.

No species were found to have good or excellent correlation with SF_5CF_3.

Carbon Monoxide (CO) – Figure 4.53a

This species has a range of anthropogenic sources, including coal combustion and vehicle exhaust fumes, and has been used by many studies as a tracer for identifying industry-influenced or polluted air masses as its emissions are well documented. CO abundances fluctuate seasonally, however, since all three Taiwanese campaigns were carried out at similar times of year, comparisons between them can be made. Median mixing ratios were similar for the 2013 and 2014 campaigns (~240 ppb) however 2015 saw a median of 200 ppb and 5 samples were observed at abundances under 100 ppb, unlike during the other years. This may indicate that fewer polluted air masses were sampled during 2015 or that pollution was transported further, resulting in increased dilution and so lower abundances.

Spikes in mixing ratios of CO that were calculated as being significant were only found on the 11th March 2013 (430 ppb) and the 19th March 2015 (620 ppb). Major potential influences suggested by NAME back trajectories on these days were China and Korea in 2013 and Taiwan in 2015. Taiwan emissions were also assessed to be a minor influence for 2013.

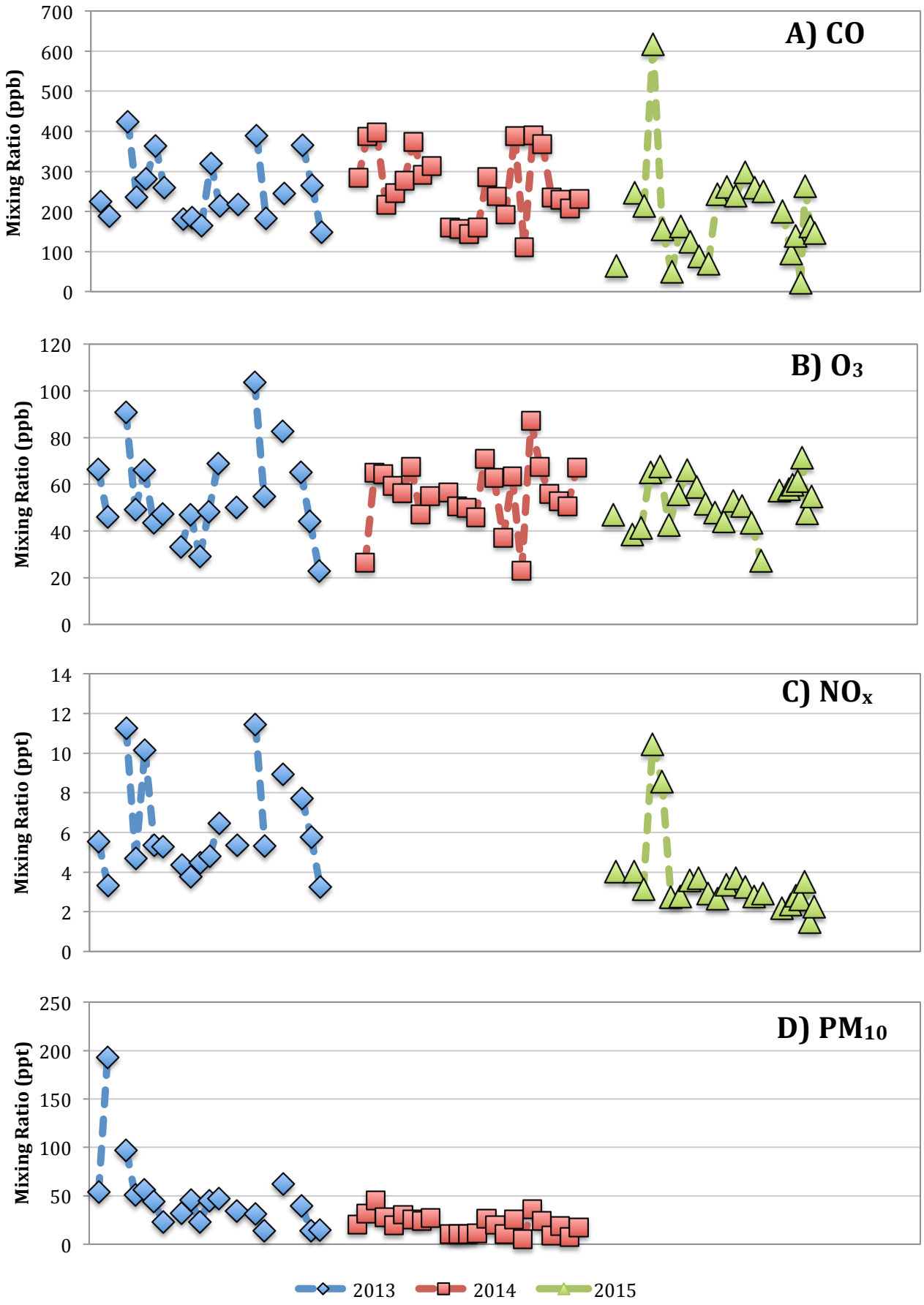

Figure 4.53: Time series spanning the three Taiwain campaigns for A) CO, B) O_3, C) NO_x and D) PM_{10} Data from 2013 is represtented in blue, 2014 in red and 2015 in green.

Meteorological data from the sampling site does not indicate impact by local emissions but, given the magnitude of the spike in 2015, it is likely that regional sources from Taiwan contributed. Good correlation with CO was only found during the 2013 campaign with HFC-125, which also appears to have sources in China. No excellent correlation with any other halocarbon species was identified.

Ozone – Figure 4.53b

Whilst stratospheric ozone is an essential part of the atmosphere, low-level tropospheric ozone is a pollutant and may be damaging to health, particularly through prolonged exposure. Although it is not produced directly from industrial sources, it is formed by the reaction of UV radiation from the sun with nitrogen oxides or hydrocarbons, which do have industry-related and vehicular sources. Like CO, ozone mixing ratios show seasonal variation and significant spikes in its abundance during the campaigns may indicate particularly polluted or local influenced samples. Median mixing ratios for ozone do have similarities between the campaigns with abundances being highest in 2014 (56 ppb) and lowest in 2013 (49 ppb), with 2015 between the two (53ppb). The larger increase between 2013 and 2014 may be related to the proximity and frequency of Chinese emissions sampled during that campaign but normal fluctuations cannot be ruled out.

Again, like CO, a significant spike in ozone mixing ratios was observed on the 11th March 2013 (91 ppb) however spikes were also seen on the 27th March 2013 (100 ppb) and the 30th March 2014 (87 ppb). None were measured in 2015. NAME back trajectories suggest these samples all had potential influences from Korea and China. Regional Taiwanese emissions may have had a minor impact during the 2013 spikes as well, however site meteorological data does not suggest a local origin for this.

No good or excellent correlation with any halocarbon species was found with ozone.

Nitrogen Oxides (NOx) – Figure 4.53c

NO_x refers to NO and NO_2 and these species formed during combustion and so have major anthropogenic sources from vehicles and industry. As such NO_x emissions in East Asia have been increasing with industrial growth. During the Taiwanese campaigns, NOx was only measured in 2013 and 2015 campaigns, both carried out at the southern site. Median mixing ratios suggested a distinct decrease in abundance, from 5.3 ppt to 2.9 ppt. These results may reflect the shift towards renewable and clean energy, particularly by areas such as Japan and South Korea (Wang et al. 2014) but may just be variability given the short lengths of the campaigns.

As with ozone, significant spikes during the 2013 campaign were detected on the 11th and 27th March (11 ppt). In 2015, the 19th and 20th March saw significant abundances (10 ppt and 8.6 ppt respectively).

Comparison with NAME back trajectories suggested China and Korea were possible major influences for the spikes in 2013 and Taiwan in 2015. Like CO, Taiwan was also a potential minor influence for the 2013 significant samples. This may indicate that regional emissions from Taiwan impact this site although meteorological data does not imply the sources are local.

No good or excellent correlation was found with NO_x for other species.

PM_{10} – Figure 4.53d

PM_{10} is a term used to describe atmospheric particulate matter with an average diameter of 10μm and this has anthropogenic sources including coal combustion, power plants and vehicles. Similar to the previously mentioned species, this can be used to identify days or periods of high pollution. PM_{10} was only measured in the 2013 and 2014 campaigns and median mixing ratios decreased from 44 ppt to 20 ppt respectively. This difference may be due to the change in sampling sites or the proximity of local sources.

Significant spikes in PM_{10} abundance were detected on the 8th March 2013 (190 ppt) and the 13th March 2014 (46 ppt). Whilst both these samples had potential major influences from China indicated by the NAME back trajectories, the 2013 spike was also assessed as having Taiwanese emissions as a minor influence. Site wind directional data for this day does suggest that transport over local populated areas may have occurred and, given the magnitude of this spike, impact from this seems likely.

Again, no good or excellent correlation was found with other species for PM_{10}.

4.9.4 Summary

In recent years the East Asian region has become a major source of halocarbon emissions due to rapid industrialisation. The Montreal and Kyoto Protocols aim to ultimately phase out the production and consumption of species that contribute to ozone depletion and global warming respectively. Halocarbon emissions are therefore changing and require regular monitoring to ensure legislation is being followed. A number of campaigns have been carried out in East Asia but many of these do not assess mainly minor compounds and very short-lived substances. Campaigns spanning multiple years have been limited and so changes in observed abundances or regional emissions are less clear as varying methods and associated uncertainties have to be considered.

This work aimed to analysis a large range of halocarbon species, including several recently detected minor species and a number of short-lived substances, during three annual short-term air sampling campaigns in Taiwan. The data contributed towards individual species inter-annual variation assessments and widened the overall knowledge of halocarbon abundances in the region. Modelled back-trajectory analysis also enables some source location estimation. Interspecies correlations were used to suggest potentially co-located or co-emitting sources.

For the major CFCs, -11 and -12, decreasing median mixing ratios were observed over the three campaigns, which agrees with the Montreal Protocol phases out. China, Korea and Japan all appeared to contribute to measured pollution events from analysis of back trajectories. A lack of significant interspecies correlation suggests widespread sources of these species are present across the East Asian region, mainly due to small bank emissions.

Only measured during 2015, the minor isomeric CFCs, -114 and 114a, were unexpectedly found not to correlate with each other indicating different sources. Continued emissions were suggested by enhancement above background abundances, particularly for CFC-114a. Back trajectory analysis and interspecies correlation suggested China as a potential source region for -114a and Korea for -114. Decreasing regional inter-annual abundances for CFC-115 and CFC-13 were observed and emissions from China were indicated to have major impact on the air masses sampled for both these species.

CFC-113, CFC-113a, halon 1211 and halon 1202 were identified as species of interest and so expansion on these results will take place in the respective sections (4.10 and 4.11). Median mixing ratios reflected decreasing regional variation between campaigns for CFC-113, halon 1211 and halon 1202 whilst increases were observed for CFC-113a. Some continued emissions were suggested however by enhancements above background mixing ratios and distinct pollution events for all of these species.

Regional inter-annual variation of the minor halons -1301 and -2402 were also observed to follow the respective increasing and decreasing global trends.

China and Korea were suggested as potential origins for -1301 emissions whilst the -2402 trajectories indicated local emissions from Taiwan. Good interspecies correlation was found with several HCFC and HFC compounds and may be due to widespread emissions of these species since their implementation as CFC and halon replacements.

Median mixing ratios of HCFC-22 and HCFC-141b declined between 2013 and 2015, suggesting regional sources of these species may be decreasing. HCFC-142b however, saw increased median abundances across the campaigns. All these compounds saw more frequent enhancement above background mixing ratios during the 2014 campaign This implies there are extensive Chinese sources for these species although interspecies correlation. Taiwanese emissions are also suggested for HCFC-141b.

The recently detected HCFC-133a has had a more varied global trend than other species and mixing ratios from these campaigns suggested the regional abundances had been decreasing, which agreed with the study from Vollmer et al. (2015). Correlation of this species with CFC-113 and CFC-113a also identified it as a compound of interest; see section 4.10 for further details.

Carbon tetrachloride and methyl chloroform were observed to have decreasing median mixing ratios across the three campaigns. Chinese emissions were suggested to have impacted the air masses sampled for both species. Sources in Japan of carbon tetrachloride and Taiwanese sources for methyl chloroform were potentially indicated as well. Halothane median mixing ratios were very similar for both years it was measured and influence from Korean emissions were implied by back-trajectories.

For the methyl halides, significant natural sources are likely part of the consistent enhancement above background mixing ratios observed. Potential source locations also varied, particularly for methyl bromide. The interspecies correlations for methyl chloride and the short-lived species imply potential Chinese sources however no firm conclusions can be drawn.

Median abundances of dichloromethane, 1,2-dichloroethane and chloroethane decreased whilst chloroform and tetrachloroethene medians increased. All 5 VSLS-Cl species have potential sources in China although both 1,2-dichloroethane and chloroethane were suggested to have Taiwanese sources as well. Interspecies correlation was generally found between these short-lived species along with other extensively used ODS.

Bromoform was the only VSLS-Br species interpreted and, no clear conclusions can be drawn given its fluctuating abundance. Back trajectories indicated the Pacific Ocean as a major source, as expected.

Increasing median abundances were observed for the HFCs, -134a, -23 and -125 whereas -143a and 152a were found to decrease. Back-trajectories for HFC-134a do not indicate any distinct source regions, likely due to the widespread emission.

China and Taiwan are all indicated as potential emissions sources for the other major HFC species. Interspecies correlations were generally seen with HCFCs and VSLS-Cl, which also have extensive uses in China.
Increasing median abundances were observed for the minor HFCs, -245fa, -227ea and 365mfc. Analysis of back-trajectories and interspecies correlations are similar to the other HFCs.

The short chain PFCs, C_2F_6 and cyclic-C_4F_8 both had observed mixing ratios that reflected the previously reported increasing growth rates of these species, along with SF_6. C_3F_8 saw decreases in median abundances suggesting regional emissions have changed. China and Korea were suggested as potential major sources through both back-trajectory analysis and interspecies correlation. Local Taiwanese influence was seen in 2014 and further details can be found in section 4.12.

Potential contamination during the 2013 campaign limited the usability of the long-chain PFC data. Median mixing ratios of C_4F_{10} and C_7F_{16} increased between 2014 and 2015. However, C_5F_{12} saw a decrease in median abundances, which may be due to changes in the sampling site and/or regional emissions. Back-trajectory and interspecies correlations comparisons indicated Chinese and Korean emissions as major influences, with some emissions from Taiwan contributing as well.

The isomers n-C_6F_{14} and iso-C_6F_{14} were only measured in 2015 and co-emission was suggested by the excellent correlation found between these compounds. Back trajectories did not indicate a clear source location but local winds indicated influences from Taiwanese sources. Cyclic-C_5F_{10} was also measured in 2015 but very little is known about its applications or emissions. Potential sources were suggested as Korea and Japan although Chinese emissions also influenced some of the observed pollution events.

Some variation was seen with median mixing ratios of carbonyl sulphide and emissions were suggested to originate in China and Korea. Median abundances for SF_5CF_3 were found to be similar each year and, given the discontinued production of this species and long atmospheric lifetime, this was not unexpected. Taiwanese emissions were suggested to be dominant on days where pollution events were seen however.

Carbon monoxide mixing ratios decreased for 2015, potentially indicating the sampling of less polluted air masses and Ozone saw variations in abundance between all the campaigns, likely due to normal fluctuations. NO_x and PM10 decreased between the two campaigns they were respectively measured in. Back-trajectory analysis suggested influence from Chinese, Korean and Taiwanese emissions for these species.

4.9.5 Further Analysis

These campaigns have helped to highlight the potential of Taiwan to play a major role in the assessment of atmospheric halocarbon monitoring for the East Asian region however, their scope was limited due to sampling time and analysis constraints. As such, there is still a long way to go to fully utilise this location.

The large data set established from this work may contribute to the wider knowledge of East Asian halocarbons, especially for newly detected and minor species, where only limited data is available. Whilst global control measures appear to be followed for many species, continued monitoring is still necessary to confirm and ensure this continues and to observe changes in species just beginning their phase out schedules.

The establishment of a continuous monitoring site in Taiwan would aid global assessments due to its advantageous location for assessment of continental outflow in the region. Collection of data for a range of halocarbon species over a number of years would better identify variation in atmospheric trends from inter-annual changes and constrain background abundances for the region more robustly, allowing for better interpretation.

Future campaigns would benefit from the assessment of boundary layer variation and more regular local meteorological data to better identify the air masses sampled in comparison to modelled results. A significantly more quantitative analysis of backwards trajectories established NAME would also further improve and strengthen the conclusions able to drawn in terms of potential sources of emissions.

4.10 Case Study 1: CFC-113, CFC-113a and HCFC-133a

4.10.1 Introduction

CFC-113 (CCl_2FCClF_2, Figure 4.54a) is the third most abundant CFC in the atmosphere and has had widespread uses in aerosols, dry cleaning and refrigeration as well as having applications as a foam-blowing agent (EIA, 2009) and solvent (Kim et al. 2011). Like all CFCs, the high volatility combined with low flammability and low toxicity of CFC-113 made it a very useful compound industrially but the negative effects on the atmosphere led to its inclusion in the Montreal Protocol. This resulted in the global phase out of its production and use by 2010 (UNEP, 2016) in all but Russian Federation aerospace applications, which are currently exempt whilst alternatives are developed and introduced (UNEP, 2015b). Atmospheric mixing ratios peaked in the late 1990s (see Figure 4.55) at ~83 ppt but have been decreasing ever since, at a rate of ~0.7 ppt yr^{-1}. In recent years, global emissions have been regularly less than 5 Gg/yr (Carpenter and Reimann, 2014).

Whilst much is known about the uses and production of the regularly monitored CFC-113, considerably little is known about its isomer CFC-113a (CCl_3CF_3, Figure 4.54b) that has only recently been detected in the atmosphere (Laube et al. 2014). Though also covered under the Montreal Protocol, there are no publicly accessible reports to UNEP of CFC-113a production and industrial applications are unclear.

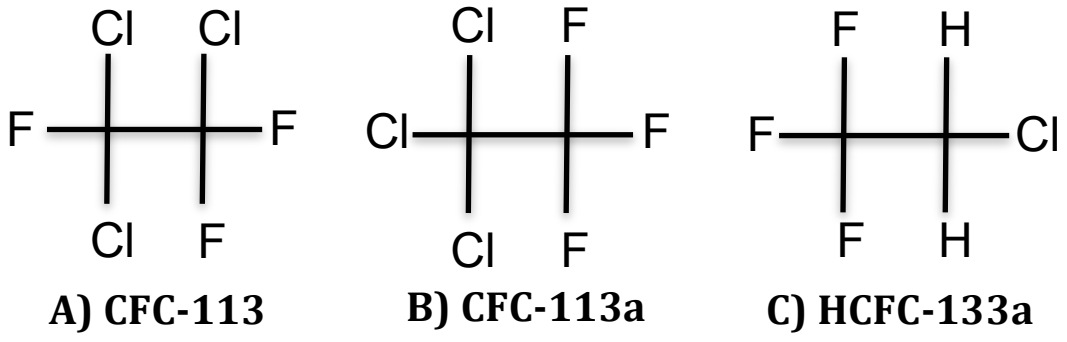

Figure 4.54: Chemical structures of the CFCs A) -113 and B) -113a as well as the HCFC C) -133a.

It should be noted that the Montreal Protocol includes both official exemptions for specific uses of a number of species and limitations as to what does and does not have to be reported. When used as a chemical feedstock, production does have to be reported to UNEP but this information is not allowed to be released to the public. Feedstock usage is also considered to be only a minor contributor to emissions and so is not controlled.

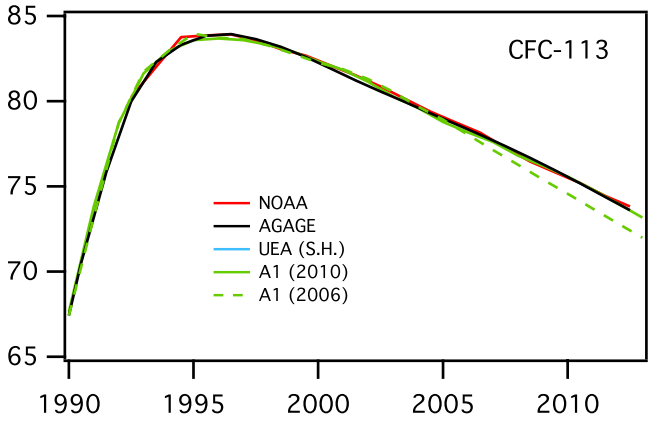

Figure 4.55: Global mole fraction of CFC-113 from 1990 to 2012. Taken from Carpenter and Reimann, 2014.

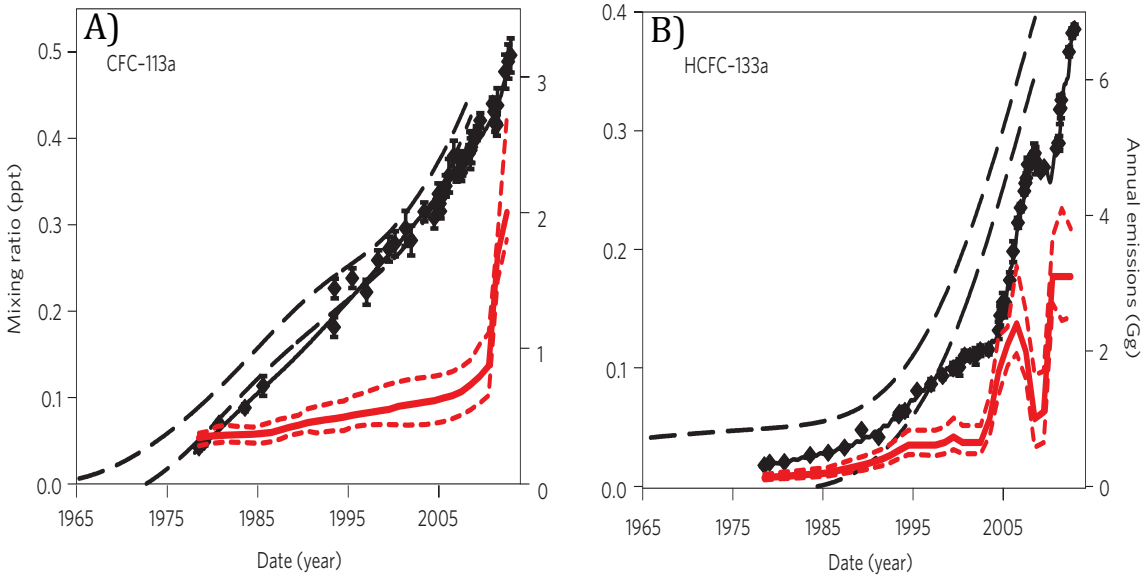

Figure 4.56: Global trend of mixing ratios and annual emissions for A) CFC-113a and B) HCFC-133a. Black dashed lines reflect the range of northern hemispheric trend, reconstructed from firn samples. Black diamonds represent average individual samples collected at Cape Grim and the black solid line is the model fit through this data set that was used to estimate emissions (red line, right hand axis). Dashed red lines indicate 1σ uncertainties. From Laube et al. 2014

During the manufacture of other ODS, production of intermediate species, estimates of trace amounts released or fugitive emissions do not have to be reported. With isomers, production does not have to be reported separately so in the case of CFC-113a, this may have been reported along with CFC-113 (Laube et al. 2014). In 2003, CFC-113a was added to the list of Montreal Protocol exemptions as an 'agrochemical intermediate for the manufacture of synthetic pyrethroids' likely in relation to its use in the cyhalotrin and tefluthrin production (Cuzzato et al. 2002). It is also a known intermediate in the manufacturing processes of the widely used HFC-134a (Manzer, L.E. 1990) and HFC-125 (Kuijpers and Seki, 2013).

Detected concentrations of CFC-113a in clean, southern hemispheric air, were only 0.48 ppt in late 2012 (Laube et al. 2014) and so its contribution to total tropospheric chlorine mixing ratios is extremely low (less than 0.1%). However, what is most concerning about this compound is that atmospheric abundances are still increasing (see Figure 4.56a) and in recent years the rate has increased, in contrast to all other CFCs and without any apparent slowdown (Laube et al. 2014). Drawing conclusions as to the origin of emissions resulting in these abundances is complicated especially due to the collection of air samples away from sources at remote sites. Feedstock and chemical immediate use as well as fugitive emissions from these applications and the potential of non-sanctioned production mean further campaigns are necessary to assess potential source locations.

Also, recently detected in the same study, at 0.37 ppt in late 2012, was HCFC-133a (CF_3CH_2Cl, Figure 4.54c). HCFCs were mainly utilised in the replacement of CFCs and halons. However, Figure 4.56b shows HCFC-133a appeared in the atmosphere before the large-scale substitution began suggesting that the sources are not entirely related to the CFC phase-out. Another unusual behaviour of this compound is the period of interrupted growth between mid-2008 to mid-2010. Before this period mixing ratios of HCFC-133a were increasing and from 2004 to 2008 the rate of growth also increased. After the slight drop that continued until mid-2010, the abundance increased again into 2012. However, in order for these turnarounds to occur and be measurable, huge changes in emissions are required. Potential causes for this interruption may be changes in production procedures by one or more large industrial emitters and/or changes in the range of products manufactured (Laube et al. 2014). Like CFC-113a, information on the applications of HCFC-133a is minimal and it too is a known intermediate in the production of HFC-134a (McCulloch and Lindley, 2003) and HFC-125 though through a different production process. It is also used in the manufacture of HFC-143a (Shanthan Rao et al. 2015) as well as pharmaceuticals, agrochemicals and halothane, a now phased out anaesthetic (Vollmer et al. 2015b).

While emissions of HCFC-133a were ~3 Gg in 2012 (Laube et al. 2014), a more recent study by Vollmer et al. (2015) found emissions to have since declined sharply to 1.5 Gg yr^{-1} in 2014. The suggestion for this decrease is better catalytic conversion and containment during production since the manufacture of HFCs, where HCFC-133a is produced as an intermediate, has increased. Regional emissions analysis also suggested that HCFC-133a is unlikely to be an impurity in HFC products and thus emissions would be from HFC manufacturing sites rather than their widespread applications. Between 2012 and 2015, northern hemispheric mixing ratios appear to have begun to increase again suggesting a further turn around in emissions. Further campaigns looking into the exact reason for these variations in emissions and observed mixing ratios, intentional or not, is needed along with continued monitoring to assess further changes or stabilisation in abundance (Vollmer et al. 2015).

Data from the 2013 and 2014 Taiwan campaigns was included in the Vollmer et al. (2015) study and observed pollution events, resulting in enhanced HCFC-133a mixing ratios, were found to be in line with similar events measured at the European stations Jungfraujoch and Dubendorf, Switzerland. This supports the validity of the data from Taiwan as completely different calibration scales were used to calculate mixing ratios from the sites in the Vollmer et al. (2015) study but good agreement was still seen.

In this case study the concentrations, correlations, back trajectories and variation between these three compounds during the 2013 and 2014 campaigns will be compared and potential explanations for their relationships and impacts discussed. Issues with the 2015 analysis of CFC-113 means there is no data currently and there was not time available for reanalysis. 2015 data is however, presented for CFC-113a and HCFC-133a

4.10.2 Results

Figures 4.57a-c show a side-by-side comparison of the time series results during the 2013 and 2014 for all three of the compounds mentioned above. What can be seen are distinct similarities between days when pollution events resulted in spikes in concentration. It also shows this relationship continuing into the 2015 campaign, at least between CFC-113a and HCFC-133a. As such, correlations between all three compounds were calculated and also plotted (Figures 4.58a-c) to show the associations for each campaign.

What is most notable from Figures 4.57 and 4.58 is the apparent correlation between CFC-113 and CFC-113a during the first two campaigns, with coefficients of 0.88 in 2013 and 0.96 in 2014 (see Table 4.7). Also, the slopes of the linear best-fit lines are similar, with 0.34 in 2013 and 0.36 in 2014 indicating very similar relationships between the two species for both years. This suggests co-emission or at least very good co-location of sources of these isomers, which has never previously been reported. This is particularly unexpected as CFC-113a has not been detected as a by-product or contaminant of CFC-113 emissions like isomers of other species. There are also no reports of their use in the same applications though, as considered before, there is very little information on uses of CFC-113a so this correlation could be the result of a previously unreported joint application.

Table 4.7: Comparison of the correlation coefficients and R^2 values between CFC-113, CFC-113a and HCFC-133a.

Compound	Formula	Campaign Year	Correlation Coefficient			R^2 Value		
			CFC-113	CFC-113a	HCFC-133a	CFC-113	CFC-113a	HCFC-133a
CFC-113	CCl_2FCClF_2	2013		0.88	0.92		0.78	0.84
		2014		0.96	0.90		0.91	0.80
		2015						
CFC-113a	CCl_3CF_3	2013	0.88		0.92	0.78		0.85
		2014	0.96		0.96	0.91		0.92
		2015			0.94			0.89
HCFC-133a	CF_3CH_2Cl	2013	0.92	0.92		0.84	0.85	
		2014	0.903	0.96		0.80	0.92	
		2015		0.944			0.89	

While production and consumption of CFCs should have ceased, both CFC-113 and -113a were detected at above background mixing ratios. Continued emissions of CFC-113 are likely explained by the presence of banks in refrigeration and foam applications however there is no information of the likelihood of CFC-113a banks. Given what is known about -113a applications, long-term storage and later release currently seems unlikely but this is still a largely unknown area. Since atmospheric concentrations have been increasing for CFC-113a from the 1960s and are still continuing to do so during these campaigns, this does suggest a continued emissions source. CFC-113 abundances, on the other hand, are relatively stable and show only a very slight decrease between 2013 and 2014 suggesting that the phase out of this compound was successful and emissions are very minimal.

Whilst this lack of evidence of emissions could imply that the detected source of CFC-113a is not related to CFC-113, it should be noted that this does not agree with the correlation seen and, the abundance of CFC-113 is considerably larger at ~75ppt compared to ~0.8ppt on average for CFC-113a. As such somewhat larger emissions of CFC-113 are needed to show a change in trend than in the case of -113a.

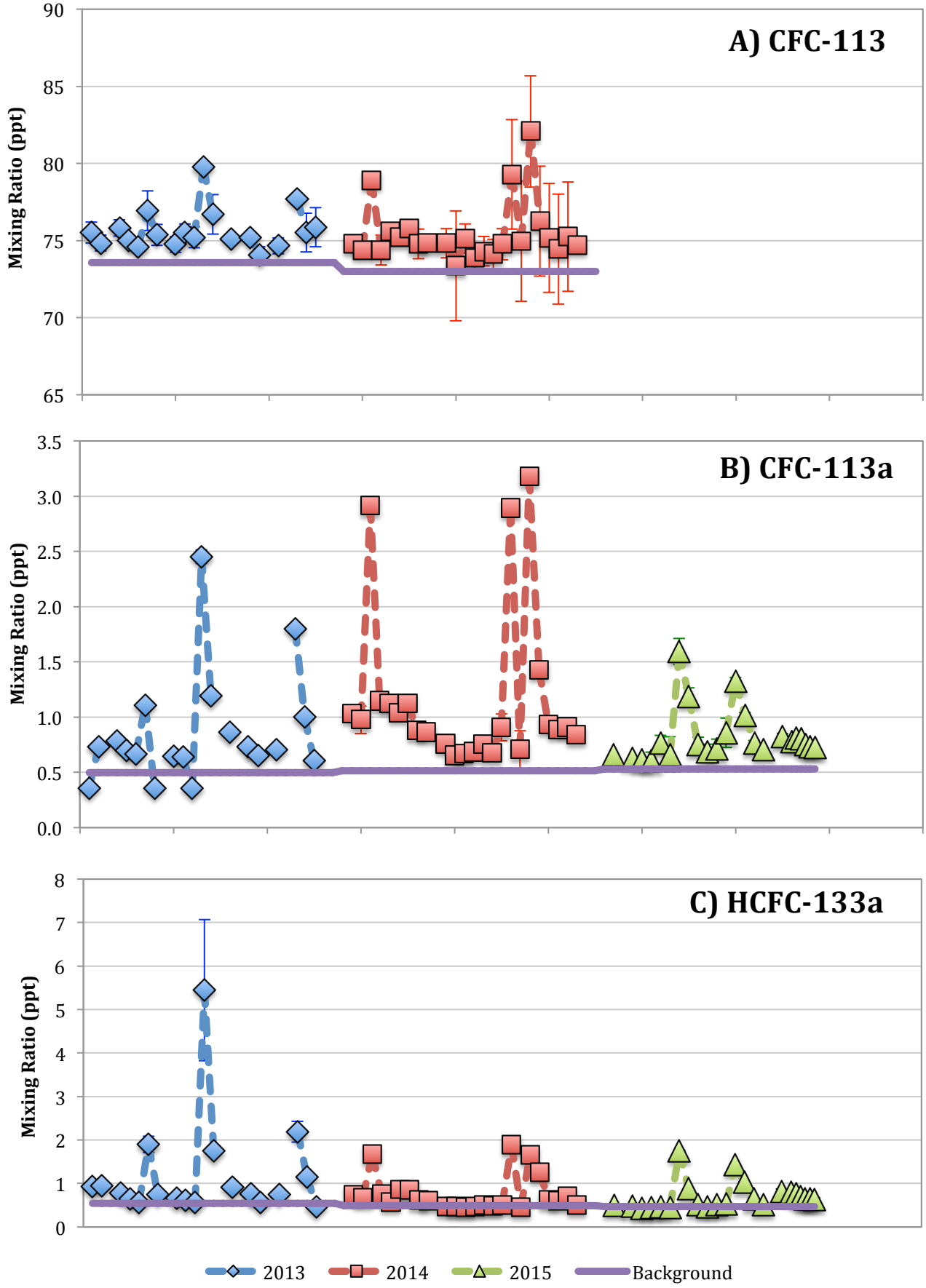

Figure 4.57: Time series spanning the three Taiwain campaigns for A) CFC-113, B) CFC-113a and C) HCFC-133a. Data from 2013 is represtented in blue, 2014 in red and 2015 in green. Background abundances are shown in purple. Error bars indicate the total uncertainty calculated for the samples.

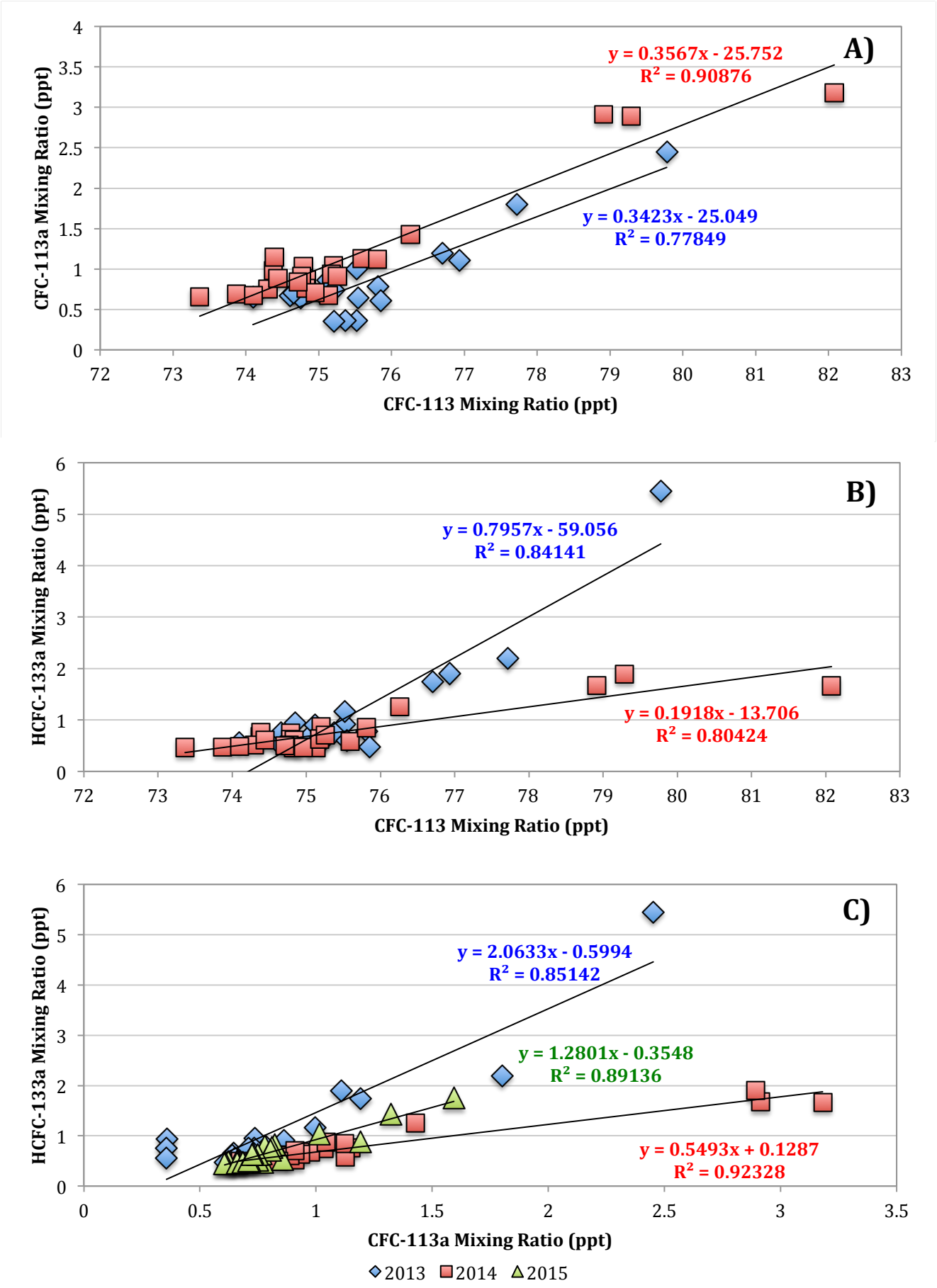

Figure 4.58: Correlation between A) CFC-113 and CFC-113a, B) CFC-113 and HCFC-133a, and C) CFC-113a and HCFC-133a, for the three Taiwan campaigns. Data from 2013 is represented in blue, 2014 in red and 2015 in green.

For HCFC-133a, correlation coefficients with CFC-113a are even higher than those previously mentioned with 0.92 in 2013, 0.96 in 2014 and 0.94 in 2015 (see Table 4.7). Correlation coefficients with CFC-113 are only slightly less (0.92 in 2013 and 0.90 in 2014). The slopes of the lines of best fit for HCFC-133a vary considerably more than was observed between CFC-113 and -113a suggesting there were significant changes in this species' emissions. With CFC-113 (Figure 4.58b), the slope was 0.80 in 2013 but shifted to 0.19 in 2014 whilst correlation coefficients remained comparable. Similarly, with CFC-113a (Figure 5.58c) the slope changed from 2.06 in 2013, to 0.55 in 2014 and finally to 1.28 in 2015. These decreasing gradients between 2013 and 2014 may be due to a large reduction in emissions of HCFC-133a and this is consistent with the abundance observations of Vollmer *et al*. (2015). The increase in gradients between 2014 and 2015 is also consistent with the apparent rise in mixing ratios detected at northern hemispheric sites in 2015 by the same study, which is likely tied to another increase in HCFC-133a emissions. These differences, which were not seen between the CFCs, indicate that source co-location of HCFC-133a with CFCs -113 and -113a is more likely than co-emission. Since HCFC-133a is a relatively newly detected compound, this has not been previously reported and, like CFC-113a, there are few clear indications of its uses and applications. However, HCFC-133a is an intermediate in the production of the same HFCs as CFC-113a, though the chemical processes are different.

In HFC-134a production, CFC-113 is isomerised to form CFC-113a and then this is then fluorinated to produce CFC-114a (Rao, 1994), which is then hydrogenolysed to HFC-134a. For HCFC-133a the process involves production from trichloroethene and then the substitution of the final chlorine atom. Whilst all three compounds of interest are utilised in this production, both these processes are totally enclosed and gases recycled or treated rather than vented so fugitive emissions from this source should be minimal (McCulloch and Lindley, 2003).

In the production of HFC-125, CFC-113, CFC-113a and HCFC-133a can all be produced as by-products by the fluorination and recycling of starting materials HCFC-123 or HCFC-124. However, the CFCs are often fluorinated further to CFC-114a or CFC-115 in the reactor (Kono et al. 2002) so whilst the generation rate for CFCs maybe ~2% depending on the methods and catalysts used, this is unlikely to be made up of CFC-113 or -113a (Takahashi et al. 2002). Nevertheless, CFC-113a and HCFC-133a were found to have good correlation with CFC-114a and some correlation with CFC-115. This indicates that there is an observed relationship with all these compounds and at least some co-location of emissions, likely from this process. Mixing ratios of CFC-115 were found to be relatively stable over the three campaigns and are no longer increasing. This suggests that the abundances detected for -113a and -133a are either not entirely from this source, which is plausible, or that emissions mainly occur before further fluorination occurs, which seems unlikely.

Both CFC-113a and HCFC-133a have applications in the manufacture of agrochemicals (TEAP, 2014) but since specifics for this are unavailable, it is unclear whether sources from this industry would be collocated and what the likelihood of fugitive emissions would be. Also, the use of CFC-113 in this area has not been reported and so these potential sources do not explain the correlation of CFC-113 that indicates co-emission with CFC-113a and co-location with HCFC-133a. As such, this would suggest agrochemicals are unlikely to be the cause of the detected emissions, at least during the 2013 and 2014 campaigns.

With this information, leaks from HFC-134a production whilst unlikely, seem to be the most feasible explanation for the correlation detected however other uses and applications of these compounds need to be investigated further through continued sampling before a more evidence-based conclusion can be reached.

In terms of abundances detected, all three compounds were found to be enhanced above background mixing ratios in the majority of samples measured. Several days of significant enhancement were seen during each campaign and Table 4.8 lists the largest of these, all of which correspond with each of these species.

Some near background abundances were detected as well, particularly for HCFC-133a, from 26% of samples in 2013 to 42% in 2014 and 28% in 2015. These backgrounds reflect HCFC-133a mixing ratios in Jungfraujoch, Switzerland, a remote Northern Hemispheric sampling station, and are taken from Vollmer et al. (2015). This increase in close to background concentrations suggests that the atmospheric trend for HCFC-133a has started decreasing again, which agrees with the Vollmer et al. (2015) study.

Table 4.8: Mixing ratio and wind data for pollution events occurring during the three Taiwanese campaigns for CFC-113, CFC-113a and HCFC-133a.

Campaign	Date	Mixing Ratio (ppt)			Winds	
		CFC-113	CFC-113a	HCFC-133a	NAME Trajectory	Local
2013	14/03/13	76.9	1.1	1.9	China/Korea	ENE
	21/03/13	79.8	2.5	5.5	China/Korea	ENE
	22/03/13	76.7	1.2	1.8	Korea/Pacific	NNW
	03/04/13	77.7	1.8	2.2	China	ENE
2014	13/03/14	78.9	2.9	1.7	China	ENE
	28/03/14	79.3	2.9	1.9	China/Japan/Pacific	SSE
	30/03/14	82.1	3.2	1.7	China	ESE
	31/03/14	76.2	1.4	1.3	China	NNW
2015	22/03/15		1.6	1.8	China/Korea	ENE
	23/04/15		1.2	0.88	China	ENE
	28/03/15		1.3	1.4	China/Japan	ENE
	29/03/15		1.0	1.0	China/Taiwan/Japan	ENE

Still, distinct pollution events are visible and these too appear to show variation that may be due to the impact of decreasing emissions since the largest enhancements (5.44 ppt and 2.19 ppt) were seen in 2013 and spikes in the campaigns after that are progressively lower (maximum of 1.89 ppt in 2014 and 1.75 ppt in 2015).

This is different to both CFC-113 and CFC-113a who see their largest enhancements in 2014 (82.1 ppt and 3.2 ppt respectively). The results for CFC-113 collected during these campaigns agree with its global trend, with median mixing ratios decreasing slightly from 75.4 ppt in 2013 to 74.8 ppt in 2014 (see Appendix 3.4) although this may be due to inter-annual variation. Still, enhancements above background seen in 2014 were up to 4% larger than those in 2013, against the atmospheric trend. Again, this may be due to inter-annual variation or this could be the origin of the emissions being sampled during the campaigns and so the NAME trajectories and local winds for each of the main identified spikes were considered (see Table 4.8).

What is most notable about the trajectories that correspond with the largest spikes in concentration of these three compounds is that all bar one appear to have some influence from Chinese emissions. This implies that China is the predominant source region for these species. The day without impact from China is the 22nd March 2013 and sees air masses travelling from Korea and the Pacific Ocean. While abundances of CFC-113, -113a and HCFC-133a were all markedly enhanced above background on these days, the sample for the previous day (21st March) saw even more significant enhancement and its NAME backwards trajectory saw major influences from both China and Korea. The difference between these two samples and comparison with the other two main spikes during this campaign may indicate that, whilst there are potentially sources of all three species in Korea, emissions are not a large as those from China. Whilst HFC 125 and 134a production estimates are unavailable for Korea, 78 Gg yr^{-1} and 118 Gg yr^{-1} respectively were reported for Chinese production in 2013, giving some indication as to the extent of this industry and so potential sources (Fang et al. 2016).

To investigate this further, samples with back trajectories suggesting major emissions contributions from China only from all three campaigns were compared and their correlations calculated (see Table 4.9). Whilst only some correlation was found with HCFC-133a for both CFC species, good correlation was found between CFC-113 and CFC-113a suggesting co-located sources. The lower coefficient of HCFC-133a is not unexpected given its wider known sources however, given the back trajectories of these samples, this indicates that the currently unknown sources of CFC-113a are likely to be in China and potentially near sources of CFC-113 as well. Further sampling would be necessary to confirm this relationship and more specific source locations, along with the testing of any CFC-113 banks for potential contamination.

Table 4.9: Comparison of the correlation coefficients and R^2 values between CFC-113, CFC-113a and HCFC-133a for samples with major emission contributions from China from NAME analysis of all three Taiwan campaigns

Compound	Pearson Correlation Coefficient			R^2 Value with CFC-113
	CFC-113	CFC-113a	HCFC-133a	
CFC-113		0.902	0.699	
CFC-113a	0.902		0.603	0.81
HCFC-133a	0.699	0.603		0.49

Local winds on the 22nd March 2013 also varied compared to the other three days considered - this day saw local winds travelling from the NNW rather than the ENE. The winds from the east are indicative of the katabatic winds previously discussed and so are likely to contain evidence of long range transport but may have picked up some local influences before reaching the site. Several other days during the 2013 campaign saw similar easterly winds and no consistent patterns in enhancement were noticeable suggesting that local influence for these compounds would be minimal. The fact that comparable correlation and slopes were also seen at completely different sampling sites for CFC-113 and -113a also suggests that these spikes in abundances were not local in origin. Comparable correlation coefficients were seen with HCFC-133a between sites as well and variation in slopes can be explained by the changes in emissions discussed previously, which indicates a lack of local sources for this species too.

The 2014 campaign saw trajectories of predominantly Chinese origin on three of the four days with particular enhancement. The other day, the 28th March 2014, had potential impacts from Japan and the Pacific Ocean. Overall, this campaign saw the largest frequency of trajectories originating in China and CFC-113a particularly appears more enhanced in general during this time with median mixing ratios having increased by 0.2 ppt (~35%) compared to 2013. For CFC-113 the decrease in median abundances was only 0.5 ppt, which is very similar to the decrease between background values over the same time period (0.58 ppt). This suggests that, this species is following the global trend even though the consistent enhancement above background seen in the previous campaign continued. Substantial local influences impacting these findings seems unlikely as local winds did indicate a number of days that may be affected (see Case Study 3 for further information) and spikes in concentrations do not correspond for these compounds. As such, this implies that air masses impacted by Chinese emissions are mostly responsible for the enhancements detected and so the major sources are likely located in this area.

The results from the 2015 campaign also suggest China as the main source location though trajectories also show potential influences from Korea and Japan as well. This year did see smaller spikes for CFC-113a than previous years (maximum of 1.6 ppt) and median concentrations were lower than the previous year as well (0.75 ppt as opposed to 0.91 ppt in 2014).

Whilst this may be due to inter-annual variation, a reduction in emissions may be due to the same changes that caused the reduction in HCFC-133a mixing ratios since the two species appear to be linked. Part of this decrease however may be due to the higher frequency of air masses from Korea during this campaign, rather than those from China, resulting in less significant enhancements being sampled. However, consistent above median enhancements were seen for both species at the end of this campaign (22nd-25th April) and the predominant major influence during this period was Korea. Local wind speeds and directions corresponded with the rest of the campaign so influence from local sources was not anticipated. This suggests emissions from Korea are continuing but these may not be large as those from China or are being substantially diluted during transport before reaching Taiwan. As such, further campaigns would need to be carried out before a conclusion can be drawn on this particular matter.

4.10.3 Summary and Further Analysis

During the three Taiwan campaigns, concentrations of the novel species CFC-113a and HCFC-133a were detected at enhanced mixing ratios and found to be well correlated with one another. CFC-113 also showed correlation with both species where data was available suggesting all three are being co-emitted or are very closely collocated. The isomers, CFC-113 and -113a, have not been reported as having correlating previously but very little is known about the sources or quantities of CFC-113a emissions, similarly with HCFC-133a. Agrochemical production uses both CFC-113a and HCFC-133a but there is a lack of available information and no indication of CFC-113 to explain the correlation. All three species are utilised in the production of HFC-134a and HFC-125 and while the nature of the processes and preventative measures put in place make this appear to be an unlikely source, the leaks during the production of HFC-134a in particular currently seems the most feasible explanation for what has been detected.

NAME back trajectories and increased species concentrations suggest that East Asia is a major source region for these species and the most likely source location for the emissions sampled is China, although there is potential for sources in Korea and possibly Japan. CFC-113 appears to be decreasing slightly in the atmosphere along with the global trend. HCFC-133a also looks to have started to decrease again, as suggested in Vollmer et al. (2015). CFC-113a may have begun to decrease in abundance between the campaigns but differences in the proportion of air masses sampled that originate in China and Korea and more dilution during transport at the southern site may be the cause of the noted decline.

Further campaigns are needed into the uses and application of CFC-113a and HCFC-133a in order to find and assess sources. Regular and widespread monitoring would be of particular use and would aid in gauging whether the recent change in HCFC-133a trend is going to continue and if the CFC-113a trend is following.

4.11 Case Study 2: Halon 1211 and Halon 1202

4.11.1 Introduction

The most abundant halon in the atmosphere, halon 1211 ($CBrClF_2$, Figure 4.59a), has been steadily decreasing in atmospheric concentration since the mid 2000s due to the control measure of the Montreal Protocol (Carpenter and Reimann, 2014). With major uses in fire-fighting and explosion protection (HTOC, 1991), sources were widespread but as of 2010 its production and consumption have been phased out. However these uses mean that large banks of halon 1211 exist and so continued emissions are expected (Carpenter and Reimann, 2014). Even though developing nations like China and Korea stopped production of 1211 in 2005 and 2009 respectively (HTOC, 2011), these bank emissions indicate the atmospheric impact of the phase out will not be immediately observed.

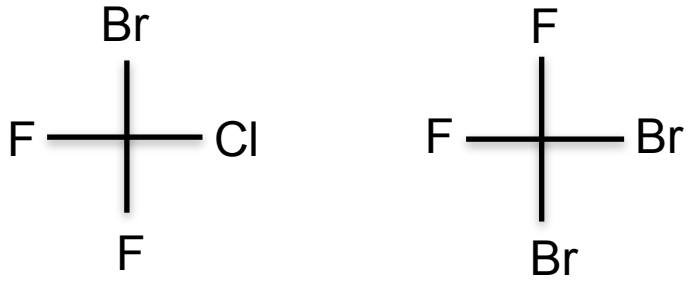

A) Halon 1211 **B) Halon 1202**

Figure 4.59: Chemical structures of A) Halon 1211 and B) Halon 1202

Also, decreasing in abundance is halon 1202 (CBr_2F_2, Figure 4.59b), a more minor species whose major source is believed to be a by-product formed by over-bromination of $CHClF_2$ (HCFC-22) during halon 1211 production (HTOC, 1999, Fraser et al. 1999). However, halon 1202 was used in very few industrial applications and not in portable fire extinguishers due to its high toxicity. The US Air Force utilised it in the protection of military aircraft engines (Grant, 2016) and it has been used both as a reagent (Rodriguez., 2002) and chemical feedstock (Surya Prakash et al. 2005) in laboratories. Newland et al. (2013) found that emissions of halon 1202 had not decreased to zero in 2010 when halon 1211 production was ceased. This suggested either a continued significant source of halon 1211 or other sources of halon 1202 not linked to halon 1211 production. They suggested that a large continued source was unlikely at previously reported halon 1202 production efficiencies however a smaller, less efficient source could be a possibility. Its use in military aircraft would have created a bank that may be released after the completion of halon 1211 production and that could result in continued emissions.

There is also the potential that halon 1202 wasn't completely separated from halon 1211 during production and so would remain as a low level contaminant in banks and be emitted at a later date (Newland et al. 2013).

This case study will compare the concentrations, correlations, back trajectories and inter-annual variation of both halon 1211 and halon 1202 in order to assess potential relationships and origins of these species.

4.11.2 Results

Figures 4.60a and b show a side-by-side comparison of the time series results during the three Taiwan campaigns. Both species were mainly enhanced above background abundances indicating there are continued emissions. While not as clear as those in the previous case study, there are some similarities between a number of days when spikes in concentration from detected pollution events were seen, particularly in the later campaigns. To look at potential relationships, the correlation between species was calculated and the results from each campaign plotted against each other (Figure 4.61).

What is clear from both the graphs and the calculated correlations (see Table 4.10) is the lack of relationship between halon 1211 and halon 1202 during the 2013 campaign (coefficient of 0.33). Since the main source of halon 1202 is believed to be halon 1211 production, this would not be unexpected as this production was ceased globally by 2010. However, mixing ratios of halon 1202 are still above background (by 68%, 53% and 50% in the respective campaigns) and there are distinct spikes suggesting the continued presence of emissions, which agrees with the study by Newland et al. (2013). Their suggestion of a small and less efficient halon 1211 production source as a potential explanation or halon 1202 being present as a low level contaminant in -1211 banks seems unlikely in this scenario since more correlation would be expected. Release from halon 1202 banks seems more reasonable however these are mainly known to be controlled by the US military. There is a significant military presence from the US, particularly in South Korea where around 28,500 troops are based (Woods, D.L. ed., 2015), and so this may be a source of the halon 1202 emissions detected.

Table 4.10: Comparison of the correlation coefficients and R^2 values between Halon 1211 and Halon 1202

Compound	Formula	Campaign	Correlation Coefficient		R^2 Value	
			Halon 1211	Halon 1202	Halon 1211	Halon 1202
Halon 1211	$CBrClF_2$	2013		0.33		0.109
		2014		0.749		0.428
		2015		0.653		0.561
Halon 1202	CBr_2F_2	2013	0.33		0.109	
		2014	0.749		0.428	
		2015	0.653		0.561	

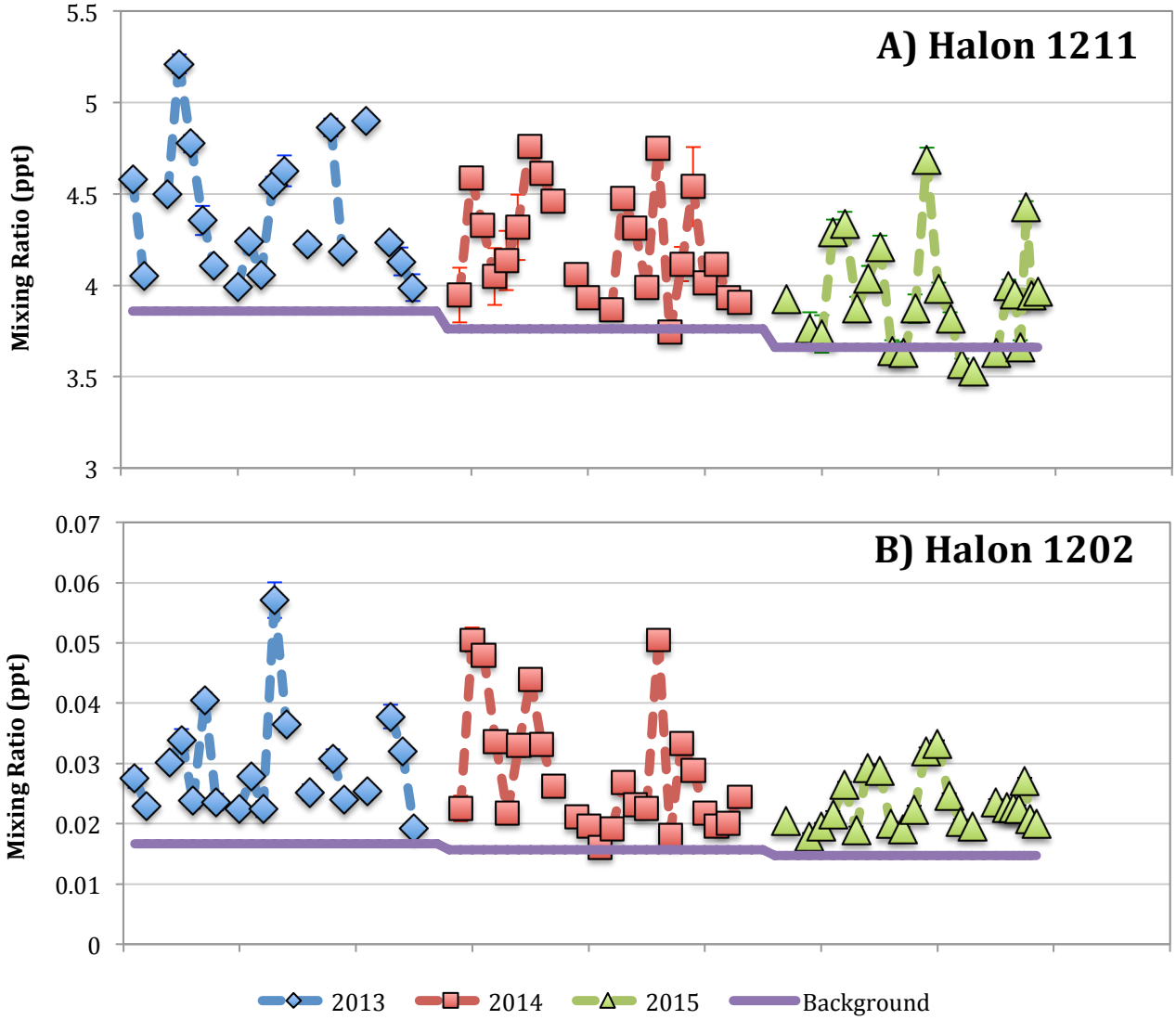

Figure 4.60: Time series spanning the three Taiwain campaigns for A) Halon 1211 and B) Halon 1202. Data from 2013 is represtented in blue, 2014 in red and 2015 in green. Background abundances are shown in purple. Error bars indicate the total uncertainty calculated for the samples.

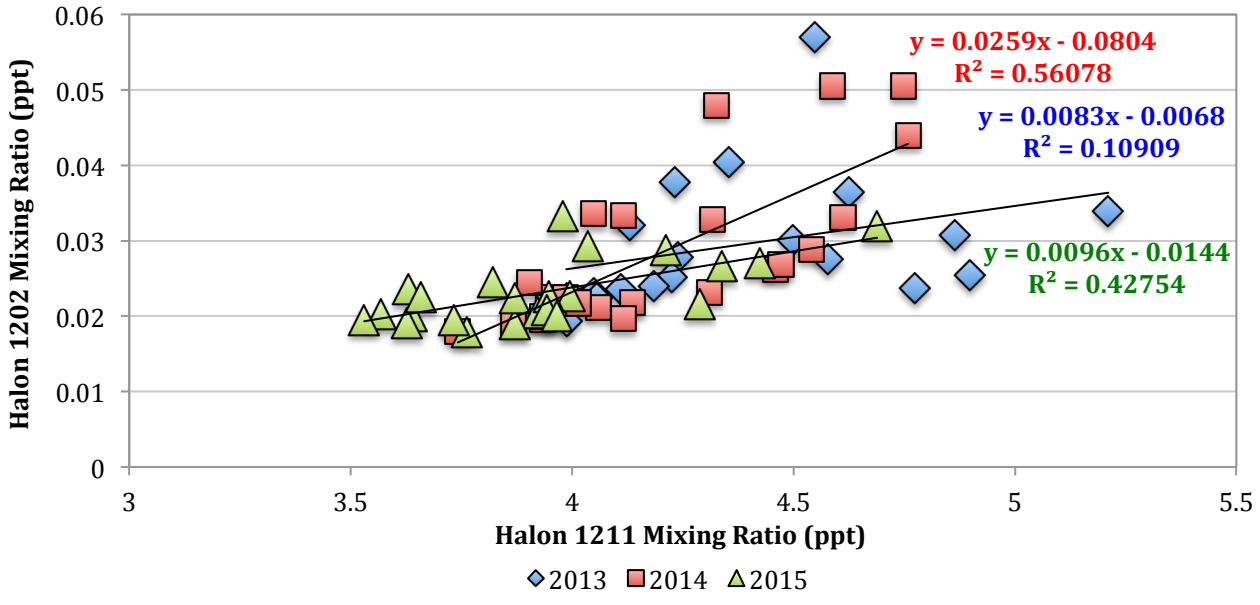

Figure 4.61: Correlation between Halon 1211 and Halon 1202 for the three Taiwan campaigns. Data from 2013 is represtented in blue, 2014 in red and 2015 in green.

However, for 2014 and 2015, the correlation coefficients between halon 1211 and halon 1202 increased to 0.75 and 0.65 respectively. Although not as high as correlations of some other species seen during these campaigns, this still implies some co-emission or similar co-location of sources. This could indicate that the previously posited suggestions of a continued halon 1211 production source, bank contamination or US military sources are more plausible for these campaigns. Comparison of the slopes for the best-fit lines added to Figure 4.61 were found to be similar for the 2013 and 2015 campaigns (0.010 and 0.008 respectively). However, the slope of the 2014 campaign is notably different at 0.026. This suggests that the different sampling sites saw different relationships between these species indicating that some different sources may have been sampled. As the 2014 campaign was impacted by more local sources for other species, this may also be true of these halons and result in the differing relationships described above. In terms of local halon-1202 sources, there is no US military presence in Taiwan but US military equipment is sold to Taiwan (Woods, D.L. ed., 2015), so this may still be a potential source. For all three campaigns, back trajectory analysis may indicate a potential area for a continued production source. However, conclusions in regards to bank contamination are unable to be confirmed until samples of these have been analysed to assess whether there is any halon 1202 present.

Comparison of NAME back trajectories on days where concentrations of both compounds spiked highest above background can be found in Table 4.11. For 2013, only two days saw notable enhancement in both compounds and both of these have influence from Korean emissions. If only the halon 1202 spikes are considered, air masses from Korea still impact the majority of these samples (see Table 4.12). This, as suggested before, may be explained by the large US military presence in South Korea. Days with trajectories also suggesting influence from Chinese emissions tended to be higher than those with just Korean influence. These were also days that saw typical katabatic winds and so could pick up local emissions before reaching the site. Given the known sources of halon 1202, and with the uncertainty of its presence in -1211 banks, sources from the relatively residential area near to the sampling site seem unlikely. Thus, while there are apparent emissions of halon 1202 being transported from Korea, there also may be transport from China and both may be sources unrelated to halon 1211.

Table 4.11: Mixing ratio and wind data for pollution events occurring during the three Taiwanese campaigns for Halon 1211 and Halon 1202

Campaign	Date	Mixing Ratio (ppt)		Winds	
		Halon 1211	Halon 1202	NAME Trajectory	Local
2013	21/03/13	4.6	0.06	China/Korea	ENE
	22/03/13	4.6	0.04	Korea/Pacific	NNW
2014	12/03/14	4.6	0.05	Taiwan/China/Korea	WSW
	17/03/14	4.8	0.04	Taiwan	WSW
	28/03/14	4.8	0.05	China/Japan/Pacific	SSE
2015	23/03/15	4.2	0.03	China	ENE
	27/03/15	4.7	0.320	Korea/Japan	NNE
	24/04/15	4.4	0.03	Korea/Japan	SSE

Table 4.12: Mixing ratios and wind data for pollution events occurring during the 2013 Taiwan campaign for Halon 1202

Date	Halon 1202 Mixing Ratio (ppt)	Winds NAME Trajectory	Local
12/03/13	0.03	Korea	SSW
14/03/13	0.04	China/Korea	ENE
21/03/13	0.06	China/Korea	ENE
22/03/13	0.04	Korea/Pacific	NNW
03/04/13	0.04	China	ENE

For 2014, NAME trajectories suggest Taiwanese influence on two out of the three days considered. Local winds are also coming from the southwest on these days, which is inland of the sampling site and in the direction of industrial areas. However, the magnitude of these spikes is very similar to others in this campaign, which would not be typical of relatively local sources since little dilution during transport would have occurred. So whilst these results could indicate potential local sources of halon 1211 and halon 1202, this would require further sampling and campaigns.

In 2015, two out of the three enhanced samples considered had suggested influence from Korean or Japanese emissions. Since Japan is much further into the Montreal Protocol phase out schedule due to its status as a developed country, it seems unlikely that this would be an area with a continued production source. Korea did have a potential source of halon 1202 in 2013 but not halon 1211. It also seems unlikely that a production source of -1211 would have started in the time between campaigns suggesting perhaps this source is bank related. The other enhanced sample from this campaign was indicted to originate from China along with the final enhanced sample from the 2014 campaign, again suggested possible sources in this area as well. Clearly, further campaigns would be required to establish both the nature and source location of the emissions sampled in these years.

One other aspect that is well-defined in Figure 4.60, particularly for halon 1211, is that both species do have decreasing median mixing ratios, as would be expected since the phase out. These decreased from 4.2 ppt to 3.9 ppt for halon 1211 and from 0.03 ppt to 0.02 ppt for halon 1202. The magnitude of pollution events appears to have decreased slightly as well for halon 1202, with a range of 0.015 ppt observed in 2015 compared to a range of 0.021 ppt in 2013. Both these features would be indicative of reduced emissions but may also be due to normal inter-annual variation.

4.11.3 Summary and Further Analysis

Whilst the main source of halon 1202 may have been from halon 1211 production, detection of continued emissions after the Montreal Protocol phase out suggested the presence of other sources (Newland et al. 2013) but little corresponding information is available. The 2013 Taiwan campaign saw potential evidence of these other sources, as there was a lack of correlation between species in samples with notable halon 1202 enhancement. Back trajectory analysis suggested Korea as the main possible influence for the corresponding air masses, likely due to US military sources. These would be unlikely to also be sources of halon 1211 and so explains the lack of correlation seen. Highest correlations with halon 1202 were found with DCM (0.88) and PCE (0.91) for this campaign, which have extensive Chinese sources. However, specific sources or applications that would result in this relationship between halon 1202 and these species are currently unclear.

The 2014 and 2015 campaigns on the other hand saw relatively good correlation between halon 1211 and halon 1202 during both campaigns. Back trajectories and local winds in 2014 implied there were potential Taiwanese sources, potentially from US-sold military equipment. Korea was indicated again in 2015 and best-fit slopes for the data reinforced this as distinct similarities with 2013 were seen. China also was a potential influence during both campaigns. However, emissions for both species appear to be decreasing as detected atmospheric concentrations have lessened each year along with background mixing ratios.

Further campaigns are needed to consider potential sources of halon 1202 including the testing of halon 1211 banks to establish whether it is a contaminant. A more in depth analysis of likely source regions is also necessary as no clear indications other than US military presence in Korea were found through these campaigns. More regular monitoring of halon 1202 concentrations simultaneously with halon 1211 would be advantageous.

4.12 Case Study 3: Short Chain Perfluorocarbons and SF_6 in Taiwan

4.12.1 Introduction

The fully fluorinated PFCs are a range of very stable compounds whose inert, non-flammable and non-toxic properties make them particularly suited to a range of applications including semiconductor manufacture, dry etching and electronics cleaning (Tsai, 2002) as well as being a by-product of the aluminium industry (Carpenter and Reimann, 2014). C_2F_6, C_3F_8 and c-C_4F_8 (see Figure 4.62a-c) are all defined here as short chain PFCs and are all anthropogenic in origin. Whilst their lack of chlorine or bromine atoms means they do not contribute to ozone depletion, they are strong absorbers of infrared radiation and so impact global warming. Emissions may be relatively small when compared to other anthropogenic global warming sources but PFCs have exceptionally long atmospheric lifetimes and GWPs so their impact is very long lived (Tsai, 2002).

Similarly, SF_6 (Figure 4.62d) is also a fully fluorinated compound, used in electronic switchgear (Carpenter and Reimann, 2014) and in high voltage smelting (Bernstein et al. 2007). It too is anthropogenic in origin, has a long atmospheric lifetime and a high global warming potential. As such, the PFCs and SF_6 both fall under the F-Gases class of compound and control measures were implemented under the Kyoto protocol. However, atmospheric concentrations for all these compounds are increasing (Carpenter and Reimann, 2014).

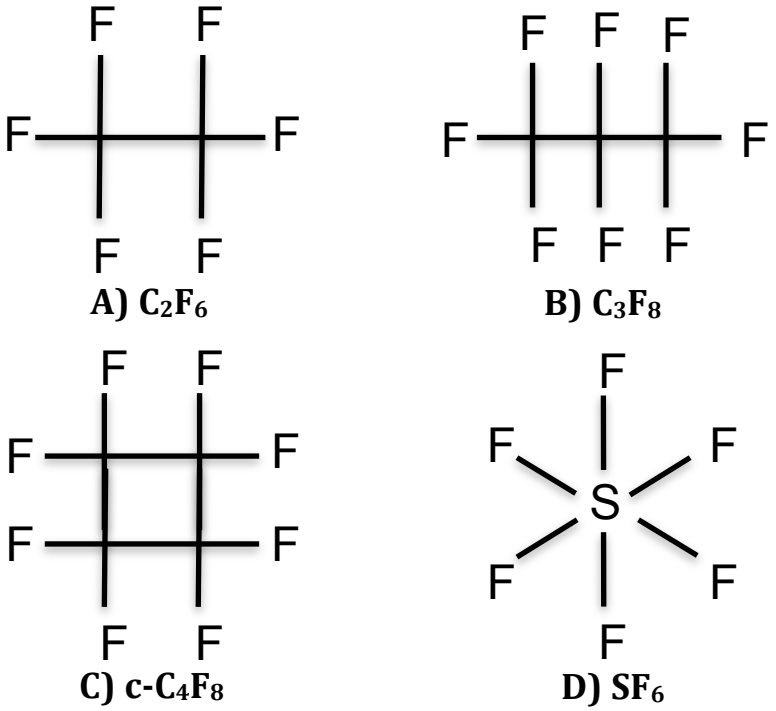

Figure 4.12: Chemical structures of A) C_2F_6, B) C_3F_8, C) c-C_4F_8 and D) SF_6.

The East Asian region has a large range of PFC and SF_6 utilising industries, spread across the different countries. Saito et al. (2014) found China to be the prevalent emitter of PFCs in the region, being the largest aluminium producer in the world as well as having a rapidly growing semiconductor industry (Saito et al. 2010). Taiwan, however, is a known hub for the electronics and semiconductor industry and Taiwanese emissions are likely to reflect this with their potentially high concentrations of PFCs and SF_6.

In this case study the concentrations, correlations and back trajectories between the previously mentioned short chain PFCs and SF_6 during the 2014 campaign will be compared and relationships discussed. This campaign was chosen as local wind data suggested several days were potentially impacted by Taiwanese emissions. An overview of the 2013 and 2015 campaigns for these species, as well as comparisons of all three years in relation to the global trends, can be found in section 4.9.3.2.2.

4.12.2 Results

In Figure 4.63a-d, side-by side time series for the three short chain PFCs and SF_6 during the 2014 campaign can be seen. All these species saw enhanced and near background concentrations except for c-C_4F_8 which was consistently above background. All the background abundances in Figure 4.63, aside from SF_6, are extrapolated from literature (Laube et al. 2012) and reflect the continued growth of mixing ratios at the previously reported rate. The consistent enhancement seen for c-C_4F_8 may indicate that the growth rate has changed since publication but a wider investigation would be necessary to confirm this is the case.

What is most noticeable between these graphs is the similarities between spikes in concentration seen on the 12th, 17th, 25th and 26th for all four compounds. To compare the relationships between them, correlations were calculated and these can be found in Table 4.13. The time series' for C_3F_8, c-C_4F_8 and SF_6 were also plotted against that of C_2F_6 (Figure 4.64a).

Table 4.13: Comparison of the correlation coefficients and R^2 values between the short chain PFCs and SF_6 during the 2014 Taiwan Campaign

Compound	Pearson Correlation Coefficient				R^2 Value with C_2F_6
	C_2F_6	C_3F_8	cC_4F_8	SF_6	
C_2F_6		0.993	0.988	0.819	
C_3F_8	0.993		0.969	0.824	0.985
cC_4F_8	0.988	0.969		0.802	0.976
SF_6	0.819	0.824	0.802		0.706

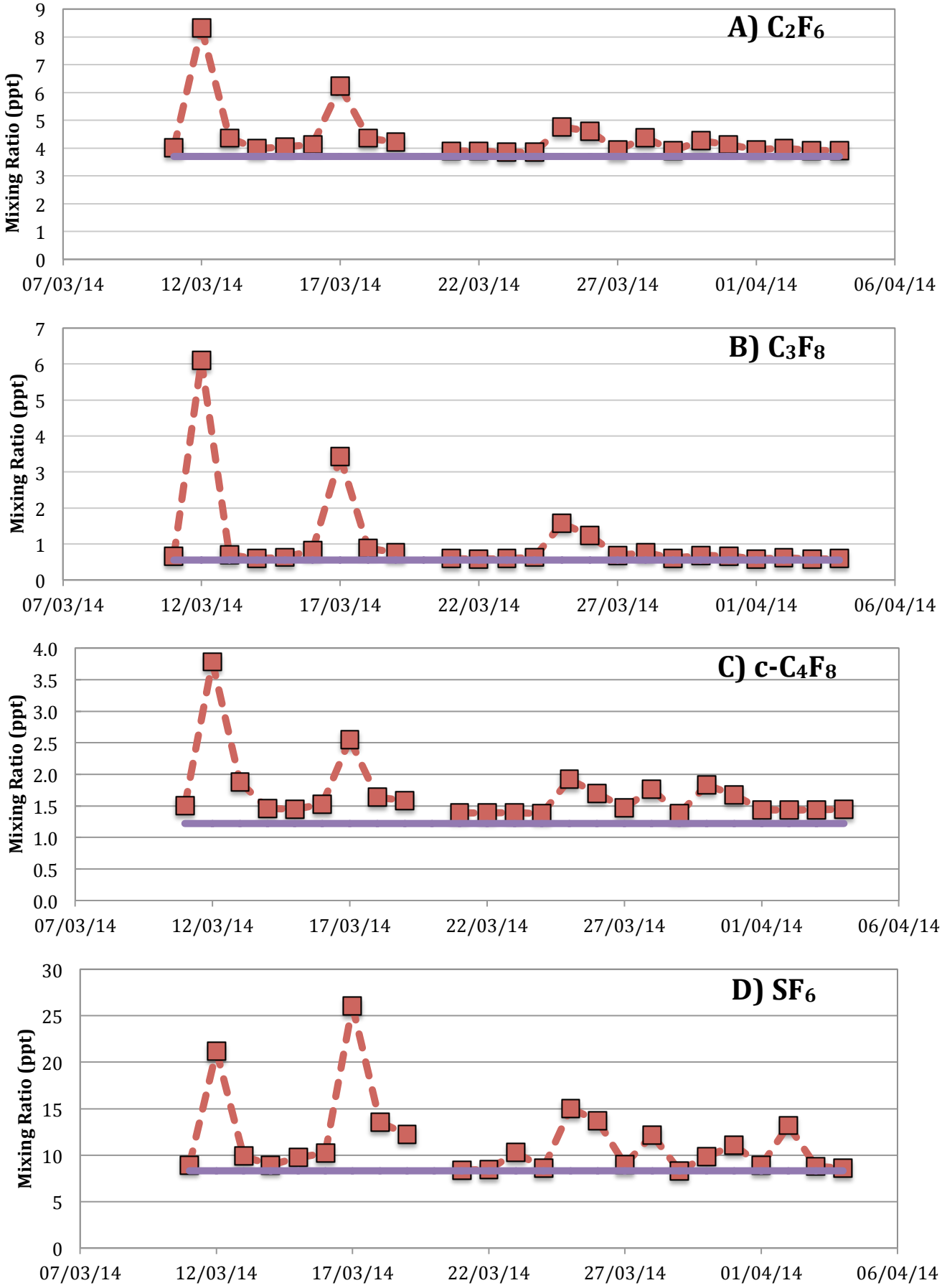

Figure 4.63: Time series of the 2014 Taiwain campaigns for A) C_2F_6, B) C_3F_8, C) c-C_4F_8 and D) SF_6. Background abundances are shown in purple.

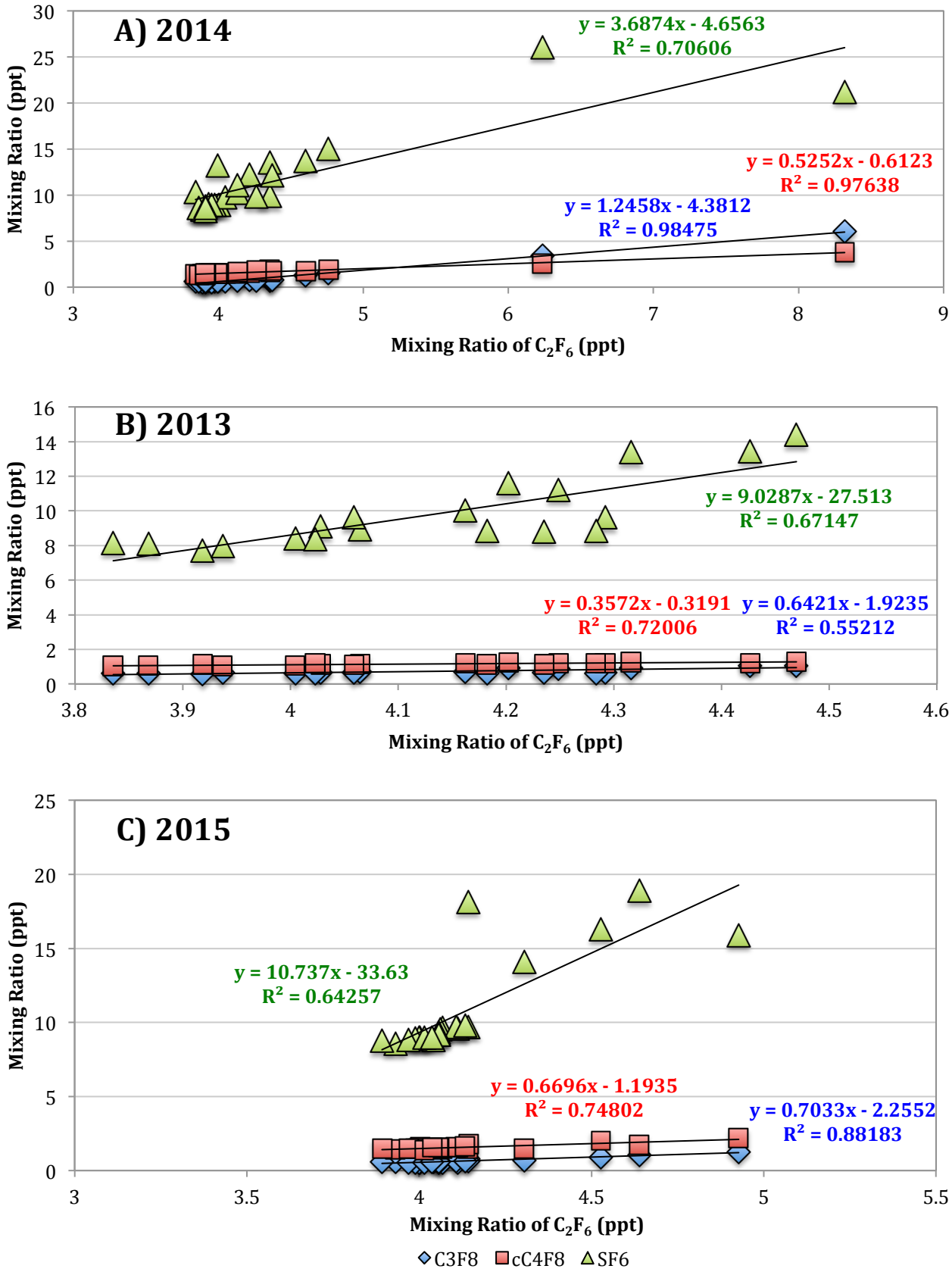

Figure 4.64: Correlation of the other short-chain PFCs with C_2F_6 from the Taiwan campaigns during A) 2014, B) 2013 and C) 2015. The most correlation between species was seen in 2014 driven by the larger range of C_2F_6 mixing ratios due to influence from local emissions.

Between all the short chain PFCs, correlation coefficients were seen consistently over 0.95, clearly indicating co-emission of these species. However, these correlations are likely to have been influenced by the corresponding spikes in abundance. As such those four dates were removed and the correlation coefficients recalculated (see Table 4.14). This shows that the short chain PFCs no longer exhibit coefficients over 0.95 and so indicate co-emission of species, however correlation between C_2F_6 with C_3F_8 (0.79) and c-C_4F_8 (0.91) is still good and so suggests potential co-location. The coefficients between C_3F_8 and c-C_4F_8 on the other hand is only 0.57 and so could imply their co-location with C_2F_6 may be more widely spread.

Table 4.14: Comparison of the correlation coefficients and R^2 values between the short chain PFCs and SF_6 during the 2014 Taiwan Campaign after the removal of locally influenced samples

Compound	Pearson Correlation Coefficient				R^2 Value with C_2F_6
	C_2F_6	C_3F_8	cC_4F_8	SF_6	
C_2F_6		0.793	0.910	0.658	
C_3F_8	0.793		0.578	0.679	0.629
cC_4F_8	0.910	0.578		0.444	0.829
SF_6	0.658	0.679	0.444		0.433

In Table 4.13, correlation with SF_6 was ~0.8 with the PFC compounds suggesting that whilst there is likely co-location of sources, there also may be some separate sources. When compared with Table 4.14, after the removal of significant spikes, this reduced to correlation coefficients of 0.66 and 0.68 with C_2F_6 and C_3F_8 respectively. Correlation with c-C_4F_8 decreased further to 0.44. This suggest, whilst there is some correlation, there is no clear consistent co-location of sources with SF_6.

Overall, this appears to suggest that the short chain PFCs and SF_6 are all likely co-emitted on the days where meteorological data indicated local sources during 2014 but for the rest of the campaign there is only co-location of some short chain PFCs and not SF_6.

The impact of other non-co-located sources of SF_6 is visible in the difference between the time series in Figure 4.63. For the short chain PFCs, on the 17th March, a spike in concentration was seen but this concentration was lower than that of the spike seen previously on the 12th. For SF_6 the opposite is true. There is also notable enhancement on the 2nd April, similar in magnitude to that seen on the 26th March however there is only minimal enhancement for the short chain PFCs in this sample. This appears to confirm that, whilst SF_6 does have common sources with PFC species due to their overlapping applications and detected correlations, there are also other emissions bases that were sampled during this campaign.

The slopes of the short chain PFCs when plotted against C_2F_6 for the 2014 campaign (Figure 4.64a) were compared with those for the 2013 (Figure 4.64b) and 2015 (Figure 4.64c) campaigns to assess whether different sources may have been sampled. Whilst a mixture of sources cannot be ruled out for any of the campaigns, distinct differences in these slopes can indicate at least one different source. Given that proximity of the potential local sources identified during the 2014 campaign, differences were expected.

For C_3F_8, slopes of 0.64 and 0.70 were found in 2013 and 2015 but a slope of 1.25 was seen in 2014. Similarly, for SF_6, the 2013 and 2015 campaigns saw slopes of 9.03 and 10.74 but the 2014 data was found to have a slope of 3.69. The variations between the 2013 and 2015 are not unexpected as the back trajectories of the sampled air masses differed between campaigns and there is active effort to reduce PFC emissions, which would ultimately affect the sources observed. However, the significant differences seen in 2014 for both these species suggests that at least one different source is being measured and, as the effect would likely be more distinct with proximity, this is potentially relatively local to the sampling site. For c-C_4F_8, slopes were found to be 0.36 in 2013, 0.53 in 2014 and 0.67 in 2015, which indicates some differences in sources throughout the campaigns. However, there is no clear suggestion of a different and local source in 2014 but it also does not rule out the presence of one, particularly given the previously discussed correlation observed and the similarities in time series with the other short chain PFCs.

As before, the 4 days which indicate significant local influence were removed from the 2014 data set and the R^2 values with C_2F_6 were recalculated. C_3F_8 decreased significantly to 0.38 whereas c-C_4F_8 and SF_6 both had increased gradients of 0.79 and 6.08 respectively. Again, given the differences in sampling sites and so back trajectories, this variation in slopes is not unexpected. It also suggests that the local source is not the only different source being sampled in 2014.

When comparing the NAME back trajectories for the four days that saw distinct enhancement in all these compounds (see Table 4.15), it is apparent that Taiwanese emissions may have impacted the sampling site on these days. This is further corroborated when the data for the local winds on these days is considered as this indicates three out of the four experienced winds from the WSW. Taiwan is known for its large electronics and semiconductor industries, which would utilise PFCs and SF_6, and the majority of these sites can be found along the west coast of the island. Figure 4.65 shows a map of Taiwan from 2013, indicating the locations of industrial parks, and this shows around 10 different parks located to the southwest of the sampling site on the northern tip. As such, emissions from any number of these industrial areas could have been transported and sampled on these days.

Table 4.15: Mixing ratios and wind data for pollution events of the short chain PFCs during the 2014 Taiwan campaign

Date	Mixing Ratio (ppt)				Winds	
	C_2F_6	C_3F_8	cC_4F_8	SF_6	NAME Trajectory	Local
12/03/14	8.32	6.1	3.8	21.2	Taiwan/China/Korea	WSW
17/03/14	6.23	3.4	2.6	26.0	Taiwan	WSW
25/03/14	4.76	1.6	1.9	15.1	Taiwan/Japan	ESE
26/03/14	4.6	1.2	1.7	13.7	Taiwan/China/Japan	WSW

The magnitudes of the mixing ratios detected, particularly on the 12th and 17th, do also suggest a lack of dilution during transport thus indicating more local sources.

For the 25th March as well as the 2nd April, when SF_6 was found to be enhanced, local winds were detected from the ESE and Figure 4.65 does show two industrial parks located in this region. Whilst NAME trajectories for the 2nd April do not indicate Taiwanese impact on this day, the local wind data does suggest emissions may still have been transported from this area. This could indicate that one of these parks contains a source of SF_6 that does not co-emit short chains PFCs or does so at a distinctly different ratio to the other. The peak on the 25th March is seen by all four compounds and so implies that there likely is a PFC source in this area.

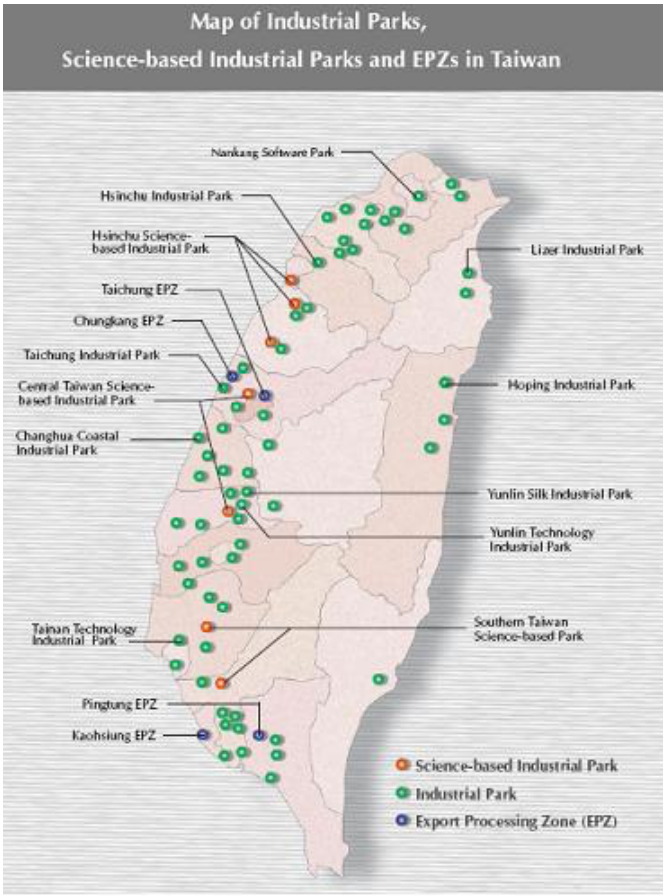

Figure 4.65: Map of Industrial Park locations in Taiwan from 2013 (Nossent, K. 2013)

Several other days during this campaign also saw ESE local winds but not the enhancements. This may be because air masses did not travel over the industrial parks in this area, considering there are notably less to the west, or that trajectories suggested by NAME were coming from a different source and these air masses were more predominantly sampled. While efforts were made to collect local wind speed and direction at a similar time sampling, the system in place took hourly measurements of each and so the data has been time averaged to better reflect sampling conditions. As such, there may be some associated differences that could impact the conclusions drawn here. A more focussed study on PFC emissions in Taiwan could result in a clearer explanation of some of the occurrences seen during this campaign.

4.12.3 Summary and Further Analysis

For the short chain PFCs; C_2F_6, C_3F_8 and c-C_4F_8, common applications include use in the manufacture of electronics and semiconductors, an area where the similarly fully fluorinated SF_6 is also utilised. Whilst China has been found to be the largest emitter of these compounds (Saito et al. 2010), Taiwan also has extensive industry in these fields.

In 2014, a number of days were sampled were both NAME back trajectories and local wind data suggested that emissions from Taiwanese sources would impact the concentrations of compounds detected. It was on these days, the 12th, 17th, 25th and 26th March, high mixing ratios of the short chain PFC were found, all of which correlated extremely well with one another indicating they likely came from the same source. Increased mixing ratios were also detected for SF_6 on these days although correlations were slightly lower with the PFCs due to indications of separate sources as well as co-located ones.

Comparison between slopes from when C_2F_6 was plotted against the other short chain PFCs for all three campaigns found distinct differences for C_3F_8 and SF_6 suggesting at least one different and potentially local source was sampled in 2014 comparative to the other years. Variation was seen for c-C_4F_8 as well but differences were less significant between campaigns and so conclusions are less clear for this species.

Comparison with reported locations of Taiwanese industrial parks suggested potential locations for the emissions sampled on these days however further campaigns would be required to both confirm and identify individual sources, both for the short chains PFCs and SF_6. As only one campaign detected the large pollution events associated with these local emissions, further campaigns at the Northern site would enable more comparison between observed abundances and relationships of short and long-range emissions.

4.13 Key Findings

Of the results presented here, the key findings of the three Taiwanese sampling campaigns are:

- Taiwan is an ideal location to monitor continental outflow in East Asia. Modelled NAME backwards trajectories indicate air masses from China, Korea, Japan and the Pacific ocean were all sampled during the campaigns and an extensive range of halocarbon species, both long and short-lived were measurable.
- Local emissions from Taiwanese industry were seen to impact measurements and local meteorological information was utilised to clearly identify this. Assessment of local impact would be improved through regular boundary layer analysis throughout the sampling campaign.
- The majority of halocarbon species saw enhancement above background mixing ratios in all three campaigns. This was expected given the polluted air masses being sampled however the lack of available regional background measurements limited the significance of these results.
- CFC-113 and its isomer CFC-113a were found to have strong correlation throughout the three campaigns suggesting co-location of sources. This has not been previously reported and comparison with back trajectories suggests sources may be found in China. HCFC-133a was also found to be have good correlation with both species although its sources were less clear, potentially due to more widespread use.
- The isomers CFC-114 and CFC-114a were not found to correlate when measured during the 2015 campaign. This was unexpected as CFC-114a as co-emission has previously been assumed and these results suggest potential sources of -114a in China and -114 in Korea.
- Correlations between halon 1211 and halon 1202 were assessed as previous studies had suggested potentially separate sources. Results from the Taiwan campaigns were variable however Korea was identified as an apparent source of -1202, potentially from the US military present based there.
- Good correlation was identified between the short chain PFC species and SF_6. Local sources that indicate co-emission were identified in the 2014 campaign at the northern end of the island. If this site is utilised for future campaigns, the potential impact of this nearby industry needs to be considered.
- Cyclic C_5F_{10} was measured for the first time in 2015 however little is known about potential sources. No clear correlations were identified.
- Isomers n-C_6F_{14} and iso-C_6F_{14} were measured separately during the 2015 campaign and their correlation suggests co-emission indicating sources of C_6F_{14} are likely mixtures of both species.
- The development of a continuous monitoring station would be beneficial to continue monitoring halocarbon species in the region to fully establish long-term trend data, seasonal variability and identify potential source locations for compounds of interest.

Chapter 5: Long-range transport of Ozone Depleting Substances to Bachok, Malaysia

5.1 Bachok and Malaysia

Southeast Asia is a sub-region of the Asian continent that consists of those countries found north of Australia, south of China, between India and New Guinea. The area is split into two further regions known as Mainland Southeast Asia (or Indochina) and Maritime Southeast Asia (or the Malay Archipelago). Indochina includes Cambodia, Thailand, Vietnam and Peninsular Malaysia whereas Maritime Southeast Asia includes Indonesia, the Philippines, Singapore and East Malaysia. With the majority of Southeast Asia falling within tropical and subtropical latitudes, the climate is generally hot and humid all year round with regular monsoon weather systems. The South China Sea (SCS) is the main body of water in the area and this borders the East Asian region at its most northerly part.

Similarly to East Asia, industrialisation has increased rapidly in recent decades with agricultural processing, textiles and electronics manufacture dominating employment. Mining for tin, nickel and copper have also been major industries in this region (Frederick, 2015). As was discussed in the previous chapter, the use of halocarbons in industry is widespread and there is limited knowledge on their emissions and transport across Asia. To this end, further and regular monitoring is necessary and so new sites, such as the one recently built in Bachok, Malaysia, are of great importance to the global network.

Situated on the east coast of peninsular Malaysia, in the Kelantan province (6.009°N, 102.425°E, see Figure 5.1), the Bachok Marine Research Station was recently constructed as part of the Institute of Ocean and Earth Sciences (IOES) at the University of Malaya (UM). Using a NERC International Opportunities Fund award, the Universities of Cambridge and East Anglia, along with the National Centre for Atmospheric Science, worked to assist the development of measurement capabilities at the site. The ultimate goal for Bachok is to join the WMO GAW Programme and become an integral part of the global monitoring network. Currently the station is able to measure a range of parameters including methane, CO and NO_x as well as O_3, SO_2 and VOCs, with capabilities still being adjusted and improved.

An atmospheric observation tower was built at the station (see Figure 5.2) with the specific purpose of being used in the study of long-range transport of pollution (along with coastal meteorology and air sea exchange). It is the extent of this transport that is of particular interest in assessing halocarbon mixing ratios and sources.

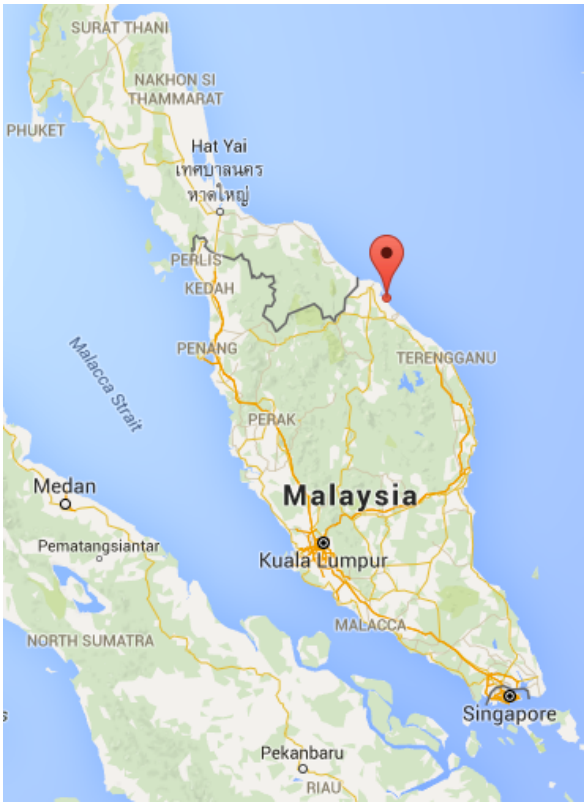

Figure 5.1: Map showing the location of the Bachok sampling site on the east coast of Malaysia.

Figure 5.2: The atmospheric observation tower, purpose built for studying the long-range transportation of pollution to Bachok.

In 2014, a 'demonstration activity' of joint measurements was carried out at the site for a three-week period from 20th January to 9th February (NCAS, 2015) and during this time a number of flask samples were collected from the tower to be analysed for halocarbon content. As was seen with Taiwan in the previous chapter, this time of year sees winter monsoon conditions, where strong winds predominantly travel across the region from the northeast. and can result in long range transport of continental outflows in East Asia. Although Taiwan is around 3000km away from Bachok, distinct weather patterns known as cold surges have the potential to travel this distance and bring with them polluted air masses. It is hoped that regular campaigns at the Bachok site will enable monitoring of this transport during cold surges and increase understanding as to the potential impacts of any increased pollution it causes. Further information about the conditions that produce a cold surge and importance of investigating them can be found in the section below.

5.2 Cold Surges

During the winter months, generally November to March, the East Asian region and the South China Sea (SCS) experience numerous cold surge weather events as part of the East Asian Winter Monsoon (EAWM). This seasonal phenomenon is influenced by the annual formation of a large anticyclone over Siberia, causing strong north-easterly winds that may travel as far south as Singapore and Malaysia (Ashfold et al. 2015).

A cold surge is a sub-system of the winter monsoon that occurs approximately 10 times each winter (Chen et al. 2004). They cause abrupt drops in temperature that can have serious socio-economic impacts on affected East Asian countries, bringing heavy snowfall in some regions and inducing strong convective activity over the SCS (Park et al. 2008). The origin of these cold surges is a semi-permanent, cold core, high-pressure system known as the Siberian High (see Figure 5.3) (Park et al. 2011). It is the amplification and expansion of this system due to upper tropospheric disturbances (Park et al. 2008) that results in extremely cold air from north of the Tibetan plateau abruptly migrating southwards towards East Asia (Jeong et al. 2006). A well-known feature of these disturbances is the shortwave train that occurs over Lake Baikal in south-eastern Siberia. This is where a short-wave trough ahead of a ridge aloft over the lake deepens due to the establishment of a north-westerly flow and propagation across northeast Asia. The upper-troposphere ridge-trough structure formed intensifies the surface anticyclone and causes southward surface cold air to break out from the eastern Siberian high (Chen et al. 2002). This results in strong north-easterly winds in the lower troposphere (Park et al. 2008) and sharply increases surface pressure (Yokoi and Matsumoto, 2008) which strengthens cold advection in the Siberian High, along the eastern edge, resulting in lower wind chill temperatures (Park et al. 2011b). These conditions lead to an acute drop in temperature over several days but extreme cold conditions have, in recent years, lasted as long as a month (Park et al. 2008).

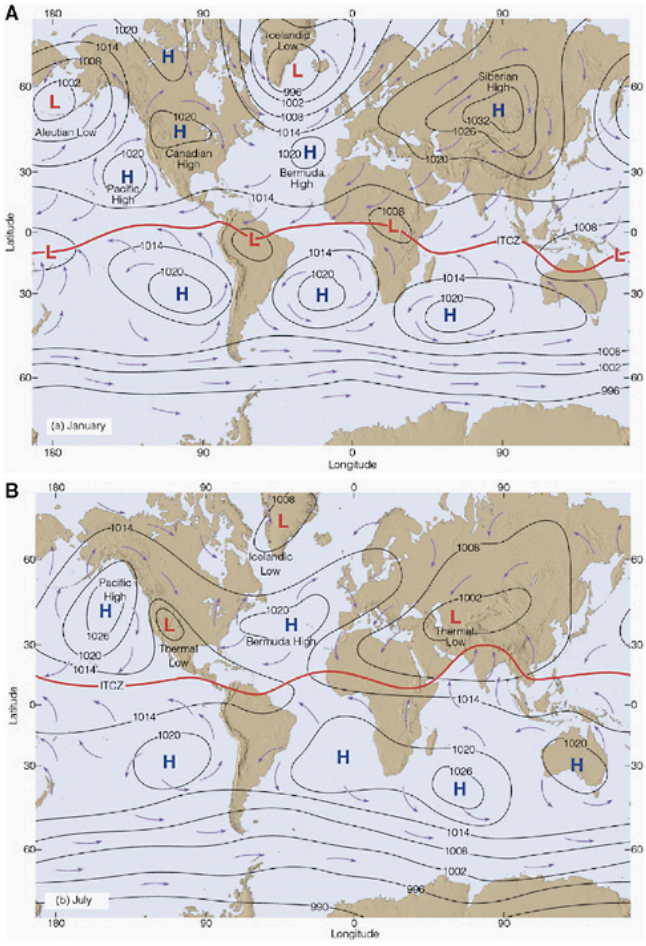

Figure 5.3: Charts showing the differences between A) Winter (January) and B) Summer (July) global mean sea-level pressure and winds. The red line near the equator marks the Intertropical Convergence Zone (ITCZ). The Siberian High that causes the cold surge conditions discussed in this chapter can be seen on Chart A (Ahrens, 2008).

Studies have found that there are a variety of upper-level circulations that influence the formation of cold surges (Jeong et al. 2006, Takaya and Nakamura, 2005, Takaya and Nakamura 2005b) and that interannual differences in these circulations during the EAWM can have considerable impact on the severity and regularity of cold surge occurrences (Park et al. 2008). Global increases in surface temperatures have reduced the severity of cold days (daily average temperatures) since the 1970s, however since cold surges are associated with daily temperature variability, a separate property, a similar decrease in frequency or severity due to warming appears unlikely. Walsh et al. (2001) suggested European and North American historical observations did not indicate a long-term trend towards fewer cold surge occurrences due to global warming, further studies are still required to assess any potential impact (Park et al. 2011b).

Investigations into the variability and frequency of cold surges are particularly necessary as a further consequence of these events is the transport of air masses from regions such as mainland China, by the strengthened north-easterly winds towards the tropics and across areas of increased convection (Ashfold et al, 2015). With the rapid industrialisation of China and other countries in the region, these air masses are likely to contain relatively high levels of pollution including halocarbon species that can deplete stratospheric ozone and contribute to global warming. Recent theoretical investigations into this transport mechanism from Ashfold et al. (2015) suggested that in only 4 days, significant amounts of pollution from East Asia (>35°N) reached the tropics.

Trajectory calculations from the same study indicated that there could be subsequent transport of the polluted air masses out of the boundary layer and into the tropical upper troposphere (>200hPa). Increased regional convection from cold surge events can enhance this process and so transport may occur in less than 10 days. From the upper tropical troposphere and tropical tropopause layer (TTL), pollutants may enter the lower stratosphere. This means that any ODS, particularly those very short lived substances (VSLS) that would not normally reach the stratosphere or would but in very small amounts, may start to be photolysed and begin the catalytic cycles that result in the breakdown of ozone. With cold surge events lasting for several days and occurring regularly throughout the winter months (Chen et al. 2004), the impact of ODS transport during these periods may be larger than previously anticipated.

Whilst the investigation by Ashfold et al. (2015) was theoretical, Oram et al. (in preparation, 2016) found the first evidence supporting this mechanism for a number of VSLS using samples collected during a ground-based sampling campaign in Bachok, Malaysia. This campaign sampled air both during and after a cold surge event and reported enhanced concentrations during, suggesting the predicted transport of pollutants from East Asia (further indicated by back trajectories calculated using the NAME model) had occurred. Oram et al. (in preparation, 2016) also used data from aircraft flights in the region, as part of the CARABIC project, to confirm rapid vertical transport of these species as well.

5.3 The Research Gap

Whilst identifying the effect of increased regional convection during cold surge events is particularly important in assessing the impact for short-lived species, other ODS will still reach the upper troposphere. As such, investigations considering a wider range of species are necessary to confirm the extent of pollutants from East Asia potentially reaching the stratosphere. A campaign during the winter months that is able to successfully measure a cold surge could would both aid in the understanding and assessment of cold surge impact and set up a precedent for future campaigns to expand on these findings. As well as this, non-cold surge period analysis may help in the wider evaluation of the general atmospheric effect of East and South East Asian emissions as well.

5.4 This Study

In this chapter, results from the ground-based sampling campaign in Bachok, Malaysia, including those VSLS that contributed to the paper by Oram et al. (in preparation, 2016), will be assessed. The concentrations of a large range of ODS will be compared along with NAME back trajectories to evaluate the long-range transport of pollution across the SCS during cold surge events. Equivalent chlorine (ECl – see section 1.12) levels will be calculated for all 31 ODS measured (see Table 5.2) and used to estimate the potential concentrations reaching the upper troposphere. These will then be contrasted with previously published data (Carpenter and Reimann, 2014) although the Bachok estimate include contributions from chloroethane, bromoethane and halothane mixing ratios which are not available from Carpenter and Reimann (2014).Any differences between the published and campaign-based ECl estimates will be quantified in order to assess the possibility of underestimation in ODS influence and this could indicate the need for further control measures. These results from the Bachok campaign can also contribute to knowledge of halocarbon levels in East and South East Asia as well as potentially indicating species or groups that may benefit from further campaigns, given that this was only a case study based on one campaign.

5.5 Sample Collection and Analysis

During the Bachok campaign, 25 samples were collected by the same method as described in the previous chapter (see section 4.6). Only 12 of these were fully analysed (see Table 5.1), as with the Taiwan samples, using both the AutoSpec (the high sensitivity gas chromatography mass spectrometry suite, with a proven detection limit of <1 attomole - see section 2.2.6 for a full description) and Entech (a gas chromatography-electron ionisation mass spectrometer - see section 2.2.5 for a full description) systems due to timing and sample volume constraints. These samples include all those collected during the cold surge event and several other days expected to be more consistent with background conditions. The cold surge occurred between 19th-26th January and was identified by meteorological data that indicate increased wind speeds and decreased surface air temperatures, typical of these events.

Appendix 5.1 contains a full list of the samples collected during the Bachok campaign, with those highlighted being the ones selected for further analysis and discussion in this chapter.

To increase available data sets for the region, these samples were analysed for all of the halocarbon species also measured in the Taiwan campaigns (see previous chapter) however this chapter will only focus on those compounds considered to be ODS. Table 5.2 contains a list of these species and indicates which instrument they were measured with as well as their associated calibration scales. Again, most halocarbons were calibrated to a NOAA scale (see section 2.2.6.4) but some minor species utilised UEA calibrations instead. Other species are currently awaiting full calibration and so have been calculated relative to the standard and us such cannot be fully interpreted. This data will be made available for future work should the associated calibration scales be established.

As in the previous chapter, backwards trajectories were calculated by Matt Ashfold (University of Nottingham) for each of the samples analysed using the UK Meteorological Office Numerical Atmospheric Modelling Environment (NAME v4). For each sample, this Lagrangian dispersion model released batches of 60,000 inert particles from the measurement site. The trajectories were tthen calculated backwards, recording those particles within an altitude of 0-100m every 15 minutes. The trajectories were started throughout a 3-hour period that surrounding the sampling time and were measured for a 12-day period. More details on the specifications for this can be found in section 2.3.

Table 5.1: Times, dates and NAME results of the 12 out of 25 samples fully analysed as part of the Bachok campaign.

Date	Time		NAME Trajectory	
	Local	UTC	Major	Minor
20/01/14	12:05	04:05	China/Taiwan	Korea/Vietnam
20/01/14	16:10	08:10	China/Taiwan	Korea/Vietnam
21/01/14	12:10	04:10	China/Taiwan/ Vietnam/Cambodia	Korea
22/01/14	11:45	03:45	China/Taiwan	Vietnam
23/01/14	11:50	03:50	China/Taiwan/ Vietnam/Cambodia	
24/01/14	17:40	09:40	China/Taiwan	Korea/Japan/ Philippines/Vietnam
25/01/14	12:08	04:08	China/Taiwan	Korea/Japan/ Philippines/Vietnam
26/01/14	12:15	04:15	China/Taiwan/ Vietnam/Cambodia	Korea/Japan/Philippines
27/01/14	17:55	09:55	Taiwan/Philippines	China/Japan/Vietnam
28/01/14	12:25	04:25	Philippines/Japan/Korea	Taiwan
30/01/14	23:59	15:59	Taiwan/Philippines/Korea	China/Japan
02/02/14	12:10	04:10	Taiwan/Philippines	Korea/Japan/Vietnam

Table 5.2: Overview of ozone depleting substances measured during the Bachok campaign, the calibration scales and ions used to establish mixing ratios as well as the instrument used for the analysis.

Compound		Calibration Scale	Instrument		Ions Measured		
Group	**Name**		**Entech**	**AutoSpec**	**1**	**2**	**3**
CFCs	11	NOAA	✓	✓	101	103	
	12	NOAA	✓	✓	101	103	
	13	UEA		✓	85	87	
	113	NOAA	✓	✓	101	103	117
	113a	UEA		✓	103	117	
	114	Estimate	✓	✓	85	87	135
	114a	UEA		✓	85	87	135
	115	UEA	✓	✓	85	87	
Halons	1211	NOAA	✓	✓	85	129	131
	1202	UEA		✓	129	131	
	1301	NOAA	✓	✓	69	129	131
	2402	UEA	✓	✓	129	179	181
HCFCs	22	NOAA	✓		67		
	133a	UEA	✓	✓	118	120	
	141b	NOAA	✓		81	101	103
	142b	NOAA	✓		65		
VSLS-Cl	PCE	NOAA	✓		129	166	
	DCE	UEA		✓	62	64	
	CH_2Cl_2	NOAA	✓	✓	83	84	
	Chloroform	No Scale	✓		83	117	119
	C_2H_5Cl	UEA		✓	64	66	
VSLS-Br	CH_2Br_2	NOAA	✓		174		
	Bromoform	NOAA	✓		173		
	$CHClBr_2$	NOAA	✓		127	129	
	C_2H_5Br	UEA		✓	108	110	
	CH_2ClBr	NOAA		✓	128	130	
Chlorocarbons	CCl_4	NOAA	✓	✓	117	119	
	CH_3CCl_3	NOAA	✓		97	117	
	Halothane	UEA		✓	196	198	
Methyl Halides	CH_3Cl	NOAA	✓	✓	49	50	51
	CH_3Br	NOAA	✓	✓	94	96	

5.6 Results

5.6.1 NAME Analysis

As before, the trajectories were assessed to establish which countries the air mass had passed over, between 0-100m, and so could have potentially contributed emissions. The corresponding trajectories for the collected samples can be found in Appendix 5.2. In the 12 trajectories considered, multiple countries are likely to have added to each of the sampled air masses and Figure 5.4 indicates the approximate suggested regions for each of the different areas considered. Table 5.1 includes a list of these countries separated into major and minor influences:

Major being where the **particle density** in the model **is highest (>10^{-7} g s m^{-3})** and over the **majority (>70%) of the country,**

Minor being where a **significant proportion (50-70%) of the country** is covered by a **relatively high density of particles (10^{-8} – 10^{-7} g s m^{-3}).**

Emissions from countries assessed as being potential major influences for a specific sample are expected to impact the variation and concentration of the halocarbon species detected. Minor influences are also anticipated to have an impact but their contribution is likely to be less substantial.

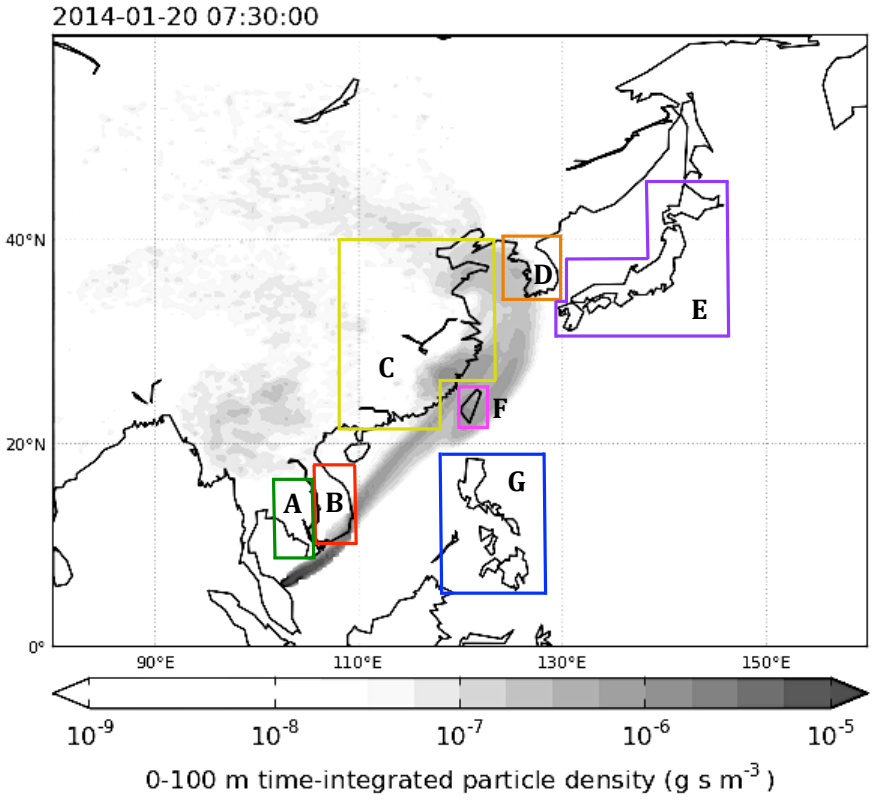

Figure 5.4: Potential source locations from analysis of NAME back-trajectories from the Bachok campaign. Approximate suggested regions are A) Cambodia, B) Vietnam, C) China, D) Korea, E) Japan, F) Taiwan and G) Philippines.

Since the campaign took place during the EAWM, prevailing winds from the northeast were expected and these are apparent from back trajectories throughout the campaign. In terms of major influences, during the 7-day cold surge event at the beginning of the campaign, the trajectories (see Appendix 5.2 A-H) suggest that, before reaching Bachok, air masses travelled over mainland China and Taiwan for all 8 samples. 3 of the 8 trajectories (21st, 23rd and 26th January, Appendix 5.2 C,E and H) also show potential major influences from air mass transport over Vietnam and Cambodia, where further emissions could be picked up.

Those days where Vietnam is not considered a major influence during the cold surge, do have it included as a possible minor influence (see Table 5.1), as indicated by the NAME trajectories. Korea was also assessed as being a minor influence for all but two of the cold surge samples (22nd and 23rd January [Figures 5.5a and b]). These are also days that saw some of the least widespread trajectories (i.e. particle density $>10^{-7}$g s m^2 only for a further distance than other trajectories) of the 7-day period meaning potential influences for these days were clearer to assess. Both saw transport over mainland China however the back-trajectory for the 23rd January (Figure 5.5b) suggests that winds had shifted more northerly and emissions from further inland, away from the south-east coast and Taiwan, may have impacted. This is the only day sampled with this inland China trajectory and so any differences in the species measured in the corresponding sample may be due to this shift. Large areas of Vietnam and Cambodia were also part of the NAME-trajectory, which is likely to have an impact on the halocarbons sampled as well. However, similar coverage of these countries was seen on the 21st January (see Appendix 5.2C) so variations possibly caused by inland China emissions may still be identified on the 23rd January.

Towards the end of the cold surge event, the NAME back trajectories suggest the prevailing winds swung further east and south which can be seen with the inclusion of Japan as a minor influence for the 24th, 25th and 26th January (Appendix 5.2 F, G and H) as well as the Philippines which sees some coverage from the model on these days also. This shift is further apparent after the cold surge event when more EAWM background air would be expected. None of the 5 days measured were assessed as having China as a potentially major influence to the air mass and only 2 of those days (27th and 30th January [Appendix 5.2 I and K]) suggested it could be a minor influence. Countries whose emissions were likely to have the largest impact in this period were the Philippines and Taiwan. Korea was also considered a major influence on the 28th and 30th January (Appendix 5.2 J and K) however without the increased winds present during a cold surge event, the magnitude of any impact from this region may be decreased due to transport time and dilution. Emissions from Japan are likely similarly affected though this was only assessed as being a potentially major influence on the 28th January and a minor influence on the other 4 days. The closer proximity of Vietnam to Bachok makes its impact unlikely to be affected by dilution, however the NAME back-trajectories indicate it is only a possible minor influence and only on 2 of the 5 days (27th and 2nd February [Appendix 5.2 I and L]).

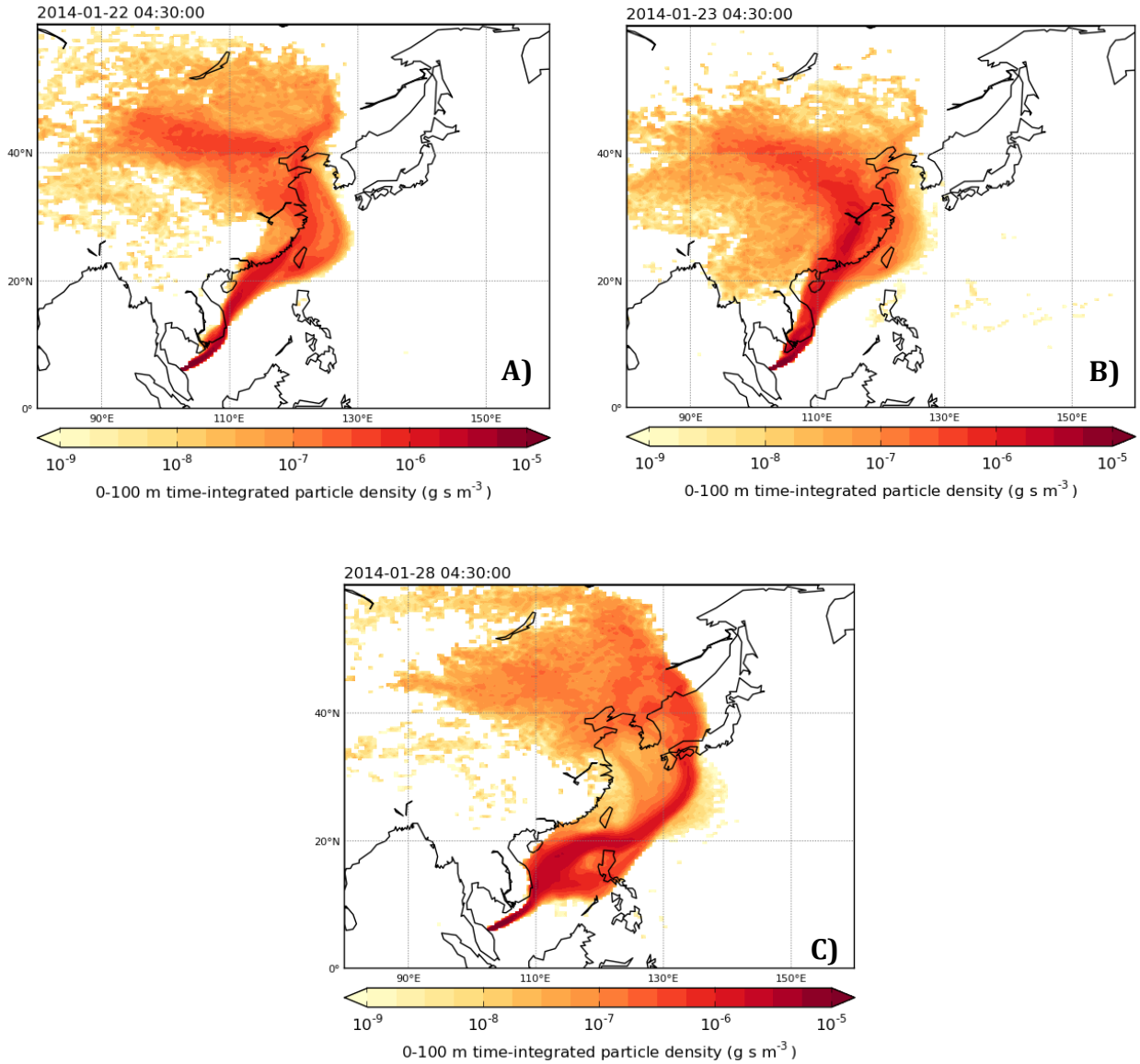

Figure 5.5: Examples of NAME back-trajectories for samples taken during the Bachok campaign on A) 22nd January 2014, B) 23rd January 2014 and C) 28th January 2014. A) and B) were during the identified cold surge period and the difference in trajectory seen in C) reflects that this weather system had ended by the 28th.

Overall, the back-trajectories calculated by the NAME model suggest that whilst there is a prevailing north-easterly wind throughout the campaign, as would be expected during the EAWM, there is a shift further east and south during the latter stages. In the cold surge event mainland China is a potential major influence on the air masses sampled whereas the Philippines appear more influential afterwards. Taiwan is the only region to be consistently part of the analysed trajectories and was only assessed as not being a possible major influence on the 28th January (Figure 5.5c), although it is still considered minor. However, Taiwan is comparatively small and so the impact of these emissions is likely to be less distinct than those of China.

Given the potential differences in sources Vietnam and Cambodia appear to have a potentially more significant impact during the cold surge period but Vietnam in particular, still features after.

5.6.2 Overview of Halocarbon Observations

This section will give an overview of all the 31 ODS measured from the two halves of the Bachok campaign; during the cold surge event and after the cold surge event. These summaries will be organised by compound group and Appendix 5.3 indicates the mean and range mixing ratios (in ppt) for the campaign as a whole as well as specifically for during and after the cold surge. Similarly, Appendix 5.4 utilises this mixing ratio data to give a percentage value of any enhancement above the known background concentrations of a species and the key below the table corresponds to the origin of the background value. Not all the compounds measured currently have representative background data available and so percentage enhancements have only been calculated for 20 species.

As in the previous chapter, the background mixing ratios are primarily taken from NOAA Mauna Loa Observatory in Hawaii (19.536°N, 155.576°W) and when these are not available AGAGE backgrounds are taken from Ragged Point, Barbados (13.165°N, 59.432°W). Both of these are remote stations closest in latitude to Bachok and abundances from January were utilised. Other species use abundances from literature or the Air Archive from Cape Grim, Tasmania (40.683°S, 144.690°E) and are referenced accordingly. Due to the southern hemispheric location of Cape Grim, mixing ratios were selected ~6 months later than the Bachok campaign to reflect the time taken for the gradient to shift between the tropics and the southern hemisphere.

As with the Taiwan campaigns, a limitation of this study was the lack of available background data within the region of analysis. Lack of local stations extrapolation was not feasible and, as previously mentioned, the closest AGAGE stations in Korea and Japan were not forthcoming when contacted for data. As such there was little choice but to use the robust background mixing ratios available from the sites described above, which generally reflect remote northern hemispheric abundances. However, it is hoped that the successful development of the Bachok atmospheric measurement station will lead to a continuous measurement site in the region that may be utilised to better constrain background data for future campaigns.

Also included in Appendix 5.3 is mixing ratio data for carbon monoxide, a species often used as a tracer compound for industrial source regions. CO does have natural sources however such as biomass burning and so calculations using known emissions of CO have been carried out to estimate the mixing ratio proportion associated with industrial sources. It is therefore suggested that the difference between these two values is potentially caused by other, including natural, emissions and as such, will behave differently.

5.6.2.1 Chlorofluorocarbons

During the Cold Surge Event – 20th January 2014 to 26th January 2014

Since these species have been phased out under the Montreal Protocol, mixing ratios were expected to be at close to background levels regardless of the cold surge event due to minimal emissions and their decades long atmospheric lifetimes. Whilst some variation is expected, significant spikes would not be anticipated.

CFC-11 and CFC-12, the two most abundant species in this group, were detected at mixing ratios both above and below background concentrations (235 ppt for CFC-11 and 521 ppt for CFC-12) during the cold surge period (see Figures 5.6a and b). The main variation is characterised by alternating sharp increases and decreases in mixing ratio between the 23rd and 28th January. Whilst the fluctuation in CFC-12 mixing ratios saw only a range 10 ppt (±1%) which is inside the margin of error, a wider range of 20 ppt (±5%) was detected for CFC-11. Although both the highest and lowest data points were during the cold surge, this variation continues for two days after the 26th and does not appear in line with any variations in NAME back-trajectory suggesting it is most likely unrelated to this weather system. CFC-13 (Figure 5.6c) saw variation of around ±5% (3.8-4.1 ppt,), which continues after the 26th very similar to that of CFC-11. However, it was observed to be enhanced above background levels on all days except the 24th January. The use of a southern hemispheric background due to the lack of regular measurement of this species may have contributed to this difference however the background was taken from July 2014 rather than January in order to compensate for the hemispheric gradient. As such, this enhancement may be more reflective of continued small emissions in East Asia, likely from banks.

CFC-113 (Figure 5.7a) was consistently detected at levels between 1 and 4% above background (73 ppt) throughout the cold surge event, which is within the levels of enhancement detected for this compound during the Taiwan campaigns. This similarity could suggest that there may be transport of emissions of this species, potentially from bank release or possibly from the chemical industry as suggested in section 4.10, in East Asia to Bachok. Although the median enhancement is slightly lower than was seen in the Taiwan campaigns (1.9% as opposed to around 2.5%), this is likely explained by dilution during transport. There is a similar pattern of alternating variation between the 23rd and 26th January, as seen with the other CFCs, however this appears less pronounced than was seen for CFC-11 and mixing ratios of CFC-113 overall still seem to increase during the cold surge.

For CFC-113a (Figure 5.7b), the newly detected and only strongly increasing CFC in the atmosphere, a notably different pattern is apparent that corresponds with the cold surge period. Like its isomer CFC-113, CFC-113a was detected at concentrations above background through the cold surge however these ranged from 39-95% enhancement (Appendix 5.4).

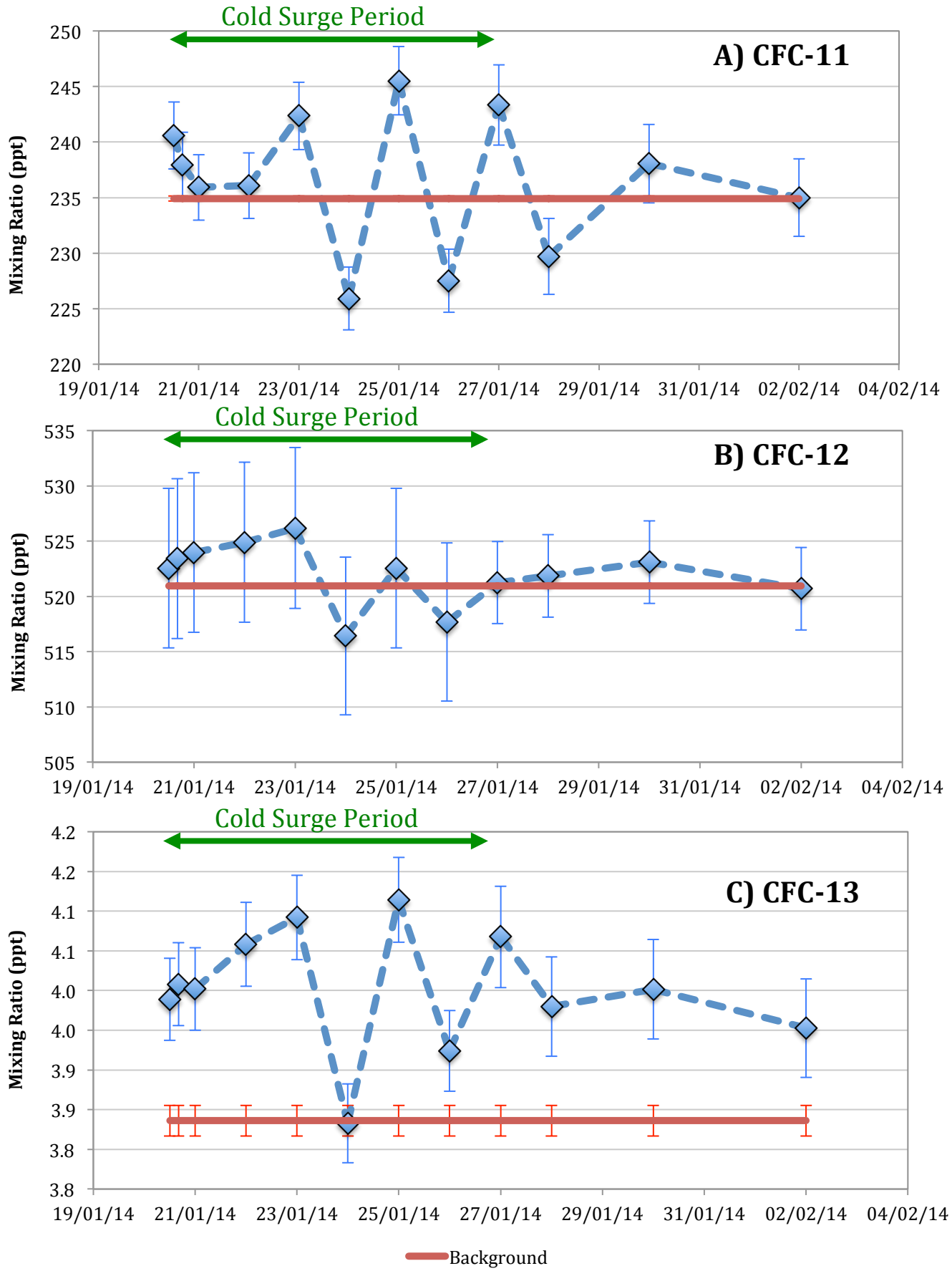

Figure 5.6: Time series of the CFCs, A) CFC-11, B) CFC-12 and C) CFC-13, observed during the Bachok campaign. Background mixing ratios are shown in red and error bars represent total calculated uncertainty.

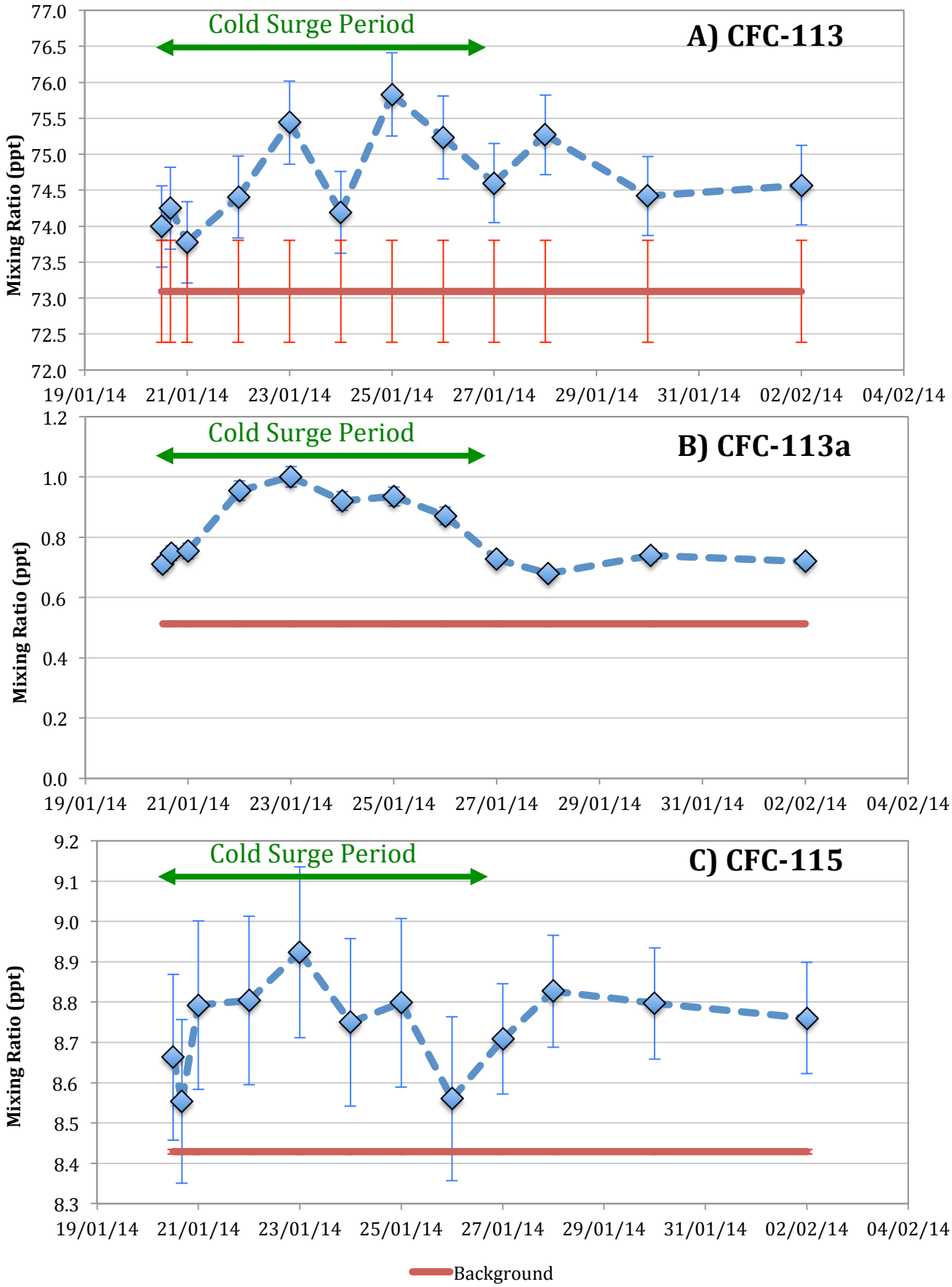

Figure 5.7: Time series of the CFCs, A) CFC-113, B) CFC-113a and C) CFC-115, observed during the Bachok campaign. Background mixing ratios are shown in red, with that of CFC-113a being extrapolated from Laube *et al.* (2014) and error bars represent total calculated uncertainty.

There is also still a decrease in mixing ratios between the 23rd and 24th followed by an increase on the 25th as seen with the other CFCs but this is much less pronounced for this species. What is most noticeable is that mixing ratios increase from the 20th January to a peak of 1 ppt on the 23rd and then overall, they decrease until the 28th January (0.68 ppt). Whilst other CFC species have shown several days of enhanced concentrations over this period, this well-defined change in concentration in time with the cold surge event clearly indicates that this species is transported from East Asia by the weather phenomenon. The peak on the 23rd also corresponds with the NAME back-trajectory where further inland emissions from China are a potential major influence and this agrees with the conclusions drawn in the previous chapter that China is a likely source region for CFC-113a.

With the isomers CFC-114 and CFC-114a (Figures 5.8a and 5.8b) the pronounced variation in mixing ratios between the 23rd and 26th previously mentioned for the other CFC species is apparent mainly for CFC-114. CFC-114a was enhanced for the majority of the cold surge period but saw a drop in mixing ratio back to near background abundance on the 24th January, similar to that seen for CFC-13. CFC-114 also decreased but dropped nearly 0.5 ppt below background mixing ratios. This sharp difference in abundance was observed for several ODS but saw a spike with the VSLS-Br species and so potential reasoning will be discussed further in section 5.6.2.6. CFC-114a saw more enhancement above background (1.0 ppt) than CFC-114 (15 ppt) with a median enhancement of 11% compared to 5.1%. Overlaying the time series for both these species (Figure 5.8c) shows distinct similarities in peaks and troughs suggesting there may be some potential co-location of sources. This is somewhat different to the relationship observed in the Taiwan 2015 campaign (see section 4.9.3.1.1) but may be a reflection of increased mixing during long-range transport or different sources being sampled. As such, a future campaign focusing on locating sources of these isomers through targeting sampling locations and a more quantitative modelling approach may be beneficial in assessing their relationship and emissions.

CFC-115 (Figure 5.7c) exhibited a similar change in concentration during the cold surge event as CFC-113a, with a peak on the 23rd January (8.9 ppt) followed by an overall decrease to the 26th. This species was also enhanced above background concentrations between 1.5% and 5.9% throughout the cold surge and saw the same pattern of variation between the 23rd and 26th as was apparent for the other CFCs although again, like CFC-113a, this was somewhat less pronounced. Whilst this general increase in mixing ratios that corresponds with the cold surge does suggest CFC-115 is one of the species being transported from sources in East Asia, concentrations increase again after the cold surge is over, the implications of which will be explained in the next section.

After the Cold Surge Event – 27th January to 2nd February

The peaks and troughs in mixing ratios continue on the 27th and 28th January, to some extent, for all but two CFCs where by concentrations continue to decrease for CFC-113a and conversely continue to increase for CFC-115.

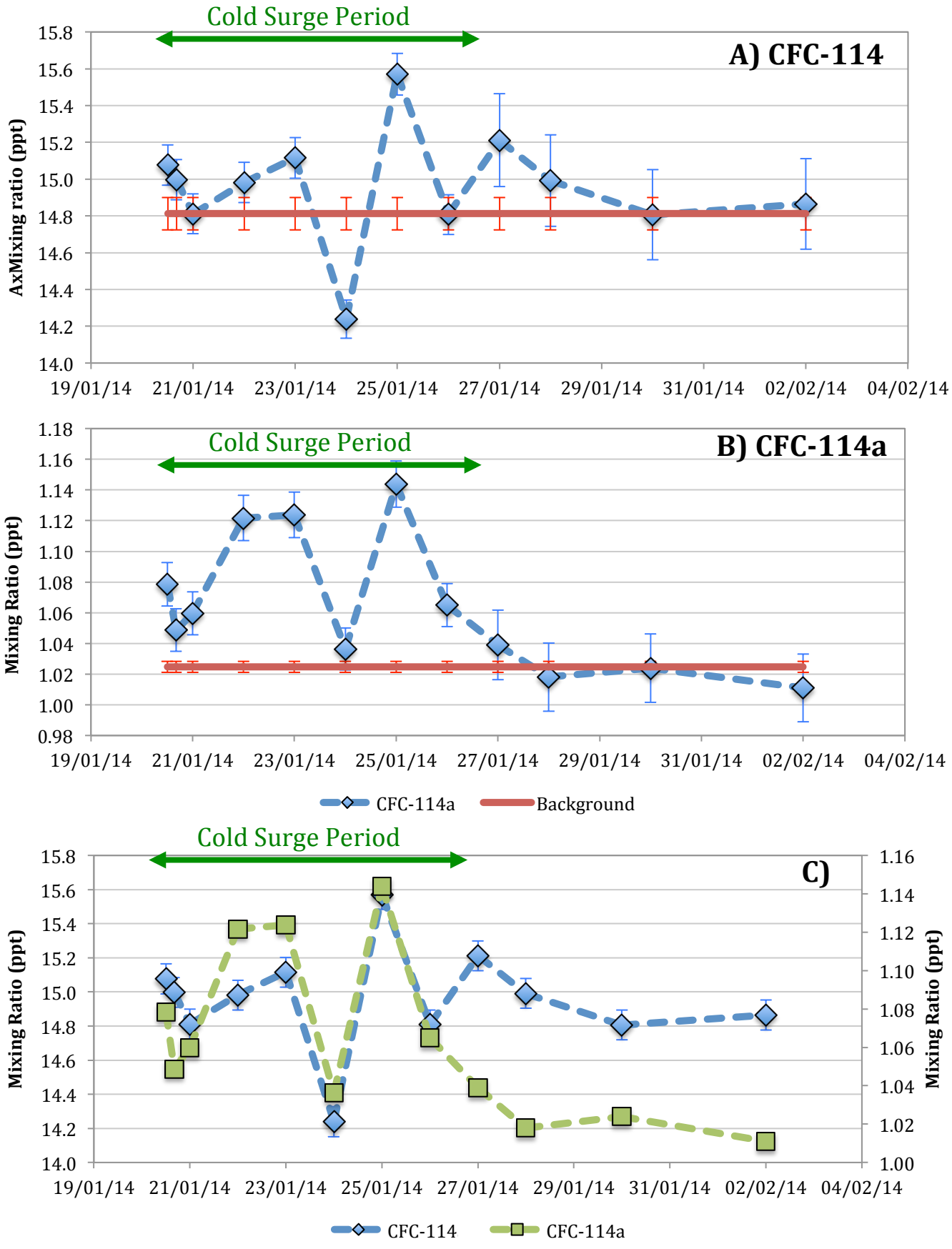

Figure 5.8: Time series of the isomers A) CFC-114 and B) CFC-114a as well as the overlayed time series for both speries C). Background mixing ratios are shown in red and error bars represent total calculated uncertainty.

Although the end of the cold surge and reduced long range transport explains the decrease in CFC-113a, the increase of CFC-115 back to mid-cold surge levels of over 8.8 ppt, suggests the presence of another emissions source. NAME back-trajectories do indicate a difference in contributing regions during and post-cold surge, from Chinese and Taiwanese dominated trajectories to those that still travel over Taiwan but have more major influences from the Philippines and Korea. However, further campaigns would be necessary to identify specific source areas. After the 28th, no substantial variation in concentration is seen for any of the CFC species.

5.6.2.2 Halons

During the Cold Surge Event – 20th January 2014 to 26th January 2014

Phased out along with the CFCs and having similar properties, the halons were also expected to be detected at close to background mixing ratios even during the cold surge period. Given their long lifetimes these species are generally well-mixed in the atmosphere and so whilst some variation in abundance is anticipated, significant spikes were not expected.

For Halon 1211 (Figure 5.9a), the most widely utilised halon species, the cold surge event appeared to considerably affect mixing ratios. These increased from the 20th January to a peak of 4.4 ppt on the 23rd, over 16% enhancement (see Appendix 5.4) above the background concentration. A sharp decrease to 3.9 ppt, much like those seen for the CFCs previously, occurred on the 24th but concentrations increased again on the 25th before continuing to decrease until the 28th. Aside from this trough, the general change in concentration in-line with the cold surge event does indicate the long-range transport of halon 1211. While continued emissions of this compound are expected due to sizeable banks, these are potentially larger in heavily populated regions such as mainland China and so mixing ratios transported and detected from this area would likely be above background (3.8 ppt).

Similarly, Halon 1202 (Figure 5.9b) is also enhanced above background concentrations (41-174%) during the cold surge period and also exhibits a peak on the 23rd at 0.05 ppt (compared to a background mixing ratio of 0.016 ppt). Unlike previously considered species, whilst there is a subsequent drop in concentration after this peak, there is one before on the 22nd January from 0.03 ppt on the 21st to 0.02 ppt. Still, the general change over the cold surge period indicates there is long-range transport of halon 1202. Given the good correlation and possible by-product relationship with halon 1211 found and discussed in the previous chapter, the co-location of sources resulting in both species being transported during a cold surge event is likely. Analysis of the Taiwanese data did suggest potential source locations of Korea, likely from US military sources, and Taiwan both of which are major or minor influences throughout the Bachok campaign.

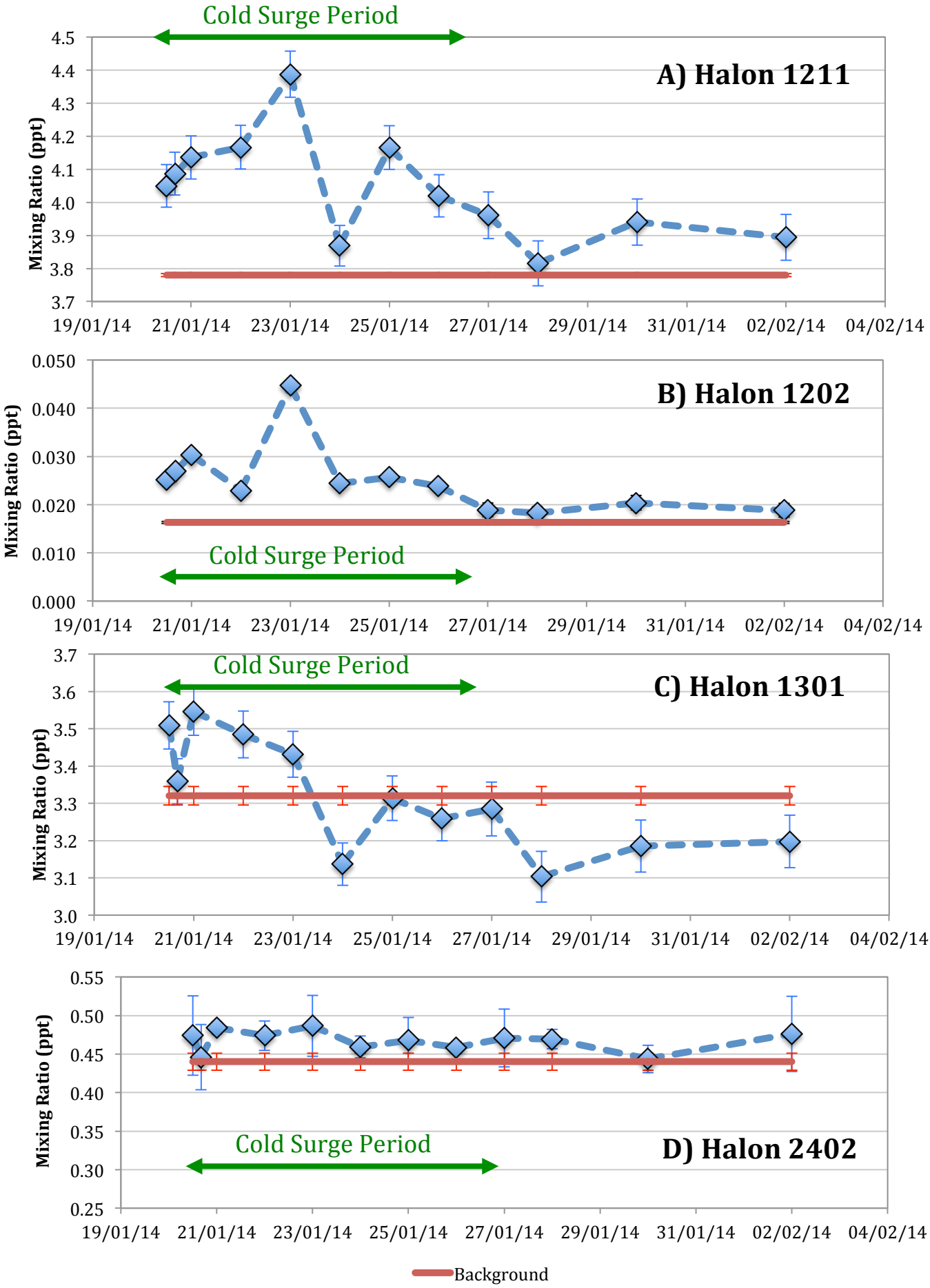

Figure 5.9: Time series of the halons, A) halon 1211, B) halon 1202, C) halon 1301 and D) halon 2402, observed during the Bachok campaign. Background mixing ratios are shown in red and error bars represent total calculated uncertainty.

Halon 1301 and halon 2402 (Figures 5.9c and 5.9d) both display considerably different time series to the other CFC and halon species. While halon 1301 starts at concentrations above the background 3.32 ppt, after the dip on the 24th January seen in many other species, it does not return above the background again. Even so, mixing ratios are higher during the cold surge period than after suggesting there is more transport of this compound during that time.

Halon 2402 however, is consistently enhanced above the background of 0.44 ppt although this enhancement only ranges from 0.9% to 10.6%. There are no significant peaks and troughs, which suggests no consistency or changes in transport related to the cold surge event. This may suggest that the background used may be too low for this species in this region, particularly as a recent study by Vollmer et al (2016) detected Halon 2402 in frequent pollution events at Gosan, Korea with potential sources around the Sea of Japan/East Sea and the Russian Federation. Although backwards trajectories during this campaign do see influences from Korea and Japan, the observed mixing ratios do not indicate increased source impact from these regions. This may, at least partially, be attributed to dilution during long- range transport.

After the Cold Surge Event – 27th January to 2nd February

Both halon 1211 and 1202 exhibit the near background concentrations, within the margin of error, which were originally expected for these species. This further indicates that the sources of these species are considerable distances from Bachok and so may mainly be transported as far without undergoing dilution to the hemispheric background mixing ratio during cold surge events.

Halon 1301 continued to be measured under background levels with no significant changes in abundance, which suggests that sources are long-range. No clear conclusions can currently be drawn about sources of halon 2402.

5.6.2.3 Hydrochlorofluorocarbons

During the Cold Surge Event – 20th January 2014 to 26th January 2014

Due to their use as replacements for CFCs and halons, mixing ratios of HCFCs are still increasing and sources are widespread in East Asia so evidence of long-range transport through increased mixing ratios during the cold surge period is expected.

All 4 of the HCFCs measured, HCFC-22, -133a, -141b and 142b during this campaign were detected at concentrations that generally increased until a peak on the 23rd January (to 267 ppt, 0.99 ppt, 33 ppt and 23 ppt respectively) and then decreased until the 28th, following the cold surge event (see Figures 5.10a, b, c and d). The peak on the 23rd corresponds with the back-trajectory suggesting mainland China is more of a major influence than on other days sampled. This difference appears evident when considering the peak concentrations of which HCFC-133a and -142b showed some significance (between 1 and 2σ) and HCFC-22 and -141b were statistically significant (over 2σ) unlike other days sampled.

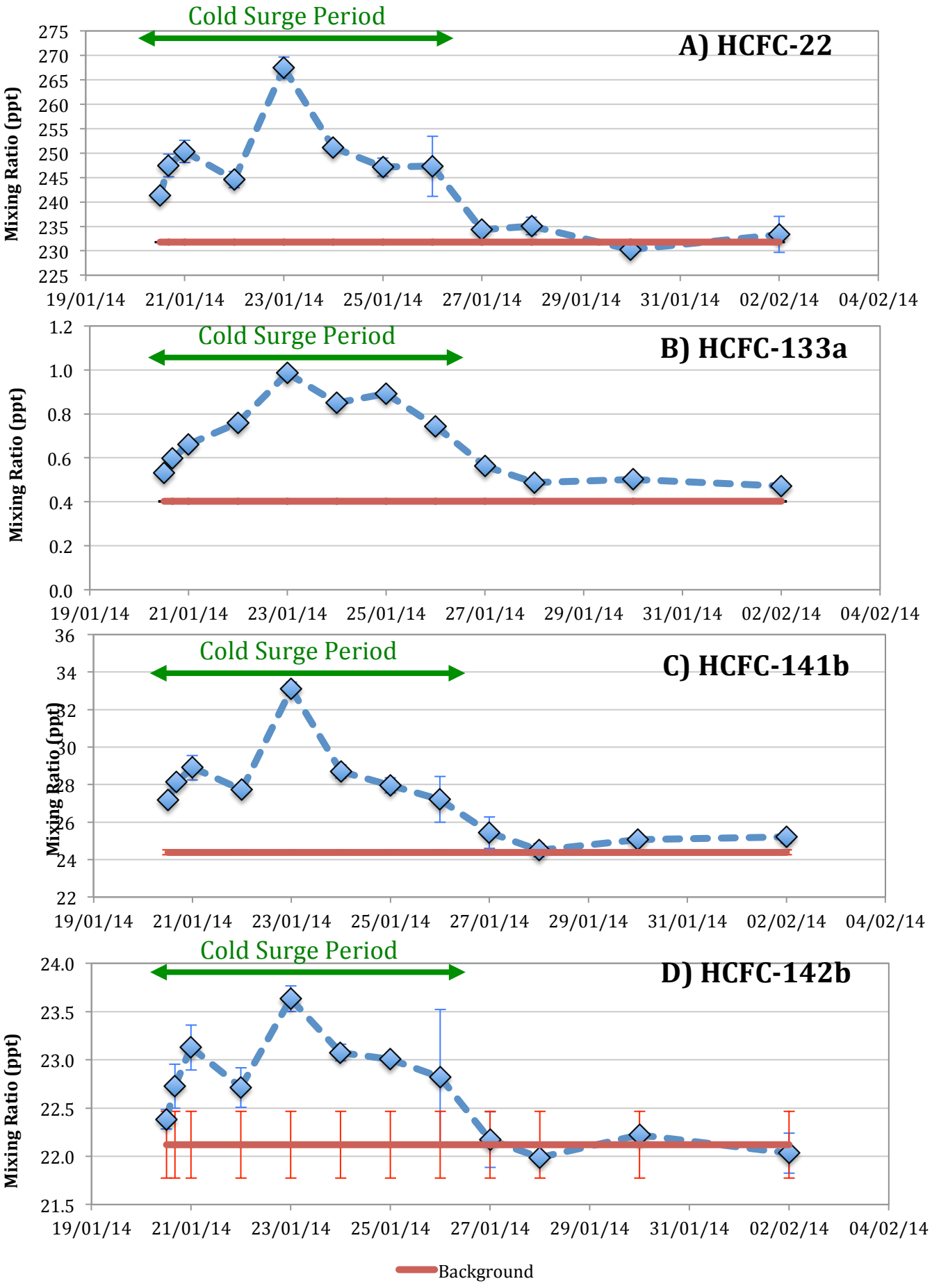

Figure 5.10: Time series of the HCFCs, A) HCFC-22, B) HCFC-133a, C) HCFC-141b and D) HCFC-142b, observed during the Bachok campaign. Background mixing ratios are shown in red and error bars represent total calculated uncertainty.

This indicates that there are emissions from this more inland region of China that have undergone long-range transport due to the cold surge conditions since no other days had this area as a potential influence or saw this magnitude of detected species.

HCFC-22, -141b and -142b all saw a dip in concentration before the 23rd similar to halon 1202 however HCFC-133a exhibited a very similar time series to CFC-113a. This is unsurprising given the correlation and probable co-emission between these species suggested in the previous chapter. All 4 species were also enhanced above their background concentrations during the cold surge (see Appendix 5.4), further indicating transport of emissions.

After the Cold Surge Event – 27th January to 2nd February

Comparative to during the cold surge period, little variation in mixing ratios was seen in the period after. HCFC-22 decreased to 230 ppt (below the background of 232 ppt) on the 30th January but increased slightly to 233 ppt afterwards although this was within error margins. Similarly, HCFC-141b and -142b both saw their lowest abundances on the 28th January (24 ppt and 22 ppt respectively), however both increased slightly afterwards. HCFC-141b stayed above background (24 ppt) with minimal variation whereas HCFC-142b decreased below background (22 ppt) but again, this was within error margins.

HCFC-133a stayed enhanced above the background concentration of 0.40 ppt and continued to decrease after the 26th January before seeing very little variation (a range of just over 0.03 ppt) for the last three samples.

As such for all the HCFCs measured, the variation in concentration between during and after the cold surge event further emphasises that the sources of these species are long range in origin. Transport of these emissions without dilution to near background levels does not appear to occur without the increased winds of the cold surge.

5.6.2.4 Chlorocarbons

These chlorinated species have longer lifetimes than the VSLS and are controlled by the Montreal Protocol so emissions should be minimal, with banks being the main potential source. However these are likely found in East Asia and so increased mixing ratios during the cold surge period and near background level after would be expected.

During the Cold Surge Event – 20th January 2014 to 26th January 2014

Carbon tetrachloride (Figure 5.11a) exhibited a similar pattern on peaks and troughs during the cold surge as was seen for many of the CFC species. The largest enhancement is 12% above background (84.8 ppt) on the 25th January before concentrations start to decrease consistently, likely due to the end of the cold surge.

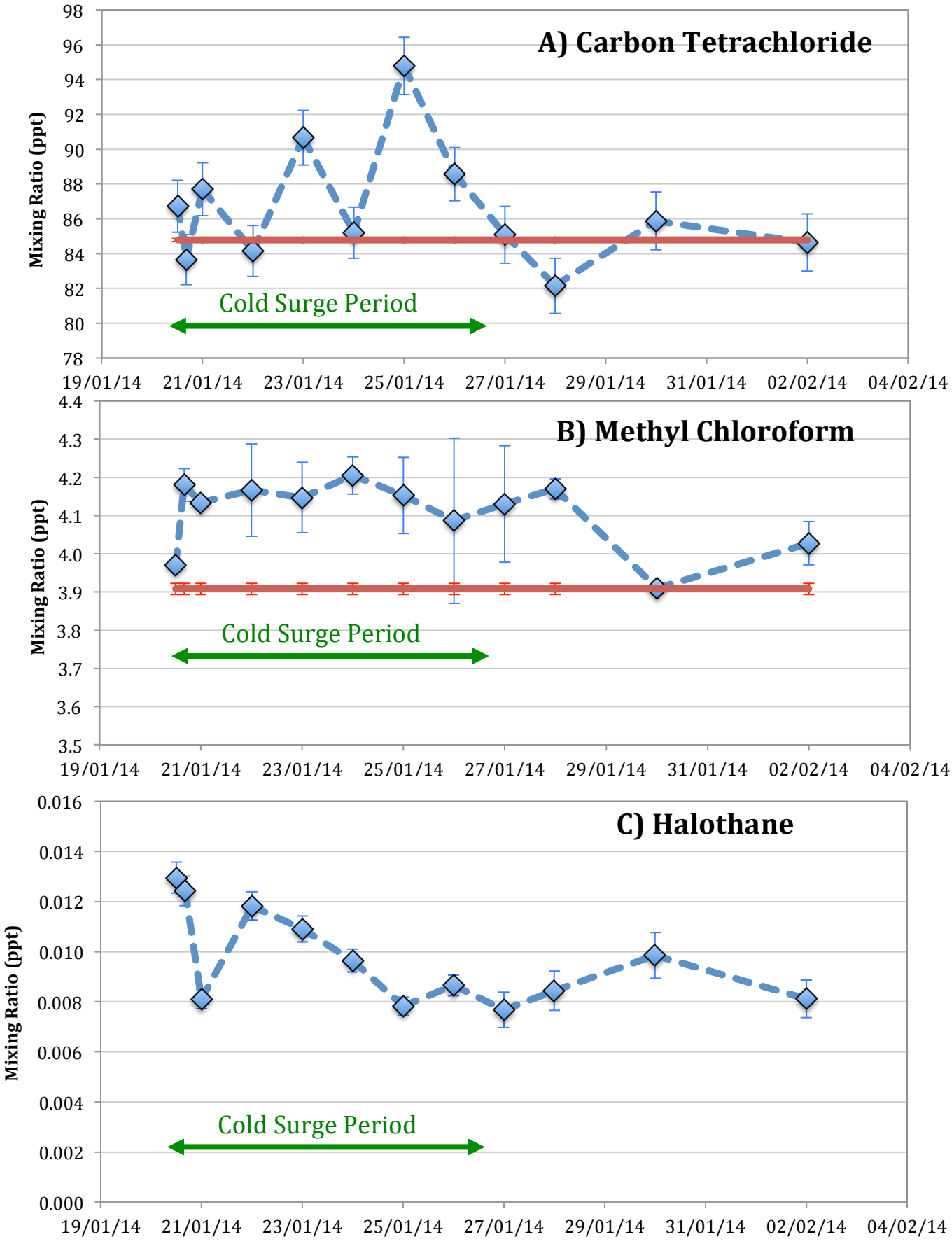

Figure 5.11: Time series of the chlorocarbons, A) carbon tetrachloride, B) methyl chloroform and C) halothane, observed during the Bachok campaign. Background mixing ratios are shown in red and error bars represent total calculated uncertainty.

As previously discussed, the NAME trajectory does not suggest a reason for this variation as potential regional influences are very similar throughout the cold surge event. However the detected troughs appear to be within the error margins for near background levels indicating periods of clean air may have been sampled but the range of compounds sampled and measured at enhanced concentrations during the weather event would suggest this is unlikely.

For methyl chloroform (Figure 5.11b) samples collected during the cold surge were enhanced up to 7.6% above the 3.9 ppt background suggesting that emissions were being measured. Halothane (Figure 5.11c) was also detected however there is currently no background data available for this species and so potential enhancements due to the cold surge are unable to be quantified. However, the time series produced is very similar to that of CH_2ClBr and the two show good correlation (see section 5.6.3) although halothane is anthropogenic in origin. Still, concentrations are generally higher for this species during the cold surge period indicating that some long-range transport of emissions may occur.

After the Cold Surge Event – 27th January to 2nd February

Whilst both carbon tetrachloride and halothane do have decreasing mixing ratios after the cold surge, both increase again on the 30th January by 3.7ppt and 0.001 ppt respectively. This brings carbon tetrachloride back above background (84.8 ppt) and causes a slight spike in halothane abundance that is still lower than concentrations measured during the cold surge. Similar to carbon tetrachloride, methyl chloroform mixing ratios decrease to below background, outside of error margins, for one sample, however this is the 30th January as opposed to the 28th. Overall the indication for all 3 chlorocarbon species is that they do undergo some transport during the cold surge period and concentrations return to near background values after.

5.6.2.5 Very Short Lived Species – Chlorine Based

These species – dichloromethane, 1,2-dichloroethane (DCE), tetrachloroethene (PCE), chloroform and chloroethane, all have atmospheric lifetimes less than 6 months and so remain in the troposphere for much less time than the other ODS measured during this campaign. As such, long-range transport of these species without substantial dilution or breakdown is minimal and so, whilst anthropogenic emissions sources are apparent in East Asia, transport across the SCS during non-cold surge periods is expected to be limited. Dichloromethane, DCE, chloroform and chloroethane all also have natural sources from biomass burning (Carpenter and Reimann, 2014) that may originate closer to the sampling site and potentially impact the concentrations detected.

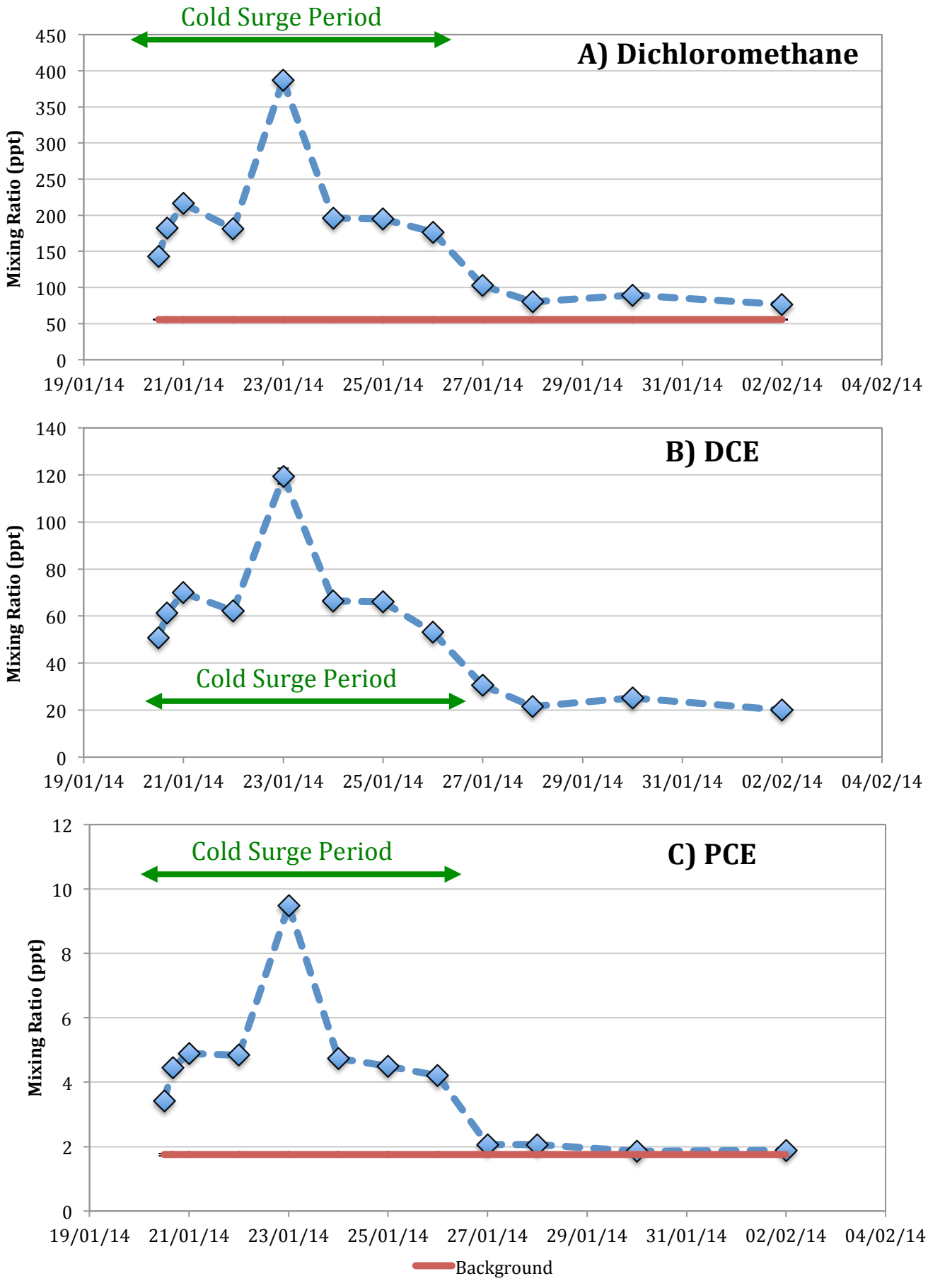

Figure 5.12: Time series of A) dichloromethane, B) DCE and C) PCE observed during the Bachok campaign. Background mixing ratios are shown in red and error bars (not visible due to the large range of mixing ratios detected) represent total calculated uncertainty.

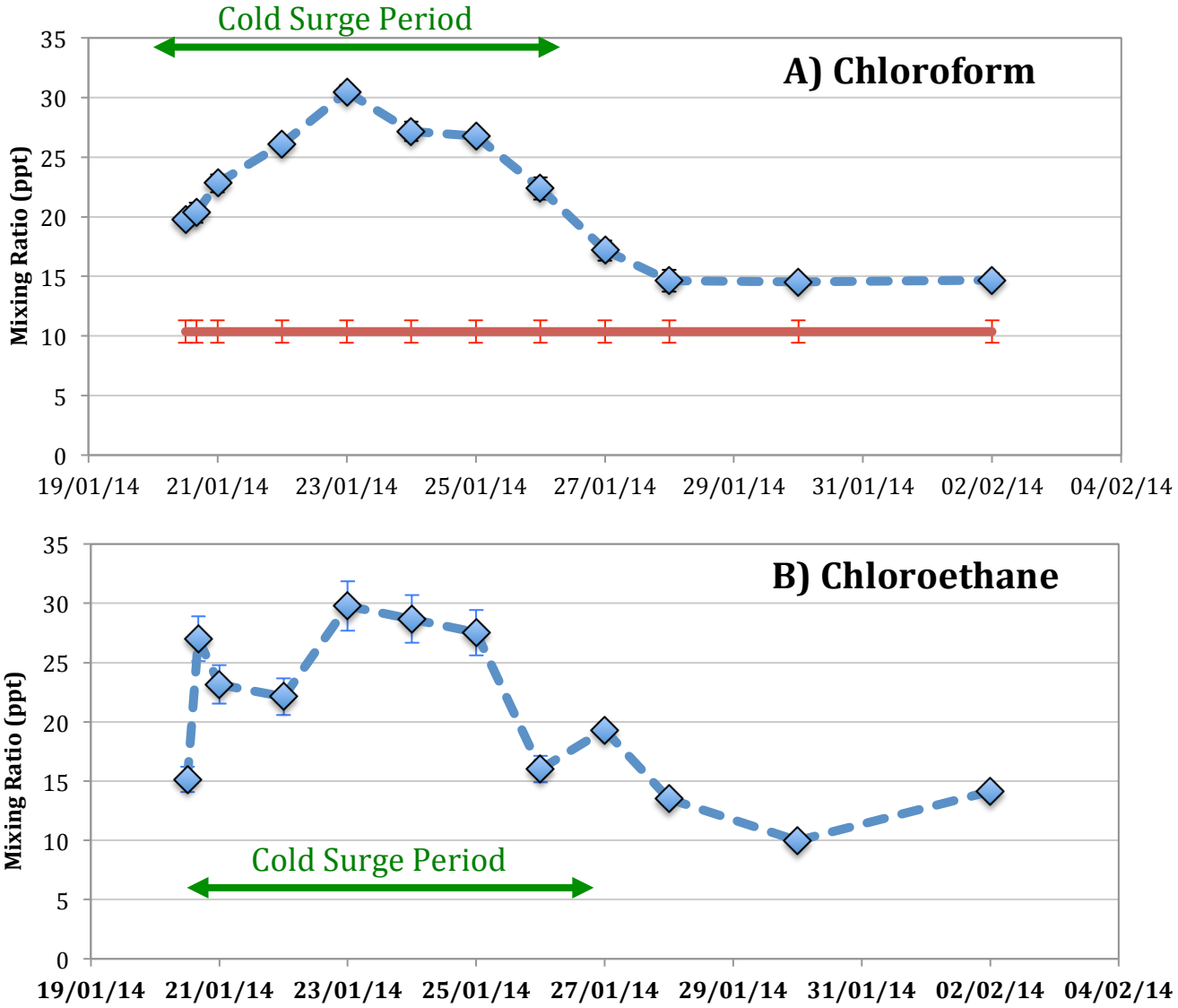

Figure 5.13: Time series of A) chloroform and B) chloroethane observed during the Bachok campaign. Background mixing ratios are shown in red and error bars represent total calculated uncertainty.

During the Cold Surge Event – 20th January 2014 to 26th January 2014

Dichloromethane, DCE and PCE all exhibited very similar time series during the cold surge period (Figures 5.12a, b and c). Though background data is not available for DCE due to limited measurements, both dichloromethane and PCE were enhanced above their respective background concentrations (55.5 ppt and 1.75 ppt) during this phase of the campaign. All 3 compounds saw a distinct spike, like that seen previously with the HCFCs, on the 23rd January (to 390 ppt, 120 ppt and 9.5 ppt respectively) after generally increasing concentrations beforehand, followed by a decrease to the 27th.

Similar features were seen for chloroform and chloroethane (Figures 5.13a and b) however they were less pronounced for these species although the time series for chloroform was comparable with that produced for CFC-113a and HCFC-133a. This is reflected in the calculated correlation coefficients and will be expanded on further, along with the several other HCFCs and VSLS-Cl species that share notable correlation, in section 5.6.3 of this chapter.

Unlike the other compounds mentioned, chloroethane sees a spike in abundance (to 27 ppt) on the 2nd sample from the 20th January, collected only 4 hours after the first. Whilst overall the NAME back-trajectories are very similar for both these samples and the subsequent one, there is potential for some impact from Vietnam and, given the 12 ppt difference in concentration during a 4-hour period, a short-range emission source seems more feasible. Biomass burning could be a possible origin and methyl bromide, another indicator of this kind of source, was also detected at increased concentrations for this sample.. Concentrations of other biomass burning related species, methyl chloride and CO, are less clear and so this cannot be confirmed as the likely source for this spike.

Overall, these results suggest that high levels of VSLS-Cl species from sources in East Asia, are being transported across the SCS to Bachok in a relatively short time period during this cold surge event.

After the Cold Surge Event – 27th January to 2nd February

All VSLS-Cl species measured decreased in concentration after the 27th January and all but chloroethane exhibited a minimal range of mixing ratios after that day (10ppt for dichloromethane, 5ppt for DCE and 0.2 ppt for both PCE and chloroform). Chloroethane does have a shorter atmospheric lifetime than the other species and so this may contribute to its wider variation in abundance. Dichloromethane and chloroform both remained enhanced above background mixing ratios (56 ppt and 10 ppt respectively) however PCE decreased to within error margins of the 1.8 ppt background by the 30th January.

Chloroethane decreased in concentration until the 30th January before increasing by over 4ppt by the 2nd February, the next sample. However, since there is not currently background data for this species it is unclear as to how much enhancement this corresponds but the 14 ppt reached on this day is still a lower mixing ratio than was seen throughout the cold surge period. As such, this further emphasises that the higher levels seen for this species and the other VSLS-Cl are likely due to cold surge related transport and the lack of variation after indicates a lack of local sources for most compounds.

5.6.2.6 Very Short Lived Species – Bromine Based

The VSLS-Br species also have short atmospheric lifetimes of less than 6 months but their sources are primarily of natural oceanic origin (Carpenter and Reimann,. 2014). There are some minor anthropogenic emissions of bromoform ($CHBr_3$) from power plant cooling water and the chlorination of drinking water (Worton et al. 2006). Since during the EAWM air mass travel over the SCS then oceanic emissions may be picked up during transport so identifying anthropogenic sources is likely to be difficult, even during a cold surge when rapid long-range transport may occur.

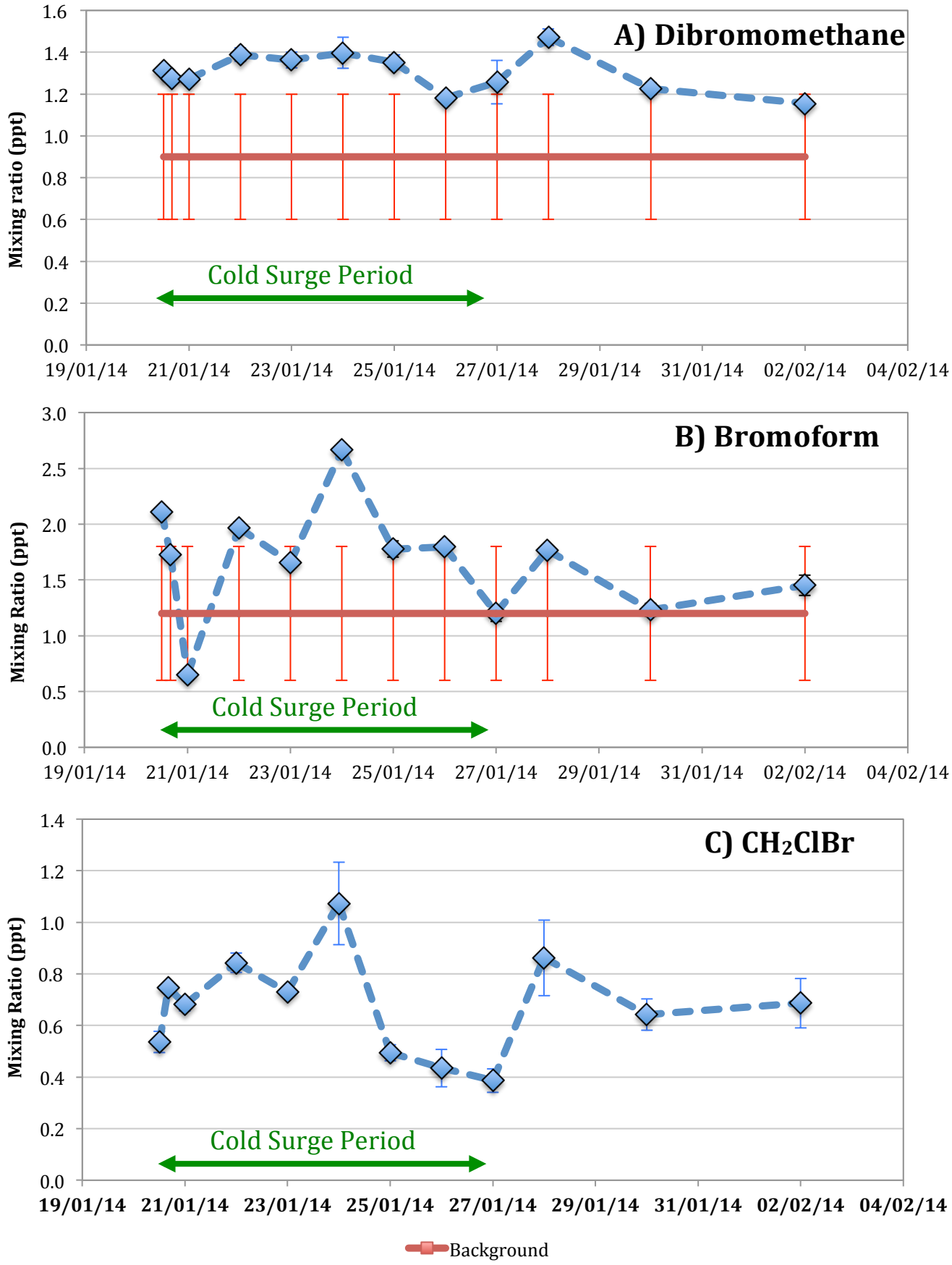

Figure 5.14: Time series of A) dibromomethane, B) bromoform and C) CH_2ClBr observed during the Bachok campaign. Background mixing ratios are shown in red and error bars represent total calculated uncertainty.

During the Cold Surge Event – 20th January 2014 to 26th January 2014

There is currently no background data for any of the VSLS-Br compounds so assessing potential enhancements in concentration that can be associated with the cold surge is difficult. Dibromomethane, bromoform and CH_2ClBr all have reported median Marine Boundary Layer (MBL) abundances in (Carpenter and Reimann, 2014) and these have been added to their respective figures (Figure 5.14a, b and c).

Both dibromomethane and CH_2ClBr are consistently enhanced above these medians (by at least 0.28 ppt and 0.07 ppt respectively). However, whilst enhancements above the MBL median of 1.2 ppt for bromoform were seen, the sample on the 21st January was detected 0.55 ppt lower. As this compound is so short-lived (24 days – see Table 1.6), proximity to sources is likely to impact observed levels significantly and so variation such as this is not unexpected. The 21st January saw influences from Vietnam and Cambodia along with China and Taiwan, as did the 23rd January. These are also both samples where mixing ratios for bromoform decreased comparative to the surrounding days. This may be due to the air masses passing over more land and so less ocean than on other days before reaching Bachok.

Bromoform, bromoethane and CH_2ClBr (Figure 5.14b, 5.15a and b) all have spikes on the 24th January that are 0.9 ppt, 0.4 ppt and 0.5 ppt higher respectively than the median concentrations during the cold surge period for these species. Dibromomethane (Figure 5.14a) also appears to have slight increased concentrations on this day however, the previous and subsequent mixing ratios are only slightly lower so this may fall within error margins. The 24th is day when the majority of ODS previously mentioned saw a sharp decrease in mixing ratios although NAME back-trajectories appeared to have similar influences to the surrounding days. The higher levels of these VSLS-Br could indicate a stronger oceanic influence on the air mass suggesting less travel over populated areas took place hence the decreased anthropogenic compound level mentioned before.

Also, similar to chloroethane, bromoethane saw a spike on the 2nd sample for the 20th January. Only one other compound was found to clearly have this feature (methyl bromide) indicating that it may be from a biomass burning source however concentrations of both CO and methyl chloride are less clearly enhanced so confirmation of this is not currently possible.

$CHClBr_2$ (Figure 5.15b) has a spike on the 1st sample of the 20th January and whilst several other species including dibromomethane and bromoform do show increased concentrations on this day they are not to the same magnitude, comparative to the rest of the samples, which then decrease. Comparison with the NAME back-trajectory does not suggest any obvious source location except Vietnam mostly due to the size of the increase and the lack of continued enhancement throughout the rest of the cold surge indicating short-range transport would be more likely.

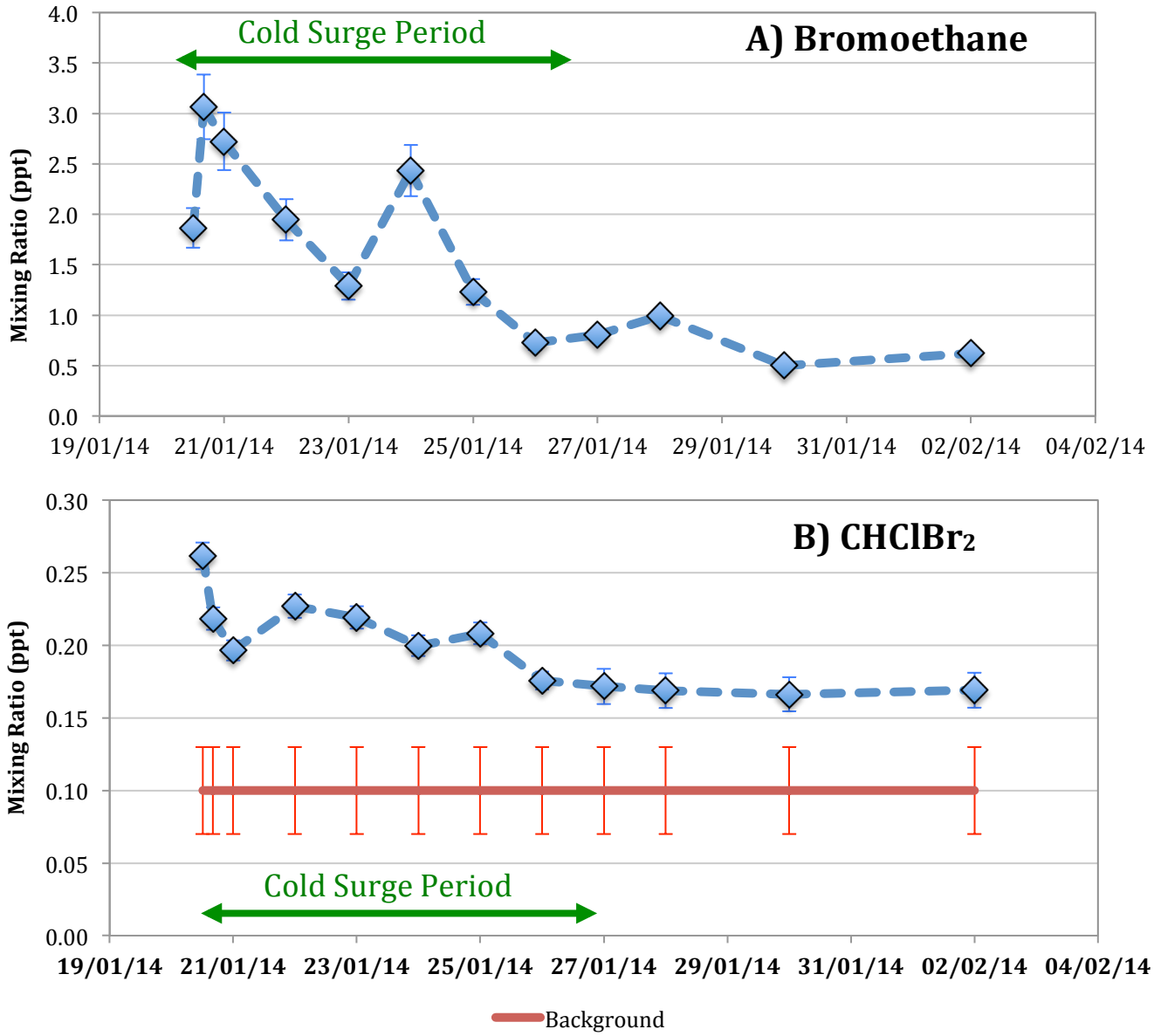

Figure 5.15: Time series of A) bromoethane and B) $CHClBr_2$ observed during the Bachok campaign. Background mixing ratios are shown in red and error bars represent total calculated uncertainty.

Whilst not as clear as many of the other ODS measured, likely due to their natural sources, for all of the VSLS-Br detected there does appear to be some consistent increases in concentration that could be related to the cold surge event however further study would be required to fully confirm this.

After the Cold Surge Event – 27th January to 2nd February

Concentrations of dibromomethane, $CHClBr_2$ and CH_2ClBr appear similar in the time after the cold surge as they did during, with median mixing ratios not being significantly lower (0.04 ppt, 0.05 ppt and 0.04 ppt respectively, see Appendix 5.3). Bromoform and bromoethane see larger decreases in median mixing ratios (0.35 ppt and 1.2 ppt respectively) but neither of these are significant differences either.

However, all of these compounds except CH_2ClBr do exhibit a spike in mixing ratios on the 28th January, which for dibromomethane is the highest concentration measured during this campaign at 1.5 ppt.

Comparison with the NAME back-trajectory indicates that the path of this air mass was mainly over ocean, which may explain some of the increased concentrations seen however these were still lower than those seen in the cold surge period for most of the VSLS-Br. This again could suggest that cold surge events do result in increased levels of bromine based short-lived species but a long-running measurement campaign throughout several cold surges would be necessary to affirm this.

5.6.2.7 Methyl Halides

The final group of ODS measured in this campaign were the methyl halides of which there are both anthropogenic and natural sources including biomass burning, rice paddies and oceans. As such, similar to the VSLS-Br, identifying any increase in concentration caused by the cold surge aided long-range transport of anthropogenic emissions is likely to be difficult.

During the Cold Surge Event – 20th January 2014 to 26th January 2014

For methyl chloride (Figure 5.16a) clear enhancements above the background concentration by between 33% and 47% can be seen during the cold surge period with a peak reached on the 23rd January at around 880 ppt. Like many other species measured, the concentration drop the next day (to 780 ppt) before increasing again (to 860 ppt) on the 25th and then decreases steadily as the cold surge abates. Methyl bromide (Figure 5.16b) also sees clear enhancements, between 63% and 307%, above the background mixing ratio of 7.0 ppt during the cold surge event,. However, the peak concentration of 28 ppt is reached on the 24th January, a day when the majority of species have seen decreases. Other compounds that had spikes on this day were the VSLS-Br species and as previously mentioned, this could indicate that emissions from the ocean rather than anthropogenic sources dominated on this day.

A spike to 23 ppt was also measured for methyl bromide in the 2nd sample from the 20th and this corresponds with spikes seen for chloroethane and bromoethane. Comparison with NAME back-trajectories and given the magnitude of this enhancement, short-range transport of biomass burning emissions from Vietnam could be a potential source. Methyl chloride mixing ratios are enhanced for this sample as well however it is not clear as to whether that is due to the transport of anthropogenic emissions, biomass burning emissions or a combination of the two. Unfortunately CO concentrations for this sample appear to decrease so there is no firm indication as to whether biomass burning is the cause of this spike. Emissions of methyl halides from vegetation such as tropical, subtropical and mangrove forests may also contribute to air masses travelling over land regions like Vietnam however the spike in methyl bromide does suggest a less stable source.

Generally, the mixing ratios of both methyl halide species measured appear to be impacted by the increased transport of anthropogenic emissions during the cold surge period. Emissions from natural sources, such as those from vegetation, may have also been sampled during this period due to most air masses travelling over more land including Vietnam during this period. However, this source is unlikely to account for significant changes in observed mixing ratios but may potentially account for part of the more consistent, above background abundances detected.

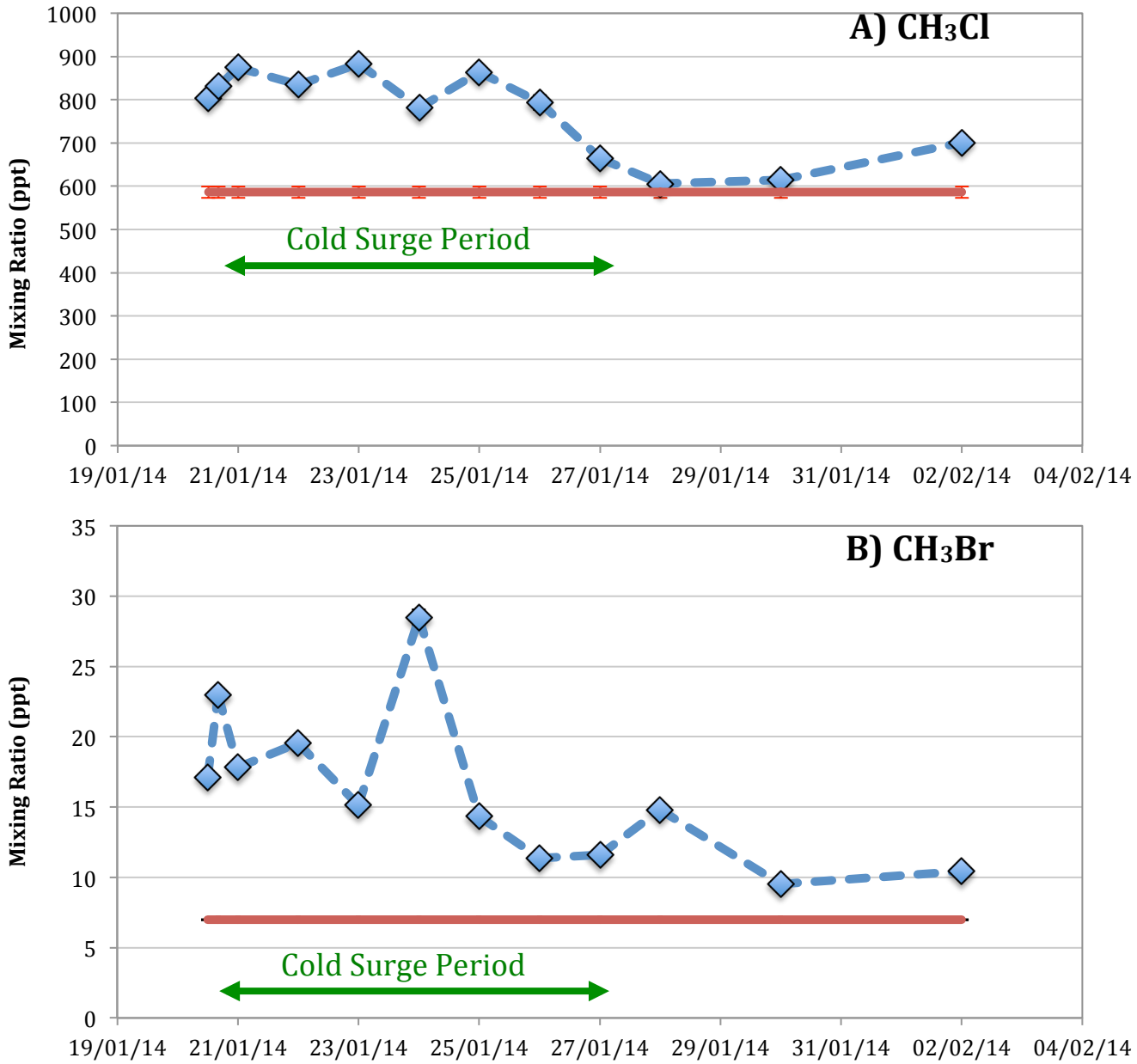

Figure 5.16: Time series of the methyl halides, A) methyl chloride and B) methyl bromide, observed during the Bachok campaign. Background mixing ratios are shown in red and error bars represent total calculated uncertainty.

After the Cold Surge Event – 27th January to 2nd February

Methyl chloride concentrations decrease to a median of 9% enhancement above the background (590 ppt) after the cold surge has finished but appear to increase again after the 30th January. This is more likely due to the significant tropical sources of methyl chloride, particularly from tropical forests and plants (Saito et al. 2008), as opposed to anthropogenic sources. Methyl bromide behaves similarly however there is a slight spike to 15 ppt on the 28th, which corresponds with spikes seen during the analysis of the VSLS-Br and a NAME back-trajectory that suggests this is most likely due to oceanic emissions rather than anthropogenic.

5.6.2.8 Carbon Monoxide

Also, measured during the Bachok campaign was carbon monoxide, a compound often emitted from similar sources of anthropogenic ODS and also used as a tracer for industrial air. Emissions of CO are generally well documented and so estimates of emissions for other species may be calculated provided there is good correlation between the two. For the CO data utilised in this campaign, records of industrial emissions were used to calculate the proportion of the CO concentrations detected each day associated with industry from latitudes greater than 20°N. This enables correlations with other species to be assessed without disparities caused by short-range and potentially natural CO sources. The remaining difference between the total CO and the industrial CO should be a reflection of natural sources including biomass burning so further species correlations can be assessed. The process of estimating emissions for correlating species can be found later in this chapter (see section 5.6.4).

During the Cold Surge Event – 20th January 2014 to 26th January 2014

Figure 5.17 shows the time series for total CO, industrial CO and short-range/natural CO on the same graph. During the cold surge, it clear that there are increased CO levels from industrial sources while the natural CO remains relatively stable with a range of only 5 ppb compared to that of 57 ppb for industrial CO. A slight spike in short-range/natural CO is seen on the 21st of January but other species that share this feature are the HCFCs and VSLSs potentially suggesting that not all the industrial CO was separated in the calculation. However, the significant spike (over 2σ) on the 23rd January is only present in the industrial CO data and corresponds with a large number of ODS previously mentioned. This further emphasises that significantly high levels of ODS of industrial origin are being transported by cold surge events, from mainland China to Bachok.

After the Cold Surge Event – 27th January to 2nd February

From the 27th January, industrial CO levels did increase again by around 7ppb but this is substantially less than during the cold surge period and concentrations decreased again before the end of the campaign.

Short-range/natural CO, on the other hand, continued to increase from the 28th January and was, in the last analysed sample from the 2nd February, 4 ppb higher than the industrially sourced CO. This suggests that, without the stronger winds of the cold surge event, shorter-range natural emissions sources are more dominant and less diluted during transport than those from industry. Comparison with the NAME back-trajectories for this time indicate that Vietnam, a region known to have areas of biomass burning, may be a potential source region for this natural CO.

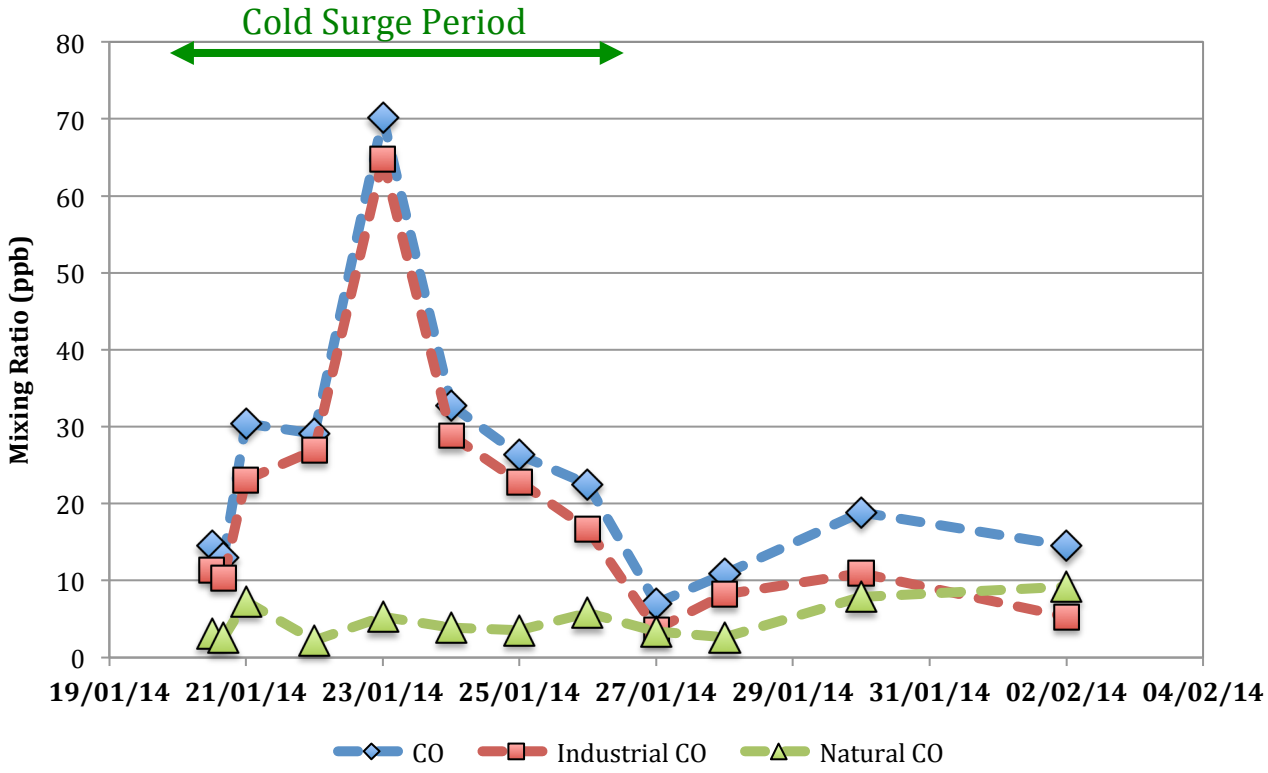

Figure 5.17: Time series of total CO as well as the established industrial and natural CO portions, observed during the Bachok campaign.

5.6.3 Correlation Overview

For all the ODS measured, interspecies correlations were assessed using the Pearson correlation coefficients, calculated utilising the equation 4.1.

$$r = \frac{\sum (x - \bar{x})(y - \bar{y})}{\sqrt{\sum (x - \bar{x})^2 \sum (y - \bar{y})^2}}$$ Equation 4.1

Where ***r*** is the Pearson correlation coefficient, ***x*** is the mixing ratio of one halocarbon species and ***y*** is the mixing ratio of a second halocarbon species. The coefficient quantifies the linear correlation between the two variables and is a built-in function of Excel which aided data processing. Species were separated as having some, good or excellent correlation using the following criteria:

Some correlation = Pearson coefficient **between 0.5 and 0.75**

Good correlation = Pearson coefficient **between 0.75 and 0.95**

Excellent correlation = Pearson coefficient **above 0.95**

Table 5.3 lists those species with good or excellent (highlighted in red) correlation. In the previous chapter, good correlation was an indication of co-location of sources whereas excellent correlation suggested co-emission. However, given the distance between Bachok and the likely sources of these ODS, there is much greater uncertainty with these conclusions and so only excellent correlation in this chapter is used as an indication of source co-location and potential co-emission. Described below are main interspecies relationships that this assessment and the previous overview highlighted.

Table 5.3a: Good and Excellent interspecies correlations for the CFCs, halons and HCFCs during the Bachok campaign.

Compound Group	Compound Name	Correlation (Good = 0.75-0.95 Excellent = >0.95)						
CFCs	11	CFC-13	CFC-114					
	12	CFC-13						
	13	CFC-11	CFC-12	CFC-114	CFC-114a			
	113a	HCFC-133a	HCFC-142b	CH_2Cl_2	DCE			
		PCE	Chloroform	CO	Industrial CO			
	114	CFC-11	CFC-13	CFC-114a				
	114a	CFC-13	CFC-114	Halon 1211				
Halons	1211	CFC-114a	Halon 1202	Halon 1301	HCFC-22	HCFC-141b	HCFC-142b	
		CH_2Cl_2	DCE	PCE	CH3Cl	Industrial CO		
	1202	Halon 1211	HCFC-22	HCFC-141b	HCFC-142b	CH_2Cl_2		
		DCE	PCE	CO	Industrial CO			
	1301	Halon 1211						
HCFCs	22	Halon 1211	Halon 1202	HCFC-133a	HCFC-141b	HCFC-142b	CH_2Cl_2	DCE
		PCE	Chloroform	Ethyl-Cl	CH_3Cl	CO	Industrial CO	
	133a	CFC-113a	HCFC-22	HCFC-141b	HCFC-142b	CH_2Cl_2	DCE	
		PCE	Chloroform	Ethyl-Cl	CO	Industrial CO		
	141b	Halon 1211	Halon 1202	HCFC-22	HCFC-133a	HCFC-142b	CH_2Cl_2	DCE
		PCE	Chloroform	Ethyl-Cl	CH_3Cl	CO	Industrial CO	
	142b	CFC-113a	Halon 1211	Halon 1202	HCFC-22	HCFC-133a	HCFC-141b	CH2Cl2
		DCE	PCE	Chloroform	Ethyl-Cl	CH_3Cl	CO	Industrial CO

Table 5.3b: Good and Excellent interspecies correlations for the chlorinated and brominated VSLS, chlorocarbons, methyl halides and CO during the Bachok campaign.

Compound		Correlation						
Group	Name	Good = 0.75-0.95 Excellent = >0.95						
VSLS-Cl	CH_2Cl_2	CFC-113a	Halon 1211	Halon 1202	HCFC-22	HCFC-133a	HCFC-141b	HCFC-142b
		DCE	PCE	Chloroform	Ethyl-Cl	CH_3Cl	CO	Industrial CO
	DCE	CFC-113a	Halon 1211	Halon 1202	HCFC-22	HCFC-133a	HCFC-141b	HCFC-142b
		CH_2Cl_2	PCE	Chloroform	Ethyl-Cl	CH_3Cl	CO	Industrial CO
	PCE	CFC-113a	Halon 1211	Halon 1202	HCFC-22	HCFC-133a	HCFC-141b	HCFC-142b
		CH_2Cl_2	DCE	Chloroform	Ethyl-Cl	CH_3Cl	CO	Industrial CO
	Chloroform	CFC-113a	HCFC-22	HCFC-133a	HCFC-141b	HCFC-142b	CH_2Cl_2	
		DCE	PCE	Ethyl-Cl	CO	Industrial CO		
	C2H5Cl	HCFC-22	HCFC-133a	HCFC-141b	HCFC-142b			
		CH_2Cl_2	DCE	PCE	Chloroform			
VSLS-Br	CH_2ClBr	Halothane						
Chlorocarbons	Halothane	CH_2ClBr						
Methyl Halides	CH_3Cl	Halon 1211	HCFC-22	HCFC-141b	HCFC-142b	CH_2Cl_2		
		DCE	PCE	Chloroform	Ethyl-Cl			
	CH_3Br	Ethyl-Br						
CO	Total CO	CFC-113a	Halon 1202	HCFC-22	HCFC-133a	HCFC-141b	HCFC-142b	
		CH_2Cl_2	DCE	PCE	Chloroform	Industrial CO		
	Industrial CO	CFC-113a	Halon 1211	Halon 1202	HCFC-22	HCFC-133a	HCFC-141b	
		HCFC-142b	CH_2Cl_2	DCE	PCE	Chloroform	CO	

The good Pearson correlation coefficient (verging on excellent) of 0.949 between CFC-113a and HCFC-133a was not unexpected given the relationship identified during the Taiwan campaign and discussed in the previous chapter (see Chapter 5, Case Study 1). What was noticeable however was the slightly different time series produced by these species during the Bachok campaign when compared to the other CFC and HCFC compounds, particularly CFC-113, and the very prominent peaks visible in their time series. Whilst both compounds do exhibit good correlation with a number of other species including HCFCs and VSLS, the only other compound with a similar time series is chloroform. Unlike during the Taiwan campaigns, the correlation with these species and CFC-113 is minimal suggesting a different source may have been sampled. This implies there are multiple sources of CFC-113a and HCFC-133a in East Asia and emphasises the need for further campaigns and continued measurement in order to identify them, particularly given the status of CFC production and consumption under the Montreal Protocol.

Also, conversely to the Taiwan campaign, CFC-114 and CFC-114a where found to have good correlation, with a coefficient of 0.77, suggesting there may be similarly located sources of these species. However, given the long-range transport from potential source regions, significant mixing and dilution may have occurred resulting in their similar time series. As such, more measurements of both short-range and long-range transported emissions would be necessary before firm conclusions on source location can be drawn.

Chloroform was calculated to have Pearson correlation coefficients of 0.91 with CFC-113a and 0.96 with HCFC-133a, indicating the species have good correlation and excellent correlation respectively and this can be seen in Figure 5.18. This level of correlation with HCFC-133a, suggests source co-location and potential co-emission with this species. This relationship was not previously apparent during the Taiwan campaigns and should be compared by future campaigns at both sites before any firm conclusions as to this are drawn.

The other species exhibiting excellent correlations were the main HCFCs and VSLS-Cl. Like before, whilst the co-location of emissions sources of these species is apparent, potential co-emission is less clear given the long-range transport of the air sampled. Figure 5.19 shows HCFC-22 plotted on the x-axis against HCFC-141b, -142b, dichloromethane, DCE and PCE, indicating the clear relationships seen between mixing ratios of these species. Similarly, Figure 5.20 shows dichloromethane plotted on the x-axis against abundances of HCFC-141b, -142b, DCE and PCE, suggesting associated source locations for these species as well.

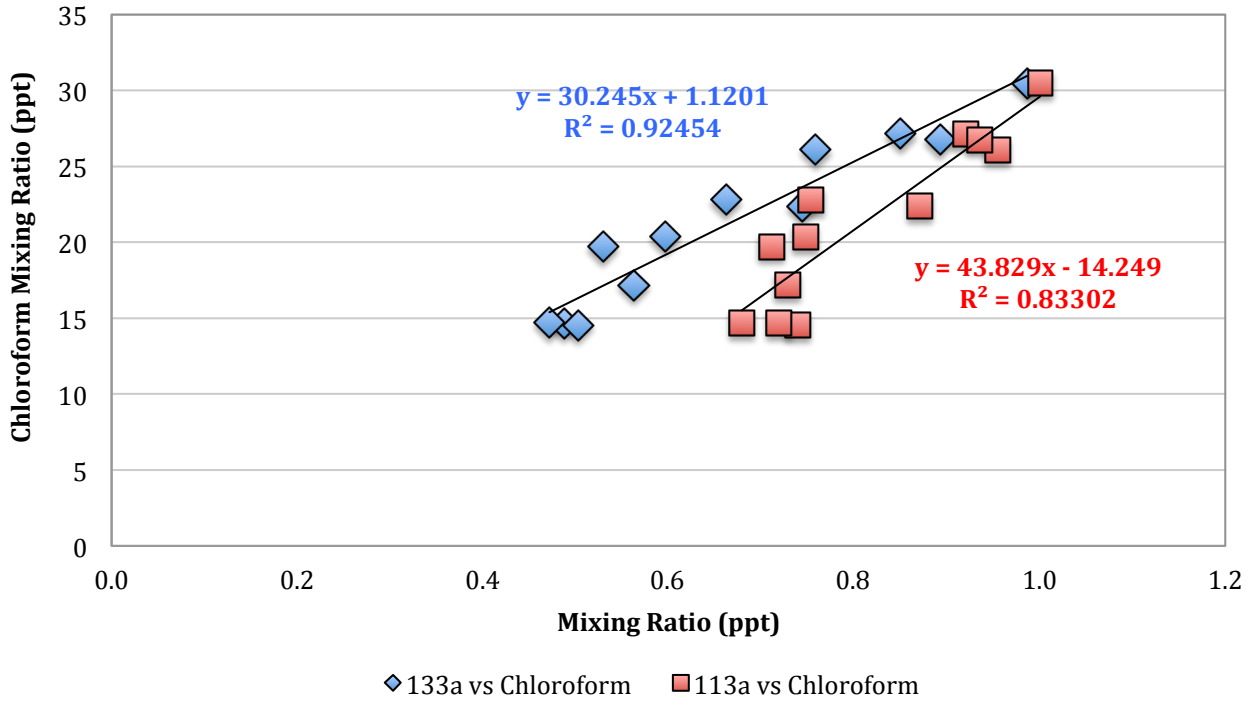

Figure 5.18: Interspecies correlation between chloroform and CFC-113a and HCFC-133a during the Bachok campaign.

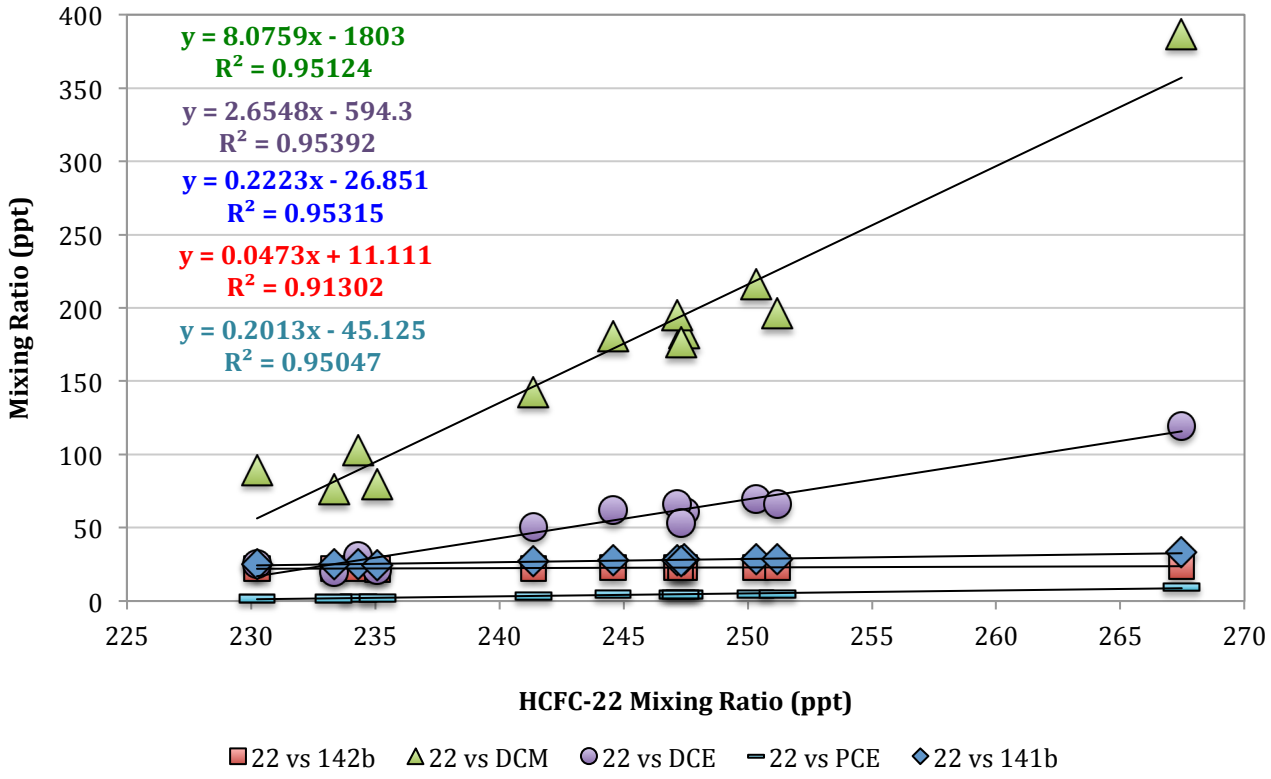

Figure 5.19: Interspecies correlation between HCFC-22 and HCFC-141b, HCFC-142b, dichloromethane, DCE and PCE during the Bachok campaign.

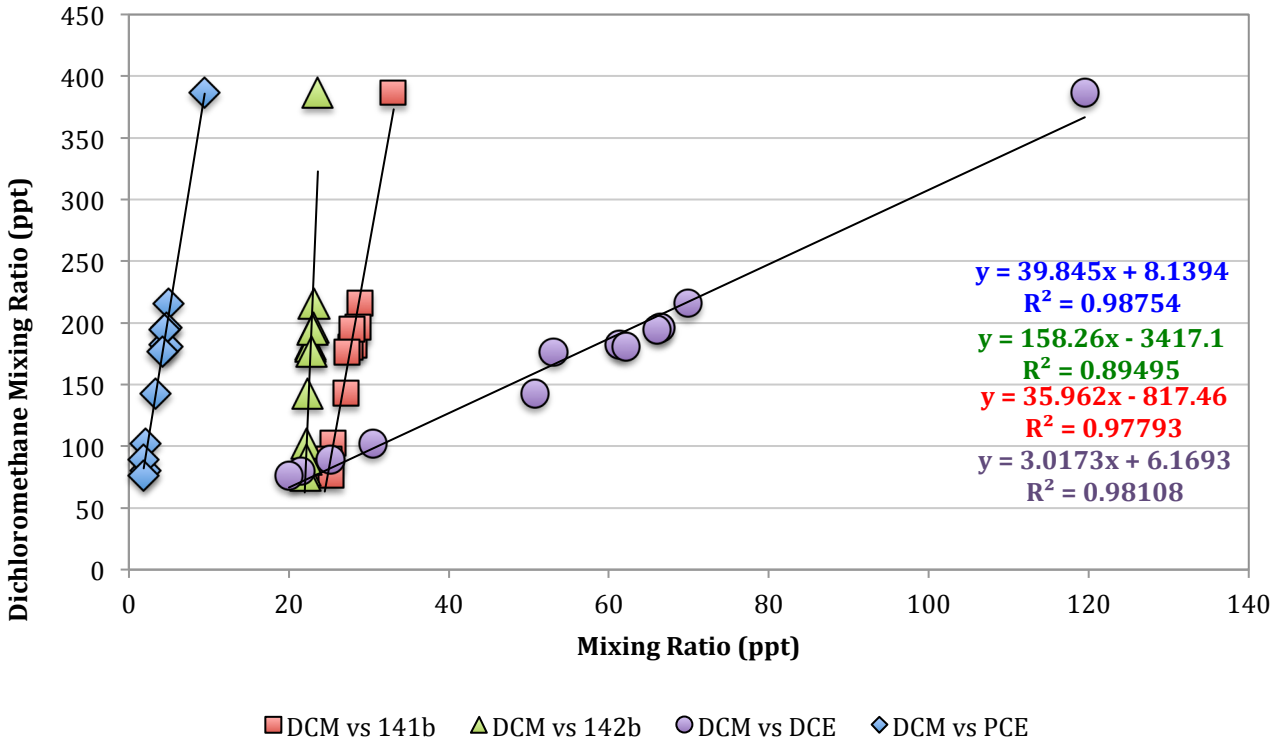

Figure 5.20: Interspecies correlation between dichloromethane and HCFC-141b, HCFC-142b, DCE and PCE during the Bachok campaign.

5.6.4 Estimating Emissions through CO correlation

Whilst no species were found to have excellent interspecies correlation with CO, CFC-113a, halon 1211, halon 1202, HCFCs -22, -133a, 141b and 142b were all calculated to have good correlation as well as dichloromethane, DCE, PCE and chloroform. As such, utilising the emissions data used to separate the CO mixing ratios into industrial and natural sources, emissions estimates for these species are able to be calculated.

Shao et al. (2011) and Wang et al. (2014), studies discussed in chapter 5, both utilised measured CO and assumed an inherent relationship between CO and a number of halocarbon species in order to estimate emissions. This method uses the slope of the linear regression line between the halocarbon species (X) and CO as the molar ratio of the halocarbon relative to CO (X/CO). This is then used in Equation 5.1 to calculate emissions for the halocarbon species.

$$E_x = E_{\mathrm{CO}} \times (X/\mathrm{CO}) \times (M_X/M_{\mathrm{CO}}) \times 10^{-3} \qquad \text{Equation 5.1}$$

Where CO is expressed in ppb and X in ppt and E_{CO} is the inventory emission of CO. As X/CO is a molar ratio, the molecular weights of the species (M_X and M_{CO}) have to be taken into account.

For this work the same equation will be used however, rather than using measured CO, the E_{CO} uses modelled CO. This may be advantageous as it reflects only recently emitted industrial CO from >20°N rather than including local CO or emissions of CO from biomass burning in Indochina. The emitted industrial CO used by Matt Ashfold to calculate the NAME CO tracer values was 80 Tg yr^{-1} for the East Asian region (20-70°N, 70-170°E). Table 5.4 lists the X/CO molar ratios for the 11 halocarbon species found to have good correlation with CO. Whilst these values may appear small, however this is due to the difference of CO being measured in ppb and the other halocarbon species being measured in ppt. Table 5.5 shows the emissions estimated for these species using Equation 6.1 and compares them with previous studies.

Table 5.4: X/CO molar ratios for halocarbon species with good CO correlation

Compound	X/CO
CFC-113a	6.00 x10^{-6}
Halon 1211	7.00 x10^{-6}
Halon 1202	4.00 x10^{-7}
HCFC-22	5.50 x10^{-4}
HCFC-133a	9.00 x10^{-6}
HCFC-141b	1.30 x10^{-4}
HCFC-142b	3.00 x10^{-5}
Dichloromethane	4.82 x10^{-3}
DCE	1.54 x10^{-3}
PCE	1.20 x10^{-4}
Chloroform	2.80 x10^{-4}

Table 5.5: Estimated emissions of halocarbon species with good CO correlation and comparisons with estimates from previous studies in China (2010-2011) and globally (2012)

Compound	E_X (Gg yr^{-1})		
	This Study (Jan 2014)	**China (2010-2011)[a]**	**Global (2012)[b]**
CFC-113a	3.2		2.0 ± 0.7[c]
Halon 1211	3.3		4.8 ±4.5
Halon 1202	0.2		0.26[d]
HCFC-22	135.9	129.3 ± 106.5	366 ±50
HCFC-133a	3.0		3.1 ± 0.7[c]
HCFC-141b	4.5		66 ±8
HCFC-142b	8.6		29 ±6
Dichloromethane	1170.6	284.4 ± 206.6	796.5 ± 180
DCE	435.6	147.2 ±108	
PCE	56.9	40.7 ± 30.5	158.5 ± 31.5
Chloroform	95.6	50.7 ± 38.1	285 ±53

a – Wang et al. 2014 b – Carpenter and Reimann, 2014 c – Laube et al. 2014
d – Newland et al. 2013

When compared with previously estimated emissions for China from Wang et al. (2014), estimates from this study for both HCFC-22 (135.9 Gg yr^{-1}) and PCE (56.9 Gg yr^{-1}) are within uncertainties whereas chloroform (95.6 Gg yr^{-1}) was slightly higher than the upper limit (88.8 Gg yr^{-1}). Dichloromethane (1170.6 Gg yr^{-1}) and DCE (435.6 Gg yr^{-1}) were estimated well outside the range of estimates suggested in literature. Whilst the mixing ratios of these species observed during the Bachok campaign were generally lower than those measured in Wang et. al. (2014), these compounds did have the widest range of detected mixing ratios which resulted in steeper slopes. This may be impacted by their short lifetimes and dilution during long-range transport resulting in a range of abundances where as Wang et al. (2014) measured relatively short-range transport. It may also suggest other sources of these short-lived species may have been sampled during the Bachok campaign, potentially from Taiwan or Vietnam. However, for dichloromethane, the estimated emissions from this campaign were higher than those estimated globally for 2012 (796.5 ± 180 Gg yr^{-1}, Carpenter and Reimann, 2014) suggesting this may be an overestimation anyway.

The other 6 species considered in this study were not measured in Wang et al. (2014) and so have been compared to global estimates for 2012 instead. CFC-113a (3.2 Gg yr^{-1}) was estimated to have slightly higher emissions than those suggested by Laube et al. (2014) and, considering this species is known to be increasing in the atmosphere and its sources are not well known, this could be feasible. HCFC-133a (3.0 Gg yr^{-1}) was also compared to estimates from Laube et al. (2014) and is in line (3.1 Gg yr^{-1}), however Vollmer et al. (2015) found global emissions to be rapidly decreasing for this species after 2011. The data collected during the Taiwan campaigns (see chapter 5) did suggest co-emission of CFC-113a and HCFC-133a, which implies they would both at least partially increase and decrease together.

As such, campaigns to identify the sources and locations of these species are necessary before firm conclusions as to these emissions estimates can be drawn.

Halon 1211 (3.3 Gg yr^{-1}) and halon 1202 (0.2 Gg yr^{-1}) are both estimated to have emissions lower than the global estimates for 2012. As both these species are known to have been phased out under the Montreal Protocol this is as expected. Whilst the estimates for the Bachok campaign would reflect a large portion of the global estimate, this is also feasible as the East Asian region was one of the last areas to phase out these species and has a lot of large banks that may continue to emit for decades to come.

HCFC-141b (4.5 Gg yr-1) and -142b (8.6 Gg yr-1) have global emissions estimates considerably higher than those estimated for the Bachok campaign. Given the global sources of these species as the phase out in developed countries is not yet completed, this is not unexpected and emissions would be expected to be increasing.

Overall, most of the estimated emissions for these halocarbon species appear to be within reasonable limits, aside from those of dichloromethane and DCE. Similar utilisation of this estimation method on other data sets would help to fully assess the limitations and comparison with further studies may aid in evaluating its accuracy. The area for which the modelled CO emissions are calculated may also be refined as it currently includes some areas of India, which are not crossed by the Bachok back-trajectories and so would not contribute to the CO as a tracer species during the campaign.

Given the short-term nature of the campaign, it is also likely that photolysis rates and OH concentrations experienced may have impacted the data collected, particularly in comparison to a global average (Carpenter and Reimann, 2014) or the summer campaign (July-October) of Wang *et al*. (2014). Photolysis rates are higher during the summer months along with hydroxyl radical concentrations (Vaughan *et al*. 2012) both of which contribute to the breakdown of some halocarbon species, particularly the VSLS. As such, the loss of these species before measurement in Wang *et al*. (2014) is likely to have been greater than that seen during the winter campaign at Bachok and so may have led to an overestimation of emissions in comparison. For this estimate, negligible loss was also assumed between emission and measurement, which may be less reflective of summer conditions. With the limited range of emissions studies in the East and Southeast Asian region, coordinated campaigns may be required to fully assess the accuracy of these measurements and any seasonal variation in emissions and their estimates.

Long term campaigns or continued measurement in the region may better identify potential variation in industrial activity as well given that emissions, particularly in China, are known to increase during the winter months. Whilst government restrictions are in place for power plants and vehicles, coal and biomass burning is still widespread, including from residential sources (Lui *et al*. 2016).

This introduces more CO into the atmosphere during the winter months and this difference would need to be quantified and factored into the CO tracer emission value in order to better constrain potential impact to estimates in future winter campaigns.

5.6.5 Calculating an Equivalent Chlorine Budget for the Bachok Campaign

In order to quantify the amount of chlorine potentially being rapidly transported to the upper troposphere during these cold surge events, an equivalent chlorine budget was calculated using all the ODS measured during this campaign.

To achieve this, mixing ratios for each species were multiplied by the number of chlorine atoms in said species for each sample. With bromine-based compounds, at this point the number was also multiplied by 60 as bromine atoms have, on average, 60 times the effect of chlorine atoms on stratospheric ozone (Daniel and Velders, 2007). These values were then combined for each species in a particular compound group for each day sampling took place (average errors for each species also underwent the same process to enable an error margin to also be calculated). This data can be found in Appendix 5.3 and was plotted in Figure 5.21.

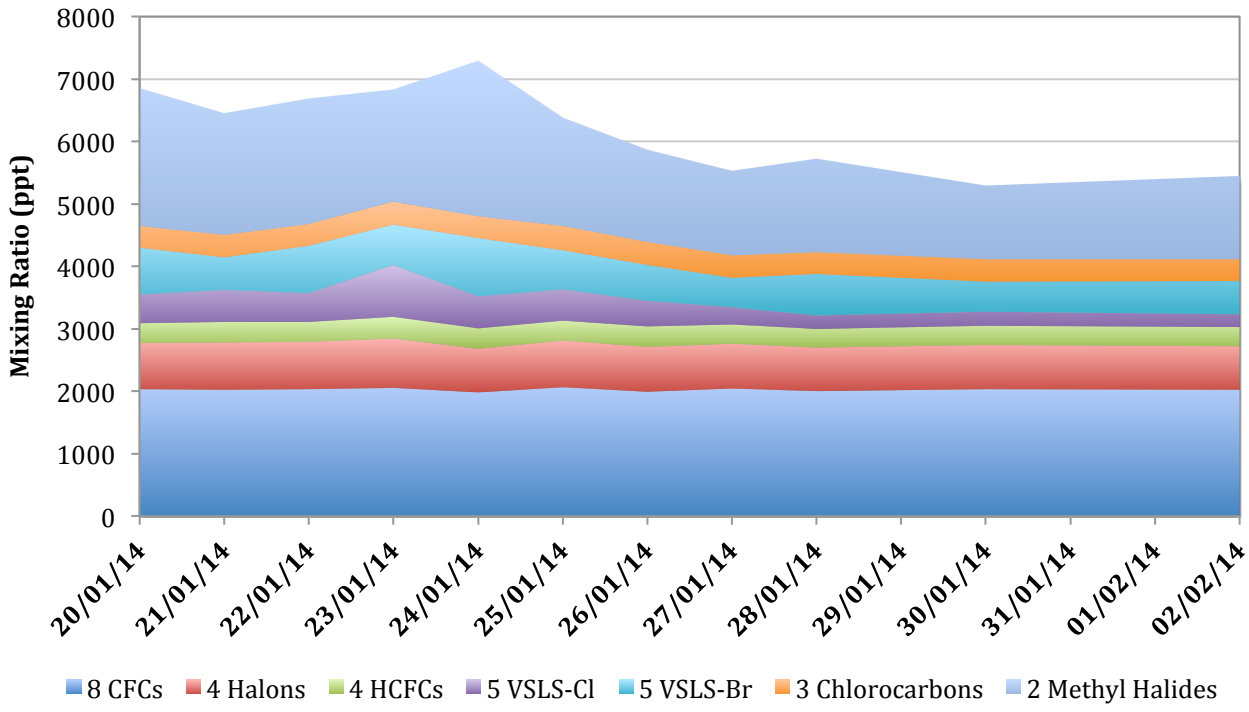

Figure 5.21: Total equivalent chlorine observed in each sample from the Bachok campaign, separated into compound groups.

The equivalent chlorine budget graph shows that the longer lived species i.e. the CFCs and halons, are less affected by the cold surge period and their chlorine contribution is relatively consistent throughout the campaign.

The largest variation is seen in the proportion of chlorine from the short-lived species, particularly during the cold surge when there was increased transport of these species. The methyl halides also contribute a large proportion of equivalent chlorine however, unlike most of the other ODS that make up the graph, a considerable part of that is natural in origin. This is particularly clear as the peak in methyl halide concentrations can be seen on the 24th January, a day when oceanic emissions appeared to dominate, whereas the other groups peak on the 23rd January, when pollution was transported from mainland China.

Whilst this graph does indicate the compound groups most impacted during the cold surge event it also shows that during this period an average of 6594ppt of equivalent chlorine was measured and this decreased to 5500ppt once it was over. To put this into context, the expected global abundance of equivalent chlorine at the marine boundary layer (MBL) was calculated using information from Carpenter and Reimann (2014) for 2012 (see Appendix 5.3). This stated that the contribution from ODS was 3203 ppt with a further addition of 1139 ppt for bromine-based species, 92 ppt for VSLS-Cl and 366 ppt for VSLS-Br. This only totals 4801 ppt, which is around 700 ppt of equivalent chlorine lower than the observations from this campaign during a non-cold surge period, when chlorine concentrations are at their lowest. Figure 5.22 shows a plot of the total equivalent chlorine values calculated from the campaign data, average for the whole campaign as well as averages specifically for the cold surge and non-cold surge period along with the Carpenter and Reimann (2014) 2012 total. Average error margins were calculated for all the Bachok data, Carpenter and Reimann (2014) error margins were combined from those in the report.

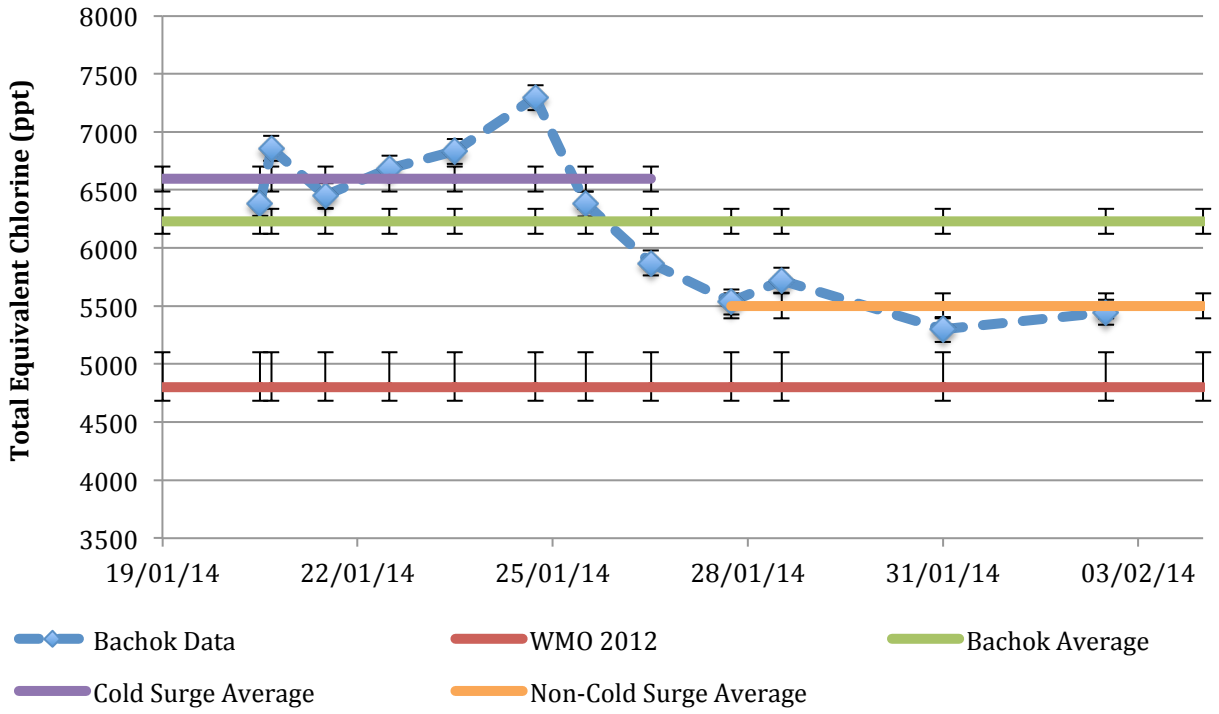

Figure 5.22: Summary of the total equivalent chlorine calculated for the Bachok data (blue) and Bachok average (green) as well as the average for the cold surge period (purple) and the average after (orange). Also shown is the 2012 average total equivalent chlorine as calculated from the WMO report of 2014 (Carpenter and Reimann, 2014). Error bars indicate total calculated uncertainty.

From Figure 5.22 it is clear that, even with error margins, the Carpenter and Reimann (2014) published average global level of equivalent chlorine in the MBL is significantly lower (over 2σ) than the average observed equivalent chlorine level at Bachok (6229ppt). This could be due to the Carpenter and Reimann (2014) data being for 2012 as opposed to being for January 2014 however the total tropospheric chlorine levels have been decreasing in recent years, which would only make this difference more pronounced. What is particularly noticeable is that, comparative to this campaign, Carpenter and Reimann (2014) appears to underestimate the VSLS species. Whilst data from the MBL is not reflective of the mixing ratios that reach the stratosphere, more short-lived chlorinated species (~60%) are transported to the stratospheric entry region than the brominated short-lived species (~36%) due to tropospheric sinks (Carpenter and Reimann, 2014). However, this does indicate that these species may still have significant impact on ozone depletion.

The average VSLS-Cl during the Bachok campaign was ~415 ppt and Oram et al. (in preparation, 2016) reported aircraft data from the CARIBIC (Civil Aircraft for the Regular Investigation of the atmosphere Based on an Instrument Container) project within Southeast Asia to be between 48-330 ppt. Assuming 60% of the Bachok VSLS-Cl would reach this altitude results in an abundance of ~249 ppt which is well within this range. Table 5.6 directly compares the estimated TTL abundance of the individual VSLS-Cl species with observations reported in Carpenter and Reimann (2014) for the level of zero radiative heating, which occurs at approximately 15 km altitude. Air masses at this level are generally considered to enter the stratosphere and so it can be used to derive stratospheric input. This comparison indicates significant differences for all 4 VSLS-Cl species reported, particularly for DCE. However, it is noted in Carpenter and Reimann (2014) that measurements in this region are limited and so data has been scaled to reflect the trends of the boundary layer. Also, the regions in which these reported measurement were collected are not those where the majority tropospheric to stratospheric transport occurs. As such, differences are not unexpected however the magnitude, particularly for DCE, does suggest that this contribution is substantially underestimated.

Table 5.6: Comparison between estimated TTL abundance of VSLS-Cl from the Bachok campaign with reported level of zero radiated heating (LZRH) observations.

VSLS-Cl Species	Estimated TTL abundance from Bachok Campaign (ppt)	LZRH observations (Carpenter and Reimann et al. 2014) (ppt)
DCM	101.2	46.4
DCE	64.6	5.4
Chloroform	51.4	17.1
PCE	7.3	2.8

The average VSLS-Br was also measured at 641ppt during the campaign, which can be used to estimate ~231 ppt would be transported to the TTL. Table 5,7 compares the individual species to observations at the LZRH (Carpenter and Reimann, 2014). Whilst CH_2Br_2 and CH_2ClBr were estimated below the reported abundances, bromoform and $CHClBr_2$ were both estimated above, with bromoform suggested as being almost 70 ppt higher during the Bachok campaign. Given this variation between species, the Bachok campaign only estimates an extra 20 ppt in total more than Carpenter and Reimann (2014). However, the enhanced effect of bromine on stratospheric ozone does means a difference of this size would be a significant contribution to ozone depletion.

Table 5.7: Comparison between estimated TTL abundance of VSLS-Br from the Bachok campaign with reported level of zero radiated heating (LzRH) observations.

VSLS-Br Species	Estimated TTL abundance from Bachok Campaign (ppt)	LZRH observations (Carpenter and Reimann et al. 2014) (ppt)
CH_2Br_2	56.3	88.8
Bromoform	108.0	39.6
$CHClBr_2$	29.5	7.26
CH_2ClBr	4.4	6.1

Given the recent findings of Ashfold et al. (2015) and Oram et al. (in preparation, 2016) in regards to swift long-range transport of pollution to the tropics and then rapid vertical transport to the TTL, this suggests that the impact of short-lived chlorinated and brominated species in the troposphere may not be fully appreciated and further consideration of these species is necessary.

To put this into perspective, Chen e*t al*. (2012) used Lagrangian modelling to estimate around 20% of boundary layer sources for major polluted regions of the Indian subcontinent crossed the tropopause during the summer monsoon. Whilst they state polluted regions of Eastern China had a somewhat smaller contribution, they identified that the Western Pacific, South China and Philippines Seas were the most dominant source domain in the area. Although the summer and winter monsoons of Asia differ in a number of ways, they both have associated weather patterns that result in rapid convection. The majority of studies have focused on the summer monsoon (Ha *et al*. 2012) and little data is available in regards to transport to the tropopause during this period. As such, in order to estimate potential differences between global averages and observations from Bachok, the estimate from Chen *et al*. (2012) will be utilised to suggest an upper bound for potential stratospheric transport.

Given that the following estimate is for a cold surge period when rapid vertical transport occurs, long-lived species were assumed to have only negligible loss during transport. Whilst the VSLS are likely to undergo more substantial loss in this time, the previously mentioned percentages that reach the stratospheric entry region (60% for VSLS-Cl and 36% for VSLS-Br, Carpenter and Reimann, 2014) were utilised again for this calculation.

As such the global average MBL equivalent chlorine mixing ratio from Carpenter and Reimann (2014) was adjusted to 4508 ppt and the average observered cold surge equivalent chlorine mixing ratio was adjusted to 5948 ppt accordingly (see Table 5.8). 20% of each of these values was then found to represent the maximum abundance transported from the boundary layer to the TTL of 902 ppt and 1190 ppt respectively.

Tissier and Legras (2016) suggested that for the North Asian Pacific Ocean, where these convective events occur during cold surges, the average upwards mass flux through the TTL (and so likely to enter the stratosphere) in January is $2.5x10^{9}$ kg s^{-1}. Given that the cold surge measured at Bachok lasted for 6 days, this is an approximate upwards mass flux of $4.8x10^{8}$ kg s^{-1} (see Table 5.9). To estimate what proportion of this may contain the previously calculated equivalent chlorine abundances, these were converted into g L^{-1} values (see Table 5.8). Using the density of dry air at 15 km, the percentage of equivalent chlorine in TTL air was then worked out for both data sets (see Table 5.8). This was then combined with the previously calculated upwards mass flux of a 6 period in January to estimate the mass of equivalent chlorine being potentially transported into the stratosphere (see Table 5.8). For the Carpenter and Reimann (2014) based values, an upwards mass flux of 2.34 kg s^{-1} was estimated whereas the Bachok data was estimated at 3.09 kg s^{-1}, producing a difference of +0.75 kg s^{-1} from observations (see Table 5.9).

Table 5.8: Summary of calculations to estimate upwards mass flux through the TTL for global averaged and observed cold surge equivalent chlorine.

	Carpenter and Reimann (2014)	**Bachok Observations**
Equivalent Chlorine (ppt)	4800.9	6594.0
VSLS Adjusted Equivalent Chlorine (ppt)	4508.5	6391.1
20% (ppt)	901.7	1189.6
20% (g L^{-1})	$9.02x10^{-10}$	$1.19x10^{-9}$
Equivalent Chlorine in TTL air (%)	$4.83x10^{-7}$	$6.38x10^{-7}$
Upwards mass flux through TTL (kg s^{-1})	2.34	3.09
Difference in upwards mass flux (kg s^{-1})	0.75	

Table 5.9: Summary of calculations using data from Tissier and Legras (2016) to estimate the upwards mass flux through the TTL for a 6 day period in January from the North Asian Pacific Ocean Region.

Upwards mass flux through the TTL for North Asian Pacific Ocean (kg s^{-1})	
January	$2.5x10^9$
6 days	$4.84x10^8$

Whilst a difference in this direction was expected, this still suggests nearly that a cold surge may provide nearly a third more additional equivalent chlorine to the stratosphere than that of average global conditions. Cold surges occur around 10 times (Chen *et al.* 2004) during each winter monsoon and so this could represent a significant source of ozone destruction. However, assumptions were made in the production of this estimate and so this would reflect the upper end of a potential stratospheric contribution. Further modelling and campaigns during winter monsoons would be necessary to confirm and fully quantify the difference in stratospheric impact from anticipated and observed equivalent tropospheric chlorine. Increased measurements of VSLS species in the East and South East Asian region would also to be useful in order to reassess their true environmental effect and instigate control measures accordingly.

5.7 Summary and Further Analysis

Overall, many of the ODS measured during this campaign do exhibit increased concentrations during the identified cold surge period and these concentrations do decrease closer to background values once the event is over. This suggests that the increase is due to the transport of emissions from further afield that, due to the stronger wind speeds, are carried faster and so are less diluted when the reach the sampling site.

Concentrations of only one CFC were clearly affected by the cold surge period and that was CFC-113a, the only CFC known to still be strongly increasing in the atmosphere. This was observed at a median of 0.90 ppt during the cold surge, which corresponds to an median enhancement of 75% above the background of 0.51 ppt. Of the halons, the major halon 1211 and the minor halon 1202 both were both impacted by the cold surge with median enhancements above background being 0.19 ppt (5.1%) and 0.007 ppt (40.1%) higher during this period than after. However, halon 1202 also shared distinct similarities in its time series with the three main HCFC species, HCFC-22, -141b and -142b along with the VSLS species dichloromethane, DCE and PCE. The HCFC, -133a, was also influenced by the cold surge period and saw a median enhancement of 0.75 ppt (87 %) above background but its time series was similar with those of CFC-113a and chloroform. For the VSLS-Br compounds, there was some evidence of cold surge impact however days with strong oceanic emissions resulted in the largest spikes in concentrations, as was the case with methyl bromide. Methyl chloride saw clear enhancement due to cold surge conditions as did industrial sourced CO however the measurements for the chlorocarbon species were less well defined.

The main days of interest within this campaign were the 23rd, 24th and 28th January. The 23rd saw significant peak mixing ratios for many of the ODS species transported during the cold surge and was the only day to have a corresponding NAME back-trajectory indicating major influences from further inland of mainland China. The 24th and 28th were both found to be days when emissions from oceanic sources appeared to dominate and, in the case of the 24th, resulted in noticeable decreases in the mixing ratios of many anthropogenic species also measured for that day.

Interspecies correlation during the campaign found excellent correlation coefficients (>0.95) between the three main HCFCs (HCFC-22, -141b and 142b) and the three main VSLS-Cl (dichloromethane, DCE and PCE) suggesting emission sources of all of these species are co-located. Correlation coefficients between CFC-113a, HCFC-133a also indicated co-location of sources for these compounds. Conclusions as to potential co-emission were unable to be clearly drawn to the long-range transport from source regions. Other species that were found to have good correlation coefficients (between 0.75-0.95) with multiple species were halon 1211, methyl chloride and industrial CO.

11 ODS species were found to have good correlation with industrial CO and so the modelled CO emissions were used, along with X/CO molar ratio established from linear regression slopes, to estimate emissions for these species.

The emissions were then compared to similar estimates for China in 2010-2011 (Wang et al. 2014) and global estimates for 2012 (Carpenter and Reimann, 2014, Laube et al. 2014 and Newland et al. 2013). In general, estimates appeared to be within reasonable limits except for dichloromethane (1170.6 Gg yr^{-1}) and DCE (435.6 Gg yr^{-1}), which were significantly above Chinese emissions estimates and, in the case of dichloromethane, above global estimates. HCFC-22 (135.9 Gg yr^{-1}) and PCE (56.9 Gg yr^{-1}) were found to be in line with Chinese estimates from Wang et al. (2014) whereas HCFC-133a was in line with the global estimate for Laube et al. (2014) although the study of Vollmer et al. (2015) would suggest a decrease would have been expected. Further utilisation of this method on other data sets and refinement of the modelled CO emissions is necessary to assess limitations, including increased industrial activity during winter and seasonal variation of photolysis rates and hydroxyl radical concentrations.

Equivalent chlorine (ECl) abundances were calculated for the ODS measured during this campaign and the very short lived chlorine species were identified as having the most variation during and after the cold surge period. Total ECl was found to be, on average, 6229 ppt during the campaign with this increasing to 6594 ppt during the cold surge period only and decreasing to 5500 ppt afterwards. Marine Boundary Layer ECl was calculated from reported values in Carpenter and Reimann (2014) and was found to be significantly lower at 4801 ppt. Comparisons suggested that the impact of VSLS species may be being underestimated, especially given the reported rapid transport to the TTL in the tropics. Stratospheric entry region mixing ratios were calculated from the Bachok data and compared to Carpenter and Reimann (2014). All the VSLS-Cl species were significantly higher, especially DCE, however the VSLS-Br were more varied with only bromoform being notably increased. Further comparison of equivalent chlorine was also carried out, utilising an estimation for upwards mass flux through the TTL for the cold surge period. This suggested that these events may provide a third more equivalent chlorine mass into the stratospheric entry region.

Finally, whilst this campaign gives an indication of the range of ODS being rapidly transported from the mid latitudes of East Asia into the tropics and so into a region where vertical transport to the upper tropical troposphere occurs regularly, only one cold surge event was measured. As such further campaigns are needed to assess if these results are typical for a cold surge event and to establish their impact given the frequency of these systems through the winter months. Analysis of multiple cold surges will enable a more accurate quantification of the mixing ratios of ODS that are increased in the region during these periods and potentially how much may be reaching the upper troposphere.

Increased measurements of VSLS species in both East and South East Asia may help to assess the discrepancies identified between anticipated and observed concentrations through better constraining background mixing ratios and identifying seasonal variations as well as possibly enabling source location. This information could then be used to adjust and improve control measures to better minimise the impact to the stratosphere from these common compounds in this particularly critical region.

Further identification of potential natural sources and methods for separating this data out would also be required to produce a clear understanding of the role long-range transport of anthropogenic emissions is playing with regards to atmospheric composition in this region.

5.8 Key Findings

Of the results presented in this chapter, the key findings of the Bachok, Malaysis sampling campaign are:

- The sampling station in Bachok is able to measure long-range transport of ozone depleting species from East Asia, particularly during cold surge meteorological events. It is located in a region key to rapid stratospheric entry through convection and a wide range of ozone-depleting substances, both long and short-lived, were measurable in the samples collected. Modelled NAME backwards trajectories indicate air masses from China, Korea and Japan as well as Taiwan, Vietnam and the Philippines.
- During the cold surge period, many species were detected at higher abundances than after the cold surge had finished. Many of these species were also enhanced against background, where available. As with Taiwan, the lack of background data for the region limits this significance however the comparison with post-cold surge results appears to confirm these differences are due to variation in air mass and source locations.
- CFC-113a was the only CFC compound to show clear enhancement throughout the cold surge and good correlation was again found with HCFC-133a suggesting co-location of sources.
- The VSLS-Cl species dichloromethane. DCE and PCE were all enhanced during the cold surge and had good interspecies correlation with one another.
- Emissions estimates calculated through correlation with industrial CO where generally within literature ranges aside from dichloromethane and DCE which were much higher. Given the short-lived nature of these species they are potentially underestimated, particularly in global averages. However, analysis of further data sets is necessary to better constrain seasonal and industrial variability.
- Equivalent chlorine calculations and comparisons with literature saw significant differences with total equivalent chlorine being 700 ppt higher during the cold surge than that of the global average marine boundary layer equivalent chlorine.
- Comparisons of VSLS-Cl species calculated to stratospheric entry region abundances with literature were all found to be increased, particularly DCE. Whilst the data in Carpenter and Reimann (2014) for this region has its own limitations, this further suggests that the potential impact of VSLS species, especially in regions of rapid vertical transport, has not been fully recognised.

- Estimations of upwards mass flux through the tropical tropopause layer for the cold surge period suggest up to a third more mass of equivalent chlorine may be entering the region during each cold surge event.
- Continued measurement at the Bachok site will aid in the quantification of long-range transport, particularly of VSLS during meteorological events. The potential impact of these species to the stratosphere through rapid vertical transport in the region requires more data in order for an accurate and conclusive assessment to be made.

Chapter 6: Conclusions and Outlook

The focus of this thesis was on halogenated hydrocarbons in the atmosphere that act as greenhouse gases and/or deplete stratospheric ozone and the importance of sources and emissions in the East and South East Asian regions. This chapter summarises the main outcomes of this work and identifies how the resulting information may be utilised to direct further study and investigation.

6.1 Analysis of methyl halide production from plants

Methyl halides are produced from a range of plant species in significant amounts that ultimately contribute to the depletion of stratospheric ozone. Whilst human control of plant-based emissions is limited, agriculturally grown crops such as rice and rapeseed are of particular interest given their increasing productions in response to a growing global population. Identification and understanding of the genes that regulate methyl halide production could lead to the manipulation of crop species to develop 'ozone-safe' plants, with zero or low emissions of methyl halides. With the extensive farming of rice in the Asian region, an area identified as experiencing regular and rapid vertical air mass transport to the stratosphere, the introduction of 'ozone-safe' species could dramatically reduce methyl halide emissions and so their impact on ozone depletion.

In Chapter 3, mutant *Arabidopsis thaliana* plants, in which the *HARMLESS TO OZONE LAYER* (*HOL*) gene was inactive, were found to emit methyl chloride, methyl bromide and methyl iodide at rates on average 95% lower than those of wild type plants. This not only confirms the involvement of the gene in methyl halide production but indicates that this pathway can be successfully altered in plants without detrimental effect to their growth. This property is particularly necessary for the development of 'ozone-safe' agricultural species as poor growth, reduced yield or lack of disease-resistance would make genetically altered plants less desirable to commercial farmers.

Emissions of transgenic *A. thaliana* plants were evaluated to establish whether similarities in the genetic coding of the *HOL* gene from other species could mediate methyl halide production in *Arabidopsis*. Genes from rice, moss (*Physcomitrella patens*) and diatoms were utilised. However, only samples with the moss *HOL* gene were found to produce significant emission rates for all three methyl halide species measured, and these were between 86-120% higher than those of *A. thaliana* mutants. The lack of pronounced emissions with the rice and diatom transgenic plants is unsurprising given the variation in plant evolution resulting in the genetic coding of the *HOL* genes for these species including many differences to that of *A. thaliana*. As such, this could suggest that different species may require different genetic manipulation in order to successfully render the *HOL* gene inactive and individual procedures may need to be developed for each species of interest, requiring further time and research.

Comparison of methyl halide emissions from *P. patens* wild type plants and those with the *HOL* gene removed indicated at least partial involvement of the gene in methyl bromide production.

Given that mosses are evolutionally ancient species relative to *A. thaliana*, this indicates that methyl halide production is part of a similarly ancient mechanism in plants. As the exact purpose of this production pathway is currently unknown, this limits the understanding of how manipulation of the *HOL* gene may ultimately impact plant species during large scale growth. Phylogenetic analysis shows divergence of *P. patens* and *A. thaliana* took place over 350 million years ago, indicating the methyl halide production property must have evolved before this time. This could suggest its purpose may be related to the ancient atmosphere or ancient soil conditions which may be relatively irrelevant in the present day.

Results of preliminary experiments into the effect of temperature on methyl halide emissions indicated a positive relationship with both *A. thaliana* and *P. patens*. This suggests that the production of methyl halide species from plants may increase as global temperature rises and this increase may be larger than the 10% per 1°C higher as suggested by previously modelled studies With methyl chloride and methyl bromide both having global warming potentials higher than carbon dioxide, these emissions could further contribute to increasing global temperatures. As such the development of 'ozone-safe' plant species may help control agricultural contributions to global warming as well. Minor differences were noted in the temperature-dependent effect on *HOL*-modified plants for each species which may be due to differences in genetic coding developed during evolution however further experimentation is needed to confirm this.

Data from these experiments in Chapter 3 was utilised to establish initial estimates as to the impact of replacing the entire global rice crop with genetically modified 'ozone-safe' species. This resulted in significant reductions in emission rates of 94.7% and 97.2% for methyl chloride and methyl bromide respectively. These calculations suggest that the continued expansion of rice production in response to increasing populations when using 'ozone-safe' species would cause only a negligible increase on global methyl halide abundances. As such, continued development of these species is vital in establishing a method to control and restrict the emissions of methyl halide species from agricultural sources, particularly in regions of rapid atmospheric transport like Asia.

6.2 Halocarbon observations in Taiwan

East Asia is a region that, in recent years, has undergone rapid industrialisation and so is a major source of halocarbon emissions. Although a number of field campaigns have been carried out in East Asia, many of these do not assess the wide range of detected halocarbon species, particularly minor compounds and very short-lived substances. Multi-year campaigns have also been limited and so changes in detected abundances or emissions are less clear due to the consideration of multiple methods and their associated uncertainties.

The work in Chapter 4 analysed a wide range of halocarbon species, including a number of recently detected minor species and several short-lived substances, over three short-term air sampling campaigns based in Taiwan. This data is able to widen the overall knowledge of halocarbon mixing ratios in the East Asian region and provide reference for future campaigns. Similarly, comparison of abundances with other campaigns outside of Asia is also possible, as was the case with the study of HCFC-133a by Vollmer *et al*. (2015).

Backwards trajectory analysis utilising the Numerical Atmospheric-dispersion Modelling Environment (NAME) allowed for estimation of potential source locations. China, Korea and more locally Taiwan were regularly identified as probable origins of halocarbon species throughout all three campaigns. Interspecies correlations were also utilised similarly to previous studies to suggest the presence of potentially co-located or co-emitting sources.

The majority of the halocarbon species measured were detected at abundances that reflected Montreal Protocol phase out schedules or were similar to comparative background values. Summarised below are the main findings for these species.

The major CFCs, -11 and -12 along with the minor CFCs, -13 and -115, were detected at abundances that reflected the legislative phase out of these species. Modelling suggested China, Korea and Japan as potential source locations for pollution events however the lack of interspecies correlation found for these compounds reflects their previously widespread use across the region and so varied potential origins as well as the lack of pronounced pollution events.

The halons -1301 and -2402 were also measured at concentrations in line with global legislation whilst China and Korea were indicated as a potential source of -1301 and Taiwan for -2402. Interspecies correlation was identified with several HCFC and HFC species, likely due to their widespread use as CFC and halon replacements.

Detected abundances suggested regional sources of HCFC-22 and -141b were decreasing, conversely to HCFC-142b. All 3 species saw increased enhancement during the 2014 campaign reinforcing the likelihood of extensive Chinese sources.

Carbon tetrachloride, methyl chloroform and halothane were all indicated as having potential sources in China as well as Japan, Taiwan and Korea respectively.

Enhancement above background mixing ratios of methyl chloride and methyl bromide were both likely influenced by natural sources (see examples in Chapter 3) although interspecies correlation with very short-lived species indicates potential industrial Chinese sources as well.

The VSLS species, dichloromethane, 1,2-dichlorethane, chloroethane, chloroform and tetrachloroethane were identified as having likely sources in China along with possible emissions originating in Taiwan for 1,2-dichloroethane and chloroethane. Interspecies correlation was found between these species and other extensively used ozone depleting substances.

HFCs -134a, -23, -125, 143a and 152a along with the minor -245fa, 227ea and 365mfc were generally observed to have increasing median abundances across the 3 campaign and backwards trajectories suggested China and Taiwan for all species. Interspecies correlations were identified with HCFCs and VSLS species.

Of the PFCs measured, only observations of C_3F_8 and C_5F_{12} suggested changes in regional emissions. C_2F_6, cyclic-C_4F_8, C_4F_{10} and C_7F_{16} were detected at abundances reflecting previously reported growth rates. Modelling and interspecies correlation indicated potential Chinese and Korean sources for all PFC species. Also, the isomers n-C_6F_{14} and iso-C_6F_{14} were measured during the 2015 campaign and their excellent correlation with each other implies these species are co-emitted.

Finally, carbonyl sulphide was suggested to have emission originated in China and Korea whilst SF_5CF_3 saw influence from Taiwan when pollution events occurred. Carbon monoxide abundances suggested less polluted air masses were sampled in 2015 and ozone fluctuations were likely due to normal fluctuations, for a region heavily influenced by pollution, across all 3 campaigns.

However, the minor CFCs, -113, -113a, -114 and -114a, along with halon-1211, halon-1202 and HCFC-133a, were detected at unanticipated concentrations or were found to exhibit unexpected interspecies correlations. As well as this, a number of short-chain PFCs were measured during significant pollution events in the 2014 campaign and the relatively unknown c-C_5F_{10} was detected during the 2015 campaign. The conclusions drawn from the data for each of these species is summarised below.

The minor isomeric CFCs, -114 and 114a, were only measured during the 2015 campaign and were found not to correlate with each other indicating the likelihood of different sources and so a lack of co-emission in contrast to what would be expected for many isomers. Enhancement above background abundances was seen, particularly for CFC-114a, suggesting there may be continued emissions in the region. Emissions of isomeric compounds are reported combined by countries and so sources of CFC-114a are less well known. As such, if emissions are continuing then identification of source locations is particularly important in order to ensure Montreal Protocol restrictions are being followed. NAME analysis suggests China as a potential source region however a more quantified analysis would enable confirmation and possibly identify a specific region to focus a more targeted sampling campaign in. These results were published as part of Laube *et al*. (2016)

A relationship between the isomeric CFC-113 and CFC-113a and HCFC-133a was identified during the Taiwan campaigns. Consistent enhancements above background mixing ratios suggested continued emissions of all three species in the region. The very good to excellent correlation between these species indicated potential co-emission or at least very close co-location of sources, which has not previously been reported. Knowledge on the exact sources and quantities of CFC-113a and HCFC-133a emissions are limited however all three of these species are utilised in the production of the HFCs -134a and -125. These HFCs are both extensively used across East Asia and whilst preventative measures are in place to minimise fugitive emissions during production, the correlation observed suggests this could be a potential source. Given that CFCs have been phased out by the Montreal Protocol and HCFCs are currently being phased out, the identification of sources is imperative in ensuring full compliance in East Asia, particularly as global abundances for CFC-113a are still increasing. Preliminary back trajectory comparisons indicate Chinese and Korean emissions as being the main influences on days when pollution events were detected for these species. Regular monitoring within the region would help confirm this and also enable better detection of any further changes in the global trend for HCFC-133a, as suggested in Vollmer et al. (2015) who found global emissions of this compound peaked in 2006 and 2011 followed by declines into 2009 and 2015 respectively. Future comparison of this trend with those of CFC-113 and -113a may improve understanding as to the relationship between these species and their sources as well.

The relationship between the major and minor halons, -1211 and -1202 respectively, was also considered. The main source of halon-1202 emissions has previously been suggested as a by-product during halon-1211 production and given the completed phase-out of the halons, enhanced abundances and correlation between the two species was not expected. During the 2013 campaign there was little evidence of this correlation and back trajectories indicated that halon-1202 pollution events were likely due to Korean emissions, potentially from US military sources. However, good correlations were observed during the 2014 and 2015 campaigns and given that contamination of halon-1211 banks has not previously reported, this could potentially be an indication of continued production of halon-1211, which would go against global control measures. However, regional emissions for both species appear to be decreasing as abundances have lessened each year although this could reflect interannual variability as well. Continued emissions of these halons would contribute to both ozone depletion and global warming and so, as the exact sources of halon-1202 are not well known, further campaigns into locating and analysing these would be beneficial. Also, establishing whether there is a -1202 presence in -1211 banks, is necessary to ensure legislation is being adhered to in the East Asian region.

For the very short-lived chlorinated substances, the three campaigns in Taiwan saw median abundances of dichloromethane, 1,2-dichloroethane and chloroethane decreased whilst chloroform and tetrachloroethene medians increased over this period. Preliminary analysis indicated that all 5 species have sources in China although both 1,2-dichloroethane and chloroethane were suggested to potentially have local Taiwanese sources as well. Correlation was generally found between these short-lived species along with other ozone depleting substances used extensively in Chinese industry.

Given that VSLS species are currently not controlled by global legislation and the importance of the East Asian region in the rapid stratospheric transport of air masses, the large emissions suggested for some of these species by these campaigns may be particularly damaging to the ozone layer. Regular regional monitoring and comparison with meteorological events would be useful in estimating the impact these species may have. Further campaigns would enable trends to be assessed and emphasise the need for VSLS to be added to the Montreal Protocol.

Significant pollution events occurred amongst the short-chain PFCs, C_2F_6, C_3F_8, c-C_4F_8 and SF_6, during the 2014 campaign. Local wind data and back-trajectories were compared and emissions from Taiwanese sources were suggested as impacting these specific days. Very good and excellent correlation between these species also indicated there were co-located sources, which is plausible given their similar applications. Comparing the location of local industrial parks with the directional wind data for the samples, which exhibited these high abundances identified potential locations for sources of these emissions. As Taiwan has extensive semi-conductor and electronic manufacturing industries that utilise PFCs and only one campaign was measured at the northern site, further campaigns in this area would be desirable to fully assess the full influence of these potential sources and the associated emissions rates. As the impact of PFCs on the environment is significantly long-term due to their atmospheric lifetimes, efforts to quantify and minimise emissions are needed at both an industrial level as well as through global legislation.

Cyclic-C_5F_{10} was measured during 2015 only and very little is known about the applications or emissions of this species. The preliminary location of potential sources was suggested by NAME as being Korea and Japan although Chinese emissions were also suggested to influence some of the pollution events observed. Some interspecies correlation was found with compounds have also been suggested to have potential Chinese sources. As this is a relatively novel species, understanding as to its potential environmental impact is limited and so continued monitoring and analysis would be required to ensure appropriate control measures are implemented in the future.

6.3 Long-range transport of ozone depleting substances to Bachok, Malaysia

In Chapter 5, a recently established atmospheric monitoring site in Bachok, Malaysia was utilised in an air sampling campaign to assess the abundances of ozone depleting substances during a weather phenomenon known as a cold surge. This weather system occurs multiple times a year during the East Asian winter monsoon and cause abrupt drops in temperature and very strong winds that across the South China sea and so may transport pollution to Malaysia. Recent studies have suggested that air masses transported into the tropics may subsequently be rapidly transported to the upper troposphere through convection, which is increased during these cold surge periods. This means that ozone depleting substances, particularly those short-lived species usually considered to have minimal impact, may reach the stratosphere more quickly and so result in more ozone being destroyed than previously anticipated. This work aimed to assess the abundances of these species during and after a cold surge event and compare this data with previously reported contributions to identify if there was a significant difference.

In general, the majority of ozone depleting substances measured were found to exhibit increased contributions during the cold surge period of the sampling campaign. CFC-113a saw a median abundance during this period of 0.90 ppt, 25% above the post cold surge median whilst halons -1211 and -1202 were observed at medians of 4.1 ppt (+5.1%) and 0.03 ppt (+40.1%) respectively. Similarly, the HCFCs all saw increased abundances during the cold surge with HCFC-133a seeing the largest median enhancement of 50% to 0.75 ppt, compared to after the cold surge event, whilst HCFC-22 reached 247 ppt (+5.6%), -141b rose to 28 ppt (+12%) and -142b reached 23 ppt (+4.5%). This indicates there is increased long-range transport of emissions due to the stronger winds and so the proportion of pollution with the potential to be rapidly transported to the stratosphere is higher than during non-cold surge periods. This suggests contributions to both ozone depletion and global warming will also increase during these events.

Short-lived chlorinated species in particular saw significant enhancement above background mixing ratios, which did decline post-cold-surge but remained elevated as compared to expected background levels. Specifically, dichloromethane was observed at a median abundance of 190 ppt during the cold surge, 224% higher than the post-cold surge median abundance of 85 ppt. Likewise during the cold surge, 1,2-dichloroethane had a median concentration of 64 ppt (+278%), PCE rose to 4.6 ppt (+230%), chloroform reached a median of 24 ppt (+160%) and chloroethane rose to 25 ppt (+179%), compared to the post-cold surge medians. Given that these species are not currently controlled by global legislation, the abundances detected suggest substantial emissions which, due to the potential rapid vertical transport in the region, could significantly impact ozone depletion despite their short atmospheric lifetimes.

NAME analysis was utilised and potential sources were suggested across the East Asian region, including China, Korea, Japan and Taiwan. Interspecies correlation was also compared and the suggested co-location of some halocarbons, particularly for species of interest such as the minor CFC-113a and its isomer -113, may further be confirmed or identified by a more quantitative NAME approach.

Correlation of a number of halocarbon species with industrial CO was used to estimate emissions, which were then compared to previous studies, both regionally and globally. Most species estimated were found to be within reasonable limits. However the short-lived species, dichloromethane and 1,2-dichloroethane, were found to be significantly higher than earlier estimates at 1170.6 Gg yr^{-1} (+412% on 2010-2011 estimated Chinese emissions, Wang *et al*. 2014) and 435.6 Gg yr^{-1} (+296% compared to Wang *et al.* 2014 also) respectively. This suggests that emissions of these species may have been underestimated previously or may still be growing, particularly given the lack of restrictions in place for their production and consumption. As discussed previously, given the convective transport in the region, the proportion of these species reaching the stratosphere may be much higher than anticipated thus further impacting ozone depletion.

Calculations as to the equivalent chlorine abundance for the ozone depleting substances measured was found to be highest during the cold surge period and this was significantly larger (+1793.2 ppt) than that estimated from reported tropical tropopause layer mixing ratios taken from the most recent WMO study (Carpenter and Reimann, 2014). Similarly, comparison of calculated stratospheric entry region mixing ratios and an estimation for upwards mass flux through the tropical tropopause layer during the cold surge period both indicated increased equivalent chlorine concentrations and large contributions from very short-lived species. This suggests that the impact of these species may have been underestimated and highlights the need for their introduction into global legislation. Controls on their production and use in an important stratospheric entry region like East Asia would aid the continuing recovery of the ozone layer.

6.4 Thesis Outcomes

The individual chapters of this thesis were linked through their relation to the emissions and observations of halocarbon species and the East and South East Asian regions. Identified within this work, through air sampling, were a wide range of compounds, both of natural and anthropogenic origin, that can contribute to ozone depletion and global warming. The data sets produced by in Chapters 4 and 5 have extended knowledge, particularly of anthropogenic halocarbons utilised within the region, through the measurement of minor and novel species whilst the study on genetic modification of plants has considered the natural emissions of methyl halides and their potential impact in this area.

The combination of these chapters highlights the importance of this region in regards to the further degradation of the ozone layer. When considered alongside the rapid vertical atmospheric transport discussed in Chapter 5, the emissions of halocarbon compounds indicated in Chapters 3 and 4 have the potential to undergo this process and so may have a larger contribution to ozone depletion that previously anticipated. Evidence of continued emissions and long-range transport is necessary to assess and implement the control measures needed to reduce this. The results of Chapter 3 have suggested a long-term method of minimising emissions from rice crops in Asia whereas those of Chapters 4 and 5 have emphasised species that require further monitoring or addition to global legislation, such as CFC-113a and the chlorinated VSLS compounds, in order to reduce atmospheric impact from emissions. Without intervention such as this, previous progress made in the reduction of ozone destruction is at risk of being slowed or eventually reversed.

Ultimately it is hoped that the results and conclusions discussed in this thesis can be utilised and extended through future campaigns to better constrain and monitor halocarbon species emitted and transported throughout this region.

6.5 Suggestions for Future Work

Chapter 3 – Analysis of methyl halide production in plants

Before the development of 'ozone-safe' crops can fully come to fruition, there is much that still needs to be done. A clearer understanding of the purpose of methyl halide production in plants is necessary to predict and counteract any potential impact on plant growth or health from deactivating the genes involved in the pathway. Experimentation involving the related glucosinolate pathway and the measurement of emissions of related species such as acetonitrile in plant species with and without genetic modification may shed further light onto methyl halide production.

Further comparison of the genetic coding for the *HOL* gene between different species may help to identify key sections related to function and evaluate differences that could result in different procedures needed to fully deactivate said gene. Continued study into developing excessive expression of the *HOL* gene (i.e. increased methyl halide production) outside of *A. thaliana* may also allow for more widespread analysis of species of interest as well.

Finally, confirmation of the relationship of methyl halide production and temperature is required through further experimentation and analysis. Comparison of *A. thaliana* and *P. patens* results with those of a more ancient species such as Liverwort could not only increase understanding of *HOL* gene evolution but suggest a potential purpose for methyl halide production linked with environmental conditions. Research into the changing global ecosystem since the evolution of this pathway could suggest why it evolved and may indicate current day impact if widespread cultivation of 'ozone-safe' species were to occur.

Chapter 4 – Halocarbon observations in Taiwan

Overall, whilst the short-term sampling campaigns in Taiwan provided abundance data for a wide range of halocarbon species, further campaigns are needed to better identify potential trends from interannual variation. Regular, long-term monitoring through the construction of a continuous sampling site in Taiwan would both aid this and enable the calculation of a robust background more relative for the region. Comparative to Europe and the United States, widespread sampling in East Asia is limited and this study has shown Taiwan's location to be useful in assessing continental outflow. As such global assessments for both major and minor halocarbon species would benefit from a from a site such as this.

Combined with a more quantitative analysis of modelled backwards trajectories from NAME, this may also allow for better identification of source locations during pollution events. This could help to better constrain previously unknown or potentially unregulated sources as well as allowing for comparison with emission inventories within the region. Further understanding of the uses and locations of particular species of interest may enable better control and management through regional and global legislation.

Chapter 5 – Long-range transport of ozone depleting substances to Bachok, Malaysia

Overall, this campaign established a wide range of ozone depleting species are rapidly transported to the tropics from the mid-latitudes of East Asia. As only one cold surge event was measured during this campaign it is imperative that further campaigns assess the impact of more cold surges before firm conclusions can be drawn. Continuous monitoring at Bachok would both identify if the results established from this campaign proved typical and allow for more robust background abundances for the region to be developed. Air-based sampling campaigns to measure vertical transport would also be desirable and aid in quantifying the abundances of species reaching the upper troposphere and so potentially the stratosphere. Regular measurement of both minor and short-lived species in particular would aid the understanding of long-range anthropogenic emission transport in the region and its reflection on the atmospheric composition of the area. Data such as this could provide evidence to support the addition of short-lived halocarbon species to global legislation.

A further quantitative analysis of the NAME modelled data for this and future campaigns would better constrain potential sources and enable comparison of known emissions data with detected halocarbon abundances. This in turn may aid in the further control through production and consumption restrictions of ozone depleting species.

Also, comparison of emissions estimates calculated from further and future data sets and refinement of the modelled CO emissions is necessary in order to better constrain the limitations of the model and so improve the reliability of the data produced. This could then be used in contrast with known emissions inventories to identify potential discrepancies that may need to be addressed in order to ensure global legislation is being fully adhered to.

References

A

Agarwal, R. S., et al. (2002) *2002 report of the refrigeration, air conditioning and heat pumps technical options committee*, 193–197, United Nations Environment Programme, Ozone Secretariat, Nairobi, Kenya.

Agilent Technology (2016) *GS-GasPro Specifications* [Online] Available on: https://www.agilent.com/en-us/products/gas-chromatography/gc-columns/capillary/gs-gaspro [Accessed on 3rd May 2016].

Agilent Technology (2016b) *GS-GasPro Column Information* [Online] Available on: http://www.agilent.com/en-us/products/gas-chromatography/gc-columns/capillary/gs-gaspro/gs-gaspro [Accessed on 3rd May 2016]

Agilent Technology (2016c) *CP-Al_2O_3/KCl Specifications* [Online] Available on: http://www.agilent.com/en-us/products/gas-chromatography/gc-columns/capillary/cp-al2o3-kcl [Accessed on 3rd May 2016].

Ahrens, C.D. (2008) *Essential of Meteorology: An Invitation to the Atmosphere*. Thomson Brooks/Cole, California, USA.

Allin, S.J. (2015) *Trace gases in Antarctic and Greenland firn and ice: a record of carbonyl sulphide and the isotopologues of chlorofluorocarbons.* Doctoral Thesis, University of East Anglia.

Allin, S.J., Laube, J.C., Witrant, E., Kaiser, J., McKenna, E., Dennis, P., Mulvaney, R., Capron, E., Martinerie, P., Röckmann, T. and Blunier, T. (2015) Chlorine isotope composition in chlorofluorocarbons CFC-11, CFC-12 and CFC-113 in firn, stratospheric and tropospheric air. *Atmospheric Chemistry and Physics*. **15** (12), 6867-6877.

Amachi, S., Kamagata, Y., Kanagawa, T. and Muramatsu, Y. (2001) Bacteria mediate methylation of iodine in marine and terrestrial environments. Applied and Environmental *Microbiology*. **67**, 2718-2722.

Amsden, A. H. (1995) Like the rest: South-East Asia's 'late' industrialization. *Journal of International Development*. **7** (5), 791-799.

An, X., Henne, S., Yao, B., Vollmer, M.K., Zhou, L. and Li, Y. (2012) Estimating emissions of HCFC-22 and CFC-11 in China by atmospheric observations and inverse modelling. *Science China*. **55** (10), 2233-2241.

Andreae, M. O. and Crutzen, P. J. (1997) Atmospheric aerosols: Biogeochemical sources and role in atmospheric chemistry, *Science*, **276** (5315), 1052-1058.

Armeanu-D'Souza, K. (2009) *Saving the ozone layer from oilseed rape*. MSc Thesis. University of East Anglia. Norwich, UK.

Armstrong, D.W., Reid, G.L. and Luong, J. (1996) Gas Separations: A Comparision of GasPro™ and Aluminium Oxide PLOT Columns for the Separation of Highly Volatile Compounds. *Current Separations*, **15**, 5-11.

Arnold, T., Ivy, D.J., Harth, C.M., Vollmer, M.K., Muhle, J., Salameh, P.K., Steele, L.P., Krummel, P.B., Wang, R.H.J., Young, D., Lunder, C.R., Hermansen, O., Rhee, T.S., Kim, J., Reimann, S., O'Doherty, S., Fraser, P.J., Simmonds, P.G., Prinn, R.G. and Weiss, R.F. (2014) HFC-43-10,ee atmospheric abundances and global emissions estimates. *Geophysical Research Letters*. **41**, 2228-2235.

Ashfold, M.J., N.R.P. Harris, A.J. Manning, A.D. Robinson, N.J. Warwick, and J.A. Pyle, (2014) Estimates of tropical bromoform emissions using an inversion method, *Atmospheric Chemistry and Physics*. **14** (2), 979-994.

Ashfold, M.J., Pyle, J.A., Robinson, A.D., Meneguz, E., Nadzir, M.S.M, Phang, S.M., Samah, A.A., Ong, S., Ung, H.E., Peng, L.K., Yong, S.E. and Harris, N.R.P. (2015) Rapid transport of East Asian pollution to the deep tropics. *Atmospheric Chemistry and Physics*. **15**, 3565-3573.

ATSDR [Agency for Toxic Substances and Disease Registry] (1998) *Toxicological Profile for Chloromethane (Update).*U.S. Public Health Service, U.S. Department of Health and Human Services, Atlanta, GA.

Attieh, J. M., Hanson, A. D. and Saini, H. S. (1995) Purification and characterization of a novel methyltransferase responsible for biosynthesis of halomethanes and methanethiol in *Brassica oleracea*. Journal of *Biological Chemistry*. **270**, 9250-9257.

Attieh, J., Kleppinger-Sparace, K. F., Nunes, C., Sparace, S. A. and Saini, H. S. (2000) Evidence implicating a novel thiol methyltransferase in the detoxification of glucosinolate hydrolysis products in *Brassica oleracea* L. *Plant Cell and Environment.* **23**, 165-174.

Attieh, J., Djiana, R., Koonjul, P., Etienne, C., Sparace, S. A. and Saini, H. S. (2002). Cloning and functional expression of two plant thiol methyltransferases: a new class of enzymes involved in the biosynthesis of sulfur volatiles. *Plant Molecular Biology.* **50**, 511-521.

Aydin, M., Williams, M. B., Tatum, C., and Saltzman, E. S. (2008) Carbonyl sulfide in air extracted from a South Pole ice core: a 2000 year record, *Atmospheric Chemistry and Physics*, 8, 24, 7533-7542.

B

Bais, H. P., Weir, T. L., Perry, L. G., Gilroy, S. and Vivanco, J. M. (2006) The role of root exudates in rhizosphere interations with plants and other organisms. *Annual Review of Plant Biology.* **57**, 233-266.

Barletta, B., Meinardi, S., Simpson, I.J., Atlas, E.L., Beyersdorf, A.J., Baker, A.K., Blake, N.J., Yang, M., Midyett, J.R., Novak, B.J., McKeachie, R.J., Fuelberg, H.E., Sachse, G.W., Avery, M.A., Campos, T., Weinheimer, A.J., Rowland, F.S. and Blake, D.R. (2009) Characterization of volatile organic compounds (VOCs) in Asia and north America pollution plumes during INTEX-B: identification of specific Chines air mass tracers. *Atmospheric Chemistry and Physics*. **9**, 5371-5388.

Bernstein, L., Roy, J., Delhotal, K.C., Harnisch, J., Matsuhashi, R., Price, L., Tanaka, K., Worrell, E., Yamba, F., and Fengqi, Z. (2007) Industry. In: Metz, B., Davidson, O.R., Bosch, P.R., Dave, R. and Meyer, L.A. eds. *Climate Change 2007: Mitigation. Contribution of Working Group III to the Fourth Assessment Report of the Intergovernmental Panel on Climate Change*. Cambridge University Press, Cambridge, United Kingdom.

Bonner, C.S., Ashley, M.C.B, Cui, X., Feng, L., Gong, X., Lawrence, J.S., Luong-Van, D.M., Shang, Z., Storey, J.W.V., Wang, L., Yang, H., Zhou, X. and Zhu, Z. (2010) Thickness of the atmospheric boundary layer above dome A, Antarctica, during 2009. *Astronomical Society of the Pacific*. **122**, 1122-1131.

Boucher, O., Haigh, J., Hauglustaine, D., Haywood, J., Myhre, G., Nakajima, T., Shi, G.Y. and Solomon, S. (2001) Radiative Forcing of Climate Change. In: *Climate Change 2001: The Scientific Basis* [Houghton, J.T., Ding, Y., Griggs, D.J., Nouger, M., van der Linden, P.J., Dai, X., Maskell, K. and Johnson, C.A. (eds.)], Cambridge University Press, Cambridge.

Brioude, J., Portmann, R.W., Danial, J.S., Cooper, O.R., Frost, G.J., Rosenlof, K.H., Granier, C., Ravishankara, A.R., Montzka, S.A. and Stohl, A. (2010) Variations in ozone depletion potentials of very short-lived substances with season and emission region. *Geophysical Research Letters*. **37** (L19804), 1-5.

Bruhl, C., Lelieveld, J., Crutzen, P.J. and Tost, H. (2012) The role of carbonyl sulphide as a source of stratospheric sulphate aerosol and its impact on climate. *Atmospheric Chemistry and Physics*. **12**, 1239-1253.

Butler, J.H., Battle, M., Bender, M.L., Montzka, S.A., Clarke, A.D., Saltzman, E.S., Sucher, C.M., Severinghaus, J.P. and Elkins, J.W. (1999) A record of atmospheric halocarbons during the twentieth century from polar firn air. *Nature*. **399**, 749-755.

C

Calm, J.M. (2008) The next generation of refrigerants – Historical review, considerations, and outlook. *International Journal of Refrigeration*. **31**, 1123-1133.

Carpenter, L.J. and Reimann, S. [Lead Authors] (2014), Ozone-Depleting Substances (ODSs) and Other Gases of Interest to the Montreal Protocol, Chapter 1 in *Scientific Assessment of Ozone Depletion: 2014*, Global Ozone Research and Monitoring Project-Report No. 55, World Meteorological Organization, Geneva, Switzerland

Chapman, S. (1930) A theory of upper-atmospheric ozone, *Memoirs of the Royal Meteorological Society*. **3**, 26, 103-125.

Chen, T.S., Yen, M.C., Huang, W.R. and Gallus, W.A. (2002) An East Asian Cold Surge: Case Study. *Monthly Weather Review*. **130**, 2271-2290.

Chen, T.S., Huang, W.R. and Yoon, J.H (2004) Interannual Variation of the East Asian Cold Surge Activity. *Journal of Climate.* **17**, 401-413.

Chen, B., Xu, X.D., Yang, S., and Zhao, T.L. (2012) Climatological perspectives of air transport from atmospheric boundary layer to tropopause layer over Asian monsoon regions during boreal summer inferred from Lagrangian approach. *Atmospheric Chemistry and Physics*. **12**, 5827-5839.

Chipperfield, M.P., Liang, Q., Strahan, S.E., Morgenstern, O., Dhomse, S.S., Abraham, N.L., Archibald, A.T., Bekki, S., Braesicke, P., Di Genova, G., Fleming, E.L., Hardiman, S.C., Iachetti, D., Jackman, C.H., Kinnison, D.E., Marchand, M., Pitari, G., Pyle, J.A., Rozanov, E., Stenke, A. and Tummon, F. (2014), Multimodel estimates of atmospheric lifetimes of long-lived ozone-depleting substances: Present and future, *Journal of Geophysical. Research. Atmospheres.,* **119**, 2555–2573

Chiras, D.D. (2001) *Environmental Science: Creating a Sustainable Future*. 6th Edition. Jones and Bartlett Publishers Inc., Sudbury, Massachusetts,

CIA (Central Intelligence Agency) 2016. *The World Factbook 2015-16*. Washington, DC.

Clough, S. J. and Bent, A. F. (1998) Floral dip: a simplified method for Agrobacterium- mediated transformation of *Arabidopsis thaliana*. *Plant Journal*. **16**, 735-743.

Coffey, M. and Brasseur, G. (1999) Middle Atmospheric Ozone in *Atmospheric Chemistry and Global Change*, Chapter 14, Oxford University Press.

Cuzzato, P. and Bragante, L. (2002) *Process to obtain CFC-113a from CFC-113*. US Patent Application 2002/0151755

D

D'Amours R. (1998) Modeling the ETEX plume dispersion with the Canadian emergency response model. *Atmospheric Environment.* **32** (24): 4335–4341.

Daniels, J.S. and Velders, G.J.M [Lead Authors] (2007) Halocarbon Scenarios, Ozone Depletion Potentials, and Gobal Warming Potentials. Chapter 8 in *Scientific Assessment of Ozone Depletion: 2006*, Global Ozone Research and Monitoring Project-Report No. 50, World Meteorological Organization, Geneva, Switzerland

Davis, M.E., Bernard, F., McGillen, M.R., Fleming, E.L. and Burkholder, J.B. (in review, 2016) UV and Infrared Absorption Spectra, Atmospheric Lifetimes and Ozone Depletion and Global Warming Potentials for CCl2FCCl2F (CFC-112), CCl3CClF (CFC-112a), CCl3CF3 (CFC-113a) and CCl2FCF3 (CFC-114a). *Atmospheric Chemistry and Physics Discussions*.

Devenish, B.J., Thomson, D.J., Marenco, F., Leadbetter, S.J., Ricketts, H. and Dacre, H.F. (2012) A study of the arrival over the United Kingdom in April 2010 of the Eyajafjallajokull ash cloud using ground-based lidar and numerical simulations. *Atmospheric Environment*, **48**, 152-164.

Dore, A.J., Carslaw, D.C., Braban, C., Cain, M., Chemel, C., Conolly, C., Derwent, R.G., Griffiths, S.J., Hall, J., Hayman, G., Lawrence, S., Metcalfe, S.E., Redington, A., Simpson, D., Sutton, M.A., Sutton, P., Tang, Y.S., Vieno, M., Werner, M. and Whyatt, J.D. (2015) Evaluation of the performance of different atmospheric chemical transport models and inter-comparison of nitrogen and sulphur deposition estimates for the UK. *Atmospheric Environment.* **119**, 131-143.

E

EC-JRC/PBL [European Commission, Joint Research Centre (JRC)/Netherlands Environmental Assessment Agency (PBL)] (2009) *Emission Database for Global Atmospheric Research (EDGAR)*. Release Version 4.0. http://edgar.jrc.ec.europa.eu.

Ehhalt, D., Prather, M., Dentener, F. Derwent, R. Dlugokencky, E., Holland, E. Isaksen, I., Katima, H., Kirchhoff, V., Matson, P., Midgley, P. and Wand M. (2001) Atmospheric Chemistry and Greenhouse Gases. In: Houghton, J.T., Y. Ding, D.J. Griggs, M. Noguer, P.J. van der Linden, X. Dai, K. Maskell, and C.A. Johnson eds. *Climate Change 2001: The Scientific Basis. Contribution of Working Group I to the Third Assessment Report of the Intergovernmental Panel on Climate Change*. Cambridge University Press, Cambridge, United Kingdom and New York, NY, USA.

EIA [Environmental Investigation Agency] (2009) *The HFC imperative – Essential action for global climate protection*. EIA, London, United Kingdom.

EPA [Environmental Protection Agency] R.O.C [Republic of China (Taiwan)] (2015a) *Vienna Convention and Montreal Protocol*. Available on: http://unfccc.epa.gov.tw/unfccc/english/04_our_efforts/0821_convention.html [Accessed on 26th April 2016]

EPA [Environmental Protection Agency] R.O.C [Republic of China (Taiwan)] (2015b) *Towards UNFCCC FAQ*. Available on: http://unfccc.epa.gov.tw/unfccc/english/05_faq/01_faq.html [Accessed on 26th April 2016]

Etminan, M., Highwood, E.J., Laube, J.C., McPheat, R., Marston, G., Shine, K.P. and Smith, K.M. (2014) Infrared Absorption Spectra, Radiative Efficiencies, and Global Warming Potentials of Newly-Detected Halogenated Compounds: CFC-113a, CFC-112 and HCFC-133a. *Atmosphere*. **5** (3), 473-483.

F

Fang, X., Wu, J., Xu, J., Huang, D., Shi, Y., Wan, D., Wu, H., Shao, M. and Hu, J. (2012a) Ambient mixing ratios of chlorofluorocarbons, hydrochlorofluorocarbons and hydrofluorocarbons in 46 Chinese cities. *Atmospheric Environment*. **54**, 387-392.

Fang, X. Wu, J., Su, S., Han, J. Wu, Y., Si, Y. Wan, D. Sun, X., Zhang, J. and Hu, J. (2012b) Estimates of major anthropogenic halocarbon emissions from China based on interspecies correlations. *Atmospheric Environment*. **62**, 26-33.

Fang, X., Thompson, R.L., Saito, T., Yokouchi, Y., Kim, J., Li, S., Kim, K.R., Park, S., Graziosi, F. and Stohl. A. (2014) Sulfur hexafluoride (SF_6) emissions in East Asia determined by inverse modelling. *Atmospheric Chemistry and Physics*. **14**, 4779-4791.

FAOSTAT (2014) Global Crop Production 1961-2013 [Online] Available at: http://faostat.fao.org (Accessed on 3rd May 2016)

Farman, J. C., Gardiner, B. G., and Shanklin, J. D. (1985) Large losses of total ozone in Antarctica reveal seasonal ClO_X/NO_X interaction, *Nature*, **315** (6016) 207-210.

Flowers, T.J. (2004). Improving crop salt tolerance. *Journal of Experimental Botany.* **55**, 307- 319.

Forster, P., V. Ramaswamy, P. Artaxo, T. Berntsen, R. Betts, D.W. Fahey, J. Haywood, J. Lean, D.C. Lowe, G. Myhre, J. Nganga, R. Prinn, G. Raga, M. Schulz and R. Van Dorland, (2007) Changes in Atmospheric Constituents and in Radiative Forcing. In: *Climate Change 2007: The Physical Science Basis. Contribution of Working Group I to the Fourth Assessment Report of the Intergovernmental Panel on Climate Change* [Solomon, S., D. Qin, M. Manning, Z. Chen, M. Marquis, K.B. Averyt, M.Tignor and H.L. Miller (eds.)]. Cambridge University Press, Cambridge, United Kingdom and New York, NY, USA

Fortems-Cheiney, A., Chevallier, F., Saunois, M., Pison, I., Bousquet, P., Cressot, C., Wang, H.J., Yokouchi, Y. and Artuso, F. (2013) HCFC-22 emissions at global and regional scales between 1995 and 2010: Trends and variability. *Journal of Geophysical research: Atmospheres*. **118**, 7379-7388.

Fraser, P.J., Oram, D.E., Reeves, C.E., Penkett, S.A., and McCulloch, A. (1999) Southern hemispheric halon trends (1978–1998) and global halon emissions. Journal of Geophysical Research. **104**, 15985–15999.

Frederick, W.H. (2015) Southeast Asia. *Encyclopaedia Britannica*. London, Encyclopaedia Britannica Ltd.

Fthenakis, V., Clark, D.O., Moalem, M., Chandler, P., Ridgeway, R.G., Hulbert, F.E., Cooper, D.B. and Maroulis, P.J. (2010) Life-Cycle Nitrogen Trifluoride Emissions from Photovoltaics. *Environmental Science* Technology. **44**, 8750-8757.

G

Gan, J., Yates, S.R., Ohr, H.D. and Sims, J.J. (1998) Production of methyl bromide by terrestrial higher plants. *Geophysical Research Letters*. **25**, 3595-3598.

Gloster, J., Champion, H.J., Sørensen, J.H., Mikkelsen, T., Ryall, D.B., Astrup, P., Alexandersen, S., and Donaldson, A.I., (2003) Airborne transmission of foot-and-mouth disease virus from Burnside Farm, Heddon-on-the-Wall, Northumberland during the 2001 epidemic in the United Kingdom, *Veterinary Record* **152**, 525-533.

Grant, C.C. (2016) Halon Design Calculations. In: Hurley, M.J. ed. *SFPE Handbook of Fore Protection Engineering*. New York, Springer Science+Business Media, 1450-1482.

Guo, H., Ding, A.J., Wang. T., Simpson, I.J., Blake, D.R., Barletta., B., Meinardi, S., Rowland, F.S., Saunders, S.M., Fu., T.M., Hung, W.T. and Li, Y.S. (2009) Source origins, modelled profiles, and apportionments of halogenated hydrocarbons in the greater Pearl River Delta region, southern China. *Journal of Geophysical Research*. **114**, (D11302) 1-19.

H

Ha, K.J., Heo, K.Y., Lee, S.S., Yun, K.S. and Jhun, J.G. Variability in the East Asian Monsoon: a review. *Meteorological Applications*. **19**, 200-215.

Halpern, D.F. (1993) Recent developments in fluorine substituted volatile anesthetic. In: Filler, R., Kobayashi, Y. and Yagupolskii, M. eds. *Organofluorine Compounds in Medicinal Chemistry and Biomedical Applications*. Elsevier, Amsterdam, Netherlands. 101-133.

Hegglin, M. I., Fahey, D. W., McFarland, M., Montzka, S.A. and Nash, E.R. (2015) *Twenty Questions and Answers about the Ozone Layer: 2014 Update, Scientific Assessment of Ozone Depletion.* World Meterological Organization, Geneva, Switzerland.

Hennemuth, B. and Lammert, A. (2006) Determination of the atmospheric boundary layer height from radiosonde and lidar backscatter. *Boundary-Layer Meteorology*. **120** (1), 181-200.

Hodnebrog, Ø., Etminan, M., Fuglestvedt, J.S., Marston, G., Myhre, G., Nielsen, C.J., Shine, K.P. and Wallington, T.J. (2013) Global Warming Potentials and Radiative Effeciencies of Halocarbons and Related Compounds: A Comprehensive Review. *Reviews of Geophysics*. **51** (2), 300-378.

Holloway A.M. and Wayne R.P. (2010) *Atmospheric Chemistry*. Royal Society of Chemistry, 1st edition. Cambridge, UK.

Hossaini, R., M.P. Chipperfield, S. Dhomse, C. Ordoñez, A. Saiz-Lopez, N.L. Abraham, A. Archibald, P. Braesicke, P. Telford, N. Warwick, X. Yang, and J. Pyle (2012a) Modelling future changes to the stratospheric source gas injection of biogenic bromocarbons, *Geophysical Research Letters.* **39** (20), L20813

Hossaini, R., Chipperfield, M.P., Feng, W., Breider, T.J., Atlas, E., Montzka, S.A., Miller, B.R., Moore, F. and Elkins, J., (2012b). The contribution of natural and anthropogenic very short-lived species to stratospheric bromine. *Atmospheric Chemistry and Physics*, **12** (1), 371-380.

Hossaini, R., Chipperfield, M.P. Montzka, S.A., Rap, A., Dhomse, S. and Feng, W. (2015) Efficiency of short-lived halogens at influencing climate through depletion of stratospheric ozone. *Nature Geoscience*. **8**, 186-190.

HTOC [Halon Technical Options Committee] (1991) *1991 Assessment Report of the Halons Technical Options Committee*. UNEP Technology and Economic Assessment Panel/UNEP Ozone Secretariat, Nairobi, Kenya.

HTOC [Halon Technical Options Committee] (1999) Assessment Report of the Halons Technical Options Committee 1998, Ozone Secretariat, UNEP, Nairobi, Kenya.

HTOC [Halon Technical Options Committee] (2007) *Technical Note #1 – Revision 3 – New Technology Halon Alternatives*. UNEP Technology and Economic Assessment Panel/UNEP Ozone Secretariat, Nairobi, Kenya.

HTOC (Halon Technical Options Committee) (2011) Assessment Report of the Halon Technical Options Committee 2010, Ozone Secretariat, UNEP, Nairobi, Kenya.

Hu, L., Yvon-Lewis, S.A., Butler, J.H., Lobert, J.M. and King, D.B. (2013). An improved oceanic budget for methyl chloride. *Journal of Geophysical Research: Oceans*, **118** (2), 715-725.

Hu, L., Montzka, S.A., Miller, B.R., Andrews, A.E., Miller, J.B., Lehman, S.J., Sweeney, C., Miller, S.M., Thoning, K., Siso, C. and Atlas, E.L., 2016. Continued emissions of carbon tetrachloride from the United States nearly two decades after its phaseout for dispersive uses. *Proceedings of the National Academy of Sciences*, **113** (11), 2880-2885.

Hubschmann H.J. (2009) *Handbook of GC/MS*. Wiley-VCH Verlag GmBH, Weinheim, 2nd edition.

I

IPCC/TEAP [Intergovernmental Panel on Climate Change/Technology and Economic Assessment Panel] (2005) *IPCC/TEAP Special Report: Safeguarding the Ozone Layer and the Global Climate System*. *Issues Related to Hydrofluorocarbons and Perfluorocarbons*. [Metz, B., Kuijpers, L., Solomon, S., Andersen, S.O., Davidson, O., Pons, J., de Jager, D., Kestin, T., Manning, M. and Meyer, L. (Eds)]. Cambridge University Press, UK.

Ivy, D.J., Arnold, T., Harth, C.M., Steele, L.P., Mühle, J., Rigby, M., Salameh, P.K., Leist, M., Krummel, P.B., Fraser, P.J., Weiss, R.F. and Prinn, R.G. (2012) Atmospheric histories and growth trends C_4F_{10}, C_5F_{12}, C_6F_{14}, C_7F_{16}, C_8F_{18}. *Atmospheric Chemistry and Physics*. **12**, 4313-4325.

Ivy, D.J., Rigby, M., Baasandorj, M., Burkholder, J.B. and Prinn, R.G. (2012b) Global emissions estimates and radiative impact of C_4F_{10}, C_5F_{12}, C_6F_{14}, C_7F_{16} and C_8F_{18}. *Atmopsheric Chemistry and Physics*. **12**, 7635-7645.

J

James A.T. and Martin A.J.P. (1952) Gas-liquid partition chromatography: the separation and microestimation of volatile fatty acids from formic acid to dodecanoic acid. *Biochemistry Journal*. **50**, 679-90,

Jeong, J.H., Kim, B.M., Ho, C.H., Chen, D. and Lim, G.H. (2006) Stratospheric origin of cold surge occurrence in East Asia. *Geophysical Research Letters*. **33** (L14710), 1-5.

Jiao, Y., Wickett, N. J., Ayyampalayam, S., Chanderbali, A. S., Landherr, L., Ralph, P. E., Tomsho, L. P., Hu, Y., Liang, H., Soltis, P. S., Soltis, D. E., Clifton, S. W., Schlarbaum, S. E., Schuster, S. C., Ma, H., Leebens-Mack, J. and dePamphilis, C. W. (2011) Ancestral polyploidy in seed plants and angiosperms. *Nature*. **473**, 97-U113.

Jones A., Thomson D., Hort M., Devenish B. (2007) The U.K. Met Office's Next-Generation Atmospheric Dispersion Model, NAME III. In: Borrego C., Norman AL. (eds) *Air Pollution Modeling and Its Application XVII*. Springer, Boston, MA

K

Khan, M.A.H., Whelan, M.E. and Rhew, R.C. (2012). Effects of temperature and soil moisture on methyl halide and chloroform fluxes from drained peatland pasture soils. *Journal of Environmental Monitoring*. **14**, 241-249.

Kjeldsen, P., Scheutz, C., Fredenslund, A.M. and Poulsen, H. (2003). *Release and attenuation of fluorocarbons in landfills*. Ninth International Waste Management and Landfill Symposium, Italy.

Kim, J., Shanlan, L., Kim, K.R., Stohl, A., Muhle, J., Kim, S.K., Park, M.K., Kang, D.J., Lee, G., Harth, C.M., Salameh., P.K. and Weiss, R.F. (2010) Regional atmospheric emissions determined from measurements at Jeju Island, Korea: Halogenated from China. *Geophysical Research Letters*. **37**, (L12801), 1-5.

Kim, K., Shon, Z., Nguyen, H.T. and Jeon, E. (2011) A review of major chlorofluorocarbons and their halocarbon alternatives in the air. *Atmospheric Environment*. **45**, 1369-1382.

Kim, J., Li, S., Muhle, J., Stohl, A., Kim, S.K., Park, S., Park, M.K., Weiss, R.F., and Kim, K.R. (2012) Overview of the findings from measurement of halogenated compounds at Gosan (Jeju Island, Korea) quantifying emissions in East Asia. *Journal of Integrative Environmental Sciences.* **9** (Sup 1), 71-80.

Kim, J., Fraser, P.J., Li, S., Muhle, J., Ganesan, A.L., Krummel, P.B., Steele, L.P., Park, S., Kim, S.K., Park, M.K., Arnold, T., Harth, C.M., Salameh, P.K., Prinn, R.G., Weiss, R.F. and Kim, K.R. (2014) Quantifying aluminium and semiconductor industry perfluorocarbon emissions from atmospheric measurements. **41**, 4787-4794.

Kloss, C., Newland, M.J., Oram, D.E., Fraser, P.J., Brenninkmeijer, C.A.M, Rockmann, T. and Laube, J.C. (2014) Atmospheric Abundances, Trends and Emissions of CFC-216ba, 216ca and HCFC-225ca. *Atmosphere*. **5**, 420-434.

Ko, M.K.W., Sze, N.D., Wang, W., Shia, G., Goldman, A., Murcray, F.J., Murcray, D.G. and Rinsland, C.P. (1993) Atmospheric Sulfur Haxafluoride: Sources, Sinks and Greenhouse Warming. *Journal of Geophysical Research*. **98**, 10,499-10,507.

Koerner, E. (2012) *Evolution, function and manipulation of methyl halide production in plants.* Doctoral Thesis, University of East Anglia.

Kono, S., Yoshimura, T. and Shibanuma, T. (2002) *Process for producing 1,1,1,2,2-pentafluoroethane*. US 6392106 B1.

Kremser, S., N. B. Jones, M. Palm, B. Lejeune, Y. Wang, D. Smale, and N. M. Deutscher (2015), Positive trends in Southern Hemisphere carbonyl sulfide, *Geophysical Research Letters*, **42**, 9473–9480.

Krysztofiak, G., Catoire, V., Poulet, G., Marécal, V., Pirre, M., Louis, F., Canneaux, S. and Josse, B. (2012) Detailed modeling of the atmospheric degradation mechanism of very-short lived brominated species, Atmospheric Environment, 59, 514-532.

Kuijpers, L. & Seki, M. (2013) *UNEP Report of the Technology and Economic Assessment Panel Vol. 1*. UNEP Ozone Secretariat, Nairobi, Kenya.

Kusky, T. (2005) *Encyclopedia of Earth Science*. New York, U.S.A, Facts on File Inc.

L

Langbein, T., Sonntag, H., Trapp, D., Hoffman, A., Malms, W., Roth, E.P., Mors, V. and Zellner, R. (1999) Volatile anaesthetics and the atmosphere: Atmospheric lifetimes and atmospheric effects of halothane, enflurane, isoflurane, desflurane and sevoflurane. *British Journal of Anaesthesia*. **82** (1), 66-73.

Larsson, L. and Odham, G. (1984) Gas Chromatography. In: *Gas Chromatography Mass Spectrometry Applications in Microbiology*. Plenum Press, New York.

Lateb, M., Meroney, R.N., Yataghene, M., Fellouan, H., Saleh, F. and Boufadel, M.C. (2016) On the use of numerical modelling for near-field pollutant dispersion in urban environments – A review. *Environmental Pollution*. **208** (A), 271-283.

Laube, J.C., Engel, A., Bönisch, H., Möbius, T., Worton, D.R., Sturges, W.T., Grunow, K. and Schmidt, U. (2008) Contribution of very short-lived organic substances to stratospheric chlorine and bromine in the tropics–a case study. *Atmospheric Chemistry and Physics*, **8** (23),7325-7334.

Laube, J.C., Martinerie, P., Witrant, E., Blunier, T., Schwander, J., Brenninkmeijer, C.A.M., Schuck, T.J., Bolder, M., Röckmann, T., van der Veen, C., Bönisch, H., Engel, A., Mills, G.P., Newland, M.J., Oram, D.E., Reeves, C.E. and Sturges, W.T. (2010) Accelerating growth of HFC-227ea (1,1,1,2,3,3,3-heptafluoropropane) in the atmosphere. *Atmospheric Chemistry and Physics.* **10**, 5903-5910.

Laube, J.C., Hogan, C., Newland, M.J., Mani, F.S., Fraser, P.J., Brenninkmeijer, C.A.M., Martinerie, P., Oram, D.E., Röckmann, T., Schwander, J., Witrant, E., Mills, G.P., Reeves, C.E. and Sturges, W.T. (2012) Distributions, long term trends and emissions of four perfluorocarbons in remote parts of the atmosphere and firn air. *Atmospheric Chemistry and Physics*. **12**, 4081-4090.

Laube, J.C., Newland, M.J., Hogan, C., Brenninkmeijer, C.A.M., Fraser, P.J., Martinerie, P., Oram, D.E., Reeves, C.E., Rockmann, T., Schwander, J., Witrant, E. and Sturges, W.T. (2014) Newly detected ozone-depleting substances in the atmosphere. *Nature Geoscience*. **7**, 266-269.

Law, K.S. and Sturges, W.T. [Lead Authors] (2007) Halogenated very short-lived substances, Chapter 2 in: *Scientific Assessment of Ozone Depletion: 2006*, Global Ozone Research and Monitoring Project–Report No. 50. World Meteorological Organization, Geneva, Switzerland.

Lee-Taylor, J. and Redeker, K.R. (2005) Reevaluation of global emissions from rice paddies of methyl iodide and other species. *Geophysical Research Letters*. **32** (15).

Leedham, E.C., C. Hughes, F.S.L. Keng, S.-M. Phang, G. Malin, and W.T. Sturges (2013) Emission of atmospherically significant halocarbons by naturally occurring and farmed tropical macroalgae, *Biogeosciences*, **10** (6), 3615-3633

Leedham-Elvidge, E.C., Oram, D.E., Laube, J.C., Baker, A.K. Baker, Montzka, S.A., Humphrey, S., O'Sullivan, D.A. and Brennikmeijer, C.A.M. (2014) Increasing concentrations of dichloromethane, CH_2Cl_2, inferred from CARIBIC air samples collected 1998-2012. *Atmospheric Chemistry Physics*. **15**, 1939-1958.

Levin, I., Naegler, T., Heinz, R., Osusko, D., Cuevas, E., Engel, A., Ilmberger, J., Langenfelds, R.L., Neininger, B., v. Rohden, C., Steele, L.P., Weller, R., Worhty, D.E. and Zimov, S.A. (2010) The global SF6 source inferred from long-term high precision atmospheric measurements and its comparison with emission inventories. *Atmospheric Chemistry and Physics*. **10**, 2655-2662.

Li, S., Kim, J., Kim, K.R., Muhle, J., Kim, S.K., Park, M.K., Stohl, A., Kang, D.J., Arnold, T., Harth, C.M., Salameh, P.K. and Weiss, R.F. (2011). Emissions of Halogenated Compounds in East Asia Determined from Measurements at Jeju Island, Korea. *Environmental Science & Technology*. **45**, 5668-5675

Lindley, A.A. and McCulloch, A. (2005) Regulating to reduce emissions of fluorinated greenhouse gases. *Journal of Fluorine Chemistry*. **126**, 1457-1462.

Lindow, S. E. and Brandl, M. T. (2003). Microbiology of the phyllosphere. *Applied and Environmental Microbiology*. **69**, 1875-1883.

Liu, S. and Ridley, B. (1999) Tropospheric Ozone in *Atmospheric Chemistry and Global Change*, Chapter 13, Oxford University Press.

Liu, J., Mauzerall, D.L., Chen, Q., Zhang, Q., Song, Y., Peng, W., Klimont, Z.m Qiu, X., Zhang, S., Hu, M., Lin, W., Smith, K.R.. and Zhu, T. (2012) Air pollutant emissions from Chinese households: A major and underappreciated ambient pollution source. *Proceedings of the National Academy of Sciences of the United States of America*. **113** (28), 7756-7761.

M

Mahieu, E., R. Zander, P.F. Bernath, C.D. Boone, and K.A. Walker,(2013) Recent trend anomaly of hydrogen chloride (HCl) at northern mid-latitudes derived from Jungfraujoch, HALOE and ACE-FTS Infrared solar observations, in *The Atmospheric Chemistry Experiment ACE at 10: A Solar Occultation Anthology*, [Bernath, P.F. (eds.)], 239-249, A. Deepak Publishing, Hampton, Virginia.

Manley, S.L. (2002). Phytogenesis of halomethanes: A product of selection or a metabolic accident? *Biogeochemistry*. **60**, 163-180.

Manley, S. L., Wang, N. Y., Walser, M. L. and Cicerone, R. J. (2006) Coastal salt marshes as global methyl halide sources from determinations of intrinsic production by marsh plants. *Global Biogeochemical Cycles*. **20**.

Manley, S. L., Wang, N.-Y., Walser, M. L. and Cicerone, R. J. (2007). Methyl halide emissions from greenhouse-grown mangroves. *Geophysical Research Letters*. **34**.

Manning, A. J., Ryall, D. B., Derwent, R. G., Simmonds, P. G., and O'Doherty, S. (2003) Estimating European emissions of ozone-depleting and greenhouse gases using observations and a modelling back-attribution technique, Journal of Geophysical Research. **108**, 4405.

Manning, A.J. (2011) The challenge of estimating regional trace gases from atmospheric observations. *Mathematical, Physical and Engineering Sciences*. **369**, 1943-1954.

Manzer, L. E. (1990) The CFC-ozone issue: Progress on the development of alternatives to CFCs.*Science* **249**, 31–35.

McCulloch, A. (1999) CFC and Halon replacements in the environment. *Journal of Fluorine Chemistry*. **100**, 163-173.

McCulloch, A. (2003) Fluorocarbons in the global environment: a review of the important interactions with atmospheric chemistry and physics. *Journal of Fluorine Chemistry*. **123**, 21-29.

Metcalfe, S.E., Whyatt, J.D., Broughton, R., Derwent, R.G., Finnegan, D., Hall, J., Mineter, M., O'Donoghue, M., Sutton, M.A., (2001) Developing the Hull Acid Rain Model: its validation and implications for policy makers. *Environmental Science Policy*. **4**, 25-37

Molina M and Rowland F. (1974) Stratospheric sink for chlorouoromethanes: chlorine atom-catalysed destruction of ozone. *Nature*, 249, 810–812.

Montzka, S.A. and Fraser, P.J. [Lead Authors] (2003) Controlled Substances and Other Source Gases. In: *Scientific Assessment of Ozone Depletion: 2002*, Global Ozone Research and Monitoring Project-Report No. 47, World Meteorological Organization, Geneva, Switzerland

Montzka, S. A., Aydin, M., Battle, M., Butler, J. H., Saltzman. E. S., Hall, B. D., Clarke, A. D., Mondeel, D., and Elkins, J. W. (2004) A 350-year atmospheric history of carbonyl sulfide inferred from Antarctic firn air and air trapped in ice, *Journal of Geophysical Research – Atmospheres*, **109** (D22), D22302
Montzka, S.A., Calvert, P., Hall, B.D., Elkins, J.W., Conway, T.J., Tans, P.P. and Sweeney, C. (2007) On the global distribution, seasonality and budget of atmospheric carbonyl sulphide (COS) and some similarities to CO_2. *Journal of Geophysical Research*. **112** (D09302), 1-15.

Montzka, S.A. (2011) Source gases that effect stratospheric ozone. In: Muller, R. ed. *Stratospheric Ozone Depletion and Climate Change*. Cambridge, The Royal Society of Chemistry, 33-77.

Montzka, S. A. and Reimann, S. [Lead Authors] (2011) Ozone depleting substances (ODSs) and related chemicals. In: *Scientific Assessment of Ozone Depletion*, Global Ozone Research and Monitoring Project-Report No. 52, World Meteorological Organization, Geneva, Switzerland World Meteorological Organisation, Geneva, Switzerland.

Mu, Y. J., Wu, H., Zhang, X. S., and Jiang, G. B. (2002) Impact of anthropogenic sources on carbonyl sulfide in Beijing City. *Journal of Geophysical Research – Atmospheres*, **107** (D24), 4769.

Mühle, J., Ganesan, A.L., Miller, B.R., Salameh, P.K., Harth, C.M., Greally, B.R., Rigby, M., Porter, L.W., Steele, L.P., Trudinger, C.M., Krummel, P.B., O'Doherty, S., Fraser, P.J., Simmonds, P.G., Prinn, R.G. and Weiss, R.F. (2010) Perfluorocarbons in global atmosphere: tetrafluoromethane, hexafluoroethane and octafluoropropane. *Atmospheric Chemistry and Physics*. **10**, 5145-5164.

Murashige T. and Skoog F. (1962) A revised medium for rapid growth and bioassays with tobacco tissue cultures. *Physiologia Plantarum*, **15**, 473-497.

Muthayya, S., Sugimoto, J.D., Montgomery, S. and Maberly, G.F. (2014) An overview of global rice production, supply, trade and consumption. *Annals of the New York Academy of Sciences*. **1324**, 7-14.

Myhre, G., D. Shindell, F.-M. Bréon, W. Collins, J. Fuglestvedt, J. Huang, D. Koch, J.-F. Lamarque, D. Lee, B. Mendoza, T. Nakajima, A. Robock, G. Stephens, T. Takemura and H. Zhang, (2013) Anthropogenic and Natural Radiative Forcing. In: *Climate Change 2013: The Physical Science Basis. Contribution of Working Group I to the Fifth Assessment Report of the Intergovernmental Panel on Climate Change* [Stocker, T.F., D. Qin, G.-K. Plattner, M. Tignor, S.K. Allen, J. Boschung, A. Nauels, Y. Xia, V. Bex and P.M. Midgley (eds.)]. Cambridge University Press, Cambridge, United Kingdom and New York, NY, USA

N

Nadalig, T., Farhan Ul Haque, M., Roselli, S., Schaller, H., Bringel, F. and Vuilleumier, S. (2011) Detection and isolation of chloromethane-degrading bacteria from the Arabidopsis thaliana phyllosphere, and characterization of chloromethane utilization genes. *Fems Microbiology Ecology*. **77**, 438-448.

Nagatoshi, Y. and Nakamura, T. (2009) Arabidopsis HARMLESS TO OZONE LAYER protein methylates a glucosinolate breakdown product and functions in resistance to *Pseudomonas syringae* pv. *maculicola*. *Journal of Biological Chemistry*. **284**, 19301- 19309.

NCAS [National Centre for Atmospheric Science] (2015) *Bachok Research Station: Opportunities for Atmospheric Measurements*. Available at: https://www.ncas.ac.uk/index.php/en/bachok-research-station [Accessed on 26th April 2016].

Newland, M.J., Reeves, C.J., Oram, D.E., Laube, J.C., Sturges, W.T., Hogan, C., Begley, P. and Fraser, P.J. (2013) Southern hemispheric halon trends and global halon emissions 1978-2011. *Atmospheric Chemistry and Physics*. **13**, 5551-5565.

Ni, X. H. and Hager, L. P. (1998) cDNA cloning of *Batis maritima* methyl chloride transferase and purification of the enzyme. *Proceedings of the National Academy of Sciences of the United States of America*. **95**, 12866-12871.

Ni, X. H. and Hager, L. P. (1999). Expression of *Batis maritima* methyl chloride transferase in *Escherichia coli*. *Proceedings of the National Academy of Sciences of the United States of America*. **96**, 3611-3615.

NIST/EPA/NIH (2005) The NIST Spectral Search Program for the NIST/EPA/NIH Mass Spectral Library. Version 2.0. U.S.A.

Noakes, T. (2002) Medical aerosol propellants. *Journal of Fluorine Chemistry*. **118**, 35-45.

Nossent, K. (2013) *High Tech Kansen Taiwan*. NL Agency, Ministry of Economic Affairs. Available from: http://www.rvo.nl/sites/default/files/HTSM%20Taiwan.pdf (Last Accessed 1st June 2016)

O

O'Doherty, S.J. and Carpenter, L.J. (2007) Halogenated Volatile Organic Compounds. In: Koppmann, R. ed. *Volatile Organic Compounds in the Atmosphere*. Oxford, Blackwell, 173-220.

Oh, C.H., Ko, S.J., Shin, D.K. and Jeong, Y.Y. (2012) Improving Eco-Efficiency Via Elimination of Greenhouse Gases from Semiconductor Dry Cleaning Processes. *Advanced Semiconductor*. **12,** 257-260.

Ohr, H. D., Sims, J. J., Grech, N. M., Becker, J. O. and McGiffen, M. E. (1996) Methyl iodide, an ozone-safe alternative to methyl bromide as a soil fumigant. *Plant Disease*. **80**, 731-735.

Ooki, A. and Yokouchi, Y. (2011) Dichloromethane in the Indian Ocean: Evidence for in-situ production in seawater. *Marine Chemistry*. **124** (1-4), 119-124.

Oram, D.E., Mani, F.S., Laube, J.C., Newland, M.J., Reeves, C.E., Sturges, W.T., Penkett, S.A., Brenninkmeijer, C.A.M., Rockmann, T. and Fraser, P.J. (2012) Long-term tropospheric trend of octafluorocyclobutane (c-C_4F_8 or PFC-318). *Atmospheric Chemistry and Physics*. **12**, 261-269.

Oram, D.E., Ashfold, M.J., Laube, J.C., Gooch, L.J., Humphrey, S. Sturges, W.T., Leedham-Elvidge, E., Forster, G.L., Harris, N.R.P., Mead, M.I., Samah, A.A., Phang, S.M, Ou-Yang, C.F., Lin, N.H., Wang, J.L., Baker, A.K. and Brenninkmeijer, C.A.M. (in preparation, 2016) A new threat to the ozone layer from short-lived anthropogenic chlorocarbons.

Orkin, V.L., Khamaganov, V.G., Kozlov, S.N. and Kurylo, M.J. (2013) Measurements of Rate Constants for the OH Reactions with Bromoform ($CHBr_3$), $CHBr_2Cl$, $CHBrCl_2$, and Epichlorohydrin (C_3H_5ClO). *The Journal of Physical Chemistry*. **117**, 3809-3818.

Ou-Yang, C-F, Hsieh, H-C, Wang, S-H, Lin, N-H, Lee, C-T, Sheu, G-R and Wang, J-L (2012) Influence of Asian continental outflow on the regional background ozone level in northern South China Sea. *Atmospheric Environment*. **78**, 144-253.

P

Pagano, L.E. (2010) *A Comparative Study between FLEXPART-WRF and HYSPLIT in an Operational Setting: Analysis of Fire Emissions across complex geography using WRF*. Masters Thesis, North Carolina State University.

Palmer, P.I., Jacob, D.J., Mickley, L.J., Blake, D.R., Sachse, G.W., Fuelberg, H.E. and Kiley, C.M. (2003) Eastern Asian emissions of anthropogenic halocarbons deduced from aircraft concentration data. *Journal of Geophysical Research*. **108**, (D24), 4753-4762.

Pantina, P., Tsay, S.C., Hsiao, T.C., Loftus, A.M., Kuo, F., Ou-Yang, C.F., Sayer, A.M., Wang, S.H., Lin, N.H., Hsu, N.C., Janjai, S., Chantara, S. and Nguyen, A.X. (2016) COMMIT in 7-SEAS/BASELInE: Operation of and Observation from a Novel Mobile Laboratory for Measuring *In-Situ* Properties of Aerosols and Gases. *Aerosol and Air Quality Research*. **26**, 2728-2741.

Papadimitriou, V.C., Portmann, R.W., Fahey, D.W., Mühle, J., Weiss, R.F. and Burkholder, J.B. (2008) Experimental and Theoretical Study of the Atmospheric Chemistry and Global Warming Potential of SO_2F_2. *Journal of Physical Chemistry*. **122**, 12657-12666.

Papanastasiou, D.K., McKeen, S.A. and Burkholder, J.B. (2014) The very short-lived ozone depleting substance $CHBr_3$ (bromoform): revised UV absorption spectrum, atmospheric lifetime and ozone depletion potential. *Atmospheric Chemistry and Physics*. **14**, 3017-3025.

Park, T.W., Jeong, J.H., Ho, C.H. and Kim, S.J. (2008) Characteristics of Atmospheric Circulation Associated with Cold Surge Occurrences in East Asia: A Case Study During 2005/06 Winter. *Advances in Atmospheric Sciences*. **25** (5), 791-804.
Park, T.W., Ho, C.H. and Yang, S. (2011) Relationship between the Artic Oscillation and Cold Surges over East Asia. *Journal of Climate*. **24**, 68-83.

Park, T.W., Ho, C.H., Jeong, S.J., Choi, Y.S., Park, S.K. and Song, C.K. (2011b) Different characteristics of cold day and cold surge frequency over East Asia in a global warming situation. *Journal of Geophysical Research*. **116** (D12118), 1-12.

Pisso, I., Haynes, P.H. and Law, K.S. (2010) Emission location dependent ozone depleting potentials for very short-lived halogenated species. *Atmospheric Chemistry and Physics.* **10**, 12025-12036.

Prather, M.J. and Hsu, J. (2008) NF3, the greenhouse gas missing from Kyoto. *Geophysical Research Letters*. **35**, 1-3.

Q

Qin, D. (2007) Decline in the concentrations of chlorofluorocarbons (CFC-11, CFC-12 and CFC-113) in an urban area of Bejing, China. *Atmospheric Environment*. **41**, 8424-8430.

R

Raaijmakers, J. M., Paulitz, T. C., Steinberg, C., Alabouvette, C. and Moenne-Loccoz, Y. (2009) The rhizosphere: a playground and battlefield for soilborne pathogens and beneficial microorganisms. *Plant and Soil*. **321**, 341-361.

Rao, V.N.M. (1994) Alternatives to Chlorofluorocarbons (CFCs). In: Banks, R.E., Smart, B.E. and Tatlow, J.C. eds. *Organofluorine Chemistry: principles and Commercial Applications*. New York, Springer Science+Business Media, 162-165.

Ray, D.K., Mueller, N.D., West, P.C. and Foley, J.A. (2013) Yield Trends Are Insufficient to Double Global Crop Production by 2050. PLOS ONE 8(6): e66428.

Redeker, K. R. and Cicerone, R. J. (2004). Environmental controls over methyl halide emissions from rice paddies. *Global Biogeochemical Cycles.* **18**: Gb1027.

Reeves, C.E., Sturges, W.T., Sturrock, G.A., Preston, K., Oram, D.E., Schwander, J., Mulvaney, R., Barnola, J.-M. and J. Chappellaz (2005) Trends of halon gases in polar firn air: implications for their emission distributions. *Atmospheric Chemistry and Physics*. **5**, 2055-2064.

Rhew, R. C., Miller, B. R. and Weiss, R. F. (2000) Natural methyl bromide and methyl chloride emissions from coastal salt marshes. *Nature*. **403**, 292-295.

Rhew, R. C., Østergaard, L., Saltzman, E. S. and Yanofsky, M. F. (2003). Genetic control of methyl halide production in Arabidopsis. *Current Biology*. **13**, 1809-1813.

Ristaino, J. B. and Thomas, W. (1997) Agriculture, methyl bromide, and the ozone hole: Can we fill the gaps? *Plant Disease*. **81**, 964-977.
Rodriguez, I. (2002) The disposal of environmentally harmful laboratory chemicals. *Green Chemistry*. **4**, G51-G52.

Rozema, J. and Flowers, T. (2008) Crops for a salinized world. *Science*. **322** (5907), 1478-1480.

S

Saikawa, E., Rigby, M., Prinn, R.G., Montzka, S.A., Miller, B.R., Kuijpers, L.J.M., Fraser, P.J.B., Vollmer, M.K., Saito, T., Yokouchi, Y., Harth, C.M., Muhle, J., Weiss, R.F., Salameh, P.K., Kim, J., Li, S., Park, S., Kim, K.R., Young, D., O'Doherty, S., Simmonds, P.G., McCulloch, A., Krummel, P.B., Steele, L.P., Lunder, C., Hermansen, O., Malone, M., Arduini, J., Yao, B., Zhou, L.X., Wang, H.J., Elkins, J.W. and Hall, B. (2012) Global and regional emissions estimates for HCFC-22. *Atmospheric Chemistry and Physics Discussions*. **12**, 18243-18285.

Saito, T., Yokouchi, Y., Kosugi, Y., Tani, M., Philip, E. and Okuda, T. (2008) Methyl chloride and isoprene emissions from tropical rain forest in Southeast Asia. *Atmospheric Science*. **35** (L19812), 1-6.

Saito, T., Yokouchi, Y., Stohl, A., Taguchi, S. and Mukai, H. (2010) Large Emissions of Perfluorocarbons in East Asia Deduced from Continuous Atmospheric Measurements. *Environmental Science Technology*. **44**, 4089-4095.

Sandu I, Bompay F, Stefan S. (2003) Validation of atmospheric dispersion models using ETEX data. *International Journal of Environment and Pollution*. **19** (4): 367–389.

Santee, M.L., Livesey, N.J., Manney, G.L., Lambert, A. and Read, W.G. (2013). Methyl chloride from the Aura Microwave Limb Sounder: First global climatology and assessment of variability in the upper troposphere and stratosphere. *Journal of Geophysical Research: Atmospheres*, ***118*** 13,532–13,560.

Schäfer, H., Miller, L. G., Oremland, R. S. and Murrell, J. C. (2007) Bacterial cycling of methyl halides. *Advances in Applied Microbiology*. **61**, 307-346.

Scheutz, C., Fredenslund, A.M., Nedenskov, J. and Kjeldsen, P. (2010). Release and fate of fluorocarbon in a shredder residue landfill: 2. Field investigations. *Waste Management*. **30**, 2163-2169.

Schmidt, A., Witham, C.S., Theys, N., Richards, N.A.D., Thordarson, T., Szpek, K., Feng, W., Hort, M.C.., Woolley, A.M., Jones, A.R., Redington, A.L., Johnson, B.T., Hayward, C.L. and Carslaw, K.S. (2014), Assessing hazards to aviation from sulfur dioxide emitted by explosive Icelandic eruptions, *Journal of Geophysical Research Atmospheres*. **119** (14) 180–196.

Schoenenberger, F., Vollmer, M.K., Rigby, M., Hill, M., Fraser, P.J., Krummel, P.B., Langenfelds, R.L., Rhee, T.S., Peter, T. and Reimann, S. (2015) First observations, trends, and emissions of HCFC-31 (CH_2ClF) in the global atmosphere. *Geophysical Research Letters*, **42** (18),7817-7824.

Shao, M. Huang, D., Gu, D., Lu, S., Chang, C. and Wang, J. (2011) Estimate of anthropogenic halocarbon emission based on measured ratio relative to CO in the Pearl River Delta region, China. *Atmospheric Chemistry and Physics*. **11**, 5011-5025.

Simpson, I.J., Akagi, S.K., Barletta, B., Blake, N.J., Choi, Y., Diskin, G.S., Fried, A., Fuelberg, H.E., Meinardi, S., Rowland, F.S., Vay, S.A., Weinheimer, A.J., Wennberg, P.O., Wieberg, P., Wisthaler, A., Yang, M., Yokelson, R.J. and Blake, D.R. (2011) Boreal forest fire emissions in fresh Canadian smoke plumes: C_1-C_{10} volatile organic compounds (VOCs), CO_2, CO, NO_2, NO, HCN and CH_3CN. *Atmospheric Chemistry and Physics*. **11**, 6445-6463.

Singles, R.J., Sutton, M.A., Weston, K.J., (1998) A multi-layer model to describe the atmospheric transport and deposition of ammonia in Great Britain. *Atmospheric. Environment*. **32**, 393-399.

Skoog, D. A., West, D. M., Holler, F. J., and Crouch, S. R. (2004) *Fundamentals of Analytical Chemistry*. Saunders College Publishing.

Soloman, S. (1999) Stratospheric Ozone Depletion: A review of concepts and history. *Reviews of Geophysics*. **37**, (3) 275-316.

SPARC (2016), SPARC Report on the Mystery of Carbon Tetrachloride. Q. Liang, P.A. Newman, S. Reimann (Eds.), SPARC Report No. 7, WCRP-13/2016.

Stein, A.F., Draxler, R.R., Rolph, G.D., Stunder, B.J.B. and Cohen, M.D. (2015) NOAA's HYSPLIT Atmospheric Transport and Dispersion Modelling System. *Bulletin of the American Meteorological Society.* 96 (12) 2059-2077.

Stohl, A., Forster, C., Frank, A., Seibert, P. and Wotawa, G. (2005) Technical note: the Lagrangian particle dispersion model FLEXPART version 6.2. *Atmospheric Chemistry and Physics*. **5**, 2461-2474.

Stohl, A., Kim, J. Li, S. O'Doherty, S., Muhle, J., Salameh, P.K., Saito, T., Vollmer, M.K., Wan, D., Weiss, R.F., Yao, B., Yokouchi, Y. and Zhou, L.X. (2010) Hydrochlorofluorocarbon and hydrofluorocarbon emissions in East Asia determined by inverse modelling. *Atmospheric Chemistry and Physics*. **10**, 3545-3560.

Stolarski, R.S. and Cicerone, R.J., 1974. Stratospheric chlorine: a possible sink for ozone. *Canadian journal of Chemistry*, ***52*** (8), pp.1610-1615.

Sturges, W.T., Wallington, T.J., Hurley, M.D., Shine, K.P., Sihra, K., Engel, A., Oram, D.E., Penkett, S.A., Mulvaney, R. and Brenninkmeijer, C.A.M. (2000) A Potent Greenhouse Gas Identified in the Atmosphere: SF_5CF_3. *Science*. **289**, 611-613.

Sturges, W.T., Oram, D.E., Laube, J.C., Reeves, C.E., Newland, M.J., Hogan, C., Martinerie, P., Witrant, E., Brenninkmeijer, C.A.M., Schuck, T.J. and Fraser, P.J. (2012) Emissions halted of the potent greenhouse gas SF_5CF_3. *Atmospheric Chemistry and Physics*, **12**, 3653-3658.

Sturrock, G.A., Etheridge, D.M., Trudinger, C.M., Fraser, P.J. and Smith, A.M. (2002) Atmospheric histories of halocarbons from analysis of Antarctic firn air: Major Montreal Protocol species. *Journal of Geophysical Research*. **107**, 4765-4779.

Surya Prakash, G.K., Hu, J., Wang, Y. and Olah, G.A. (2005) Fluoride-induced nucleophilic (phenylthio)difluoromethylation of carbonyl compounds with [difluoro(phenylthio)methyl]trimethylsilane (TMS-CF_2SPh). *Journal of Fluorine Chemistry*. **126** (4), 527-532.

T

Takahashi, H., and Luo, Z.J., (2014) Characterizing tropical overshooting deep convection from joint analysis of CloudSat and geostationary satellite observations, *Journal of Geophysical Research*., **119** (1), 112–121.

Takahashi, K., Kono, S. and Shibanuma, T. (2002) *Manufacturing method for fluorine-containing ethane*. US 6455745 B1.

Takaya, K. and Nakamura, H. (2005) Mechanisms of Intraseasonal Amplification of the Cold Siberian High. *Journal of the Atmospheric Sciences*. **62**, 4423-4440.

Takaya, K. and Nakamura, H. (2005b) Geographical Dependence of Upper-Level Blocking Formation Associated with Intraseasonal Amplification of the Siberian High. *Journal of the Atmospheric Sciences*. **62**, 4441-4449.

Takekawa, Y. and Nakamura, T. (2012). Rice OsHOL1 and OsHOL2 proteins have S- adenosyl-L-methionine-dependent methyltransferase activities toward iodide ions. *Plant Biotechnology*. **29**, 103-108.

Taylor, R. W. D. (1994) Methyl bromide - Is there any future for this noteworthy fumigant. *Journal of Stored Products Research.* 30, 253-260.

TEAP [Technology and Economic Assessment Panel] (2009) Assessment of Alternatives to HCFCs and HFCs and Update of the TEAP 2005 Supplement Report Data. *Task Force Decisions XX/8 Report*. UNEP Technology and Economic Assessment Panel/UNEP Ozone Secretariat, Nairobi, Kenya.

TEAP [Technology and Economic Assessment Panel] (2013) 2013 Chemicals TOC (CTOC) Progress Report. In: *Report of the Technology Assessment Panel, Volume 1 Progress Report*. UNEP Technology and Economic Assessment Panel/UNEP Ozone Secretariat, Nairobi, Kenya.

TEAP [Technology and Economic Assessment Panel] (2014) Chemicals TOC (CTOC) Progress Report. In: *Report of the Technology Assessment Panel, Volume 1 Progress Report*. UNEP Technology and Economic Assessment Panel/UNEP Ozone Secretariat, Nairobi, Kenya.

Tissier, A.S. and Legras, B. (2016) Convective sources of trajectories traversing the tropical tropopause layer. *Atmospheric Chemistry and Physics*. **16**, 3383-3398.

Toda, H. and Itoh, N. (2011) Isolation and characterization of a gene encoding a S-adenosyl-L-methionine-dependent halide/thiol methyltransferase (HTMT) from the marine diatom *Phaeodactylum tricornutum*: Biogenic mechanism of CH_3I emissions in oceans. *Phytochemistry*. **72**, 337-343.

Travnikov, O., Angot, H., Artaxo, P., Bencardino, M., Bieser, J., D'Amore, F., Dastoor, A., De, Simone, F., Diequez, M.d.C., Dommergue, A., Ebinghaus, R., Feng, X.B., Gencarelli, C.N., Hedgecock, I.M., Magand, O., Martin, L., Matthias, V., Mashyanov, N., Pirrone, N., Ramachandran, R., Read, K.A., Selin, N.E., Sena, F., Song, S., Sprovieri, F., Wip, D., Wangberg, I. and Yang, X. (2016) Multi-model study of mercury dispersion in the atmosphere: Atmospheric processes and model evaluation. *Atmospheric Chemistry and Physics Discussions*. 1-37.

Trudinger, C.M., Etheridge, D.M, Sturrock, G.A., Fraser, P.J., Krummel, P.B. and McCulloch, A. (2004) Atmospheric histories of halocarbons from analysis of Antarctic firn air: Methyl bromide, methyl chloride, chloroform, and dichloromethane. *Journal of Geophysical Research*. **109** (D22310), 1-15.

Tsai, W. (2002) A review of environmental hazards and adsorption recovery of cleaning solvent hydrochlorofluorocarbons (HCFCs) *Journal of Loss Prevention in the Process Industries.* **15**, 147-157.

Tsai, W. (2005) An overview of environmental hazards and exposure risk of hydrofluorocarbons (HFCs). *Chemosphere*. **61**, 1539-1547.

Tsai, W. (2005b) Environmental risk assessment of hydrofluoroethers (HFEs). *Journal of Hazardous Materials*. **A119**, 69-78.

Tsai, W.T. (2006) Energy and environmental policies relating to hydrofluorocarbons (HFCs) emissions mitigation and energy conservation in Taiwan. *Energy Conversion and Management*. **47** (15-16), 2308-2318.

Tsai, W. (2011) Environmental Property Modeling of Perfluorodecalin and its Implications for Environmental Fate and Hazards. *Aerosol and Air Quality Research*. **11**, 903-907.

U

UNEP [United Nations Environment Programme] (1992) *The Montreal Protocol on Substances that Deplete the Ozone Layer as either adjusted and/or amended in London 1990, Copehagen 1992*. UNEP Ozone Secretariat, Nairobi, Kenya.

UNEP [United Nations Environment Programme] (2007) *Report of the Nineteenth Meeting of Parties to the Montreal Protocol on Substances that Deplete the Ozone Layer*. UNEP Ozone Secretariat, Nairobi, Kenya.

UNEP [United Nations Environment Programme] (2009) *Report on Emission Reduction and Phase-Out of CTC (Decision 55/45).* UNEP Ozone Secretariat, Nairobi, Kenya.

UNEP [United Nations Environment Programme] (2013) *Register of the Status of Ratification of the Montreal Protocol and its Amendments as at 14 November 2013*. Department of the Environment, Australian Government.

UNEP [United Nations Environment Programme] (2014) *Assessment for Decision-Makers: Scientific Assessment of Ozone Depletion: 2014*, World Meteorological Organization, Global Ozone Research and Monitoring Project – Report No. 56, Geneva, Switzerland

UNEP [United Nations Environment Programme] (2015) *Article 5 Parties Status*. [Online] Available at: http://ozone.unep.org/en/article-5-parties-status [Accessed on 26th April 2016]

UNEP [United Nations Environment Programme] (2015b) *Decision XXVI/3: Essential-use exemption for chlorofluorocarbon-113 for aerospace applications in the Russian Federation*. UNEP Ozone Secretariat, Nairobi, Kenya.

UNEP [United Nations Environment Programme] (2016) *The Montreal Protocol on substances that deplete the ozone layer*. Tenth edition, UNEP Ozone Secretariat, Nairobi, Kenya.

UNEP [United Nations Environment Programme] (2017a) *Treaties and Decisions*. [Online] Avilable at: http://ozone.unep.org/en/treaties-and-decisions [Accessed on 11th April 2017]

UNEP [United Nations Environment Programme] (2017b) *Frequently Asked Questions relating to the Kigali Amendment to the Montreal Protocol*. Fouth edition, UNEP Ozone Secretariat, Nairobi, Kenya.

UNFCCC [United Nations Framework Convention on Climate Change] (2012) *Doha Amendment to the Kyoto Protocol*. UNFCCC Secretariat, Germany.

UNFCCC [United Nations Framework Convention on Climate Change] (2014) *What is the CDM?* [Online] Available at: https://cdm.unfccc.int/about/index.html [Accessed on 26th April 2016]

UNFCCC [United Nations Framework Convention on Climate Change] (2015) *Adoption of the Paris Agreement*. Available at: https://unfccc.int/resource/docs/2015/cop21/eng/l09r01.pdf [Accessed on 27th April 2016]

UNIDO [United Nations Industrial Development Organization] (2009) Preparing for HCFC phase-out: Fundamentals of uses, alternatives, implications and funding for Article 5 countries. UNIDO Secretariat, Vienna, Austria.

V

Vaughan, S., Ingham, T., Whailey, L.K., Stone, D., Evans, M.J., Read, K.A., Lee, J.D., Moller, S.J., Carpenter, L.J., Lewis, A.C., Fleming Z.L. and Heard, D.E. (2012) Seasonal observation of OH and HO_2 in the remote tropical marine boundary layer. *Atmospheric Chemistry and Physics*. **12**, 2149-2172.

Vollmer, M.K., Zhou, L.X., Greally, B.R., Henne, S., Yao, B., Reimann, S., Stordal, F., Cunnold, D.M., Zhang, X.C., Maione, M., Zhang, F., Huang, J. and Simmonds, P.G. (2009) Emissions of ozone-depleting halocarbons from China. *Geophysical Research Letters*. **36**, (L15823), 1-5.

Vollmer, M.K., Rigby, M., Laube, J.C., Henne, S., Rhee, T.S., Gooch, L.J., Wenger, A., Young, D., Steele, L.P., Langenfelds, R.L., Brenninkmeijer, C.A.M., Wang, J.L., Ou-Yanf, C.F., Wyss, S.A., Hill, M., Oram, D.E., Krummel, P.B., Schoenenberger, F., Zellweger, C., Fraser, P.J., Sturges, W.T., O'Doherty, S. and Reimann, S. (2015) Abrubt reversal in emission and atmospheric abundance of HCFC-133a (CF_3CH_2Cl). *Geophysical Research Letters*. **42**, 8702-8710.

Vollmer, M. K., T. S. Rhee, M. Rigby, D. Hofstetter, M. Hill, F. Schoenenberger, and S. Reimann (2015b), Modern inhalation anesthetics: Potent greenhouse gases in the global atmosphere, *Geophysical Research Letters*. **42**, 1606–1611.

Vollmer, M.K., Mühle, J., Trudinger, C.M., Rigby, M., Montzka, S.A., Harth, C.M., Miller, B.R., Henne, S., Krummel, P.B., Hall, B.D. and Young, D. (2016) Atmospheric histories and global emissions of halons H-1211 ($CBrClF_2$), H-1301 ($CBrF_3$), and H-2402 ($CBrF_2CBrF_2$). *Journal of Geophysical Research: Atmospheres*. **121**, 3663-3686.

W

Wallace J.M. & Hobbs P.V. (1977) *Atmospheric Science an Introductory Survey* Academic Press Inc., London, U.K., 1st edition.

Walsh, J.E., Phillips, A.S., Portis, D.H. and Chapman, W.L. (2001) Extreme Cold Outbreaks in the United States and Europe, 1948-99. *Journal of Climate*. **14**, 2642-2658.

Wang, S.X., Zhao, B., Cai, S.Y., Klimont, Z., Nielsen, C.P., Morikawa, T., Woo, J.H., Kim, Y., Fu, X., Xu, J.Y., Hao, J.M. and He, K.B. (2014) Emission trends and mitigation options for air pollutants in East Asia. *Atmospheric Chemistry and Physics*. **14**, 6571-6603.

Warneck, P. (1999) Fundamentals. In: *Global Aspects of Atmospheric Chemistry* [Baumgärtel, H., Grünbein, W. and Hensel, F. (eds.)] Darmstadt, Steinkopff, New York, Springer.

Watson, J.T. and Sparkman, O.D. (2007) *Introduction to Mass Spectrometry: Instrumentation, Applications and Strategies for Data Interpretation.* 4th edition. John Wiley & Sons, Ltd., Chichester.

Weiss, R.F., Mühle, J., Salameh, P.K. and Harth, C.M. (2008) Nitrogen trifluoride in the global atmosphere. *Geophysical Research Letters*. **35**, 1-3.

Whitam, C.S., Hort, M.C., Potts, R., Servranckx, R., Husson, P. and Bonnardot, F. (2007) Comparison of VAAC atmospheric dispersion models using the 1 November 2004 Grimsvotn eruption. *Meterological Applications*. **14**, 27-38.

Williams, J. (2006) Mass Spectrometric Methods for Atmospheric Trace Gases in *Analytical Techniques for Atmospheric Measurements*. Wiley-Blackwell.

Wood, D.L. ed. (2015) Assessing the Global Operating Environment: Asia. In: *2015 Index of U.S. Military Strength*. Washington D.C., The Heritage Foundation, 131-145.

Worton, D.R., Sturges, W.T., Schwander, J., Mulvaney, R., Barnola, J.M. and Chappellaz, J. (2006) 20th century trends and budget implications of chloroform and related tri- and dihalomethanes inferred from firn air. *Atmospheric Chemistry and Physics*. **6** (10), 2847-2863.

Wuosmaa, A. M. and Hager, L. P. (1990). Methyl chloride transferase - a carbocation route for biosynthesis of halometabolites. *Science*. **249**, 160-162.

Y

Yao, B., Vollmer, M.K., Zhou, L.X., Henne, S., Reimann, S., Li, P.C., Wenger, A. and Hill, M. (2012) In-situ measurements of atmospheric hydrofluorocarbons (HFCs) and perfluorocarbons (PFCs) at the Shangdianzi regional background station, China. *Atmospheric Chemistry and Physics*. **12**, 10181-10193.

Yokoi, S. and Matsumoto, J. (2008) Collaborative Effects of Cold Surge and Tropical Depression-Type Disturbance on Heavy Rainfall in Central Vietnam. *Monthly Weather Review*. **136**, 3275-3287.

Yokouchi, Y., Noijiri, Y., Barrie, L. A., Toom-Sauntry, D., Machida, T., Inuzuka, Y., Akimoto, H., Li, H. J., Fujinuma, Y. and Aoki, S. (2000) A strong source of methyl chloride to the atmosphere from tropical coastal land. *Nature*. **403**, 295-298.

Yokouchi, Y., Inagaki, T., Yazawa, K., Tamaru, T., Enomoto, T. and Izumi, K. (2005) Estimates of ratios of anthropogenic halocarbon emissions from Japan based on aircraft monitoring over Sagami Bay, Japan. *Journal of Geophysical Research.* **110** (D06301), 1-7.

Yokouchi, Y., Taguchi, S., Saito, T., Tohjima, Y., Tanimoto, H. and Mukai, H. (2006) High frequency measurements of HFCs at a remote site in east Asia and their implications for Chinese emissions. *Geophysical Research Letters*. **33** (L21814), 1-4.

Z

Zifan, A. (2015) *Countries by Population Density in 2015* [Online]. Available at: https://commons.wikimedia.org/wiki/File:Countries_by_Population_Density_in_2015.svg [Accessed: 26th April 2016]

Ziska, F., B. Quack, K. Abrahamsson, S.D. Archer, E. Atlas, T. Bell, J.H. Butler, L.J. Carpenter, C.E. Jones, N.R.P. Harris, H. Hepach, K.G. Heumann, C. Hughes, J. Kuss, K. Krüger, P. Liss, R.M. Moore, A. Orlikowska, S. Raimund, C.E. Reeves, W. Reifenhäuser, A.D. Robinson, C. Schall, T. Tanhua, S. Tegtmeier, S. Turner, L. Wang, D. Wallace, J. Williams, H. Yamamoto, S. Yvon-Lewis, and Y. Yokouchi. (2013) Global sea-to-air flux climatology for bromoform, dibromomethane and methyl iodide, *Atmospheric Chemistry and Physics*. **13** (17), 8915-8934

Appendices

1.1 Abbreviations

ABL	**Atmospheric Boundary Layer**
AGAGE	Advanced Global Atmospheric Gases Experiment
CaMV	Cauliflower Mosaic Virus
CARIBIC	Civil Aircraft for the Regular Investigation of the atmosphere Based on an Instrument Container
CDM	Clean Development Mechanism
CFC	Chlorofluorocarbon
CI	Chemical Ionisation
DC	Direct Current
DCE	1,2-Dichloroethane
DCM	Dichloromethane
EAWM	East Asian Winter Monsoon
ECD	Electron Capture Detectors
ECl	Equivalent Chlorine
EESC	Equivalent Effective Stratospheric Chlorine
EI	Electron Ionisation
ESRL	Earth System Research Laboratory
FID	Flame Ionisation Detector
FPD	Flame Photometric Detectors
GAW	Global Atmosphere Watch
GC	Gas Chromatography
GC-MS	Gas Chromatography Mass Spectrometry
GHG	Greenhouse Gases
GL	Glucosinnolate
GWP	Global Warming Potential
HCFC	Hydrochlorofluorocarbon
HFC	Hydrofluorocarbon
HOL	Harmless to Ozone Layer
HTMT	Halide Thiol Methyl Transferase
ID	Internal diameter
IOES	Institute of Ocean and Earth Sciences
ITCZ	Intertropical Convergence Zone
IFC	Iodofluorocarbons
JIC	John Innes Centre
MBL	Marine Boundary Layer
MT	Methyl Transferase
MS	Mass Spectrometry
m/z	Mass to charge ratio
NAME	Numerical Atmospheric Modelling Environment
NCAS	Nation Centre for Atmospheric Science
NCU	National Central University
NDC	National Determined Contribution
NERC	National Environemtal Research Council
NIST	National Institute of Standards and Technology

NOAA	National Oceanic and Atmospheric Administration
ODP	Ozone Depletion Potential
ODS	Ozone Depleting Substances
OFN	Oxygen Free Nitrogen
OZS	Ozone Safe
PCE	Perfluoroethene (tetrachloroethene)
PFC	Perfluorocarbon
PLOT	Porous Layer Open Tubular
ppm	Parts per million
ppb	Parts per billion
ppt	Parts per trillion
PSC	**Polar Stratospheric Clouds**
QMF	Quadrupole Mass Filter
RF	Radio Frequency
SAM	S-adenosyl-L-methionine
SCS	South China Sea
SD	Standard Deviation
SIM	Single Ion Monitoring
TCE	Trichloroethene
TTL	Tropical Tropopause Layer
UEA	University of East Anglia
UM	Unified Model or University of Malaya
UNFCCC	United Nations Framework Convention on Climate Change
UTC	Coordinated Universal Time
VSLS	Very Short Lived Substance
WCOT	Wall Coated Open Tubular
WMO	World Meteorological Organisation
WT	Wild Type

1.2 List of Figures

1.3 List of Tables

Chapter 5

2.1a Murashige and Skoog Basal Salt Mixture

Macro Elements	mg/L
$CaCl_2$	332.02
KH_2PO_4	170.00
KNO_3	1900.00
$MgSO_4$	180.54
NH_4NO_3	1650.00
Micro Elements	**mg/L**
$CoCl_2.6H_2O$	0.025
$CuSO_4.5H_2O$	0.025
FeNaEDTA	36.70
H_3BO_3	6.20
KI	0.83
$MnSO_4.H_2O$	16.90
$Na_2MoO_4.2H_2O$	0.25
$ZnSO_4.7H_2O$	8.60

2.1b PPNO3 Media

Compound	mg/L
$CaNO_3.4H_2O$	0.80
$MgSO_4.7H_2O$	0.25
$FeSO_4.7H_2O$	0.0125
$CuSO_4.5H_2O$	0.055
$ZnSO_4.7H_2O$	0.055
H_3BO_3	0.614
$MnCl_2.4H_2O$	0.389
$CoCl_2.6H_2O$	0.055
KI	0.028
$Na_2MoO_4.2H_2O$	0.025
KH_2PO_4	0.25
Agar	7000

2.2 Sample Enclosure Timings

October 2013

Sample	Time Covered	Time Collected	Total time (hrs)
BLANK 1	09:52	09:41	23:49
BLANK 2	09:53	09:45	23:52
BLANK 3	09:54	09:47	23:53
COL-01	09:37	10:07	24:30
COL-02	09:38	10:08	24:30
COL-03	09:39	10:09	24:30
HOL-1 1	09:30	09:50	24:20
HOL-1 2	09:31	09:52	24:21
HOL-1 3	09:32	09:54	24:22
HOL-1 4	09:33	09:55	24:22
Os HOL 1	09:45	10:01	24:16
Os HOL 2	09:46	10:03	24:17
Os HOL 3	09:47	10:04	24:17
Os HOL 4	09:48	10:06	24:18

November 2013

Sample	Time Covered	Time Collected	Total time (hrs)
Blank 1	16:43	16:16	23:33
Blank 2	16:43	16:43	24:00
Blank 3	16:43	16:45	24:02
Blank 4	16:43	16:48	24:05
HOL-1	16:20	16:18	23:58
HOL-1 2	16:20	16:20	24:00
HOL-1 3	16:20	16:21	24:01
HOL-1 4	16:20	16:23	24:03
Pp HOL 1	16:25	16:34	24:09
Pp HOL 2	16:25	16:36	24:11
Pp HOL 3	16:25	16:38	24:13
Pp HOL 4	16:25	16:40	24:15
Pt HOL 1	16:37	16:24	23:47
Pt HOL 2	16:37	16:28	23:51
Pt HOL 3	16:37	16:29	23:52
Pt HOL 4	16:37	16:32	23:55

December 2013

Sample	Time Covered	Time Collected	Total time (hrs)
Blank 1	14:30	15:37	49:07
Blank 2	14:32	15:44	49:12
Blank 3	14:34	15:40	49:06
Blank 4	15:00	16:20	49:20
WT 1	14:36	15:46	49:10
WT 2	14:38	15:46	49:08
WT 3	14:40	15:52	49:12
WT 4	14:42	15:54	49:12
Pp HOL4-1	14:44	15:38	48:54
Pp HOL4-2	14:46	16:00	49:14
Pp HOL4-3	14:58	16:05	49:07
Pp HOL4-4	14:48	16:08	49:20
Pp HOL9-1	14:50	16:10	49:20
Pp HOL9-2	14:52	16:15	49:23
Pp HOL9-3	14:54	16:17	49:23
Pp HOL9-4	14:56	16:19	49:23

June 2014

Sample	Time Covered	Time Collected	Total time (hrs)
Blank 1	10:00	11:10	49:10
WT1	09:15	11:15	50:00
WT2	09:18	11:25	50:07
WT3	09:21	11:31	50:10
PpHOL-4 1	09:24	11:22	49:58
PpHOL-4 2	09:27	11:27	50:00
PpHOL-4 3	09:30	11:31	50:01
Blank 1 27°C	10:05	11:38	49:33
WT4 27°C	09:34	11:51	50:17
WT5 27°C	09:38	11:41	50:03
WT6 27°C	09:42	11:55	50:13
Blank 2 27°C	10:10	11:56	49:46
PpHOL-4 4 27°C	09:46	11:48	50:02
PpHOL-4 5 27°C	09:50	11:45	49:55
PpHOL-4 6 27°C	09:54	11:43	49:49

December 2014

Sample	Time Covered	Time Collected	Total time (hrs)
Blank 1 27°C	08:50	14:50	6:00
Blank 2 27°C	08:52	14:52	6:00
WT1 27°C	08:30	14:35	6:05
WT2 27°C	08:36	14:43	6:07
WT3 27°C	08:42	14:46	6:04
HOL-1 27°C	08:33	14:40	6:07
HOL-2 27°C	09:39	14:45	5:06
HOL-3 27°C	08:45	14:48	6:03
Blank 1	09:30	15:06	5:36
WT-1 22°C	09:05	14:57	5:52
WT-2 22°C	09:12	15:00	5:48
WT-3 22°C	09:20	15:03	5:43
HOL-1 22°C	09:08	14:59	5:51
HOL-2 22°C	09:15	15:02	5:47
HOL-3 22°C	09:25	15:05	5:40

2.3 Wild Type and PpHOL knockout line emissions for methyl chloride and methyl iodide

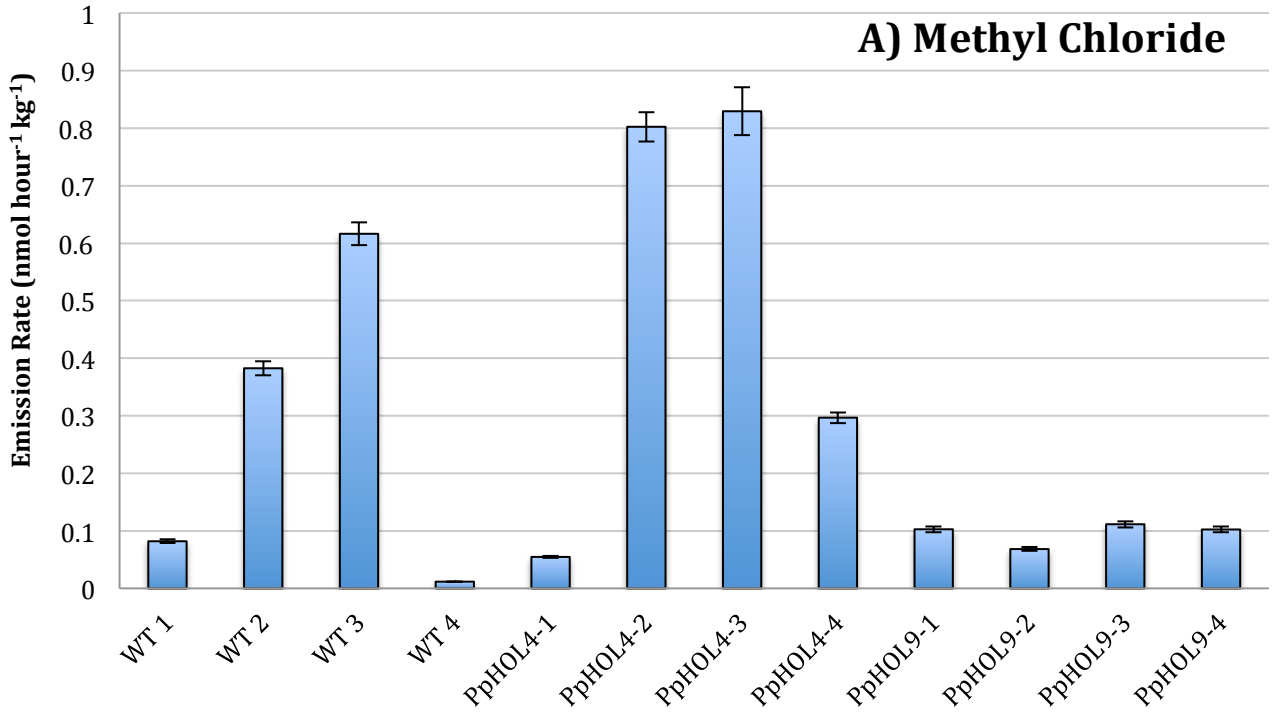

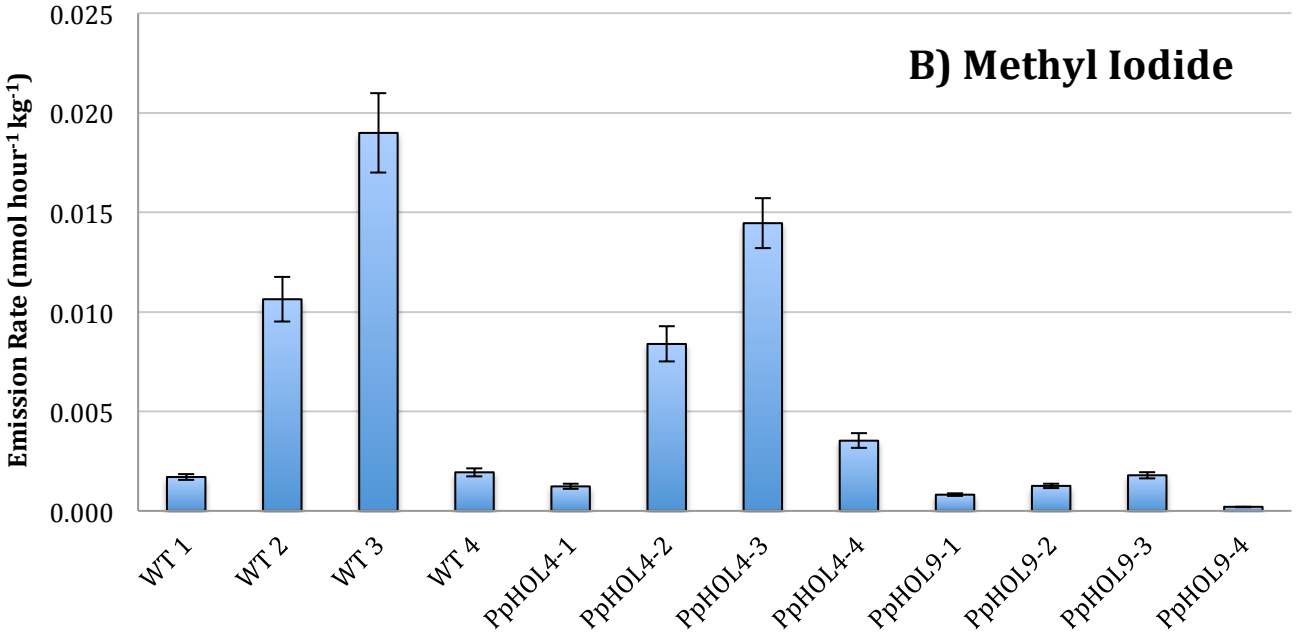

Appendix 3: Construction and Testing of a Semi-automated Inlet System for GC-MS

The overall aims of this section were to build a new operational inlet system for a GC-MS system, carry out preliminary testing to assess it functionality before installing it on the AutoSpec for high-throughput, high-sensitivity, air sample analysis. The work detailed below was mainly carried out during the first year of the PhD process however problems arose during testing. Time constraints meant that full trials and installation were never completed due to prioritisation of the work described in chapter 3, 4 and 5. As such, this section details the what was completed and summarises the conclusions found from the testing that did take place.

The main objectives were:

- Physically construct the inlet system from previously designed plans and parts.
- Test and optimise the two cryotrapping systems – submerged and headspace.
- Test and optimise the conditions for electronic heating cycles.
- Create a basic GC-MS method for sample analysis that covers a range of ion masses and species with varied abundances.
- Identify an appropriate switchback time to ensure back-flushing does not interfere with compound elution.
- Trap and analyse a dilution series to assess the linearity of the system with both cryotrapping methods.
- Assess system precision through repeated sample analysis with both cryotrapping methods.
- Identify areas in need of further testing or improvement.

3.1 Introduction

The high sensitivity AutoSpec mass spectrometry suite described in the previous chapters and utilised to collect the majority of measurements discussed in this thesis has, for over 10 years, been connected to a specially constructed manual inlet system to prepare and trap samples ready for analysis (see Figure 2.3 for the schematic). Whilst this set up has proved effective for numerous studies collecting high precision measurements from small air samples at pmol mol^{-1} levels (e.g. Laube et al. 2014, Allin et al. 2015, Sturges et al. 2012 and Laube et al. 2010), certain limitations are apparent. As such, development of an automated inlet system to ultimately replace the manual system was started prior to the commencement of this studentship.

The main advantages of fully automating the sample preparation, trapping and injection procedures include improving accuracy of measurements through minimising human-based influences.

Differences in flow rates during trapping, and time spent switching between cooling and heating cycles, will not only vary person to person but also between samples. This can impact the retention times and concentrations of detected species, particularly those that elute early in the analysis process.

Another benefit of automation is the potential for overnight analysis, which would improve comparability of samples as instrument performance can fluctuate day to day through differences in tuning and mass calibration. Currently, the number of samples able to be run per day is dependent on the amount of time a person is available to operate the instrument. With the analysis time of a sample being anywhere between 20 minutes to over an hour, depending on the method being used, this manual and labour intensive system can become a major limitation in terms of throughput. Automation, coupled with computer control and remote monitoring, would enable the system to continue to analyse samples overnight without compromising the reliability of the data collected. This increased processing of samples would also help reduce waiting time for the AutoSpec suite, which is often in high demand, and allow a wider range of samples and projects to be analysed accordingly.

As well as this, automation and electronic control of the heating process, used to inject compounds desorbed on the sample loop into the GC for separation, enables for higher temperatures to be utilised. One of main restrictions of the current system is that the use of hot water (~95°C) does not result in the complete desorption of compounds with boiling points above this from the Hayesep D within the sample loop. This means species such as bromoform and dichlorobenzene are unable to be measured on this system reliably. Therefore, data sets for these compounds have to be produced using less sensitive and precise instrumentation which have lower mass resolutions and, as such, higher probability of interferences as well as requiring larger volumes of samples.

Increasing the range and reliability of the AutoSpec through its automation will help increase knowledge and aid understanding of a wide variety of air measurement applications. This appendix will discuss the progress of the automated inlet system and the results of the first tests when connected to a GC-MS set up.

3.2 Designs and Plans

The early ideas and designs for the new inlet system were developed by Graham Mills, Bill Sturges and Johannes Laube, who frequently utilise manual GC-MS based set ups and understand the requirements necessary to produce an effective replacement system. In collaboration with the UEA Mechanics and Electronics workshops, these designs were further adjusted and advanced before testing and construction began, and before the contribution of this studentship started.

The basic structure required a system of electronically controlled pneumatic valves, connected via stainless steel tubing in a similar arrangement to the current manual system. Figure 3.1 shows one of the designs of this set up and indicates the two main sections of the system.

3.2.1 Section A - The Sample Rack

This section enables the connection of up to 9 samples with the inlet system at any one time, each with individual valves (valves 1-9). This means that, as well as a standard, 8 other samples can be analysed via the opening and closing of these valves without the need for manual changing in between runs, a particularly useful feature for unattended or overnight analysis. This section is also connected to a sensor that enables the pressure of the sample being analysed to be monitored and to a helium line (valve 10) connected to the same ultra-pure helium canister as the GC carrier gas, which allows the system to be flushed and can be used in blank analysis.

3.2.2 Section B – The Inlet System

This section is connected to the sample rack before valves 11 and 12, and after an inline pressure regulator. Valve 12 connects to the vacuum pump which enables the sample rack to be under vacuum even when the rest of the system is not. Valve 11 is followed by the needle valve used to control the flow rate in the system and the magnesium perchlorate ($Mg(ClO_4)_2$) drier used to remove any water from the air being sampled. Valve 13 also connects to the vacuum pump and multiple connections like this at strategic points allow different areas of the system to be closed off and evacuated.

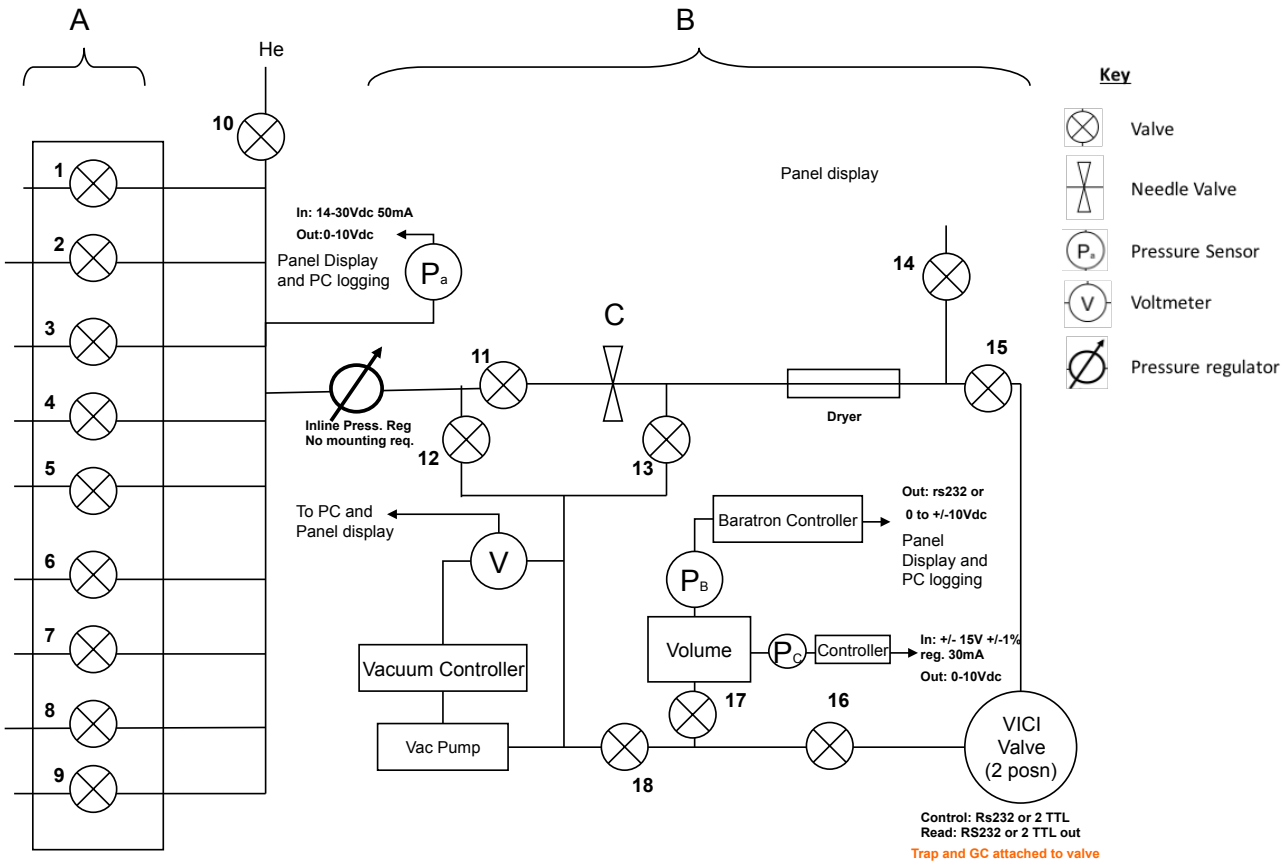

Figure 1.1: Design plan for the semi-automated inlet system, showing the two main sections. Section A indicates the sampling rack and section B indicates the inlet system itself.

This can be very useful in the determination of system leaks and to help prevent contamination. Valve 14, in this diagram, does not appear to connect to anything specific but this spare connection enables additions to the system to be easily made without a complete redesign occurring, such as the addition of an additional pressure sensor to verify the principal one is functioning correctly. Valves 15 and 16 are either side of the multiport valve that connects to the GC-MS system and the sample loop. The multiport valve can be in either two positions, load or inject, and this too can be controlled electronically. Valve 17 is after the sample loop and before the reference volume and the pressure sensors either side. These are used to monitor the change in pressure during trapping which is proportional to the volume of air being trapped e.g.. a pressure of 1 Torr corresponds to a trapped volume of 8 mL of air. Finally valve 18 also connects to the vacuum pump and so will allow for the system to be pumped down from the other side of the sample loop when necessary, and helps speed up evacuation as the adsorbent filled loop is the main restriction in the system. Outputs from all the sensors connected, as well as valve positions, are displayed on a control panel situated on the rack containing the electronic boards and controls as well as on a computer based counterpart once software development is completed.

What is not shown in Figure 3.1 is the electronically heated and controlled Dewar set up that was designed to be situated around the sample loop and multiport valve.

This enables a Dewar containing a dry ice/ethanol mixture (for submerged cryotrapping at -79°C) or liquid nitrogen (for headspace cryotrapping at approximately -125°C) to be pneumatically raised around the sample loop to chill it. Temperature sensors connected to the loop itself are able to display on the control panel the trapping temperature. In the case of headspace cryotrapping, a feedback loop can be set up around a specific chill point temperature and a small boiler, at the base of the Dewar, switched on and off to adjust the temperature accordingly. With the dry ice/ethanol, a change in temperature would likely indicate the need for the mixture to be topped up as the sample loop may no longer be entirely submerged.

When cryotrapping is complete and a heating cycle for injection started, the Dewar is then pneumatically lowered and the sample loop itself heated electronically. This is done via resistive heating of the metal sample loop and requires the loop to be electronically and thermally insulated from the rest of the system. It allows a wide range of heating set points to be available and feedback loops can again be set up to control any overshoots or fluctuations. The volume above the Dewar and sample loop, containing the multiport valve and connections to the GC-MS system, was also designed to maintain a set temperature of 60°C in order to prevent gases desorbing off the sample loop from condensing before reaching the GC oven.

3.3 Development and Construction

The contribution of this studentship in the development of this inlet system began in November 2012, and the sampling rack, Dewar set up and electronics rack had already been constructed as well as a base for all the valves to connect to.

The first task was to connect all of the individual valves to the base and then join them together using stainless steel tubing and Swagelok connections (see Figure 3.2). Also connected were the needle valve, reference volume and vacuum pump. A combination of $^1/_4$, $^1/_8$ and $^1/_{16}$ inch tubing was used depending on the space and flexibility required between valves. The magnesium perchlorate drier was not added at this point as the glass tube may break under high pressure and a pressure monitor had not yet been connected. The valve layout, at this point, was relatively unchanged from the earlier designs.

Next, the air sampling rack was mounted onto the base and a series of pneumatic control switches were attached to the side (see Figure 3.3). On one side, these control valves were designed to be connected to a compressed air line. However, during the testing process, one was not available so oxygen-free nitrogen (OFN) canisters were used instead at a pressure of 50 bar. On the other side, plastic tubing was used to connect each of the pneumatic control switches to the corresponding valve on the system base (see Figures 3.4 and 3.5). The Electronics workshop were then able to wire the control switches into the electronics rack meaning that the valves could be opened and closed using the buttons on the rack's display (see Figures 3.6 and 3.7).

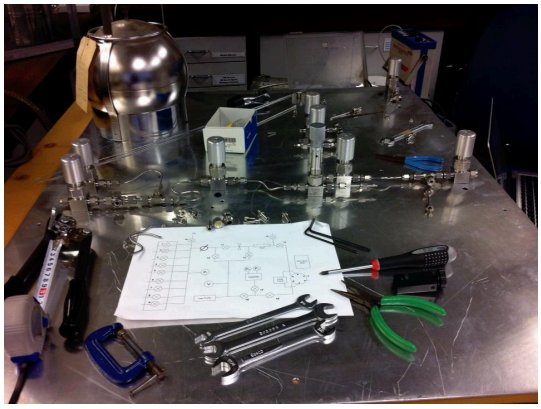

Figure 3.2: Valves were attached to the metal base of the inlet system and connected together via stainless steel tubing and Swagelok.

Figure 3.3: The air sampling rack and 6L reference volume were also positioned onto the metal base. The pneumatic control switches for the valves were attached to the side of the sampling rack.

Figure 3.4: Plastic tubing was used to connect the pneumatic control switches to the valves themselves. These were all also connected to an oxygen-free nitrogen supply.

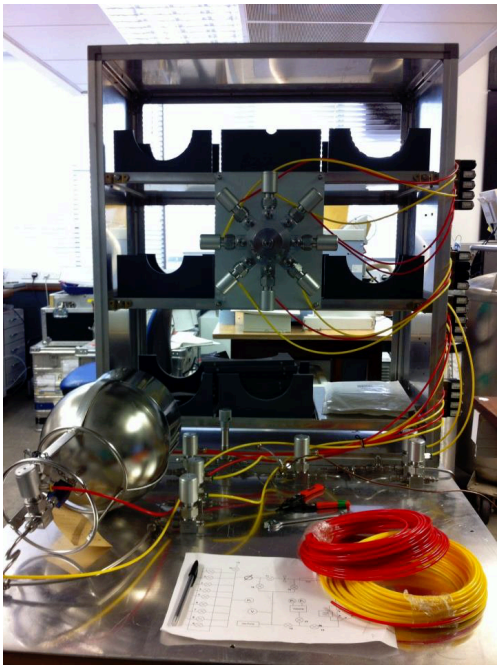

Figure 3.5: Full connections of the plastic tubing to the corresponding valves.

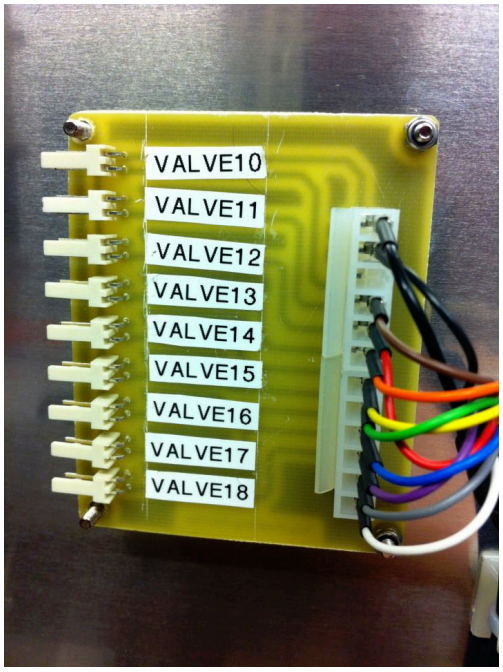

Figure 3.6: Electronic wiring used to connect the pneumatic control switches to the electronics rack to enable semi-automated control.

Figure 3.7: The electronic rack for the inlet system. The top half displays a schematic of the system and buttons correspond and connect to valves, enabling them to be opened and closed.

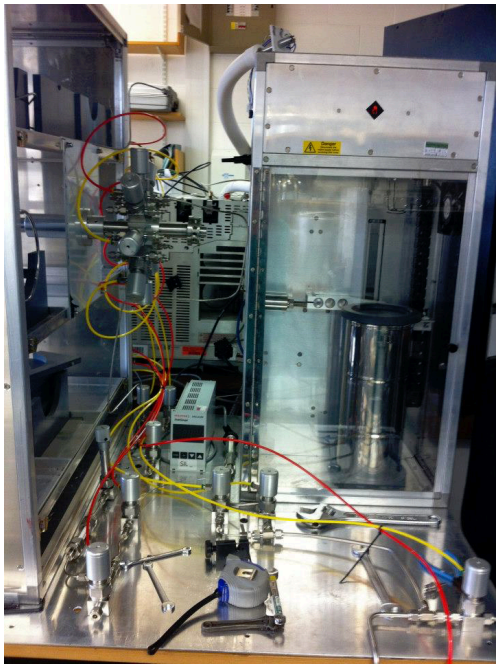

Figure 3.8: The Dewar setup was positioned on the metal base and the reference volume moved onto the shelf below.

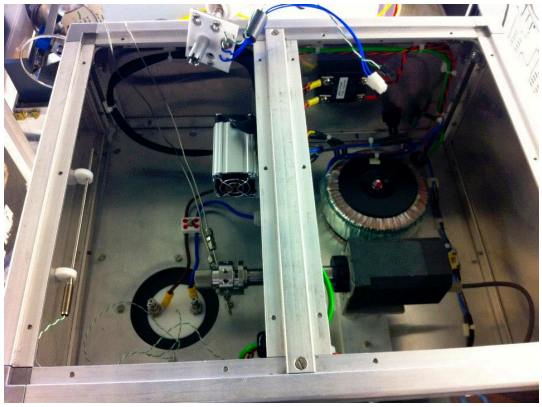

Figure 3.9: The inside of the top box above the Dewar setup. The lefthand side contains the connections between the sample loop and inlet system as well as the multiport valve that enables transport from the inlet system to the GC-MS. The righthand side contains the electronics for the heater of the box and the controls for the switching of the multiport valve.

A pressure gauge was then connected and the system pumped down to a vacuum in order to assess any leaks present. Systematic opening and closing of specific valve combinations enabled areas that were leaking, and so not maintain vacuum conditions, to be identified. Leaks at this point were mainly caused through Swagelock connections not being tight enough. Filling the system with helium and using a helium leak detector to check each part of the construction found more exact locations of small leaks.

Once the tubing system was considered to be leak tight and the valves all tested, the reference volume was moved to a shelf beneath the rest of the system to make space for the Dewar set up to be installed (see Figure 3.8). Like the valves, the Dewar uses pneumatics to be able to raise and lower at the push of a button but it too was designed to be connected to a compressed air line. Whilst connection to an OFN canister was successful, large leaks were found in the internal connections. Significant time was spent attempting to reduce these leaks and replace parts in order to minimise OFN use, however these still have not been fully solved. The leak rate is minimal but unless the OFN canister is fully shut when the system is not in use, i.e. overnight or during weekends, a considerable amount of pressure is lost. In this state, overnight runs would still be possible but careful planning and monitoring of the OFN levels would be required.

The Dewar set up is programmed, for safety, to not be able to start a heating cycle without a chill cycled occurring first and, in order for a chill cycle to occur, the Dewar must be detected as being at least half full. To ensure that the pneumatic connections were fully operational despite a minor leak, dry ice/ethanol mixture was added to the Dewar and an empty sample loop of $^{1}/_{16}$ inch stainless steel was installed and connected to the temperature sensor. This allowed a full chill and heat cycle to occur without damaging or contaminating other parts of the system.

The next stage was to fully connect the inlet system to the Dewar set up by installing $^{1}/_{16}$ inch tubing from valves 15 and 16 to the box above the Dewar itself (see Figure 3.9). The left hand side of the box is where the connections between the sample loop, inlet system and GC-MS are made via the multiport valve. The right hand side is the electronic control for the multiport valve switch and the heater to maintain the temperature in that top box. Once valves 15 and 16 were connected into adjacent ports, and the position of the multiport valve was identified as being in ‘inject’ mode, leak checks of the whole inlet system were carried out. Figure 3.10 shows diagrams of the two positions of the multiport valve, firstly in ‘load’ and then in ‘inject’. For checking this connection, the inject position was required as it bypasses the sample loop that was not connected at that time. Once a suitable vacuum was being held, the magnesium perchlorate trap was also added to the system and a leak check took place again.

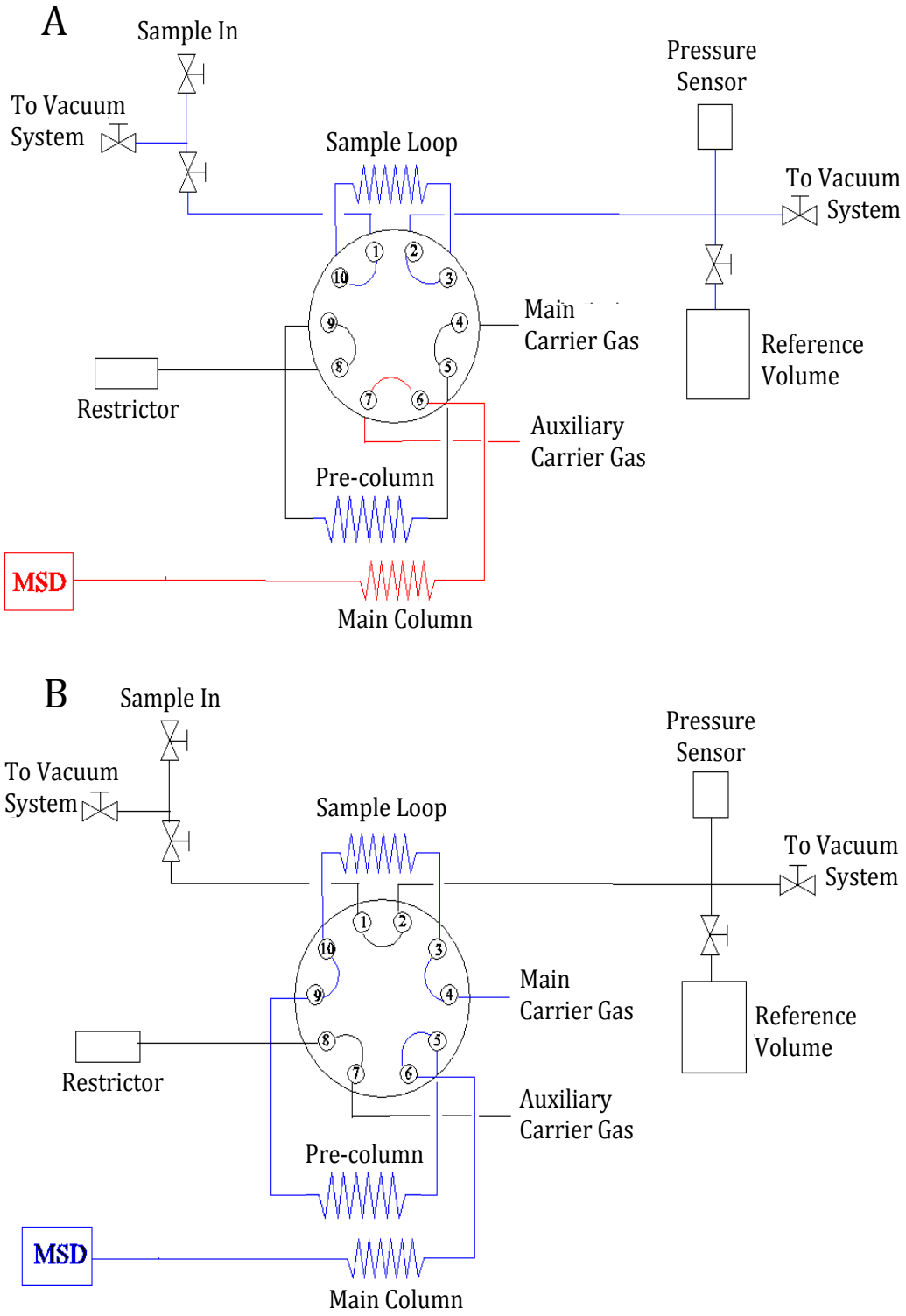

Figure 3.10: Schematic of the connections to the multiport valve in the box above the Dewar setup in A) Load position and B) Inject position. When in position A, the inlet system is connected to the sample loop and so samples may be trapped. The pre- and main columns have the helium carrier gas passing through them. In position B the helium gas flow passes through the sample loop before travelling through the two columns to the detector, thus enabling analysis of the previously trapped sample.

With the main section of the system installed and leak tight, focus moved onto installing the rest of the connections to the multiport valve in the box above the Dewar, as indicated in Figure 3.10. Before this could occur, coordination with the Mechanics workshop took place to properly mount the heated transfer line that would contain the capillaries travelling from the multiport valve to and from the GC. Without proper support, they could potentially move and snap whilst testing occurred. Figure 3.11 shows the heated transfer line in position and connecting into the GC. Since the inlet system was still in the testing stages, it should be noted it was not connected to the AutoSpec at this point. Instead it was connected to a Agilent 6890 GC and 5973 MS (Figure 3.12). Seeing as the AutoSpec is in high demand, and is particularly sensitive to contamination, this GC-MS was considered to be more robust and convenient for testing purposes. As such, to aid later removal and repositioning, the heating element of transfer was not yet connected into the electronics rack or display. An external power supply with a variable voltage was used and a temperature of ~95°C could be maintained by a 17V supply. With the transfer line in place, three capillaries could be carefully threaded from the multiport valve, through to the GC oven.

A further difference between this inlet system and the current set up on the AutoSpec is that this system allowed for the installation of a pre-column. This pre-column is a short (7m) section of GS-GasPro (ID 0.32mm) installed in the GC oven along with the main column (GS-GasPro, 20m, ID 0.32mm). During the injection process the sample travels along the transfer capillary to the pre-column, then back down a second transfer capillary to the multiport valve before then travelling down the third transfer capillary and into the main column (see Figure 3.13). This process prevents high-boiling point species from accumulating in the main column and potentially interfering with subsequent analysis and, in addition, increases the lifetime of the main column. Also, the system is set up so that when the multiport valve is switched back to the load position, the pre-column is backflushed with helium carrier gas, removing any low-volatility compounds that had previously been retained.

Also installed in the multiport valve were the two connections that bring helium carrier gas from the GC and several metres of $^{1}/_{16}$ inch tubing and a needle valve to act as a restrictor as shown in Figure 3.10. This tubing prevents back diffusion of ambient air into the system, as internal and external concentration gradients are quite large, particularly for nitrogen and oxygen. The restrictor stimulates the same resistance as the column in order to not introduce a pressure surge when switching between carrier gas supplies. These carrier gas flows are only of the order of 2mL/min. Capillaries were carefully connected from the valve to the two bulkheads that join the sample loop into the system. These contain small metal filters that prevent the sample loop filling from being transported into the multiport valve and damaging it. With the limited space and tight connections, considerable time was taken to install these parts without causing damage. Once fully connected, tests switching the multiport valve between load and inject mode resulted in the capillaries to the sample loop breaking.

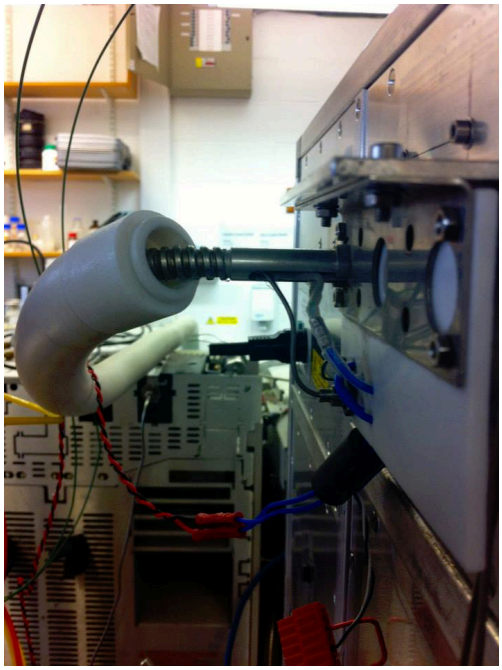

Figure 3.11: Position and support of the heated transfer line from the box above the Dewar setup to the GC-MS.

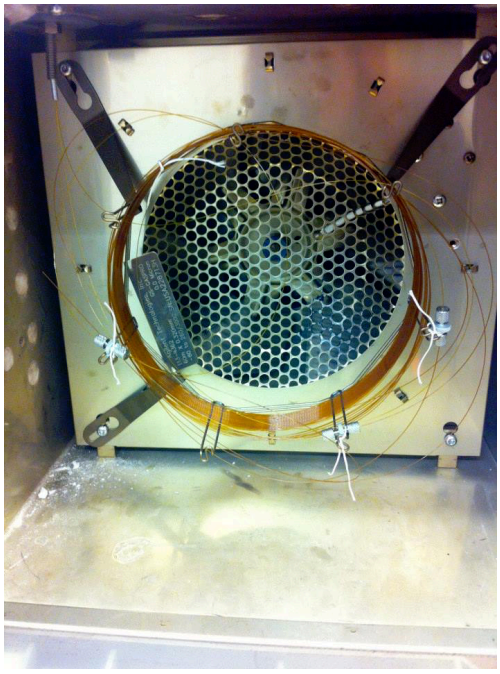

Figure 3.13: The pre-column and main column in the GC oven. Capillaries from the transfer line enter at the top left of the oven.

Figure 3.12: The Agilent 6890 GC (on the right) and 5973 MS (on the left) attached to the inlet system for preliminary analysis. This quadrupole system is not as high sensitivity as the AutoSpec that the inlet system will ultimately be installed on. However, the sensitivity and resolution is sufficient for the testing discussed in this appendix.

These were deemed to have been too short, resulting in tight bending angles, and were replaced with longer pieces. During this aspect of the system construction, damage to the multiport valve and several other connections occurred. Further time was lost acquiring replacements parts and ensuring no lasting damage to the rest of the system transpired.

The system was then leak-checked again using both vacuum pressure and helium flushing. Since the GC-MS was now connected to the system, when leaks appeared minimal using those methods, levels of oxygen, nitrogen and water were observed as these give good indications of the presence of air. Given that the inlet system had been exposed for the majority of its construction, the concentrations of these species did decrease through baking out the GC oven and maintaining higher temperatures throughout the transfer line and the top box, as well as tightening some connections. To fully confirm if a leak was present in the top box, this area was filled with argon and an ion mass of 40 was monitored through the GC-MS and adjustments to connections made accordingly.

By July 2013, all sections of the inlet system were considered leak tight and work began on optimising the heating and cooling cycles.

3.4 Cooling and Heating Cycle Testing

With the automation of the inlet set up, an integrated system of first cooling the sample loop and then electronically heating it within defined parameters was programmed to occur with the push of a button on the electronics rack. Both aspects, however, were relatively untested with respect to the limitations necessary to maintain the precision and reproducibility currently available manually on the AutoSpec system.

3.4.1 Cooling

As mentioned previously, the inlet system is set up to use either a dry ice/ethanol mixture for submerged cryotrapping or liquid nitrogen for headspace cryotrapping and both methods were found to have some drawbacks during initial tests.

Whilst the dry ice/ethanol mixture does maintain the sample loop at -78°C when fully immersed, the Dewar itself is quite large in comparison to the one currently in use on the AutoSpec. This means a larger volume of ethanol is required and, since the Dewar is controlled pneumatically, the height to which it reaches cannot be adjusted manually. The result of this is that as the level of the mixture decreases during the day, when the ethanol boils off, less of the sample loop is submerged and so cooling is not consistent. This became apparent in the concentrations detected from analysis using the system. Regular top ups to the mixture throughout the period of use were then required to minimise this impact, making overnight autonomous running with this method near impossible. Ethanol is also highly flammable and having a large volume situated very near a hot sample loop is not ideal. Whilst a lid over the mixture is automatically put in place once the heat cycle starts and the Dewar lowers, any risk may still be avoided by using headspace cryotrapping instead.

Although the liquid nitrogen method enables trapping to occur at lower temperatures than the dry ice/ethanol, and comparatively minimises risk, maintaining a consistent chill point proved difficult in early tests. When the Dewar was relatively full at the beginning of the day, the chill point was often overshot with the sample loop becoming colder than required, resulting in significant time spent waiting for it to return to the appropriate level. As the day progressed, and the headspace temperature increased, the feedback system programmed into the electronics would turn on the boiler in the base of the Dewar causing cold nitrogen to reach the headspace and cool the loop again. Control of this feedback system was problematic as there was no built in means of slightly heating the headspace when it got too cold again meaning further waiting occurred which, in turn, would limit the amount of samples able to be run that day.

These difficulties with controlling the temperature of the headspace cryotrapping meant that, for the majority of further testing carried out in 2013, the dry ice/ethanol mixture was utilised instead. However, when work on the inlet system was resumed in 2015 (the explanation for which can be found in Section 3.5.1), a discussion and collaboration with Graham Mills resulted in the construction of an improved feedback system for the liquid nitrogen method, a diagram of which can be seen in Figure 3.14. This system works by using an external power supply that is always on to provide 1-2W to the sample loop, heating it to between 30-40°C when not being chilled. Tubing, attached to a valve and nitrogen line, is also coiled and positioned within the Dewar so nitrogen can cool in the liquid nitrogen at the bottom before travelling further and being released directly into the headspace area. A temperature sensor attached to the sample loop controls the valve to this nitrogen line and the required set point can be programmed in. When the headspace temperature increases above the set point, the valve is opened and cold nitrogen is released and cools the loop. Any overshoot is quickly overcome by the consistent heating of the loop from the external power supply. Testing of this set up found it to be more responsive than the originally installed arrangement and set points were quickly maintained within an estimated ±0.5°C. As such both dry ice/ethanol and liquid nitrogen cryotrapping methods were used in the 2015 analysis of air samples.

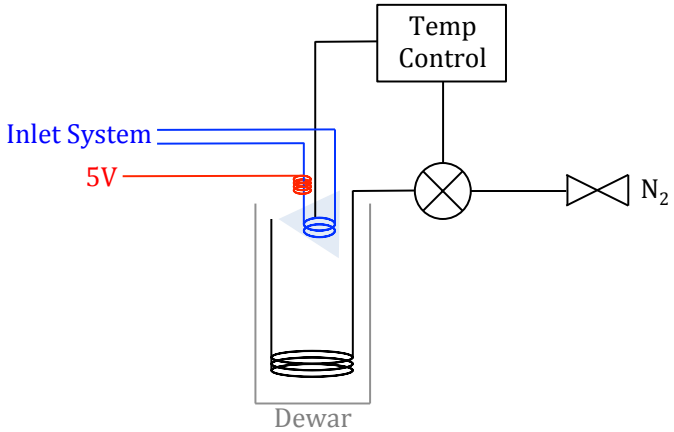

Figure 3.14: The feedback system for the liquid nitrogen headspace cryotrapping designed by Graham Mills. The blue line indicates the sample loop connected to the inlet system. The red line indicates the external power supply to heat the sample loop. The light blue triangle indicates the spray of cold nitrogen to the headspace.

3.4.2 Heating

As the electronic system had increased the temperature range available, the requirements for the heating cycle were more varied than those needed for cryotrapping. In order to keep the system in line and comparable with other available set ups, the set point for the heating cycle needed to be reached within 60 seconds. Also, although feedback systems to control the power causing the heating were programmed, an initial larger overshoot was expected followed by minor fluctuations around the set point, similar to what was seen in the cooling cycle. However, this initial overshoot needed to be minimal as a Hayesep D-filled sample loop would eventually be installed in the system and any unintentional heating above its maximum working temperature (260°C) may result in degradation. Fluctuations of ±5°C around the set point were deemed to be acceptable as well so these conditions were worked towards during testing.

The first trials of the heating cycle revealed that the output power level to the sample loop was too high, resulting in large overshoots and fluctuations, although the set point was reached very quickly. As such, the power level was systematically lowered and tested until an acceptable response was found. A cycle with a set point of 150°C and a heating time of 120 seconds was carried out 5 times with each percentage power level, with temperatures being recorded every 15 seconds. An overview of these tests, where the sample loop had previously been cooled by using dry ice/ethanol, can be found in Table 3.1 and Figure 3.15.

Firstly, what is noticeable in Figure 3.15 about the higher power levels (10-15%) is that they all see significant overshoots of over 20°C making them unsuitable for use with this cycle. The overshoots for the other levels tested averaged out lower but a record of the highest temperature recorded out of the 5 cycles run can be found in Table 3.1. 5-8% all saw overshoots of over 10°C whereas 2-4% were only up to 8°C. Standard deviations between the highest temperatures reached were also calculated and these suggested that the most variation was seen with the higher power levels (between 2.68 and 3.83 for 10% and 15% respectively). 3 and 4%, on the other hand, were calculated at 0.84 and 0.71 and recorded fluctuations in temperature after the 60 second point are only ~±2°C.

Figure 3.16 also shows that all of the tested power levels reached the set point of 150°C by the 60 second point except for 2 and 3%. However, the gradient at which the temperature increases is different for any level of 8% and above. Whilst these higher power levels resulted in quick increases to 150°C, those at 6% and under slowed between the 15 and 30 second points, continuing to 45 seconds for the lowest levels. When the temperatures recorded at these times were compared, it was found that it was around this period when the boiling point of ethanol (78.4°C) was reached. Therefore, this slow down is thought to be caused by any remaining droplets of ethanol present on the sample loop being boiled off.

Table 3.1: Heating cycle tests with dry ice/ethanol mixture cryotrapping. The temperature setpoint was 150°C and the heating time was set to 2 minutes.

Output Level (%)	Average Temperature (°C) After (mins): 0	0.25	0.5	0.75	1	1.25	1.5	1.75	2	Highest Temp (°C)	S.D. of Highest Temp
15	-67.8	76.8	180.0	157.4	155.2	157.8	159.8	159.2	158.0	191	3.83
12	-73.4	75.6	178.0	155.4	156.0	158.0	157.0	152.4	154.6	185	3.70
10	-74.0	73.8	171.4	154.8	156.0	154.0	154.0	156.6	158.4	175	2.68
8	-74.0	64.0	143.4	152.6	156.6	156.2	153.0	151.8	154.4	168	2.74
6	-74.2	43.6	76.8	155.4	154.0	152.8	151.4	151.0	150.8	162	1.30
5	-75.0	41.6	84.4	153.4	152.4	151.6	151.8	151.8	151.8	163	2.35
4	-74.2	33.2	71.4	134.6	152.0	152.2	151.8	151.8	150.6	158	0.71
3	-75.0	23.6	57.0	75.2	142.6	150.8	150.0	152.4	151.0	157	0.84
2	-75.0	14.0	43.0	57.4	102.6	137.0	146.8	146.2	151.0	157	1.22

Table 3.2: Heating cycle tests with liquid nitrogen cryotrapping. The temperature setpoint was 150°C and the heating time was set to 2 minutes.

Output Level (%)	Average Temperature (°C) After (mins): 0	0.25	0.5	0.75	1	1.25	1.5	1.75	2	Highest Temp (°C)	S.D. of Highest Temp
12	-68.8	158.0	155.2	155.4	153.4	155.2	154.6	152.8	155.6	167	1.89
10	-114.4	152.6	151.6	153.2	153.8	152.6	153.4	154.4	155.2	167	3.32
7	-80.4	130.6	152.2	151.6	152.6	155.4	154.6	151.4	151.8	161	0.96
5	-70.6	92.4	151.2	150.8	152.0	152.2	152.8	149.8	152.2	158	0.96
4	-79.0	69.4	142.4	150.2	150.6	149.2	148.0	150.2	152.6	156	0.58
3	-82.2	51.0	112.8	134.8	145.0	148.4	148.4	148.8	148.8	152	1.26

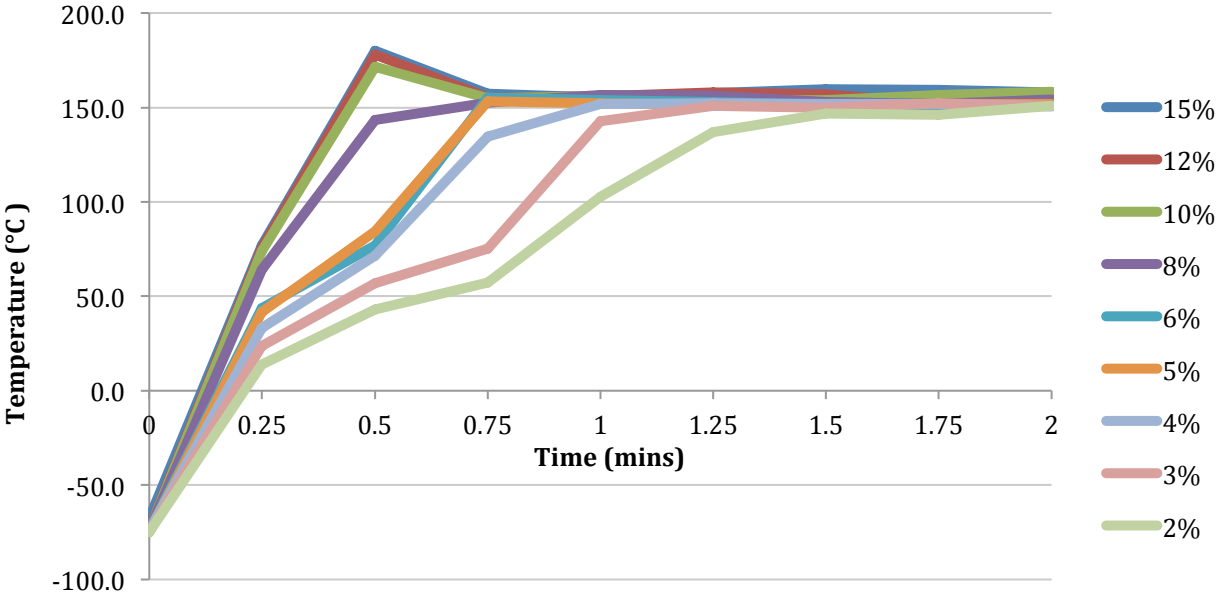

Figure 3.15: Graphical representation of the heating cycle tests after dry ice/ethanol cryo-trapping. Each colour line indicates a different output power level and measurements were taken every 15 seconds over a 2 minute period.

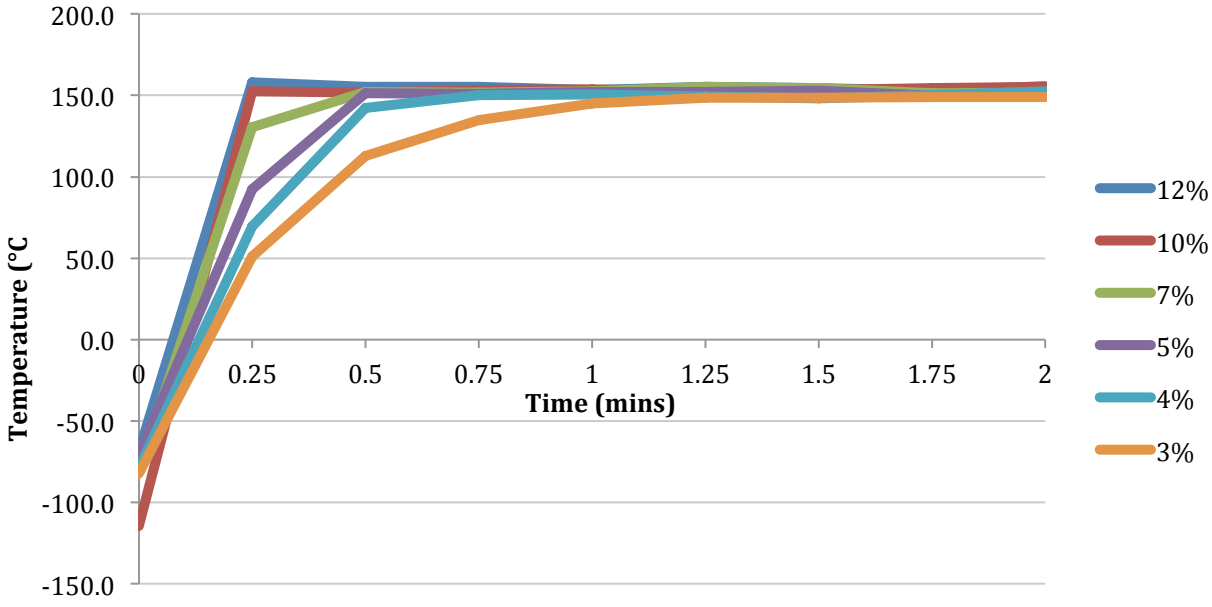

Figure 3.16: Graphical representation of the heating cycle tests after liquid nitrogen cryo-trapping. Each colour line indicates a different output power level and measurements were taken every 15 seconds over a 2 minute period.

This is further confirmed when compared to the results of the same tests run using the liquid nitrogen headspace cryotrapping method instead (see Figure 3.16). Here, whilst a slight slow down in temperature increase is seen (as expected) when the power level decreases, there is no indication of the significant changes seen with the dry ice/ethanol mixture, suggesting that it is the cryotrapping method causing this change and not the low power levels.

Similarly to the dry ice/ethanol results, highest temperatures were recorded for the headspace cryotrapped cycles (see Table 3.2) and overshoots of over 10°C were seen between 7-12% output power levels. Standard deviations were calculated up to 3.32 for the 10% level. Fluctuations for all of the power levels measured after 60 seconds were within ±5°C and all but the 3% reach the 150°C set point in the target 60 seconds. However, the 3% was, on average, at 145°C at this point. Also, although a wider variation is seen in the starting temperature due to the difficulties in maintaining the headspace chill point when these tests were carried out, this did not appear to affect how successful the heating cycles were or how quickly the set point was reached.

One other thing that did become apparent during the heating cycle tests was that, if the door to the Dewar set up was not firmly closed, it could open during the heating process. This would cause cooler air to reach the sample loop and could prevent it from reaching the set point, particularly at lower power levels. As such, efforts were made to ensure the door remained closed throughout the chilling and heating process with the aid of strong adhesive tape.

After comparing both these sets of results from the heating cycle test, an output power level of 4% was chosen as the best level to meet the required conditions, particularly in terms of overshoots and fluctuations. As the dry ice/ethanol mixture was planned on being used for the cryotrapping in further testing, changes to the sample loop design were made in an attempt to minimise potential areas for ethanol droplets to remain when the heating cycle began. This involved reshaping the sample loop from horizontal coils to vertical ones.

Future considerations that may also help reduce impact from remaining ethanol include potentially reprogramming some of the electronics to employ a two-stage power level ramp, starting higher at potentially 8% and then reducing to 4% after approximately 30 seconds. This would hopefully enable the sample loop temperature to get past the 78.4°C without significant slow down but still prevent too large an overshoot or fluctuations from occurring.

3.5 Air Sample Analysis

3.5.1 2013

In November 2013, the system was considered ready to test the first air samples and so a HayeSep D sample loop, like the one used on the AutoSpec, was conditioned and installed, replacing the empty $^1/_{16}$ inch stainless steel tubing previously in place. A large canister of air collected locally on the UEA campus was connected to the inlet system and a basic wide-ranging scan method was set up on the MS. As for the GC, the flow rate was set a 2mL/min and the oven was set up to hold at -10°C for 2 minutes, then ramped up by 10°C/min until a final temperature of 200°C was reached and held. At least 1L of air was trapped using the dry ice/ethanol method, whilst peaks detected and identified as halocarbons from this scan were then used to help create a selective ion method for further testing.

Table 3.3 shows the compounds identified from the scan and their retention times. Since the AutoSpec uses the same column as this GC system, the relationship between retention times was expected to be linear and this can clearly be seen in Figure 3.17. This correlation was then used to estimate the retention times of a range of halocarbon species from their AutoSpec counterparts and a selective ion method was set up. However, before this could be fully tested, the rotor within the multiport valve became scratched, and a replacement ordered, and a leak developed in the inlet system that proved hard to locate. In the interests of time, the testing and development of the inlet system was put on hold and analysis of the data discussed in Chapters 3, 4 and 5 was prioritised.

During this time the MS system was also removed and utilised on a different instrument and so work only resumed in September 2015 after the MS had been returned and the rotor replaced. Significant leak checking was also required, due to the length of time the system had been out of use, whilst the column in the GC oven had suffered some damage and so was shortened meaning the previously established retention times would no longer be accurate.

Table 3.3: Compounds identified from a scan MS analysis of an air sample standard, trapped using the inlet system, in November 2013

Compound	AutoSpec Pre-2014 RT	Inlet System RT
CFC-12	10.145	7.92
CH_3Cl	11.805	10.21
HFC-227ea	13.37	11.41
CFC-11	14.615	12.79
CH_2Cl_2	16.2	14.7
CFC-113	17.375	15.4
Halon 2402	17.695	15.61
Chloroform	18.09	16.2
Benzene	21.24	19.17

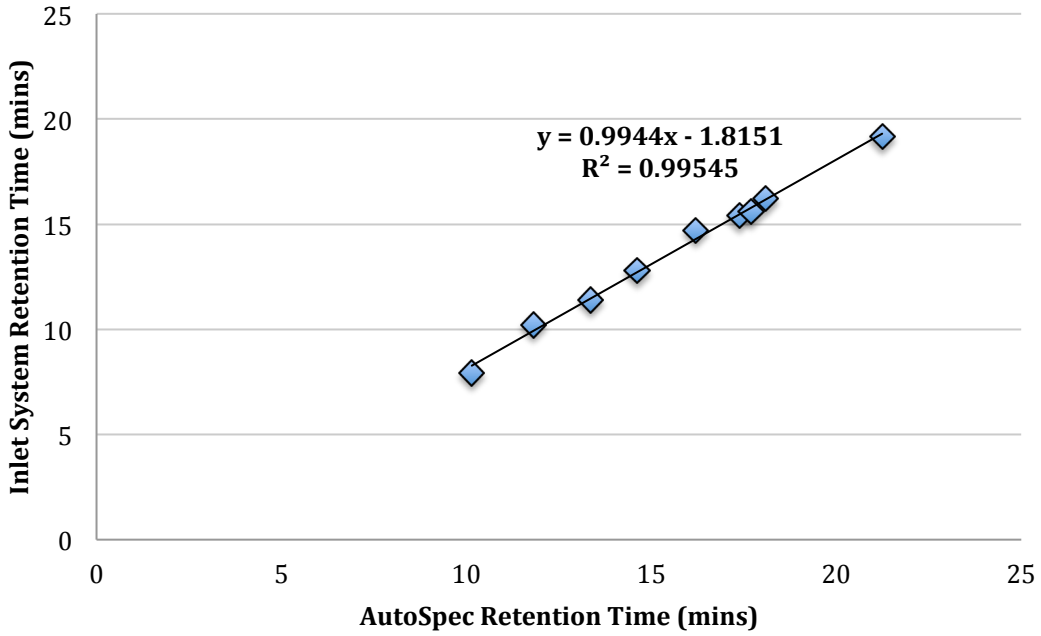

Figure 3.17: Relationship between selected retention times of compounds detected using the established AutoSpec system and the Inlet system in November 2013.

3.5.2 2015

Aside from the changes in column length, by 2015 a different sample was available to test the inlet system with. This was SX-0706077, which was collected at Niwot Ridge in 2009 and has been utilised as an in-house standard so the concentrations of a wide range of halocarbons species present are known. These are calibrated on UEA-internal scales as well as internationally recognised NOAA-ESRL scales. Using this information, several basic selective ion methods were created and run to find out the retention of several major compounds. As before, these times were plotted against the corresponding times on the AutoSpec (see Table 3.4) and the relationship plotted (see Figure 3.18). Unsurprisingly, this again shows excellent linear correlation and comparisons with the AutoSpec retention times was used to develop the selective ion method found in Table 3.5. This method covers not only a range of halocarbon species but also a variety of ion masses, retention times and abundances which should help in the assessment of the capabilities of the new inlet system. Compounds such as bromoform and 1,2-dichlorobenzene are particularly late eluters that are not currently able to be measured on the AutoSpec and so are target species for this system.

Before the performance of the inlet system could be quantified, several factors had to be considered and optimised to achieve the best response from the analysis. Firstly, the heating cycle was considered.

In previous tests, set points had been 150°C however, since several of the compounds of interest were high boiling (such as bromoform at 149°C and 1,2-dichlorobenzene at 180°C), this was increased to 200°C. In order to ensure this temperature was still reached within 60 seconds, the output power level was steadily increased to 7%. The sample loop was heated to 230°C after injection and multiple standards were run to ensure that any overshoot did not reach this temperature at this level and fluctuations were still within acceptable limits (±5°C). Also, with the installation of the different feedback system for headspace cryotrapping, both liquid nitrogen and dry ice/ethanol were able to be used for analysis in quick succession. To maintain comparability between the two methods, all heat cycling conditions were kept the same and the chill point was set at -79°C for both methods. This meant the same species should be trapped and an assessment of which was the better method for the system could be carried out.

Table 3.4: Compounds identified from a scan MS analysis of an air sample standard, trapped using the inlet system, in October 2015

Compound	AutoSpec Early 2014 RT	Inlet System RT
C_2F_6	5.99	10.3
SF_6	6.43	10.8
HFC-23	6.92	11.2
COS	9.04	13.1
Halon 1301	9.32	13.4
C_3F_8	9.93	14.0
CFC-115	10.67	14.8
HFC-125	11.07	15.2
HFC-143a	11.21	15.4
CFC-12	11.56	15.6
HCFC-22	11.58	15.7
HFC-134a	12.86	17.0
CH_3Cl	12.99	17.1
Halon 1211	13.94	18.0
F114+a	14.75	18.8
CH_3Br	14.85	18.9
HCFC-142b	14.86	18.9
CFC-11	15.85	20.0
CH_2Cl_2	17.33	21.6
HCFC-123	18.40	21.9
CFC-113	18.40	22.0
CCl_4	19.50	23.4
Benzene	22.00	25.9
PCE	22.06	26.0

Table 3.5: Selective ion method developed using the relationship of retention times (RT) between the inlet system and the AutoSpec, for air sample analysis.

Function	Window		Compound	RT	Mass	Qualifiers	
	Start	Finish					
1	5.0	11.0	C_2F_6	10.3	119		
			SF_6	10.8	127		
2	11.0	13.3	HFC-23	11.2	50		
			COS	13.1	62		
3	13.3	14.5	C_3F_8	14.0	169		
4	14.5	15.3	CFC-115	14.8	102		
			HFC-125	15.2	101		
5	15.3	16.8	HFC-143a	15.4	65		
			CFC-12	15.6	85		
			HCFC-22	15.7	67		
6	16.8	17.7	HFC-134a	17.0	83		
			CH_3Cl	17.1	50		
7	17.7	18.5	Halon 1211	18.0	129		
8	18.5	21.0	CFC-114+a	18.8	87		
			CH_3Br	18.9	94		
			HCFC-142b	18.9	65		
			CFC-11	20.0	101		
9	21.0	24.5	CH_2Cl_2	21.6	83		
			F113	22.0	85	101	
10	24.5	26.5	Benzene	25.9	73		
			PCE	26.0	166		
11	26.5	29.5	Bromoform	28.9	173	175	
			Chlorobenzene		112	114	
12	29.5	34.0	Dichlorobenze	30.9	146	148	150

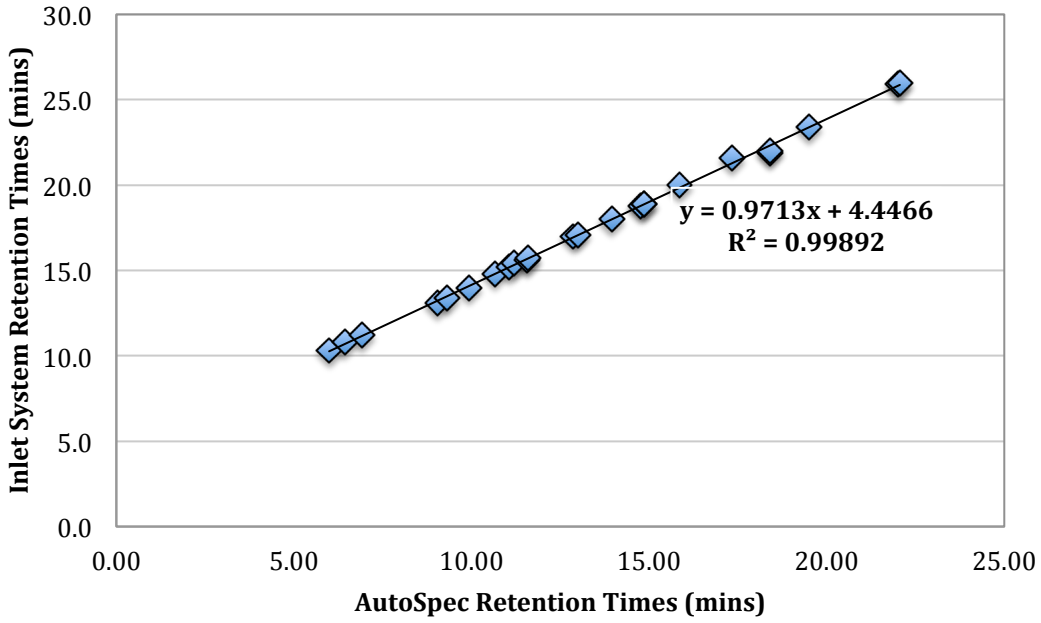

Figure 3.18: Relationship between retention times of compounds detected using the established AutoSpec system and the Inlet system in October 2015.

To ensure that the low volatility species were desorbed from the sample loop, the heat cycle time was increased, from the 15 minutes of heating utilised on the AutoSpec, to 20 minutes with the new inlet system. This would also be the point when the multiport valve would usually be switched back into the load position when using the AutoSpec. However, since a pre-column is installed on this inlet system it is necessary to wait longer in order to elute the high boiling point compounds before backflushing. 20, 25 and 27 minutes were all tested as potential switchback times. 26 minutes was settled on as this still provided baseline after the final peak of interest (1,2-dichlorobenzene) but before the sudden shift in baseline that indicates the switchback point. This also still allowed time to begin the chill and trapping procedure for the next sample before the MS acquisition actually finished at 34 minutes.

The volume trapped was also considered as the AutoSpec is capable of analysing smaller volumes due to its higher sensitivity than the current GC-MS set up attached to the inlet system. As such ~500mL was trapped for the majority of samples to ensure a detectable signal was produced by some of the less abundance species such as bromoform. When ~250mL was trapped, peaks were still apparent for all species of interest, however several signals could be lost if concentrations in a sample were 50% lower.

In summary, the results of these minor tests were, that for samples to quantify the performance of the new inlet system, ~500ml of air was to be cryotrapped using both the submerged dry ice/ethanol method and the headspace liquid nitrogen method with a chill point set at -79°C. The sample loop would be heated to 200°C, with an output power level of 7%, for 20 minutes and the multiport valve would be switched back to load at 26 minutes to allow for back flushing of the pre-column. Each run was to be completed at 34 minutes. .

3.6 Reproducibility and Linearity Testing

In order to assess the performance of the inlet system, along with both available methods of cryotrapping, the precision and linearity of the response of the set up were analysed using the SX-0706077 standard to assign mixing ratios to samples. Repeat runs of standards bracketed no more than three samples and all concentrations are helium blank and drift corrected using linear interpolation of the two nearest standards as with the AutoSpec (see section 2.2.6.4). Nine halocarbon species (CFCs -11, -12 and -113, Halon-1211, HCFC-22, HFC-134a, dichloromethane, PCE and 1,2-dichlorobenzene) were considered in these tests, representing a range of mass-to-charge (*m/z*) ratios of the detected fragment ions and retention times (see Figure 3.19).

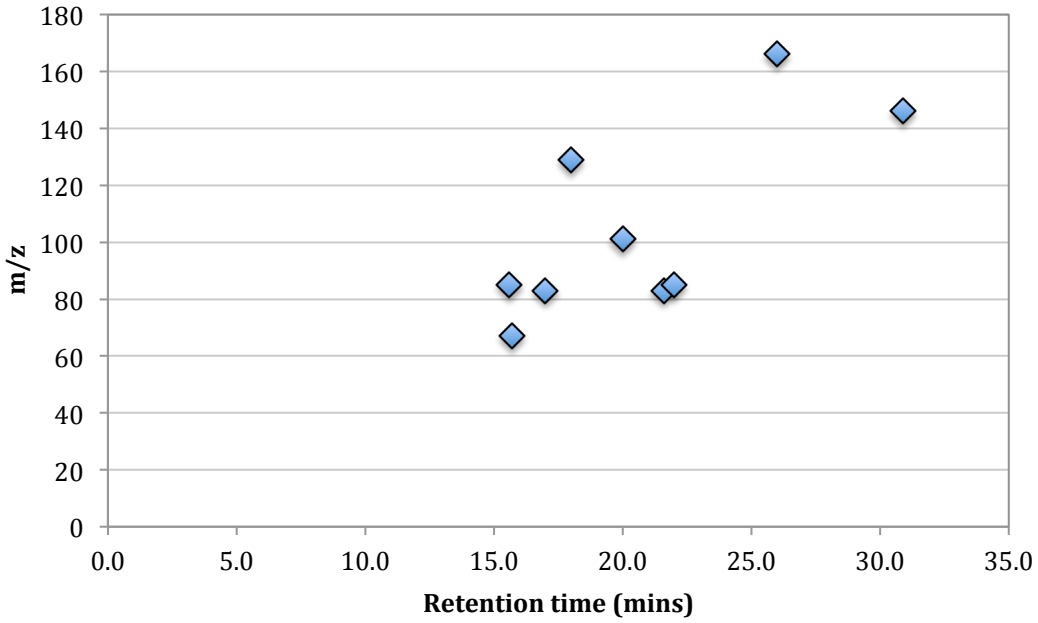

Figure 3.19: Comparison of mass-to-charge ratios (*m/z*) and the retention times of the ions used for the reproducibility and linearity testing.

3.6.1 Reproducibility

Measurement precision is an important part of instrument characterisation so, to assess this component, 4 runs of SX-0706077 on two separate days were retrieved as if they had been samples and bracketed by other SX-0706077 runs. These were corrected for drift and assigned individual mixing ratios for 9 specific compounds. The first day samples were trapped using dry ice/ethanol and the second using liquid nitrogen. Figure 3.20(a. and b.) displays, for each compound, the variation between detected concentrations in each of the four samples for each trapping method, along with the known mixing ratio of SX-0706077. Table 3.6 summarises the average detected concentration, percentage standard deviation and sample precision for each trapping method.

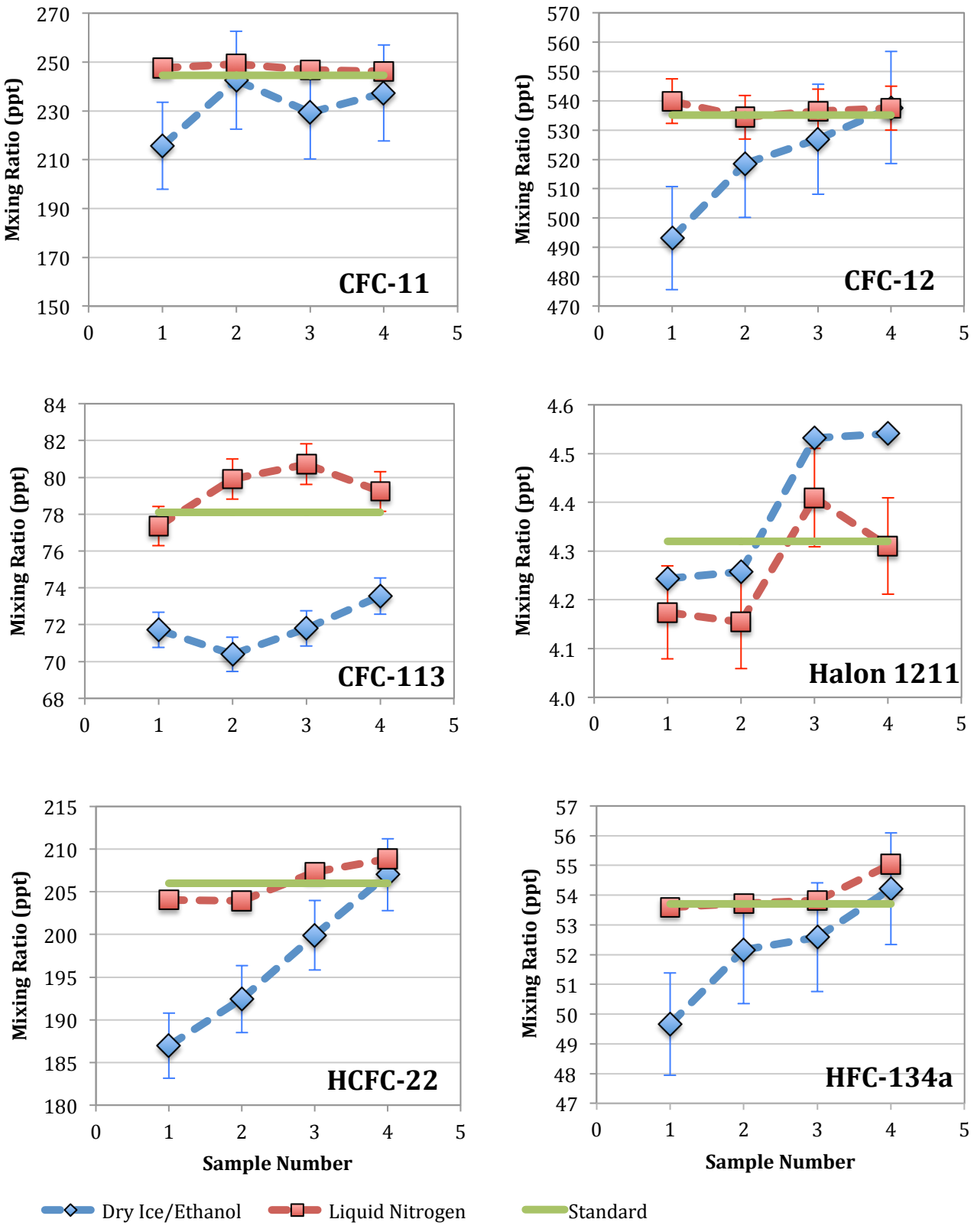

Figure 3.20a: Reproducibility testing of the inlet system for CFC-11, CFC-12, CFC-113, Halon 1211, HCFC-22 and HFC-134a. Blue points represent samples trapped using the dry ice/ethanol mixture and red points represent samples trapped using liquid nitrogen. The green line corresponds to the known mixing ratio present in the SX-0706077 standard being analysed.

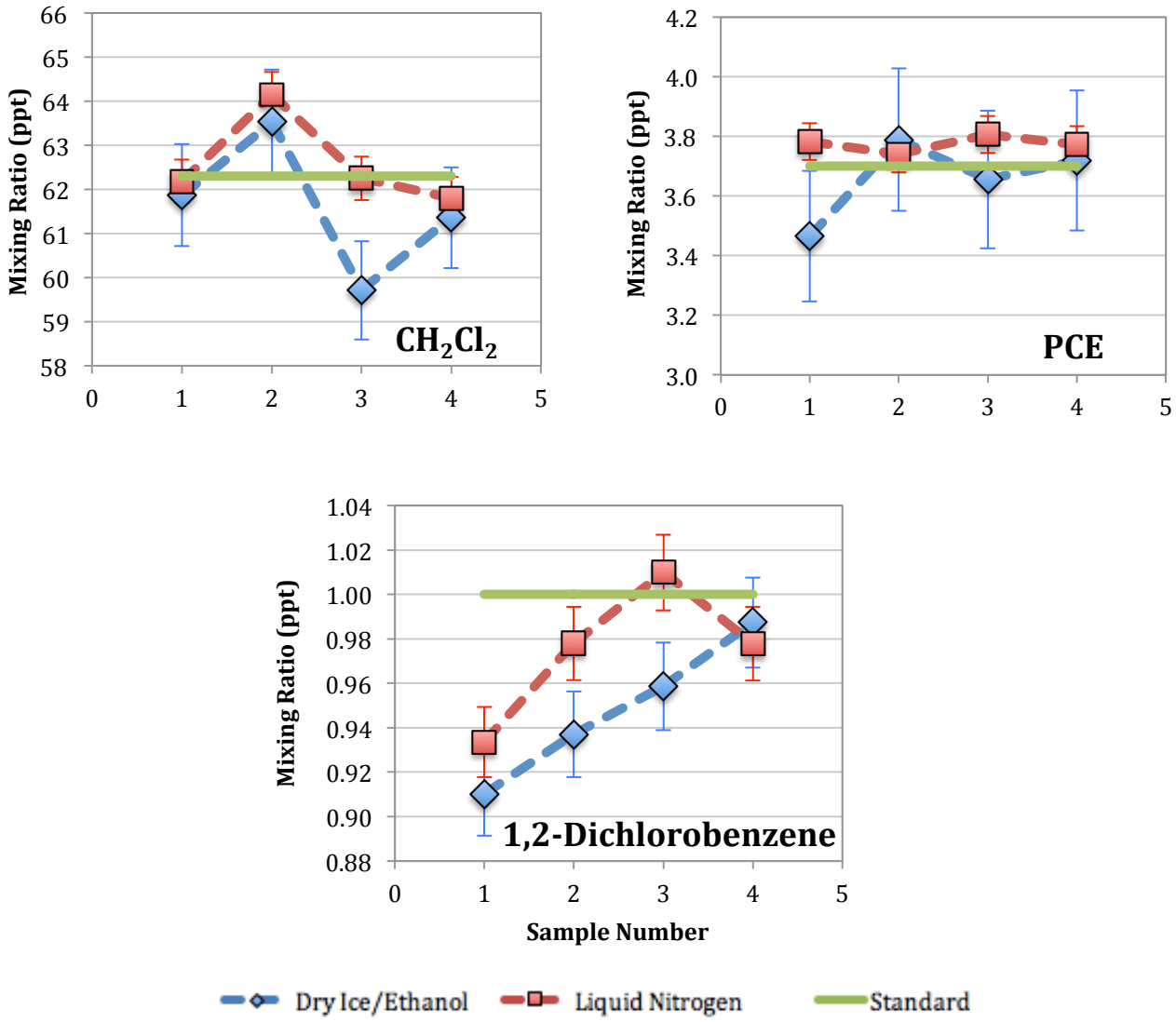

Figure 3.20b: Reproducibility testing of the inlet system for dichloromethane, PCE and 1,2-dichlorobenzene. Blue points represent samples trapped using the dry ice/ethanol mixture and red points represent samples trapped using liquid nitrogen. The green line corresponds to the known mixing ratio present in the SX-0706077 standard being analysed.

What is most noticeable in Figure 3.20, across all 9 species, is that the results from the liquid nitrogen trapping are generally detected closer to known standard concentrations. Table 3.6 similarly indicates all the percentage standard deviations are lower when headspace trapping is used, 0.42%-3.22% compared to 1.8-5.05% for the dry ice/ethanol method. This suggests that this method is producing more consistent results which is most likely due to the feedback system in place that helps control the chill point throughout the trapping process, something that is not possible with the dry ice/ethanol mixture. Whilst some of the lowest variations (0.53 and 0.42%) are detected with the two most abundant CFCs, -11 and -12, when trapped with liquid nitrogen, these compounds were found to have some of the largest variations (5.05 and 3.65%) with dry ice ethanol trapping. Given that these species both have particularly high mixing ratios, this could potentially indicate slight non-linearities for these compounds when the submerged cryotrapping method is used and this is further discussed below.

Table 3.6: Comparison of the reproducibility testing of the inlet system carried out with two cryotrapping methods for 9 halocarbon species.

Compound	Trapping Method	Standard Mixing Ratio (ppt)	Average Mixing Ratio (ppt)	S.D (%)	Sample Precision (%)
CFC-11	Dry Ice/Ethanol	244.5	231.22	5.05	8.28
	Liquid N_2		247.38	0.53	0.28
CFC-12	Dry Ice/Ethanol	535.1	519.08	3.65	3.56
	Liquid N_2		537.07	0.42	1.4
CFC-113	Dry Ice/Ethanol	78.1	71.86	1.80	1.33
	Liquid N_2		79.30	1.81	1.37
Halon 1211	Dry Ice/Ethanol	4.32	4.39	3.76	0.24
	Liquid N_2		4.26	2.82	2.29
HCFC-22	Dry Ice/Ethanol	206	196.58	4.45	2.04
	Liquid N_2		206.04	1.18	0.26
HFC-134a	Dry Ice/Ethanol	53.7	52.16	3.61	3.47
	Liquid N_2		54.04	1.24	0.48
Dichloromethane	Dry Ice/Ethanol	62.3	61.62	2.55	1.87
	Liquid N_2		62.60	1.69	0.79
PCE	Dry Ice/Ethanol	3.7	3.66	3.81	6.32
	Liquid N_2		3.78	0.72	1.64
Dichlorobenzene	Dry Ice/Ethanol	1	0.95	3.45	2.06
	Liquid N_2		0.97	3.22	1.69

3.6.2 Linearity

GC-MS systems are ideally expected to respond linearly to the mixing ratio of an injected sample, however non-linearities may arise through a number of factors including non-quantitative trapping of high concentration species or non-quantitative desorption from pre-concentration systems. In order to assess the response of the new inlet system in terms of linearity, a serial dilution of the SX-0706077 standard was trapped by both methods and analysed.

This series was statically diluted from the original standard with pure nitrogen and the dilution factors were estimated using pressure sensors. Anna Ridley, another PhD student within the department, produced five dilutions and these represented 3.34%, 7.11%, 15.15%, 30.38% and 68.11% of the standard. The same 9 halocarbon species were assigned mixing ratios for each of the dilution as well as one 100% sample. As with the precision analysis, one day was spent trapping the series with dry ice/ethanol, the other with liquid nitrogen. Table 3.7 indicates the Pearson correlation coefficients of the mixing ratios with the dilution concentrations and suggests none of the compounds were affected by non-linearities given the very high (over 0.98) coefficients calculated. Correlation appears better with the dry ice/ethanol method, however differences are not significant.

Even so, this method of comparison does not accurately indicate the variation seen with the different dilutions and so normalised fractional responses were determined.

Table 3.7: Summary of the Pearson Correlation Coeffcients for the linearity testing of 9 halocarbon species using the inlet system and two cryotrapping methods.

Compound	Pearson Correlation Coeffcient	
	Dry Ice/Ethanol	Liquid N_2
CFC-11	0.9998	0.9996
CFC-12	0.9996	0.9992
CFC-113	0.9992	0.9995
Halon 1211	0.9998	0.9978
HCFC-22	0.9996	0.9994
HFC-134a	0.9987	0.9986
Dichloromethane	0.9995	0.9988
PCE	0.9996	0.9998
Dichlorobenzene	0.9975	0.9831

Figure 3.21(a. to c.) displays the results for each of these compounds in terms of the normalised response, calculated as the relative change from the known standard abundance at each dilution, although some of the less abundant species were not detected in the lower dilutions. Results from the dry ice/ethanol trapping are in blue and the liquid nitrogen trapping is in red. In an ideal linear system, the normalised responses for all the dilutions should lie on the y = 1, within error margins. For the majority of the considered species, deviation from the ideal response is within 10% down to the 15.15% dilution, with only CFC-12 seeing more variation (~20% with dry ice/ethanol, ~30% with liquid nitrogen) in the 68.11% dilution. Wider deviation is seen with most species in the 7.11% and 3.34% dilutions and for the more abundant species (CFC-11, CFC-12, CFC-113, HCFC-22 and HFC-134a) these deviations are negative for the 7.11% and positive for the 3.34%. Less abundant species, such as halon-1211, PCE and 1,2-dichlorobenzene, were not measured in the 3.34% dilution, likely due to limits of detection for these species being reached. However, their lack of significant deviation in the 7.11% dilution, unlike the more abundant species, suggests that it is not mixing ratio alone that may be affecting linearity. Further investigation would be necessary to identify whether a combination of factors contribute to the differences seen, potentially utilising a more sensitive mass spectrometer and analysing a volume series as well. Overall, linearity appears good for the system when analysing less diluted samples.

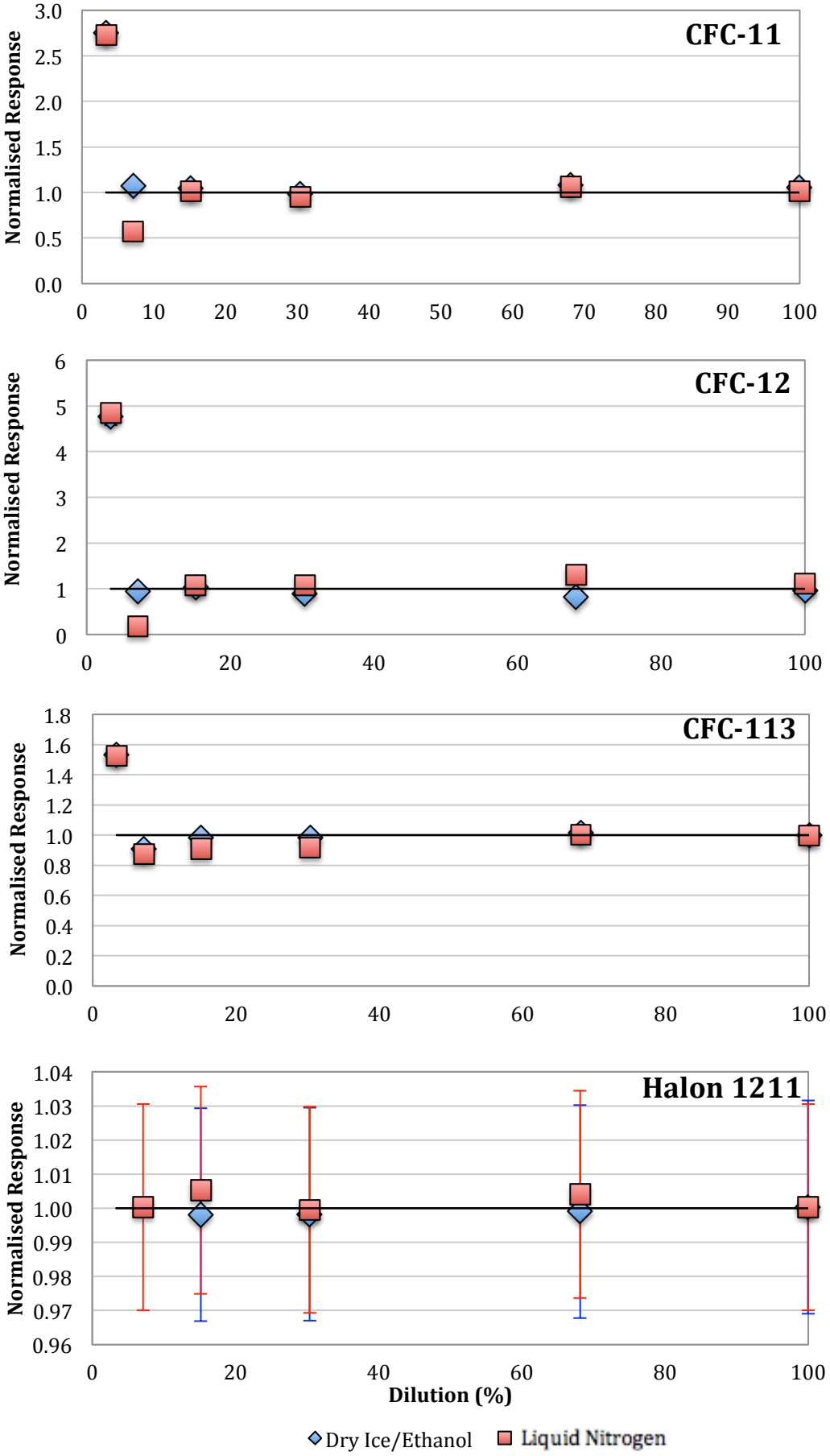

Figure 3.21a: Graphical summary of the normalised response of an SX-0706077 dilution series for CFC-11, CFC-12, CFC-113 and Halon 1211, analysed on the inlet system. Blue diamonds represent samples cryo-trapped by a dry ice/ethanol mixture, red squares represents samples cryo-trapped by liquid nitrogen.

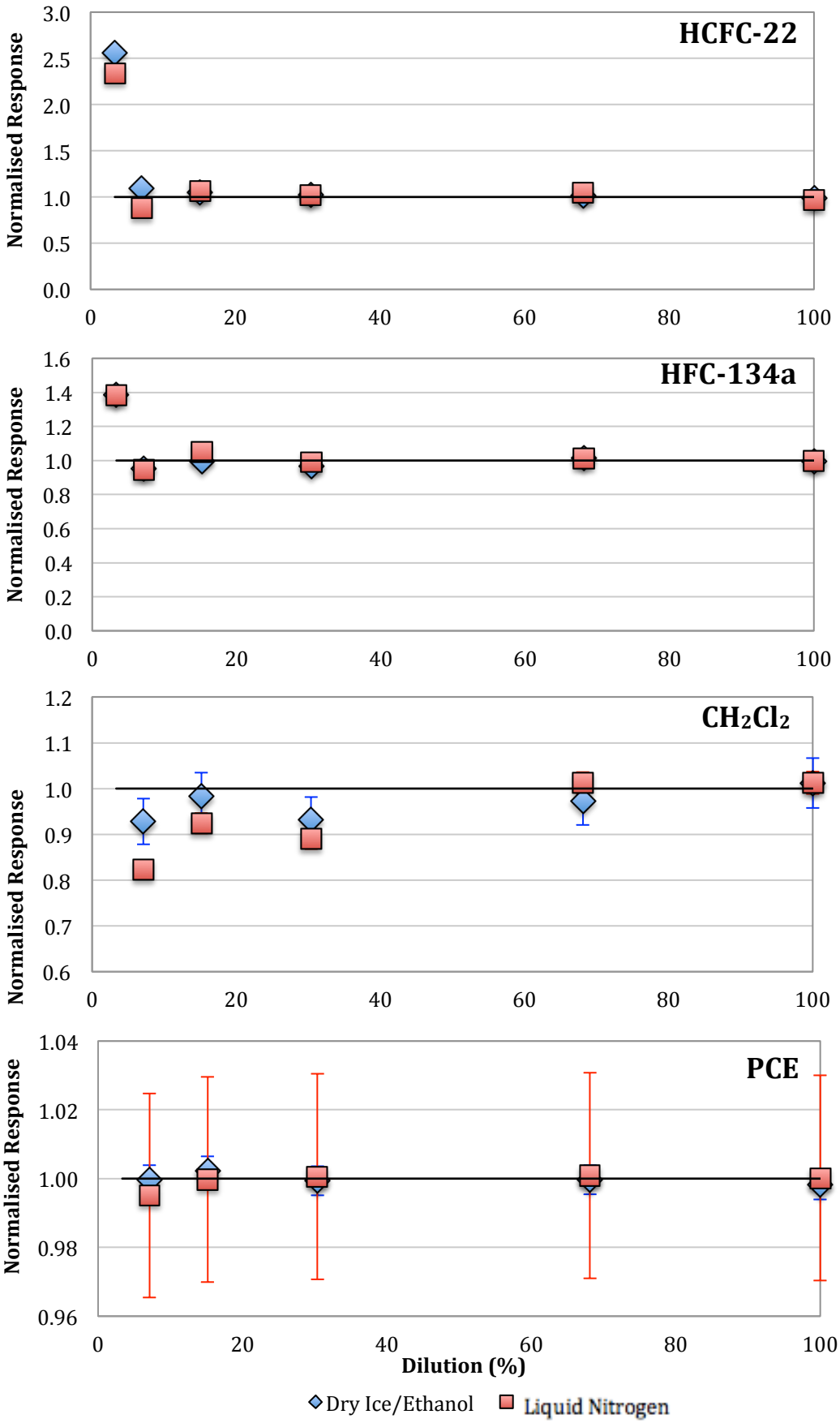

Figure 3.21b: Graphical summary of the normalised response of an SX-0706077 dilution series for HCFC-22, HFC-134, dichloromethane and PCE, analysed on the inlet system. Blue diamonds represent samples cryo-trapped by a dry ice/ethanol mixture, red squares represents samples cryo-trapped by liquid nitrogen.

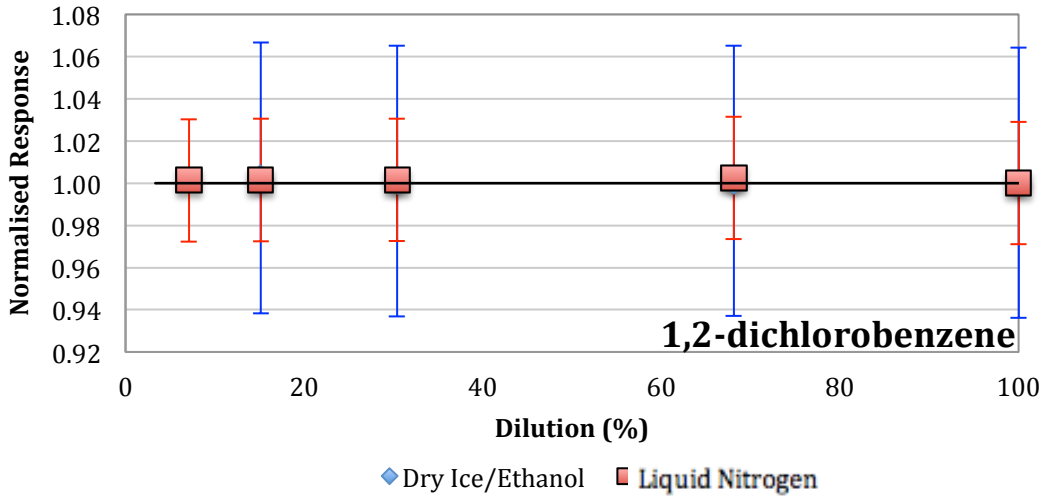

Figure 3.21c: Graphical summary of the normalised response of an SX-0706077 dilution series for 1,2-dichlorobenzene analysed on the inlet system. Blue diamonds represent samples cryo-trapped by a dry ice/ethanol mixture, red squares represents samples cryo-trapped by liquid nitrogen.

3.7 Summary and Further Investigations

Since November 2012, the automated inlet system has been constructed from a series of valves, tubing and electronics into a functional GC-MS trapping and injection system. Minor changes to valve positions since the early designs have been made but, other than the addition of an improved system for the headspace cryotrapping, few significant changes to the design have occurred. This modification however, has resulted in the liquid nitrogen trapping becoming the more consistent of the two processes. It also allows for a much wider variation in trapping temperatures, requires topping up less frequently and has less associated risks than large volumes of ethanol. Further testing to assess the range and limitations available using liquid nitrogen trapping is necessary, both in terms of temperature and unattended running.

Although preliminary testing has been carried out, and a basic method for trapping, injecting and analysing air samples has been prepared, more testing and adjustments will be needed before the system is fully automated and able to be installed on the AutoSpec system. Whilst linearity appears good for the majority of higher mixing ratio samples, further assessment of the cause of non-linearities at lower abundances and determining reproducibility using a larger sample set is necessary. However, problems during construction of the system prevented there from being enough time to do this. A wider range of species should also be investigated, with particular focus on the high boiling compounds so an upper limit for the system can be determined. As well as this, although bromoform was detected with dry ice/ethanol cryotrapping during testing, it was not found in any of the liquid nitrogen trapped samples. Since bromoform is a particular species of interest, further examination of this occurrence is suggested.

A potential reason for this could be the variability in trapping temperature associated with the liquid nitrogen cooling method as, since colder temperatures can be reached, the chill point may fluctuate cooler which is not seen with the dry ice/ethanol mixture. A cooler chill temperature may result in more CO_2 being trapped on the sample loop which could impact other species trapped, particularly those that produce only small peaks when analysed, like bromoform.

Finally, further programming of the electronics and associated computer systems as well as an emphasis towards potential remote control is essential to continue the automation process. Installation of a Stirling cooler is being considered in order to give the system independence from solvents and further facilitate overnight running.

4.1 NAME Backwards Trajectories for the Taiwan 2013 Campaign

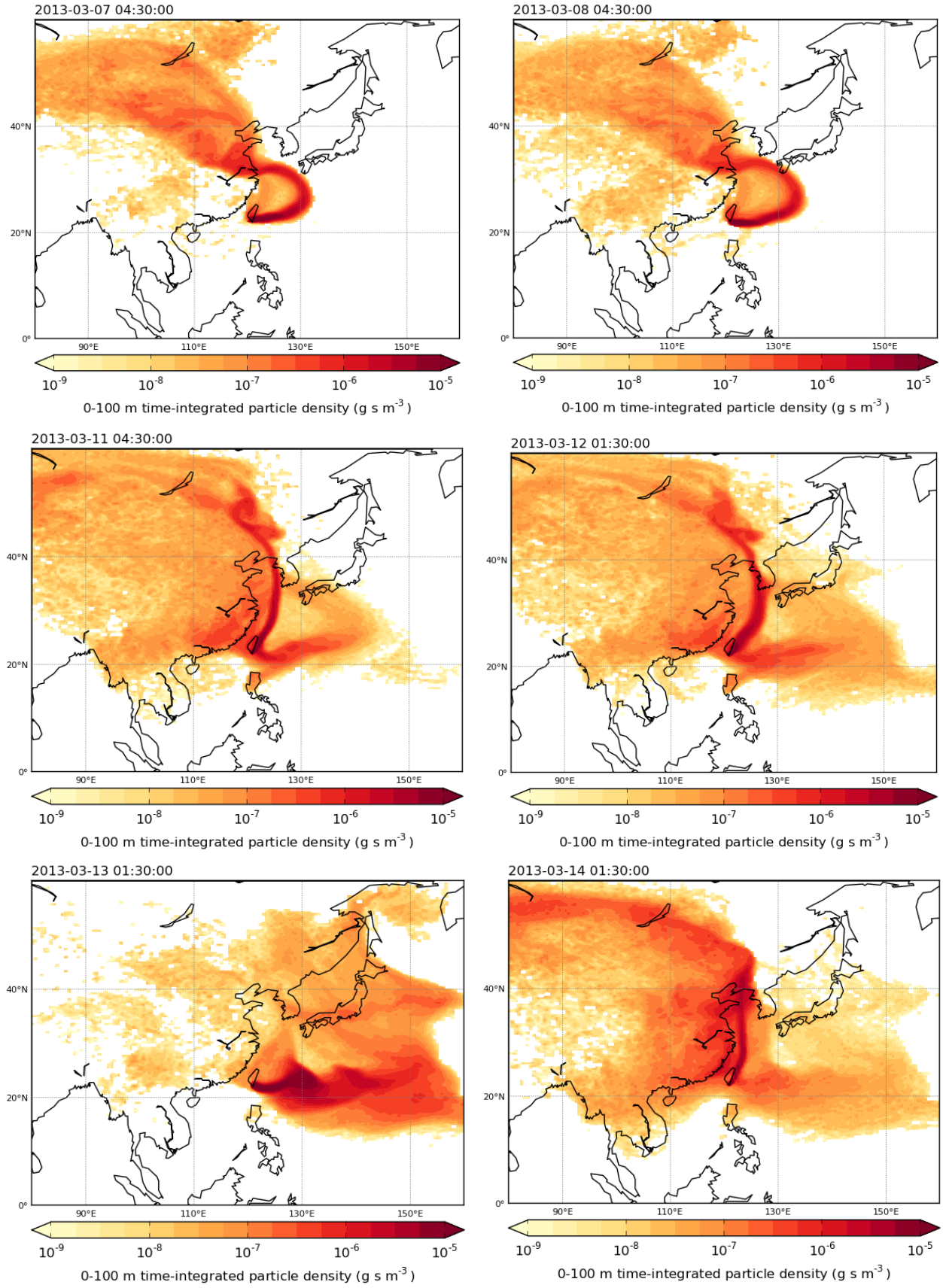

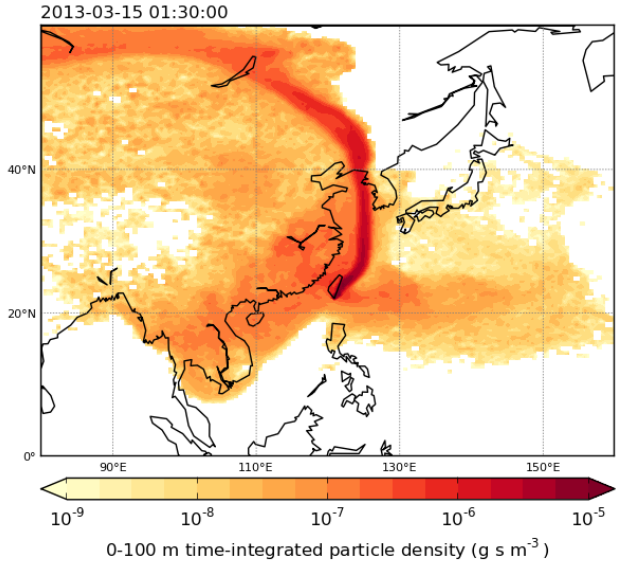
2013-03-15 01:30:00
40°N
20°N
0°
90°E
110°E
130°E
150°E
10^-9
10^-8
10^-7
10^-6
10^-5
0-100 m time-integrated particle density (g s m^-3)

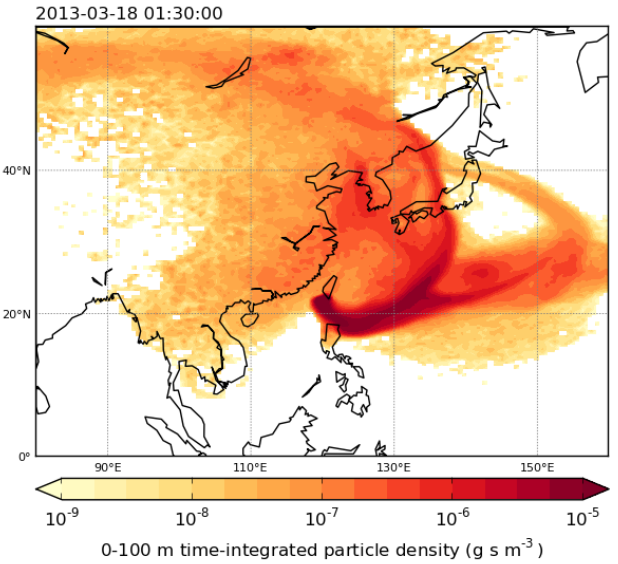
2013-03-18 01:30:00
40°N
20°N
0°
90°E
110°E
130°E
150°E
10^-9
10^-8
10^-7
10^-6
10^-5
0-100 m time-integrated particle density (g s m^-3)

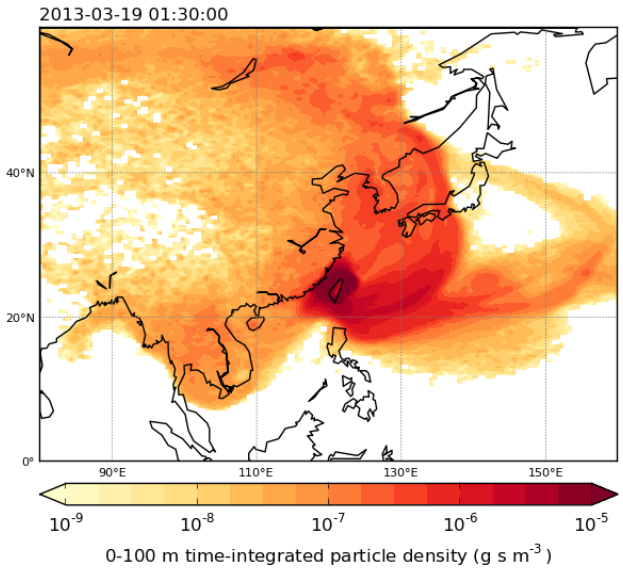
2013-03-19 01:30:00
40°N
20°N
0°
90°E
110°E
130°E
150°E
10^-9
10^-8
10^-7
10^-6
10^-5
0-100 m time-integrated particle density (g s m^-3)

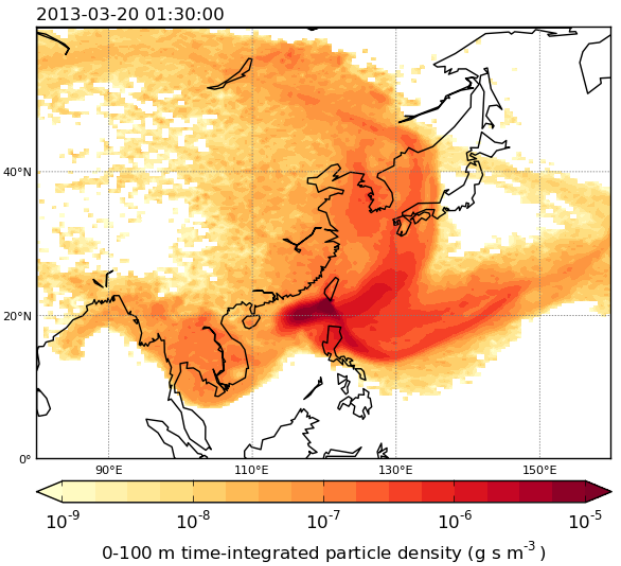
2013-03-20 01:30:00
40°N
20°N
0°
90°E
110°E
130°E
150°E
10^-9
10^-8
10^-7
10^-6
10^-5
0-100 m time-integrated particle density (g s m^-3)

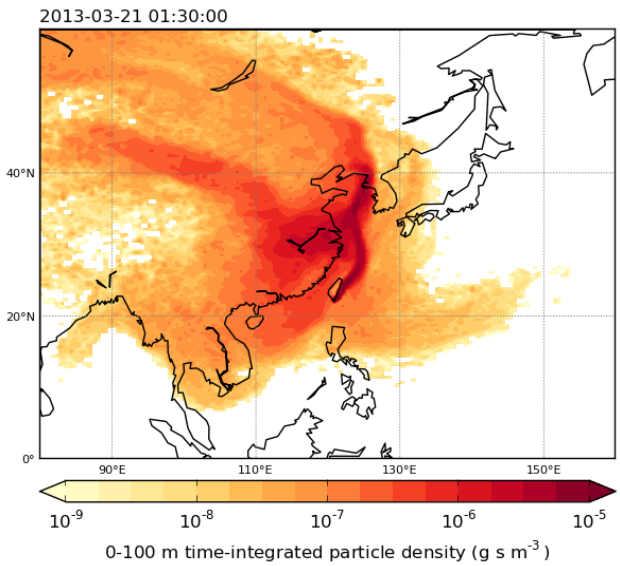
2013-03-21 01:30:00
40°N
20°N
0°
90°E
110°E
130°E
150°E
10^-9
10^-8
10^-7
10^-6
10^-5
0-100 m time-integrated particle density (g s m^-3)

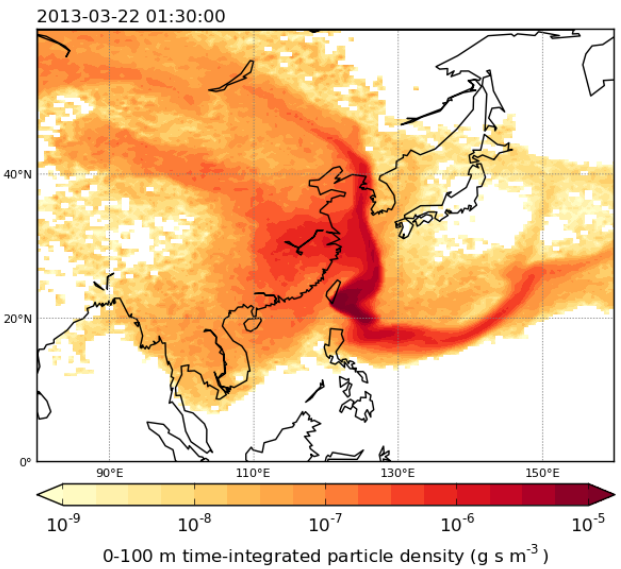
2013-03-22 01:30:00
40°N
20°N
0°
90°E
110°E
130°E
150°E
10^-9
10^-8
10^-7
10^-6
10^-5
0-100 m time-integrated particle density (g s m^-3)

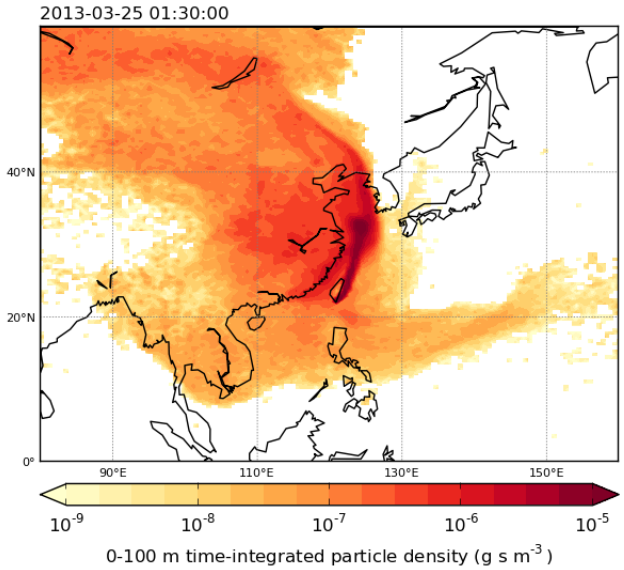
2013-03-25 01:30:00
40°N
20°N
0°
90°E
110°E
130°E
150°E
10-9
10-8
10-7
10-6
10-5
0-100 m time-integrated particle density (g s m-3)

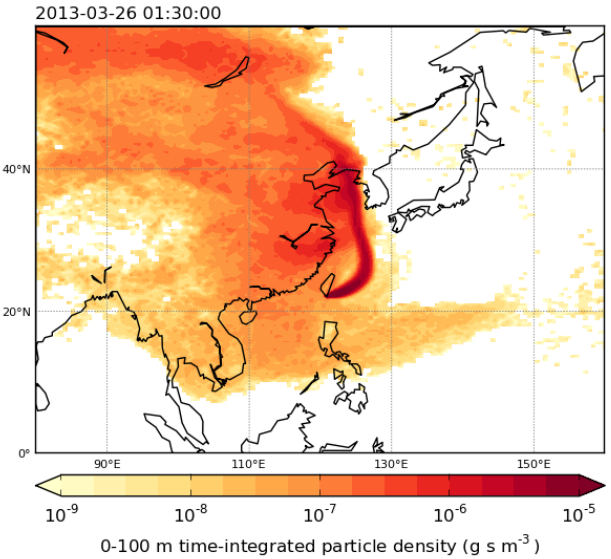
2013-03-26 01:30:00
40°N
20°N
0°
90°E
110°E
130°E
150°E
10-9
10-8
10-7
10-6
10-5
0-100 m time-integrated particle density (g s m-3)

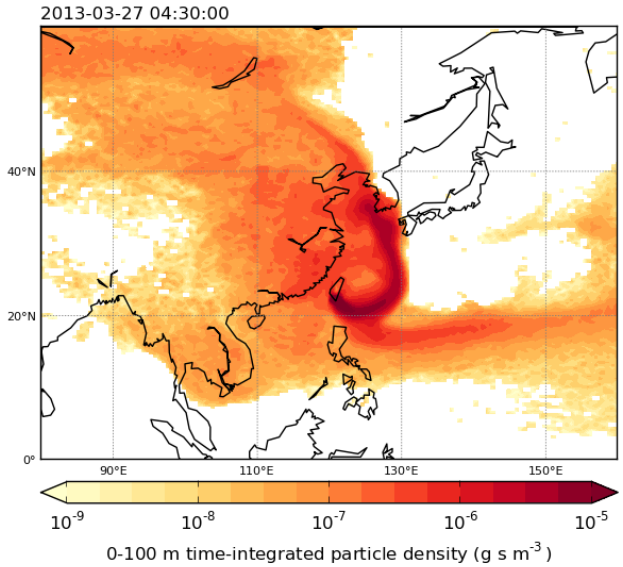
2013-03-27 04:30:00
40°N
20°N
0°
90°E
110°E
130°E
150°E
10-9
10-8
10-7
10-6
10-5
0-100 m time-integrated particle density (g s m-3)

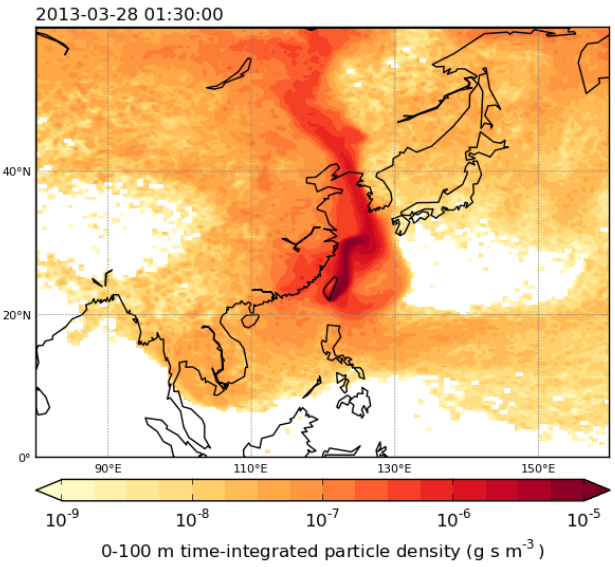
2013-03-28 01:30:00
40°N
20°N
0°
90°E
110°E
130°E
150°E
10-9
10-8
10-7
10-6
10-5
0-100 m time-integrated particle density (g s m-3)

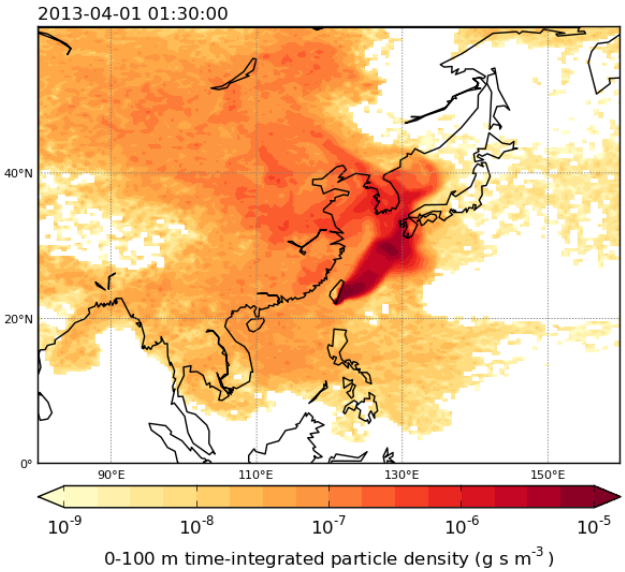
2013-04-01 01:30:00
40°N
20°N
0°
90°E
110°E
130°E
150°E
10-9
10-8
10-7
10-6
10-5
0-100 m time-integrated particle density (g s m-3)

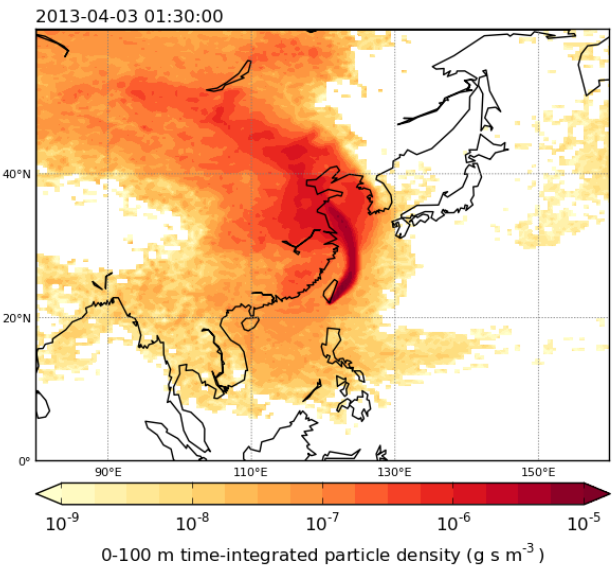
2013-04-03 01:30:00
40°N
20°N
0°
90°E
110°E
130°E
150°E
10-9
10-8
10-7
10-6
10-5
0-100 m time-integrated particle density (g s m-3)

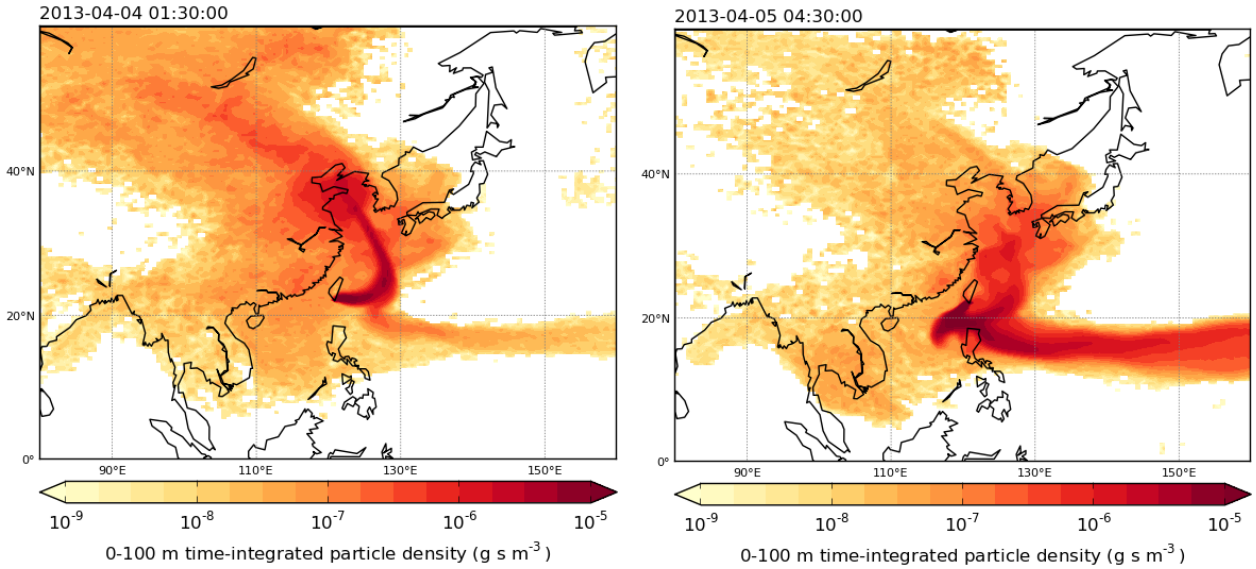

4.2 NAME Backward Trajectories for the Taiwan 2014 Campaign

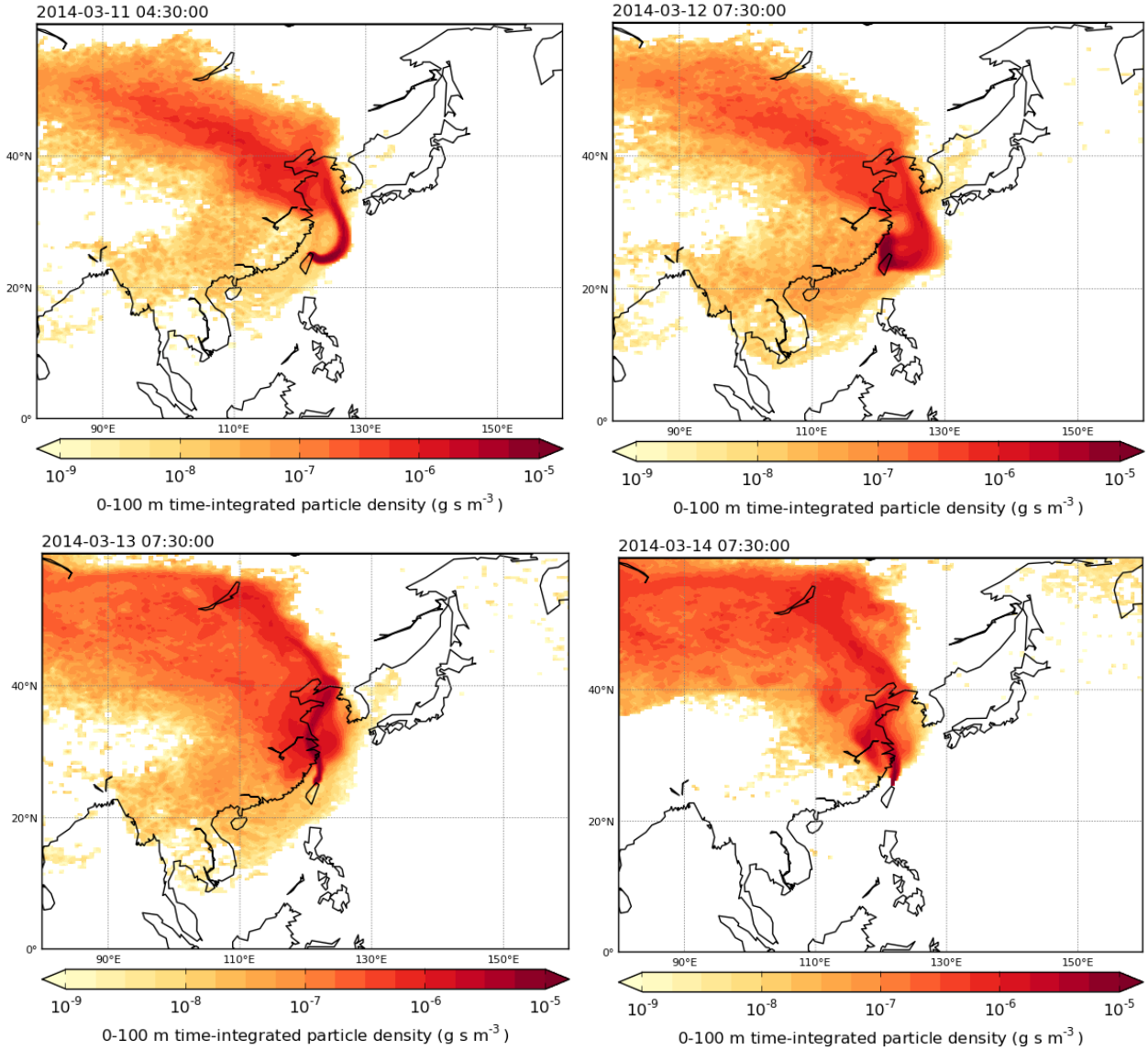

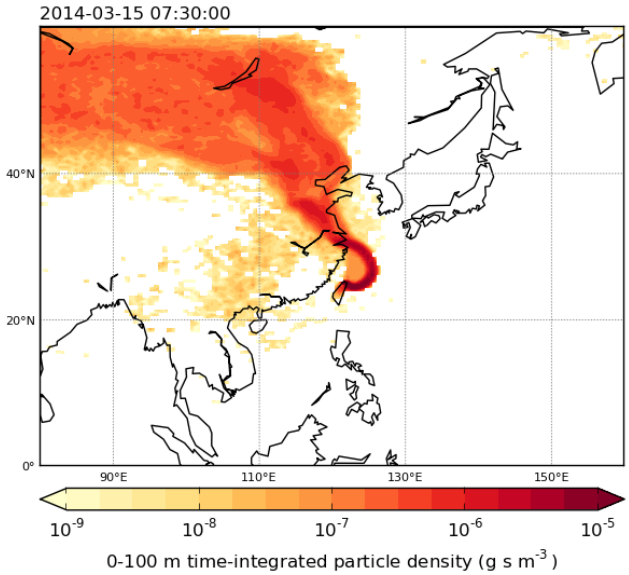
2014-03-15 07:30:00
40°N
20°N
0°
90°E
110°E
130°E
150°E
10-9
10-8
10-7
10-6
10-5
0-100 m time-integrated particle density (g s m-3)

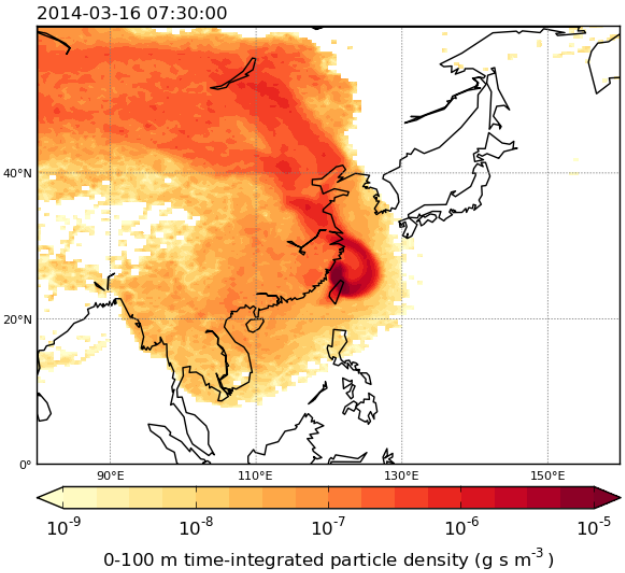
2014-03-16 07:30:00
40°N
20°N
0°
90°E
110°E
130°E
150°E
10-9
10-8
10-7
10-6
10-5
0-100 m time-integrated particle density (g s m-3)

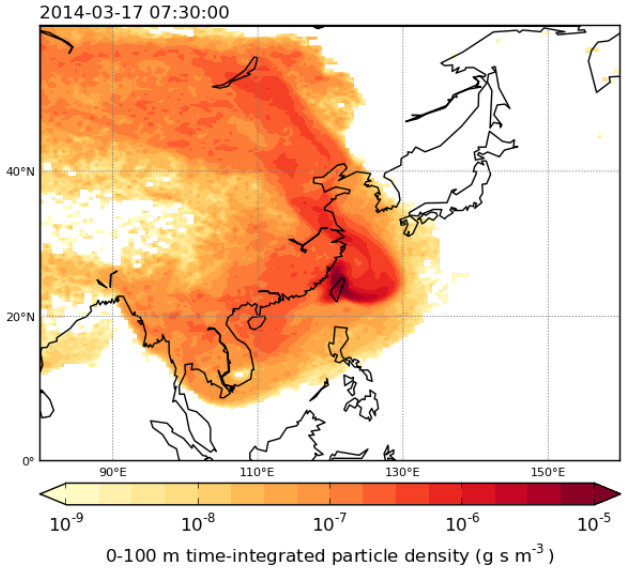
2014-03-17 07:30:00
40°N
20°N
0°
90°E
110°E
130°E
150°E
10-9
10-8
10-7
10-6
10-5
0-100 m time-integrated particle density (g s m-3)

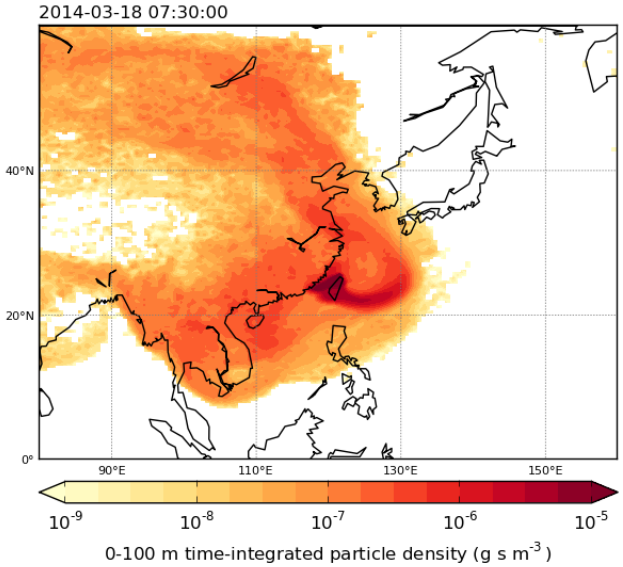
2014-03-18 07:30:00
40°N
20°N
0°
90°E
110°E
130°E
150°E
10-9
10-8
10-7
10-6
10-5
0-100 m time-integrated particle density (g s m-3)

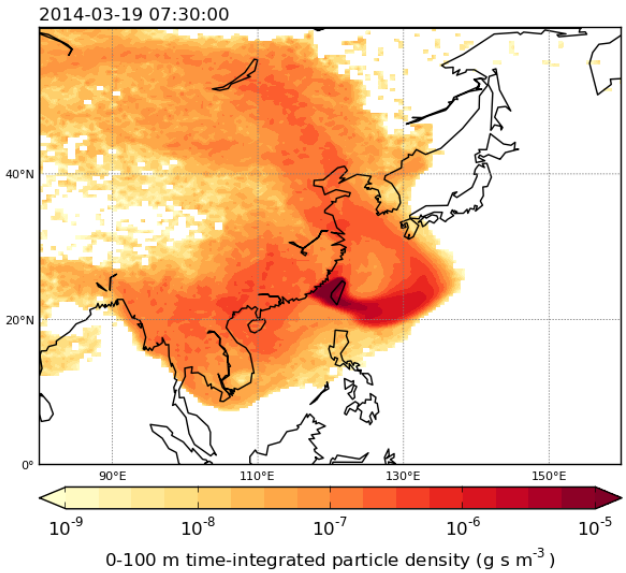
2014-03-19 07:30:00
40°N
20°N
0°
90°E
110°E
130°E
150°E
10-9
10-8
10-7
10-6
10-5
0-100 m time-integrated particle density (g s m-3)

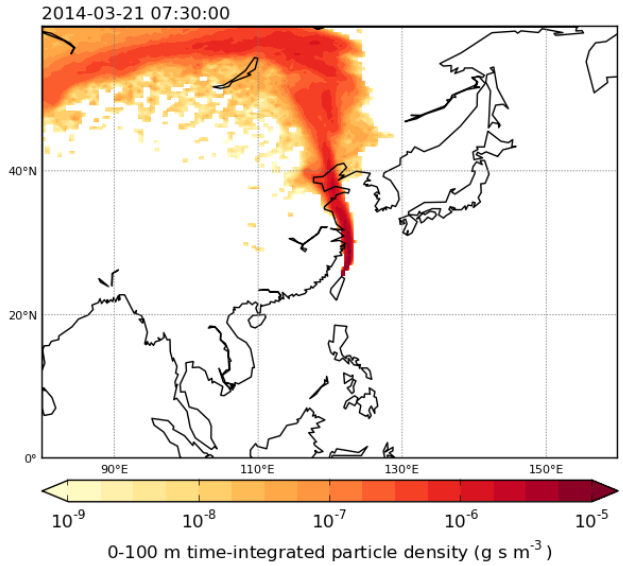
2014-03-21 07:30:00
40°N
20°N
0°
90°E
110°E
130°E
150°E
10-9
10-8
10-7
10-6
10-5
0-100 m time-integrated particle density (g s m-3)

L

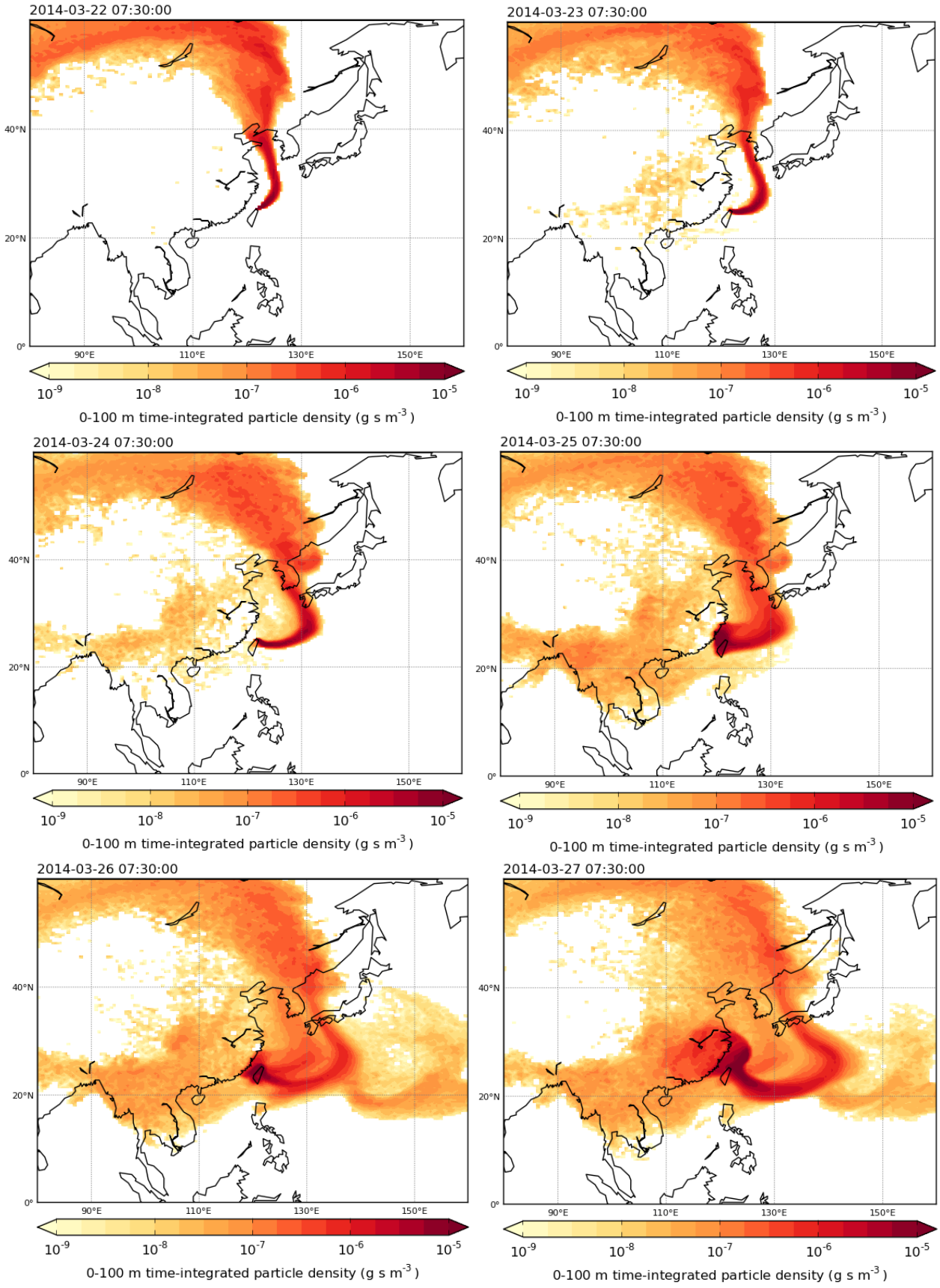
2014-03-22 07:30:00
2014-03-23 07:30:00
2014-03-24 07:30:00
2014-03-25 07:30:00
2014-03-26 07:30:00
2014-03-27 07:30:00
40°N
20°N
0°
90°E
110°E
130°E
150°E
10-9
10-8
10-7
10-6
10-5
0-100 m time-integrated particle density (g s m-3)

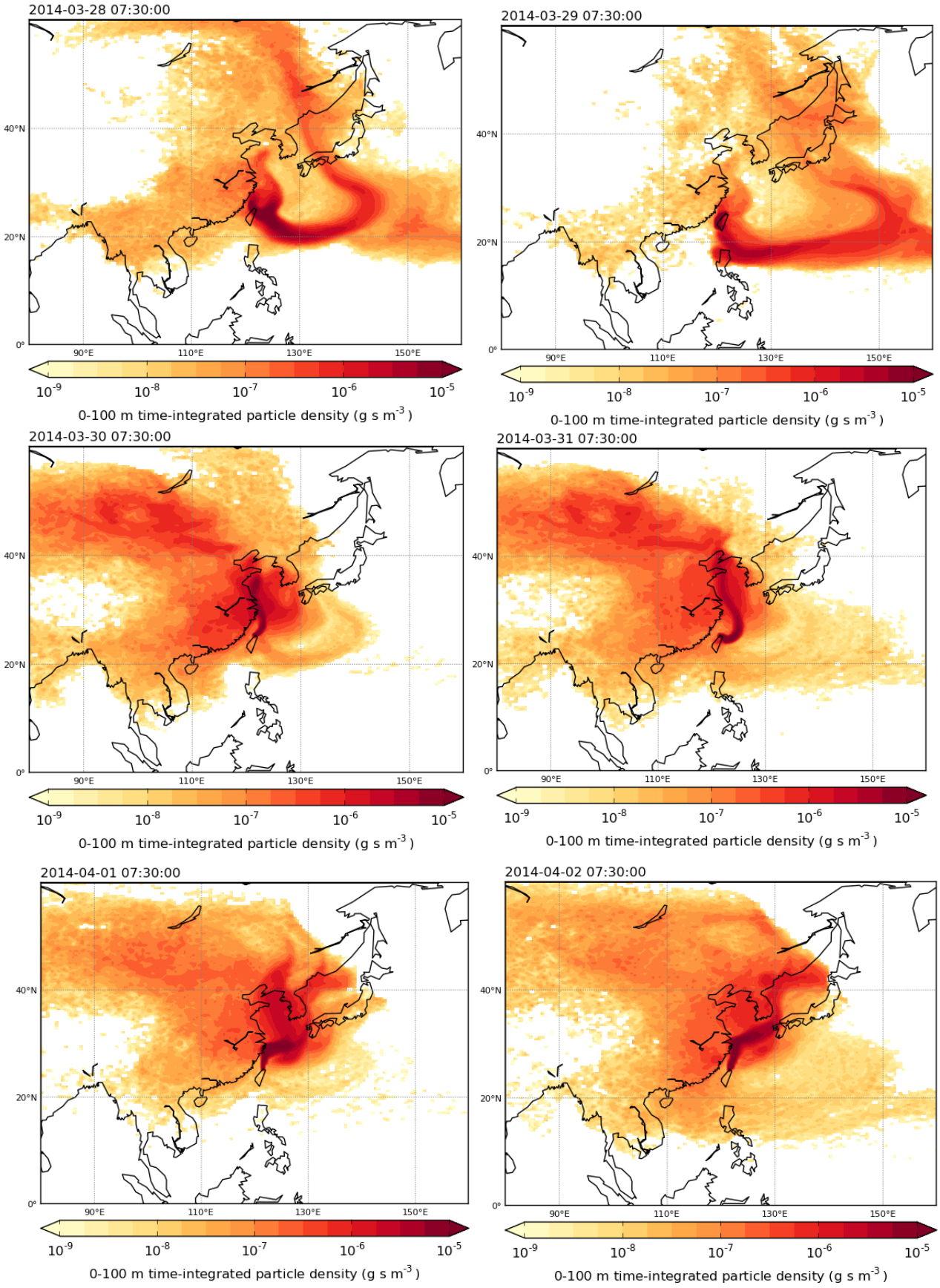
2014-03-28 07:30:00
2014-03-29 07:30:00
2014-03-30 07:30:00
2014-03-31 07:30:00
2014-04-01 07:30:00
2014-04-02 07:30:00
40°N
20°N
0°
90°E
110°E
130°E
150°E
10-9
10-8
10-7
10-6
10-5
0-100 m time-integrated particle density (g s m-3)

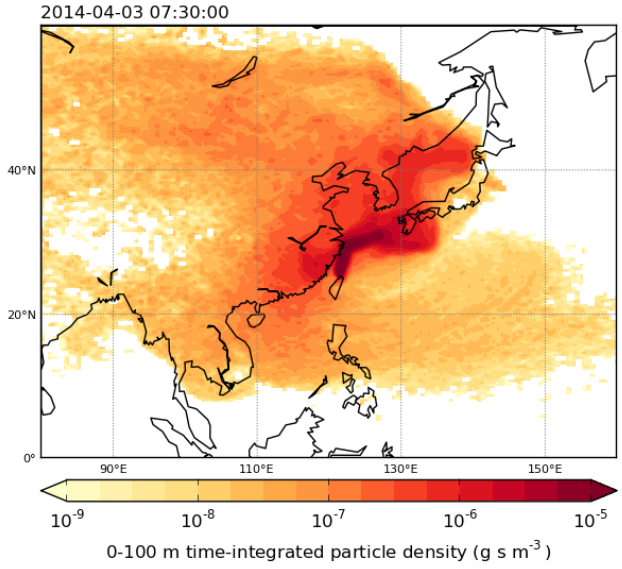

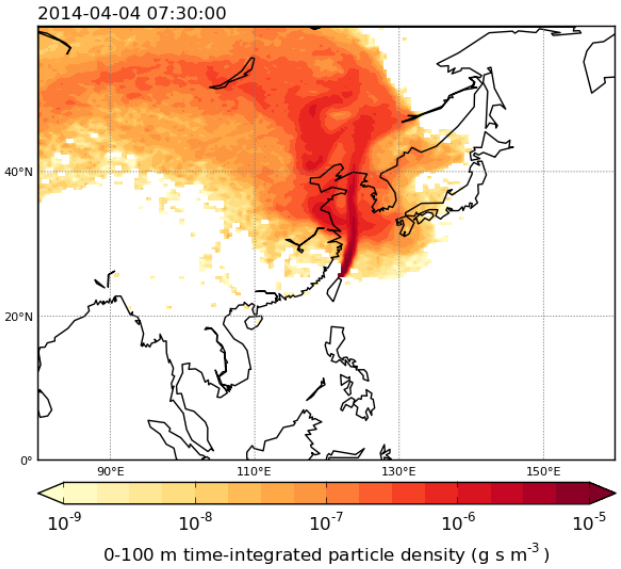

4.3 NAME Backwards Trajectories for the Taiwan 2015 Campaign

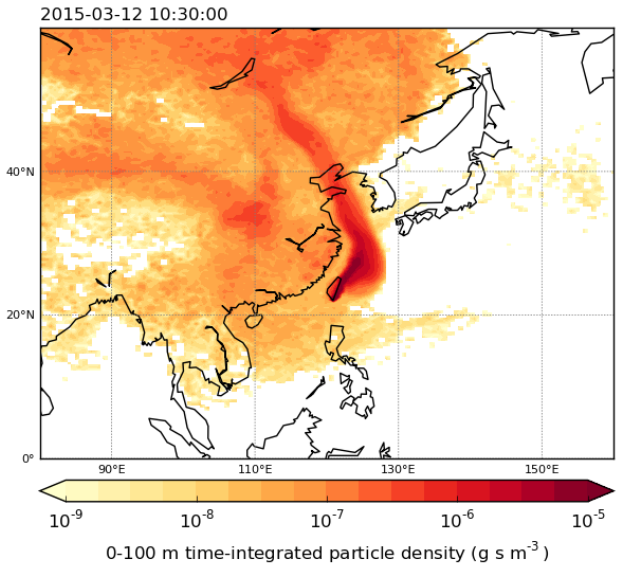

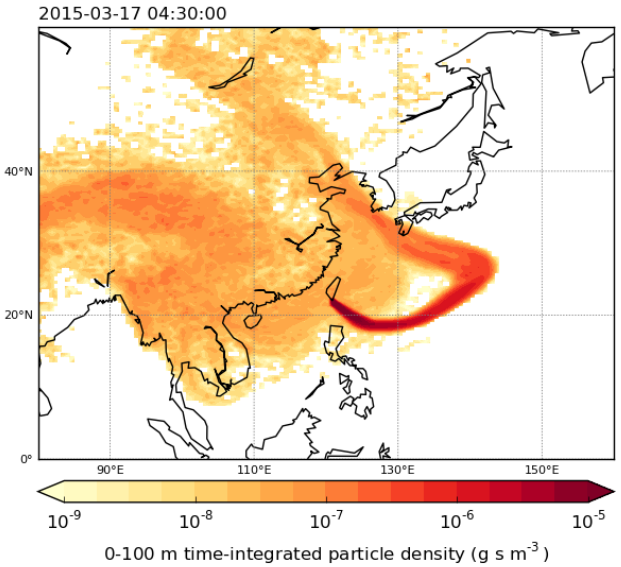

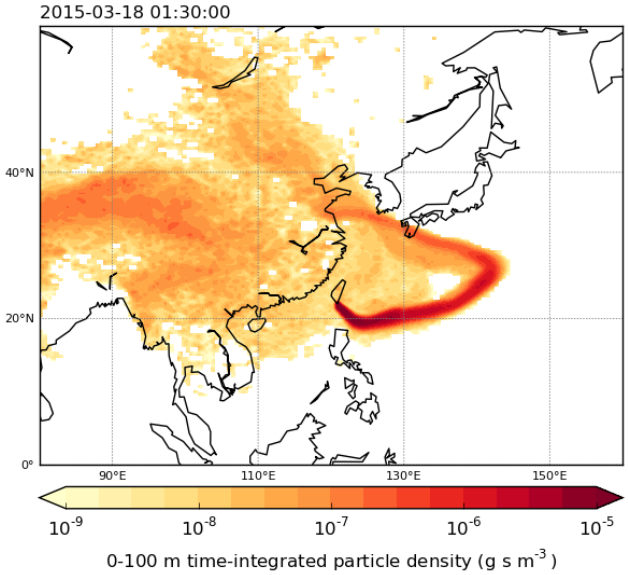

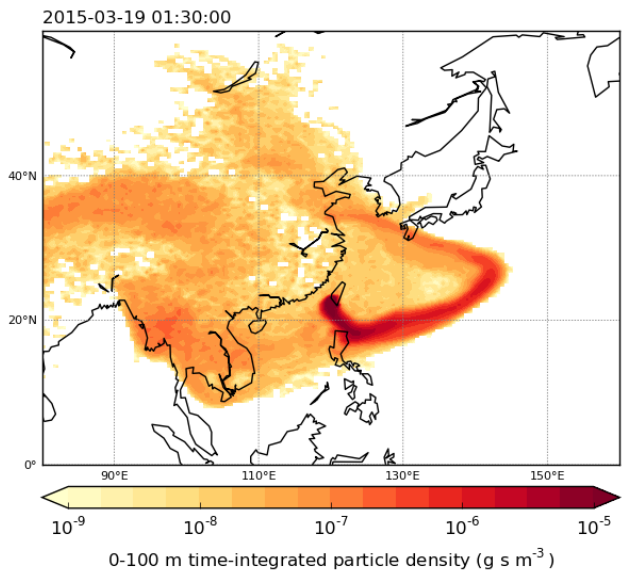

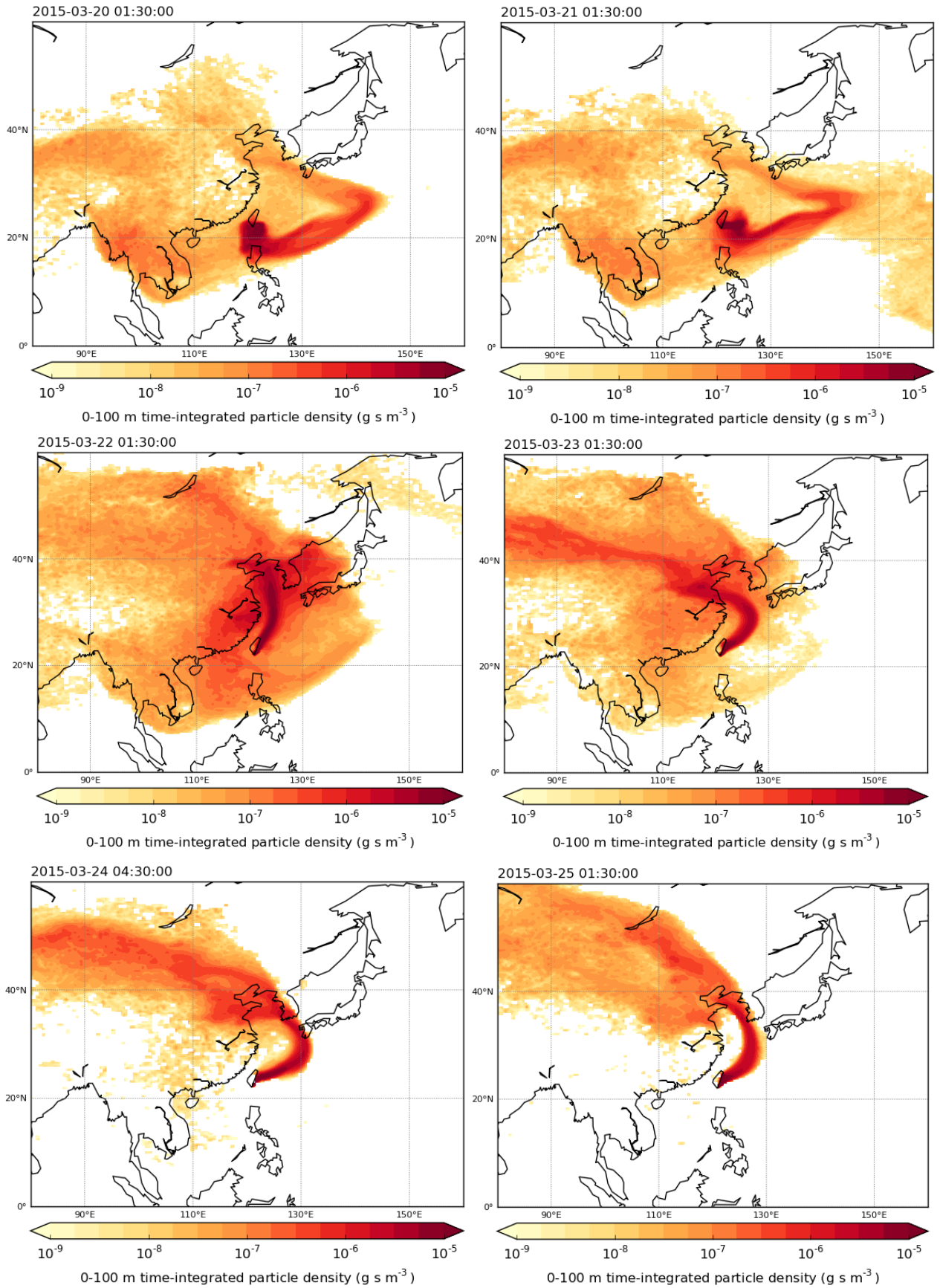
2015-03-20 01:30:00
2015-03-21 01:30:00
2015-03-22 01:30:00
2015-03-23 01:30:00
2015-03-24 04:30:00
2015-03-25 01:30:00
40°N
20°N
0°
90°E
110°E
130°E
150°E
10^{-9}
10^{-8}
10^{-7}
10^{-6}
10^{-5}
0-100 m time-integrated particle density (g s m^{-3})

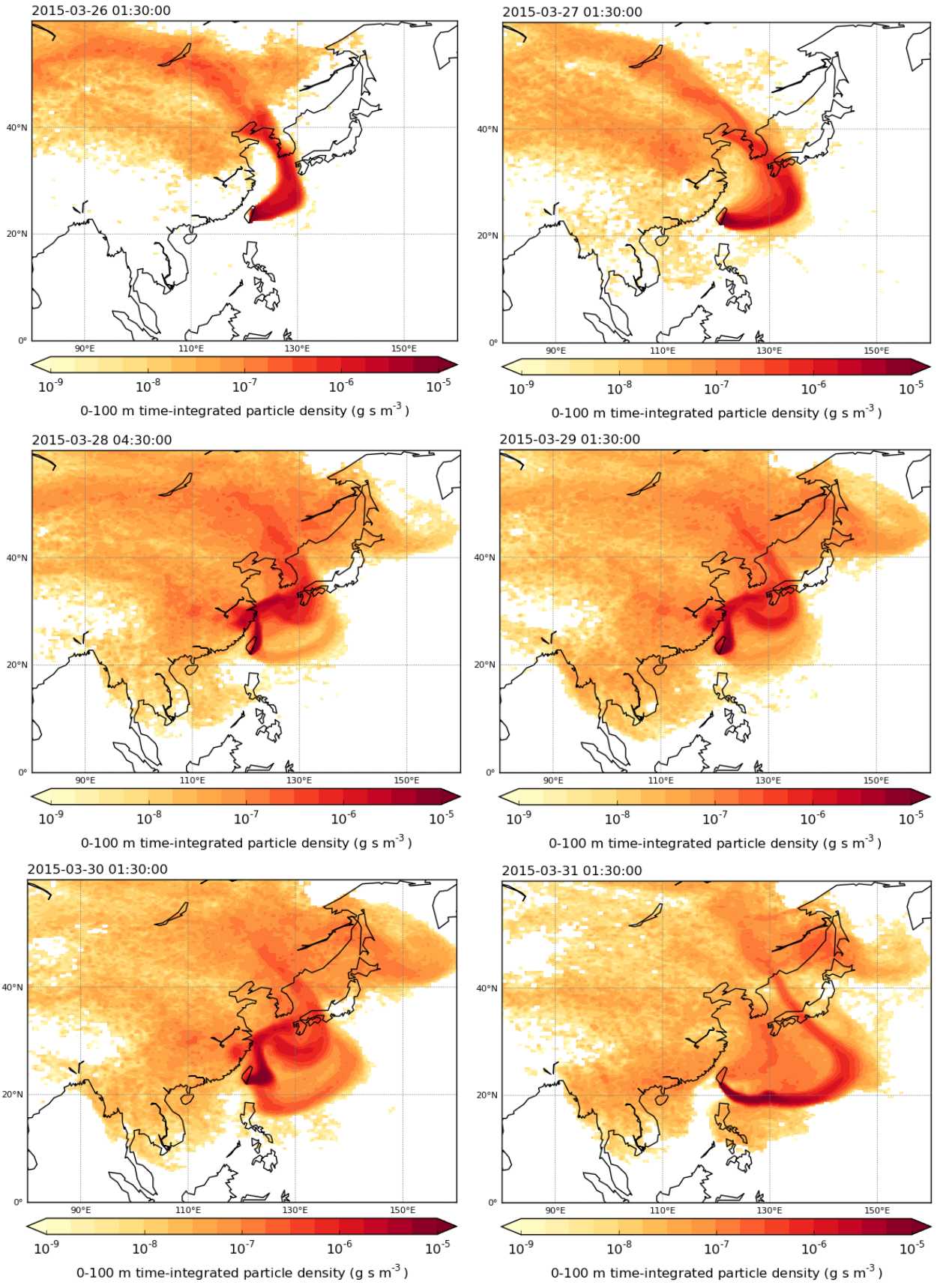
2015-03-26 01:30:00
2015-03-27 01:30:00
2015-03-28 04:30:00
2015-03-29 01:30:00
2015-03-30 01:30:00
2015-03-31 01:30:00
40°N
20°N
0°
90°E
110°E
130°E
150°E
10-9
10-8
10-7
10-6
10-5
0-100 m time-integrated particle density (g s m-3)

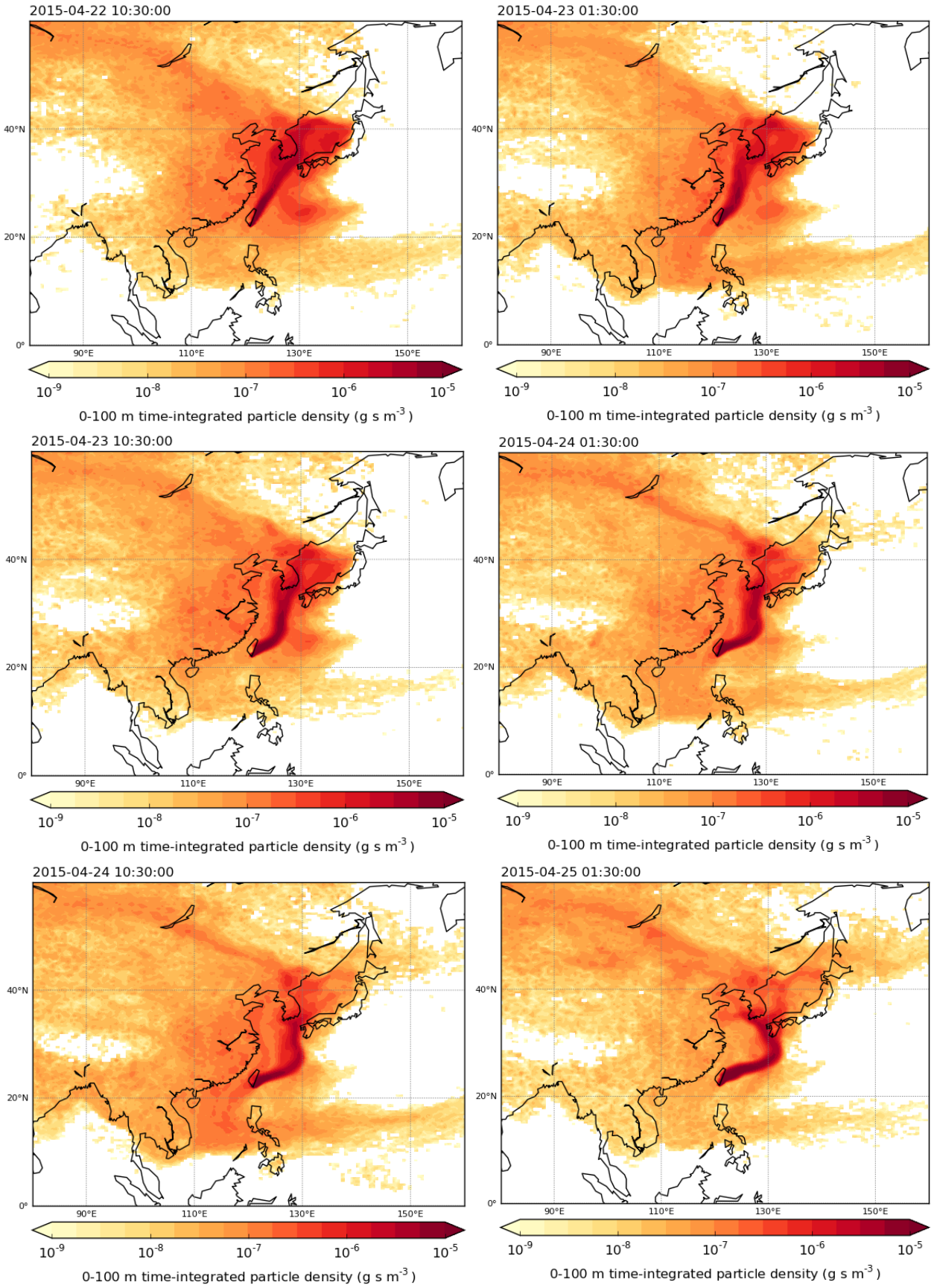
2015-04-22 10:30:00
2015-04-23 01:30:00
2015-04-23 10:30:00
2015-04-24 01:30:00
2015-04-24 10:30:00
2015-04-25 01:30:00
40°N
20°N
0°
90°E
110°E
130°E
150°E
10-9
10-8
10-7
10-6
10-5
0-100 m time-integrated particle density (g s m-3)

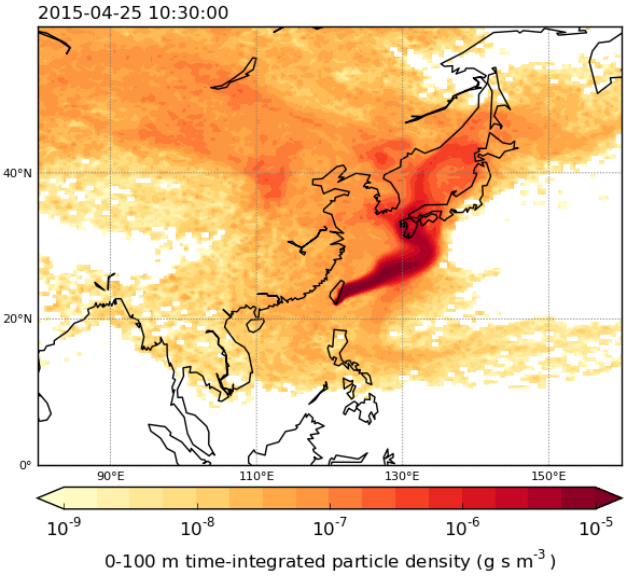
2015-04-25 10:30:00
40°N
20°N
0°
90°E
110°E
130°E
150°E
10-9
10-8
10-7
10-6
10-5
0-100 m time-integrated particle density (g s m-3)

4.4a Summary of the range and median mixing ratios for the CFCs and halons measured during the 2013, 2014 and 2015 Taiwan campaigns.

Compound		Campaign Mixing Ratios (ppt)								
Group	Name	2013			2014			2015		
		Min	Median	Max	Min	Median	Max	Min	Median	Max
CFCs	11	249	256	304	229	237	249	231	238	757
	12	511	526	543	519	524	530	513	519	533
	13	4.0	4.1	4.7				4.0	4.0	4.1
	113	74.1	75.4	79.8	73.4	74.8	82.1			
	113a	0.4	0.7	1.8	0.7	0.9	3.2	0.6	0.8	1.6
	114							14.7	15.0	15.3
	114a							1.05	1.08	1.20
	115	8.7	8.8	9.0	8.4	8.7	9.0	8.5	8.8	9.2
Halons	1211	4.0	4.2	5.2	3.7	4.1	4.8	3.5	3.9	4.7
	1202	0.02	0.03	0.04	0.02	0.02	0.05	0.02	0.02	0.03
	1301	3.0	3.2	3.5	3.2	3.3	3.5	3.1	3.3	3.6
	2402	0.46	0.49	0.51	0.44	0.48	0.86	0.3	0.5	0.5

4.4b Summary of the range and median mixing ratios for the HCFCs and chlorocarbons measured during the 2013, 2014 and 2015 Taiwan campaigns. Those rows highlighted in yellow represent species not currently calibrated and so are relative to the AAL-071170 standard.

Compound		Campaign Mixing Ratios (ppt)								
		2013			2014			2015		
Group	Name	Min	Median	Max	Min	Median	Max	Min	Median	Max
HCFCs	21	1.3	2.0	4.2	1.2	2.2	8.4			
	22	230	260	350	235	267	347	242	261	2090
	31				3.7	5.6	27.6	3.2	4.5	16.5
	123				0.02	0.05	0.95	0.02	0.06	0.16
	124				0.9	0.9	1.3	0.8	1.0	1.4
	133a	0.5	0.8	5.5	0.5	0.6	1.9	0.4	0.6	1.8
	141b	25	31	48	25	33	95	25	29	40
	142b	21.2	23.0	28.2	21.7	24.1	30.0	22.0	23.5	27.0
	225cb	0.8		1.9	0.5	0.7	1.6			
Chloro-carbons	CCl_4	87.2	89.6	134	81.4	85.5	101	82.7	85.7	94.4
	CH_3CCl_3	4.7	5.0	5.5	3.7	4.0	4.4	2.9	3.3	3.7
	Halothane				0.01	0.01	0.01	0.01	0.01	0.01
	Isoflurane	1.2	1.6	2.3	0.0	1.3	1.8	1.3	1.4	2.6
	C_3H_7Cl	4.1	5.5	24.9	0.6	1.9	5.9	1.4	3.7	13.5
	C_2H_3Cl	9.7	36.7	487	2.7	15.9	93.1	4.5	9.7	239
	C_2F_3Cl	0.2	0.4	1.1	0.1	0.2	4.1			

4.4c Summary of the range and median mixing ratios for the chlorinated and brominated VSLS and methyl halides measured during the 2013, 2014 and 2015 Taiwan campaigns. Those rows highlighted in yellow represent species not currently calibrated and so are relative to the AAL-071170 standard.

Compound		Campaign Mixing Ratios (ppt)								
Group	Name	2013			2014			2015		
		Min	Median	Max	Min	Median	Max	Min	Median	Max
VSLS-Cl	PCE	1.66	4.38	10.8	1.65	5.61	18.6	1.8	4.3	8.9
	DCE	23.7	119	820	15	82	950	12.8	59.0	356
	CH_2Cl_2	76.8	239	477	75.4	265	3970	59.4	199	537
	Chloroform	11.6	33.0	199	14	36	100	12.7	28.0	125
	C_2H_5Cl	38.2	68.4	609	9.5	20.6	57.5	15.2	30.5	144
	CHClCHCl	0.0	1.3	72	0.0	0.4	3.7	0.0	1.8	13
	CH_2CCl_2	0.7	3.8	160	0.3	1.2	60	0.4	1.3	51
VSLS-Br	CH_2Br_2	1.3	1.4	1.6	1.3	1.6	2.3	0.8	1.3	3.7
	Bromoform	1.4	2.2	4.9	3.5	5.8	25	0.8	2.0	5.3
	$CHClBr_2$				0.9	1.5	4.1			
	C_2H_5Br	2.2	2.9	10	0.5	1.3	3.6	0.7	1.5	3.1
	CH_2ClBr				0.2	0.2	0.4			
Methyl Halides	CH_3Cl	756	924	1240	577	753	1090	641	770	1090
	CH_3Br	15.9	19.0	48.8	8.09	14.8	28.6	8.74	12.5	20.6
	CH_3I	1.1	1.7	3.0	0.6	1.5	2.3	0.7	1.4	2.9

4.4d Summary of the range and median mixing ratios for the HFCs measured during the 2013, 2014 and 2015 Taiwan campaigns. The row highlighted in yellow represents a species not currently calibrated and so is relative to the AAL-071170 standard.

Compound		Campaign Mixing Ratios (ppt)								
Group	Name	2013			2014			2015		
		Min	Median	Max	Min	Median	Max	Min	Median	Max
HFCs	23	27	30	82	27	32	47	27.4	31.1	43.1
	32	4.5	8.0	17.2	5.8	9.5	28	6.4	9.0	14
	125	14.0	16.7	20.7	16.1	18.7	32.0	18.1	20.3	75.8
	134a	73.2	81.7	110	81.2	86.8	116	84.2	95.5	132
	143a	15.1	16.6	22.3	16.6	18.2	22.9	15.2	16.5	24.3
	152a	10.9	42.3	25600	8.5	13	26	7.73	11.3	38.1
	227ea	0.8	0.9	1.2	1.0	1.2	1.7	1.0	1.1	1.5
	245fa	1.2	1.3	1.5	1.4	1.5	2.3	1.2	1.6	6.0
	365mfc	0.5	0.7	0.9	0.6	0.8	2.6			

4.4e Summary of the range and median mixing ratios for the PFCs and other species measured during the 2013, 2014 and 2015 Taiwan campaigns. Those rows highlighted in yellow represent species not currently calibrated and so are relative to the AAL-071170 standard. Those rows highlighted in orange represent compounds measured by NCU and so not by the same instrumentation as the other species.

Compound		Campaign Mixing Ratios (ppt)								
		2013			2014			2015		
Group	Name	Min	Median	Max	Min	Median	Max	Min	Median	Max
PFCs	C_2F_4	0.6	1.8	6.3	0.2	0.6	5.8			
	C_2F_6	3.84	4.16	4.47	3.84	4.03	8.32	3.89	4.06	4.93
	C_3F_8	0.58	0.67	1.1	0.58	0.66	6.09	0.53	0.61	1.25
	C_4F_{10}				0.17	0.19	0.24	0.18	0.19	0.20
	iso-C_4F_{10}							0.07		0.12
	c-C_4F_8	1.0	1.2	1.3	1.4	1.5	3.8	1.4	1.5	2.2
	C_5F_{12}	0.25	0.36	0.56	0.15	0.16	0.19	0.14	0.15	0.16
	c-C_5F_{10}							1.2	1.3	1.6
	C_6F_{14}	0.69	1.2	1.9				0.26	0.27	0.59
	iso-C_6F_{14}							1.1	1.3	1.6
	C_7F_{16}	0.30	0.47	0.75	0.10	0.13	0.23	0.11	0.13	0.19
	SF_6	7.70	8.94	14.4	8.33	9.84	26.0	8.56	9.36	18.9
Other	COS	629	695	865	529	642	905	523	680	919
	SF_5CF_3	0.15	0.15	0.16	0.15	0.16	0.17	0.15	0.15	0.17
	C_3H_7Br	20	46	230	4.3	24	190			
	CO (ppb)	150	240	420	110	240	400	50	200	620
	O_3	23	49	100	23	56	87	41	53	71
	NO_X	3.3	5.3	11				1.5	2.9	10.
	PM_{10}	14	44	190	5.1	20	46			

4.5a Summary of percentage enhancement above background mixing ratios of the CFCs, halons and HCFCs for the 2013, 2014 and 2015 Taiwan campaigns. Background abundances are highlighted according to source and reflect data from NOAA MLO (red), AGAGE RPB (purple), Cape Grim, Tasmania (blue) or other literature (green) as referenced below the table.

Compound		Campaign Enhancement Above Background (%)											
		2013				2014				2015			
Group	Name	Background (ppt)	Min (%)	Median (%)	Max (%)	Background (ppt)	Min (%)	Median (%)	Max (%)	Background (ppt)	Min (%)	Median (%)	Max (%)
CFCs	11	236.49	5.3	8.3	29	234.66	-2.4	1.2	6.3	233.36	-1.0	2.2	220
	12	523.71	-2.4	0.3	3.7	521.03	-0.4	0.6	1.6	517.50	-0.8	0.3	3.1
	13	3.83	3.7	6.5	24					3.84	2.9	4.3	6.8
	113	73.57	0.7	2.5	8.4	72.99	0.5	2.5	12				
	113a[1]	0.50	-28	43	260	0.51	27	77	520	0.53	14	42	200
	114									14.73	-0.3	1.8	3.8
	114a									1.04	1.2	3.7	16
	115	8.40	3.7	5.0	7.1	8.43	-1.0	3.0	6.9	8.50	0.4	3.3	8.1
Halons	1211	3.86	3.3	9.8	35	3.76	-0.5	9.5	27	3.66	-3.5	7.2	28
	1202	0.02	15	68	140	0.02	2.4	53	220	0.01	22	45	120
	1301	3.29	-7.5	-2.1	6.5	3.26	-3.0	0.4	6.3	3.27	-3.9	1.4	10
	2402	0.45	2.3	9.4	14	0.44	1.2	10	96	0.43	-21	5.4	8.6
HCFCs	22	226.88	0.0	15	54	232.16	1.3	15	49	237.01	2.0	10	780
	133a[1]	0.54	-14	39	900	0.49	-6.0	25	290	0.47	-5.9	35	270
	141b	24.21	3.3	26	98	24.27	1.4	34	290	24.73	-1.1	17	61
	142b	22.01	-3.6	4.4	28	22.10	-1.9	9.1	36	22.30	-1.5	5.2	21

1 - Laube et al. 2014

4.5b Summary of percentage enhancement above background mixing ratios of the chlorocarbonss, chlorinated VSLS, methyl halides and HFCs for the 2013, 2014 and 2015 Taiwan campaigns. Background abundances are highlighted according to source and reflect data from NOAA MLO (red), AGAGE RPB (purple), Cape Grim, Tasmania (blue) or other literature (green) as referenced below the table.

Compound		Campaign Enhancement Above Background (%)											
		2013				2014				2015			
Group	Name	Background (ppt)	Min (%)	Median (%)	Max (%)	Background (ppt)	Min (%)	Median (%)	Max (%)	Background (ppt)	Min (%)	Median (%)	Max (%)
Chloro-carbons	CCl_4	85.58	1.9	4.7	56	84.68	-3.9	0.9	19	83.47	-0.9	2.7	13
	CH_3CCl_3	4.70	0.8	7.2	16	3.87	-5.3	2.2	13	3.22	-8.9	1.4	14
VSLS-Cl	PCE	2.20	-25	99	390	2.65	-38	110	600	2.30	-22	88	290
	CH_2Cl_2	54.80	40	340	770	49.00	54	440	8000	51.60	15	280	940
	Chloroform	7.78	49	320	2500	8.61	61	310	1100	9.48	34	200	1200
Methyl Halides	CH_3Cl	576.56	31	60	110	546.17	5.6	38	99	553.71	16	39	97
	CH_3Br	7.37	120	160	560	7.13	14	110	300	6.80	29	84	200
HFCs	23	26.11	3.9	17	210	27.07	2.3	18	73	28.27	-3.0	9.6	52
	125	13.08	7.6	27	58	14.83	8.7	26	120	16.71	8.2	22	350
	134a	72.84	0.5	12	51	78.17	3.9	11	49	83.68	0.6	14	58
	143a	13.40	13	24	66	14.48	15	26	59	15.97	-4.9	3.3	52
	152a	7.77	40	440	330000	7.19	18	77	260	7.32	5.7	54	420
	227ea	0.93	-14	-3.8	32	1.01	3.4	20	70	1.11	-11	1.2	36
	245fa	1.99	-38	-33	-25	2.08	-34	-27	11	2.33	-47	-29	160
	365mfc	0.68	-24	-3.4	29	0.70	-21	15	260	0.78			

4.5c Summary of percentage enhancement above background mixing ratios of the PFCs and other species for 2013, 2014 and 2015 Taiwan campaigns. Background abundances are highlighted according to source and reflect data from NOAA MLO (red), AGAGE RPB (purple), Cape Grim, Tasmania (blue) or other literature (green) as referenced below the table.

Compound		Campaign Enhancement Above Background (%)											
		2013				2014				2015			
Group	Name	Background (ppt)	Min (%)	Median (%)	Max (%)	Background (ppt)	Min (%)	Median (%)	Max (%)	Background (ppt)	Min (%)	Median (%)	Max (%)
PFCs	C_2F_6	3.75	2.3	11	19	3.79	1.4	6.3	120	3.83	1.6	5.9	29
	C_3F_8	0.58	0.6	15	88	0.59	-2.4	11	930	0.61	-14	-0.2	100
	C_4F_{10}[1]					0.18	-7.1	4.5	33	0.18	-2.7	5.6	12.
	c-C_4F_8[2]	1.31	-21	-13	-0.2	1.34	2.3	10	180	1.37	4.1	10	58
	C_5F_{12}[1]	0.14	74	150	290	0.15	3.3	12	31	0.15	-1.5	2.3	6.8
	$C6F_{14}$[1]	0.26	170	350	640					0.26	-1.6	4.2	130
	C_7F_{16}[1]	0.12	160	300	550	0.12	-13	10	89	0.12	-9.3	6.1	59
	SF_6	7.90	-2.5	13	82	8.26	0.7	19	220	8.53	0.3	9.6	120
Other	COS	526.40	20	32	64	531.00	-0.4	21	70	522.40	0.0	30	76
	SF_5CF_3[3]	0.15	-0.7	2.7	4.9	0.15	-1.5	3.3	12	0.15	-3.2	2.7	13

1 – Laube et al. 2012 2. – Oram et al. 2012 3. – Sturges et al. 2012

4.6a Summary of uncertainties for the background mixing ratios utilised for comparison in each Taiwan campaign.

Compound		Background uncertainties (ppt)		
Group	**Name**	**2013**	**2014**	**2015**
CFCs	11	0.383	0.391	0.388
	12	0.861	0.821	0.362
	13	0.010	0.006	0.005
	113	0.015	0.004	-
	113a[1]	0.004	0.004	0.004
	114	-	-	0.3
	114a	-	-	0.01
	115	0.075	0.047	0.038
Halons	1211	0.01	0.03	0.01
	1202	0.038	0.026	0.010
	1301	0.08	0	0
	2402	0.013	0.002	0.006
HCFCs	22	0.61	0.75	0.66
	133a[1]	0.043	0.043	0.043
	141b	0.11	0.01	0.12
	142b	0.01	0.04	0.14
Chloro-carbons	CCl_4	0.323	0.291	0.247
	CH_3CCl_3	0.03	0.022	0.022
VSLS-Cl	PCE	0.09	0.01	0.01
	CH_2Cl_2	0.16	0.24	0.03
	Chloroform	0.475	0.508	0.575

4.6b Summary of uncertainties for the background mixing ratios utilised for comparison in each Taiwan campaign continued.

Compound		Background uncertainties (ppt)		
Group	**Name**	**2013**	**2014**	**2015**
Methyl Halides	CH_3Cl	0.2	0.4	0.2
	CH_3Br	0	0	0.01
HFCs	23	0.144	0.114	0.105
	125	0.07	0.52	0.43
	134a	0.08	0.07	0.02
	143a	0.3	0.35	0.58
	152a	0.02	0.05	0.09
	227ea	0.03	0.03	0.01
	245fa	0.073	0.044	0.041
	365mfc	0.003	0.005	0.023
PFCs	C_2F_6	0.027	0.020	0.012
	C_3F_8	0.03	0.03	0.03
	C_4F_{10}[1]	0.003	0.003	0.003
	c-C_4F_8[2]	0.02	0.02	0.02
	C_5F_{12}[1]	0.003	0.003	0.003
	C_6F_{14}[1]	0.007	0.007	0.007
	C_7F_{16}[1]	0.004	0.004	0.004
	SF_6	0.036	0.029	0.03
Other	COS	2.1	0.8	0.7
	SF_5CF_3[3]	0.018	0.018	0.018

5.1 Full sample list of canisters collected during the 2014 Bachok campaign.

Canister	Date	Time		Fill (psi)	Wind
		Local	UTC		
K1623	20/01/14	12:05	04:05	26	light
K1621	20/01/14	16:10	08:10	30	light
K1635	21/01/14	12:10	04:10	30	light
K1622	22/01/14	11:45	03:45	30	light
K1624	23/01/14	12:50	04:50	40	light from sea
K1633	24/01/14	17:40	09:40	40	mod from sea
K1634	25/01/14	12:08	04:08	40	light
K1527	26/01/14	12:15	04:15	40	light from sea
K1636	27/01/14	17:55	09:55	40	mod from sea
K1632	28/01/14	12:25	04:25	40	strong from sea
K1531	28/01/14	17:05	09:05	40	mod from sea
K1529	29/01/14	17:00	09:00	40	light from sea
K1518	30/01/14	11:55	03:55	40	strong from sea
K1573	30/01/14	17:45	09:45	40	light from sea
K1566	30/01/14	19:40	11:40	40	
K1572	30/01/14	23:59	16:00	40	
K1565	31/01/14	08:00	00:00	40	light from land
K1571	31/01/14	12:00	04:00	40	light from sea
K1563	31/01/14	16:00	08:00	40	light from sea
K1568	31/01/14	20:00	12:00	40	light from sea
K1584	01/02/14	08:00	00:00	40	no breeze
K1520	01/02/14	12:00	04:00	40	v light from sea
K1582	01/02/14	16:00	08:00	40	light from sea
K1567	01/02/14	20:00	12:00	40	light from sea
K1570	02/02/14	12:10	04:10	40	light from sea
K1561	03/02/14	14:15	06:15	40	mod from sea
K1581	05/02/14	17:55	09:55	45	light/mod sea

5.2a NAME Backwards Trajectories for Bachok 2014: Cold Surge Period

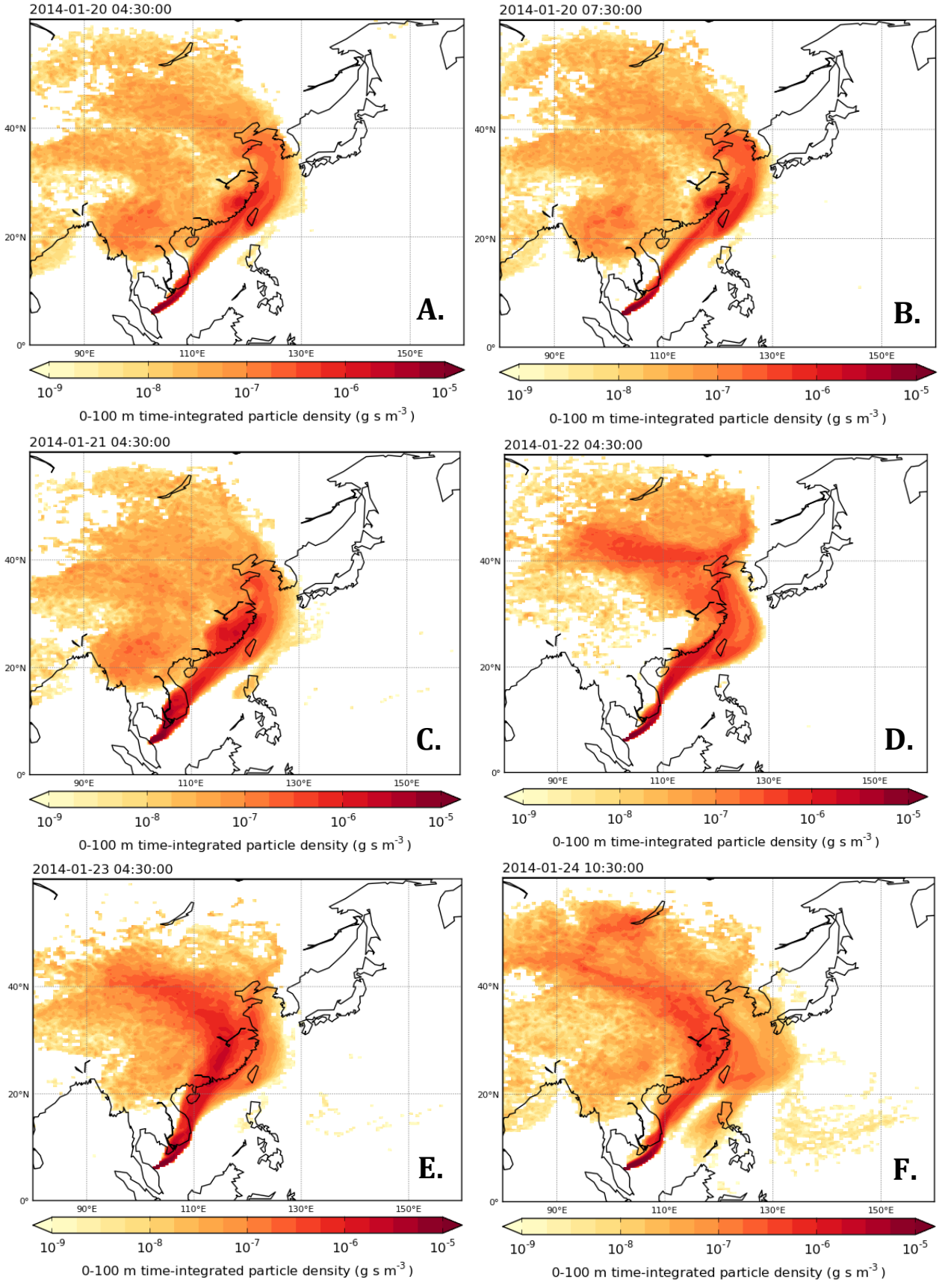

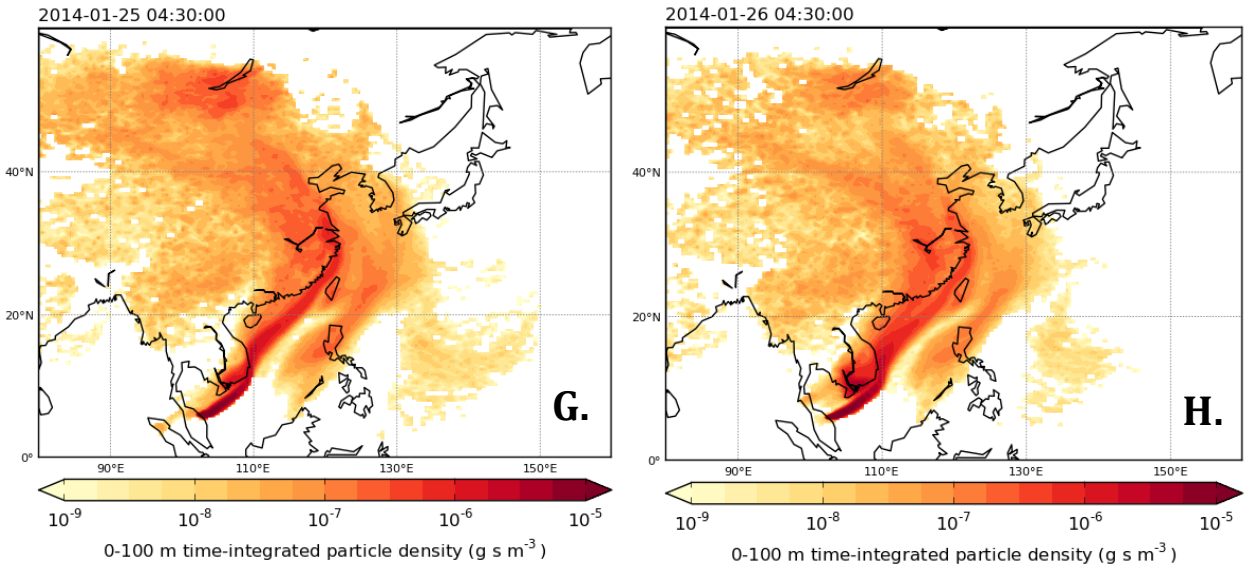

5.1b NAME Backwards Trajectories for Bachok 2014: Post-Cold Surge Period

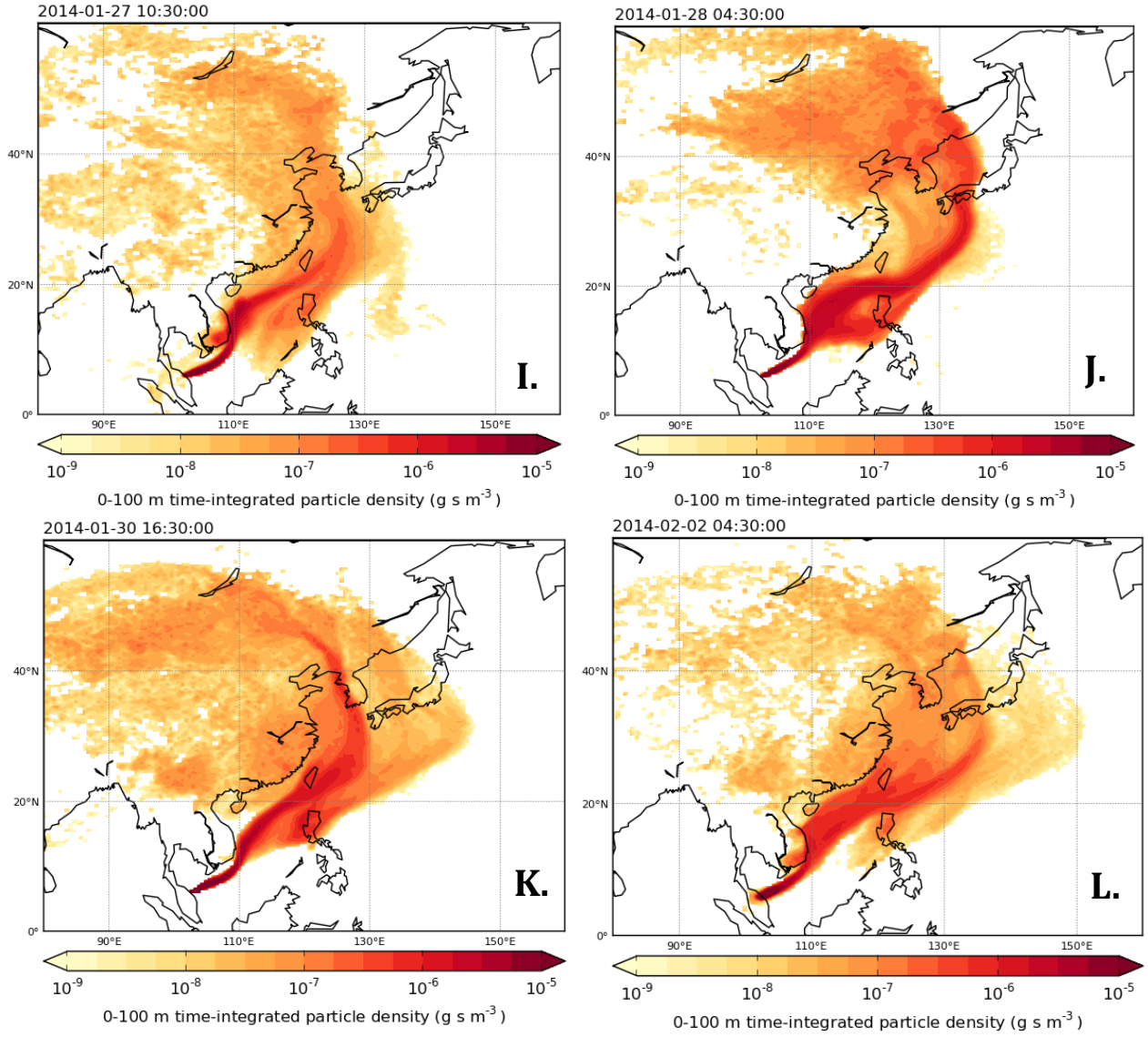

5.3a Overview of the range and median mixing ratios for CFCs, halons and HCFCs measured during the cold surge event, after the cold surge event and across the whole Bachok campaign.

Compound		Mixing Ratios (ppt)								
		Bachok Campaign			During Cold Surge Event			After Cold Surge Event		
Group	Name	Min	Median	Max	Min	Median	Max	Min	Median	Max
CFCs	11	226	237	245	226	237	246	235	237	243
	12	516	523	526	516	523	526	521	522	523
	13	3.8	4.0	4.1	3.8	4.0	4.1	4.0	4.0	4.1
	113	73.8	74.5	75.8	73.8	74.3	75.8	74.4	74.6	75.2
	113a	0.68	0.75	1.0	0.71	0.90	1.0	0.68	0.72	0.74
	114	14.2	15.0	15.6	14.2	15.0	15.6	14.8	14.9	15.2
	114a	1.0	1.1	1.1	1.0	1.1	1.1	1.0	1.0	1.0
	115	8.6	8.8	8.9	8.6	8.8	8.9	8.7	8.8	8.8
Halons	1211	3.9	4.0	4.4	3.9	4.1	4.4	3.9	3.9	4.0
	1202	0.02	0.02	0.04	0.02	0.03	0.04	0.02	0.02	0.02
	1301	3.1	3.3	3.6	3.1	3.4	3.6	3.1	3.2	3.3
	2402	0.44	0.47	0.49	0.45	0.47	0.49	0.44	0.47	0.48
HCFCs	22	230	246	267	241	247	267	230	234	235
	133a	0.47	0.63	0.99	0.53	0.75	0.99	0.47	0.50	0.56
	141b	24	27	33	27	28	33	24	25	25
	142b	22	23	24	22	23	24	22	22	22

5.3b Overview of the range and median mixing ratios for chlorinated and brominated VSLS, chlorocarbons and methyl halides as well as CO, measured during the cold surge event, after the cold surge event and across the whole Bachok campaign.

Compound		Mixing Ratios (ppt)								
		Bachok Campaign			During Cold Surge Event			After Cold Surge Event		
Group	Name	Min	Median	Max	Min	Median	Max	Min	Median	Max
VSLS-Cl	CH_2Cl_2	76	180	390	140	190	390	76	85	100
	DCE	20	57	120	51	64	120	20	23	31
	PCE	1.9	4.3	9.5	3.4	4.6	9.5	1.9	2.0	2.0
	Chloroform	15	21	30	20	24	30	15	15	17
	C_2H_5Cl	10.0	21	30	15	25	30	10	14	19
VSLS-Br	CH_2Br_2	1.2	1.3	1.5	1.2	1.3	1.4	1.2	1.2	1.5
	Bromoform	0.65	1.8	2.7	0.65	1.8	2.7	1.2	1.3	1.8
	$CHClBr_2$	0.39	0.68	1.1	0.43	0.72	1.2	0.39	0.66	0.86
	C_2H_5Br	0.50	1.3	3.1	0.73	1.9	3.2	0.50	0.71	0.99
	CH_2ClBr	0.15	0.20	0.26	0.18	0.21	0.26	0.15	0.17	0.17
Chloro-carbons	CCl_4	82	86	95	84	87	95	82	85	85
	CH_3CCl_3	3.9	4.1	4.2	4.0	4.1	4.2	3.9	4.1	4.2
	Halothane	0.01	0.01	0.01	0.01	0.01	0.01	0.01	0.01	0.01
Methyl Halides	CH_3Cl	600	800	860	780	830	860	610	640	700
	CH_3Br	9.5	15	28	11	17	28	9.5	11	14.8
CO	Total CO	7.0	21	70	12.91	27.75	70.09	7.0	13	19
	Industrial CO	3.7	14	65	10	23	65	3.7	6.7	11
	Other CO	2.2	3.7	9.2	2.2	3.7	7.3	2.6	5.6	9.2

5.4a Overview of the enhancement above background in CFC, halon and HCFC abundances during and after the cold surge event as well as across the whole Bachok campaign. Background mixing ratios highlighted in red indicates a NOAA MLO average, purple indicates an AGAGE RPB average, blue indicates a Cape Grim average and green indicates extrapolated from Laube et al. 2014

Compound		Background (ppt)	Enhancement Above Background (%)								
			Bachok Campaign			During Cold Surge Event			After Cold Surge Event		
Group	Name		Min	Median	Max	Min	Median	Max	Min	Median	Max
CFCs	11	234.91	-3.83	0.89	4.52	-3.83	0.89	4.52	0.04	0.69	3.59
	12	520.95	-0.87	0.31	1.00	-0.87	0.39	1.00	-0.05	0.11	0.41
	13	3.84	-0.08	4.3	7.3	-0.08	4.4	7.3	3.0	4.0	6.0
	113	73.09	0.93	1.92	3.75	0.93	1.69	3.75	1.8	2.0	3.0
	113a[1]	0.51	32	46	95	39	75	95	32	41	44
	114	14.81	-3.9	1.2	5.1	-3.9	1.2	5.1	-0.01	0.80	2.7
	114a	1.02	-1.4	2.5	11	1.5	4.4	11	-1.4	-0.46	1.5
	115	8.43	1.5	4.1	5.9	1.5	4.1	5.9	3.3	4.2	4.7
Halons	1211	3.78	2.1	6.7	16	2.34	8.76	16.06	2.07	3.63	4.78
	1202	0.02	12	48	170	40.55	55.92	174.29	11.78	15.83	25.03
	1301	3.32	-6.7	-0.64	6.8	-5.52	2.26	6.81	-6.74	-3.87	-1.07
	2402	0.44	0.85	6.8	11	1.33	6.96	10.57	0.85	6.82	8.23
HCFCs	22	231.78	-0.67	6.08	15.4	4.10	6.73	15.4	-0.67	0.88	1.42
	133a	0.40	17	57	150	32	87	150	17	23	40
	141b	24.38	0.46	13	36	11	15	36	0.46	3.1	4.4
	142b	22.12	-0.60	2.7	6.8	1.2	3.6	6.8	-0.60	-0.08	0.46

5.4b Overview of the enhancement above background in chlorinated and brominated VSLS, chlorocarbon and methyl halide abundances during and after the cold surge event as well as across the whole Bachok campaign. Background mixing ratios highlighted in red indicates NOAA MLO average and orange indicates MLB medians from Carpenter and Reimann, 2014.

Compound		Background (ppt)	Enhancement Above Background (%)								
			Bachok Campaign			During Cold Surge Event			After Cold Surge Event		
Group	Name		Min	Median	Max	Min	Median	Max	Min	Median	Max
VSLS-Cl	CH_2Cl_2	55.50	38	220	600	160	240	600	38	52	84
	DCE										
	PCE	1.75	6.1	150	440	95	160	440	6.1	13	18
	Chloroform	10.36	40	110	190	90	140	190	40	42	66
	C_2H_5Cl										
VSLS-Br	CH_2Br_2	0.90	28	44	64	31	48	55	28	38	63
	Bromoform	1.20	-46	45	120	-46	49	120	0.3-	11	47
	$CHClBr_2$										
	C_2H_5Br										
	CH_2ClBr	0.10	49	98	160	76	110	160	49	69	72
Chloro-carbons	CCl_4	84.79	-3.1	0.89	12	-1.3	2.9	12	-3.1	0.09	0.36
	CH_3CCl_3	3.91	0.05	5.9	7.6	1.6	6.2	7.6	0.05	4.4	6.7
	Halothane										
Methyl Halides	CH_3Cl	586.18	3.4	36	47	33	42	47	3.4	9.1	20
	CH_3Br	6.99	36	110	31-	63	150	310	36	58	110

5.5 Calculation of EECl Budget Data

Table 1: Species included in the budget calculations and their associated EECl multiplication factors

Group	Compound	Multiplication Factor
CFCs	CFC-11	3
	CFC-12	2
	CFC-13	1
	CFC-113	3
	CFC-113a	3
	CFC-114	2
	CFC-114a	2
	CFC-115	1
Halons	H1211	120
	H1202	61
	H1301	60
	H2402	120
HCFCs	HCFC-22	1
	HCFC-133a	1
	HCFC-141b	1
	HCFC-142b	2
VSLS-Cl	CH_2Cl_2	1
	DCE	2
	PCE	3
	Chloroform	4
	C_2H_5Cl	2
VSLS-Br	CH_2Br_2	120
	Bromoform	180
	$CHClBr_2$	121
	C_2H_5Br	60
	CH_2ClBr	61
Chlorocarbons	CCl_4	4
	CH_3CCl_3	3
	Halothane	61
Methyl Halides	CH_3Cl	1
	CH_3Br	60

Table 2: Total EECL for each compound group for each sample as calculated from the mixing ratios and multiplication factors. Total error was calculated using the same multiplication factors.

Sample	8 CFCs	4 Halons	4 HCFCs	5 VSLS-Cl	5 VSLS-Br	3 Chlorocarbons	2 Methyl Halides	Total
20/01/14	2039.12	744.73	313.83	363.53	729.33	359.58	1831.56	6381.69
20/01/14	2033.37	738.09	321.62	453.72	750.93	347.95	2210.33	6856.01
21/01/14	2026.95	757.37	326.14	508.17	527.53	363.69	1942.66	6452.52
22/01/14	2032.41	755.57	318.48	468.35	753.05	349.81	2008.66	6686.34
23/01/14	2057.49	784.00	348.83	835.88	640.92	375.71	1789.40	6832.22
24/01/14	1982.06	697.97	326.90	509.20	935.24	354.02	2489.93	7295.33
25/01/14	2061.61	746.89	322.00	502.67	628.49	392.06	1724.90	6378.61
26/01/14	1993.60	722.41	320.90	416.81	572.39	367.08	1476.49	5869.68
27/01/14	2046.44	719.21	304.66	276.88	473.13	353.21	1361.27	5534.80
28/01/14	2007.62	689.08	304.03	214.62	668.76	341.64	1494.77	5720.51
30/01/14	2034.09	712.55	300.24	223.37	486.49	355.84	1185.70	5298.29
02/02/14	2019.62	704.27	303.06	209.18	530.80	351.12	1326.99	5445.03
Total Error	23.93	12.65	2.82	9.75	27.91	6.48	24.29	107.84

Table 3: 2012 avergae EECl for compound groups as established from Carpenter and Reimann, 2014.

	Cl-ODS	Br-ODS	VSLS-Cl	VSLS-Br	Total
2012 Average	3203.2	1139.3	91.9	366.4	4800.9